USGS
science for a changing world

Proceedings
UJNR WORKSHOP ON
SOIL-STRUCTURE INTERACTION

Menlo Park, California
September 22-23, 1998

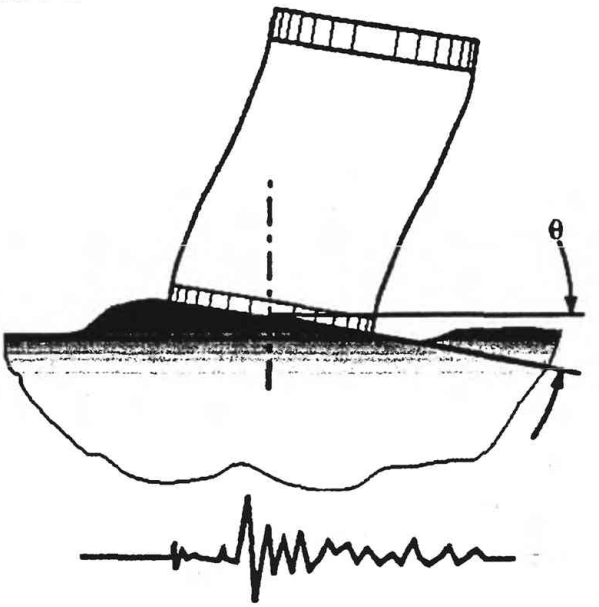

Editors & Conveners:

Mehmet Çelebi[1]
and
Izuru Okawa[2]

Open-File Report 99-142
1999

U.S. Department of the Interior
U.S. Geological Survey

---

[1] U. S. Geological Survey (MS977), 345 Middlefield Rd., Menlo Park, Ca. 94025
[2] IISEE, Building Research Institute, Tsukuba, Japan

ACKNOWLEDGEMENTS

The workshop was sponsored by both United States (US) and Japan. On the US side, the National Science Foundation (CMS-980762) and the United States Geological Survey (USGS) were the main sponsors. On the Japan side, several institutions including the Building Research Institute (BRI) and the Public Works Research Institute (PWRI) of the Ministry of Construction of Japan provided funds in support of this workshop. The conveners gratefully acknowledge the financial support that enabled successful planning and execution of the workshop

Mehmet Çelebi (USGS, Menlo Park, Ca.)
Izuru Okawa (BRI, Japan)

DISCLAIMER

The technical papers presented in this document are the responsibility of the authors. The United States Geological Survey does bear any responsibility for the accuracy of the calculations, figures and presentations contained in individual papers.

TABLE OF CONTENTS

TECHNICAL PAPERS OF THE WORKSHOP

FORWARD

During the May 1997 meeting of the Panel on Wind and Seismic Effects of the United States – Japan Natural Resources Development Program (UJNR) held in Tsukuba, Japan, it was decided to hold a workshop on "Soil-Structure Interaction " (SSI) in 1998. The panel assigned Dr.` M. Celebi of USGS, Menlo Park, Ca., and Dr. I. Okawa from BRI, Tsukuba, Japan to serve as organizers of the workshop. Subsequently, the organizers decided to hold this workshop in Menlo Park, California on
September 22-23, 1998.

The workshop participants who are experts in the field from Japan and the United States met in Menlo Park, California, presented technical papers and discussed topics including but not limited to (a) current methods of SSI used in design/analyses processes in both Japan and the United States, (b) recent research that is being carried out, (c) experimental SSI research arrays and/or facilities developed and that are in the process of being developed and (d) searching ways to cooperate on future SSI research. The aim of the workshop was to cover the following topics:

1. Current Methods of Practice of SSI in the US and Japan
    a. Geotechnical Point of View
    b. Structural Point of View
2. Code Provisions and Limitations.
3. Observed Data.
4. Observational Arrays and Testing Facilities – Current Status and Future Needs.
5. Recent Research Results and How To Implement Them Into Practice.
6. Additional Research Needed.
7. Additional Observational Arrays and Testing Facilities Needed.

While it was impossible to cover all of these subjects, the workshop provided a venue to discuss a variety of issues related to soil-structure interaction. One of the important issues revealed during these discussions, summarized in Section XX (?) of the proceedings, is that funding for SSI research has not increased in either the US or Japan. Consequently, the number of published papers related to SSI research has been steady and has not increased during the last few years. A recommendation made by the participants to organize an International Association for Soil-Structure Interaction (IASSI) is aimed to improve the funding for SSI research and improve the communication between the researchers and the practicing engineers. Furthermore, it was pointed out that should such an organization be formalized, it would be a means to organize special purpose conferences and workshops on the specific subject.

As the host convener of the workshop, I thank all of the participants for their attendance and enthusiastic presentations and discussions. I look forward to future UJNR-SSI Workshops.

Mehmet Çelebi
Menlo Park, Ca.
September 1998

RESOLUTION OF PARTICIPANTS

U.S. - Japan Workshop on Soil-Structure Interaction
Menlo Park, California, September 22-23, 1998

WHEREAS, soil-structure interaction can have major influence on the seismic performance of important structures, such as buildings, dams, bridges, and nuclear power plants, and thus affect public safety; and

WHEREAS, the methodologies for including soil-structure interaction effects in assessing seismic performance of such structures are inadequate; and

WHEREAS, present-day design codes provide little guidance for treating soil-structure interaction effects;

NOW THEREFORE BE IT RESOLVED THAT

(1) research to advance soil-structure interaction methodologies be given high priority and that design provisions related thereto be introduced into the codes, thus enhancing the seismic safety of structures designed accordingly, and

(2) cooperation between the U.S. and Japan, with focus on advancing both state-of-the-art and state-of-the-practice of treating soil-structure interaction be strengthened, and

(3) future additional UJNR-SSI meetings be organized, and

(4) an international organization be established to promote research, education, and improved design practice as related to soil-structure interaction.

Participants
US-Japan Workshop on SSI,
Menlo Park, Ca.
September 22-23, 1998

SUMMARY OF DISCUSSIONS AND RECOMMENDATIONS

Soil-structure-interaction (SSI) effects may be either beneficial or detrimental to the performance of structures. When beneficial, by incorporating SSI effects in the seismic code calculations, more cost-effective designs are possible. For some situations, such as the design or retrofitting of bridges, dams or buried structures, etc., an appropriate inclusion of SSI effects in seismic calculations may bring large design cost savings to our society. There is an urgent need for performing comparative cost-benefit reviews with and without considering rigorously the SSI effects for different types of constructions. On the other hand, when it is determined by calculations that SSI effects can be detrimental to the performance of structures, by mere recognition and taking effective measures, safety and better performance can be achieved.

1. Present Status of SSI:

- To promote practical application of SSI evaluation procedures, practicing engineers must first be convinced of the need for SSI evaluations. To render such evaluations a necessity, SSI evaluation procedures must become an integral part of the total seismic analysis and design process. Current building codes, which are based on SSI response behavior of a single-degree-of–freedom (SDOF) SSI system and have incorporated only the SSI effects of period elongation and damping increase for the fundamental mode of a structure system, do not address the total effect of SSI (such as the additional effects of "scattered" seismic input motions, and global as well as local soil non-linearity); as such, they do not promote the use of proper SSI evaluation procedures in the design process.

- In the past, SSI research has concentrated on solutions for gross dynamic response behaviors of simple linear SSI systems. Recent research also tends to focus on studying the SSI problems that can be solved with simple linear theories. To further the SSI research, it is time that the research be advanced beyond the studies of simple linear SSI systems and should start to develop realistic SSI evaluation procedures needed for practical design purposes, e.g. evaluations of nonlinear soil-resistance behaviors and soil-foundation interface pressures.

- To date, evaluation of seismic SSI effects has placed emphasis on seismic system demand, i.e., seismic SSI system response behavior. It is time to extend evaluation to SSI system performance, which requires the evaluation of not only the system demands but also the corresponding (strength and ductility) capacities. In the context of SSI, the system capacities of interest are the capacities of the soil-foundation interaction system. In fact, any realistic evaluation of the SSI system demand must incorporate realistic constitutive behavior of the soil-foundation system up to its allowable capacity limit.

- Experimental research should not be limited to the confirmation of SSI system response behavior. It must be designed and conducted in a manner in order to improve the SSI system modeling and to facilitate assessment of the SSI system performance up to its performance limit.

- To facilitate practical applications, SSI researchers must also develop and make available to practicing engineers a set of reliable and easy-to-use computer software for them to conduct realistic SSI evaluations.
- The number of papers on SSI both in Japan and US has been steady during the last few years. This implies that support for SSI research has not increased in recent years.
- SSI is interdisciplinary (geotechnical and structural) and hence tends to be poorly understood by both sides. There is a big gap between SOA (state-of-the-art) and the knowledge of practicing engineers.
- SSI is too complex to define exactly. We can define conditions where SSI is not important, however. Let's define what we know, where contributions can be made, and improve our knowledge transfer. We should not emphasize code-oriented research too much, we need to communicate to practitioners the essential aspects of the problem.
- Need to distinguish between heavy nuclear power plants and ordinary buildings. Nuclear plants are already being designed with consideration of SSI. For buildings, there are cases where SSI is not important. These cases should be identified.
- Our knowledge of ordinary building structures is limited, so there is a need to emphasize SSI research for ordinary types of buildings.
- There are virtually no full-scale experiments on buildings.
- Single-degree-of-freedom (SDOF) structure with rigid foundation is the most common type of research topic. Much research has been done on this subject.
- Flexible foundations with multi-degree-of-freedom (MDOF) structures are difficult to analyze and there is very little research done on this topic.
- Individual footings beneath each column are also difficult to analyze, and there is very little work done on this subject.
- There is virtually no field performance data on SSI. Existing data is inadequate. Interpretation of field data from earthquakes is important to verify methodologies.
- There is a lot of research on pile foundations. However, there is great need to translate that accumulated knowledge into practice.
- We need more detailed experiments.
- In general, Linear Elastic Analysis is good for:
    i. buildings on surface foundations
    ii. building-soil-building interaction
    iii. single building with embedded foundation

- Linear analyses is not so bad. Past experience shows linear models are here to stay. They've been around for a long time, despite some nonlinear alternatives, and they will remain. However, linear elastic analysis has shortcomings for building-soil-building interaction when the foundations are embedded.

- The standpoint of practitioners: Is SSI a necessary aspect of the design process? We think it is, but how do we demonstrate that? Need more than period lengthening and foundation damping; these are not useful to practicing engineers. We need to translate our research results into better demand predictions for structures. SSI enters the design process through pressure on foundations. Need further research on this.

- SSI is significant in the context of performance-based design.

- Community studying SSI is shrinking due to limited funding priority place on SSI by NSF. If we speak as one voice, we can make an impact on the NSF (like the structural control and tsunami people). Let's create a web site to advance the issue (post research findings, etc.).

- Design of Nuclear Power Plants was a major stimulus to SSI. Since practically no new nuclear plants are being design, such stimulus has vanished.

- Recent earthquakes show that there is a high level of nonlinearity in soil over broad area. This nonlinearity may have lead to SSI effects which saved these buildings. We need to investigate this.

- Need dialogue between experimentalists and analysts.

2. Additional SSI Research:

- Seismic earth pressures against retaining walls, considering non-linear aspects such as gapping.
- Comparative studies of non-linear vs. linear SSI to evaluate where non-linear analysis is important.
- More work is needed on pile foundations. For example, observed damage of piles due to soil displacement suggests that we need to consider soil displacement, not just structural inertia, when designing piles. How the two actions can be superimposed is of vital importance.
- More work is needed for underground structures such as tunnels and pipelines.
- How do we estimate the degree of nonlinearity in soil and its effects.
- Need more work on flexible foundations.
- More work needs to be done on seismic soil pressures against walls
- SSI is more involved than just the first mode period lengthening ratio ($\tilde{T} / T$) due to interaction and ground motion variability. The load paths for inertial load, especially near the ground line need to be considered.

- Nonlinear SSI may be very important for severe earthquakes. Need simple models for nonlinear SSI
- We are only recently getting accustomed to > 1g ground motions. Pushover is becoming more common, need to properly account for SSI in such analyses, especially near the failure state.
- If the movement is towards Performance Based Design, then we need to understand the uncertainties.
- There is a need for SSI research for near field ground motions. Such effects may be very localized.
- From the geotechnical point of view, an important issue is the damage in piles at soil boundaries significantly below the ground surface due to lateral flow. Before liquefaction, soil is fairly elastic and strains are important in determining soil properties. After liquefaction, soil behaves as liquid. Need to distinguish between liquefied and non-liquefied soil in our SSI formulations.
- Energy absorption by liquefied soil is significant, adds extra damping.
- Level of energy dissipation depends on when liquefaction occurs in the time history. Liquefaction doesn't help much if it occurs late. There is evidence of this from Wildlife Liquefaction Site (*see* Holzer, T. L., Youd, T. L., and Hanks, T. C., 1989, Dynamics of Liquefaction during the 1987 Superstition hills, California, earthquake, **Science**, v. 244, pp. 56-69).
- We need to be concerned about 5-to-10 story buildings subjected to near-field pulses. The long period energy content of these motions means that period lengthening would increase the base shear.
- There is a need to address in future engineering activities the large uncertainty associated with SSI. We know that the earthquake motions are random, the soil properties are random, local motion spatial variation is random, etc. So, there is an objective need in the future to approach these aspects more consistently using probabilistic models. In addition, for improving a seismic design or for a costly retrofit of a highway concrete bridge, it is essential to do some probabilistic SSI analyses, and try to calibrate the deterministic design based on risk assessment comparisons. Therefore, it is important that NSF envisions this need for future.

3. Better Field Observations:

- In general, there have been some successes in experimental work and use of observed data. These can be summarized in three ways: (a) Lotung-type of experiment with very good instrumentation for a specific type of structure, lots of comparisons between theory and experiment, (b) in-depth studies of typical building structures and (c) studies of many buildings, look at trends that can be easily understood by many engineers (e.g. Stewart, Ph.D. thesis – Stewart, J.P., and Stewart, A. F., 1997, Analysis of soil-structure interaction effects on building response from earthquake strong motion recordings at 58 sites, Report No: UCB/EERC 97/01, Richmond, Ca.). However, there is still great need for developing and/or improving the current field observation systems such that these systems will better enable
    - experimental verification of analytical procedures (e.g., in Europe, the research is on verifying SSI provisions in Eurocode.).

- interpretation of available field data
- additional instrumentation to obtain proper SSI response data (e.g. most instrumented buildings have inadequate vertical sensors to calculate rocking effects, and in some cases, if physically possible, additional free-field instruments and downhole accelerographs should be deployed).
- evaluation of the influence of free-field displacements on piles.
- understanding the soil pressures against foundation elements such as basement walls. More work needs to be done on seismic soil pressures against walls.

- We need reliable experimental data for verification of simple analysis schemes

4. Transfer of Knowledge:

- There is a big gap between state-of-the-art and the knowledge of practicing engineers. Therefore,
  - it is necessary to simply be able to demonstrate to the practicing engineers when and if SSI is important.
  - simple and practical tools and procedures are needed for transfer of knowledge to practicing engineers.
  - efforts should be made to include SSI in building codes.
  - efforts should be made to incorporate SSI methodologies in favorite computer software such as SAP.
  - efforts should be made to demonstrate to the profession the usefulness in incorporating SSI in their designs. The design engineers should be appraised of the fact that incorporation of SSI procedures can be, in some cases, financially beneficial.

- There is considerable research on pile foundations. However, there is great need to translate that accumulated knowledge into practice.

- There is a significant need for knowledge transfer on the issue of damping.

- Graduate students need to be taught SSI – this will help bridge that gap between researchers and practitioners. All grad student qualifying exams should have SSI questions.

- Need practical tools and agreed-upon computer codes.

- The data should not be used to calibrate a design code. Rather, we need to understand simple problems well, then develop good code formulations for design based on the insight gained from these simple models. Instrumentation needs to be detailed enough to guide us through the process.

5. Data Exchange Between US and Japan:

- This is of vital importance for researchers on both sides. As an example, Professor Iguchi wrote a book (along with 21 authors) on SSI. Two-thousand (2000) copies of this book were distributed in Japan through lectures to engineers. The US side may desire to have the book translated.
- There are impressive experiments in Japan for SSI, we need to become more familiar with them.
- We should recommend that there be better information exchange between US and Japan
- Japanese experimental data is extremely valuable – must relate it to available theoretical models. Perhaps we in the US could contribute our expertise to such an effort.

6. Other Issues:

- SSI practices should be pushed into the codes. In that case, the industry will use it. Thus, it will be necessary to teach it. Under these conditions, funding agencies will have to fund such activities. The code committees are receptive now to SSI. Therefore, this should be followed to fruition.
- We need an inside advocate in the NSF and USGS to get SSI funding. Let's speak as one voice to develop this inside advocacy. We should also look into new funding sources such as the insurance industry, and gas and oil companies.
- Funding for SSI research will increase when the industry has a demand for SSI, e.g. nuclear industry in 1970-1980s. Our models should not just be elastic, but should consider soil strength.
- There is an acute need for an international organization to promote SSI. The workshop participants agreed that it is important to promote research, education and design applications of soil-structure interaction, and to initiate specific steps towards its mandatory implementation in the design codes. Maria Todorovska proposed that an international association be set up to serve as an organizational framework to carry out this important task. The workshop participants endorsed this idea and agreed to promote the establishment of such an organization. It was further agreed that Maria Todorovska will contact the leading researchers in the US and abroad to discuss this idea further and to take specific steps towards its completion. The Japanese workshop participants agreed to contact other researchers in Japan.
- It was agreed that the 12WCEE (to be held in Auckland, New Zeland, in year 2000) is a convenient place for a meeting which can finalize the creation of an International Association. A special session on soil-structure interaction at this conference would be appropriate. Maria Todorovska proposed to organize such a session.

PROGRAM
UJNR-SSI WORKSHOP
Vallombrosa Center, 250 Oak Grove Avenue, Menlo Park, Ca

MONDAY – SEPTEMBER 21, 1998

Japanese participants arrive in the morning. US participants arrive in the afternoon/evening and the following morning.

TUESDAY - SEPTEMBER 22, 1998

8:00 - 9:00 AM	Breakfast & Registration
	[Session Chairs: Okawa, Celebi]
9:00 - 9:20 AM	Welcome Comments by Mehmet Celebi & Izuru Okawa
9:20 - 10:00 AM	(1) "States of the Arts on the Research on SSI in Japan" (Iguchi)
10:00 - 10:20 AM	**Coffee Break**
	[Session Chairs: Iiba, Veletsos]
10:20 - 11:00 AM	(2" Lateral seismic soil pressure" (Ostadan)
11:00 - 11:30 AM	(3) " On the design of pile foundation using response deformation method (Sugimuro & Karkee)
11:30 - 12:00 AM	(4) "Dynamic Soil-Foundation Structure Interaction Analyses of Large Caissons" (Mok)
12:00 - 13:00	**Lunch at Vallombrosa Center**
	[Session Chairs: Kitagawa, Ostadan]
13:00 - 13:30 PM	(5) "Dynamic Response of Cantilever Retaining Walls" (Veletsos)
13:30 - 14:00 PM	(6) "Dynamic behavior of pile foundation in liquefied Process-Shaking Table Tests Utilized Big Shear Box" (Iiba)
14:00 - 14:30 PM	(7) "Energy Dissipation in Soil-Structure Interaction" (Crouse)
14:30 - 15:00 PM	(8) "Empirical Assessment of SSI Effects from Strong Motion Recordings" (Stewart)
15:00 - 15:30 PM	**Coffee Break**
	[Session Chairs: Iguchi, Crouse]
15:30 – 16:00 PM	(9) "Dynamic Response of Soil-pile-building Interaction System in Large Strain Levels" (Tamori)
16:00 – 16:30 PM	(10) "Non-linear SSI Analyses" (Borja)
16:30 – 17:00 PM	(11) "SSI Effects on damping and natural frequency and effective input motion" (Fukuwa)
17:00 - 17:30 PM	(12) "The use of nolinear response spectra to seismic design" (Nakao)
17:30 - 18:00 PM	Discussions & Recommendations
18:00 – 19:00 PM	**Barbacue Dinner at Vallombrosa Center**
19:30 - 20:30 PM	Review Discussion of Draft Resolution & Reseach Issues

WEDNESDAY 23, SEPTEMBER, 1998

8:00 - 9:00 AM	Breakfast
	[Session Chairs: Fukuwa, Stewart]
9:00 - 9:30 AM	(13) "Reliability & Probabilistic Methods in SSI based on Observational Data" (Ghanem)
9:30 - 10:00 AM	(14) "Methods of analysis of SSI Effects in Bldgs & Underground Structures" (Luco)
10:00 - 10:30 AM	**Coffee Break**
	[Session Chairs: Tamori, Bielak]
10:30 - 11:00 AM	(15) "Soil-structure Interaction Effect on an NPP Reactor Building (Testing by NUPEC, Achievements and the Current Status)" (Kinoshita)
11:00 - 11:30 AM	(16) "Uncertainties in SSI Analysis: Modeling and Examples" (Ghiocel)
11:30 - 12:00 AM	(17) "Soil-structure interaction analysis via fixed-based system subjected to a modified ground motion" (Aydinoglu)
12:00 - 13:00	**Lunch at Vallombrosa Center**
	[Session Chairs: Sugimori, Todorovska]
13:00 - 13:30 PM	(18) "Seismic Design Procedure of Building Structures including SSI Effect" (Kitagawa)
13:30 - 14:00 PM	(19) "Experimental Facilities in the US that are being (and can be) used for SSI Research" (Ashford)
14:00 – 14:30 PM	(20) "Some full-scale experimental results on soil-structure interaction" (Todorovska & Trifunac)
14:30 – 15:00 PM	(21) "Soil-Foundation structure Interaction of bridges" (Tseng & Penzien)
15:00 - 15:30 PM	**Coffee Break**
	[Session Chairs:Karkee, Ashford]
15:30 - 16:00 PM	(22) "Three dimensional response of building-foundation systems" (Bielak)
16:00 - 16:30 PM	(23) "Dense Instrumentation in the BRI building and surrounding soil" (Okawa)
16:30 - 17:00 PM	(24) " Development of an SSI Experiment" (Celebi)
17:00 - 18:00 PM	Discussions & Recommendations
18:00 – 19:00 PM	**Dinner at Vallombrosa Center**

THURSDAY 24, SEPTEMBER, 1998

8:00 - 9:00 AM	Breakfast
9:00 -10:00 AM	Current Research Issues on Soil Structure Interaction
10:00 -10:15 AM	Coffee Break
10:15 -12:00 AM	Future Needs in Observation and Research (Analysis and Experiments)/Adoption of Resolution/Conclusion
12:00 - 14:00	**Lunch**
14:00 - 17:30 PM	Visit to USGS/Menlo Park

FRIDAY 25, SEPTEMBER, 1998

8:00 AM	Breakfast
9:00 -12:30 AM	John Blume Earthquake Eng. Center, Stanford university & Lunch
PM	Visit to Nearby Experiment Sites is being arranged for the participants

Adjourn

LIST OF PARTICIPANTS

U.S. PARTICIPANTS

Professor Scott Ashford
Structural Engineering.
9500 Gilman Dr., Mail 0085
University of California at San Diego,
La Jolla, Ca. 92093-0085
(T) 619-822-0431, (F) 619-534-6373
sashford@ames.ucsd.edu

Professor Jacobo Bielak
Dept. of Civil & Environ. Eng.
Carnegie-Mellon University
Pittsburg, PA 15213
(T) 412-268-2958, (F) 412-268-7813
jbielak@cmu.edu

Professor Ronaldo I. Borja
Dept. of Civil and Environmental Engineering
Stanford University
Stanford, CA 94305-4020
(T) 650-723-3664, (F) 650-723-7514
borja@ce.stanford.edu

Dr. Mehmet Çelebi
USGS (MS977)
345 Middlefield Rd.
Menlo Park, Ca. 94025
(T) 650-329-5623, (F) 650-329-5163
celebi@samoa.wr.usgs.gov

Dr. C. B. Crouse
Principal, Dames & Moore
2025 First Ave., Suite 500
Seattle, WA 98121
(T) 206-728-0744, (F) 206-727-3350
seacbc@dames.com

Professor Roger G. Ghanem
201 Latrobe Hall,
The John Hopkins University
Baltimore, MD 21218
(T) 410 516 7647 , (F) 410 516 7473
ghanem@jhu.edu

Dr. Dan M. Ghiocel
Stress Technology Inc
1800 Brighton-Henrietta Town Line Road
Rochester, New York 14623
(T) 716-424-2010, (F) 716-272-7201
DGHIOCEL@stresstech.com

Professor Enrique Luco
Dept. of Civil Engineering
University of California
La Jolla, Ca. 92093-0085
(T) 619-534-4338, (F) 619-822-2260
jeluco@ames.ucsd.edu

C. -M. Mok
Geomatrix Consultants Inc.
100 Pine St. , Suite 1000
San Francisco, Ca. 94111
(T)415-434-9400, (F) 415-434-1365
c.-m.mok@geomatric.com

Dr. Farhang Ostadan
Chief Engineer, Bechtel Corp.
50 Beale Street, P.O. Box 193965
San Francisco, Ca. 94119-3965
(T) 415-768-3734, (F) 415-768-3734
fostadan@bechtel.com

Professor Joseph Penzien
Internationl Civil Eng. Consultants,
1995 University Ave., Suite 119,
Berkeley, Ca. 94704
(T) 510-841-7328, (F) 510-8417438
penzien@icec.com

Professor Shahram Pezeshk
Civil Engineering Dept.
University of Memphis
Campus Box 526570
Memphis, TN 38152
(T)901-678-4727, (F)901-678-3026
spezeshk@memphis.edu

Mr. Maurice Power,
Principal Engineer
Geomatrix Consultants Inc.
100 Pine St. , Suite 1000
San Francisco, Ca. 94111
Tel: 415-434-9400,
Fax: 415-434-1365

Professor Jonathan Stewart
Civil & Environ. Eng. Dept.
5731-H Boelter Hall
University of California
Los Angeles, Ca. 90095-1593
(T) 310-206-2990, (F) 310-206-2222
jstewart@seas.ucla.edu

Professor Luis E. Suarez,
Civil Engineering Dept.
University of Puerto Rico
Mayaguez, Puerto Rico 00681-5000
(T)787-832-4040,(F)787-832-8260
lsuarez@rmce02.upr.clu.edu

Professor Maria I. Todorovska
Civil Engineering Department,
KAP 216A&D, MC 2531
Univ. of Southern California,
Los Angeles, CA 90089-2531
(T) 213-740-0616, (F) 213-744-1426
mtodorov@usc.edu

Dr. Selçuk Toprak
USGS, MS977
Menlo Park, Ca. 94025
(T)650-329-4864, (F)650-329-5163
stoprak@usgs.gov

Dr. William Joyner
USGS
345 Middlefield Road
Menlo Park, Ca. 94025
(T)650-329-5640, (F)650-329-5163
joyner@samoa.wr.usgs.gov

Professor Misha Trifunac
Civil Engineering Department,
KAP 216A&D, MC 2531
Univ. of Southern California,
Los Angeles, CA 90089-2531
(T) 213-740-0570,(F) 213-744-1426

Dr. Wen Tseng
Internationl Civil Eng. Consultants,
1995 University Ave., Suite 119,
Berkeley, Ca. 94704
(T) 510-841-7328, (F) 510-8417438
wentseng@icec.com

Professor Anestis S. Veletsos
Brown & Root Professor of Civil Eng.,
Civil Eng. Dept. P.O. Box 1892,
Rice University
Houston, Texas 77251
(T) 713-285-5291, (F) 713-285-5268

Mr. Bela Palfalvi
General Services Administration, Technical Services Branch (9PCT), Office of Property Development, 450 Golden Gate Avenue, 3rd Floor West,
San Francisco, Ca. 94102-3400
(T) 415-522-3183, (F)415- 522-3114
bela.palfalvi@gsa.gov

Dr. Roger Borcherdt
USGS
345 Middlefield Road
Menlo Park, Ca. 94025
(T)650-329-5619, (F)650-329-5163
borcherdt@samoa.wr.usgs.gov

Dr. Cliff Astill (in Absentia)
National Science Foundation
4201 Wilson Blvd.
Arlington, VA. 22230

JAPANESE PARTICIPANTS

Prof. Nobuo Fukuwa
Center for Cooperative Research in Advanced Science & Technology
Nagoya University, Furo-cho, Chikusa-ku, Nagoya 464-8603, Japan
(T) 81-52- 789-3757, (F) 81-52- 789-3768
fukuwa@sharaku.nuac.nagaoya-u.ac.jp

Dr. Masanori Iiba
Head, Geotechnical Engineering Division
Structural Engineering Department
Building Research Institute, Ministry of Construction, Tatehara-1, Tsukuba, Ibaraki 305-0802, Japan
(T)81-298- 64-6637,(F)81-298- 64-6773
Iiba@kenken.go.jp

Prof. Michio Iguchi
Dept. of Architectural Engineering, Faculty of Science and Engineering,
Science University of Tokyo,
Yamazaki 2641, Noda City 278-8510, Japan
(T) 81-471-24-1501,(F) 81-471-25-7533
Iguchi@rs.noda.sut.ac.jp

Dr. Madan Karkee
GEOTOP Corporation, Research Div.
1-16-3 Shinkawa, 4F
Chuo-ku, Tokyo, 104-0033, Japan
(T)81-3- 5543-4601,(F)81-3- 5543-4610
kar@geodec.eng.geotop.co.jp

Dr. Masamitsu Kinoshita
Nuclear Power Engineering Corporation (NUPEC), Shuwa-Kamiyacho Bldg.
Toranomon 4-3-13,
Minato-ku, Tokyo 105, Japan
(T)81-3-3434-5695,(F)81-3-3434-9487
kitada@nupec.or.jp

Prof. Yoshikazu Kitagawa
Department of Structural Engineering , Faculty of Engineering, Hiroshima University, 1-4-1,Kagamiyama,Higashi Hiroshima 739-8527,Japan
(T) 81-824- 24-7794, (F) 81-824- 24-7794
Kitaga@ipc.hiroshima-u.ac.jp

Prof. Shin-ichiro Tamori,
Department of Architecture and Civil Engineering, Faculty of Enginnering
Shinshu University, 500 Wakasato, Nagano, Nagano 380, Japan
(T) 81-26- 224 2750,(F)81-26- 224-2750
snowman@gipwc.shinshu-u.ac.jp

Dr. Yoshihiro Nakao
Ground Vibration Division,
Earthquake Disaster Prevention Research Center, Public Works Research Institute (PWRI), Ministry of Construction, 1, Asahi, Tsukuba-shi, Ibaraki-ken, 305 Japan.
(T)81-298-64-2211, (F)81-289 64-0598
nakao@pwri.go.jp

Mr. Hidemi Nakashima
Structural Design Engineer, Shimizu Corporation, [c/o EERC, University of California at Berkeley, 1301 South 46th Street, Richmond, California 94804-4698]
(T)1-510-231-9597, (F) 1-510-231-9471
hidemi@eerc.berkeley.edu /
Hidemi@ppp.bekkoame.ne.jp

Dr. Michihiro OHORI
Researcher, Obayashi Corporation
[c/o John Blume EE Center, Stanford University
Home address:
600 Willow Rd.#25,
Menlo Park, CA 94025, USA]
(T)1-650-328-9450
E-mail: ohori@pacbell.net

Dr. Izuru Okawa,
Head, Building Engineering Division
IISEE, Building Research Institute, Ministry of Construction, Tatehara-1, Tsukuba, Ibaraki 305-0802, Japan
(T)81-298-64-6758, (F)81-298- 64-6777
okawa@kenken.go.jp

Prof. Yoshihiro Sugimura
Dept. of Architecture and Building Science, Graduate School of Engineering, Tohoku University, Aoba Aramaki-06, Aobaku, Sendai, 980-8579, Japan
(T)81-22- 217-7867, (F)81-22- 217-7869
ugi@strmech.archi.tohoku.ac.jp

VISITING PARTICIPANTS

Professor Nuray Aydinoglu
Bogazici University,
Kandilli Rasathanesi,
81220 Cengelkoy, Istanbul, Turkey
(T)90-216-332-9701, (F) 90-216-308-0183
aydinogn@hamlin.boun.edu.tr

Professor Mustafa Erdik
Princeton Univ. & Bogazici University,
Kandilli Rasathanesi,
81220 Cengelkoy, Istanbul, Turkey
(T)90.216.332.1711,(F) 90.216.308.0163
erdik@hamlin.cc.boun.edu.tr

Mr. Wen Ruizhi
USGS, Menlo Park
[visiting from: IEM, Harbin, China

Dr. Li Hongjing
USGS, Menlo Park
[visiting from: IEM, Harbin, China

Seunghyun Kim
Student –UCLA

Chao-Hua Lin
Student-Stanford

Kossi Sama
Student-Stanford

Back Row: M. Trifunac, E. Luco, S. Pezeschk, R. Ghanem, I. Okawa, S. Toprak, L. Suarez, Y. Nakao, M. Kinoshita, J.Stewart (in the back), A. Veletsos, S. Ashford (in the back), H. Li (in the back), S. Tamori, M. Ohori (in the back), N. Fukuwa, M.Erdik , H. Nakashima, C.B. Crouse

Front Row: M. Çelebi, W. Tseng, J. Bielak, M. Todorovska, Y. Kitigawa, Y. Sugimura, M. Iguchi, M. Karkee, M. Iiba

STATE OF THE ART ON SOIL－STRUCTURE INTERACTION RESEARCHES RELATING TO RECENT STRONG EARTHQUAKES IN JAPAN

By Michio Iguchi [1] and Yuzuru Yasui [2]

ABSTRACT: This report reviews the soil-structure interaction (SSI) researches relating to three major earthquakes recently occurred in Japan, which include the 1993 Kushiro-oki earthquake, aftershocks of the 1993 Hokkaido-Nansei-oki earthquake and the 1995 Hyogo-ken Nanbu earthquake. The review work is focussed on the simulation analyses conducted on the basis of simultaneous earthquake records observed both in buildings and in the surrounding soil during these major earthquakes, as well as other small events observed at the site. One of the most interesting results reviewed in this report is the ratio of response spectra for the observed motions in a building to those for motions recorded on the soil surface. Marked difference of the ratios for small ground motions and for the strong motions in the Kushiro-oki earthquake is detected. It is also discussed that the nonlinear response analyses conducted with use of the two-dimensional FEM for soil-structure system have resulted in considerable deviation from the observations during the strong motions in the Kushiro-oki earthquake. Regarding the Hyogo-ken Nanbu earthquake, on the other hand, satisfactory results of the simulation analyses are overviewed. Furthermore, special emphasis is placed on a study of effective input motions into structures investigated on the basis of the simultaneous observations recorded both in structures and the surrounding soil during the Hyogo-ken Nanbu earthquake. The compared results of the peak values recorded on the foundation with those on the free-field soil surface indicate distinctly the reduction of effective input motions into structure. The effective input rates, which indicate the ratios of peak values of the effective input motion to the corresponding free-field motion, are approximately 0.7 for accelerations and 0.9 for velocities. In addition to the topics, a general trend of SSI researches for the last ten years in Japan is overviewed.

INTRODUCTION

Where is the goal of soil-structure interaction (SSI) researches? Although the objective may be set at various points, it is of no doubt that one of the goals is to improve the accuracy of assessment of structural safety against earthquakes by taking into account the SSI effects in response analyses of structures. This will lead to mitigation of earthquake damage to structures.

The seismic response analyses have become possible for complicated soil-structure models with taking into account various factors owing to great progress of SSI researches in the last three decades. As for methodology, for example, analysis methods can be chosen at our disposal among various methods (Iguchi and Akino 1993). In the analysis of an actual soil-structure system, however, we are obliged to introduce many simplifications, idealizations and assumptions in making mathematical soil models. as well as the interface between the soil and foundation. Thus, there are still a great gap between an actual system and the mathematical model.

In order to fill the gaps and to rationalize the assumptions, comparative studies between the observed and the analyzed results, so called simulation analyses must be accumulated. Furthermore, the establishment of prediction method for structural responses to strong

(1) Professor, Department of Architectural Engineering, Faculty of Science and Technology, Science University of Tokyo, Noda City, Japan.

(2) General Manager, Vibration Engineering Department, Technical Research Institute, Obayashi Corporation, Kiyose City, Japan.

earthquake ground motions with taking into account the SSI effects is also needed. In the simulation or prediction work, in either case, the accumulation of the densely observed records of soil-structure system becomes essential. In particular, the accumulation of many reliable strong motion records and the establishment of a methodology to extract the SSI effects from the records will be the key not only to capture substantially the SSI effects but also to improve the accuracy of assessment of structural safety against intense earthquakes.

In Japan, the simultaneous earthquake observations both in buildings and on the surrounding soil have been performed since the early 1970s, and many observed records have been accumulated so far. These data, however, have been scarcely made the best use of in the SSI researches. This may be due to lack of methodologies to isolate the SSI effects from the limited records or to insufficient observation records to extract the effects. Furthermore, the accumulated data are limited to those for small to medium ground motions, and there have been few strong motion records. It was not until the 1995 Hyogo-ken Nanbu earthquake that a certain number of simultaneous records have been observed for a strong earthquake and at various sites. Based on the observations, a number of studies have been presented on SSI effects for the earthquake. The objective of this report is to summarize the SSI researches relating to recent strong earthquakes including the Hyogo-ken Nanbu earthquake. Special emphasis is placed on the simulation analyses and effective input motions into structures investigated on the basis of the simultaneous observations recorded both in structures and the surrounding soil during the earthquakes. In addition to the topics, a general trend of SSI researches for the last ten years in Japan is overviewed. These will be described in the following chapters.

OVERVIEW OF CURRENT TREND OF SSI RESEARCHES IN JAPAN

A technical meeting of Architectural Institute of Japan (AIJ) is held every year and a number of papers are presented at the meeting. Many scientists, engineers and graduate students of various fields such as building science, structural mechanics, geotechnical engineering, earthquake engineering, etc. gather in one place to exchange information or to have a discussion. The papers presented at the meeting reflect the academic interest of the participants, and therefore it gives a clue to know a tendency of researches in Japan. In what follows, the current research trend on SSI in Japan is overviewed through the papers presented at the meeting. Fig. 1 shows a change of the number of papers on SSI presented at the meeting during the last ten years. As seen from the figure, the number of presented papers varies from around 60 to 80. It is noticed that a decline of the number had appeared for several years from 1992 but it has recovered soon after 1995 when Hyogo-ken Nanbu earthquake occurred. Though the interest in SSI has been unchanged among researchers, it is needed to extend the importance of SSI more widely to younger generation, as well as engineers concerned in seismic design of structures.

Fig. 2 shows the change of methodology used in SSI analyses. It is evidently seen from the figure that SSI researches relating to analytical procedures have been in decline and the thin layered element method (TLM) is gradually increasing to the contrary. The analytical solutions may have less meaning considering from practical point of view, but can play a significant roll to be

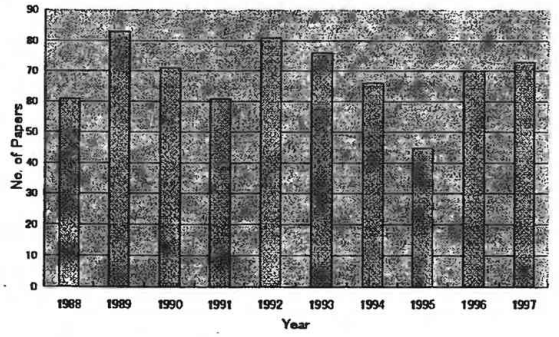

Fig. 1. The change of the number of papers presented at annual meeting of AIJ.

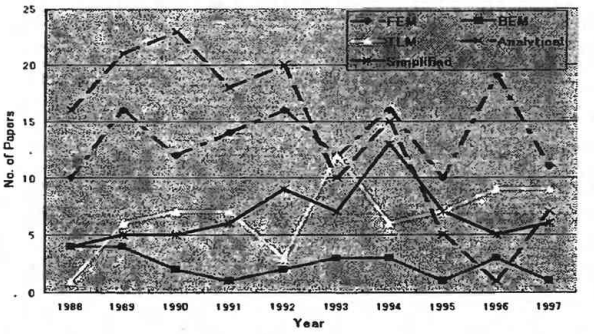

Fig. 2. The change of methodology used in SSI analyses.

the benchmark to check results obtained by other numerical procedures. The exploitation of simplified methods is important to have means to obtain results easily and quickly and the methods can be used to make up for the analytical methods. Nevertheless, the number of papers tends to be decreasing regrettably for these several years. The exploitation of simplified methods should be more evaluated.

Finally, Fig. 3 shows the change of subjects of SSI researches. It is clearly seen from the figure that the gradual increase of papers dealing with pile groups is in contrast to the decrease of papers on embedded foundations. It is also noticed from the figure that after 1995, when the Hyogo-ken Nanbu earthquake occurred, the number of papers dealing with pile groups has increased suddenly. It is also noted that the majority of papers are related to the pile groups for these two years. This is due to heavy damage to pile groups during the earthquake. At the same time, the spread of recognition of importance of soil-pile-structure interaction is another reason.

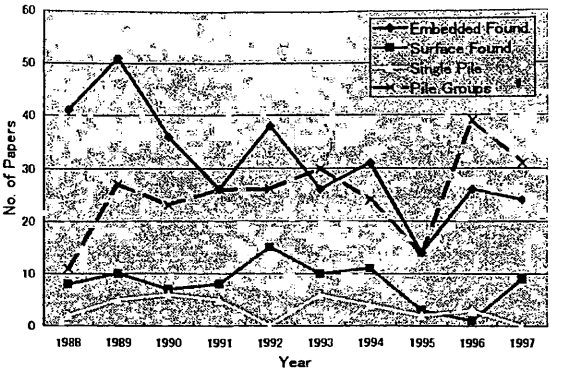

Fig. 3. The change of subjects of SSI researches.

SSI RESEARCHES ON RECENT STRONG EARTHQUAKES

The 1993 Kushiro-oki Earthquake

In January 1993, a strong earthquake struck Kushiro city in Hokkaido named the 1993 Kushiro-oki earthquake (M = 7.8). The simultaneous earthquake records were observed both in a building of Kushiro branch of the Japan Meteorological Agency (JMA) and on the soil surface at the site during the earthquake. The peak horizontal ground accelerations at the site were 711 gals (N63E) and 637 gals (N153E) recorded by a strong motion accelerometer (SMAC-MD) of the Building Research Institute (BRI). The peak accelerations observed in the building with an accelerograph (JMA-87) of JMA were 815 gals and 919 gals in north-south and east-west directions, respectively, which showed larger values than those observed on the free field. In spite of high intensity of earthquake motions, damage to structures was very slight not only at the site but also in the surrounding area. The possibilities of the intense ground motions and the slight damage had been studied from various viewpoints such as local site effects of surface geology, SSI effects, the effect of frozen soil, the strength capacities of the structures against seismic loads and so on. Some peak characteristics appeared in the response spectra of the recorded motions could be explained by using a detailed soil-structure model, but not enough to explain the magnitude of the spectra (Yasui and Takano 1994; Dan 1994). Also, the reasons of large accelerations in the building compared with the surrounding free-field motions are left unsettled. More detailed results investigated in the Extensive Research Committee on the 1993 Kushiro-oki earthquake established in the AIJ are provided elsewhere (AIJ 1994).

The earthquake motions have been observed thereafter and some other records were observed at the site. Making

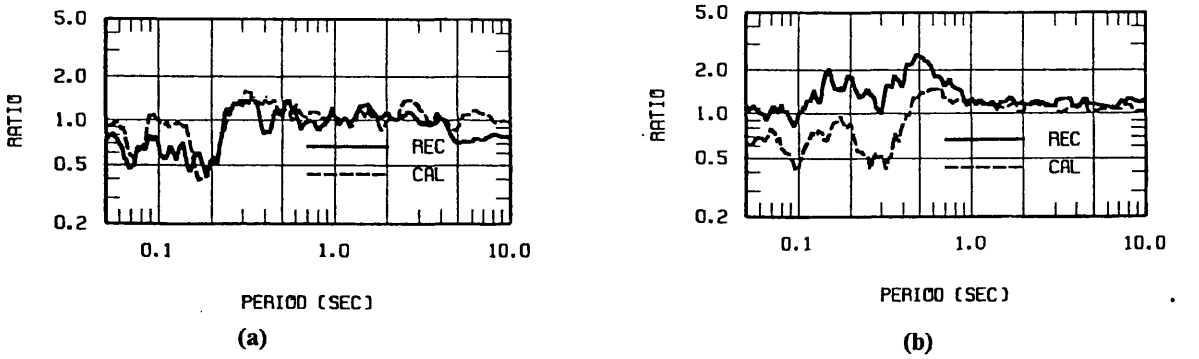

Fig. 4. Response spectral ratios (JMA/BRI) (a) for small event and (b) for Kushiro-oki earthquake (after Dan 1995).

use of these observations, comparative studies were performed on response spectra for other small events and the Kushiro-oki earthquake (Dan 1995). One of the most noticeable results presented in the paper may be found in the difference between response spectral ratios for small events and those for the strong motions of the Kushiro-oki earthquake. Fig. 4(a) and (b) show the ratios of the acceleration response spectra for the motions observed in the building (JMA) to those for the free-field motions (BRI). Fig. 4(a) is for a small event with peak acceleration (PA) of 19.3 gals and Fig. 4(b) is for the Kushiro-oki earthquake with PA of 919 gals on the soil surface. The observed results are compared in the figures with those computed by two-dimensional (2-D) FEM with taking non-linearity of the soil into account. An inspection of these results indicates that for small earthquake the ratio becomes smaller than 1.0 in shorter periods less than 0.3 sec, while for the Kushiro-oki event the ratio becomes greater than 1.0 in wider range of 0.1 to 1.0 sec. It is also noticed that the computed results can not fully explain the measured results in magnitude for the strong motions. Recalling the fact that the 2-D models tend to overestimate larger values of damping coefficients than the 3-D models (Luco and Hadjian 1974), the discrepancy might be mainly due to employment of 2-D model instead of 3-D model. It should be also noticed that the tendency recognized in the observed results in Fig. 4(b) is consistent with the parametric studies of nonlinearity effects of the surrounding soil on the structural response presented by Miyamoto et al. (1995).

The Aftershock of 1993 Hokkaido-Nansei-oki Earthquake

In July 1993, different large accelerations were observed on the ground floor of two-story school building during an aftershock (M = 6.5) of the 1993 Hokkaido-nansei-oki earthquake (M = 7.8). The peak horizontal and vertical accelerations observed were 393 gals (NS), 1,569 gals (EW) and 575 gals in UD (up-down) direction. The building is L-shaped of about 55m long in one side and supported on the soil having shear wave velocities of about 70 to 170 m/sec to the depth of 8.6m. In spite of the surprisingly large accelerations, there was no damage to structural elements of the building. Nonlinear simulation analyses of the structure were conducted with taking into consideration of SSI effects in order to explain the no structural damage to the building (Dan et al. 1997). As a consequence of detailed studies, the reason of no damage was attributed to high strength capacities of the building. The surface ground motions were also estimated based on the observed motions on the ground floor. In evaluation of the free-field motions, the foundation was assumed to be rigid in plane. The peak value of the estimated acceleration motion on the free surface was 345 gals in EW direction, which indicated large amplification of the input motion into the structure (Dan et al. 1997). It may be interpreted that the difference between the free-field motion and the records at the ground floor has resulted from SSI effects for the building. In order to confirm the large SSI effects presented in the paper, however, careful examination will be needed on effects of the location of accelerometers and the assumption of rigid foundation as well.

The 1995 Hyogo-ken Nanbu Earthquake

Some earthquake records were observed on the ground, inside of structures and simultaneously both in buildings and on the surrounding soil during the 1995 Hyogo-ken Numbu earthquake (M = 7.2). Based on the records, some simulation analyses have been conducted for heavily or slightly damaged structures with consideration of SSI effects and many suggestive results have been presented so far. Kurimoto (1996) performed a simulation analysis for a 41-story reinforced concrete building taking SSI effects into account when subjected to the observed motion at 70m below the ground surface. For this building, accelerometers are densely instrumented not only in the superstructure but also in the soil (Yasui et al. 1995). The peak horizontal accelerations observed on the ground floor during the main shock were 86.8 gals in EW and 60.7 gals in NS directions. The methodology used in the analysis was 2-D FEM incorporated with non-linearity of soil. Fairly good agreement between the observed and the computed was presented both in the soil and in the superstructure. This paper also indicates that the lateral soil of the embedded foundation becomes less effective due to non-linearity of the soil when the foundation is supported on a firm soil. Prior to this study, Fujimori et al. (1995) had studied the foundation input motions for the building subjected to ground motions observed during the Hyogo-ken Nanbu earthquake and the aftershocks as well. The comparison work indicated insignificant difference between the main and aftershocks. Perhaps, this is due to small rigidity of the lateral soil of the embedded foundation not only for the main shock but also for the aftershocks.

Tamura et al. (1996) conducted SSI analyses for damaged steel framed reinforced concrete buildings of 13-story and 11-story with embedded foundations.

Through response analyses, the horizontal motion at the base of the foundation was found to be almost same as the free-field motion at the level. This indicates a possibility of a method that the response analyses of superstructure could be evaluated with the base fixed at the bottom of the foundation and being subjected to the free-field motions at the depth of soil. Similar results have been presented by Hayashi et al. (1997). It was also pointed out that the damping factor of the SSI system associated with non-linearity of soil is dependent on the rigidity of the bearing soil (Tamura et al. 1996).

Earthquake motions were observed for buildings supported by piles and simulation analyses have been performed for the structures. Yokoyama (1996) and Kowada et al. (1997) have conducted simulation analyses of the soil-pile-structure systems subjected to the observed motions. In the analyses, Penzien's models (Penzien et al. 1964) for the soil-pile system was successfully used to explain the observed motions of superstructures.

EFFECTIVE INPUT MOTIONS IN THE HYOGO-KEN NANBU EARTHQUAKE

Review of the Researches

In addition to the findings obtained through simulation analyses, there are some noticeable studies focused on why the damage to structures had been comparatively minor in the Hyogo-ken Nanbu earthquake considering the intense earthquake ground motions. In the severely damaged Kobe City area, high intensity of accelerations (300 to 800 gals) and velocities (50 to 120 cm/sec) were observed on the ground (BRI 1996). Some of these values exceeded the earthquake intensity level which have been generally supposed in the present seismic design (the second stage of design) in Japan, i.e. about 400gals in acceleration and 40 to 50 cm/sec in velocity. Despite higher intensities of the earthquake ground motions, damage to buildings designed based on the present seismic code was not so severe. One of the possibilities of the reduced damage has been considered to be attributable to the effects of SSI. To confirm the SSI effects, some other studies have been presented in addition to the previously described simulation analyses. Hayashi et al. (1995) and Hayashi (1996) have discussed a possibility that the minor damage in the severely shaken area may be attributable to uplift of foundations.

In order to develop the discussions about the SSI effects from a different viewpoint, Hayashi et al. (1998) have performed systematically nonlinear response analyses by supposing mid-to-low-rise buildings be located in the severely damaged area in Kobe city. Through the numerical investigation, a possibility of reduction of effective input motions into structure was suggested. The reduction rates were estimated to be about 30% for accelerations and 10% for velocities. It was also shown that the reduction of effective input motions due to SSI effects is pronounced for the low-rise buildings.

The effective input motions into structure have also been studied for a different eight-story building of steel structure by assuming incident wave motions at the bedrock, 31m below the ground surface (Kaneta et al.

Table 1. Outline of structures.

	Takami Floral Bldg. (Yokoyama 1996)	Nanko power plant Smokestack (Kowada et al. 1997)	Nanko power plant Main bldg.(Doi et al. 1994)	Osaka Institute of Technology (Ooba & Mimura 1995)	Murano drinking water plant (Kobori et al. 1981)
structure type	RC frame	RC	Steel	SRC frame	RC frame
foundation type	Cast-in place Concrete piles	Upper:SC piles Lower:PHC piles	Upper:SC piles Lower:PHC piles	Cast-in place Concrete piles	Cast-in place Concrete piles
construction area	989.5 m^2	271.6	13817.0	788.0	6531.4
height of structure	98.2 m	200	31.0	65.65	37.7
depth of foundation	8.3 m	6.3	4.0~12.3	5.2	14.8
length of piles	22.75 m	64.5	62~70	20.3	12~16
diameter of piles	2.3 m	0.8	0.8	1.8, 2.0	2.0
number of piles	56	273	2449	24	422
Vs : subsurface layers	140~240m/s	160~350	160~350	130~150	-
Vs : bearing stratum	380 m/s	340	340	320	-
natural period NS,EW	1.41, 1.45 sec.	1.87(NS)	0.93(NS)	0.83, 0.92	0.437,0.439
seismometer on the ground surface	GL-1.5 m	GL-0.1 m	GL-0.1 m	GL-1.5 m	GL-1.0 m
seismometer on the foundation	1FL	GL±0 m	1FL	1FL	B2F (GL-10.8m)

1996). The analyses were performed by use of 2-D FEM incorporated with an equivalent linearization method. The numerically obtained results have indicated that the peak acceleration responses of foundation at the ground floor were reduced by 16% comparing to the surface ground motions.

To confirm the SSI effects, it is desirable to study the effects based on recorded earthquake motions. A study of the effective input motions conducted by Yasui (1996) and Yasui et al. (1998) is substantial one investigated based on the records simultaneously observed both in buildings and on the ground. One of the features of the research is that, while the sites are limited, the effective input motions into structures have been investigated for strong earthquake motions. The effective input motion is defined as the response of foundation during earthquakes, which includes the effects of inertial and kinematic interactions (Kausel et al. 1978).

Comparison of Simultaneously Observed Motions in Structures and Soil

The simultaneous records obtained both in structures and on the surrounding soil have been available at several sites in the vicinity of Kobe area. Table 1 shows an outline of the structures at four different sites, which include four buildings and one smokestack. The location of the sites is shown in Fig. 5. In this figure, location of Buildings A (Shin-Nagata Urban Complex) and Building B (NTT Kobe Ekimae Bldg) is included, which will be discussed afterward.

Fig. 6 shows the compared results of the peak accelerations recorded on the foundations with those on the soil surface. Similarly, Fig. 7 shows the compared results of the peak velocities numerically obtained by integration of the acceleration records. The location of the observation points in the ground was 0.1 to 1.5m below the soil surface and the records may be considered to be the surface motions. The seismic sensors were installed on the ground floor for three buildings and a smokestack, and the rest was instrumented on the second basement (10.8m below ground line). The results obtained on the second basement may be considered to be those on the ground floor level because of high rigidity of the basement. In Figs 6 and 7, symbols ○, □ and Δ correspond to the results of NS (north south), EW (east-west) and UD (up-down) components, respectively. The slope of the line obtained by the least-squares method is 0.7 for the observed accelerations. The value represents the weighted average ratio of peak accelerations on the foundations to

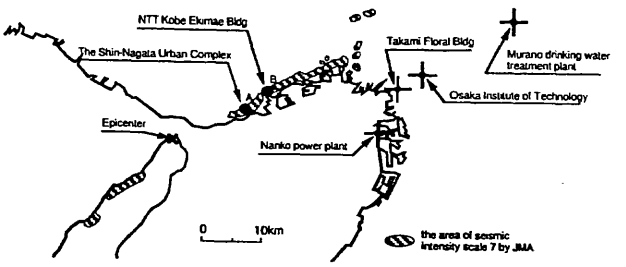

Fig.5. Location of structures.

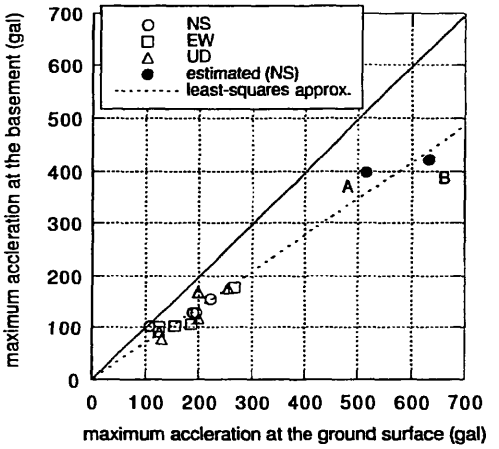

Fig. 6. Peak accelerations at the ground surface and on foundations.

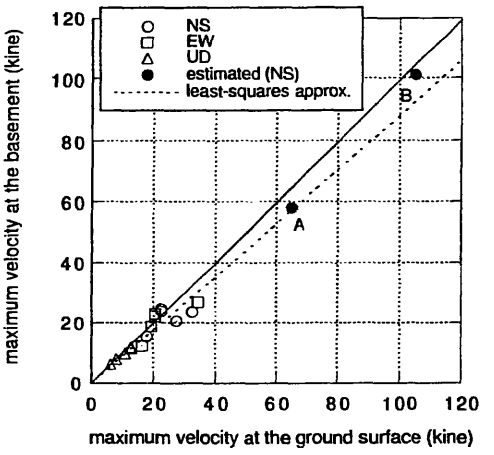

Fig. 7. Peak velocities at the ground surface and on foundations (kine = cm/sec).

those of the soil surface. In other words, the peak accelerations on foundations have reduced by 30% comparing to the surface ground motions. As for velocity,

on the other hand, the slope is 0.9, which exhibit less reduction rate comparing to the case of accelerations. It will be noticed that while the vertical components are included in above described results, the reduction rates are not affected even when they are excluded. Fig. 8 shows the comparison of response spectra (5% damping) for accelerations recorded on the foundation and on the soil surface (1.5m below soil surface) (Yokoyama 1996). Exhibited are for the records having showed the largest acceleration among the sites shown in Table 1. It is noticed from the figure that the reduction of the effective input motions can be recognized in wide range of periods less than 2 sec.

The results in the severely shocked area, so called heavily damaged belt zone, are not included in Figs 6 and 7, as the simultaneous earthquake records have not been obtained in the area. To make good the loss, the surface ground motions are estimated numerically based on records observed on the foundations. A method of backward analyses will be described in what follows (Yasui et al. 1996). In Figs 6 and 7, thus obtained results are plotted by •A and •B together with other observed results.

Estimation Method of Surface Ground Motions

The primary step is to construct a vibration model of superstructure and the restoring force characteristics of each story. Next step is to compute the inelastic response for the fixed base model when subjected to the observed motions on the foundation or alternative motions recorded on basement of the structure. Thus calculated results are compared to the observed records at different floor levels in order to confirm whether the constructed vibration model can appropriately reproduce the actual response of the structure during the earthquake.

The second step is to evaluate the impedance functions and the foundation input motions for the layered soil models at the sites. In the analyses, the thin layered element method is employed that has capability of taking into account the embedded foundations (Tajimi 1984; Takano et al. 1992). If strain dependency of soil is known a priori and the soil system could be replaced by an equivalent linear medium, the surface ground motions can be estimated by an iterative procedure described below. In the backward analyses, the followings are assumed: (1) Rocking motion is negligible; (2) incident waves impinge to foundation vertically; (3) a foundation is bonded completely to the soil; and (4) the effect of local nonlinearity on the soil surface resulting from the stresses

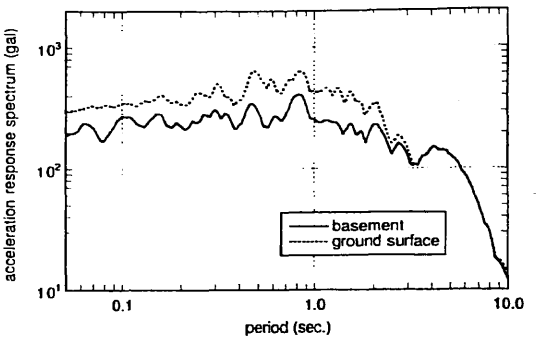

Fig. 8. Response spectra of motions on the ground surface and on the foundation (5% damping).

due to the structural vibration is negligible small comparing to the site nonlinearity or the primary nonlinearity (Roesset and Tassoulas 1982).

Letting the time histories of horizontal foundation input motion and free-field motion on the surface be $u_c(t)$ and $u_F(t)$, and corresponding Fourier transforms be $U_c(\omega)$ and $U_F(\omega)$, respectively, the foundation input motion $U_c(\omega)$ can be expressed in terms of the transfer function of the foundation input motion $H(\omega)$ as follows.

$$U_c(\omega) = H(\omega)U_F(\omega) \tag{1}$$

Let the total shear force response of the superstructure be $q(t)$ and its Fourier transform be $Q(\omega)$, which have been evaluated in the primary step, then the horizontal equation of motion of the foundation can be expressed as follows.

$$-m_0\omega^2\left(U_c(\omega)+U_0(\omega)\right)+K_H(\omega)U_0(\omega)=Q(\omega) \tag{2}$$

In which m_0 is mass of foundation, $K_H(\omega)$ is the horizontal impedance function of the foundation and $U_0(\omega)$ is the sway motion of the foundation due to the horizontal shear force. The Fourier transform of the observed horizontal motion on foundation $U_B(\omega)$ may be expressed by the sum of $U_c(\omega)$ and $U_0(\omega)$. Thus,

$$U_B(\omega) = U_c(\omega) + U_0(\omega) \tag{3}$$

Substituting from equation (3) into (2) yields,

$$U_F(\omega) = \frac{1}{H(\omega)}\left\{U_B(\omega) - \frac{1}{K_H(\omega)}\left[Q(\omega) + m_0\omega^2 U_B(\omega)\right]\right\} \tag{4}$$

The time history of ground motion on the free surface $u_F(t)$ can be calculated by an inverse Fourier transform of $U_F(\omega)$. Based on thus obtained $u_F(t)$, the free-field motions of soil system can be evaluated by an equivalent linearization method with taking into account the strain dependency of a layered soil medium. Then follows the analyses of the impedance function $K_H(\omega)$ and a transfer function of the foundation input motion $H(\omega)$ for the modified soil constants. Using the newly obtained $K_H(\omega)$ and $H(\omega)$, the free surface motions may be recalculated by equation (4). This procedure must be repeated until it converges within an admissible limit. Fig. 9 shows a schematic figure of above mentioned procedure. One of the features of this procedure is to make it possible to estimate the free-field motions on soil surface with consideration of both nonlinearities of soil and superstructure. In the above formulation, only a sway motion of the foundation is taken into account. This assumption is valid as far as following two examples are concerned, that was confirmed by observing the transfer functions of soil-structure-foundation system to an incident seismic wave with consideration of the effect of rocking motion.

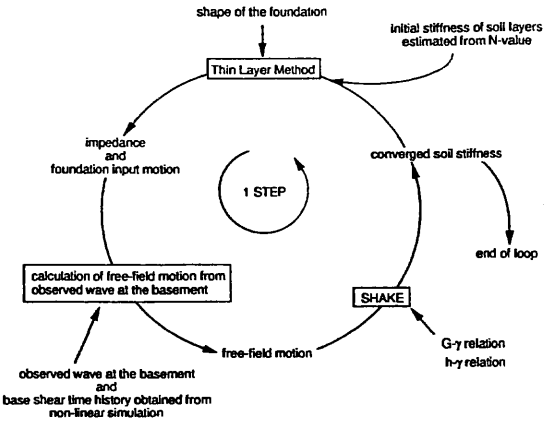

Fig. 9. Flow diagram of backward analysis.

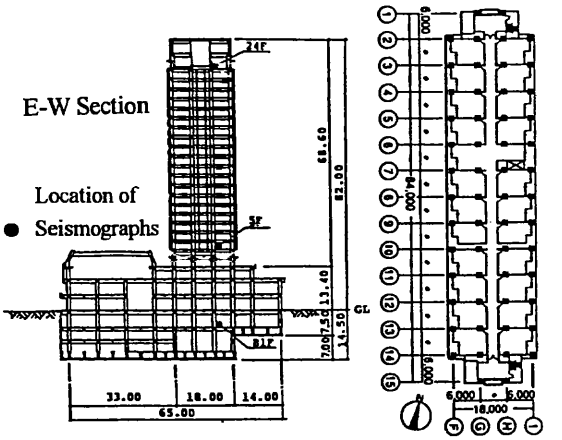

Fig. 10. Plan and section views of Building A.

Table 2. Observed maximum accelerations (gal).

	NS		EW		UD.	
	observed	Interpolated	Observed	interpolated	Observed	interpolated
24F	635*	956	302*	354	327	-
5F	379*	407	183	-	-	-
B1F	315*	354	121	-	119	-

Table 3. Soil parameters.

depth(m)	soil classification	initial		converged	
		Vs (m/sec)	density (ton/m³)	Vs' (m/sec)	h'
GL0-2.8	Fill	125.0	1.8	114-122	0.03-0.05
2.8-5.0	Sand	210.2	1.8	200	0.04
5.0-6.8	Clay	209.7	1.8	192	0.04
6.8-10.9	sand and gravel	324.3	1.9	239	0.10
10.9-14.0	Clay	229.2	1.8	198	0.06
14.0-17.4	sand and gravel	337.0	1.9	219	0.13
17.4-21.8	medium stiff clay	271.9	1.8	233-236	0.06
21.8-26.3	silty fine sand	313.9	1.8	276	0.05
26.3-29.8	medium stiff clay	278.3	1.8	233	0.07
29.8-37.0	stiff clay	296.0	1.8	250-252	0.06
37.0-40.0	gravelly fine sand	450.0	1.9	306	0.12

Estimation of Free-Field Motion for Building A –The Shin-Nagata Urban Complex of the Housing and Urban Development Corporation–

This building is built in front of Shin-Nagata station and a high rise building of 25-story with three basement floors and of steel framed reinforced concrete structure (Sawai et al. 1996). This is located in severely shaken zone of the intensity Ⅶ of JMA (the Japan Meteorological Agency) scale in the

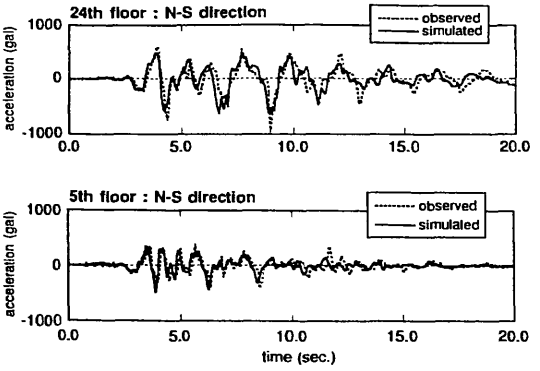

Fig. 11. Comparison of computed motions and the observed.

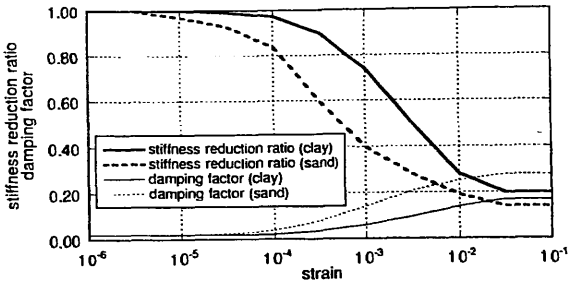

Fig. 12. Characteristics of strain dependency of soil.

Hyogo-ken Nanbu earthquake. Fig. 10 shows a plan view of an upper story and a cross section in the short direction of the structure.

As for the damage of this structure, the damage in the long side direction (NS direction) was larger than that in the short direction. The damage in the long direction was concentrated especially on beams and non-structural walls of the inner frames. There were detected large shear cracks in the non-structural walls and shear failure in beams and around openings of the partitions as well.

Accelerographs (SMA-1) have been installed in the building since it was built, and successive seismic observation has been made thereafter (Kusakabe 1997). In the Hyogo-ken Nanbu earthquake, the seismic motions were successfully recorded at three points, i.e. 24th and 5th stories, and on the first basement. Some parts of the records, however, were truncated around peaks as the peak values of the motions have largely exceeded the values expected at first. The truncated parts of the motions were interpolated by use of a spline function, and peak accelerations of the records and reproduced motions are shown in Table 2. The values with asterisks in Table 2 indicate the peak values of the truncated records. The backward analysis of the free-field surface motions at this site was made in the NS direction, which showed the maximum value among the records.

The lumped mass model of the superstructure used in inelastic response analyses was determined by a threee dimensional (3-D) static analysis of the structure when fixed at the first basement floor (Sawai et al. 1996). The 3-D model consists of six planes of structure that include two non-structural planes with beams and nonstructural walls above fifth floors. The restoring force characteristics of each story were assumed to be tri-linear type models, and were determined by the sum of those of structural frames and the nonstructural planes. The damping factor of superstructure was assumed to be 3% for the first mode and to be proportional to the initial stiffness of each story. The fundamental period of the superstructure when fixed at the first basement floor is 1.07 sec, and the system period including the effect of soil is 1.08 sec.

The inelastic response analyses were performed for the fixed model of superstructure subjected to the horizontal seismic motion recorded at the basement floor. It should be noticed that while the obtained results are for the fixed base condition, the results could be interpreted to have included the effects of SSI. This is valid as far as the rocking motion is negligible. The computed results of acceleration responses of NS component at the 24th and 5th floors are compared to the observed motions as shown in Fig. 11. It is noticed that the agreement between two is excellent up to 10 sec.

Next step is to compose a soil model. Since the soil data of wave velocities of each layer were not available around the site, the soil constants were assumed based on the standard penetration test values (SPT N-values) given in the boring logs. Table 3 shows the initial soil constants assumed in the analyses. The strain-shear modulus (G-γ) and strain-damping factor (h-γ) relationships, which are required in the equivalent linearization analysis, were determined based on the existing soil data (Ishihara 1976) as shown in Fig. 12. The free-field motions on soil surface were estimated by the aforementioned method using the soil model. Figs 13 and 14 show the horizontal impedance function and foundation input motion. The figures include

the results for the initial soil constants (step-0) and those for the successive iteration (step-1) are shown. In the iterative analyses, the equivalent soil constants have converged by a single iteration. Thus obtained results may be considered as the soil constants to have shown during the earthquake. Table 3 includes the estimated shear wave velocities V_s' and damping factor h' of each soil layer during the strong earthquake ground motions.

The estimated free-field motion on the soil surface is compared to NS component of the observed motions at the first basement as shown in Fig. 15. As for peak values, the observed peak acceleration 354 gals at the first basement level after the correction of the records using the spline function is smaller than the estimated free-field peak value 515gals, which corresponds to about 30% reduction of input motion to superstructure. Fig. 16 shows distribution of the computed peak accelerations in the soil and superstructure, and the observed peak accelerations are also included. It may be noticed that the amplification of the free-field motions above the base of foundation is significant and also the observed motions at the basement is almost same as the free-field motion at the base of foundation (Tamura et al. 1996; Hayashi et al. 1997).

In order to confirm the reduction of the effective input motions into superstructure, comparison is made for the response motions at the ground floor when subjected to the observed motion at the first basement and to the estimated motion on the free surface. Fig. 17 shows the compared results of time histories of the calculated acceleration motion on the ground floor and the estimated surface motions. As for peak values, the calculated motion on the ground floor of 398gals is about 23% smaller than the estimated value of 515gals on the soil surface. The comparison of peak velocities resulted in 65 cm/sec on the soil surface and 58 cm/sec at the ground floor, and it corresponds to about 10% reduction. These results are plotted by •A in Figs 6 and 7, which show a similar tendency as those of the observed ones. The compared results of the response spectra (5% damping) for calculated acceleration motion at the ground floor and for estimated motion on the soil surface are shown in Fig. 18. It may be observed from the figure that a slight reduction of input motions at around 1.0 sec and larger reduction may be recognized in periods below 0.4 sec. This may be interpreted as the effects of the foundation input motion shown in Fig. 14.

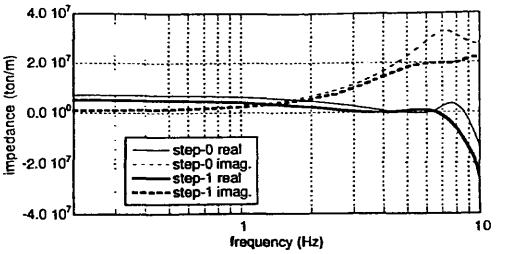

Fig. 13. Impedance functions of the foundation.

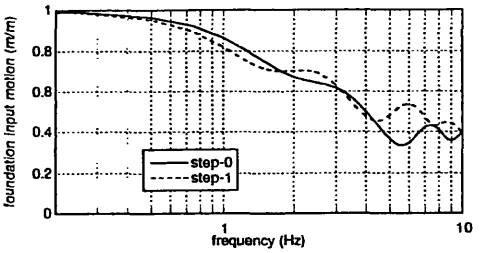

Fig. 14. Foundation input motions of the foundation.

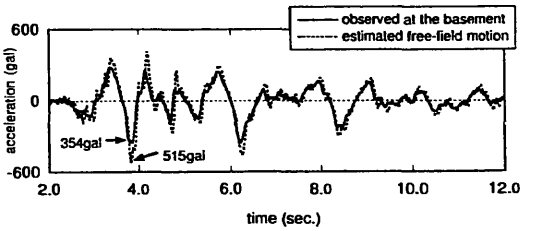

Fig. 15. Estimated Acceleration motion on the ground surface and observed motion on the first basement.

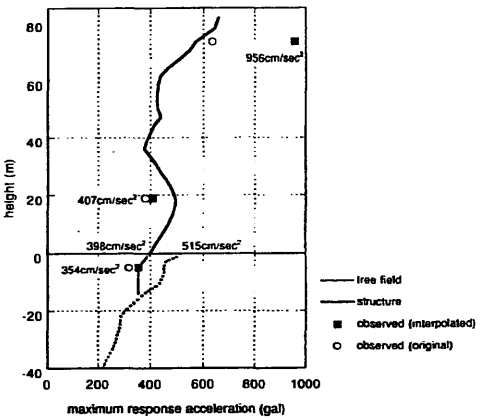

Fig. 16. Distribution of the peak accelerations of the structure and in the soil.

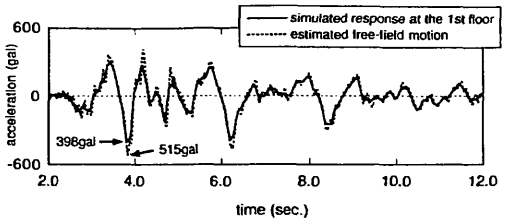

Fig. 17. Comparison of estimated surface motion and calculated motion on the ground floor.

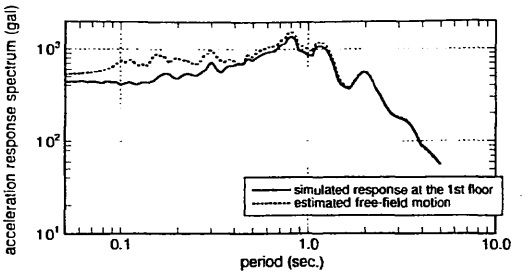

Fig. 18. Comparison of response spectra.

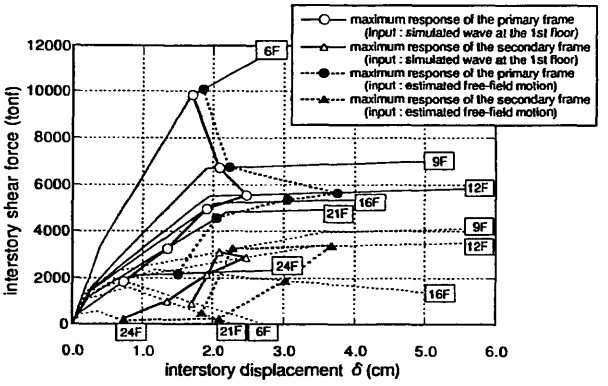

Fig. 19. Maximum shear force responses of each story.

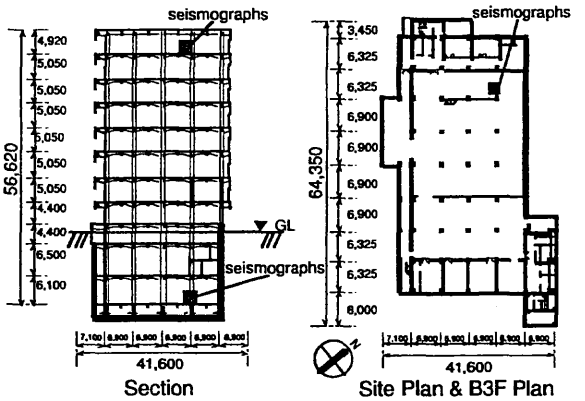

Fig. 20. Plan and section views of Building B.

In order to investigate the effects of SSI on the response of the superstructure, the response analyses were conducted for the structure when fixed at the base of the first story and excited by the estimated motion on the soil surface. The results are compared to the response to the calculated motion at the ground floor, which may be considered to be equal to the response to the observed motion at the basement level. It should be noticed that the former result does not include the effects of SSI and, on the other hand, the latter includes the effects of SSI. Therefore, the differences between these two may be interpreted as the effects of SSI. The compared results of the maximum relative displacement of each story are shown in Fig. 19. It may be seen from the figure that the difference between two is small at sixth and ninth stories. Whereas the difference between two become pronounced above 12th floors, and especially the responses at 16th and 24th stories calculated with consideration of the SSI effects are smaller than those calculated without the effects of SSI.

Estimation of Free-Field Motion for Building B –NTT Building in Front of Kobe Station–

The building is located in front of Kobe station, and is a steel framed reinforced concrete structure of eight-story above the ground and with three basement floors (Ninomiya 1996). The base of foundation is directly supported on a soil layer of gravel with sand beneath 14.5 m below the ground level. Fig. 20 shows the cross section view in east-west direction and a plan of the third basement.

The building suffered damage to shear walls with openings at the second to fifth stories in the north-south direction, and slight cracks of about 1mm width were detected in other shear walls. Accelerometers (SMAC-B2) had been installed on the third basement and on eighth story of the building since it was built, and seismic observation had been carried out successively. In the Hyogo-ken Nanbu earthquake, the seismic motions were successfully recorded, and the records of aftershocks as well. The peak accelerations observed during the Hyogo-ken Nanbu earthquake are shown in Table 4.

The backward estimation of the free-field motions was performed in the north-south direction of the structure (long side direction), which showed the largest value among the records.

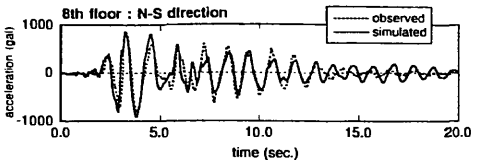

Fig. 21. Comparison of computed response at the 8th story and observed motion.

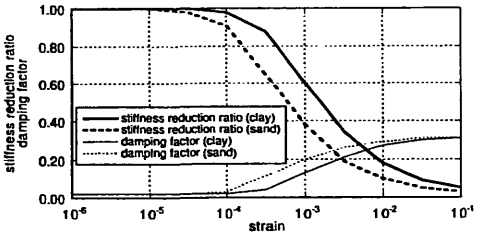

Fig. 22. Nonlinear characteristics of soil.

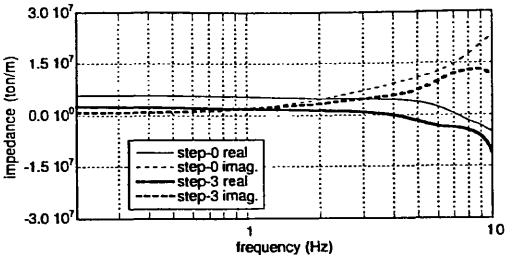

Fig. 23. Impedance functions of the foundation.

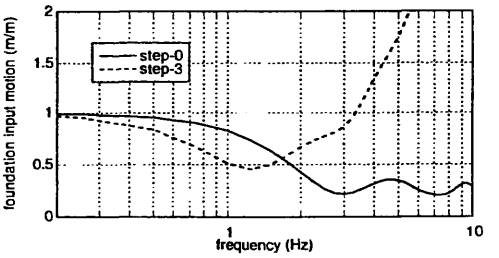

Fig. 24. Foundation input motions of the foundation.

A lumped mass system of the fixed base used in inelastic response analysis is determined on the basis of the model used in the structural design. The restoring force characteristics of each story was assumed to be of Takeda's model (Takeda et al. 1970) and determined by modifying the yield strength and the second stiffness after cracks which had been used in design of the structure. Special consideration was made in the modification so that the analyzed results correspond to the observed acceleration motions at the eighth story, as well as the relative displacement between the eighth and the third basement floor. The damping was assumed to be of viscous type. The damping factor was assumed to be 3% for the first mode and to be proportional to the initial stiffness of each story. It should be emphasized that the model is made for the purpose of a backward estimation of the free-field motions and not for evaluation of the structural design of this building. The calculated period of the structure when fixed at the bottom of the basement was 0.75 sec and the period including the effects of soil was 0.76 sec.

The inelastic response analyses were conducted for the motion recorded at the basement. The computed response motion at the eighth floor is compared to the observed

Table 4. Peak accelerations of observed motions (gal).

	NS	EW	UD
8F	881	504	408
B3F	331	154	169

Table 5. Soil parameters.

depth(m)	soil classification	Initial		converged	
		Vs (m/sec)	Density (ton/m³)	Vs' (m/sec)	h'
GL0-2.0	Fill	90.0	1.6	66-85	0.04-0.15
2.0-5.0	Sand	130.0	1.8	46-73	0.22-0.28
5.0-10.0	sand and gravel	190.0	1.9	75-105	0.22-0.27
10.0-20.0	Sand	250.0	1.9	100-134	0.23-0.27
20.0-38.0	Sand	410.0	2.0	249-294	0.16-0.20
38.0-46.0	Clay	410.0	2.0	345-351	0.09-0.10
46.0-52.0	sand and gravel	410.0	2.0	221-228	0.22-0.23
52.0-54.0	sand and gravel	360.0	1.9	147	0.27
54.0-65.0	Clay	360.0	1.9	248-259	0.16-0.17

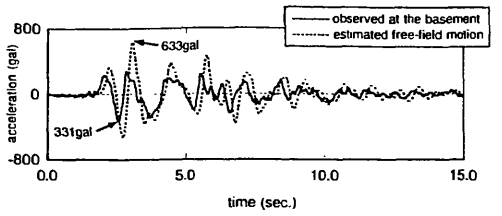

Fig. 25. Comparison of estimated surface motion and observed motion on the 1st basement.

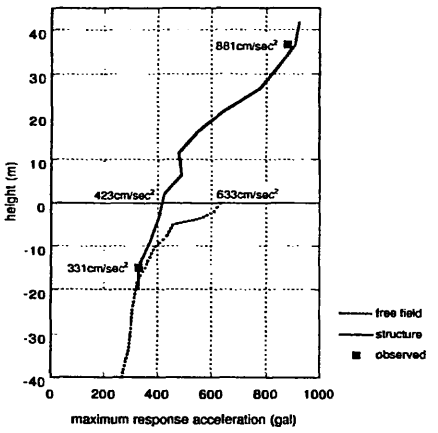

Fig. 26. Distribution of the peak accelerations of the structure and in the soil.

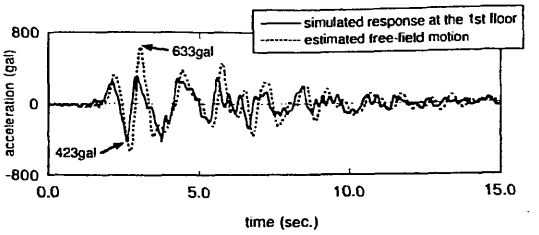

Fig. 27. Comparison of estimated surface motion and computed motion on the ground floor.

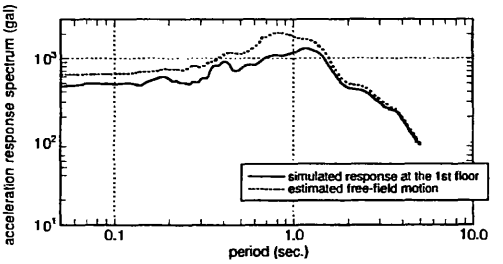

Fig. 28. Comparison of response spectra.

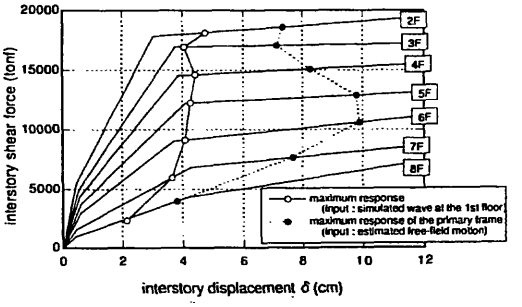

Fig. 29. Maximum shear force response of each story.

results as shown in Fig. 21. Fairly good agreement between the analyzed and the observed may be seen except the coda part of the motion after 13 sec.

The soil model, on the other hand, was determined based on the data obtained by PS logging tests that were carried out after the earthquake. Table 5 shows the initial soil constants of the soil model. As for strain dependency of soil (G-γ and h-γ relationships), a modified Ramberg-Osgood model was employed in the analyses. Fig. 22 shows the strain dependency models of silt and sand used in the backward analyses.

The Free-field motion on the soil surface was estimated by means of the iterative procedure described earlier. Figs 23 and 24 show impedance functions and foundation input motions for the foundation. In these figures, the results for the initial soil constants, which correspond to a low strain level of the soil, and those for the final soil constants after convergence are shown. In the calculation, three times of iteration was needed to converge. Table 5 shows the final shear wave velocities and damping factors of soil layers together with the corresponding initial values. Remarkable reduction of shear wave velocities from the initial values is seen.

Thus estimated free-field motion on soil surface is compared to the observed motion on the third basement floor as shown in Fig. 25. Regarding the peak values, the estimated peak acceleration on the soil surface was 633gals and has increased by 90% comparing to the observed peak on the third basement floor.

Comparing the free-field motion shown in Fig. 25 to the previous results of Building A, followings may be observed: (1) for the case of Building A, the motions on the soil surface and the associated motion in the building

are similar as shown in Fig. 15; (2) for the case of Building B, on the contrary, a pronounce difference between the motions on the soil surface and in the structure may be recognized in magnitude and in phase as well. This is mainly due to the difference of the nonlinearity rates of soil between the two cases. In other words, the nonlinearity rates have affected greatly on the results of the foundation input motions as shown in Figs 14 and 24 for Building A and Building B, respectively. It may be noticed from these figures that the foundation input motion for Building A is scarcely affected by nonlinearity of soil up to around 10 Hz. For the case of Building B, on the other hand, a pronounced difference may be detected in the results of the foundation input motion for the initial soil model and the final one. Fig. 24 indicates also that the foundation input motion is amplified by strong non-linearity of soil in frequencies more than 2 Hz.

Fig. 26 shows the distribution of peak accelerations of structure and in the soil as well. In this figure the peak values of the observed motions are also plotted. The result indicates a large amplification of the ground motions in the surface layers above –5 m. It is also noted that the observed horizontal peak value in the basement is almost same in magnitude as the free-field motion at the bottom of the foundation. This suggests that the earthquake motions transmitted to structure predominantly from the bottom of the foundation and less from the side of the foundation as far as this building is concerned.

In order to investigate the reduction effects of the effective input motions at the ground surface level, the estimated free-field motion on the soil surface is compared to the response motion on the ground floor of the structure subjected to the horizontal motion observed at the third basement. In the response analysis, the base is fixed at the base of the third basement of the structure.

Fig. 27 shows the compared results of acceleration time histories estimated on the soil surface and the computed motion on the ground floor. Observing the peak values, it may be seen that the peak value of free-field motion on the soil surface 633 gals has reduced to 423 gals at the ground floor, and the reduction rate became 33%. As for velocities, the peak value of 105 cm/sec on the soil surface reduced to 101 cm/sec on the ground floor, and the reduction rate was 4%. These values are plotted in Figs 6 and 7 by the mark •B. The reduction rates are consistent with those obtained by the observed motions for accelerations, and are somewhat smaller for velocities. In Fig. 28, the response spectra (5% damping) for the estimated free field motion and for the calculated motion on the ground floor are shown. The results indicate the reduction of the effective input motion observed through the response spectra and the reduction may be recognized in wider range of periods below 1.5 sec comparing to the case of Building A shown in Fig. 18.

Further comparison is made for the inelastic responses of superstructure with base fixed at the ground floor when subjected to both the estimated free-field motion on the soil surface and the calculated motion on the ground. The computed results of relative story displacements are shown in Fig. 29. It may be noticed from the figure that the maximum responses to the estimated motion on the free surface become large at all stories except the eighth story, especially at intermediate stories of fifth and sixth. It should be noticed that the increase of input motions as large as 30% have caused a larger difference in inelastic responses, that indicates the importance of evaluating properly the effective input motions to structures.

Summary of Discussions

The followings can be summarized based on the study described in this chapter, which is focussed on the reduction effects of effective input motions into structures during the Hyogo-ken Nanbu earthquake.

1) The compared results of the peak values recorded on the foundation with those on the free-field soil surface have indicated distinctly the reduction of effective input motions into structure. The effective input rates, which indicate the ratios of peak values of the effective input motion to the corresponding free-field motion, were approximately 0.7 for accelerations and 0.9 for velocities. It is interesting to compare the results with those for the Olive View Medical Center building during the Northridge earthquake (Ms = 6.8) of 1994 and the Whittier earthquake (Ms = 5.9) of 1987 (Celebi 1997). In the Northridge earthquake, the reduction rates of accelerations at the level of ground floor were 0.9 for NS component and 0.69 for EW component. On the other hand, the rates for the Whittier Earthquake, in which the peak accelerations at this site were about one seventh to fifteenth of those of the Northridge earthquake, were 1.0 and 1.20 for NS and EW components, respectively. Perhaps it is worth notice that the reduction rates may be affected not only the frequency characteristics of ground motions but also the intensity of the ground motions. Further substantial studies are needed to reach the firm conclusion about this subject.

2) In order to make up for the lack of the simultaneously observed data in the severely shaken area during the Hyogo-ken Nanbu earthquake, the backward analyses of the free-field motion on the soil surface on the basis of the motion observed in the structure were performed at sites of two buildings. The estimated free-field surface motions to corresponding motions in the buildings exhibited the same tendencies as those obtained based on the observed motions.
3) The reduction effects were recognized in periods less than 1.0 sec by comparing the response spectra for free-field motions and for the motions at the ground floor.
4) The horizontal peak accelerations at the base of the foundation are almost same as the peak value of the free-field motion at the corresponding level. At the same time, it will be inferred that above mentioned reduction effects are mainly due to the amplification of surface soil layers above the base of foundation.
5) To evaluate properly the effective input motions into structure is important in the inelastic response analyses of structures.

This chapter is compiled based on the paper (Yasui et al. 1998) and the summarized is outcomes of an activity done in Sub-Working Group 5-2 (chaired by Yasui) organized under the Special Research Committee of the Hyogo-ken Nanbu earthquake established in the Architectural Institute of Japan (AIJ). Many fruitful discussions exchanged among the members are gratefully acknowledged.

CONCLUDING REMARKS

It was said that the present state of SSI analyses has reached a mature stage of development (Gazetas 1983). However, it should be also noticed that due to existing limitations in each analysis method we are obliged to introduce many simplifications. idealizations and assumptions in making mathematical soil-structure models and this gives rise to a great gap between an actual system and the mathematical model. The examination of the assumptions and simplifications for validity ought to be made through simulation analyses on the basis of the earthquake motions, if possible, observed simultaneously in a building and on the surrounding soil. In particular, the accumulation of simulation analyses for strong ground motions are indispensable in order to improve the reliability for assessment of structural safety against earthquakes. From such a viewpoint, this report has reviewed the SSI researches relating to three major earthquakes recently occurred in Japan. In the review work emphasis was placed on the simulation analyses conducted based on simultaneously observed earthquake motions, as well as researches on input motions into structure for the major earthquakes and small events observed at the same sites. In most simulation analyses, 2-D FEM incorporated with non-linearity of soil has been used. Though the method seems to give satisfactory results in the simulation analyses for small ground motions, not to be acceptable for strong earthquakes.

Among the reviewed researches, the most noticeable results was the difference of response spectral ratios, that indicate the ratios of response spectra for the observed motion in a building to those for motions recorded on the soil surface, between small and strong earthquakes observed at the same site. A distinct result has been recognized between the response spectral ratio for small events and that for the Kushiro-oki earthquake at a specific site, in which the ratio showed greater than 1.0 in wide period range less than 1.0 sec.

Another emphasis was also placed on a study of effective input motions into structures investigated on the basis of the simultaneous observations recorded both in structures and the surrounding soil during the Hyogo-ken Nanbu earthquake. The compared results of the peak values recorded on the foundation with those on the free-field surface have indicated distinctly the reduction of effective input motions into structure. The effective input rates, which indicate the ratios of peak values of the effective input motion to the corresponding free-field motion, were approximately 0.7 for accelerations and 0.9 for velocities. It is worth while to notice that the result of reduced input motions into structures seen during the Hyogo-ken Nanbu earthquake is different in tendency from one observed at a specific site during the Kushiro-oki event. The distinct tendencies detected between two earthquakes, the Kushiro-oki and the Hyogo-ken Nanbu earthquakes, at the different sites may be attributed to different degree of nonlinearity of the surrounding soil.

What we have extracted from the observed motions during three major earthquakes is perhaps a portion of nonlinear SSI phenomena occurred during the earthquakes. It is desirable to increase our knowledge of nonlinear SSI effects based on the observations.

One of the remained subjects on SSI to be tackled is development of simple methods to evaluate stresses in piles with taking nonlinearity of soil into account and

input motions into superstructures supported on pile groups when subjected to strong earthquake motions. Accumulation of the observations of earth pressures on piles during intense earthquakes and strains of piles is also needed to validate the methods.

ACKNOWLEDGEMENTS

The authors would like to express their gratitude to M. Nakamura of Technical Research Institute of Obayashi Corporation and T. Mutoh of Science University of Tokyo for their helpful cooperation in preparation of this report.

REFFERENCES

Architectural Institute of Japan (1994). "A general symposium on the 1993 Kushiro-oki earthquake," The Extensive Research Committee on the 1993 Kushiro-oki Earthquake, (in Japanese).

Building Research Institute (1996). "Final reconnaissance report on the 1995 Great Hanshin-Awaji Earthquake Disaster," Building Research Institute, (in Japanese).

Celebi, M. (1997). "Response of Olive View Hospital to Northridge and Whittier Earthquakes," J. of Struct. Engrg, Proc. ASCE, Vol. 123, No. 4, pp389-396.

Dan, K. (1994). "Nonlinear interaction of soil and structure observed in the earthquake motions at the Kushiro district meteorological observatory building," A General Symposium on The 1993 Kushiro-oki Earthquake, AIJ, pp85-92, (in Japanese).

Dan, K. (1995). "Simulation of soil and structure interaction observed in the earthquake motions at the Kushiro district meteorological observatory," J. of Struct. and Constr. Engrg, AIJ, Vol. 470, pp75-84, (in Japanese).

Dan, K., M. Kikuchi, A. Fukukita and K. Nishimura (1997). "Study on large acceleration motions recorded during the largest aftershock (M6.5) of the 1993 Hokkaido-Nansei-oki earthquake," J. of Struct. and Costr. Engrg, AIJ, Vol. 495, pp45-52, (in Japanese).

Doi, T., A. Kowada, T. Matsumura, T. Kida, and N. Maeda (1994). "A study on dynamic characteristics of thermal power plant structure; (Part 1) Dynamic characteristics of turbine building," Summaries of Technical Papers of Annual Meeting, AIJ, Vol. B, pp1155-1156, (in Japanese).

Fujimori, T., Y. Yasui, K. Wakamatsu and A. Nobata (1995). "Foundation input motions of a multistory reinforced concrete structure during strong motions," Summaries of Technical Reports of Annual Meeting, AIJ, Vol. B-2, pp397-398, (in Japanese).

Gazetas, G (1983). "Analysis of machine foundation vibrations: state of the art", Int. J. of Soil Dyn. and Earthq. Engrg, Vol. 2, No. 1, pp2-42.

Hayashi, Y., M. Mori, K. Watanabe, K. Tamura, M. Kaneko, T. Saito, and H. Yokota, (1995). "Simulation analyses of a damaged building during the 1995 Hyogo-ken Nanbu Earthquake," Technical Research Report of Shimizu Corporation, Vol.62, pp.37-49, (in Japanese).

Hayashi, Y. (1996). "Damage reduction effect due to basemat uplift of buildings," J. of Struct. and Constr. Engrg, AIJ, No.485, pp.53-62, (in Japanese).

Hayashi, Y., J. Miyakoshi, K. Tamura, and H. Kawase (1997). "Peak ground velocity evaluated from damage ratio of low-rise buildings during the Hyogo-ken Nanbu Earthquake," J. of Struct. and Constr. Engrg, AIJ, No.494, pp.59-66, (in Japanese).

Hayashi, Y., T. Fujimori, Y. Yasui and M. Iguchi (1998). "Effects of soil-structure interaction in heavily damaged zone in the 1995 Hyogo-ken Nanbu Earthquake," J. of Struct. and Constr. Engrg, AIJ. (submitted).

Iguchi, M. and K. Akino (1993). "Experimental and analytical studies for soil-structure interaction: State-of-the-art Report," Principal Division Lecture at the 12th Int. Conf. on Struct. Mech. in React. Tech., (Stuttgart).

Ishihara, K. (1976). "Introduction to geological dynamics," Kajima Shuppankai, pp.199-201, (in Japanese).

Kaneta, R., M. Hisano and M. Takagi (1996). "Dynamic analysis of a damaged buildings by the 1995 Hyogoken-nanbu earthquake (Part 1 Effect of the basement floor on the input motion to the building)," Summaries of Technical Reports of Annual Meeting, AIJ, Vol. B-2, pp517-518, (in Japanese).

Kausel, E., R. V. Whitman, J. P. Morray and F. Elsabee (1978). "The spring method for embedded foundations," Nuclear Engrg and Design, Vol. 48, pp377-392.

Kobori, T., T. Kamata, and K. Kanda (1981). "Earthquake observation at a multistory water treatment plant," Proc. of Architectural Research Meetings, Kinki District, AIJ, pp.77-80, (in Japanese).

Kowada, A., N. Maeda, S. Mori, T. Ikeda and Y. Maekawa (1997). "Verification of a high smokestack for the 1995 Great Hanshin earthquake motion records; (Part 1: Characteristics of the strong motion records, the

design model and safety judgement)," Summaries of Technical Reports of Annual Meeting, AIJ, Vol. B-2, pp357-358, (in Japanese).

Kurimoto, O. (1996). "Nonlinear seismic response of 41-story reinforced concrete structure," Summaries of Technical Reports of Annual Meeting, AIJ, Vol. B-2, pp403-404, (in Japanese).

Kusakabe, K. (1997). "Earthquake response of embedded high rise building due to 1995 Hyogo-ken Nanbu earthquake," Report by the Special Research Committee of the Hyogo-Ken Nanbu Earthquake in the Kinki District, AIJ, pp179-192, (in Japanese).

Luco, J. E. and A. H. Hadjian (1974). "Two-dimensional approximations to the three-dimensional soil-structure interaction problem," Nuclear Engrg and Design, Vol. 31, pp195-203.

Miyamoto, Y., Sako, Y., Koyamada, K. and Miura, K. (1995). "Seismic response analyses of a building subjected to the 1995 Hyogo-ken Nanbu Earthquake with consideration of site condition (part-3)," Proc. of the 66th Architectural Research Meetings, 1995, Kanto District, AIJ, pp.73-76, (in Japanese).

Ninomiya, T. (1996). "NTT Kobe-Ekimae Building; -Seismic records and dynamic response analysis-," Symp. on the Hyogo-Ken Nanbu Earthquake in the Research Committee of Earthquake Resistant Structure in the Kinki District, AIJ, pp26-34, Nov., (in Japanese).

Ohba, S. and K. Mimura (1995). "Influence of intensity of ground motion on natural period of a building," Proc. of Architectural Research Meetings, Kinki District, AIJ, pp205-208, (in Japanese).

Penzien, J., C. F. Scheffy and R. A. Parmelee (1964). "Seismic analysis of bridges on long piles," J. Engrg Mech. Div., ASCE, EM3, pp223-254.

Roesset, J. M. and J. L. Tassoulas (1982). "Nonlinear structure interaction: An overview," Earthquake Ground Motion and Its Effects on Structures, ed. by S. K. Datta, AMD-Vol. 53, ASME, pp59-76.

Sawai, N., H. Eto, K. Tsuda, and K. Takata (1996). "Response analysis of a 25-story SRC building during the 1995 Hyogoken-Nanbu (Kobe) earthquake," Concrete Journal, Vol. 34, No. 11, pp.37-41, Nov., (in Japanese).

Tajimi, H. (1984). "Predicted and measured vibration characteristics of a large-scale shaking table foundation," Proc. 8th World Conf. on Earthq. Engrg, Vol. III, pp873-880.

Takano, S., H. Maeno and Y. Yasui (1992). "Seismic response analysis of grouped pile foundation using substructure method; (Part 6) Formulation of grouped pile embedded foundation case," Summaries of Technical Papers of Annual Meeting, AIJ, Vol. B, pp.595-596, (in Japanese).

Takeda, T., M. A. Sozen and N. N. Nielsen (1970). "Reinforced concrete response to simulated earthquakes," J. of Struct. Engrg, Proc. ASCE. Vol. 96, ST12, pp2557-2573.

Tamura, K., Y. Hayashi, M. Mori and I. Takahashi (1996). "Evaluation of effective input motion of damaged buildings in 1995 Hyogoken-Nanbu earthquake: (Part 2) Effective Input motion and damping," Summaries of Technical Reports of Annual Meeting, AIJ, Vol. B-2, pp515-516, (in Japanese).

Yasui, Y. and S. Takano (1994). "Analysis of soil and structure interaction on Kushiro district meteorological observatory building and the foundation of strong motion seismograph," A General Symposium on The 1993 Kushiro-oki Earthquake, AIJ, pp75-84, (in Japanese).

Yasui, Y., K. Wakamatsu, T. Fujimori and S. Yagi (1995). "Aseismic motions of 41-story reinforced concrete tube structure; Part 11: Seismic observation (2) – The Hyogo-ken Nanbu earthquake -," Summaries of Technical Reports of Annual Meeting, AIJ, Vol. B-2, pp947-948, (in Japanese).

Yasui, Y. (1996). "Effects of soil-structure interaction," First symposium on the Hyogo-Ken Nanbu Earthquake, The Special Research Committee of the Hyogo-Ken Nanbu Earthquake, AIJ, pp.19-22, (in Japanese).

Yasui, Y., S. Takano, M. Nakamura, and K. Takata (1996). "A study on observed earthquake records in a 25-story SRC residential building during the Hyogo-Ken Nanbu Earthquake," Symp. on the Hyogo-Ken Nanbu Earthquake, The Research Committee of Earthquake Resistant Structure in the Kinki District, AIJ, pp.35-44, Nov., (in Japanese).

Yasui, Y., M. Iguchi, H. Akagi, Y. Hayashi and M. Nakamura (1998). "Examination on effective input motion to structures in heavily damaged zone in the 1995 Hyogo-ken Nanbu Earthquake," J. of Struct. and Constr. Engrg, AIJ, No. 512, (to appear).

Yokoyama, H. (1996), "Earthquake observation and dynamic analysis of a high-rise RC apartment housing subjected to the Hyogo-ken Nanbu Earthquake," Symp. on the Hyogo-Ken Nanbu Earthquake, The Research Committee of Earthquake Resistant Structure in the Kinki District, AIJ, pp1-17, Nov, (in Japanese).

LATERAL SEISMIC SOIL PRESSURE

AN UPDATED APPROACH

By

Farhang Ostadan

William H. White

Bechtel National
San Francisco, California

Presented as part of

US-Japan SSI Workshop
September 22-23, 1998

United States Geological Survey
Menlo Park, California

INTRODUCTION

The effect of ground motion on retaining walls was recognized by Okabe (1924) and Mononobe and Matsuo (1929) following the great Kanto Earthquake of 1923 in Japan. The method proposed by Mononobe and Okabe, currently known as the M-O method, was based on the Coulomb's theory of static soil pressure developed more than 200 years ago. In the last 30 years, a great deal of research work both in the analytical and in experimental areas has been performed to evaluate the adequacy of the M-O method or to extend the method for specific applications. Discussion of the all the research work on the seismic soil pressure is extensive and is beyond the scope of this study. Rather, only the milestones that have influenced the design practice are described below.

Seed and Whitman (1970)

In 1970, the M-O method and the associated analytical relationships were simplified by Seed and Whitman (1970) for design of earth retaining structures for dynamic loads. Using the charts, the designer only needs to know the basic properties of the backfill (the angle of internal friction) and the peak ground acceleration to obtain the seismic soil pressure. As suggested by Seed and Whitman, the basic assumptions used in the development of the M-O method should always be considered in design applications. These assumptions are:

- The backfill materials are dry cohesionless materials.
- The retaining wall yields equally and sufficiently to produce minimum active soil pressure.
- The active soil pressure is associated with a soil wedge behind the wall which is at the point of incipient failure and the maximum shear strength is mobilized along the potential sliding surface.
- The soil behind the wall behaves as a rigid body and the acceleration is uniform in the soil wedge behind the wall.

Whitman et al. (1979, 1990, 1991)

The effect of some of the limiting assumptions used in the M-O method above has been investigated by, among others, Whitman et al. (1979, 1990, 1991) and Nadim and Whitman (1984). The non-yielding wall conditions and the amplifications of the motion in the soil mass were found to be significant in some cases. However, no practical tools were proposed for design applications to circumvent the limiting assumptions used in the M-O method. Judging from the results of model tests by several researchers, Whitman (1990) found that use of the M-O method for design of relatively simple gravity walls up to 30 ft high is acceptable. However, for higher walls and non-yielding walls, he recommended a more careful analysis be performed.

Richards and Elms (1979)

One of the more important recent developments in characterizing the seismic soil pressure for retaining walls was the work performed by Richards and Elms (1979). Using the M-O method and the Newmark's sliding-block analogy, the authors proposed a displacement-controlled method which incorporates basic ground motion parameters (maximum acceleration and maximum velocity) and reduces the seismic soil pressure based on the acceptable amount of the wall movement. In practice, the method is currently used for designing walls for which limiting horizontal displacements are of no concern.

Wood (1973)

While the M-O method was developed for yielding walls, Wood (1973) developed an equivalent static elastic solution for seismic soil pressure for non-yielding walls. The solution is based on finite element analysis of a soil-wall system for a wall resting on a rigid base and a uniform soil layer behind the wall. In general, Wood's solution amounts to a lateral force that acts about 0.63 times the height of the wall above the base of the wall which corresponds approximately to a parabolic distribution of soil pressure unlike M-O's inverted triangular distribution. Wood's solution predicts seismic soil pressure larger (by a factor of 2 to 3) than the pressure predicted by the M-O method. The elastic solution proposed by Wood has been adopted by ASCE Standards for Nuclear Structures (1986) and has been used in many applications. Wood's solution requires knowledge of the maximum ground acceleration along with the density and Poisson's ratio of the soil to obtain the seismic soil pressure behind the wall.

Matsuzawa et al. (1984), Ishibashi et al. (1985)

To address saturated backfill conditions and to include the hydrodynamic forces, the M-O method was extended by Matsuzawa et al. (1984) and Ishibashi et al. (1985). A comprehensive summary of the all the M-O based methods and their applications to various retaining wall conditions are documented in a recent US Army publication (Ebeling and Morrison, 1992).

Veletsos et al. (1994a, 1994b)

More recently, Veletsos and Younan (1994a, 1994b) developed an analytical model to compute seismic soil pressure for rigid vertical walls resting on a rigid base. The proposed model is based on the series of elastically supported semiinfinte horizontal bars with distributed mass to model the soil medium behind the wall. The model was developed for vertically propagating shear waves with the assumption that horizontal variation of vertical displacements in the soil medium is negligible. In this model, contrary to Wood's equivalent static solution, amplification of motion in the soil medium behind the wall is considered. The model highlights the effects of several parameters including the frequency of vibration on the seismic soil pressure magnitude and distribution. The model was subsequently expanded for application to cylindrical vaults and storage buildings (Veletsos and Younan, 1994c; 1995).

Significance of Seismic Soil Pressure in Design

Seed and Whitman (1970) summarized damage to wall structures during earthquakes. Damage to retaining walls with saturated backfills is typically more dramatic and is frequently reported in the literature. However, damage reports of walls above the water table are not uncommon. A number of soil retaining structures were damaged in the San Fernando earthquake of 1971. Wood (1973) reports that the walls of a large reinforced concrete underground reservoir at the Balboa Water Treatment Plant failed as a result of increased soil pressure during the earthquake. The walls were approximately 20 ft high and were restrained by the top and bottom slabs.

Damage has been reported for a number of underground reinforced concrete box-type flood control channels. Richards and Elms (1979) report damage to abutment of bridges after the 1968 earthquake in Inangahua, New Zealand. Out of the 39 bridges inspected, 24 showed measurable movement and 15 suffered damage on bridge abutments. In the Madang earthquake of 1970 in New Guinea, the damage patterns were similar. Out of 29 bridges repaired, some experienced abutment lateral movements as much as 20 inches. Reports on failed or damaged bridge abutments indicate mainly settlement of the backfill and pounding of the bridge superstructure against the abutment in longitudinal and transverse directions.

Nazarian and Hadjian (1979) also summarized damage to soil-retaining structures during past earthquakes. Damage to bridges has also been reported from various earthquakes including 1960 Chilean, 1964 Alaskan, 1964 Nigata, 1971 San Fernando, and 1974 Lima. Most of the reported damage can be attributed to the increased lateral pressure during earthquakes.

Numerous damage reports are available from recent earthquakes which report damage to the embedded walls of buildings. However, contribution of the seismic soil pressure to the damage can not be quantified since the embedded walls often carry the inertia load of the superstructure with cracks extending in all directions in the walls of the buildings. On the other hand, simple structures, such as underground box-type structures, retaining walls, and bridge abutments have suffered damage due to the increased soil pressure. All of these reports and others not mentioned highlight the significance of using appropriate seismic soil pressure in design.

RECENT EXPERIMENTS AND OBSERVATIONS

Lotung Experiment

Soil-structure interaction (SSI) effects play a significant role in the dynamic response of critical structures and internal components. Recognizing these effects, the Electric Power Research Institute (EPRI) with the cooperation from Taiwan Power Company (TPC) and the United States Nuclear Regulatory Commission (NRC) sponsored a large-scale experiment in the earthquake active area of Lotung, Taiwan. The objective

of the experiment was to evaluate the SSI analyses methodologies and to reduce uncertainties in the design. In this experiment, a 1/4-scale containment model was constructed. Instrumentation was installed both in the containment model and at the site. Since completion of the model and its instrumentation in October 1985, a number of recordings from earthquakes ranging in Richter magnitude 4.5 to 7.0 have been made at the site. The information on site condition, soil properties, and structural drawings were distributed to selected teams from the industry and academia (a total of 13 groups one which was Bechtel) to predict the responses on a round-robin basis. The results of this extensive experiment and follow up studies are published in several EPRI reports (EPRI, 1989; EPRI, 1991). The senior author also participated in the studies performed by Bechtel.

The Lotung site is a relatively flat with a relatively soft surface layer with thickness of 200 ft to 260 ft (60 m to 80 m) overlying deep alluvium stratum. The soil properties in terms of low-strain shear and compression wave velocities were measured at the site. The shear wave velocity is about 100 m/sec increasing to 250 m/sec at the depth. In addition cyclic laboratory testing was performed on soil samples and the strain-dependent soil properties were obtained.

The instrumentation for the experiment is extensive and consists of accelerometers and pressure gages in the model and in the free-field. Pressure gages were installed beneath the basemat for monitoring uplifting and bonding/de-bonding of the basemat from the supporting soil layer. In addition, pressure gages were also installed on the perimeter of the containment shell to measure seismic lateral soil pressure.

A number of earthquakes up to magnitude 7 were recorded at the site. For the purpose of this study, only the records from earthquake event LSST07 are used. The LSST07 event occurred on May 20, 1986 at about 40 miles(66.2 km) from the Lotung experiment. This event had a Richter magnitude of 6.5. The peak ground acceleration in the free-field at the ground surface were 0.16g, 0.21g, and 0.04g in the east-west, north-south, and vertical directions, respectively.

A typical recorded rime histories of seismic soil pressure is shown in Figures 1. Most time histories show a drift in the response and substantial residual pressure at the end of the shaking. Some of the pressure time histories have also been examined by Chang et al. (1990). As suggested by Chang et al., the drift in the time history and the residual pressure are attributed to the compaction of the backfill material during shaking and particle re-arrangement of the materials in the soil near the instrument. For this reason the recorded pressure time histories were corrected to eliminate the drift and the residual pressure in order to obtain the peak transient stresses. The corrected pressure time history is also shown in Figure 1 with positive sign indicating pressure and negative sign indicating extension.

The seismic soil pressure shown in Figure 1 is the normal stress component with the direction normal to the body of the containment shell in the North-South direction. The magnitude of the stress is a function of the relative motion of the containment and the surrounding soil and the soil properties. In the Lotung experiment, the relative motion was caused primarily by the rigid body rocking motion of the containment shell. To evaluate the effect of rocking motion on the lateral seismic soil pressure, frequency contents of the rocking motion are compared with the frequency contents of the pressure time history at one location, as shown in Figure 2. Comparison of the pair of spectra shows that, while the nature of the spectral amplitudes are different and are expected to have different amplitudes, the frequency content of the two motions are very similar, particularly at the rocking frequency of the containment shell (2.2 Hz).

The overall comparison of the results (see Ostadan and White, 1997) indicates that the seismic soil pressure is caused by the relative motion of the structure with respect to the surrounding soil and as such it is a SSI response. This implies that the seismic soil pressure will not only be affected by the soil properties and the characteristics of the ground motion, but also the structural properties as well as the size of the structure and its foundation embedment.

Finally, the result of the SSI analysis using the computer program SASSI (Lysmer et al., 1981) in terms of seismic soil pressure was obtained and compared with the recorded pressure in terms of spectral amplitudes in Figures 3

Other Observations From Recent Field and Experimental Data

In recent years, several field and laboratory experiments have been conducted to resolve the complexities associated with the seismic soil pressure and to develop a more realistic design parameter for the design of embedded structures. A summary of the selected recent investigations is presented below.

Case 1 - Deeply Embedded Reactor Building

Hirota et al. (1992) have collected and studied the soil pressure data from instrumented buildings since 1989. Specifically, the data from a deeply embedded reactor building (embedment depth of 120 ft) in a suburb of Tokyo have been presented and evaluated. The data from a total of eight earthquake records are presented. The principal conclusions of the study are as follows:

- The seismic soil pressure is significantly affected by the low-frequency content of the earthquake motion.
- Comparison of the pressure time history with the derived relative displacement time history between the structure and the far-field shows similar characteristics in phase and amplitude.

Case 2 - Deeply Embedded Structure

Matsumoto et al. (1991) and Watakabe et al. (1992) present the results of a study using the recorded data for a deeply embedded building in a suburb of Tokyo. The site consists of a soft alluvial layer with a thickness of 120 ft underlain by a much stiffer formation. The shear wave velocity of the upper layer ranges from 300 ft/sec to 1000 ft/sec. The building foundation rests on the stiff formation. The records from a total of 21 earthquakes have been collected and examined. The main points of the investigation are as follows:

- Frequency content of the soil pressure was examined by comparing the normalized response spectra of the soil pressure with the normalized velocity spectra of the motion in the soil layers at the respective elevations. The shapes of the normalized spectra closely matched.
- The finite element method employed was able to predict the soil-interaction effects. This conclusion confirms the use of finite element and soil-structure interaction techniques to predict seismic soil pressure.

Case 3 - Underground LNG Storage Tanks

Koyama et al. (1988,1992) collected and examined the earthquake and seismic soil pressure records from two large scale Liquid Natural Gas (LNG) underground storage tanks. The instrumented tanks are large diameter concrete tanks (200 ft diameter, 120 ft high). The site soil is a medium dense sand with a shear wave velocity of 1300 ft/sec. Over the 8-year period, records from 70 earthquakes have been collected and examined. The authors concluded that the seismic soil pressure is strongly correlated to the to the acceleration and the relative displacement of the tank and the ground.

In addition to the field experiments, a number of laboratory tests have been recently performed Kazama and Inatoi (1988) and Itoh and Nogami (1990). Evaluation of the test results showed that:

- The dynamic soil pressure is amplified near the resonant frequency of the backfill sand.
- The effect of soil nonlinearity on the peak dynamic pressure can be observed by increasing the amplitude of the vibration.
- The dynamic soil pressure distribution is consistent with the relative displacement between the ground and the caisson.
- Finite element analysis methods are able to reproduce the measured data.
- At the soil column resonant frequency, the seismic soil pressure acts in the direction of the basement movement to drive the structure, whereas at the structural resonant frequency, the dynamic pressure acts in the opposite direction of the basement movement to restrain the movement of the structure.

Recognition of the Problem and Objective of the Study

In spite of the much better understanding of the soil-wall interaction behavior that have evolved over the years, the M-O method continues to be widely used despite many criticisms and its limitations. As stated above, the method was developed for gravity retaining walls with cohesionless backfill materials. In design applications, however, the M-O method or any of its derivatives is commonly used for below ground building walls. In this regard, the M-O method is one of the most abused methods in the geotechnical practice.

In view of the overwhelming information and evidence on the dynamic behavior of buildings, some of which was outlined above, the United States Nuclear Regulatory Commission (US NRC, 1991) recently issued a position paper on the subject of the seismic soil pressure. Pertinent excerpts are quoted as follows:

> "The use of the M-O method of analysis to compute pressure on embedded walls of structures like the nuclear island (NI) structure of ..... is not considered appropriate since the development of the limit conditions in the soil requires wall movements which are most likely inappropriate for SSI conditions anticipated. The M-O approach will generally lead to a lower bound estimate for soil loads (using active state conditions in the soil) since the soil in the active wedge is assumed to transfer part of the load to the soil below through its own shear strength..."

It is the objective of this study to develop a simple and practical method to predict lateral seismic soil pressure for building walls.

- The walls of the buildings are often of the non-yielding type. The movement of the walls is limited due to the presence of the floor diaphragms, and displacements to allow development of the limit-state conditions are unlikely to develop during the design earthquake.
- The frequency content of the design motion is fully considered. Use of a single parameter as a measure of design motion such as peak ground acceleration may misrepresent the energy content of the motion, at frequencies important for soil amplifications.
- Appropriate soil properties are included in the analysis. For soil dynamic problems, the most important soil property is the shear wave velocity followed by the material damping, Poisson's ratio, and density of the soil.
- The method is flexible to allow for consideration of soil nonlinear effect where soil nonlinearity is expected to be important.
- The interaction between the soil and the building is represented. This includes consideration for the building rocking motion, amplification and variation of the motion in the soil, geometry, and embedment depth of the building.

SIMPLIFIED METHOD TO PREDICT LATERAL SEISMIC SOIL PRESSURE FOR BUILDING WALLS ON ROCK OR FIRM FOUNDATIONS

In this section, the dynamic characteristics of lateral seismic soil pressure for buildings with basemat resting on rock or firm soil layers are examined and a simplified method for predicting seismic soil pressure is presented. It is assumed that the building walls are effectively rigid. The condition that the basemat rests on a firm soil layer also simplifies the problem in that the rocking vibration of the buildings becomes insignificant. With this assumption, the embedment ratio of the building (embedment depth to basemat width) will not play a role in the results. The extension of the method for buildings embedded in deep soil layers is presented in the next section.

To investigate the characteristics of the lateral seismic soil pressure, a series of seismic soil-structure interaction analyses was performed using the Computer Program SASSI. A typical SASSI model of a building basement is shown in Figure 4. The embedment depth is designated by H and the soil layer is identified by the shear wave velocity, Vs, the Poisson's ratio, ν, total mass density, ρ, and the soil material damping, β. The basemat is resting on rock or a firm soil layer. A column of soil elements next to the wall is included in the model in order to retrieve the pressure responses from the results.

For this analysis, the acceleration time history of the input motion was specified at the top of the rock layer corresponding to the basemat elevation in the free-field. In order to characterize the dynamic behavior of the soil pressure, the most commonly used wave field consisting of vertically propagating shear waves was specified as input motion. The frequency characteristics of the pressure response were examined using harmonic shear waves for a wide range of frequencies. For each harmonic wave, the amplitude of the normal soil pressure acting on the building wall at three locations (Elements 2, 10, and 15 in Figure 4) was obtained. The pressure responses are presented in terms of pressure transfer function amplitudes which are the ratio of the amplitude of the seismic soil pressure in the respective element to the amplitude of the input motion (1g harmonic acceleration) in the free-field for each harmonic frequency. The analyses were performed for a building with embedment of 50 ft and soil shear wave velocities of 500, 1000, 1500, and 2000 ft/sec, all with the Poisson's ratio of 1/3. The material damping in the soil was specified to be 5%. The transfer function results for Element 2 (see Figure 4) are shown in Figure 5. As shown in this figure, the amplification of the pressure amplitude takes place at distinct frequencies. These frequencies increase as the soil shear wave velocity increases. The amplitude of soil pressure at low frequency was used to normalize the amplitude of the pressure transfer functions for each element. The frequency axis was also normalized using the soil column frequency which was obtained from the following relationship:

$$f = Vs / (4 \times H) \qquad (1)$$

In the above equation, Vs is the soil shear wave velocity and H is the embedment depth of the building. The normalized transfer functions are shown in Figure 6. As shown in this figure, the amplification of the pressure is about the same for all the shear wave velocities considered. In all cases the maximum amplification takes place at the frequency corresponding to the soil column frequency. Similarly, the results for points in the mid-height and bottom of the wall were examined (Ostadan and White, 1997). These results also showed the same characteristics described above.

Examining the dynamic characteristics of the normalized pressure amplitudes (such as those shown in Figure 6), it is readily evident that such characteristics are those of a single degree-of-freedom (SDOF) system. Each response begins at a value of one and increases to a peak value at a distinct frequency and subsequently reduces to a small value at high frequency. Dynamic behavior of a SDOF system is completely defined by the mass, stiffness and associated damping constant. It is generally recognized that response of a SDOF system is controlled by the stiffness at low frequency, by damping at resonant frequency, and by the inertia at high frequencies.

Following the analogy for a SDOF system and in order to characterize the stiffness component, the pressure amplitude at low frequencies for all elements (Elements 1 through 15 in Figure 4) was obtained and plotted as shown in Figure 7 in terms of the normalized height (Y/H, H=50 ft; Y is the distance from the base of the wall as shown in Figure 4). The pressure amplitudes at low frequency are almost identical for the wide range of the soil shear wave velocity profiles considered. The sudden increase shown at the top of the profile is due to the zero stress boundary condition near the ground surface and can be improved if finer elements are used. However, it is also generally recognized that soils particularly at shallow depths with low confining pressure have low shear strength and are subject to softening during vibration. For this reason, the normalized pressure profile was adjusted to have a vertical tip as shown in Figure 7. The shape of the normalized pressure will be used as a basis to determine seismic soil pressure along the height of the building wall. This will be discussed after the seismic soil pressure is examined for cases in which input motion is specified at the ground surface level.

A similar series of parametric studies were also performed by specifying the input motion at the ground surface level (Ostadan and White, 1997). The results of these studies also showed that the seismic soil pressure in normalized form can be represented by a single degree-of-freedom (SDOF) system. For both cases considered, the low frequency pressure profiles depict the same distribution of the pressure along the height of the wall as shown in Figure 7. This observation is consistent with the results of the analytical model developed by Veletsos and Younan (1994a). Since all the soil-structure interaction analyses were performed for the Poisson's ratio of 1/3, the pressure distribution was adjusted for the soil's Poisson's ratio using the factor recommended by Veletsos and Younan (1994a). The ψ_v factor is defined by:

$$\psi_\nu = \frac{2}{\sqrt{(1-\nu)(2-\nu)}} \qquad (2)$$

For the Poisson's ratio of 1/3 used in the analysis, ψ_ν is 1.897. Use of ψ_ν in the formulation allows correction of the soil pressure amplitude for various Poisson's ratios. The adjusted soil pressure distribution is also shown in Figure 7. Using the adjusted pressure distribution, a polynomial relationship was developed to fit the normalized pressure curve. The relationship in terms of normalized height, y = Y/H (Y is measured from the bottom of the wall and varies from 0 to H), is as follows:

$$p(y) = -.0015 + 5.05y - 15.84y^2 + 28.25y^3 - 24.59y^4 + 8.14y^5 \qquad (3)$$

The area under the curve can be obtained from integration of the pressure distribution over the height of the wall. The total area is 0.744 in terms of normalized wall height or 0.744H for the wall with the height H.

Having obtained the normalized shape of the pressure distribution, the amplitudes of the seismic pressure can be also obtained from the concept of a SDOF. The response of a SDOF system subjected to earthquake loading is readily obtained from the acceleration response spectrum of the input motion at the damping value and frequency corresponding to the SDOF. The total load is subsequently obtained from the product of the total mass times the acceleration spectral value at the respective frequency of the system.

To investigate the effective damping associated with the seismic soil pressure amplification and the total mass associated with the SDOF system, the system in Figure 4 with wall height of 50 ft and soil shear wave velocity of 1500 ft/sec was subjected to six different input motions in successive analyses. The motions were specified at the ground surface level in the free-field. The acceleration response spectra of the input motions at 5% are shown in Figure 8. The motions are typical design motions used for analyses of critical structures. From the set of six shown in Figure 8, two motions labeled EUS local and distant are the design motions for sites in Eastern US with locations close and far away from a major fault. The ATC S1 motion is the ATC recommended motion for S1 soil conditions. The WUS motion is the design motion for a site close to a major fault in Western US. The RG1.60 motion is the standard site-independent motion used for nuclear plant structures. Finally, the Loma Prieta motion is the recorded motion from the Loma Prieta earthquake scaled to 0.3g maximum acceleration. This motion is used in the analysis as described in later sections. All motions are scaled to 0.30g and limited to frequency cut-off of 20 Hz for use in the analysis. The cut-off frequency of 20 Hz reduces the peak ground acceleration of the EUS local motion to less than 0.30g due to high frequency content of this motion as shown in Figure 8.

The maximum seismic soil pressure values at each depth obtained from the analyses for the various input motions are shown in Figure 9. The amplitudes of the pressure vary from one motion to the other with larger values associated with use of RG1.60 motion. Using the pressure profiles in Figure 9, the lateral force acting on the wall for each input motion was computed. The lateral force represents the total inertia force of a SDOF for which the system frequency is known. The system frequency for the case under consideration is the soil column frequency which is 7.5 Hz based on Eqn (1). The total force divided by the spectral acceleration of the system at 7.5 Hz at the appropriate damping ratio amounts to the mass of the SDOF. To identify the applicable damping ratio, the acceleration response spectrum of the free-field response motions at the depth of 50 ft were computed for all six motions shown in Figure 8 for damping ratios of 5, 10, 20, 30, 40, 50, and 60 percents. Knowing the total force of the SDOF, the frequency of the system, and the input motion to the SDOF system, the relationship in the form proposed by Veletsos and Younan (1994a) was used to compute the total mass and the damping of the SDOF system. For the total mass, the relationship is

$$m = 0.50 \times \rho \times H^2 \times \psi_v \qquad (4)$$

where ρ is the mass density of the soil, H is the height of the wall, and ψ_v is the factor to account for the Poisson's ratio as defined in Eqn (2). In the analytical model developed by Veletsos and Younan, a constant coefficient of 0.543 was used in the formulation of the total mass. Study of the soil pressure transfer functions and free-field response motions at the depth of 50 ft showed that spectral values at the soil column frequency and at 30% damping have the best correlation with the forces computed directly from the SSI analysis. In the Veletsos and Younan's model, a damping of 27.5 + β percent has been proposed where β is the material damping of the soil (%). For the case of 5% soil material damping, the proposed spectral damping amounts to 32.5%. However, as shown by Ostadan and White (1997), the spectral values of the various motions considered are insensitive to the spectral damping ratios at the soil column frequency of 7.5. The various motions, however, have significantly different spectral values at the soil column frequency. This observation leads to the conclusion that while the frequency of the input motion particularly at the soil column frequency is an important component for magnitude of the seismic soil pressure, the spectral damping ratio selected is much less important in terms of pressure amplitudes. The role of soil material damping is discussed by Ostadan and White (1997).

Simplified Method: Computational Steps

To predict the lateral seismic soil pressure for below ground building walls resting on firm foundation and assuming rigid walls, the following steps should be taken:

1. Perform free-field soil column analysis and obtain the ground response motion at the depth corresponding to the base of the wall in the free-field. The response motion in terms of acceleration response spectrum at 30% damping should be obtained. The free-field soil column analysis may be performed using the Computer Program SHAKE (Schnabel et al., 1972) with input motion specified either at the ground surface or at the depth of the foundation basemat. The choice for location of control motion is an important decision that needs to be made consistent with the development of the design motion. The location of input motion may significantly affect the dynamic responses of the building and the seismic soil pressure amplitudes.

2. Use Eqn (4) to compute the total mass for a representative SDOF system using the Poisson's ratio and mass density of the soil.

3. Obtain the lateral seismic force from the product of the total mass obtained in Step 2 and the acceleration spectral value of the free-field response at the soil column frequency obtained at the depth of the bottom of the wall (Step 1).

4. Obtain the maximum lateral seismic soil pressure at the ground surface level by dividing the lateral force obtained in Step 3 by the area under the normalized seismic soil pressure, 0.744 H.

5. Obtain the pressure profile by multiplying the peak pressure with the pressure distribution relationship shown in Eqn (3).

One of the attractive aspects of the simplified method is its ability to consider soil nonlinear effect. The soil nonlinearity is commonly considered by use of the equivalent method and the strain-dependent soil properties. Depending on the intensity of the design motion and soil properties, the effect of soil nonlinearity can be important in changing the soil column frequency and therefore, amplitude of the spectral response at the soil column frequency.

Accuracy of the Simplified Method

The simplified method outlined above was tested for building walls with heights of 15, 30 and 50 ft using up to six different time histories as input motion. The results computed directly with SASSI are compared with the results obtained from the simplified solution. A typical comparison is shown in Figure 10. More extensive validation of the method is presented by Ostadan and White (1997).

Comparison to Other Commonly Uses Solutions

The seismic soil pressure results obtained for a building wall 30 ft high embedded in a soil layer with shear wave velocity of 1000 ft/sec using the M-O, Wood and the proposed simplified methods are compared in

Figure 11. For the simplified method, the input motions defined in Figure 8 were used. The M-O method results in the smallest pressure values. This is understood since this method relies on the wall movement to relieve the pressure behind the wall. Wood's solution generally results in the maximum soil pressure and is independent of the input motion as long as the peak acceleration is 0.3 g. The proposed method results in a wide range of pressure profiles depending on the frequency contents of the input motion, particularly at the soil column frequency. For those motions for which the ground response motions at the soil column frequency are about the same as the peak ground acceleration of the input motion, e.g., RG1.60 motion, the results of the proposed method are close to Wood's solution. Similar trend in the results is observed if sum of the lateral forces and the overturning moments from the above three methods are compared (Ostadan and White, 1997).

The simplified method was extended for application to soil layered system and soil deposits with parabolic distribution of the shear modulus. The extended method and its verification are discussed by Ostadan and White (1997).

SIMPLIFIED METHOD TO PREDICT LATERAL SEISMIC SOIL PRESSURE FOR BUILDINGS IN DEEP SOIL SITES

One of the distinct dynamic characteristics of a building in a deep soil site is its rocking vibration which has a significant role on distribution of the pressure depending on the embedment ratio (embedment depth versus plan dimensions), dynamic properties of the soil, and frequency contents of the ground motion under consideration.

Mita and Luco (1989) have reported the harmonic response of an embedded square foundation subjected to vertically propagating shear waves. The results adopted from the authors but modified to reflect the same nomenclature used in this report are shown in Figure 12. The results are for a square foundation with plan dimensions of 2B x 2B and embedment depth H. The halfspace is characterized by the shear wave velocity of Vs. The free-field motion has a unit amplitude at the ground surface at each harmonic frequency. The horizontal translational motion of the foundation (D) at the middle point corresponding to the basemat motion and the normalized rocking motion represented in terms of HxT are shown in terms of dimensionless frequency ratio $a_1 = \omega x H/Vs$ where T is the angle of rocking rotation and ω is the circular frequency at each harmonic frequency under consideration. The dimensionless frequency is a measure of the harmonic shear wave length as compared to the embedment depth H. The free-field motion corresponding to the basemat depth (depth of H) in the free-field shows decreasing amplitude with increasing frequency. At the soil column frequency of $f = Vs/(4xH)$, the dimensionless frequency a1 is 1.57 at which the amplitude of the free-field motion is zero. The foundation motion is a function of the frequency of vibration and the embedment ratio (H/B).

In order to examine the effect of rocking motion on seismic soil pressure, a series of SSI analyses were performed using the soil shear wave velocities of 500, 1000, 1500, and 2000 ft/sec. In all cases, the wall height considered was H=50 ft but the foundation width (2B) was changed successively from 50 ft, to 100 ft, 200 ft, and to 400 ft, resulting in embedment ratios of B/H=0.5, 1, 2, and 4. The input motion was specified at the basemat level in the free-field. A typical result in terms of amplitude of pressure transfer function is shown in Figures 13. For each soil case, the results from all three elements are clustered together with the same peak frequency which leads to the conclusion that (1) the soil column frequency continues to be the most significant frequency for the response in terms of maximum value of the seismic soil pressure, and (2) the frequency of the peak response is not affected by the embedment ratio. However, the distribution of the maximum soil pressure in terms of amplitude of the pressure in Elements 2, 5, and 10 is significantly affected by the rocking motion of the building and thus the embedment ratio. The effects of rocking motion on distribution of maximum seismic soil pressure for four different aspect ratios are shown in Figure 14. As shown, for buildings with narrow width, the rocking motion tends to reduce the amplitude of the soil pressure at top of the wall.

The results of the parametric studies performed for deep soil sites were also examined in detail. Limitation of space prohibits detail discussion of the studies performed. The computational steps for deep soil sites are, however, similar to the rigid case and consist of the following:

1. Perform free-field soil column analysis and obtain the response motion in terms of acceleration response spectrum at 30% damping at the depth corresponding to the basemat elevation in the free-field.
2. Obtain the soil column frequency using Eqn (1) and obtain the spectral value at the soil column frequency using the results of Step 1.
3. Use the following relationship to obtain the lateral force acting on the wall:

$$F = \alpha \times \rho \times H^2 \times Sa \times \Psi_v \qquad (5)$$

where ρ is the mass density of the soil, H is height of the wall, Sa is the spectral value of the free-field response obtained in Step 2, and Ψ_v is the function that considers the effect of soil Poisson's ratio and can be obtained using Eqn (2). In order to represent the effect of the embedment ratio and reduction of soil pressure due to rocking motion as well as its increase beyond the rigid base cases for wide buildings, the parameter α is defined in the equation above. This parameter was determined from back-calculation of the lateral force obtained from soil pressure and the shear stress under the basemat to hold the equilibrium of forces in the horizontal direction. Using the results of the all the parametric studies, the following values were obtained for α:

Embedment Ratio, B/H	Parameter α
0.50	0.27
1.0	0.43
2.0	0.62
4.0	0.92

4. Obtain the maximum soil pressure by dividing the lateral force obtained from Step 3 to the area under the soil pressure curve provided in Eqns(6) through (9) below depending on the embedment ratio. For an embedment ratio that falls in between the ratios considered, use interpolation.

Embedment ratio of B/H=0.50

$p(y) = -2.58y^3 + 0.32\,y^2 + 2.46\,y - 0.03$ (6)

Maximum pressure at the depth y = 0.625

Area under the curve = 0.632H

Point of application for resultant force, Y = 0.55H

Embedment ratio of B/H=1.0

$p(y) = 0.60y^3 - 3.09y^2 + 3.34y - 0.025$ (7)

Maximum pressure at the depth y = 0.625

Area under the curve = 0.77H

Point of application for resultant force, Y = 0.58H

Embedment ratio of B/H=2.0

$p(y) = -1.33y^4 + 4.38y^3 - 5.66y^2 + 3.44y + 0.17$ (8)

Maximum pressure at top of the wall y = 1

Area under the curve = 0.832H

Point of application for resultant force, Y = 0.57H

Embedment ratio of B/H=4.0

$p(y) = -0.085y^2 + 0.47y + 0.61$ (9)

Maximum pressure at top of the wall y = 1

Area under the curve = 0.82H

Point of application for resultant force, Y = 0.54H

5. Multiply the maximum lateral soil pressure from Step 4 by the relationships provided in Eqns (6) through (9) to get the pressure distribution depending on the embedment ratio of the foundation under

consideration. Judgment should be exercised to obtain the distribution for embedment ratios in between the four embedment ratios considered above.

The simplified method for deep soil sites was also tested extensively for a wide range of soil properties and foundation embedment ratios (Ostadan and White, 1997).

A comparison of the simplified method with the M-O and Wood's methods for a building with four different embedment ratios is shown in Figure 15. The results clearly demonstrates the effect of the rocking motion on distribution of the seismic soil pressure.

SUMMARY AND CONCLUSION

The Mononobe-Okabe (M-O) method was developed in the 1920's. Since then, a great deal of research work has been performed to evaluate its adequacy and to improve it. The method is, strictly speaking, applicable to gravity retaining walls which, upon experiencing seismic loading, undergo relatively large movement to initiate the sliding wedge behind the wall and to relieve the pressure to its active state. Unfortunately, the method has been and continues to be used extensively for embedded walls of the buildings as well. Recent field observations and experimental data, along with enhancements in analytical techniques have shown that hardly any of the assumptions used in the development of the M-O method are applicable to building walls. The data and the follow up detail analysis have clearly shown that the seismic soil-pressure is an outcome of the interaction between the soil and the building during the seismic excitation and as such is function of all parameters that affect soil-structure interaction (SSI) response. Some of the more recent observations and experimental data were presented in the paper. The new understanding of the attributes of seismic soil pressure prompted the United Sates Nuclear Regulatory Committee (NRC) to reject the M-O and the M-O based methods for application to critical structures. At this time, while elaborate finite element techniques are available to obtain the soil pressure for design, no simple method has been proposed for quick prediction of the maximum soil pressure, thus hindering the designer's ability to use an appropriate method in practice. To remedy this problem, the current research was conducted to develop a simple method which incorporates the main parameters affecting the seismic soil pressure for buildings.

Using the concept of the single degree-of-freedom, a simplified method was developed to predict maximum seismic soil pressures for buildings resting on firm foundation materials. The method incorporates the dynamic soil properties and the frequency content characteristics of the design motion in its formulation. It was found that the controlling frequency that determines the maximum soil pressure is that corresponding to the soil column adjacent to the embedded wall of the building. The proposed method requires the use of conventionally-used simple one-dimensional soil column analysis to obtain the relevant soil response at the base of the wall. More importantly, this approach allows soil nonlinear effects to be considered in the

process. The effect of soil nonlinearity can be important for some applications depending on the intensity of the design motion and the soil properties. Following one-dimensional soil column analysis, the proposed method involves a number of simple hand calculations in order to arrive at the distribution of the seismic soil pressure for design. The accuracy of the method relative to the more elaborate finite element analysis was verified for a wide range of soil properties, earthquake motions, and wall heights.

The method was extended to include buildings on deep soil sites . The complexity of the seismic soil pressure for such cases is compounded by the rocking motion of the structure. The rocking motion is in turn, a function of soil properties, frequency content of the design motion, and embedment ratio of the structure. A wide range of parametric studies were performed that cover many practical cases. The steps for the analysis are similar to the steps outlined for buildings on rock except that an appropriate pressure distribution curve should be selected to observe the effect of the embedment ratio. Similarly, the accuracy of the proposed method was verified against a more detailed SSI analysis.

REFERENCES

ASCE 4.86 (1986). "Seismic Analysis of Safety-Related Nuclear Structures and Commentary on Standard for Seismic Analysis of Safety Related Nuclear Structures," Published by the American Society of Civil Engineers.

Chang, C. Y., Power, M. S., Tang, Y. K., and Tang, H. T. (1990). "Analysis of Dynamic Lateral Earth Pressures Recorded on Lotung Reactor Containment Model Structure," Proceedings of 4th US National Conference on Earthquake Engineering, May 20-24, Palm Springs, CA.

Ebeling, R. M., and Morrison, Jr., E. E. (1992). "The Seismic Design of Waterfront Retaining Structures," US Army Technical Report ITL-92-11, Prepared by Information Technology Laboratory, Department of the Army, Waterways Experiment Station, Corps of Engineers, Vicksburg, Mississippi.

EPRI (1989). "Proceedings: EPRI/NRC/TPC Workshop on Seismic Soil-Structure Interaction Anslysis Techniques Using Data From Lotung, Taiwan," Electric Power Research Institute Publication No. NP-6154, 2 Volumes, March.

EPRI (1991). "Post-Earthquake Analysis and Data Correlation for the 1/4-Scale Containment Model of the Lotung Experiment," Electric Power Research Institute Publication No. NP-7305SL, October.

Hirota, M., Sugimoto, M., and Onimaru, S. (1992). "Study on Dynamic Earth Pressure Through Observation," Proceedings of 10th World Conference on Earthquake Engineering, July, Madrid, Spain.

Ishibashi, I., Matsuzawa, H., and Kawamura, M. (1985). "Generalized Apparent Seismic Coefficient for Dynamic Lateral Earth Pressure Determination," Proceedings of 2nd International Conference on Soil Dynamics and Earthquake Engineering, the Queen Elizabeth II, New York to Southampton, June/July.

Itoh, T., and Nogami, T. (1990). "Effects of Surrounding Soils on Seismic Response of Building Basements," Proceedings of 4th US National Conference on Earthquake Engineering, May 20-24, Palm Springs, CA.

Kazama, M., and Inatomi, T. (1988). "A Study on Seismic Stability of Large Embedded Rigid Structures," Proceedings of Ninth World Conference on Earthquake Engineering, August 2-9, Tokyo-Kyoto, Japan.

Koyama, K., Watanabe, O., and Kusano, N. (1988). "Seismic Behavior of In-Ground LNG Storage Tanks During Semi-Long Period Ground Motion," Proceedings of 9th World Conference on Earthquake Engineering, August 2-9, Tokyo-Kyoto, Japan.

Koyama, K., Kusano, N., Ueno, H. , and Kondoh, T. (1992). "Dynamic Earth Pressure Acting on LNG in-Ground Storage Tank During Earthquakes," Proceedings of 10th World Conference on Earthquake Engineering, July, Madrid, Spain.

Matsuzawa, H., Ishibashi, I., and Kawamura, M. (1984). "Dynamic Soil and Water Pressures of Submerged Soils," ASCE, Journal of Geotechnical Engineering, Vol. 111, No. 10, September.

Matsumoto, H., Arizumi, K., Yamanoucho, K., Kuniyoshi, H., Chiba, O., and Watakabe, M. (1991). "Earthquake Observation of Deeply Embedded Building Structure," Proceedings of 6th Canadian Conference on Earthquake Engineering, June, Toronto, Canada.

Mita, A. and Luco, J. E. (1989). "Impedance Functions and Input Motions For Embedded Square Foundations," ASCE, Journal of Geotechnical Engineering, Vol. 115, No. 4, April.

Mononobe, N. and Matuo, H. (1929). "On the Determination of Earth Pressures During Earthquakes," Proceeding of World Engineering Congress, Tokyo, Vol. 9, Paper 388.

Nadim, F. and Whitman, R.V. (1984). "Coupled Sliding and Tilting of Gravity Retaining Walls During Earthquakes," Proceedings of 8th World Conference on Earthquake Engineering, July, San Francisco, CA.

Nazarian, H., and Hadjian, A. H. (1979). "Earthquake Induced Lateral Soil Pressure on Structures," ASCE, Journal of Geotechnical Engineering, Vol. 105, No. GT9, September.

Nuclear Regulatory Commission (NRC, 1991), Proposed Staff Position on Dynamic Lateral Earth Pressures on Earth Retaining Walls and Embedded Walls of Nuclear Power Plant Structures, Civil Engineering and Geoscience Branch, Division of Engineering, Office of Nuclear Reactor Regulation.

Okabe, S. (1924). "General Theory of Earth Pressures and Seismic Stability of Retaining Wall and Dam," Journal of Japan Society of Civil Engineers, Vol. 12, No. 1.

Lysmer et al. (1981). "SASSI - A System for Analysis of Soil-Structure Interaction," Report No. UCB/GT/81-02, University of California, Department of Civil Engineering, Berkeley, California.

Ostadan, F., White, W. H. (1997). "Lateral Seismic Soil Pressure-An Updated Approach," Bechtel Technical Grant Report, Bechtel Corporation, San Francisco, California.

Richards Jr., R. and Elms, D. (1979). "Seismic Behavior of Gravity Retaining Walls," ASCE, Journal of Geotechnical Engineering, Vol. 105, No. GT4, April.

Schnabel, P. B. , Lysmer, J., Seed, H. B., "SHAKE - A Computer Program for Earthquake Response Analysis of Horizontally Layered Sites," Earthquake Engineering Research Center, University of California, Berkeley, Report No. EERC 72-12, December 1972.

Seed, H. B., and Whitman, R. V. (1970). "Design of Earth Retaining Structures for Seismic Loads," ASCE Specialty Conference on Lateral Stresses in the Ground and Design of Earth Retaining Structures, June.

Veletsos, A, and Younan, A. H. (1994a). "Dynamic Soil Pressure on Rigid Vertical Walls", Earthquake Engineering and Soil Dynamics, Vol. 23, 275-301.

Veletsos, A, and Younan, A. H. (1994b). "Dynamic Modeling and Response of Soil-Wall Systems," ASCE, Journal of Geotechnical Engineering, Vol. 120, No. 12, December.

Veletsos, A, and Younan, A. H. (1994c). "Dynamic Soil Pressures on Rigid Cylindrical Vaults," Earthquake Engineering and Structural Dynamics, Vol. 23, 645-669

Veletsos, A, and Younan, A. H. (1995). "Dynamic Modeling and Response of Rigid Embedded Cylinders," ASCE, Engineering Mechanics, October.

Veletsos, A, Parikh, V. H., Younan, A. H., and K. Bandyopadhyay (1995). "Dynamic Response of a Pair of Walls Retaining a Viscoelastic Solid," Brookhaven National Laboratory, AUI, Department of Advanced Technology, Associated Universities, Inc., UPTON, New York.

Watakabe, M., Matsumoto, H., Fukahori, Y., and Shikama, Y., Yamanouchi, K., and Kuniyoshi, H. (1992). "Earthquake Observation of Deeply Embedded Building Structure," Proceedings of 10th World Conference on Earthquake Engineering, July, Madrid, Spain.

Whitman, R. V. (1979). "Dynamic Behavior of Soils and Its Application to Civil Engineering Projects," Proceedings of 6th Pan American Conference, Lima, Peru.

Whitman, R. V., (1990). "Seismic Design and Behavior of Gravity Retaining Walls," Proceedings of a Specialty Conference on Design and Performance of Earth Retaining Structures, ASCE, Cornell University, June 18-21.

Whitman, R. V., and Christian, J. T. (1990). "Seismic Response of Retaining Structures," Pola Workshop Meeting, San Pedro, CA.

Whitman, R. V. (1991). "Seismic Design of Earth Retaining Structures," Proceedings of 2nd International Conference on Recent Advances in Geotechnical Earthquake Engineering and Soil Dynamics, March 11-15, St. Louis, Missouri.

Wood, J. H. (1973). "Earthquake Induced Soil Pressures on Structures," Doctoral Dissertation, EERL 73-05, California Institute of Technology, Pasadena, CA.

Figure 1
Original Soil Pressure Record

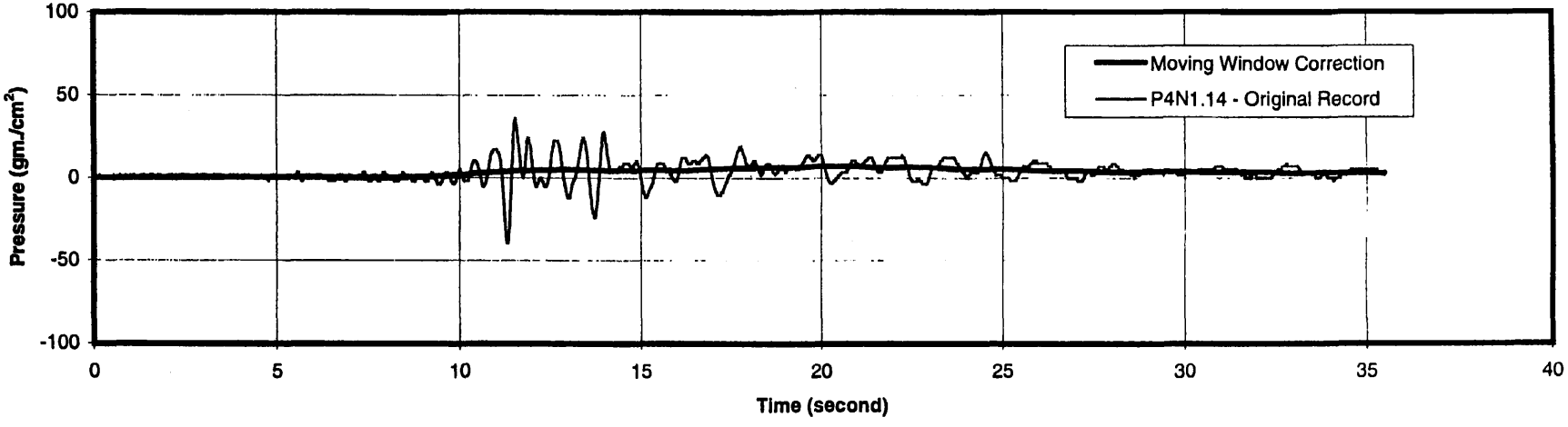

Corrected Soil Pressure Record

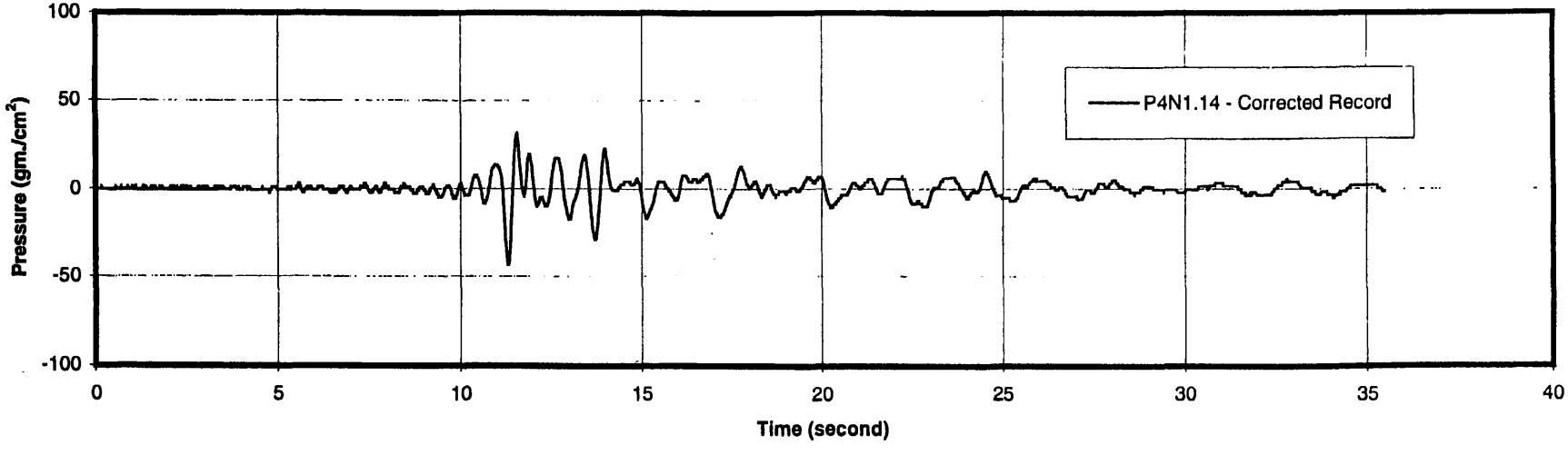

Lotungpl.xls, N114plot
7/28/98

Figure 2
Comparison of Response Spectra (5% Damping)
Lotung Records, Event LSST07. N-S Component
Rocking Motion and Soil Pressure

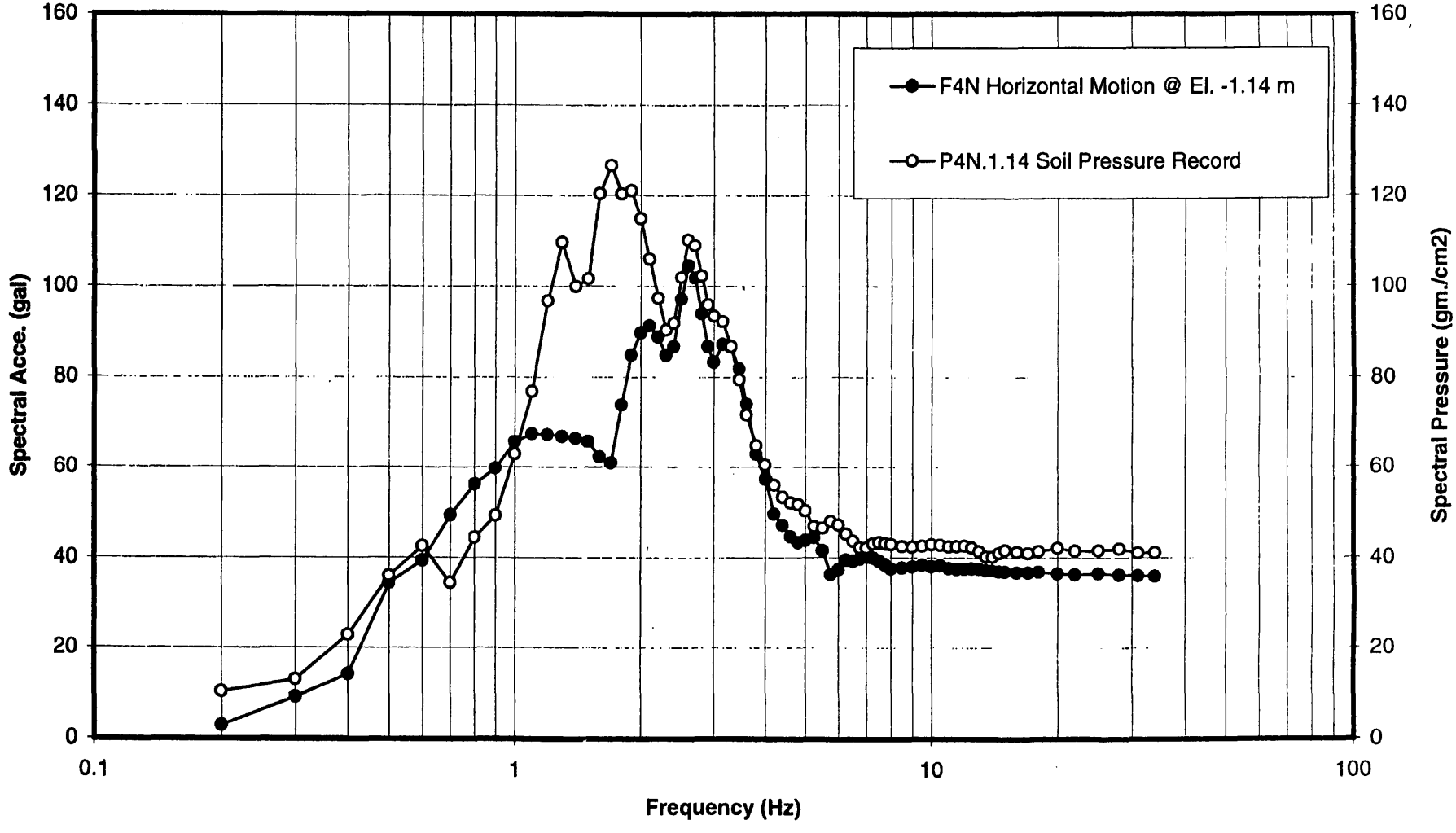

P4 f4r.xls, 4N Rck EP
7/27/98

Figure 3
Soil Pressure Response Spectra (5% Damping)
Comparison of Recorded and Computed Soil Pressure Records
EPRI Lotung 1/4 Model, Event LSST07, Station P4N1.14, N-S Direction

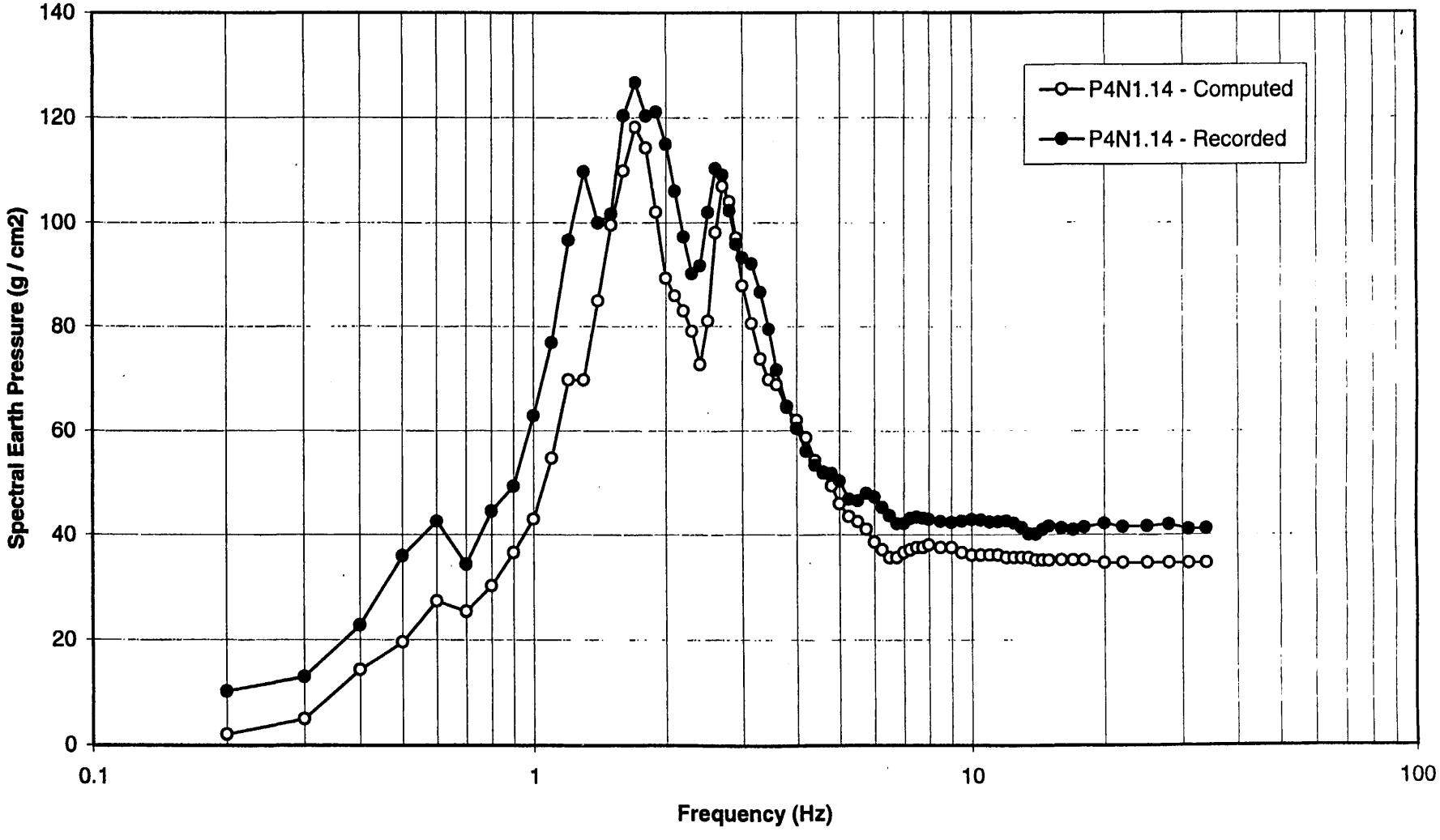

P4_ars.xls, ARS_P4N114
7/27/98

Figure 4

SASSI MODEL

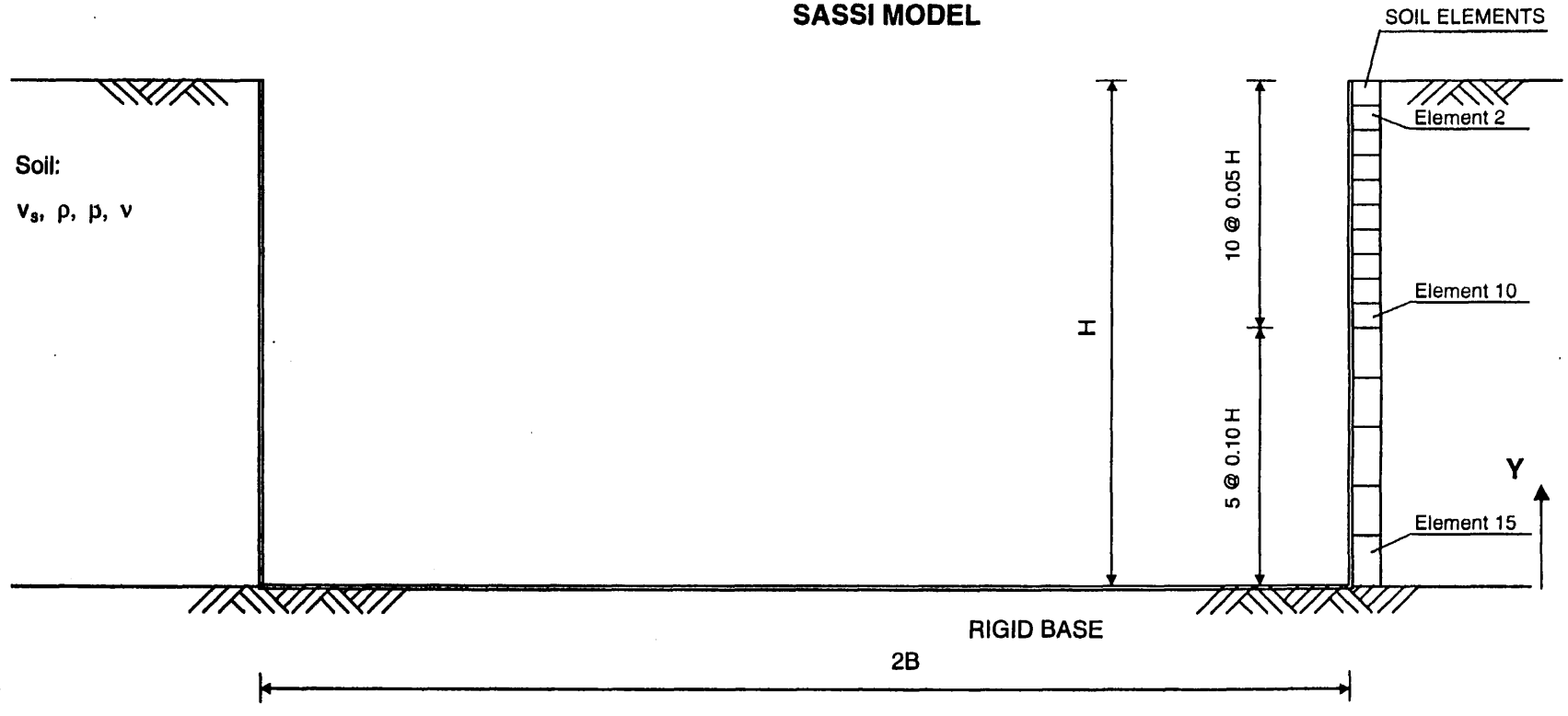

Fig31.xls, R_Base
7/27/98

Figure 5
Amplitude of Soil Pressure Transfer Functions
Rigid Halfspace. Rigid Wall. H=50 ft, ν=1/3, β=0.05
Element 2 -- D/H =0.075. Input Motion at the Base of the Wall

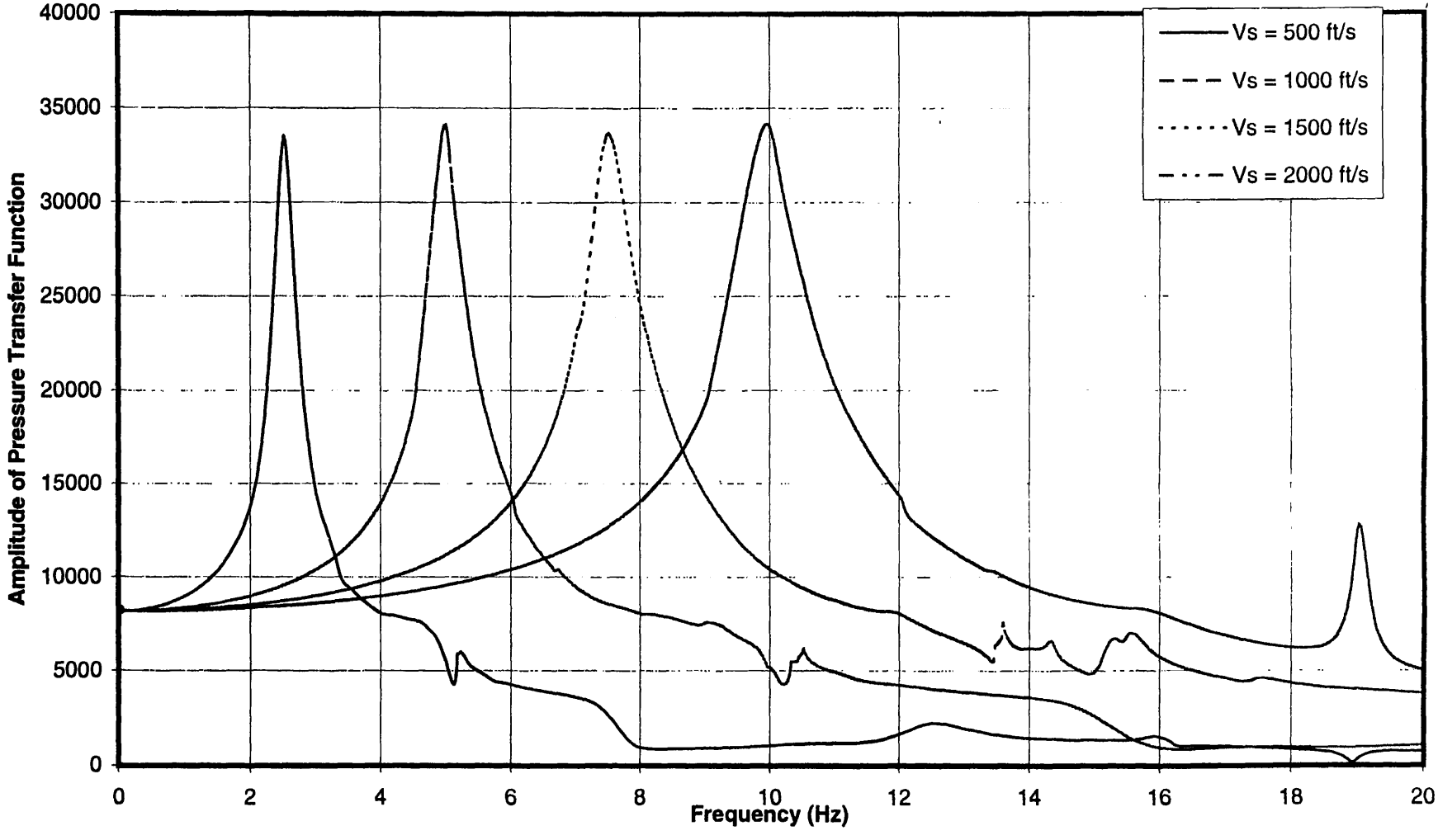

Tfbase.xls,ELEM2_T
7/27/98

Figure 6
Amplitude of Soil Pressure Transfer Functions
Rigid Halfspace, Rigid Wall, H = 50 ft, ν = 1/3, β = 0.05
Element 2 -- D/H = 0.075. Input Motion at the Base of the Wall

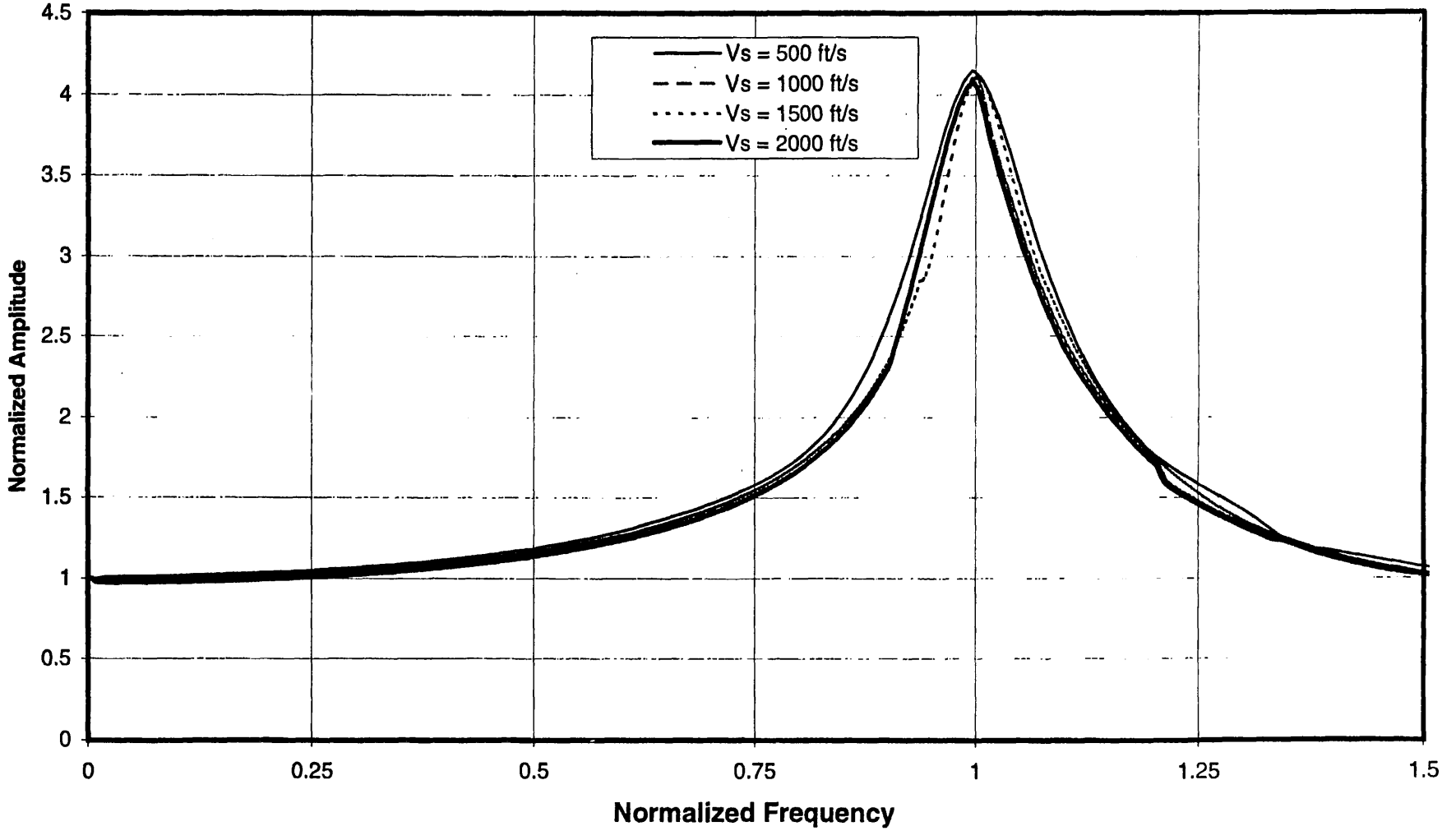

Figure 7
Amplitude of Soil Pressure Transfer Function
Rigid Halfspace, Rigid Wall. H=50 ft, ν=1/3, β=0.05
Average Amplitude in Freq. Range 0.10 - 0.25 Hz
1g Harmonic Input Motion

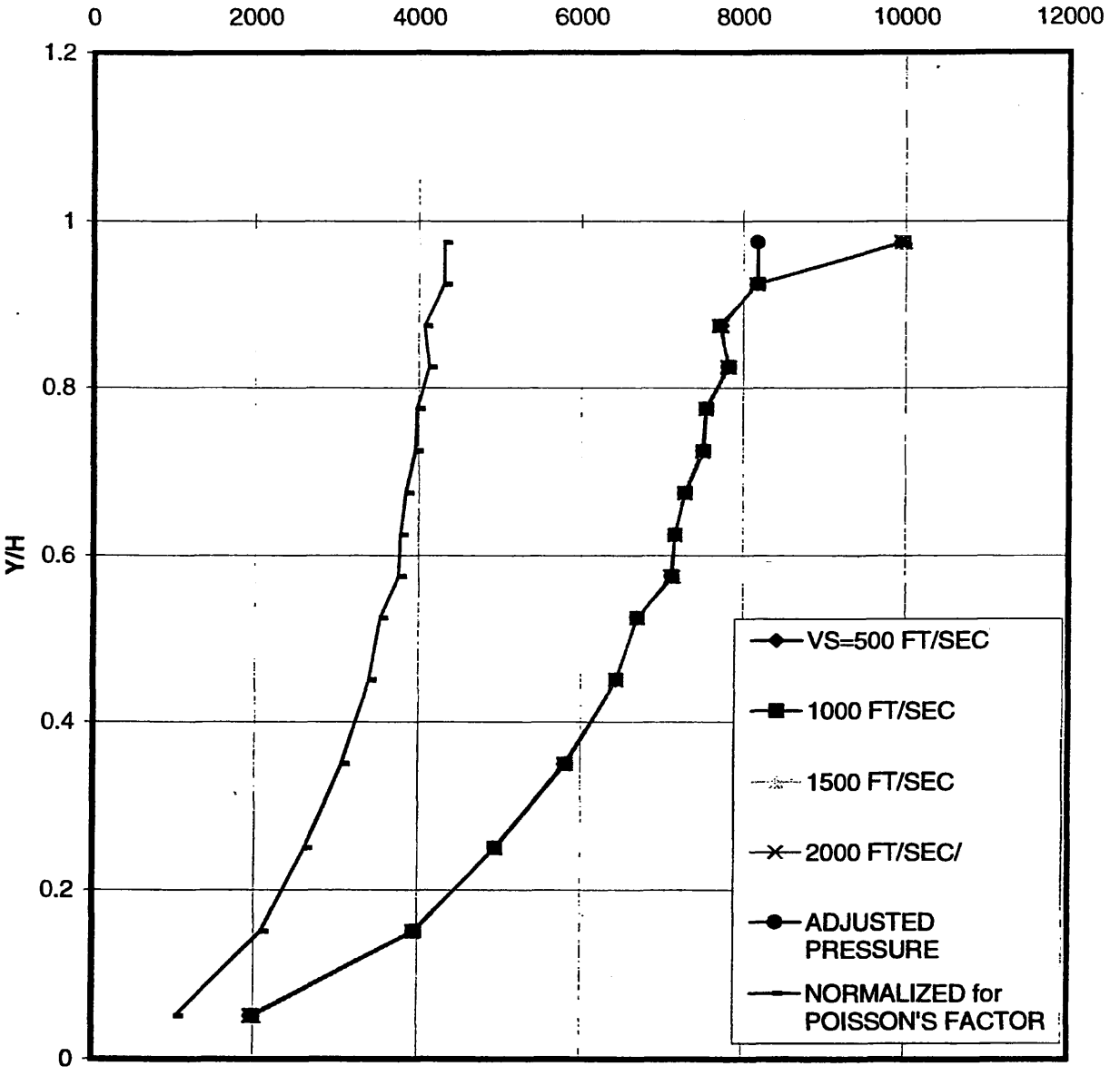

Tfsurf.xls,LOWFRQ_PRS_NORM (2)
7/27/98

Figure 8
Acceleration Response Spectra (5%)
Comparison of Different Input Earthquake Motions: Free-Field
At Ground Surface, Cutoff Freq. = 20 Hz.

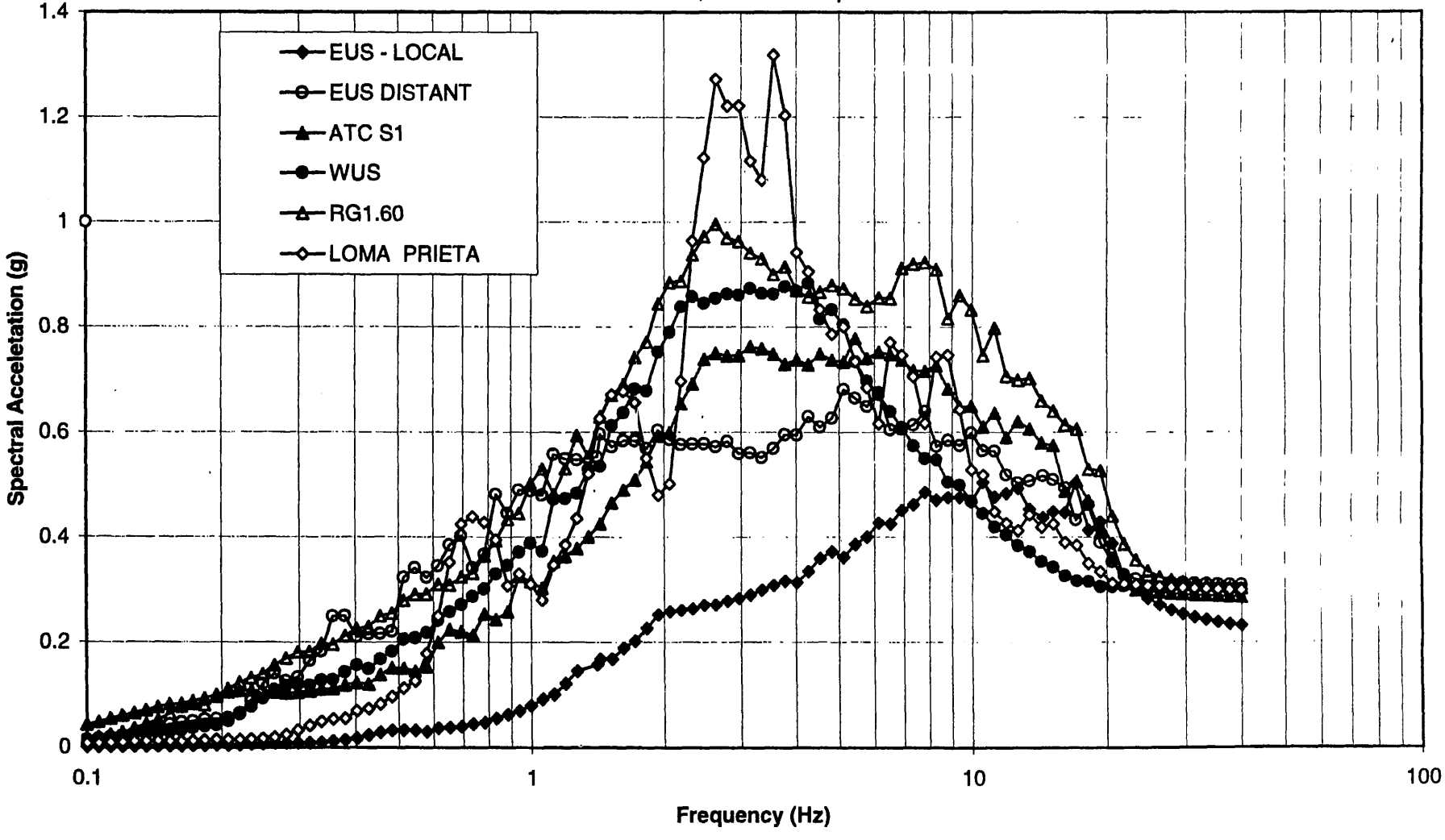

Figure 9
Maximum Seismic Soil Pressure - psf
WALL 50 ft, Vs=1500 ft/sec, ν=1/3, β=5%

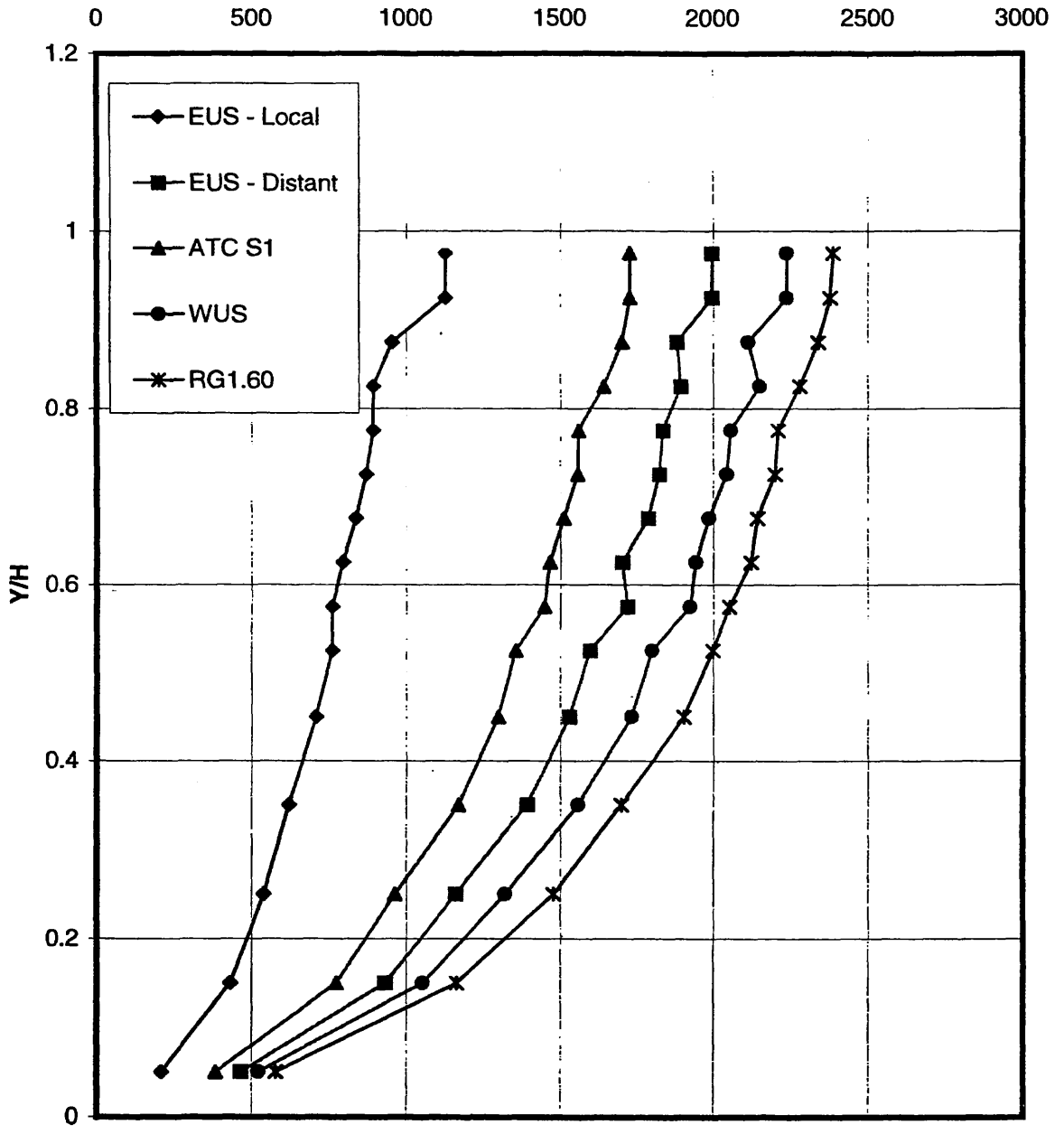

Eqs.xls,EPS_sum
7/27/98

Figure 10
Maximum Seismic Soil Pressure (psf)
WALL 30 ft, Vs=1000 ft/sec, ν=1/3, β=5%
LOMA PRIETA Motion

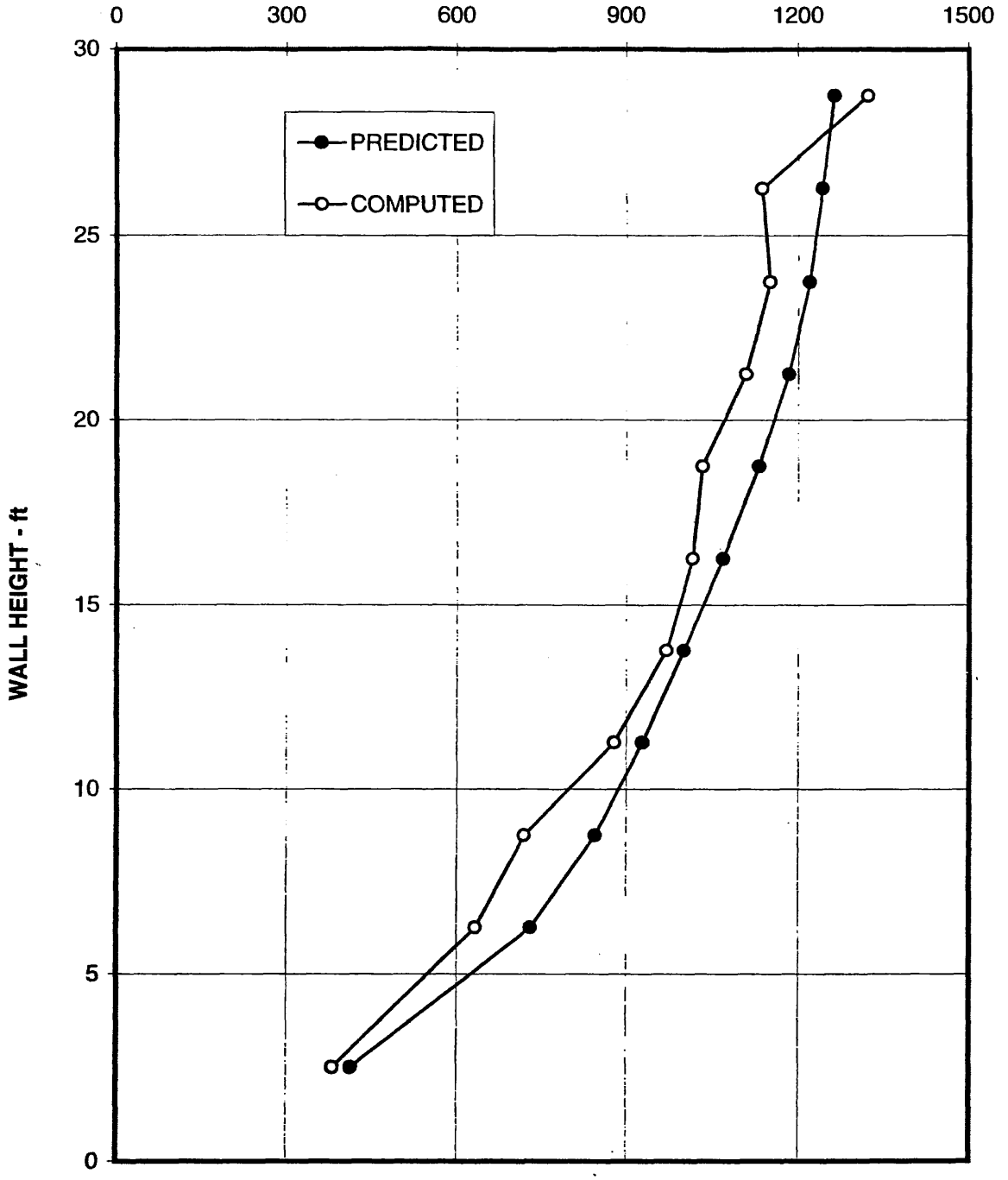

Ht_aeqs.xls,H30_LMP
7/27/98

Figure 11
Maximum Seismic Soil Pressure (psf)
WALL 15 ft, Vs=500 ft/sec, ν=1/3, β=5%
All Motions

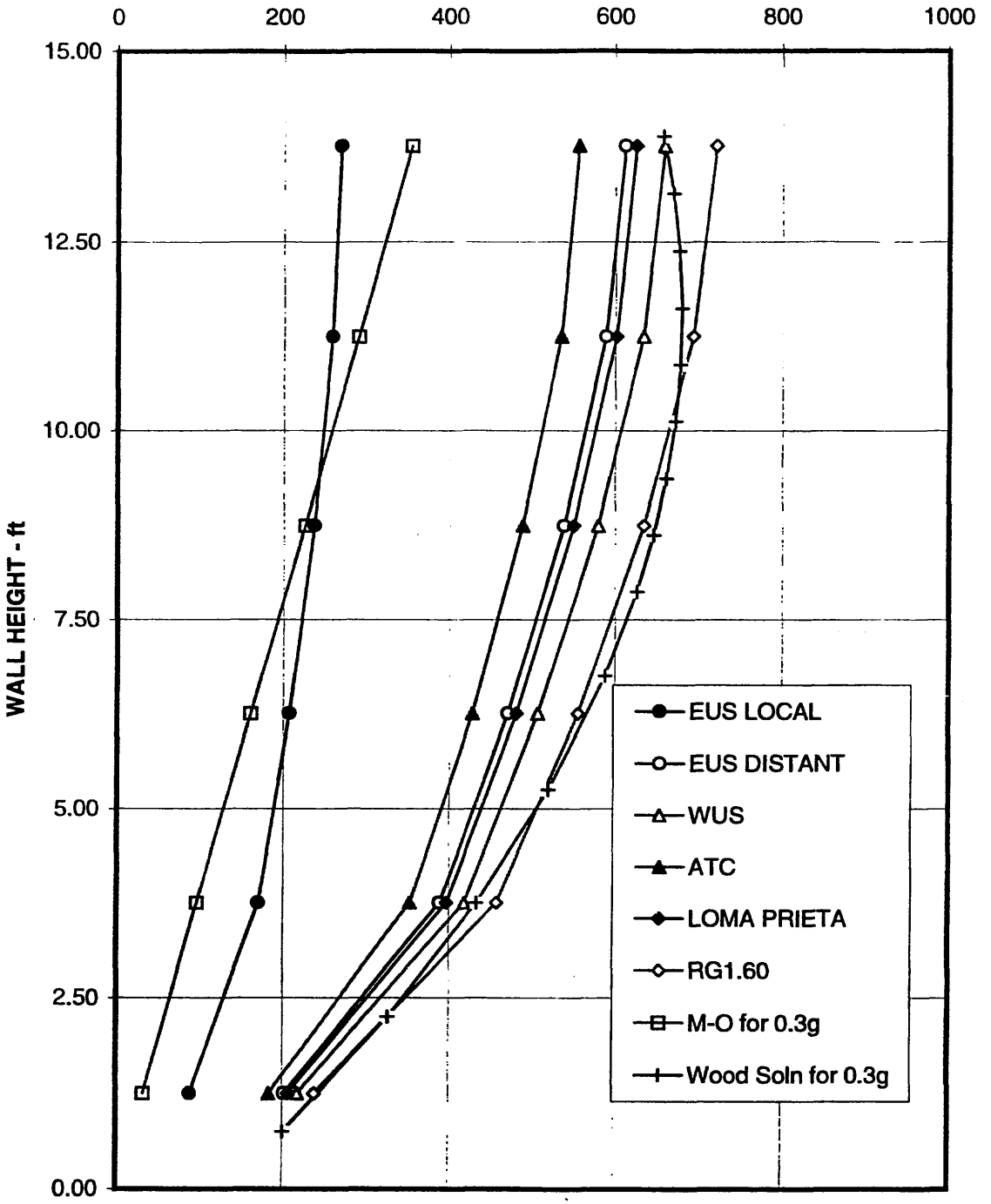

Ht_aeqs.xls,H15_ALL (2)
7/27/98

Figure 12
Normalized Amplitude Response Ratio of Horizontal D and Rocking H*T Motions For Square Embedded Foundations

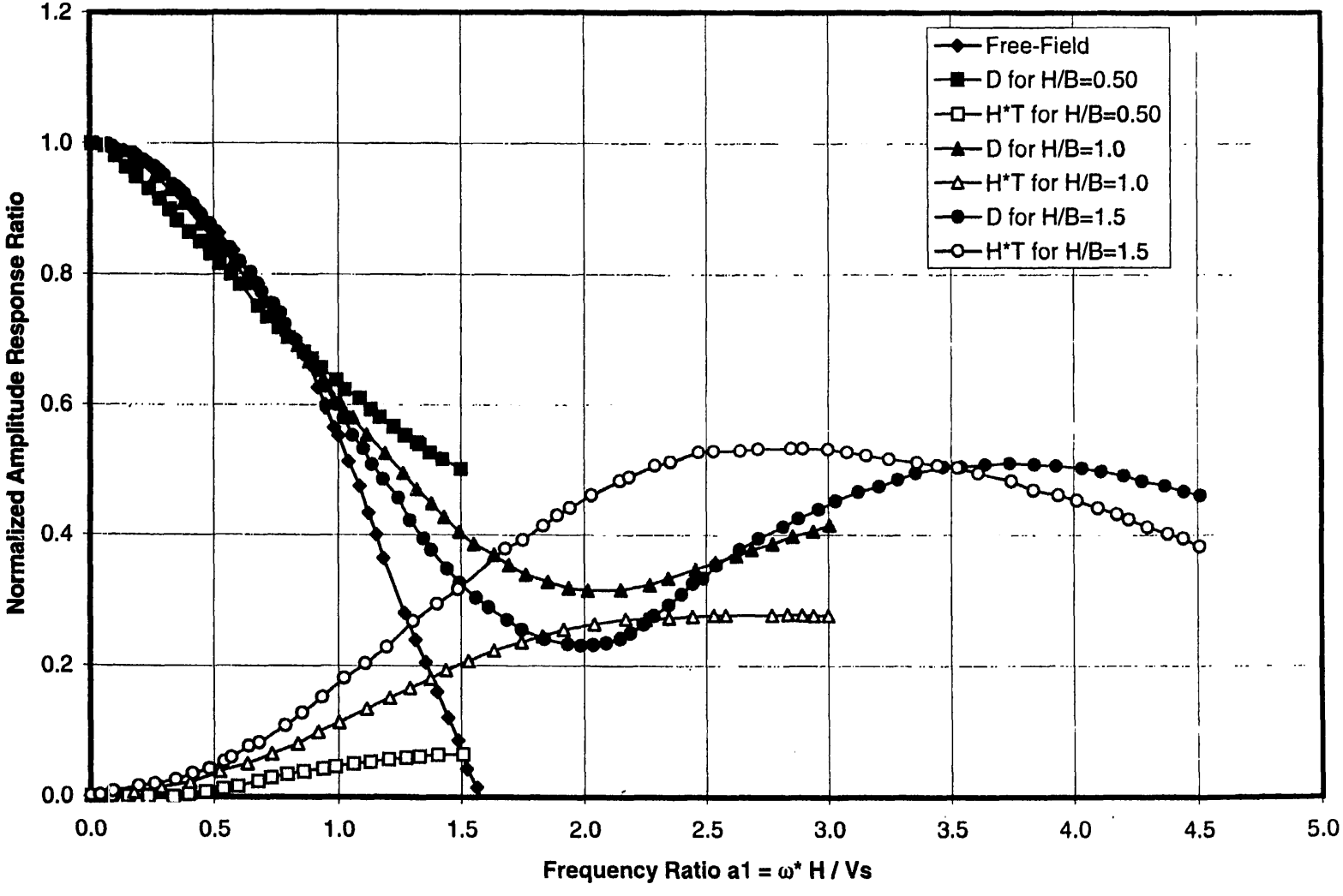

Luco.xls,luco plt
7/27/98

Figure 13
Amplitude of Soil Pressure Transfer Functions
B/H=0.50, H=50 ft, ν=1/3, β=0.05
Input Motion at the Base of the Wall

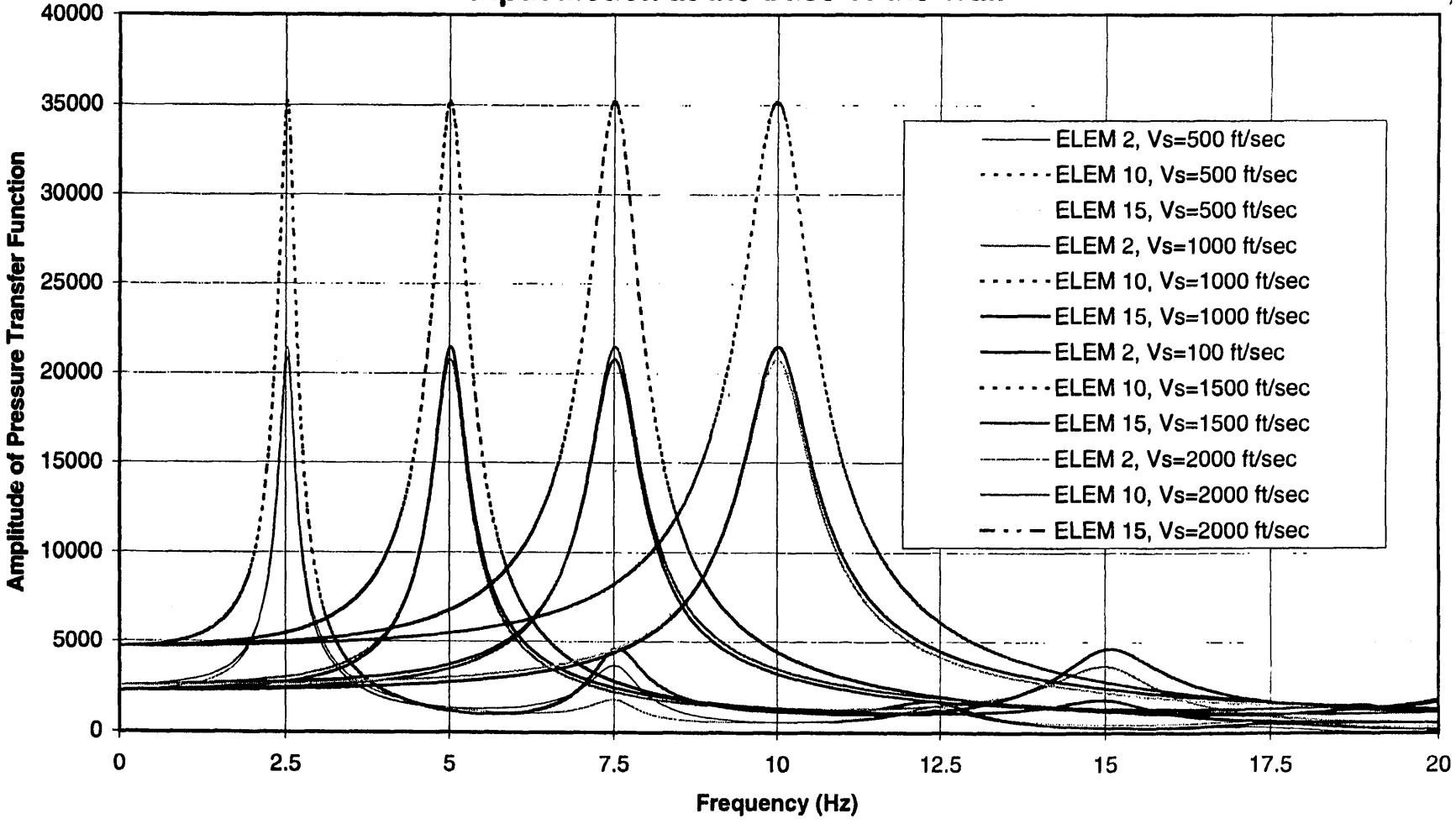

Tfst.xls,B5HAEL_PL
7/27/98

Figure 14
Maximum Seismic Soil Pressure
H=50 ft, Vs=500 ft/sec, ν=1/3, β=5%
RG1.60 Motion at the Base

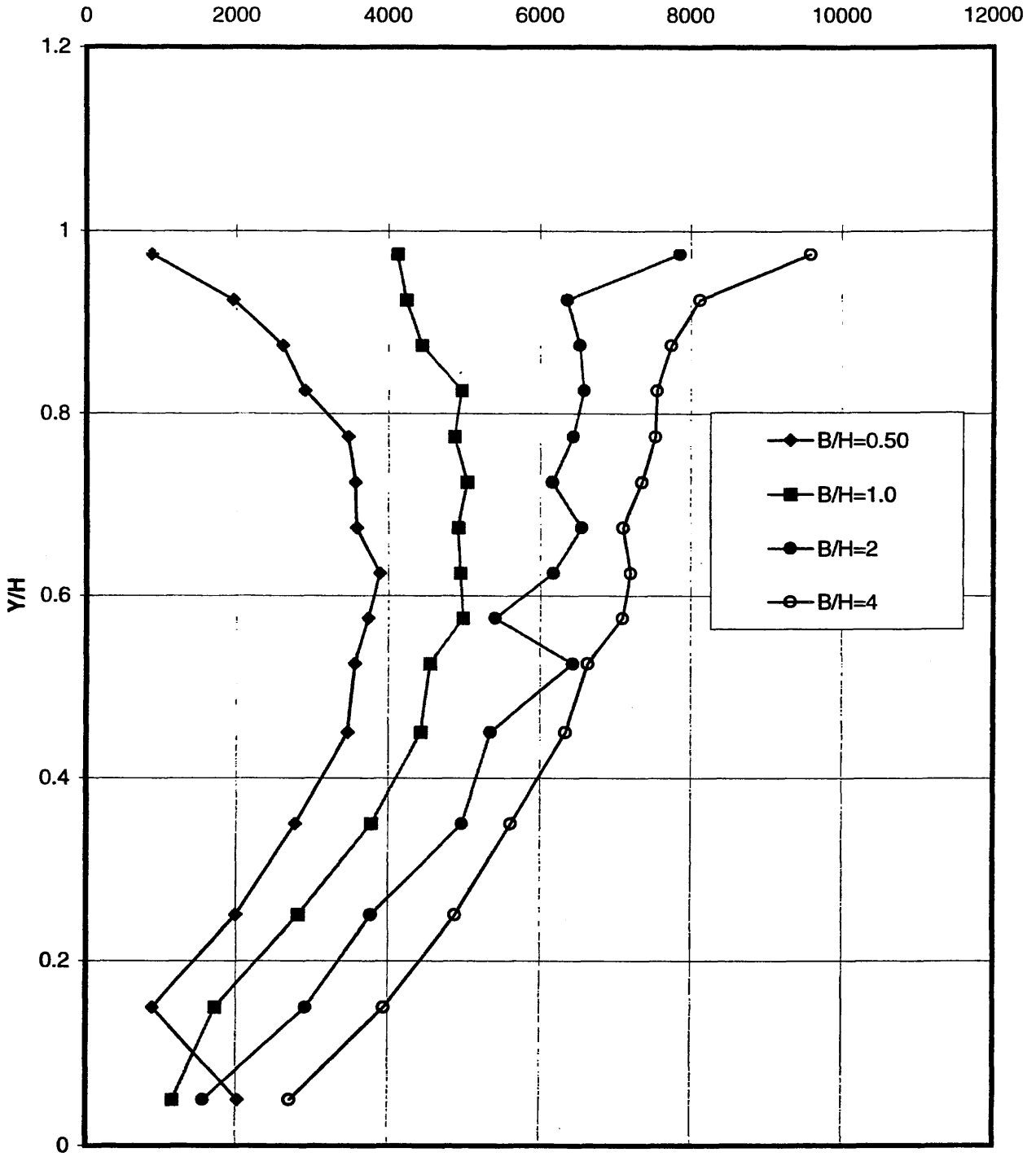

Stsum_rg.xls,v1_pl
7/27/98

Figure 15
Maximum Seismic Soil Pressure
H=50 FT, Vs=1000 ft/sec, ν=1/3, β=5%
RG1.60 Motion

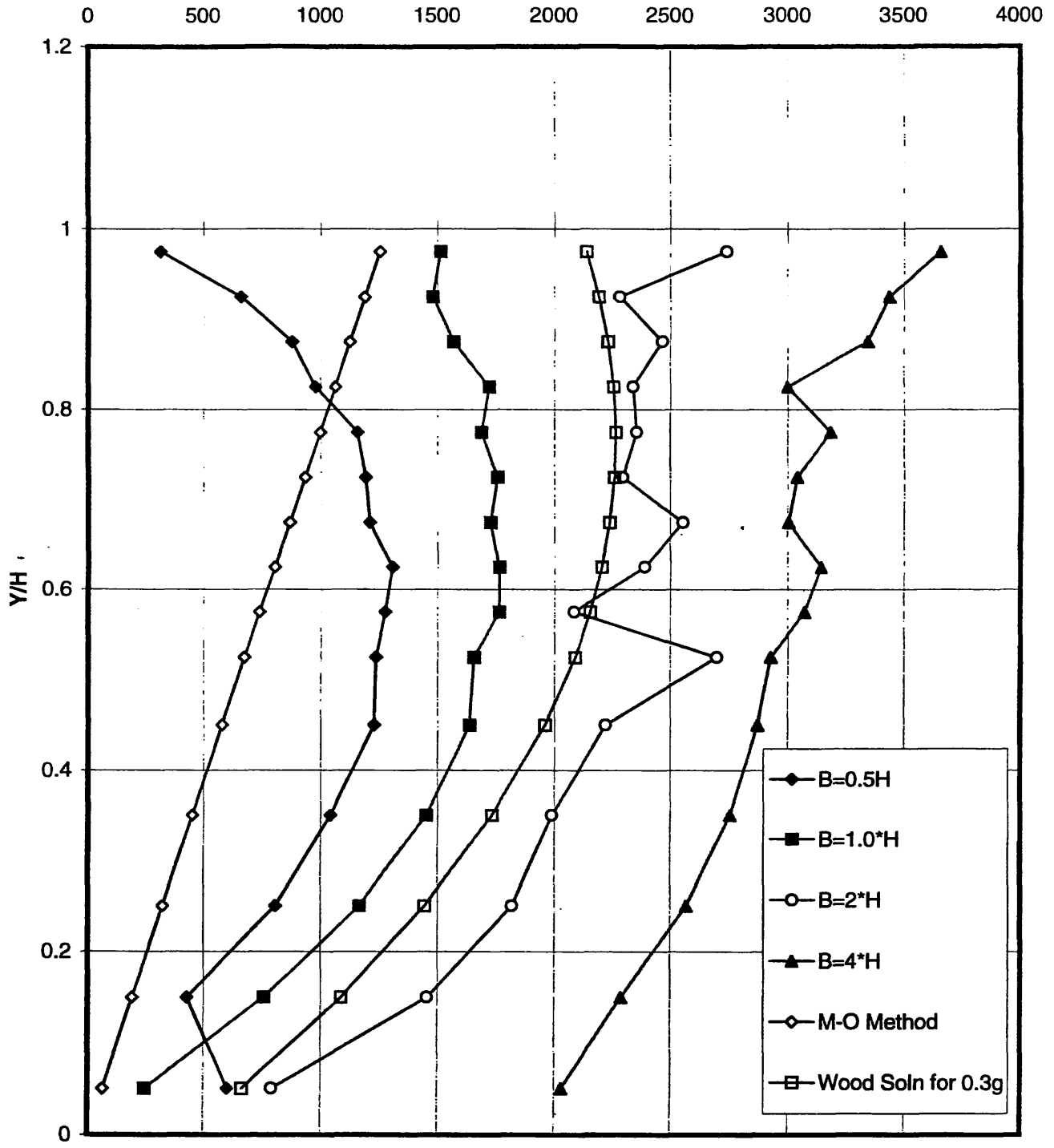

DESIGN OF PILES CONSIDERING THE DEFORMATION RESPONSE UNDER THE ACTION OF EARTHQUAKE SHAKING

By Madan B. Karkee[1], Yoshihiro Sugimura[2] and Kaoru Fujiwara[3]

ABSTRACT: There have been several instances of damage to piles at deeper part, generally near the soil layer interfaces, during the past earthquakes. Such damages are inherently difficult to detect and repair, mandating adequate provision in the design to make them as unlikely as possible. Nonlinear response analysis of soil-pile-structure system considering a two dimensional FEM model shows distinctly large ground response forces near soil layer interfaces, demonstrating the nature of stresses that may develop in piles due to distinct stiffness contrast between soil layers. While such detailed analysis is rather impractical for the general design application, current practice of designing the pile for a single concentrated load representing the inertia effect of the superstructure involves implicit disregard of the actions on piles attributable to the ground deformation response. A simple approach to account for the ground deformation response actions on piles is proposed and the potential for its use in practical design application is discussed.

INTRODUCTION

Investigations on the damage to piles during the past earthquakes provide some basic information concerning the nature of failures in piles at locations with deep soil deposit under strong ground shaking. Examples include the January 17, 1995 Hyogoken-Nambu earthquake (Karkee & Kishida 1997, Karkee et al. 1997, Matsui & Oda 1996 etc.) and the June 12, 1978 Miyagiken-oki earthquake (Sugimura 1981, 1987). Remarkably significant instance of the damage is reported to have occurred at deeper parts along the pile, particularly in relatively longer piles. Evidently, the location of pile damage at the intermediate part in longer piles also tends to coincide with changes in soil layering, giving rise to stiffness contrast interfaces.

The stresses developed in piles due to the soil-pile-structure interaction under earthquake shaking consist of the superstructure inertia effects as well as the kinematic effects of ground response. The latter effects are termed simply as 'ground response effects' in this paper. Relative magnitude of the inertial and the ground response actions depends on the ground condition as well as the level of excitation. Generally, long piles penetrating a deep layered deposit, particularly where there is a sudden change in soil stiffness, are likely to be exerted by large ground response forces. However, only the inertia effects tend to be explicitly accounted for in the seismic design practice for piles. The horizontal force to be resisted by the pile consists of the inertia of the building, and the basement if applicable (BCJ 1984), with no recognition of the ground response effects explicitly.

Results of the nonlinear response analysis on the soil-pile-building interaction system of a 35 storied reinforced concrete building based on the two-dimensional finite element model (Sugimura et al. 1997) is discussed. Considering three simple variations in soil condition, other structural details remaining the same, it is shown that the influence of soil layering on the stresses developed in piles during earthquake shaking can be very dominant. Of particular interest is the clear dependence of the building superstructure inertia itself on the nature of the soil layering system interacting with the pile. That is, for a given incident motion specified for a general region, the superstructure inertia itself depends on the different levels of excitation based on the extent of the nonlinear response (Karkee et al. 1992) depending on the local site condition. In addition, the ground deformation response for the same input earthquake motion is very dependent on the local site condition. Results of the response analysis show the need for adequate consideration of the inertia as well as the ground deformation response effects.

While the detailed finite element analysis is known to adequately depict the response of the soil-pile-structure system under earthquake excitation, computational effort can be formidable for its application to everyday design practice. Considering the current practice of utilizing a single concentrated load at the top of the pile to represent the inertial actions, there is a need to develop a simple design method that can account for the ground response effects realistically. Sugimura (1992) proposed the use of distributed load to represent the effect of ground response on piles. Presumably, the nature and the magnitude of the distributed load should reflect the local soil condition and

[1] Manager, Research Division, GEOTOP Corporation, 1-16-3 Shinkawa, 4F, Chuo-ku, Tokyo, 104-0033, Japan.
[2] Professor, Department of Architecture & Building Science, Grad. School of Engineering, Tohoku University, Sendai, Japan
[3] Sr. Managing Director, Suzuki Architectural Design Office, Yamagata, Japan

its dynamic characteristics. A simple approach for the consideration of these aspects in the estimation of the distributed load is proposed for evaluation of the ground deformation response effects to be considered in general design practice. Preliminary simulations clearly illustrate the potential of the approach to realistically represent the ground response action on piles that may be expected during earthquakes.

DAMAGE TO PILES IN PAST EARTHQUAKES

Reports on investigation of damage to foundations during past earthquakes provide ample instances of damage at the intermediate part of a pile. The location of the damage in piles may provide some indication of the dominance of either the inertia effects of the superstructure or of the kinetic effects of ground response. Generally the inertial forces may be considered to result in the failure of piles near the top, while the ground response effects may be expected to result in damages at the deeper part, particularly where there is a abrupt change in the soil stiffness.

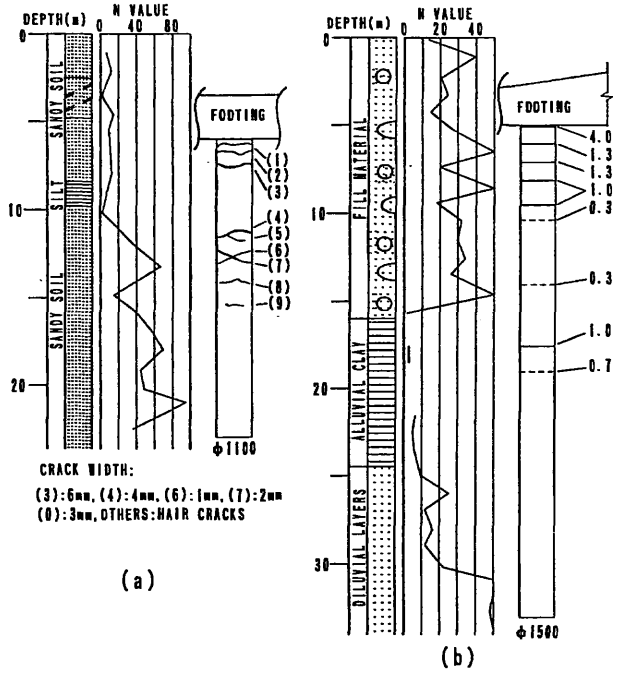

FIG. 1. Damage to piles during the Hyogoken-Nambu earthquake: (a) Building (AIJ 1996) (b) Highway (HBC 1995)

A typical case of damage to a pile supporting a building during the Hyogoken-Nambu earthquake (AIJ, 1996) is shown in relation to the ground profile in Fig. 1(a). The pile is seen to develop cracks near the top as well as at the middle part around where the soil profile changes into a stiffer layer. It seems plausible that the change from a softer to a stiffer soil layer may have contributed to the cracking at the middle part of the pile. Similarly, Fig. 1(b) shows the damage to a pile in a highway bridge (HBC, 1995). Again the pile has cracked at the middle part where the soil stiffness decreases suddenly as indicated by the N-value distribution. The cracking of the piles at deeper part noted in Fig. 1 were detected by core boring and borehole camera. Fig. 2 shows the damage to pile during the Miyagiken-oki earthquake (Sugimura & Oh-oka, 1981) in a L-shaped building where the outer corner joining the two wings had undergone a large settlement. This is a case of a pile on the inner side of one the wings. The pile foundation damage was considered to be due to inertial forces of the superstructure. However, the cracks seem to align with changes in soil layering.

Clearly, the damage to piles at deeper part is more problematic in the event of rehabilitation and recovery after the earthquake. While there are successful cases of repair of the damage to pile near the top (e.g. Karkee & Kishida 1997), damages at deeper part of the pile are by nature much more difficult to detect and repair. It is imperative that the design approach for piles at earthquake regions should particularly strive to make the damage to piles at the deeper part less likely.

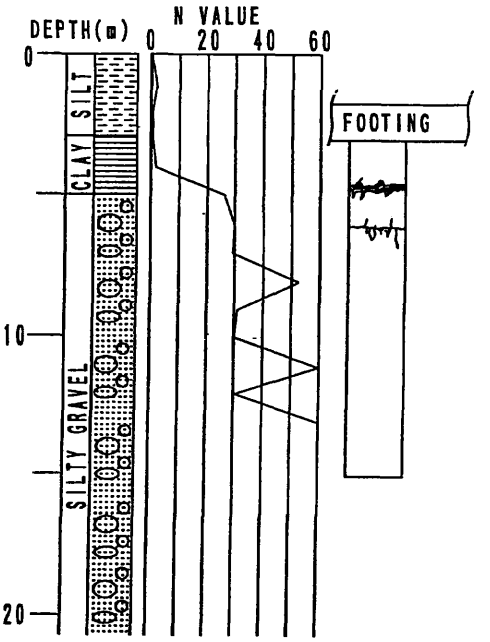

FIG. 2. Damage to pile in a building structure during the 1978 Miyagiken-oki earthquake (Sugimura & Oh-oka 1980)

Extremely large actions on piles may manifest due to failure of the ground (e.g. liquefaction) accompanied by lateral spreading (e.g. Tokimatsu et al. 1996) and detailed investigation of the local site for such possibility should be included while considering ground response effects in the seismic design of piles. Even when the complete ground failure does not occur, the excessive nonlinear response of the soft soil layer can result in large deformation response in the piles. Thus the deformation

response of piles during strong shaking can include the ground shaking effects as well as the ground failure effects.

FFINITE ELEMENT ANALYSIS FOR NONLINEAR SEISMIC RESPONSE OF THE SYSTEM

In Japan, 20 to 45 storied reinforced concrete buildings have been common for apartment building structures. The natural period of these buildings range from 1.2s to 2.5s, falling into a range in the design spectra where the spectral velocity ordinates tend to be uniform. Generally these buildings are supported on cast-in-place concrete piles with enlarged base. A 35 storied building is considered a representative of these structures and is analyzed in detail for its seismic response characteristics.

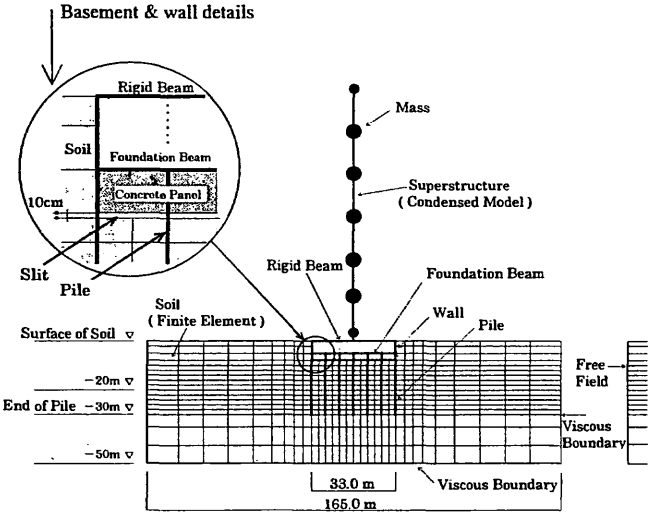

(35 stories of the building are condensed into 7 lumped masses)

FIG. 3. 2-D finite elements in combination with the lumped mass model representing the soil-pile-building system.

The schematic finite element model for nonlinear dynamic response analysis is given in Fig. 3. The basement slab in Fig. 3 is assumed to have no direct contact with the soil underneath. Three simple soil profiles shown in Fig. 4 and designated as a-soil, b-soil and c-soil overlying a sandy gravel layer, typically found in urban areas in Japan at depths of 30m or more, is considered. Three sets of response analysis are carried out for the three soil conditions, other structural details remaining the same. Details of the building structure and the method of analysis, together with the assumed nonlinear behavior of soil and concrete are as given by Sugimura et al. (1997).

Base input motion for the analysis

Two input motions are considered to investigate the effect of relative difference in the level of excitation. One is the well known El Centro NS record and the other is the Hyogoken-Nambu earthquake record of the Kobe marine observatory (Kobe JMA NS). The El Centro motion is scaled to a maximum velocity of 50cm/s while the Kobe record is used as it is. The corresponding peak accelerations are 510.8cm/s^2 and 818.0cm/s^2 respectively. The response spectra of the two input motions are given in Fig. 5, where it is seen that the spectral velocity ordinates for the Kobe record are significantly larger than those for El Centro in the period range 0.3-3.0s.

The results of the response analysis

Some of the time histories of the response forces for El Centro input are shown in Fig. 6. From the time history of the building inertia, the predominant period of the building can be noted to be about 2.9s. The corresponding period of the building was about 3.3s for Kobe JMA NS.

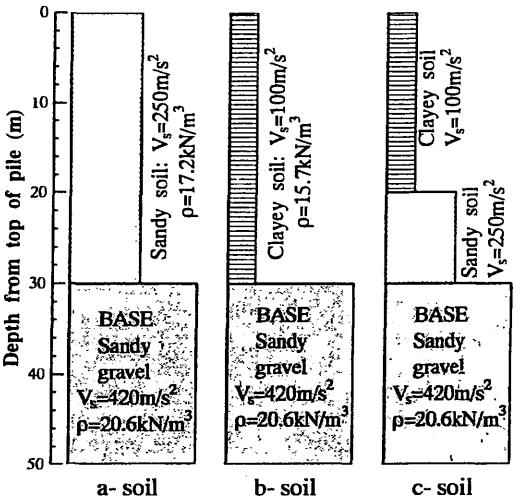

FIG. 4. Details of three soil conditions used in the analysis, the building & foundation structure remaining the same.

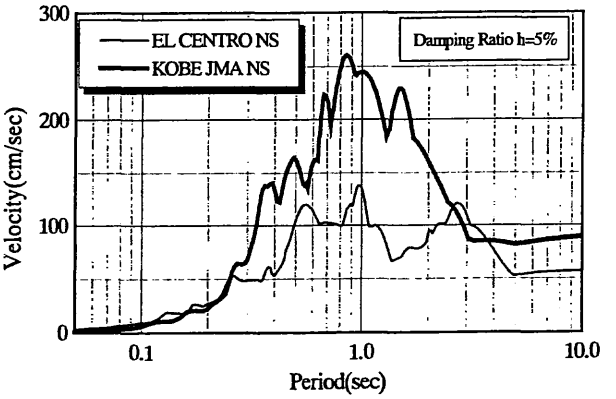

FIG. 5. Response sectra of El Centro & Kobe motions

Compared to the elastic period of 2.1s, the period of the building has elongated by a factor of 1.4 and 1.6 respectively, larger factor indicating stronger shaking in case of the Kobe input. Fig. 6 also shows that the

basement inertia is larger in stiffer soil (a-soil) compared to soft soils (b and c-soils). The time histories for pile top shear force contain long as well short period components, unlike the building inertia, where the component attributable to the predominant period of the building dominates.

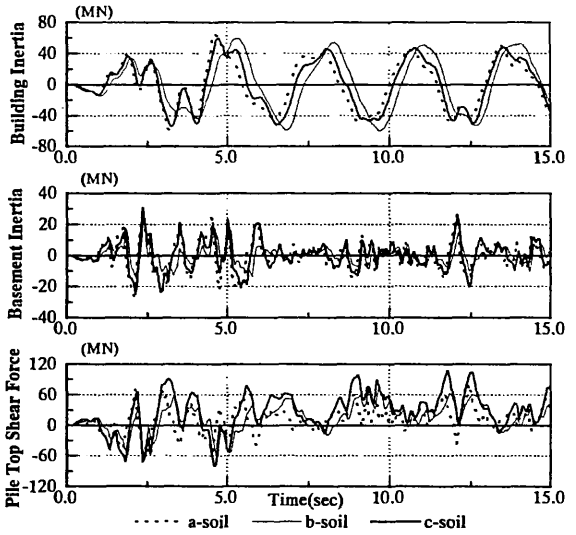

FIG. 6. Time histories of some typical response forces

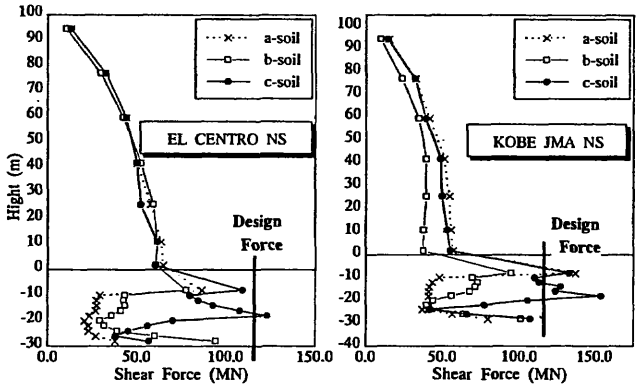

FIG. 7. Maximum shear force response of the building and the piles for the El Centro & the Kobe input motions.

Fig. 7 shows the maximum shear force response of the structure corresponding to the two incident motions. In the current design practice for the tall buildings in Japan, the piles are generally designed to have the ultimate shear capacity. The ultimate shear capacity is defined as the sum of 1.5 times the base shear capacity of the building (64.0MN) and the seismic coefficient for the basement times the weight of the basement (98.4MN). Assuming the seismic coefficient for the basement to be 0.2, the ultimate shear capacity works out to be 115.8MN. This is designated as the design force in Fig. 7.

The maximum shear force in piles is largest in case of the c-soil for both the input motions and occurs at the interface of the two soil layers. The cracking of piles at the layer interfaces observed during past earthquakes, as noted in Fig. 1, may have been caused by this tendency of large shear force around the soil stiffness contrast interfaces.

Fig. 8 shows the maximum bending moment in piles. Again a very strong influence of the soil layering is apparent from the distinctly different shape of the maximum bending moment distribution in case of the c-soil. Larger moment at the soil layer interface is seen in c-soil for both the El Centro and the Kobe input. Larger bending moment at deeper part of the pile is particularly problematic because it tends to act in combination with the decreased axial load with depth generally observed in piles. In addition to larger moment at the layer interface, it is seen in Fig. 8 that the bending moment at the pile head is also largest in case of the c-soil, for both the input motions. That is, the pile head moment as well as the moment in the intermediate part can be expected to give the worst condition when soil stiffness contrast exists over the pile length.

It may be noted that the maximum shear force, as well as the maximum bending moment, tends to large in the intermediate part of the pile when large soil stiffness contrast exists over the pile length.

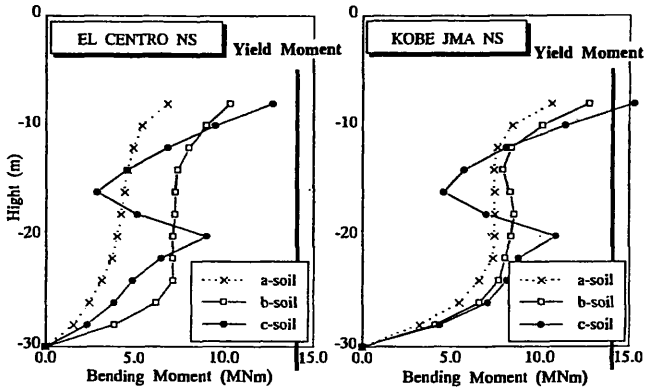

FIG. 8. Maximum bending moment distribution in piles under the action of the El Centro & the Kobe input motions

Another interesting result is that the bending moment distribution in a-soil is nearly half of that in b-soil in case of El Centro input, while the bending moment distribution for a-soil and b-soil is practically same in case of the Kobe input. This may be attributed to the much higher level of shaking in case of the Kobe input, with the increased nonlinear effect resulting in similar stiffness in a-soil and b-soil at higher level of excitation (Karkee et al. 1993, 1992). This may be considered a possibility because the soil stiffness degradation tends to saturate at

strain level attributed to the higher level of tation.

nponents of the building and the foundation -systems in the response of the total system

Attempt is made to separate (Sugimura et al. 1997) esponse of the total system into those of the building the foundation sub-systems. This is done to evaluate relative contribution of the two sub-systems to the onse of the system as a whole. The contribution of the ding superstructure and that of the soil and foundation ıe response of the total system depicted in Fig. 3 is obtained. Figs. 9 and 10 show time histories of the onse actions contributed by the building and the ıdation sub-systems respectively.

It may be noted in Fig. 9 that the building inertia and ıile top shear force tend to be in opposite phase, while . are dominated by the predominant period of the ding as noted above. Figs. 9 and 10 show that the ribution of the foundation system consists of ively short period components when compared to that of the building system. However, the contribution of both the building system and the foundation system to the pile top shear force clearly depends on the soil condition.

Fig. 11 shows distribution of the maximum shear force in a single pile. While the magnitude and the nature of distribution of maximum shear force is strongly dependent on the ground condition, the contribution of the superstructure inertia to the shear force in piles is distinctly smaller than that of the foundation system.

Thus the shear force obtained based solely on the inertia without regard to the local site condition tend to grossly underestimate the maximum shear forces that may be expected during strong ground shaking. In fact, the maximum shear force responses of the total system and that of the foundation system are seen to be practically coincident in all the three soil types in Fig. 11, particularly at deeper part, indicating domination of the foundation part. The result shows that the shear forces in piles may even be represented by the response of the foundation portion alone.

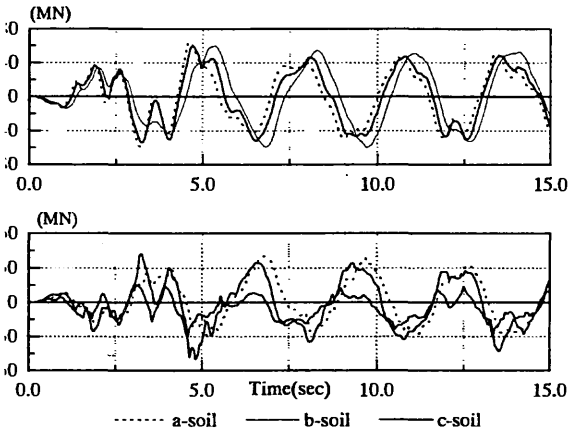

9. Response forces due to building sub-system

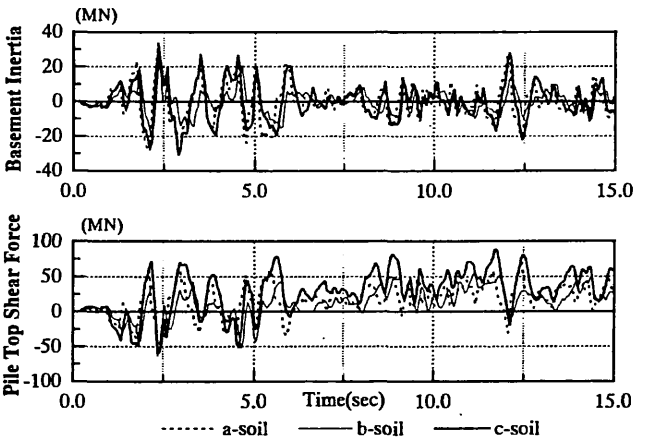

FIG. 10. Response forces due to foundation sub-system

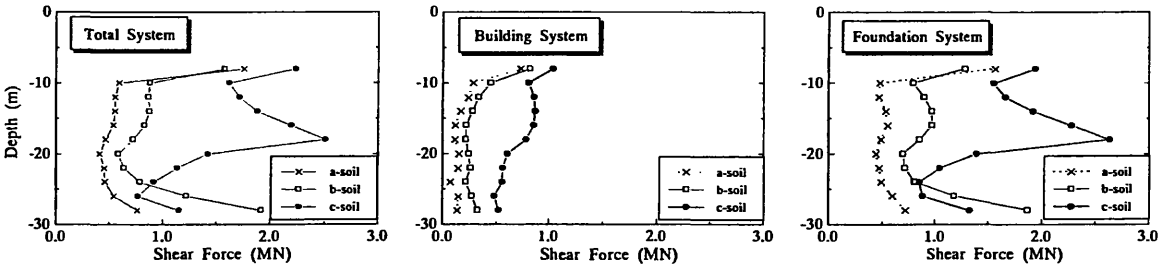

FIG.11. Maximum shear force in a pile due to the total system and the building and foundation sub-systems

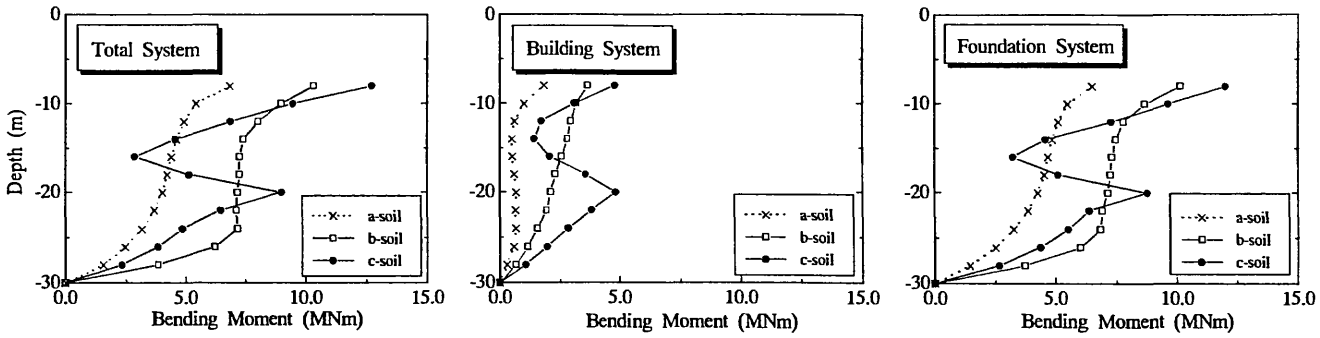

FIG. 12. Maximum bending moment in a pile due to the total system and the building and foundation sub-systems

Similar to the case of maximum shear force, Fig. 12 shows distribution of maximum bending moment in a pile. Again, the contribution of the foundation system to the maximum bending moment distribution is distinctly large and practically same as that of the total system. This follows logically from Fig. 11, because integration of shear force gives the bending moment. However, maximum bending moment does not necessarily correspond to the maximum shear force, and it is important to note strong domination of foundation system in the bending moment acting on the piles.

The results of nonlinear response analysis of the soil-pile-building system depicted in Fig. 3 clearly illustrate the inadequacy of the current practice of considering the inertia of superstructure and basement (BCJ, 1984) with implicit disregard of the soil condition in the seismic design of piles. Considering that finite element analysis discussed above is impractical for everyday design, the need to develop a suitable method to adequately account for the ground response effects is evident.

SIMPLE DESIGN APPROACH CONSIDERING GROUND RESPONSE

As mentioned above, seismic design practice in Japan allows for inertial forces to be resisted by the pile. However, the reports on damage to piles during past earthquakes, as well as the results of finite element response analysis, show strong domination of ground response effects on the internal forces developed in piles. A simple method based on the principle of beam on elastic foundation, together with an approach to evaluate the distributed load, is proposed for adequate consideration of the ground response effects in the seismic design of piles. Preliminary results indicate that the proposed approach has the potential for evaluation of the ground deformation response effects on piles.

Principle of beams on elastic foundations

Considering a Winkler soil model and assuming the pile to be a massless beam on elastic foundation, the basic equation relating the horizontal deflection y of the pile may be given by Equation 1. Here, D is the diameter, E is the Young's modulus and I is the sectional area moment of inertia of the pile. The constant k_h is the coefficient of horizontal subgrade reaction of the soil and x is the depth in soil. The soil movement $f(x)$ in Equation 1 represents the free field ground response displacement during the earthquake and equating it to zero gives the equation for the static loading case.

$$EI\frac{d^4y}{dx^4} + k_h D\{y - f(x)\} = 0 \qquad (1)$$

If $k_h Df(x)$ in Equation 1 is considered to be a force $p(x)$ at a depth x required to displace the soil there by $f(x)$, then we have:

$$EI\frac{d^4y}{dx^4} + k_h Dy = p(x) \qquad (2)$$

Equation 2 can be solved for a given distribution of load $p(x)$ along the pile length. From a practical point of view, solutions for three simple load distribution, consisting of concentrated load, uniformly distributed load and triangularly distributed load, can be appropriately combined to depict a more general distributed load approximately. These solutions are in fact already available from Hetényi (1946). This framework for the solution of a beam on elastic foundation is utilized in the proposed simple analysis method to indirectly account for the kinematic effects of ground response.

The current design method (MKS units)

Based on the Japanese design guide (Sugimura, 1988), the design external force Q_p for earthquake loading

is given in terms of the base shear Q and the number of piles n as:

$$Q_p = (1-\alpha)\frac{Q}{n}; \qquad \alpha = 1 - 0.2\frac{\sqrt{H_B}}{\sqrt[4]{H_f}} \tag{3}$$

Here, α is the participation factor of embedment given in terms of the height above ground H_B and the depth of embedment H_f, both in meters. Based on the engineering judgment derived from parametric analysis, it is recommended that the value of α should not be greater than 0.7. The design guide suggests that the internal forces and displacement can be computed based on the theory of beam on elastic foundation. For a given degree of fixity α_r at the pile head and a horizontal concentrated load Q_p acting at the top, horizontal displacement at pile head y_o is obtained from Equation 4. When not determined from horizontal loading test, it is suggested that k_h in kg/cm^3 be estimated from the Equation 6, where E_o is the elastic modulus of soil in kg/cm^2 and D is in cm.

$$y_o = \frac{Q_p}{4EI\beta^3}(2-\alpha_r) \tag{4}$$

$$\beta = \sqrt[4]{\frac{k_h D}{4EI}} \tag{5}$$

$$k_h = 0.8E_o D^{-\frac{3}{4}} \tag{6}$$

As can be noted, the design method considers only the inertia effect of the superstructure and needs to be recognized as such. While the method may be adequate to account for the inertia effects, it does not attempt to addresses the kinematic effects due to interaction between the pile and the surrounding soil that may undergo significant nonlinear response during strong ground shaking. From detailed analysis, it is noted above that the ground response effects can be very significant.

The proposed method for the evaluation of ground response effects

As is noted above in Equation 2, if the magnitude and the nature of the distributed load $p(x)$ could be determined taking into consideration the local site condition and soil nonlinearity, it may be possible to solve the problem of the beam on elastic foundation to estimate the forces acting on piles due to the kinematic effects of ground response. For this the displacement response $f(x)$ of the free field under the action of the earthquake needs to be estimated. Considering the first mode of the free field motion, the elastic fundamental period of a soil layer of thickness H and shear wave velocity V_S may be approximated by $4H/V_S$, such that the maximum displacement U_g occurring at the top of the i^{th} soil layer may be given in terms of the peak velocity of the input motion V_{max} by Equation 7.

$$U_g = V_{\max} \times \left(\frac{2H}{\pi V_S}\phi\right)_i \tag{7}$$

The parameter ϕ in Equation 7 is the 'ground period elongation factor' representing the extent of elongation in the ground period due to the nonlinear effect (Karkee et al. 1992, 1993) during strong ground shaking, such that $\phi \geqq 1$. If all the soil layers at a site are assumed to contribute equally to the ground period elongation, a constant ϕ may be assumed for all the soil layers. The introduction of the parameter ϕ constitutes an attempt to account for the effect of nonlinear soil response in a simple manner. From the dynamic analysis with the El Centro input (Sugimura et al. 1997) the, predominant ground period T_P was seen to be about twice the elastic fundamental ground period T_G. This corresponds to a value of ϕ equal to about 2.0. In comparison, the Japanese guideline (BCJ, 1992) recommends a value of 2.2 for strong shaking at bay areas with deep soil deposit. It seems reasonable to assume the overall ground period elongation factor ϕ at a deep soil site to be in the range of 2.0 to 3.0.

For a given value of the ground period elongation factor ϕ at a site, consideration of a variable value ϕ_i for different soil layers may be considered appropriate depending on the site condition. One of the way this could be done is to assume the value of ϕ_i for the i^{th} soil layer of thickness H and shear wave velocity V_S to be in proportion to the value of H/V_S such that overall ground period elongation factor ϕ remains the same. Thus, if the value of H/V_S for the i^{th} layer is defined as τ_i, then the period elongation factor ϕ_i for the layer may be given by $\theta\tau_i$, where θ is given by Equation 8.

$$\theta = \phi \times \frac{\sum_i \tau_i}{\sum_i \tau_i^2} \quad \& \quad \phi_i = \theta\tau_i \quad \textit{Where} \quad \phi_i \geq 1 \tag{8}$$

With the displacement U_g relative to the bottom of the i^{th} layer obtained from Equations 7, the ground displacement $f(z)$ relative to the bottom of the soil layer, where z varies from 0 at the top to H at the bottom of each layer, may be given by the cosine function of Equation 9. Once the displacements relative to the bottom of each layer is computed, the overall displacement $f(x)$ relative to the pile toe can be easily obtained, such that $p(x)$ is given by Equation 10.

$$f(z) = U_g \cos\left(\frac{\pi}{2H}\right)z; \quad 0 \leq z \leq H \tag{9}$$

$$p(x) = k_h D f(x); \quad 0 \leq x \leq L \tag{10}$$

One of the crucial aspect in the proposed method is the proper evaluation of the coefficient of subgrade reaction

k_h in Equation 10, because its value affects the magnitude of the distributed load $p(x)$ to a large extent once $f(x)$ is determined. In this respect, it may be noted that the elongation of the ground period by ϕ_i times noted in Equation 7 corresponds to a soil stiffness degradation by $1:\phi_i^2$. This can be adequately accounted for in estimating the value of k_h, which may be computed from the Equation 11 derived by Vesic (Poulos and Davis 1980) considering an infinite beam on elastic foundation. It may be noted that the expression for k_h by Vesic accounts for the modulus of the soil as well as that of the pile material. Evidently, the soil modulus utilized to estimate k_h should consider the extent of nonlinear response that may be expected during strong ground shaking.

$$k_h = \frac{0.65}{D}\left\{\frac{E_S}{1-\nu^2}\right\} \times \left\{\frac{E_S D^4}{EI}\right\}^{\frac{1}{12}} ; \quad \frac{E_0}{E_S} = \lambda \qquad (11)$$

In Equation 11, EI is the bending stiffness of the pile as defined earlier, ν is the Poisson's ratio of soil and λ is the 'stiffness degradation factor' indicating the extent to which the soil stiffness reduces during strong shaking resulting in the ground period elongation by ϕ_i as mentioned above. If there is a single soil layer over the pile embedment depth, the value of λ for it may be taken as equal to ϕ^2, otherwise the stiffness degradation factor λ_i for the i^{th} layer is equal to ϕ_i^2, where ϕ_i is obtained from Equation 8.

It may be noted that although the effect of soil stiffness degradation due to nonlinear response would be clearly crucial in the evaluation of the kinematic stresses in the piles due dynamic soil-pile interaction, it is also likely to be important in evaluating the inertia effects. However, the simple design method proposed here is primarily concerned with the aspects of soil response effects, and no attempt is made here to investigate the effect of soil nonlinearity on the evaluation of the inertial forces in piles.

Computation based on the proposed method

Attempt is made to compute bending moment and shear force distribution in piles for the case of c-soil by assuming the value of ϕ to be 2.0 corresponding to the El Centro input case mentioned above. As noted in Figs. 11 and 12, the ground response forces are most significant in c-soil, which consists of a clayey soil layer underlain by a stiffer sandy soil layer as shown in Fig. 4.

Fig. 13 shows the shear wave velocity profile together with the soil displacement estimated by Equation 9. Fig. 13 shows the soil displacement distribution for the constant ϕ case as well as for the variable ϕ based on Equation 8. The ground displacement depicts the shear wave velocity profile logically, giving much larger displacement of softer layer compared to the stiffer layer, with even better contrast in case of variable ϕ. The ground displacement near the pile top is about 100mm.

The coefficient of subgrade reaction k_h for the ground response effect is obtained from Equation 11 by assuming the Poisson's ratio ν of the soil to be 0.45. Resulting distribution of k_h for constant ϕ is shown in Fig. 14(a). Assumption of a variable ϕ based on Equation 8 results in a k_h distribution of Fig. 14(b). The distributed load $p(x)$ obtained from Equation 10 corresponding to the two cases of constant and variable ϕ are shown in Fig. 14(c). The cosine distribution of the load is approximated by uniformly varying loads at discrete intervals in Fig. 14(c).

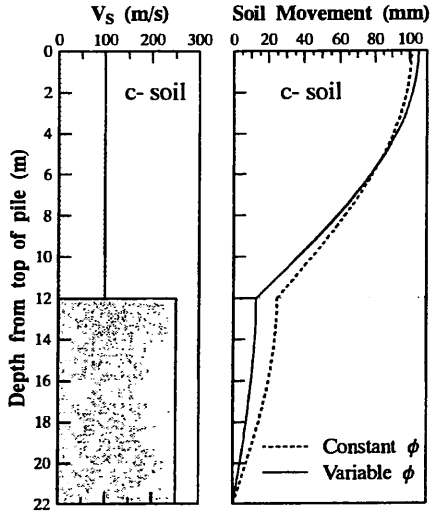

FIG. 13. Shear wave velocity profile for c-soil and the ground displacement for constant & variable values of ϕ

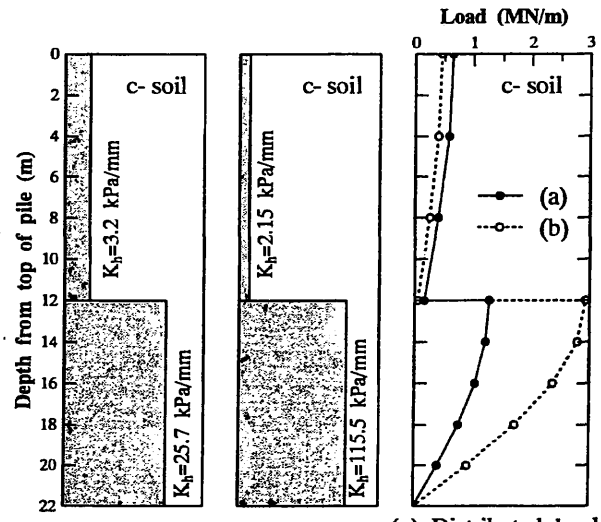

FIG. 14. Distribution of subgrade reaction for constant and variable ϕ and the corresponding distributed loads on piles

The distributed lateral load on the pile shown in Fig. 14(c) may not act all at once throughout the duration of ground shaking, specially in case of multiple soil layers. This may be understood from different possible modes of ground movement. This was previously confirmed (Sugimura et al. 1997) by the elastic eigenvalue analysis of the three systems corresponding to the three soil conditions of Fig. 4. It was found that the second mode of c-soil showed the worst of the three soil type cases, indicated by large bending moment and shear force around the two soil layers. To indirectly account for such effects in the simple design method proposed here, it would be logical to consider different combinations of distributed load over different sections of the pile length.

Fig. 15 shows three possible distributed load combinations assuming a constant value of ϕ, and in consideration to the two distinct soil layers. The shear force and bending moment diagrams for the three distributed load cases of Fig. 15 and the k_h distribution of Fig. 14(a) are given in Fig. 16.

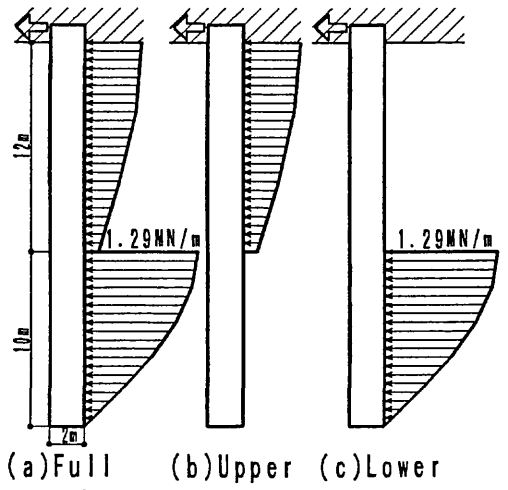

FIG. 15. Three possible distributed load cases in the c-soil consisting of two distinct soil layers over the pile length

The shear force and bending moment diagrams for the three distributed load cases representing the ground response effects is obtained by assuming the pile top to be restrained against rotation with the pile tip free. It is seen in Fig. 16 that there is a large shear force near the interface of the two soil layers similar to that seen in Fig. 11, and that the bending moment too is large around there.

It may not be logical to make a point to point quantitative comparison of the shear force and the bending moment diagrams in Fig. 16 with those for c-soil in Figs. 11 and 12, which are actually the envelop of maximum forces rather than the actual distribution. In addition, Figs. 11 and 12 also include the inertia of the basement. When this fact is recognized, the maximum shear force of about 2.5MN and the maximum bending moment of about 5.5MNm around the middle part of the pile in Fig. 16 are qualitatively comparable to those of 2.5MN and 8.0MN-m in Figs. 11 and 12 respectively. This indicates that the simple solution proposed here is capable of accounting for the ground response effects in piles that may be expected during ground shaking.

The bending moment near pile top in Fig. 16 is of the order of about 20.0MNm compared to about 13.0MNm for c-soil in Fig. 12. In contrast, the maximum bending moment of 5.5MNm at the middle part in Fig. 16 is smaller than that of about 8.0MNm in Fig. 12. This difference is most likely because of the assumption of full restraint of pile top against rotation, which is unlikely to be the case due to nonlinear response of the concrete piles during strong earthquake shaking. In fact, the yield moment of the pile is about 14.0MNm as indicated in Fig. 8. Beyond yield level the pile top would tend to rotate, resulting in only a partial restraint against rotation. When this condition is accounted for in the analysis by assuming a certain degree of restraint against rotation rather than the full restraint, the maximum bending moment obtained from the detailed nonlinear analysis can be closely approximated by the proposed simple method. For example, assuming the degree of restraint to be 0.7 in Fig. 15 would logically amounts to limiting the moment at pile top to the yield level. Under this condition, the bending moment at the middle part of the pile in Fig. 16 would be closer to about 8.0MNm obtained from the detailed nonlinear response analysis.

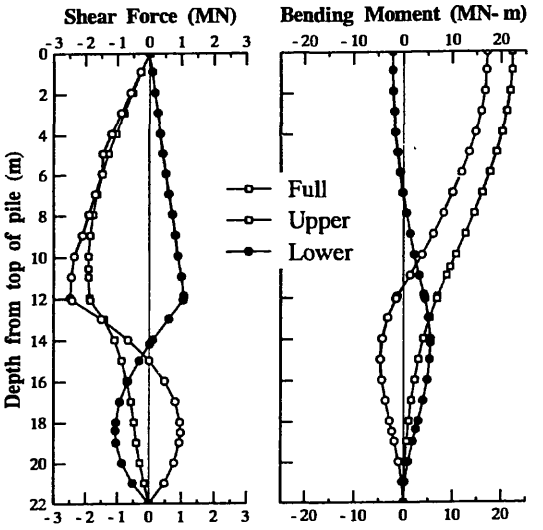

FIG. 16. Shear force and bending moment diagrams in a pile considering the three distributed load cases in Fig. 15

Investigations based on large number of simulations would be required for further refinement of the proposed method for actual application. However, the values of the coefficient of subgrade reaction k_h and the ground

displacement near pile top, applicable for realistic estimation of the ground response effects based on the proposed simple method, tend to be significantly different from those recommended in the current design practice. Evident the values of k_h recommended in Japanese code for the seismic design based on the inertial forces can not be adopted for the evaluation of ground response forces the simple method proposed here. From this standpoint, it seems logical to evaluate the inertial forces and the ground response forces separately, assuming different values of subgrade reaction k_h as applicable, and then design the pile for the envelop distribution of the largest of the two response forces along the pile length.

CONCLUSIONS

Reports on the investigation of the damage to foundations during past earthquakes show ample instances of the failure of piles that can be directly or indirectly attributed to the deformation response of the ground. Nonlinear response analysis based on the combination of a finite element and lumped mass model indicates large response forces at the soil layer interfaces. The result demonstrates the importance of ground response effects in the seismic design of piles, while also illustrating the inadequacy of the present design practice that directly accounts for the superstructure inertia effects alone.

When the response of the total soil-pile-building system is decomposed into those of the building system and the foundation system, the contribution of the foundation part is by far dominant, and comparable to that of the total system. In addition, the contribution of the building system itself is strongly dependent on the soil condition. The results clearly demonstrate the influence of the local site condition on the inertial actions as well as on the ground deformation response effects on piles.

While demonstrating the importance of considering the ground deformation response in the design of piles, the finite element response analysis also illustrates the different levels of earthquake excitation to which the building superstructure might be subjected depending on the soil condition of the site.

The proposed simple approach, based on the beam on elastic foundation framework, is seen to be promising in capturing the essence of the ground response effects on piles. The results indicate that it may be possible to evaluate the nonlinear response of a soil-pile-building system by such simple method provided the necessary parameters are selected to reflect the dynamic characteristics of the ground adequately. The essential parameters in the proposed method include peak velocity, ground period elongation factor, soil stiffness degradation factor and degree of restraint at the pile head. In addition, the dynamic characteristic of ground such as the elastic shear wave velocity, Poisson's ratio, thickness of soil layers etc are utilized.

To indirectly account for the different modes of ground movement in the proposed simple method, it is logical to consider different combinations of distributed load depending on the number of distinct soil layers over the pile length. Worst combination of the distributed load over different sections of the pile may be considered in evaluating the ground response effects.

The ground period elongation factor for a given site depends on the local site condition as well as the level of earthquake excitation. For extreme level of excitation at sites with deep soil deposit, where the ground deformation response effect is likely to dominate, may be assumed to be in the range 2.0 to 3.0. The soil stiffness degradation may be obtained from the ground period elongation factor.

The coefficient of subgrade reaction obtained based on the proposed method seems to work out to be much smaller than that recommended in the Japanese code for seismic design of piles, which directly accounts for the inertial forces alone. Further investigation is necessary for confirmation, but considering that the effects of the ground deformation response is directly related to the extent of nonlinear response of the ground, it may be logical to consider smaller value of subgrade reaction in evaluating the ground deformation response effects. This means evaluation of the inertia and the ground deformation response effects on pile by considering different values of subgrade reaction as appropriate. It may even be possible for the coefficient of subgrade reaction to assign a value of zero to depict a liquefied layer that is not expected to provide any horizontal support to the piles.

The degree of restraint of the pile head against rotation may be a major consideration in the evaluation of the bending moment distribution in piles due to ground deformation response effects. If the moment at the pile head exceeds the yield level, partial restraint at the pile top may be logically assumed to limit the moment there to the yield level. Conversely, if the moment at a section exceeds the yield moment capacity, the moment may be redistributed to limit the moment to yield level. are relevant aspects for research and investigation.

APPENDIX I. RERERENCES

AIJ (Architectural Institute of Japan). (1996). "Report on the survey of building foundation damage due to the Hyogoken-Nambu earthquake." *AIJ Kinki branch foundation group, July 1996.* (in Japanese)

BCJ (Building Center of Japan). (1992). "Guideline for evaluation of design earthquake ground motion for building design." *Published by BCJ* (in Japanese).

BCJ (Building Center of Japan). (1984). "Guideline on Seismic design of building foundation and exemplary design practice." *Published by BCJ* (in Japanese).

HBC (Highway Bridges Committee). (1995). "Survey report on damages to highway bridges during the Hyogoken-Nambu earthquake." *Committee for earthquake disaster prevention in highway bridges*, December 1995. (in Japanese)

Hetényi, M. (1946). "Beams on elastic foundation." *The university of Michigan press*, Ann Arbor.

Karkee, M. B. & Kishida, H. (1997). "Investigations on a new building with pile foundation damaged by the Hyogoken-Nambu (Kobe) earthquake." *The structural design of tall buildings, Vol. 6: 311-332*, John Wiley & Sons, Ltd.

Karkee, M. B., Nagai, K., Ogura, H. & Kishida, K. (1997). "Common behavior of building foundations during the Hyogoken-Nambu earthquake." International exchange committee, Kansai branch of JGS (ed.), *KIG forum on geotechnical engineering in recovery from urban earthquake disaster; Proc. int. symposium, Kobe, Japan, January 9-10, 1977*: 209-218.

Karkee, M. B., Sugimura, Y., Tobita, J. & Sato, K. (1993). "Potential effects of long period components in incident motion on the nonlinear ground response." *Architectural institute of Japan (AIJ); Journal of struct. constr. engng, No.449*: 69-82.

Karkee, M. B., Sugimura, Y. & Tobita, J. (1992). "Scaling a suite of ground motions for compatible levels of nonlinear ground response." *AIJ Journal of struct. constr. engng, No.440*: 29-42.

Matsui, T. & Oda, K. (1996). "Foundation damage of structures." *Soils and foundations; Special issue on geotechnical aspects of the January 17, 1995 Hyogoken-Nambu earthquake*: 189-200.

Poulos, H. G. & Davis, E. H. (1980). "Pile foundation analysis and Design." *John Wiley & Sons*, Singapore.

Sugimura, Y., Fujiwara, K., Ohgi, T. & Karkee, M. B. (1997). "Seismic behavior of piles supporting tall buildings and the consideration of ground response effects in design." *Tall buildings in seismic regions; Proc. 4th conf., Los Angeles, California, May 9-10, 1977*: 303-317.

Sugimura, Y. (1992). "A proposal on analysis of horizontal resistance of pile based on load distribution method." *Japanese society of soil mechanics and foundation engineering; Proc. 27th national conf., Kochi, June 2-4, 1992*: 1637-1640. (in Japanese)

Sugimura, Y. (1988). "Japan's foundation design guide." *Building research and practice, the journal of CIB, the int. council of building research studies and documentation*, Vol.16, No.2: 109-121.

Sugimura, Y. (1987). "Earthquake damage of pile foundation in Japan." *International society of soil mechanics and foundation engineering; Proc. 8th Asian regional conf.*, Vol.2: 245-246.

Sugimura, Y. (1981). "Earthquake damage and design method of piles." *International society of soil mechanics and foundation engineering,; Proc. 10th int. conf., Stockholm.* Vol. 2: 865-868.

Sugimura, Y. & Oh-oka, H. (1981). "Report on the damage of precast prestressed concrete piles during the 1978 off-Miyagi Prefecture earthquake." *Building research institute, ministry of construction.* (in Japanese)

Tokimatsu, K., Mizuno, H. & Kakurai, M. (1996). "Building damage associated with geotechnical problems." *Soils and foundations; special issue on geotechnical aspects of the January 17, 1995 Hyogoken-Nambu earthquake*: 219-234.

APPENDIX II. DISTRIBUTED LOAD METHOD

Based on the formulations on the beams on elastic foundations by Hetényi (1946), Sugimura (1992) has proposed the use of distributed load method for the analysis of the horizontal resistance of piles. The solutions for a pile of semi-infinite length with the top end fixed are given in the tabular form. Tables II-1, II-2 and II-3 correspond to the solutions for concentrated, uniformly distributed and triangularly distributed load cases. The solutions for the three loading cases can be readily combined to cover any general loading pattern assuming the superposition principle.

The three tables can be utilized for the computation of displacement y, rotation θ, bending moment M and shear force Q, at any point along the length of the pile, by multiplying the coefficient value χ by the multiplier μ. The explanations for the values of the multiplier given in Table II-1 are applicable to all the three Tables.

It may be noted that the relations given in Tables II-1, II-2 and II-3 are applicable for a pile of semi-infinite length with the top end fixed. Similar simple formulations can be developed for a pile of finite length and for different boundary conditions generally encountered in practice.

Table II-1: Concentrated load

Concentrated Load	Coefficient Values	Multiplier μ		Explanations
	χ	$x_c < x_a$	$x_c \geq x_a$	
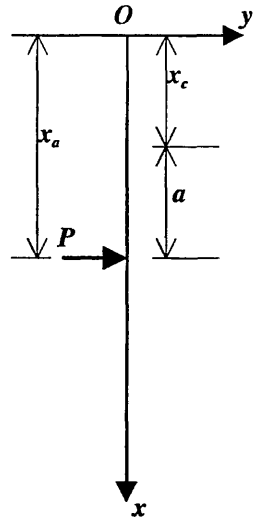 k_h : Coefficient of subgrade reaction	$y_c = \frac{P}{8EI\beta^3}$	B_{3a}	B_{3a}	$\beta = \sqrt[4]{\frac{k_h D}{4EI}}$ $a = \lvert x_c - x_a \rvert$ $b = \lvert x_c - x_b \rvert$ $B_{1a} = e^{-\beta a}\cos(\beta a)$ $B_{1b} = e^{-\beta b}\cos(\beta b)$ $B_{2a} = e^{-\beta a}\sin(\beta a)$ $B_{2b} = e^{-\beta b}\sin(\beta b)$ $B_{3a} = e^{-\beta a}\{\cos(\beta a) + \sin(\beta a)\}$ $B_{3b} = e^{-\beta b}\{\cos(\beta b) + \sin(\beta b)\}$ $B_{4a} = e^{-\beta a}\{\cos(\beta a) - \sin(\beta a)\}$ $B_{4b} = e^{-\beta b}\{\cos(\beta b) - \sin(\beta b)\}$
	$\theta_c = \frac{P}{4EI\beta^2}$	B_{2a}	$-B_{2a}$	
	$M_c = \frac{P}{4\beta}$	B_{4a}	B_{4a}	
	$Q_c = \frac{P}{2}$	B_{1a}	$-B_{1a}$	

Table II-2 : Uniformly distributed load

Uniform Load	Coefficient Values	Multiplier μ		
	χ	$x_c < x_a$	$x_a \leq x_c \leq x_b$	$x_c > x_b$
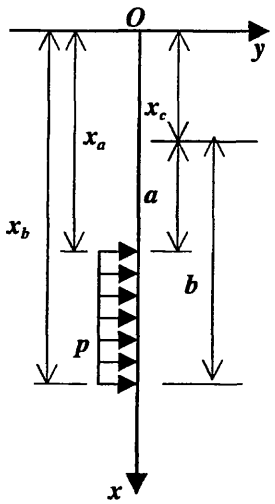	$y_c = \frac{p}{8EI\beta^4}$	$B_{1a} - B_{1b}$	$2 - B_{1a} - B_{1b}$	$B_{1b} - B_{1a}$
	$\theta_c = \frac{p}{8EI\beta^3}$	$B_{3a} - B_{3b}$	$B_{3a} - B_{3b}$	$B_{3a} - B_{3b}$
	$M_c = \frac{p}{4\beta^2}$	$B_{2b} - B_{2a}$	$B_{2a} + B_{2b}$	$B_{2a} - B_{2b}$
	$Q_c = \frac{p}{4\beta}$	$B_{4a} - B_{4b}$	$B_{4a} - B_{4b}$	$B_{4a} - B_{4b}$

Table II-3 : Triangularly distributed load

Triangular Load	Coefficient Values χ	Multiplier μ		
		$x_c < x_a$	$x_a \le x_c \le x_b$	$x_c > x_b$
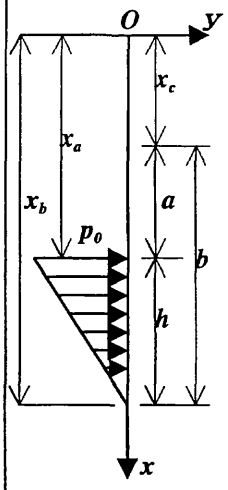	$y_c = \frac{p_0}{16EI\beta^5 h}$	$B_{4b} - B_{4a} + 2\beta h B_{1a}$	$B_{4b} - B_{4a} - 2\beta h B_{1a} + 4\beta b$	$B_{4b} - B_{4a} - 2\beta h B_{1a}$
	$\theta_c = \frac{p_0}{8EI\beta^4 h}$	$B_{1b} - B_{1a} + \beta h B_{3a}$	$B_{1a} + B_{1b} + \beta h B_{3a} - 2$	$B_{1a} - B_{1b} + \beta h B_{3a}$
	$M_c = \frac{p_0}{8\beta^3 h}$	$B_{3a} - B_{3b} - 2\beta h B_{2a}$	$B_{3a} - B_{3b} + 2\beta h B_{2a}$	$B_{3a} - B_{3b} + 2\beta h B_{2a}$
	$Q_c = \frac{p_0}{4\beta^2 h}$	$B_{2a} - B_{2b} + \beta h B_{4a}$	$-B_{2a} - B_{2b} + \beta h B_{4a}$	$B_{2b} - B_{2a} + \beta h B_{4a}$

RESPONSE TO HORIZONTAL GROUND SHAKING OF CANTILEVER RETAINING WALLS

A. S. Veletsos[1] and A. H. Younan[2]

[1] Department of Civil Engineering, Rice University, Houston, Texas, USA
[2] EQE International, Inc., Houston, Texas, USA

ABSTRACT

A broad overview is presented of the response to horizontal ground shaking of vertical, flexible cantilever walls retaining a uniform, linear viscoelastic stratum of constant thickness and semi-infinite extent in the horizontal direction. The response quantities examined include the magnitude and distribution of the dynamic wall pressures and displacements, and the maximum values of the total dynamic wall force or base shear and of the overturning base moment. Special attention is given to the effects of very long-period, effectively static excitations. The effects of an earthquake ground motion are then expressed as the products of the corresponding static effects and appropriate amplification or deamplification factors. It is shown that the flexibility of the wall may affect significantly the results, and that the maximum dynamic effects for flexible walls may be significantly smaller than those for non-deformable, rigid walls.

INTRODUCTION

Despite the multitude of studies that have been carried out over the years, the dynamic response of retaining walls is far from being well understood. There is, in particular, a lack of fundamental information on the effects of some of the major parameters that influence the dynamic response of such systems.

Previous studies of the problem may be classified into two groups: (1) elastic analyses in which the backfill is presumed to respond as a linearly elastic or viscoelastic material; and (2) limit-state analyses, such as the venerable Mononobe-Okabe approach (Mononobe and Matuo 1929, Okabe 1924), in which the wall is considered to displace sufficiently at the base to mobilize the full shearing capacity of the backfill. Detailed summaries of these contributions have been presented by Nazarian and Hadjian (1979), Prakash (1981), Whitman (1991), and Veletsos and Younan (1995).

The most comprehensive previous study of the elastic response of the system is the one presented by Wood (1973), in which the wall was considered to be rigid. In the present study, the assumption of linear response for the retained material is preserved, but the wall is considered to be flexible. The objective is to assess the effects of this flexibility on the magnitude and distribution of the wall pressures and displacements, and on the maximum values of the total wall force or base shear and of the overturning moment induced by horizontal ground shaking. The

material presented is essentially a summary of some of the more important information reported in a series of recent contributions by the authors (1994, 1995, 1997).

SYSTEM CONSIDERED

Shown in Figure 1, the system examined consists of a fixed-based, vertical cantilever wall retaining a semi-infinite stratum of uniform viscoelastic material. The wall is considered to be of uniform thickness and finite rigidity, and the retained material is considered to be free at its upper surface and bonded to a non-deformable, rigid base. The bases of the wall and stratum are presumed to experience a space-invariant horizontal motion, the acceleration of which at any time t is $\ddot{x}_g(t)$ and its maximum value is $\ddot{X}_g$. Material damping for both the medium and the wall is considered to be of the constant hysteretic type.

The properties of the soil stratum are defined by its mass density ρ, shear modulus of elasticity G, Poisson's ratio ν, and material damping factor δ, which is considered to be the same for both shearing and axial deformations. The factor δ is the same as the $\tan\delta$ factor used in some previous studies of foundation dynamics and soil-structure interaction and twice as large as the damping factor β expressed in terms of the critical coefficient of damping. The properties of the wall are defined by its thickness t_w, mass per unit of surface area μ_w, Young's modulus of elasticity E_w, Poisson's ratio ν_w, and damping factor δ_w which, like δ, is twice as large as the corresponding factor expressed in terms of the critical damping value.

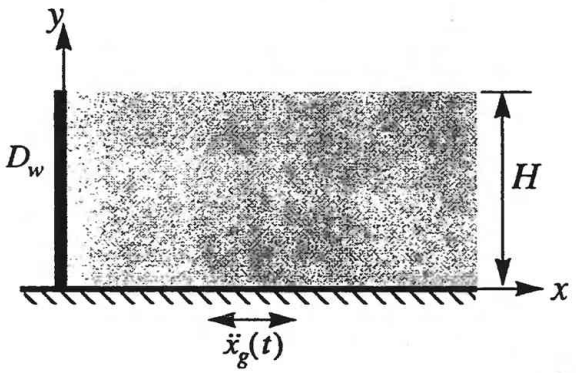

Figure 1: System considered

METHOD OF ANALYSIS

The method of analysis used has been described in Veletsos and Younan (1997) and Younan, Veletsos and Bandyopadhyay (1997), and it is summarized only briefly here.

Fundamental to the method is the assumption that, under the horizontal excitation considered, no vertical normal stresses develop anywhere in the medium, i.e. $\sigma_y = 0$. It is further assumed that the horizontal variations of the vertical displacements for the medium are negligible, so that the horizontal shearing stresses τ_{xy} can be expressed as $\tau_{xy} = G^*(\partial u/\partial y)$, where u is the horizontal displacement of an arbitrary point of the medium relative to the moving base, $G^* = G(1 + i\delta)$ is

the complex-valued shear modulus, and $i = \sqrt{-1}$. The reliability of these assumptions has been confirmed by Veletsos and Younan (1994) by comparing the solutions for rigid walls with those obtained by Wood's 'exact' solution (1973).

The steps involved in the analysis are as follows:

- First, the horizontal displacements of the medium relative to the moving base are expressed as linear combinations of the natural modes of vibration of the stratum when it is considered to act as an unconstrained, vertical cantilever shear-beam. Similarly, the relative displacements of the wall are expressed as linear combinations of its natural modes, i.e. those of a clamped-free beam. These expressions satisfy the conditions of zero displacement at the rigid base, and of zero stresses and forces at the top boundary.
- Next, the differential equation governing the motion of the medium in the horizontal direction is solved subject to the condition of compatible displacements at the interface of the medium and wall. For the purpose of satisfying this boundary condition, each natural mode of vibration of the beam is expanded in terms of the corresponding modes of the retained medium. The result of this step are medium displacements and wall pressures that are functions of the as yet undetermined wall displacements.
- Finally, the wall displacements are evaluated by satisfying the dynamic equilibrium of the forces acting on the beam using Lagrange's equations of motion.

The analysis is first implemented for harmonic excitations. The responses to arbitrary transient ground motions are then evaluated by Fourier transform techniques.

PRESENTATION OF RESULTS

Consideration is first given to the responses obtained for excitations the dominant frequencies of which are small compared to the fundamental natural frequency of the soil-wall system. This is tantamount to neglecting the dynamic amplification effects of the retained medium. Such excitations and the resulting effects will be referred to as '*static*', a term that *should not be confused* with that normally used to represent the effects of gravity forces. A maximum dynamic effect for an arbitrary excitation is then expressed as the product of the corresponding static effect and an appropriate amplification or deamplification factor.

Static Effects

In Figure 2, the total force or base shear per unit of wall length induced by the maximum static values of the lateral inertia forces, P_{st}, is plotted as a function of the dimensionless measure of the wall flexibility

$$d_w = \frac{GH^3}{D_w} \tag{1}$$

in which D_w represents the flexural rigidity per unit of wall length and is given by

$$D_w = \frac{E_w t_w^3}{12(1-\nu_w^2)} \tag{2}$$

The results are normalized with respect to $\rho \ddot{X}_g H^2$. Also shown is the distance h from the base to the line of action of the resultant of the wall force, normalized with respect to the wall height H. Referred to as the effective height, h represents the distance by which P_{st} must be multiplied to yield the static value of the overturning moment per unit of wall length. The wall in these solutions, and all others that follow, is considered to be massless, and Poisson's ratio for the retained medium is taken as $\nu = 1/3$.

It is observed that the flexibility of the wall affects significantly both the magnitude of the wall force and the line of action of its resultant. Increasing the wall flexibility reduces the horizontal extensional stiffness of the retained material relative to its shearing stiffness, and this reduction, in turn, increases the proportion of the inertia forces transmitted by horizontal shearing action to the base, and decreases the proportion transmitted to the wall. Since the effective height also decreases with increasing wall flexibility, the reduction for the overturning base moment is generally much greater than for the corresponding shear. The reductions are substantial even for rather small values of d_w. For example, P_{st} is reduced from $0.941\rho \ddot{X}_g H^2$ for a rigid wall to $0.561\rho \ddot{X}_g H^2$ for a system with $d_w = 10$. The corresponding reduction in effective height is from $0.6H$ to $0.375H$, and that for base moment is from $0.565\rho \ddot{X}_g H^3$ to $0.210\rho \ddot{X}_g H^3$.

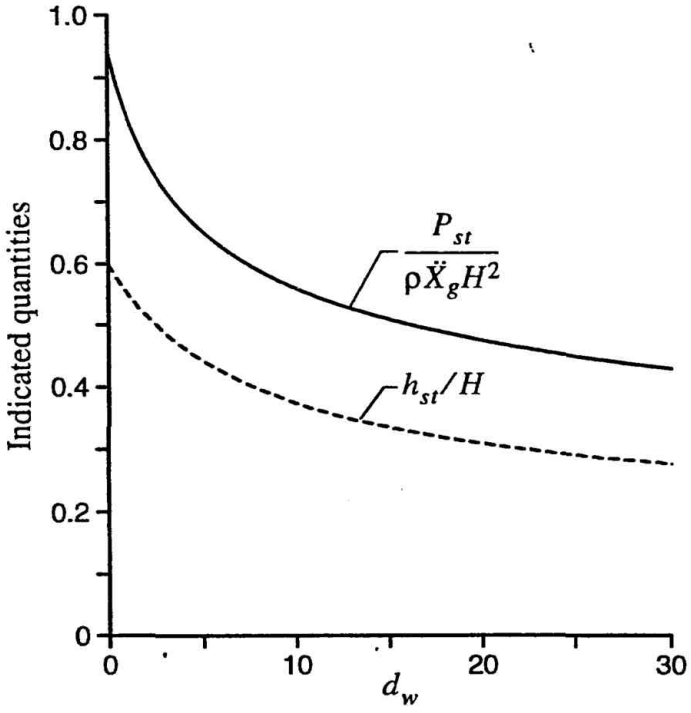

Figure 2: Normalized values of base shear and effective heights in wall of statically excited systems with different wall flexibilities; $\nu = 1/3$, $\mu_w = 0$

The effects of wall flexibility on the magnitude and distribution of the wall pressures, $p_{st}(\eta)$, is shown in Figure 3 in which $\eta = y/H$. For rigid walls ($d_w = 0$), the pressures increase almost as a quarter-sine from zero at the base to a maximum at the top, whereas for the flexible walls, there is a sharp change in the intensity of the pressure near the top, with the pressure decreasing and changing signs.

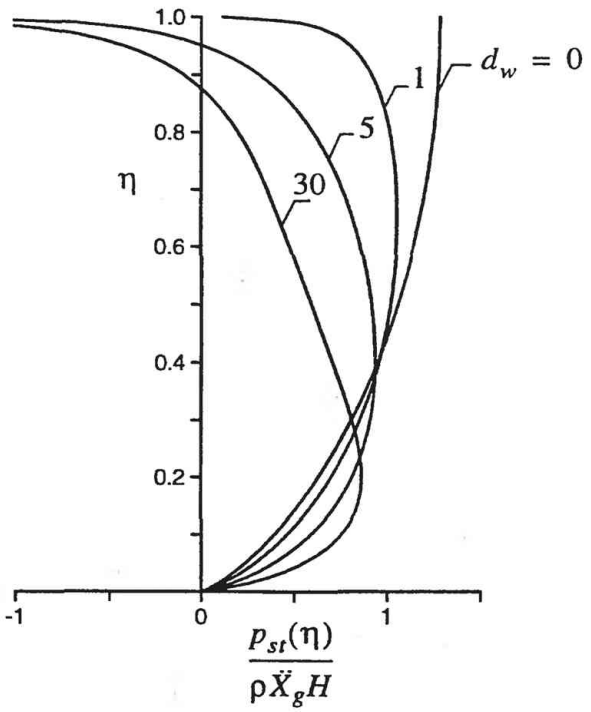

Figure 3: Distributions of wall pressures for statically excited systems; $\nu = 1/3$, $\mu_w = 0$

The maximum value of the wall displacement, which naturally occurs at the top, may be expressed either in terms of the wall properties as

$$(w_{st})_{max} = c_1 \frac{P_{st} H^3}{D_w} \tag{3}$$

or, more conveniently, in terms of the properties of the retained medium as

$$(w_{st})_{max} = c_2 \frac{\rho \ddot{X}_g H^2}{G} = c_2 \frac{\ddot{X}_g H^2}{v_s^2} \tag{4}$$

where $v_s = \sqrt{G/\rho}$ = the shear-wave velocity for the medium, and c_1 and c_2 are dimensionless factors that are functions of the wall flexibility factor d_w and are interrelated by

$$c_2 = c_1 \frac{P_{st} d_w}{\rho \ddot{X}_g H^2} \tag{5}$$

The dependence of these two coefficients on d_w is shown in Figure 4.

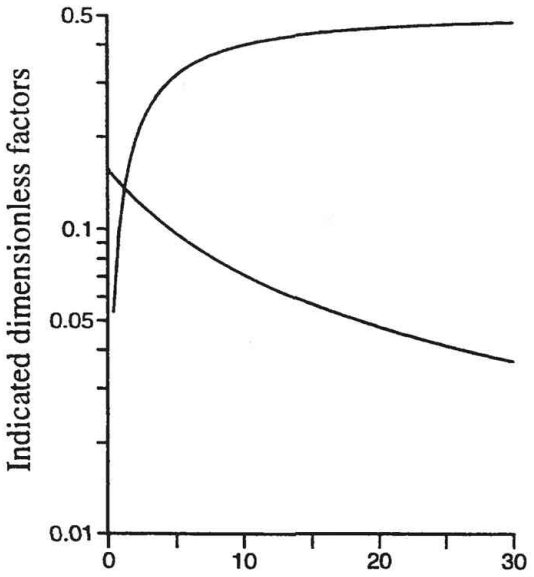

Figure 4: Coefficients c_1 and c_2 in expressions of maximum displacements relative to base for statically excited systems with different wall flexibilities; $\nu = 1/3$, $\mu_w = 0$

The deflection configurations of the wall of systems with different values of the relative flexibility factor d_w are shown in Figure 5. The results are normalized to a unit value at the top. It is observed that, within the range of d_w values examined, the results are quite similar. As $d_w \rightarrow 0$, the configuration naturally tends to that obtained for the pressures exerted on a non-deflecting, rigid wall.

As a measure of values of maximum wall displacements that may be encountered in practice, consider a concrete wall of height $H = 4.6$ m (15 ft) and thickness $t_w = 0.46$ m (1.5 ft) retaining a medium with shear-wave velocity $v_s = 122$ m/sec (400 ft/sec) and unit weight $\gamma = \rho g = 1.6$ t/m^3 (100 pcf), where g is the gravitational acceleration. With $E_w = 20684$ MPa (3000 ksi) and $\nu_w = 0.17$, the displacement factor c_2 in Equation (4) becomes 0.427; and for a peak ground acceleration $\ddot{X}_g = 0.3g$, the static value of the maximum wall displacement becomes 0.039 percent of the wall height. Even with a dynamic amplification factor of 2.0, which, based on information presented in the following sections, represents a reasonable maximum for intense earthquake ground motions, the resulting maximum dynamic displacement is below the 0.1 to 0.4 percent range widely accepted as representing the displacement values required to induce a limit state in the backfill material (Clough and Duncan, 1990). This information is offered as a confirmation of the applicability of the elastic solutions for the systems examined here.

Dynamic Effects

As already noted, the maximum dynamic effects for an arbitrary transient excitation may conveniently be expressed as the product of the corresponding static effects and appropriate

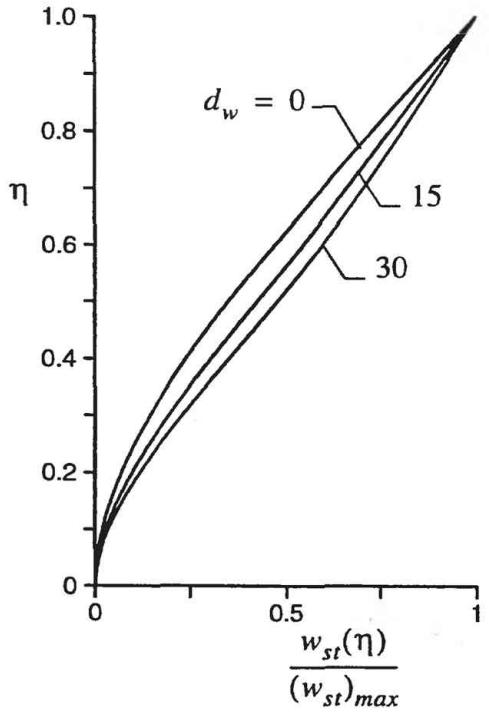

Figure 5: Distributions of wall displacements relative to base for statically excited systems with different wall flexibilities; $\nu = 1/3$, $\mu_w = 0$

amplification or deamplification factors, *AF*. Figure 6(a) shows the values of this factor for the total force or base shear per unit of wall length for systems subjected to the first 6.3 sec of the N-S component of the ground motion recorded during the 1940 El Centro, California earthquake. The peak acceleration of this motion is $\ddot{X}_g = 0.312\,g$. Four values of the wall flexibility factor d_w are considered, with the results plotted as a function of T_1, the fundamental natural period of the stratum when it is considered to respond as an unconstrained, cantilever shear-beam. This period is given by $T_1 = 4H/v_s$. The wall in these solutions is presumed to be massless, the material damping factors for the wall and retained medium are taken as $\delta_w = 0.04$ and $\delta = 0.10$ (i.e., 2 percent and 5 percent of critical damping, respectively), and Poisson's ratio for the medium is taken as $\nu = 1/3$.

The plots in Figure 6(a) are similar to, but by no means the same as, the non-dimensionalized response spectra for similarly excited, viscously damped single-degree-of-freedom systems. Specifically, for low-natural-period, stiff media, the $AF = 1$, indicating that the peak value of the dynamic base shear is equal to its corresponding static value. With increasing medium flexibility or T_1, the amplification factors increase, and after attaining nearly horizontal plateaus, they reach values that may be substantially lower than unity. Within the practically important period range of $T_1 = 0.1$ to 0.5 sec, for which the amplification factors are nearly constant, these factors are relatively small, particularly for the stiffer walls with the lower values of d_w. The average amplification factor within this range varies from 1.33 for a rigid wall to 1.68 for a wall with $d_w = 5$ and 1.82 for a wall with $d_w = 15$. These relatively low values are due to the capacity of the medium to dissipate energy by radiation of waves to the far field. The greater the wall stiffness relative to that of the retained medium, or the smaller the d_w, the greater is the capacity of the

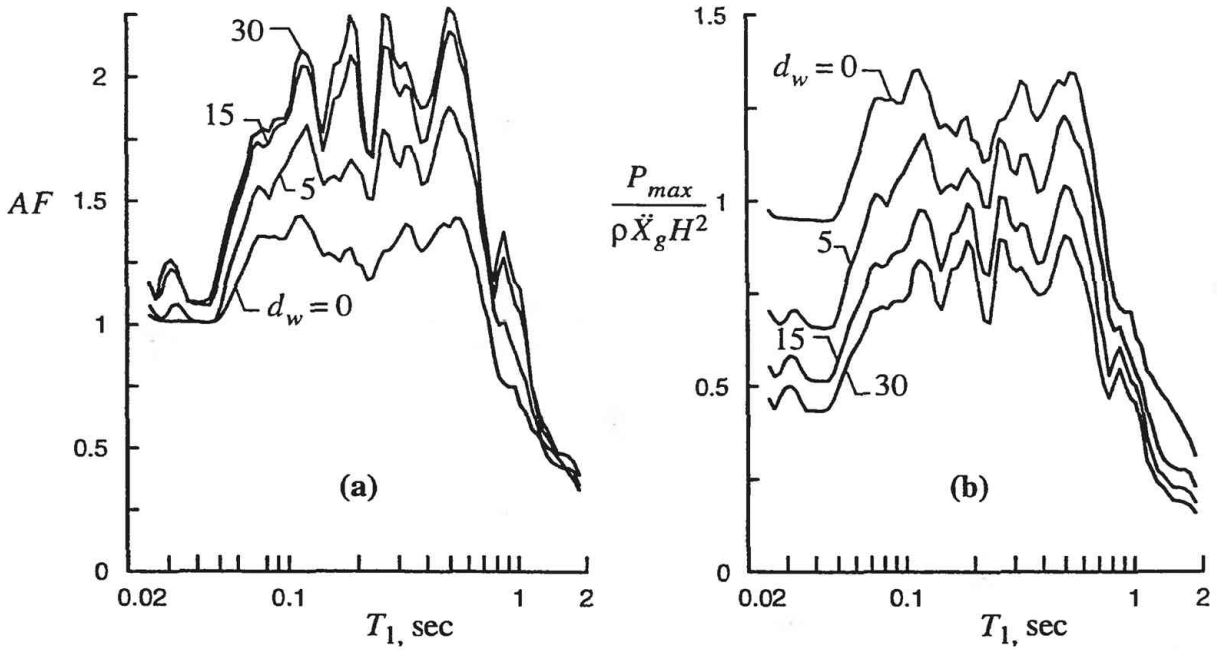

Figure 6: (a) Amplification factors for maximum wall force or base shear per unit of wall length for systems with different wall flexibilities subjected to El Centro earthquake record, and (b) Normalized values of this force; $\mu_w = 0$, $\delta_w = 0.04$, $\nu = 1/3$ and $\delta = 0.1$

wall to reflect the waves impinging on it and to dissipate them by radiation to the far field.

Further insight into the magnitude of the maximum dynamic force or base shear per unit of wall length, P_{max}, may be gained from Figure 6(b), in which this quantity is replotted normalized with respect to the common factor $\rho \ddot{X}_g H^2$. As before, four values of d_w are considered, with the results plotted as a function of the natural period of the retained medium, T_1. It is observed that increasing d_w reduces the dynamic wall force over the full range of T_1, the reductions being largest for the low and medium values of T_1.

Figure 7 shows the normalized values of the effective height h for the seismically excited systems examined. It is observed that this height, which represents the distance by which the maximum dynamic wall force or base shear must be multiplied to yield the corresponding base moment, is insensitive to variations in T_1. Accordingly, it may, for all practical purposes, be considered to have the values displayed in Figure 2 for statically excited systems. It further follows that the dynamic amplification factor for base moment may be taken equal to that for the wall force or base shear. These simple relations are consequences of the fact that the response of the system is basically dominated by its fundamental mode of vibration.

Effect of Wall Mass

For the systems examined so far, the wall was presumed to be massless. The effect of the wall mass is twofold: (1) it modifies (generally decreases) the wall pressures induced by the retained medium; and (2) it induces additional forces on the wall. The net effect is generally an increase in

the magnitude of the wall forces.

A precise evaluation of these effects is beyond the scope of this contribution. However, a reasonable approximation to the additional base shear may be obtained from the expression $m_e \ddot{X}_g(AF)$, where m_e = the effective wall mass, $\ddot{X}_g$ = is the maximum ground acceleration, and AF = the appropriate amplification factor for the massless wall. The effective mass m_e may be considered to decrease from the total wall mass for a non-deforming, rigid wall to 70 percent of the total mass for a wall with $d_w = 10$, and to 60 percent of the total mass for a wall with $d_w = 30$. In the computation of the corresponding base moment, the effective height h may be taken equal to that determined for the massless wall.

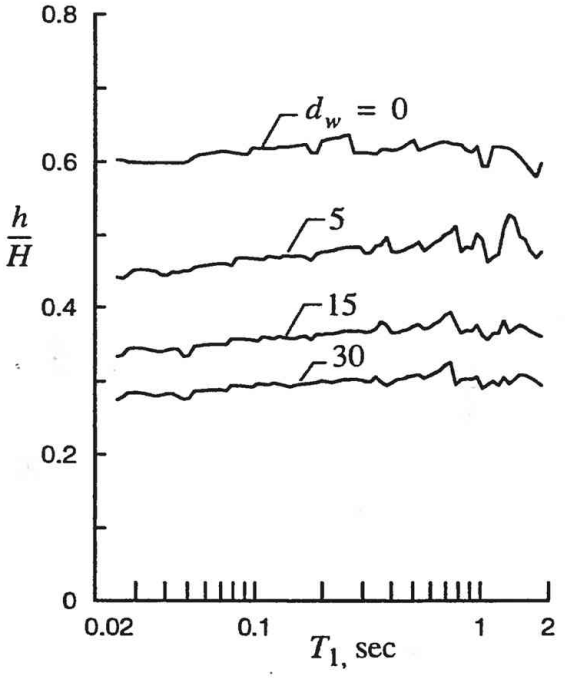

Figure 7: Normalized values of effective height for systems with different wall flexibilities subjected to El Centro earthquake record; $\mu_w = 0$, $\delta_w = 0.04$, $\nu = 1/3$ and $\delta = 0.1$

CONCLUSIONS

The magnitudes and distributions of the wall displacements, wall pressures and associated forces induced by horizontal ground shaking in the systems examined are quite sensitive to the flexibility of the wall. Increasing this flexibility reduces the horizontal extensional stiffness of the retained medium relative to its shearing stiffness, and this reduction, in turn, decreases the proportion of the soil inertia forces that gets transferred to the wall and, hence, the forces developed in it.

For realistic wall flexibilities , the total wall force or base shear may be of the order of one-half or less of that obtained for non-deformable, rigid walls, the reduction in base moment being even larger. The reduced effects may well be in reasonable agreement with those obtained by the

Mononobe-Okabe method. This agreement, however, does by no means constitute a validation of the latter method, which represents an approximate, limit-state analysis for the problem.

Even for the 1940 El Centro, California earthquake ground motion record, the maximum wall displacement relative to the moving base for realistic wall flexibilities is found to be less than the values of 0.1 to 0.4 percent of the wall height normally accepted as the minimum required to develop a limit state in the retained material.

ACKNOWLEDGMENT

This study was carried out under Projects 558223 and 568821 from Brookhaven National Laboratory, Upton, New York. This support is acknowledged gratefully.

REFERENCES

Clough, G. W. and Duncan, J. M. (1990). Earth pressures, *Foundation Engineering Handbook*, Ed. by H. Y. Fang, Chapman & Hall, NY, USA, 223-235.

Mononobe, N. and Matuo, H., On the determination of earth pressures during earthquakes. *Proc. world engrg. congress*, Tokyo, Japan, 1929, ***9***, Paper No. 388.

Nazarian, H. N., and Hadjian, A. H., Earthquake-induced lateral soil pressures on structures. *J. of the Geotech. Engrg. Div ASCE*, 1979, **105**(9), 1049-1066.

Okabe, S., General theory of earth pressure and seismic stability of retaining wall and dam. *J. Japan soc. civil engrs.*,1924, **12.**

Prakash, S., Analysis of rigid retaining walls during earthquakes, *Proc. Int. Conf. on Recent Adv. in Geotech. Earthquake Engrg. and Soil Dyn.*, University of Missouri, Rolla, MO, USA, 1981, **III**, 1-28.

Veletsos, A. S. and Younan, A. H., Dynamic modeling and response of soil-wall systems. *J. of geotech. engrg. ASCE*, 1994, **120**(12), 2155-2179.

Veletsos, A. S., and Younan, A. H., Dynamic soil pressures on vertical walls. *Proc. Third Int. Conf. on Recent Adv. in Geotech. Earthquake Engrg. and Soil Dyn.*, University of Missouri, Rolla, MO, USA, 1995, **III**, 1589-1604.

Veletsos, A. S. and Younan, A. H., Dynamic response of cantilever retaining walls. *J. of geotech. engrg. ASCE,* 1997, **123**(2), 161-172.

Whitman, R. V., Seismic design of earth retaining structures. *Proc. 2nd Int. Conf. on Recent Adv. in Geotech. Earthquake Engrg. and Soil Dyn.*, University of Missouri, Rolla, MO, USA, 1991, **II**, 1767-1777.

Wood, J. H. (1973). *Earthquake-induced soil pressures on structures*, Report EERL 73-05, Earthquake Engineering Research Laboratory, California Institute of Technology, Palo Alto, CA, USA.

Younan, A. H., Veletsos, A. S. and Bandyopadhyay, K. (1997). Dynamic response of flexible retaining walls, *Report BNL-52519*, Brookhaven National Laboratory, Upton, NY, USA.

Dynamic Behavior of Pile Foundations in Liquefaction Process - Shaking Table and Oscillator Tests Utilizing Big Shear Box -

by

Hatsukazu MIZUNO[1], Michio SUGIMOTO[2], Masanori IIBA[1], Toshihiro MORI[3] and Tsutomu HIRADE[1]

ABSTRACT : The paper presents shaking table tests and oscillator tests utilizing big shear box to clarify pile foundation behavior in liquefaction process. It is, in principle, impossible for liquefaction process to satisfy similitude ratios in reduced models of prototype water-saturated sands in centrifugally accelerated field. Therefore, we carried out shaking table tests in near-to fullscale models of water-saturated sands and piles to break through the above-mentioned bottle neck. The effect of ground water table depth on liquefaction and pile behavior is examined. And the effect of an excess pore water pressure dissipation method, that is adopted as a countermeasure against liquefaction, is also evaluated. In a case of low ground water table, the liquefaction is not so severe and bending moments of piles is reduced extremely.

INTRODUCTION

The research was conducted under a series of a activity related to a project of the Construction Technology, Research and Development(Ministry of Construction) entitled "Development of technology for earthquake disaster prevention in large metropolitan areas" in collaboration with researches and engineers of universities and private companies. Purposes of the subcommittee in the project are to clarify seismic actions to building foundations or substructures under nonlinear ground vibration and during liquefaction, and to develop the seismic design method of the building foundations or substructures through incorporating dynamic soil-structure interaction based on real phenomena. On the way, in 1995, the Hyogoken-nanbu earthquake occurred and many reports about pile damages were shown.

Contents of the subcommittee are a proposal of design model of buildings incorporating dynamic soil-structure interaction and shaking table tests of pile foundations utilizing a big shear box. The contents of the former are as follows;

1)a proposal of evaluation method on internal stresses of pile foundations based on an expanded sway and rocking model in the linear region of soil properties.

2)a proposal of evaluation method on internal stresses of pile foundations based on the Penzien model (lumped mass model) in the linear and nonlinear region of soil properties(including detailed discussion of evaluation of several constants in the model).

3)the comparison of the results between by the expanded SR model and by the Penzien method.

4)Verification through the comparison with the results of more rigorous analyses and shaking table tests on soil grounds.

The paper presents the results and discussions on the shaking table tests of the pile foundations utilizing the big shear box of about 6m, 11.6m and 3.1m in height, length and width, respectively. It is, in principle, impossible for liquefaction process to satisfy similitude ratios in reduced models of prototype water-saturated sands in centrifugally accelerated field. A main reasons for using the big shear box is to carry out the experiment in near-to fullscale models of water-saturated sands and piles.(Ref. 1) The shaking table which was used in the experiment is large shaking table(maximum weight is 500 tonf) of Disaster Prevention Research Institute of Scientific Technology Agency.

DYNAMIC PROPERTIES OF SOIL

The shaking table test on dynamic properties of the non-

1)Building Research Institute, Ministry of Construction
2)Construction Technology Institute, Takenaka-Koumuten, Inc.
3)Construction Technology Institute, Kumagai-Gumi, Inc.

liquefied ground whose soil surface is dry(in this case the height of the ground is 3.48m). The soil is called Kasumigaura sands whose physical properties are shown in Table 1. A uniformity coefficient is about 3. Figure 1 presents strain dependency of equivalent shear stiffness and equivalent damping factor base on the dynamic triaxial test(a confining pressure : 0.5kgf/cm2).

In order to investigate a change of fundamental dynamic properties of the soil ground, which is caused by soil settlement due to repeated excitation, the test of random noise excitations with maximum acceleration of 60 gal was carried out. Figure 2 presents dynamic properties(the Fourier spectrum ratio of ground surface to bottom and 1st mode shape) of the non-liquefied ground. In case of sands with dry surface, a distribution of shear stiffness of soil deposits with depth is similar to that assumed to be proportional to a square root of overburden pressure of soil. When the shear stiffness is constant with depth, the vibration mode shape is the function of cosine. Also when the shear stiffness is proportional to depth, the soil deposit has the vibration mode shape which much changes near the surface.

SHAKING TABLE TEST OF PILE FOUNDATION IN LIQUEFIED SOIL UTILIZING BIG SHEAR BOX

3.1 Experimental Series and Purpose of Experiment

The dimensions of soil deposit in the big shear box used in the experiment are about 6m, 11.6m and 3.1m in height, length and width, respectively. A model of pile foundation is made of steel and is 40cm, 10cm and 5.82m in width, thickness and length, respectively.

Table 2 shows the experimental series and purposes of each experiment. In case ①, ② and ③, the purposes are to clarify the behaviors of pile foundation during liquefaction, influences of production methods of soil deposit on the behaviors and to confirm the reproduction of dynamic behaviors by boiling production method. In case ④, that is to investigate the effect of a countermeasure against liquefaction by dissipation method of excess pore water pressure using vertical drains. In case ⑤, that is to confirm the effect of level of ground water on liquefaction process(low ground water level is an idea of the countermeasures against liquefaction).

In each case, in addition to earthquake excitation and random wave excitation with white noise, a static test, that is, horizontal force to a pile head, and an oscillator test, that is, dynamic excitation with a constant frequency to the pile head during dissipating stage of water pressure were conducted. An earthquake wave form using in the experiment is a north and south component record at 32m in depth observed in Port Island in Kobe city in 1995. The maximum acceleration of input excitation was adjusted to be 500 gals.

Production(reproduction) methods of soil deposits are a drop of sands into water(Case ①), and a boiling from bottom of soil deposit by high water pressure(Case② - ⑤). Table 3 shows heights and relative densities of produced soil deposits.

Figure 3 represents measurement points in the experiment. In this figure, a ground water level of each experimental series and a position of drains for the countermeasure against liquefaction by dissipation in case ④ are also drawn. In the ground (measured lines G-1 to G-5), accelerometers and excess pore water transducers were installed. In the piles (P-1), accelerometers, excess pore water transducers and earth pressure transducers(on the both sides perpendicular to vibration direction) were set. Also strain gauges were attached on pile surfaces (P-1 and P-2) to measure bending moments and shear forces. In the foundation and the shear box, accelerometers and displacement transducers were installed.

3.2 Dynamic Properties and Vibration Mode of Soil Ground

Dynamic properties of soil ground under random wave excitation (max. acceleration 30 gals), are drawn in Fig. 4. Predominant frequencies of soil ground are about 5.3 – 5.6 Hz and 6.85 Hz in Case① - ④, and Case ⑤, respectively.

The vibration mode at the predominant frequency in Case ① is shown in Fig. 5. In the figure, the vibration modes corresponding to the soil grounds with constant shear stiffness through depth and with stiffness proportional to overburden pressures are also drawn. The distribution of shear stiffness of produced soil ground is similar to that in the proportional stiffness to overburden pressures. The distribution in saturated soil ground is different from that in soil ground consisted of dry sand as shown in Fig. 2. Under the small vibration(acceleration),

the pore water seems to contribute the stiffness of the ground. Through the contribution of pore water to stiffness, the excess pore water will increase under the large vibration and the effective stress will decreases.

3.3 Liquefaction Phenomena Under Earthquake Excitation

(1) Comparison by Production Method of Soil Deposit

Time histories of main measuring points in Cases ① and ② are illustrated in Fig. 6. The maximum response distribution of accelerations, excess pore water pressures and pile bending moments are drawn in Fig. 7. The production method in Case ① and Cases ② and ③ are the drop of sands into water and the boiling from bottom of soil deposit by high water pressure, respectively. The difference of the process of excess pore water pressures between in Case ① and in Case ② is little except that it takes more time to increase the excess pore water pressure in depth less than 2m from the soil bottom in Case ② than in case ①. The excess pore water pressure and its process, the acceleration of foundation and the bending moment of piles have almost the same responses in Cases ② and ③ except little difference of soil ground density. From results that the distribution of maximum excess pore water pressure and, maximum acceleration of foundation and the bending moment of piles through depth in Cases ① to ③, it is clarify that the liquefied soil deposits are reproduced by the boiling.

(2) Effect of Countermeasure Against Liquefaction

The time histories of responses and the distribution of maximum responses in Cases ③ and ⑤ are shown in Figs. 8 and 9, respectively. The ground water levels are the ground surface and 1.4m in depth from the surface in Cases ③ and ⑤, respectively. In Case ③, all of the soil deposit is saturated. On the other hand, the soil deposit in depth less than 1.4m is not saturated and the soil deposit in depth more than 1.4m is saturated, in Case ⑤. The amount of increase of excess pore water pressures in saturated soil ground of case ③ is larger than that in soil ground with non-saturated soil layer of Case ⑤. In Case ⑤, there is little increase of excess pore water pressures in non-saturated soil layers. The maximum acceleration of soil deposit is larger in Case ⑤ than that in Case ③. On the contrary, The maximum bending moment of piles is less. As the decrease of the effective stress, that is, the decrease of the shear stiffness is less in the soil deposit with non-saturated soil layer, the displacement responses of soil deposit is less. The displacement of the shear box in Case ⑤ is about one fourth of that in Case ③. The amount of pole bending moments is corresponding to the difference of the displacement of shear box.

From a result of comparison of responses between in Cases ③ and ④, the excess pore water pressure and its build-up process, the acceleration of foundation and the bending moment of piles have the similar responses. It shows that the effect of reducing increase of excess pore water pressure by vertical drains is not remarkable under the earthquake level in the experiment. However, in the dissipation process of the excess pore water pressures after the excitation, the dissipation rate is 4 times by vertical drains, as shown in Fig. 10.

(3) Behavior of Piles

The distribution of bending moment of piles and excess pore water pressures at several stages of excess pore water pressure level are drawn in Fig. 11. During the increase process of excess pore water pressures, the distribution that the amount of bending moments is large in the depth near ground surface(shallow depth) can be seen. There are enough subgrade reactions to piles in deeper soil layers. After the increase of excess pore water pressures in all of the layers, the bending moment distribution of piles is linearly changed and the reduction of subgrade reactions due to liquefaction is verified.

OSCILLATOR TEST OF PILE FOUNDATION

In order to investigate relationships between the subgrade reaction of the soil and the excess pore water pressure, an oscillator(an eccentric moment is 100kg.cm) was installed on the footing of the pile foundation. After the earthquake excitation, the oscillator test was conducted in several stages of dissipated process of the soil deposit. A excited way of the oscillator is a sweep excitation with increase or decrease of frequency between 3 and 16 Hz in time period of 50 seconds. Following results are those under the frequency increase excitation in the dissipated process of Case ②.

(1)Responses of Footing and Pile

The time history of excess pore water pressure in the dissipated process after the earthquake excitation are

shown in Fig. 12. The broken lines means a time period when the excess pore water pressures were not measured just after the earthquake excitation and during final stage of dissipation. The excess pore water pressure is zero before the earthquake excitation. Symbols T1 to T6 means several stages in dissipating process. Though the increase of excess pore water pressure occurs during the oscillation test, the influence on the whole dissipation process seems to be little. The distributions of excess pore water pressures at the several stages are drawn in Fig. 13. In the figure, the distribution of the maximum excess pore water pressures during earthquake excitation is plotted. The dissipation of excess pore water pressures starts in the deeper layer and the dissipated layers move to shallow layers gradually with time.

Resonant curves of the foundation displacement at the stages T1 to T6 are illustrated in Fig. 14. With the dissipation, the resonant frequencies are high and the amplitudes at the resonant frequencies is low. When the dissipation goes to a certain extent, the resonance of the soil deposit(about 5 Hz) appears again by getting the shear stiffness of the soil. The distribution of the pile bending moments at the resonant frequencies of each stage is shown in Fig. 15. The maximum of pile bending moments occurs at the pile head in every case. The second maximum points of bending moments are 2.5 to 4 m from ground bottom and are more shallow with dissipation.

(2)Subgrade Reaction During Dissipation

The subgrade reactions and coefficients of subgrade reaction to piles are estimated from the data of bending moments of piles.

The distribution of earth pressures to the pile at the resonant frequencies of each stage is presented in Fig. 16. The earth pressure transducers were installed at the both sides in the excitation direction. The earth pressures are obtained from values of outer and inner transducers(difference between two). The depth at the maximum earth pressures moves at shallow depth with the dissipation. The change of depth at the maximum bending moments and the maximum earth pressures in the ground means the reappearance of soil stiffness with dissipation.

The distribution of bending moments is approximately expressed by a polynomial equation. The subgrade reactions do not act to the piles in the depth where the settlement of ground surface occurs during dissipation. The subgrade reactions are obtained to be differentiated twice with respect to a time t. The displacements are obtained to be integrated twice with respect to a time. Boundary condition of the displacement at the pile tip is zero and that at pie head is equal to the displacement of the footing measured in the experiment. The coefficient of the subgrade reaction is a division of the subgrade reaction by the displacement and the pile width.

The distributions of the pile displacements and the subgrade reactions obtained from the pile bending moments are shown in Fig. 17. In the figure, the distribution of displacement obtained from the measured acceleration and the distribution of subgrade reaction obtained from the measured earth pressures. The approximate polynomial equations are compatible to the distribution of measured data except a little difference of values. The coefficients of the subgrade reactions is drawn in Fig. 18. The coefficient of subgrade reactions with nearly zero displacement is omitted in the graph. In early dissipation stage, the coefficients are large in the relatively deep layers. With reproducing shear modulus of soil, the depth at the maximum of the coefficients is gradually shallow.

CONCLUSIONS

The results of the shaking table tests of the pile foundation during liquefaction and the oscillator tests of that during dissipation are summarized as follows.

1) It is clarify that the liquefied soil deposits are reproduced by the boiling except little difference of soil ground density.
2) The effect of low ground water level on preventing from liquefaction is remarkable.
3) The effect of the vertical drains(the countermeasure method against liquefaction) is not remarkable in the increasing process of excess pore water pressure during liquefaction. But the vertical drains are effective on dissipating the excess pore water pressure after excitation.
4) The subrgade reaction is reproduced with dissipation. The deeper layers are early reproduced.
5) The shear stiffness is reproduced with dissipation and the resonant frequency of the soil ground appears.

AKNOWLEDGEMENT

The research was conducted in a subcommittee under the project entitled "Development of Technology for Earthquake Disaster Prevention in Large Metropolitan Areas" in collaboration among Building Research Institute, Housing & Urban Development Corporation and Building Construction Society(The subcommittee of design for earthquake resistance of building foundations, chairman is Dr. Yutaka Matsushima, Professor of Tsukuba University) The experiment was carried out a working group under the subcommittee (chairman is Dr. Michio Iguchi, Professor of Science University of Tokyo). The authors express our thanks members of the subcommittee and the working group for their sincere advice to conduct the experiment.

REFERENCES

1)Building Research Institute : reports of a subcommittee of the design for earthquake resistance (building part) in the Development of Technology for Earthquake Disaster Prevention in Large Metropolitan Areas, annual reports of 1993 - 1997 (in Japanese)

2)Ishihara K., T. Kagawa and C. Minowa et al. : Design and Setup of Large scale Liquefaction Reproducing Facilities, Proc. of 31th presentation of the Japanese Society of Soil Mechanics and Foundation Engineering, 1996.6, pp.1189-1190 (in Japanese)

3)Iguchi M. et al. : Evaluation of Seismic Behavior of Pile Foundation and Seismic Action on Piles by Shaking Table Test of Large-scale Shear Box, Summary of annual meetings of Architectural Institute of Japan, 1997.9, pp.369-396 (in Japanese)

4)Mizuno H. et al. : Dynamic Behavior of Pile Foundations in Liquefaction Process - Shaking Table Tests Utilizing Big Shear Box -, Proc. of 10th Japan Earthquake Engineering Symposium, 1998.11 (in Japanese, now adjusting the paper for final submission)

Table1 Soil Test Result

Test item	Result
density (g/cm³)	2.718
gravel fraction (%)	0.8
sand fraction (%)	94.8
silt fraction (%)	3.5
clay fraction (%)	0.9
uniformity coefficient	3.01
D50 (mm)	0.311
natural water content	5.71

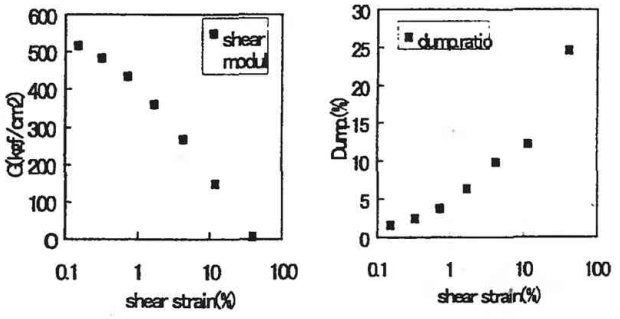

Fig.1 Equivalent Shear Modules & Dumping

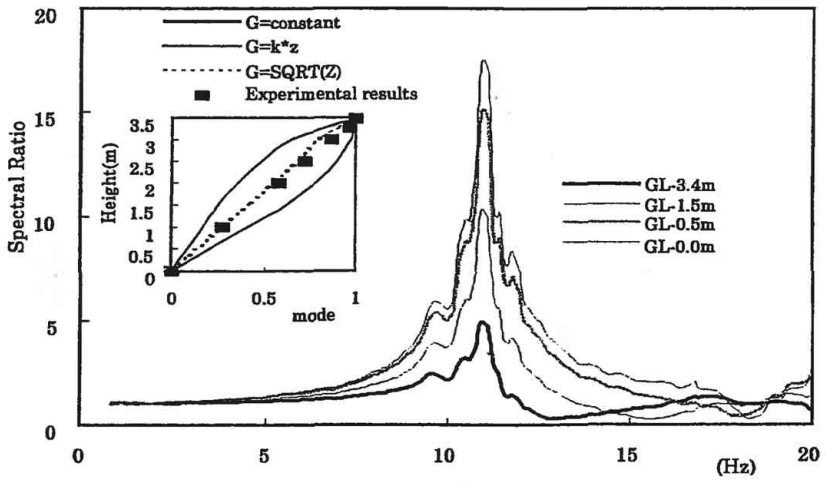

Fig.2 Spectral Ratio on Random Wave(60gal)

Table2 Test Series and Objects

Test Case & Test Ground Condition	Shaking Table Test(○:input)				Static Load (before shake table)	Oscil-later Test	Object
	Ran-dom 30gal	Earthquake wave ,gal (Port island GL-32m,Ns)					
		500	200	re-500			
Case ① Drop of Sand into Water, water level G.L.	○2,5	○3			○1,4	○7 at dissipation	check the liquefaction seismic behavior of ground & foundations
		○6*350gal,time scale=1/2					
Case ② Produced by boiling, water level G.L.	○2,6	○3		○7 *600gal	○1,5	○4 at dissipation	seismic behavior of ground & foundations (compare Case ①)
Case ③ Reproduced by boiling, water level G.L.	○3,7,9	○4	○8	○10	○2,8	○1,5 before earthquake wave	reappearance of seismic behavior of ground & foundations (compare Case ②)
		measured dissipation					
Case ④ Reproduced by boiling with drain, water level G.L.	○2,4,6	○3	○5	○7	○1		seismic behavior of ground & foundations under the drain (compare Case ③)
		measured dissipation					
Case ⑤ Reproduced by boiling, water level G.L.-1.4m	○2,6,7	○3	○8	○8	○1,5	○4 at dissipation	seismic behavior of ground & foundations at low water level (compare Case ②,③)
		measured dissipation					

○index : Test Order

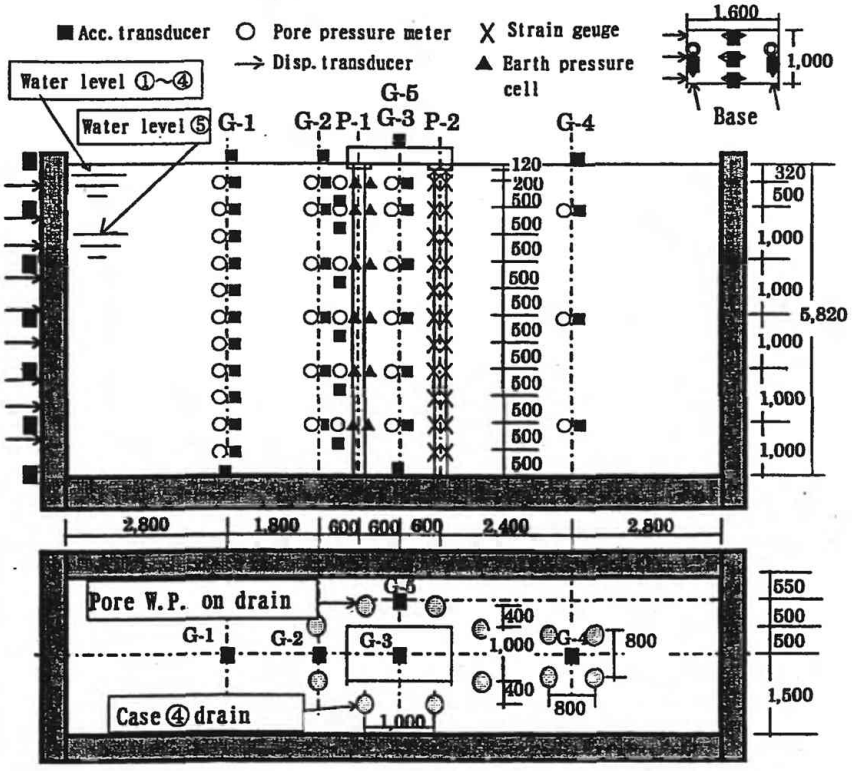

Fig.3 Outline of Test Specimen and Measurement

Table3 Ground Condition

Test Case	Surface Level(m)	Dry density (g/cm³)	Void ratio	Wet density (g/cm³)	Relative density (%)	Water Level(m)
①	5.82	1.50	0.81	1.95	38.7	surface
②	5.65	1.59	0.71	2.00	63	surface
③	5.54	1.62	0.68	2.02	71.7	surface
④	5.52	1.62	0.67	2.03	73.3	surface
⑤	5.39	1.68	0.64	2.05	83.3	surface-1.4

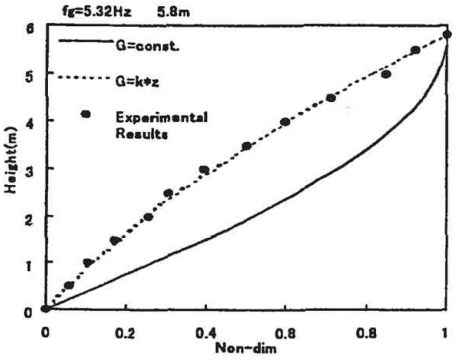

Fig.5 Vibration Mode

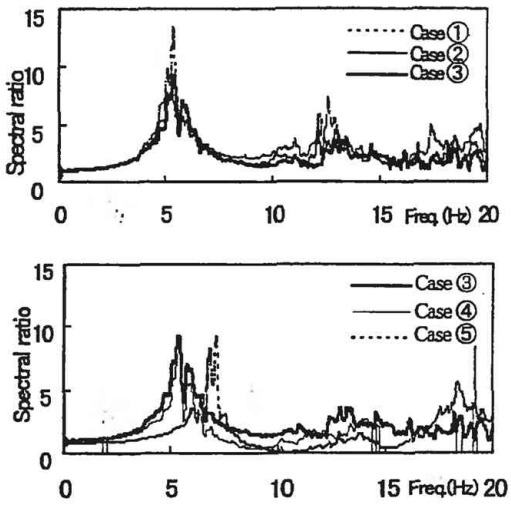

Fig.4 Spectral Ratio due to Random Wave(30gal)

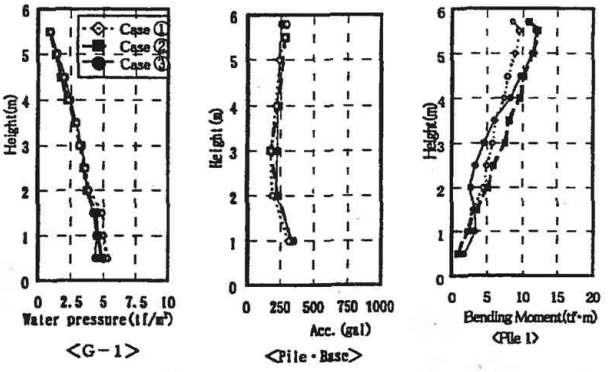

Fig.7 Max. Distribution of Pore Water Pressure, Acceleration and Bending Moment (Case ①~③)

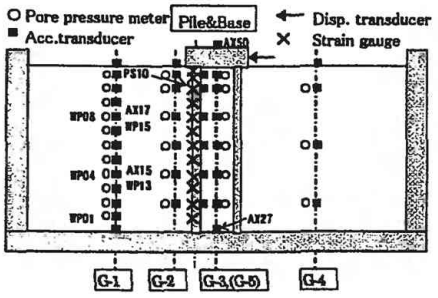

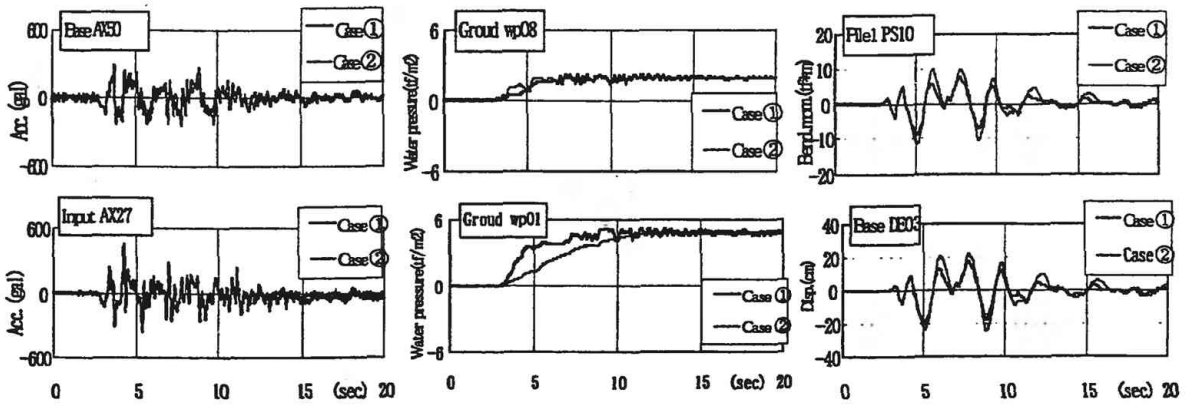

Fig.6 Time History due to Earthquake Excitation (Case ①, ②)

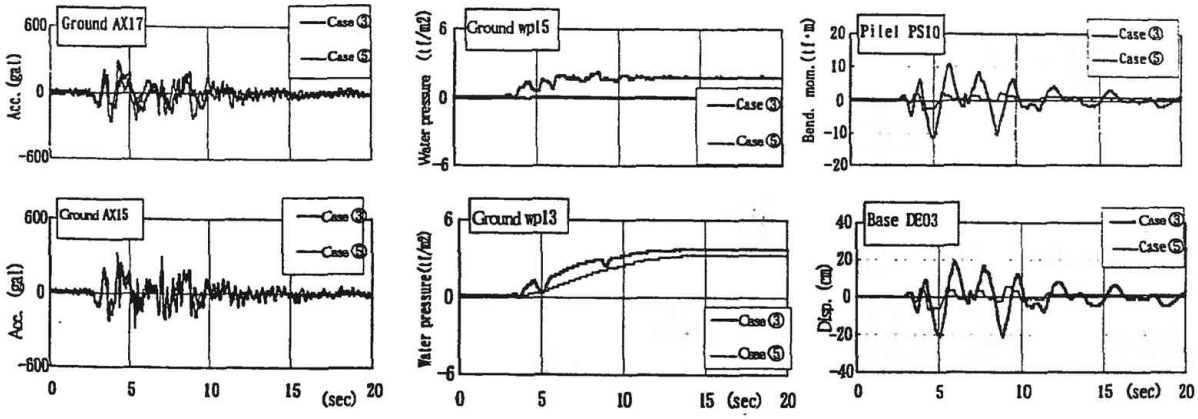

Fig.8 Time History due to Earthquake Excitation (Case ③, ⑤)

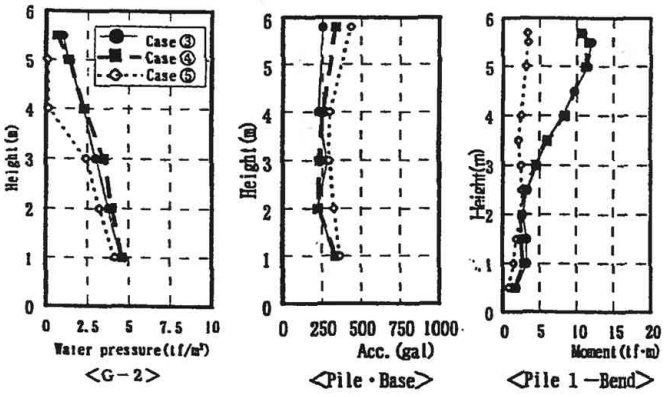

Fig.9 Comparison of Max. Response Distribution with Ground Water Level (Case ③, ⑤)

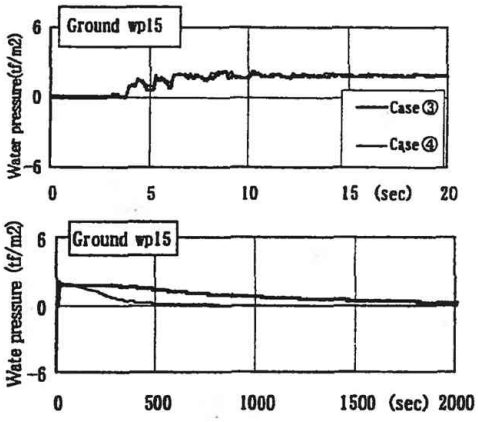

Fig.10 Pore Water Pressure During Dissipation with and without Drains (Case ③, ④)

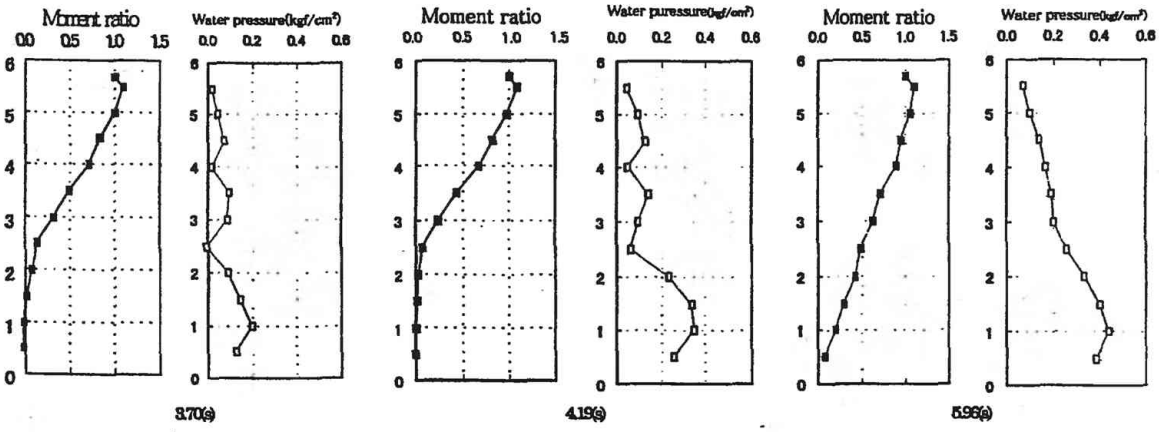

Fig.11 Distribution of Bending Moment Ratio & Pore Water Pressure at Several Times During Liquefaction (Case ①)

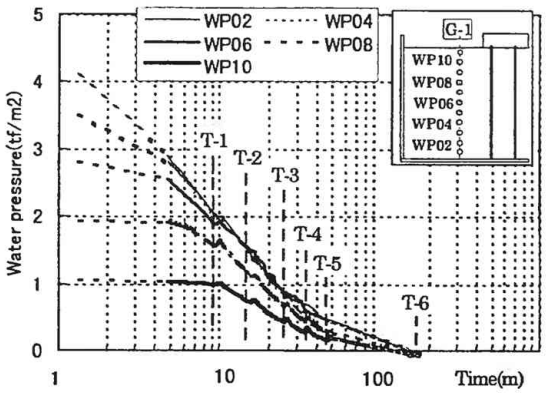

Fig.12 Pore Water Pressure in Dissipation process after Earthquake Excitation

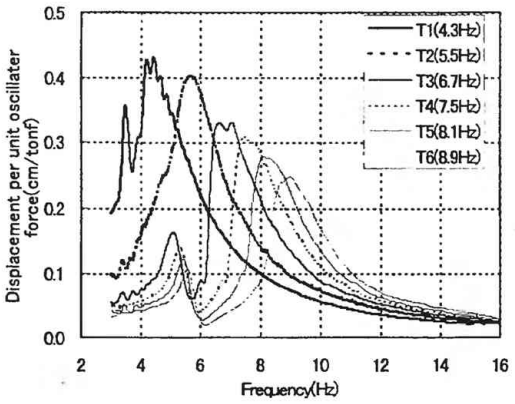

Fig.14 Resonant Curves of Footing Displacement

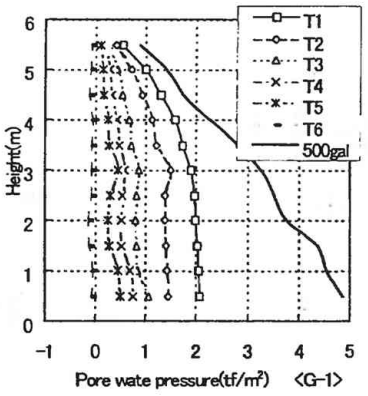

Fig.13 Distribution of Pore Water Pressure at several stages

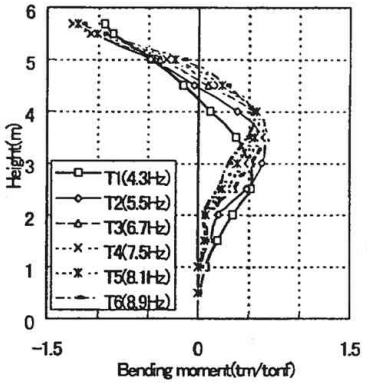

Fig.15 Distribution of Bending Moment at several stages(Pile2)

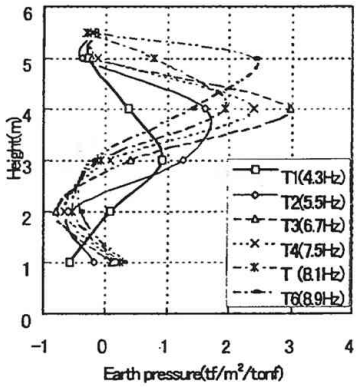

Fig.16 Distribution of Earth Pressure at several stages(Pile1)

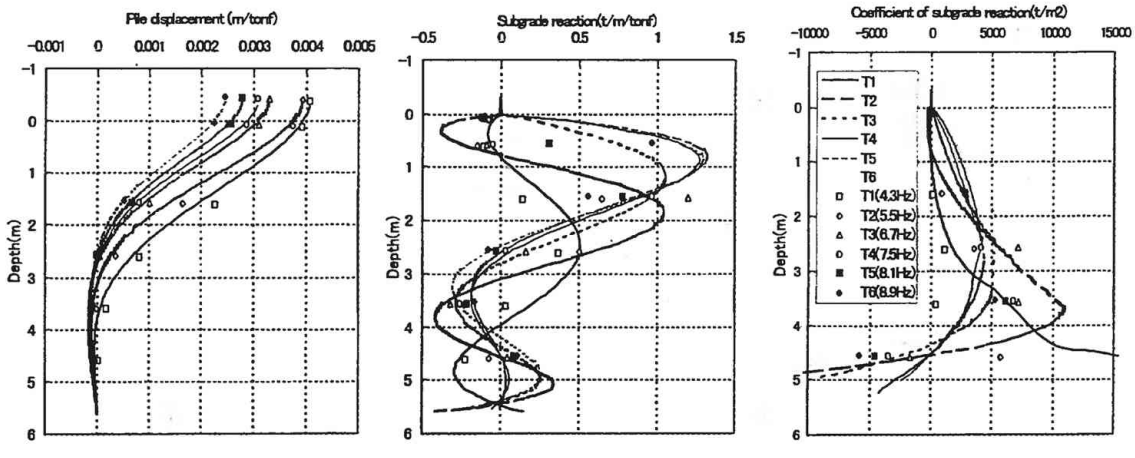

Fig.17 Pile Displacement, Subgrade Reaction, Coefficient of Subgrade Reaction obtained by Polynomial Approximation

ENERGY DISSIPATION IN SOIL-STRUCTURE INTERACTION: A CONSULTANT'S PERSPECTIVE

By: C.B. Crouse[1]

ABSTRACT: Energy dissipation as a means of reducing the seismic response of structures has become a popular topic among researchers and structural engineers who have developed and implemented devices, such as friction dampers, fluid dampers, and isolators, in the retrofit of structures. However, a natural source of energy dissipation is the interaction between a structure, its foundation, and the supporting soil medium. This interaction can be significant and potentially beneficial in certain situations, resulting in large reductions in seismic response. Unfortunately, this phenomenon is often ignored by many structural engineers because of their lack of knowledge of (1) theoretical principles governing soil-structure interaction (SSI), (2) circumstances when SSI is potentially important, (3) the field measurements of modal damping ratios, and (4) methods to estimate modal damping ratios in soil-structure systems. This knowledge gap exists primarily because the SSI subject is not generally taught at the undergraduate or graduate levels in university civil engineering departments. The theoretical principles, involving wave-propagation theory, boundary-value problems, and soil and structural mechanics/dynamics, are daunting to most civil engineering students with design-oriented career goals. Nevertheless, assuming the frequency-dependent foundation impedance functions can be obtained for a particular SSI system from the literature or from a consultant, relatively simple and practical systems-identification methods can be used to estimate the composite modal damping ratios for the significant modes of vibration. SSI experiments and theoretical calculations using these simple models have yielded relatively large modal damping ratios in certain situations for structures such as short-span bridges, offshore concrete gravity platforms, nuclear power plant containments, fuel storage tanks, short to mid-rise buildings, and nuclear waste processing plants.

[1] Principal Engineer, Dames & Moore, 500 Market Place Tower, 2025 First Avenue, Seattle, Washington 98121

INTRODUCTION

This paper, which is intended primarily for the professional structural engineer engaged in seismic design, first reviews the general state of SSI practice in the consulting engineering/structural design professions from the standpoint of energy dissipation in SSI systems. In dynamic analysis of structures, modal damping ratios between 0.03 and 0.07 (with a nominal value of 0.05) are typically used in practice. These values are generally acknowledged as structural damping ratios and are usually valid for a rigid or nearly rigid-base model of the structure. However, these values are often used in flexible-base models, which can result in an overestimation of the seismic loads.

In the section, Composite Modal Damping. technical justification for higher damping ratios for flexible-base models is provided by reviewing the concept of composite modal damping for soil-structure systems and the factors that affect it. Next, experimental data on modal damping of soil-structure systems are reviewed in the section, Measurements of Composite Modal Damping. In the subsequent section, Estimate of Composite Modal Damping, a simple systems identification procedure is described for estimating modal damping ratios in SSI systems with one or more foundations and frequency-dependent foundation impedance functions. Details of an example calculation of the modal damping ratios illustrating this procedure for a liquid fuel storage tank are described at the end of this section. A discussion of the implications of energy dissipation in SSI for seismic design is presented in the last section of this paper.

STATE OF PRACTICE

The state of the practice for modeling energy dissipation in SSI analysis for structures other than nuclear power plants is typically as follows. The structural engineer usually performs the analysis and constructs a model of the structure from the element library in a commercial software program for structural dynamics. Most of these element libraries have rotational and translational springs of constant stiffness that can be attached to the base of the structural model to simulate the foundation-soil interaction. The structural engineer will usually consult a geotechnical engineer for these foundation stiffnesses, but will not usually request estimates of the foundation damping. The structural analysis software typically solves the equations of motion using modal superposition.

The input motion is usually defined by the geotechnical engineer or engineering seismologist and consists of design spectra corresponding to damping ratios specified by the structural engineer, who typically selects values in the aforementioned 0.03 – 0.07 range.

This practice of incorporating SSI effects has remained fairly constant during the last 20 years. While more structural engineers recognize the importance of including foundation flexibility in their models, there has been a reluctance to properly incorporate the damping into the system. Most popular commercial structural dynamics software programs do not include viscous damping

elements. Even if the provision for specifying the element damping were available in these programs, most engineers would have difficulty specifying the viscous damping constants for each element because, unlike the relatively simple methods for generating the element stiffnesses, the procedures for estimating the values of a system damping matrix, are more complex. Available procedures are obscure, unknown, or difficult to understand by many structural engineers. Until they become familiar and comfortable with these procedures, the usual practice of arbitrarily adopting modal damping values around 0.05 will continue.

Many structural engineers are presently using software for nonlinear inelastic dynamic analysis of structures. The hysteretic damping from the specification of the load-deflection characteristics of the structural elements is automatically included in the structural models, but the damping for the foundation elements is more difficult to specify because of the anelastic (hysteretic) damping of the soil and the frequency-dependent radiation damping of the foundation-soil medium.

In the penultimate section of this paper, a simple example is provided illustrating the calculation of modal damping ratios for the fundamental mode of vibration of a tank-foundation system. Even in this example, the geotechnical engineer needed to recognize and properly estimate the two components of foundation damping (hysteretic and radiation).

COMPOSITE MODAL DAMPING

The composite modal damping ratio for each mode of vibration of a soil-structure system depends on the foundation damping, the structural damping, and the nature and degree of interaction between the structure and supporting soil. The foundation damping consists of the material (or hysteretic) damping of the soil and the radiation damping associated with the generation and propagation of seismic waves into the soil medium by the motion of the foundation relative to the free-field earthquake motion. The material damping primarily depends on strain induced in the soil during the shaking (e.g., Seed and Idriss, 1970), whereas the radiation damping depends on the elastic properties of the surrounding soil and the shape and embedment of the foundation. For a given soil profile and foundation geometry, the radiation damping depends on the mode of foundation vibration, e.g., vertical translation, horizontal translation, rotation, or a combination of translation and rotation (Richart et al., 1970; Gazetas, 1983).

Generally, foundation damping is highest for vertical and horizontal vibration and lowest for rocking motion. However, even for rocking modes, the damping ratios can be significantly larger than the nominal 5% critical damping ratio typically assumed for structures such as buildings and bridges. Thus, foundation damping is normally much higher than structural damping. In qualitative terms, the composite modal damping for a given soil-structure system with given amounts of foundation and structural damping will depend on the amount of deformation in the structure relative to the foundation movement. For example, the composite modal damping for stiff

structures on flexible soils is expected to be greater than the composite modal damping for flexible structures on stiff soils. This conclusion is easily seen in the limiting cases of an infinitely rigid structure on a flexible soil or a flexible structure founded on hard bedrock (i.e., rigid-base structure).

The next two sections discuss the measurement and prediction, respectively, of composite modal damping.

MEASUREMENTS OF COMPOSITE MODAL DAMPING

Composite modal damping ratios have been measured in a variety of soil-structure systems including simple footings, pile foundations, multistory buildings, bridges, and a scale-model nuclear plant containment structure. These damping ratios were obtained from soil-structure responses measured during forced vibration tests or earthquake excitations. The results for several soil-foundation and soil-foundation-structural systems familiar to the author are presented below. A comprehensive compilation of SSI parameters (including modal damping ratios) estimated from earthquake responses recorded at 58 building sites is presented in Stewart and Stewart (1997).

Concrete Footings

Forced harmonic vibration tests were conducted on small rectangular footings, approximately 1.2m x 1.2m in plan dimensions with thicknesses ranging from 0.1 m to 0.6m. The footings, to which strong-motion accelerographs were attached to measure earthquake ground motions, were underlain by moderately stiff soil with shear-wave velocities on the order of 150 m/s. One test was conducted in Jenkinsville, South Carolina (Crouse et al., 1984) and the others were conducted in southern California (Crouse and Hushmand, 1989). The Jenkinsville footing, which is 0.6 m thick and embedded approximately 0.45 m in the surrounding soil, is shown in Figure 1, and the southern California footings are shown in Figure 2. The modal damping ratios for these footings are summarized in Table 1 below.

TABLE 1. Measured Modal Damping Ratios for 1.2m x 1.2m Concrete Footings

Location	Damping Ratio
Jenkinsville, SC	0.20 - 0.21
Parkfield, CA	0.30 - 0.40
El Centro, CA	0.30 - 0.40

The vibration modes corresponding to these damping ratios were coupled translation-rocking.

A similar vibration test was conducted in El Centro, California on a larger rectangular foundation with dimensions of 2.44m x 2.44m x 0.10m thick (Crouse and Hushmand, 1989, 1990). This foundation, also founded on soil with a shear-wave velocity of approximately 150 m/s, supported an 2.44m high rigid masonry block structure (Figure 3). The modal damping ratio for this system was approximately 0.29 (Crouse et al., 1992).

Scale-Model Concrete Containment Structure

In 1985 the Electric Power Research Institute (EPRI) and Taiwan Power Company (TPC) constructed a 1/4 scale-model of a nuclear power plant containment structure (Figure 4) in Lotung, Taiwan. The containment structure was a cylindrical reinforced concrete shell (outer radius = 5.25m) that was 15.2m high and attached to a 0.91m thick circular concrete mat. The average shear-wave velocity measured in the upper 6.1m of soil was approximately 150 m/s. The Nuclear Regulatory Commission (NRC) conducted forced harmonic vibration tests on the structure. The instrumentation on the structure also recorded motions from several earthquakes.

The modal damping ratios measured during the forced vibration test and during the May 20, 1986 earthquake of magnitude 6.5 are listed in Table 2 (Tajimi Engineering Services, Ltd, 1989).

TABLE 2. Measured Modal Damping Ratios for Concrete Containment Structure

Event	Estimation Method	Damping Ratio
Forced Vibration Test	Bandwidth	0.10
	Resonant Amplification	0.15 – 0.17
	Energy	0.13 – 0.21
5/20/86 Earthquake	System Identification	0.22

The mode of vibration yielding these damping ratios was primarily foundation rocking with a relatively small component of sway deformation of the containment. The associated resonant frequency was 3.8 Hz during the forced vibration test and 2.3 Hz during the earthquake. The lower frequency and higher damping during the earthquake is attributed to greater nonlinear (hysteretic) soil behavior.

Bridges

Vibration measurements on bridges during forced vibration tests and during a large earthquake were used to estimate modal damping ratios for three bridge-foundation-soil systems. Analysis of these data appears in a paper by Crouse and Werner (1995). Table 1 from that reference (reproduced with minor edits as Table 3 below) lists the relevant information about the bridges, Horsethief, Meloland Road Overcrossing (MRO), and Moses Lake, which are one, two, and three

spans, respectively, and which are supported on moderately stiff soil at their abutments and pier foundations.

TABLE 3. Characteristics of Bridges

Name and Location	Length (m)	Type of Construction	Type of Abutment	Foundation Type		Foundation Soils	
				Abutment	Pier	Abutment	Pier
Horsethief Corona, CA	31.4	RC box girder	Monolithic	Footing	-	Stiff sand	-
MRO El Centro, CA	63.4	RC box girder	Monolithic	Wood Piles	Wood Piles	Stiff clay	Mod. stiff sand, clay and sand
Moses Lake, WA	43.3	RC I girder	Seat	Footing	Footing	Dense silty sand	Very stiff sandy silt

The mode shapes, natural frequencies, and modal damping values were compiled from the test data and the strong motion records. Table 4 contains the relevant modal data from each bridge-vibration data set; only the data from modes with a significant transverse component are included in the table. In these modes, the SSI was thought to be potentially significant. Listed in the third through seventh columns of Table 4 are the natural frequencies, selected modal deflections, and modal damping ratios. The modal deflections listed are the average transverse translation of the abutments ($\overline{R}_a^t$), the maximum transverse deflection of the deck (R_d^t), and the maximum vertical deflection of the deck (R_d^v). For these data sets, R_d^v was primarily due to torsion of the deck about the longitudinal axis. The transverse modal deflections at the pier foundations of the MRO and Moses Lake bridges were not included in Table 4 because they were roughly an order of magnitude smaller than the abutment deflections, ($\overline{R}_a^t$).

A parameter, θ, was defined to characterize the amount of SSI in each mode of vibration of the bridge-foundation-soil system in terms of the modal deflection terms:

$$\theta = \frac{\overline{R}_a^t}{(R_d^t + R_d^v)} \tag{1}$$

The rationale for this expression is as follows. The experimental data for bridges reveal high damping in transverse modes of vibration where the abutment transverse deflection is a significant fraction of the transverse deck deflection. In these modes, the vertical deflection of the deck is relatively small. Modes with vertical deflections that are much larger than the transverse deflections of the abutment have relatively small damping. Longitudinal modes of vibration are expected to have fairly large damping also, but these modes are difficult to excite and are not considered to be as important as transverse modes from the standpoint of earthquake performance. Thus, the parameter θ does not incorporate longitudinal deflection terms.

If significant soil-structure interaction is defined as values of $\theta \geq 0.1$, then all modes satisfying this criterion in Table 4 have modal damping ratios $\zeta > 6\%$. The range of ζ is between 6% and 26%. For $0.05 \leq \theta < 0.1$, modal damping ratios, $\zeta > 6\%$ were also observed for the second transverse mode of the MRO. For $\theta < 0.05$, $\zeta < 0.05$ for the data in Table 4. The correlation between θ and ζ is clearly seen in these data, which strongly suggest that damping ratios $\zeta > 0.05$ are justified for bridges in cases where the SSI is significant.

TABLE 4. Modal Damping Ratios for Transverse Modes of Vibration of Bridges

Bridge Test Case	Transverse Mode No.	Natural Frequency (Hz)	Modal Deflections			Modal Damping, ζ (%)	SSI Parameter θ
			$\overline{R}_a^t$	R_d^t	R_d^v		
1. MRO-vib. test (quick release - 21 kip load)	1 2 3	3.3 12.7 22.1	0.11 0.029 ~0	0.31 0.096 0.19	0.18 0.30 0.38	6.2 8.8 3.2	0.22 0.073 ~0
2. MRO-vib. test (quick release - 141 kip load)	1 2 3	3.2 13.2 22.4	0.094 0.02 ~0	0.33 0.10 0.96	0.14 0.32 0.34	6.5 11.6 3.4	0.2 0.05 ~0
3. MRO-1979 EQ	1	2.5	0.66	1.0	0.37	10-26	0.48
4. Horsethief (forced harmonic vibration)	1 2	6.4 8.2	< 0.01 0.8	0.03 1.25	0.27 0.39	3.5 15.0	~0 0.49
5. Moses Lake (forced harmonic vibration - test 1)	1 2	6.6 7.4	0.31 0.26	1.0 1.0	0.22 0.45	9.1 6.8	0.25 0.18
6. Moses Lake (forced harmonic vibration - test 2)	1 2	6.5 7.1	0.24 0.40	1.0 1.0	0.26 0.42	6.2 8.5	0.19 0.28

ESTIMATION OF COMPOSITE MODAL DAMPING

This section first describes a systems-identification method for the estimation of modal damping in SSI systems where the foundation impedance functions are frequency and strain dependent. Next, the method is illustrated in an example calculation of composite modal damping for a liquid natural gas (LNG) tank.

Systems-Identification Method

Systems-identification methods typically have been used to estimate system parameters (e.g., natural frequencies, damping ratios, and foundation stiffnesses) from response data recorded during vibration tests or earthquakes. These methods also can be adapted to SSI analyses for structures in the design stage in cases where the structures are supported on multiple foundations and/or where the frequency dependence of the foundation impedance functions is significant. For such cases, closed-form solutions for modal damping ratios do not presently exist, although solutions have been developed for the case of single foundations supported on a medium in which the foundation impedance functions (stiffness and damping coefficients) are frequency independent (e.g., Luco, 1981; ASCE, 1986).

The systems-identification method, presented herein, is applicable to linear SSI systems and is as follows. Equations of motion are derived in the frequency domain for the SSI system in generalized spatial coordinates and in modal coordinates. These two sets of equations are used to develop transfer functions (one for generalized coordinates and another for modal coordinates) that express the ratio of the motion at some point on the structure to the free-field motion as a function of frequency. The transfer function of the model in generalized coordinates is presumed to be known because the structural masses, moments of inertia, stiffnesses and damping constants, as well as the foundation impedance functions, are known or can be computed. On the other hand, the natural frequencies and damping ratios in the transfer function for the SSI model based on modal coordinates are unknown. The values of these parameters are varied until the two transfer functions are similar.

In the generalized coordinate system, the specification of the structural damping is straightforward for a 1 degree-of-freedom (d.o.f.) representation of the structure, which is an acceptable approximation for a number of SSI systems. In this case, the damping coefficient, c, is computed using the formula, $c=2\varsigma\sqrt{km}$, for a 1 d.o.f. oscillator, where ζ is the assumed modal damping ratio for the oscillator (fixed-base structure), and k and m are the known oscillator stiffness and mass, respectively. In cases where a multi-d.o.f. model is required for the structure, the structural damping matrix can be computed by fairly simple matrix algebra (e.g., Tsai, 1969) by (1) assigning modal damping ratios (ζ_i) for each mode of vibration of the fixed-base model of the structure, and (2) assuming these ratios are factors in the diagonal elements, $2\ \omega_i\zeta_i$, of the diagonal damping matrix of the modal equivalent of the fixed-base structure, which is assumed to possess classical normal modes.

For many applications in practice, the foundation impedance functions can be obtained from the literature (see Appendix A of WSDOT (1993)) or from commercially available computer codes, e.g., DYNA3 (Novak et al, 1991), SUPELM (Kausel, 1992).

The impedance functions in the literature are usually presented in graphs or tables for assumed values of the material damping of the soil. In the case of uniform material damping of the soil medium, the published impedance functions can be easily adjusted to account for a different material damping (Wong and Luco, 1981). This material damping ratio can be estimated from published strain-dependent damping ratio curves or can be derived from laboratory tests on soil samples. In either case, the effective shear strain in the soil must be estimated based on the design ground motion.

Example Calculation of Composite Modal Damping for a LNG Tank

Dames & Moore recently participated in a project involving the seismic design of a large cylindrical steel flat-bottom LNG tank in a region of moderate seismic activity. The tank was to be supported on a mat foundation resting on the surface of improved soil. The structural designer was planning to conduct a linear dynamic analysis using the design response spectra corresponding to the appropriate modal damping ratios associated with the impulsive and convective modes of the tank-fluid-foundation-soil system.

The composite modal damping of primary interest was for the fundamental impulsive mode. The model used to compute this ratio was similar to the model of Veletsos and Tang (1990). It consisted of a single-degree-of-freedom oscillator representing the impulsive mode of the fixed-base tank attached to a circular foundation mat supported on a visco-elastic half space. The relevant parameters of the model for the Operating Basis Earthquake (OBE) and Safe Shutdown Earthquake (SSE) levels of shaking (0.2 g and 0.4 g, respectively) are summarized in Table 5.

TABLE 5. Model Parameters for LNG Tank Example

Model Element	Parameter	Parameter Value	
		OBE	SSE
Tank Shell & Fluid	Impulsive Liquid Mass	3.35×10^7 kg	3.35×10^7 kg
	Impulsive Mode Frequency	3.9 Hz	3.9 Hz
	Impulsive Mode Damping Ratio	0.03	0.07
	Height of Impulsive Mass	11.9 m	11.9 m
	Height of Liquid, H	31.8 m	31.8 m
	Inner Tank Radius, a	40.0 m	40.0 m
Tank Foundation	Radius	44.5 m	44.5 m
	Mass	1.23×10^7 kg	1.23×10^7 kg
	Mass Moment of Inertia	7.10×10^9 kg-m^2	7.10×10^9 kg-m^2
Half Space	Shear-Wave Velocity	263 m/s	204 m/s
	Density	1.76 gm/cc	1.76 gm/cc
	Poisson's Ratio	0.3	0.3
	Material Damping Ratio	0.10	0.15

The modal damping ratio was estimated by deriving equations for the Transfer Function (TF) between the tank-displacement motion and the free-field, ground-displacement motion induced by the earthquake. One TF was expressed in terms of the generalized coordinates, mass, damping, and stiffness quantities, while the other TF was expressed in terms of the modal quantities (i.e., natural frequencies, modal damping ratios, mode shapes, and participation factors). The material damping ratio of the soil was incorporated by modifying the foundation impedance functions for a circular disc on an elastic half space without material damping. The procedure for the modification is given in Gazetas (1983) or Wong and Luco (1981).

The modal damping ratio for the fundamental mode of the system that provided similarity in the moduli of the two TFs was estimated. Using best estimates for the parameters of the tank-foundation soil model (Table 5), modal damping ratios of 0.19 and 0.28 were estimated for the OBE and SSE, respectively. Comparisons between the resulting two TFs of the OBE and SSE are shown in Figures 5a and 5b, respectively.

The relatively high modal damping ratios estimated for the OBE and SSE are the result of the significant interaction between the tank foundation and underlying soil. These results are consistent with those in Veletsos and Tang (1990) in the sense that composite modal damping values much higher than the structural damping value are expected for tanks with small liquid height to inner tank radius ratios (H/a) on relatively flexible soils.

DISCUSSION

Experimental test results and predictions from theoretical models clearly demonstrate that relatively large composite modal damping ratios are possible when SSI effects are significant. Furthermore, when properly substantiated by appropriate SSI analysis procedures, the use of relatively large composite damping values for the computation of seismic loads is accepted practice in the U.S. nuclear power industry. All of this experimental/theoretical evidence and the nuclear industry precedent suggest that in the case of other important structures, composite modal damping values larger than the structural damping ratios should be considered in the calculation of the seismic loads. However, the composite modal damping values determined by theoretical models are not necessarily those that should be used in final design. The final modal damping values should consider uncertainties associated with the SSI model and its parameters, relevant experimental data, and the degree of conservatism desired for the design.

One potentially beneficial effect that was not considered in the SSI model for the tank example is the filtering or reduction in high frequency ground motion by the passage of seismic waves across the tank foundation. During the last 25 years, this effect has been observed in buildings with foundation areas similar to that of the example tank. The high-frequency filtering phenomenon for foundations of this size on soils of roughly the same stiffness has been observed for frequencies

greater than about 2 Hz (e.g., Yamahara, 1970; Crouse and Jennings, 1975; Newmark et al., 1977; Fenves and Serino, 1992; Stewart and Stewart, 1997). The filtering, or kinematic interaction, is caused by (1) incoming seismic waves at angles of incidence less than 90° (vertical propagation), and (2) incoherence in the ground motion due to wave scattering from inhomogeneities in the local geology and anelastic attenuation.

The size of the example tank foundation (~ 80 m diameter), the flexibility of the underlying soil, and the estimated fundamental impulsive frequency of the tank-soil system (~ 3½ Hz) were factors collectively suggesting that filtering of ground motion at this frequency may occur, thus reducing the impulsive seismic load on the tank. The observational data indicate that a modest reduction in the OBE and SSE design spectra at short periods to account for this effect (which is equivalent to increasing the damping) was appropriate. However, the inclusion of this effect in the development of site-specific design spectra for particular structures should be coordinated with the structural engineer performing the dynamic analysis and design. The basis and amount of any reduction in the design spectra due to kinematic interaction should be well documented by the professional developing the design spectra.

APPENDIX. REFERENCES

ASCE, 1986. Seismic Analysis of Safety-Related Nuclear Structures and Commentary on Standard for Seismic Analysis of Safety-Related Nuclear Structures: American Society of Civil Engineers, ASCE Standard 4-86, September.

Crouse, C.B., and B. Hushmand, 1989. Soil-structure interaction at CDMG and USGS accelograph stations: Bull. Seism. Soc. Am., Vol. 79, No. 1, February, p. 1-14.

Crouse, C.B. and B. Hushmand, 1990. Soil-structure interaction and nonlinear site response at the Differential Array accelerograph station: Proceedings of 4th U.S. National Conf. on Earthq. Eng., Palm Springs, CA, May, Vol. 3, p. 815-823.

Crouse, C.B. and S.D. Werner, 1995. Estimation of modal damping for bridges: Proceedings of 4th U.S. Conf. on Lifeline Earthq. Eng., San Francisco, CA, August, p. 408-415.

Crouse, C.B., and P.C. Jennings, 1975. Soil-structure interaction during the San Fernando earthquake: Bull. Seism. Soc. Am., Vol. 65, No. 1, February, p. 13-36.

Crouse, C.B., E. Trahern, and T. Price, 1992. Nonlinear site response at the Differential Array station during the 1979 Imperial Valley, California, earthquake: Report to U.S. Nuclear Regulatory Commission and National Science Foundation, March.

Crouse, C.B., G.C. Liang, and G.R. Martin, 1984. Experimental study of soil-structure interaction at an accelograph station: Bull. Seism. Soc. Am., Vol. 74, No. 5, October, p. 1995-2013.

Fenves, G.L. and G. Serino, 1992. Evaluation of soil-structure interaction in buildings during earthquakes: Calif. Strong Motion Instrumentation Program, CSMIP/92-01, June.

Gazetas, G., 1983. Analysis of machine foundation vibrations, state of art: J. Soil Dyn. and Earthq. Eng., Vol. 2, No. 1, p. 2-42.

Kausel, E., 1992. SUPELM, Ver. 2.0, Foundations embedded in layered media: Dynamic stiffnesses and response to seismic waves.

Luco, J.E., 1981. Linear soil-structure interaction: Lawrence Livermore Laboratory Report (UCRL-53011) to U.S. Nuclear Regulatory Commission (NUREG/CR-1780).

Newmark, N.M., W.J. Hall, and J.R. Morgan, 1977. Comparison of building response and free-field motion in earthquakes: Proceedings 6th World Conf. Earthq. Eng., New Delhi, India, Vol. 3, p. 972-978.

Novak, M., M. Sheta, L. El-Hifnawy, H. El-Marsafawi, and O. Ramadan, 1991. DYNA3, A Computer Program for Calculation of Foundation Response to Dynamic Loads, User Manual: Univ. of Western Ontario Geotechnical Research Centre, Rept. No. GEOP90-02, Vol. 1, Rev. 2

Richart, F.E., J.R. Hall and R.D. Woods, 1970. Vibrations of Soils and Foundations. Prentice-Hall, Englewood Cliffs, NJ.

Seed, H.B. and I.M. Idriss, 1970. Soil moduli and damping factors for dynamic response analysis. University of California, Berkeley, Earthquake Engineering Research Center, ERRC 70-10.

Stewart, J.P. and A.F. Stewart, 1997. Analysis of soil-structure interaction effects on building response from earthquake strong motion recordings at 58 sites. University of California, Berkeley, Earthquake Engineering Research Center, Report No. UBC/EERC-97/01, February.

Tajimi Engineering Services, Ltd., 1989. Lotung SSI analysis using a 3-D harmonic Green's function method: Proceedings EPRI/NRC/TPC Workshop on Seismic Soil-Structure Interaction Analysis Techniques using Data from Lotung, Taiwan, Vol. 2, EPRI NP-6154, March, p. 16-1 to 16-50.

Tsai, N-C, 1969. Influence of Local Geology on Earthquake Ground Motion: Ph.D. Thesis, California Institute of Technology, Pasadena, CA, 201 p.

Veletsos, A.S. and Y. Tang, 1990. Soil-structure interaction effects for laterally excited liquid storage tanks: J. Earthq. Eng. and Struct. Dyn., Vol. 19, p. 473-496.

WSDOT (Washington State Department of Transportation), 1993. Manual of Practice, Foundation-Soil Interaction Analysis of Bridges, Vol. 1, Report by Dames & Moore and Inca Engineers.

Wong, H.L. and J.E. Luco, 1981. Identification of sensitive parameters for soil-structure interaction: Lawrence Livermore Laboratory Report (UCRL-15493) to U.S. Nuclear Regulatory Commission (NUREG/CR-3044).

Yamahara, H., 1970. Ground motions during earthquakes and the input loss of power to an excitation of buildings: Soils and Foundations, Vol. 10, No. 2, Tokyo, Japan, p. 145-161.

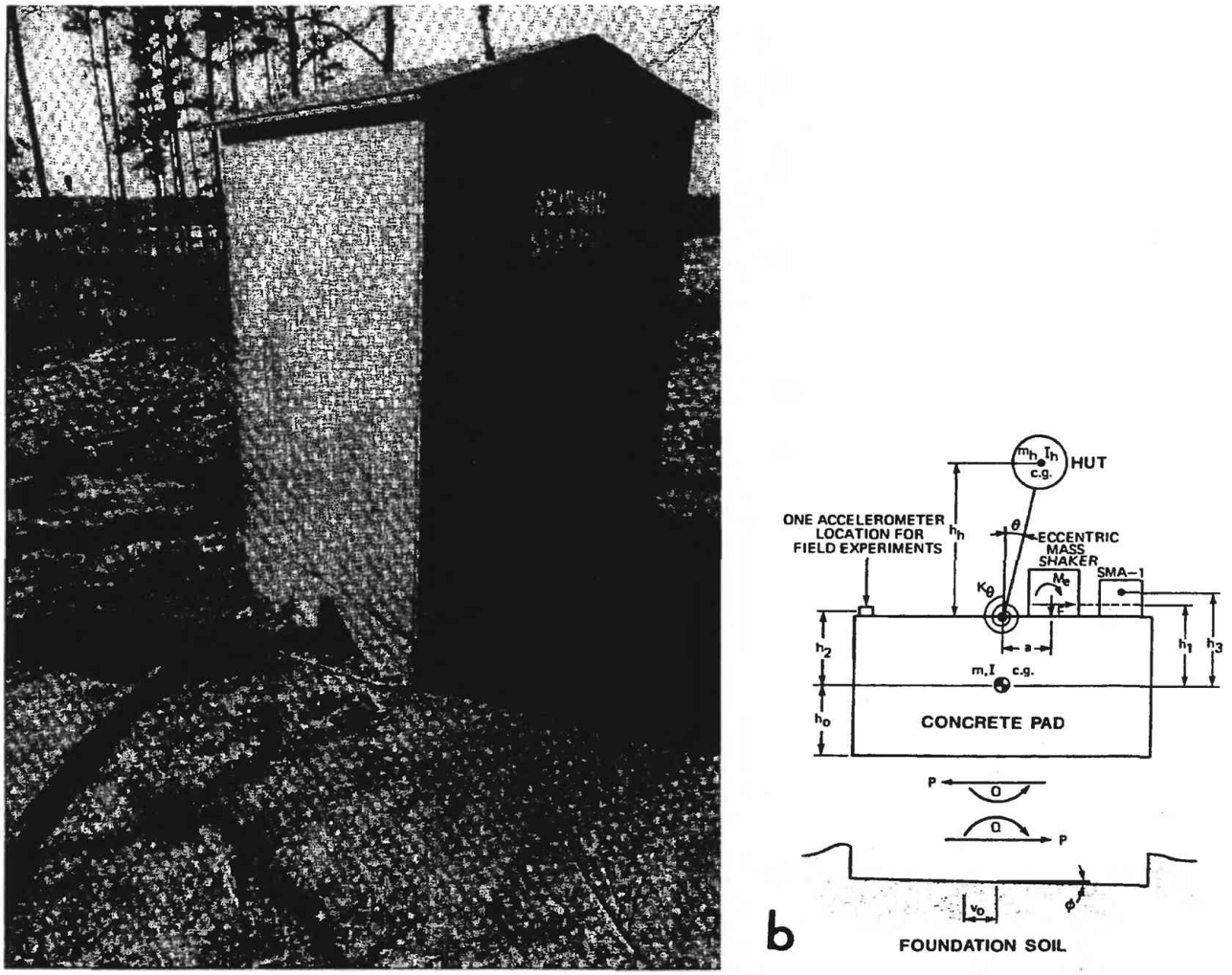

Fig 1. (a) Jenkinsville, South Carolina, accelerograph station. (b) Soil-structure interaction model of station.

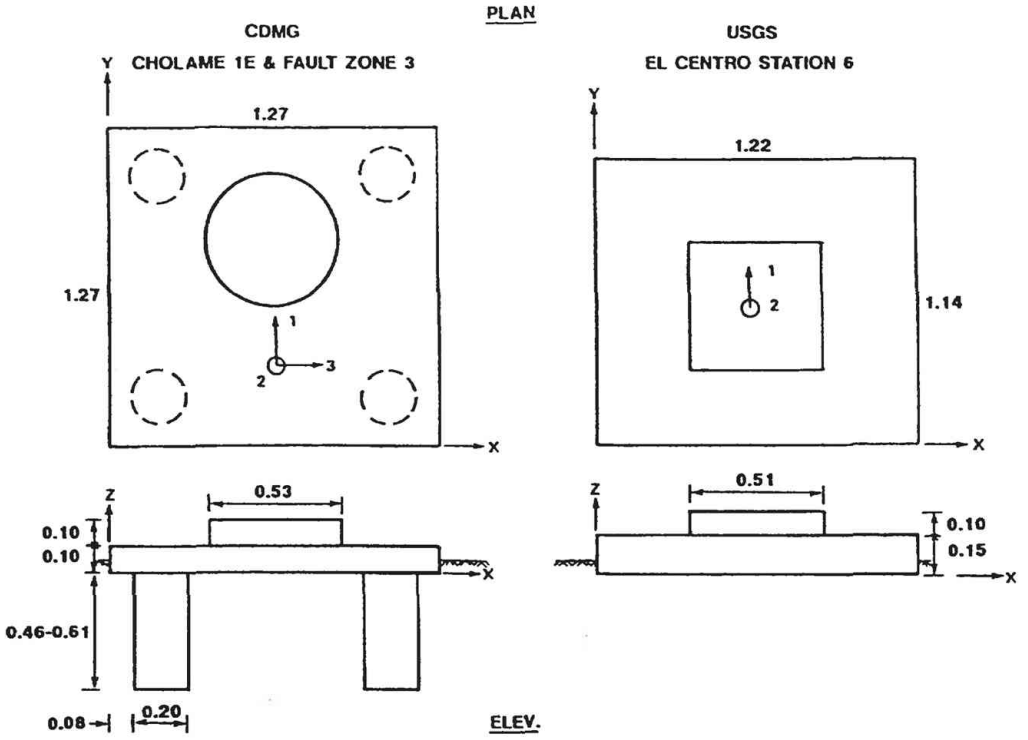

Fig. 2. Foundations of CDMG (Cholame 1E and Fault Zone 3) and USGS (Station 6) accelerograph stations. Numbered arrows indicate locations and directions of applied shaker forces. Dimensions in meters.

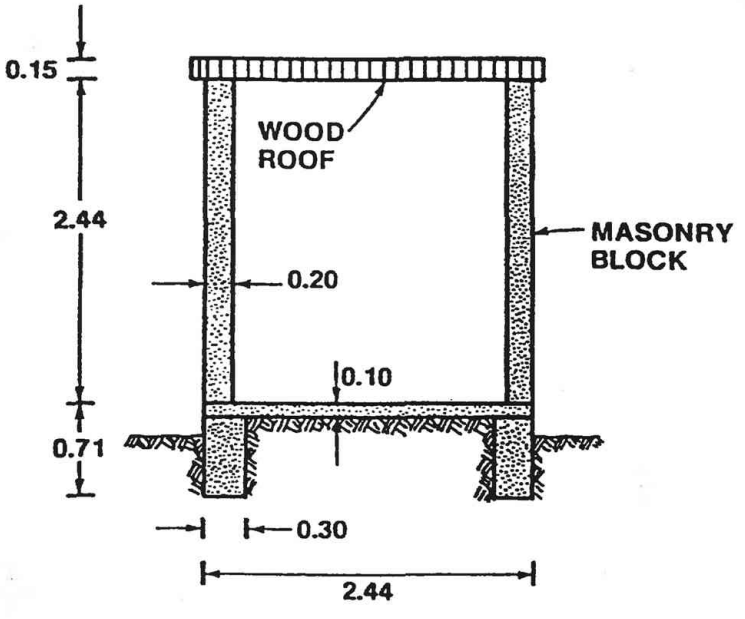

Fig. 3. Differential Array station. Dimensions in meters.

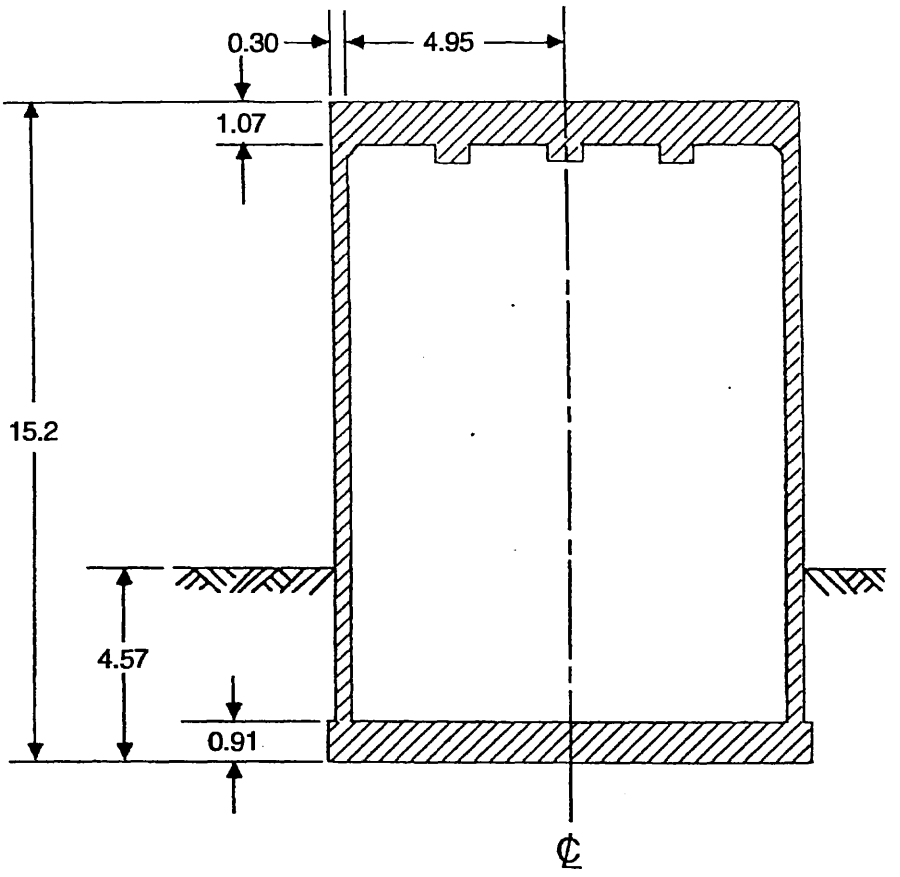

Fig. 4. Cross section of 1/4-scale containment model. Dimensions in meters.

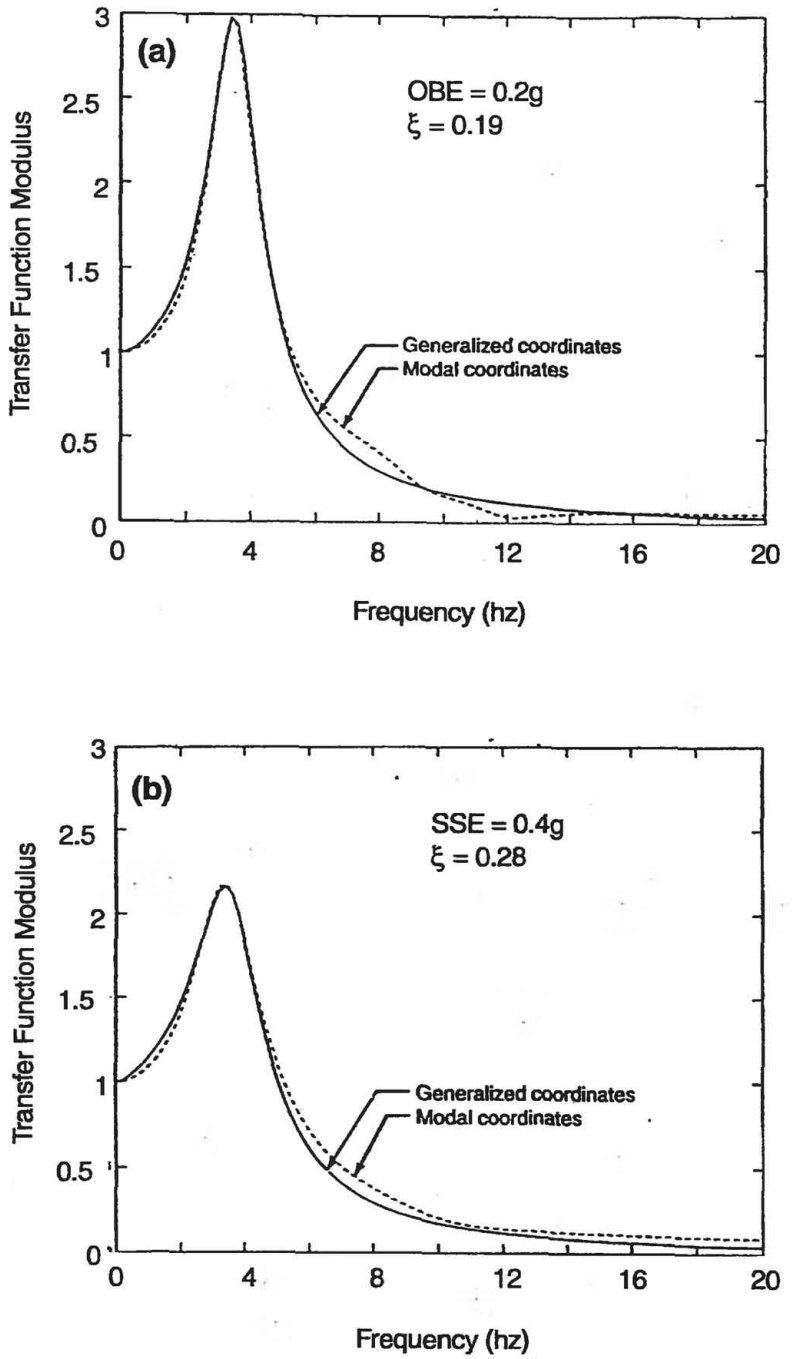

Fig. 5. Transfer functions and fundamental modal damping ratios for tank example for: (a) OBE, and (b) SSE.

EMPIRICAL ASSESSMENT OF SOIL-STRUCTURE INTERACTION EFFECTS FROM STRONG MOTION RECORDINGS

Jonathan P. Stewart[1]

Abstract: System identification analyses are used to evaluate soil-structure interaction effects for 77 strong motion data sets at 57 building sites which encompass a wide range of structural and geotechnical conditions. Kinematic interaction effects on the "input" motion at the bases of structures are found to be relatively modest in many cases, whereas inertial interaction effects on the structural response to these motions can be significant. To quantify inertial interaction effects, fixed- and flexible-base modal vibration parameters are used to evaluate first-mode period lengthening ratios ($\tilde{T}/T$) and foundation damping factors ($\tilde{\zeta}_0$). The response of some structures is dominated by inertial interaction (e.g. $\tilde{T}/T \approx 4$, $\tilde{\zeta}_0 \approx 30\%$), whereas others undergo negligible SSI (e.g. $\tilde{T}/T \approx 1$, $\tilde{\zeta}_0 \approx 0$). Simplified analytical formulations adapted from Veletsos and Nair (1975) and Bielak (1975) are used to predict inertial interaction effects, and are found to be reasonably accurate relative to empirical results, with some limitations for long-period structures. A collective examination of the empirical and predicted results reveals a pronounced influence of structure-to-soil stiffness ratio on inertial interaction, as well as secondary influences from structure aspect ratio and foundation embedment, type, shape, and flexibility.

INTRODUCTION

Documentation of seismic case history data is a critically important step towards understanding and reliably characterizing complex problems in geotechnical earthquake engineering. Few empirical studies of soil-structure interaction (SSI) have been performed due to the previously limited amount of strong motion data from sites with instrumented structures and free-field accelerographs. In contrast, analytical formulations for SSI are numerous, ranging from complex, three-dimensional finite element analysis procedures capable of incorporating fully nonlinear dynamic soil modeling (e.g. Borja, 1992) to simplified substructure techniques suitable for implementation in building codes (e.g. Veletsos and Nair, 1975). While some sophisticated analytical models have been verified using recorded data from nuclear reactor structures or scaled models thereof (e.g. Valera et al., 1977; Bechtel, 1991), empirical studies incorporating a large number of building sites with strong motion recordings are lacking.

In this paper available earthquake strong motion data, much of which has only recently become available, are analyzed to evaluate the effects of inertial interaction on structural

[1] Asst. Prof., Civil and Env. Engrg. Dept., University of California, Los Angeles, CA 90095-1593

response for a range of geotechnical and structural conditions. The results are used to verify simplified inertial interaction analysis procedures modified from Veletsos and Nair (1975) and Bielak (1975). Kinematic interaction, which modifies foundation-level motions relative to free-field motions, is a second order effect for many buildings, and is not the primary subject of this paper. The paper is organized into separate sections describing the analysis procedures, database, empirical data, and the calibration of the SSI design procedures. These results are a summary of the findings in Stewart et al. (1998).

ANALYSIS METHODS

Overview of Design Procedure for SSI

For analysis of inertial interaction effects, the objectives are predictions of first-mode period lengthening ratio $\tilde{T}/T$ and foundation damping factor $\tilde{\zeta}_0$. As shown in Fig. 1, simple procedures for evaluating these effects employ a model consisting of a single degree-of-freedom structure resting on a foundation-soil system represented by an impedance function. The impedance function is calculated for a rigid disk foundation resting either at the surface of (Veletsos and Nair, 1975) or embedded into (Bielak, 1975) a uniform visco-elastic halfspace.

As shown in Fig. 2, the motivation for characterizing $\tilde{T}/T$ and $\tilde{\zeta}_0$ is that they can be used to estimate flexible-base modal parameters ($\tilde{T}$, $\tilde{\zeta}$), which in turn are used in response spectrum-based approaches for evaluating design-level seismic base shear forces and deformations in structures. The parameters needed for analysis of $\tilde{T}/T$ and $\tilde{\zeta}_0$ are:

- Soil conditions: shear wave velocity V_S and hysteretic damping ratio β which are representative of the site stratigraphy and the level of ground shaking; representative soil Poisson's ratio ν.
- Structure/Foundation Characteristics: effective height of structure above foundation level, *h*; embedment, *e*; and foundation radii which match the area and moment of inertia of the actual foundation, r_u and r_θ.
- Fixed Base 1st Mode Parameters: period and damping ratio, T and ζ.

Using these data, the impedance function is evaluated at the flexible-base period of the structure, $\tilde{T}$. The frequency dependent and complex-valued impedance terms are expressed in the form

$$\bar{k}_j = k_j(a_0,\upsilon) + i\omega c_j(a_0,\upsilon) \quad (1)$$

where *j* denotes either deformation mode u (translation) or θ (rocking), ω is angular frequency (radians/sec.), a_0 is a dimensionless frequency defined by $a_0 = \omega r/V_S$, r = foundation radius, V_S =

soil shear wave velocity, and υ = soil Poisson ratio. Terms k_j and c_j consist of a combination of static foundation stiffness (K_j) and dynamic modifiers α_j and β_j as follows:

$$k_j = \alpha_j K_j \qquad c_j = \beta_j \frac{K_j r}{V_s} \tag{2}$$

The terms α_j and β_j express the frequency dependence of the impedance, and are computed differently for surface (Veletsos and Verbic, 1975) and embedded (Bielak, 1975) foundations. Foundation radii are computed separately for translational and rotational deformation modes to match the area (A_f) and moment of inertia (I_f) of the actual foundation (i.e. $r_u = \sqrt{A_f/\pi}$, $r_\theta = \sqrt[4]{4I_f/\pi}$). The Bielak formulation includes a rigorous model of dynamic basement wall-soil interaction, assuming perfect wall-soil bonding. An approximate analysis of embedment effects can be made with the Veletsos and Nair model by increasing the static stiffness according to the well known guidelines of Kausel (1974), and using α_j and β_j terms for surface foundations (Elsabee and Moray, 1977).

Stewart et al. (1998) outlined several considerations associated with the application of these procedures to realistic foundation and soil conditions. These can be summarized as follows:

1. *Representation of nonlinear soil response and nonuniform soil profiles as a visco-elastic halfspace.* Strain dependent soil properties are evaluated with site response analyses which are used to calculate an equivalent hysteretic damping ratio and a degraded shear wave velocity profile. The effective profile velocity is taken as the profile depth divided by the shear wave travel time through the degraded profile. Profile depth is taken as r_u.
2. *Representation of non-circular foundations.* While noncircular foundations with aspect ratios < 4:1 can generally be represented as equivalent disks (Roesset, 1980), radiation dashpot coefficients for rocking can be underestimated by such procedures (Dobry and Gazetas, 1986). Correction factors can be adapted from the Dobry and Gazetas results.
3. *Representation of flexible foundations.* The impedance of flexible base mats with thin perimeter walls or rigid concentric interior and perimeter walls can be reasonable well represented by rigid foundation models (Liou and Huang, 1994; Riggs and Waas, 1985). However, the rigid disk model is inadequate for buildings with rigid central cores, and should be modified according to the results of Iguchi and Luco (1982).

The basic procedures for rigid disk foundations on or in halfspaces were modified according to (1) to (3) above, and are subsequently referred to as the "modified Veletsos" (MV) and "modified Bielak" (MB) formulations.

Use of System Identification to Evaluate SSI Effects

The objective of system identification analyses is to evaluate the unknown properties of a system using a known input into, and output from, that system. For analyses of seismic structural

response, the "system" has an unknown flexibility that generates a known difference between pairs of input and output strong motion recordings. For example, as indicated in Fig. 3, parameters describing the fixed-base system are evaluated from input/output pairs that differ only by the structural deformation (u). Likewise, parameters describing the flexible base system are evaluated from strong motion pairs whose difference results from foundation flexibility in translation (u_f) and rocking (θ), as well as structural flexibility. A comparison of fixed- and flexible-base modal parameters provides a direct quantification of SSI effects.

There are two principal system identification procedures:

1. Nonparametric procedures evaluate complex-valued transmissibility functions from the input and output recordings without fitting an underlying model. These transmissibility functions represent an estimate of the ratio of output to input motion in the frequency domain, and are computed from smoothed power and cross-power spectral density functions of the input and output motions. Modal frequencies and damping ratios are estimated from peaks in the transmissibility function amplitude (Pandit, 1991; Ljung, 1987; Fenves and DesRoches, 1994).

2. Parametric procedures develop numerical models of transfer functions, which represent the ratio of output to input motion in the Laplace domain. The amplitude of the transfer function is a surface in the Laplace domain. The locations of peaks (or poles) on this surface can be related to modal frequencies and damping ratios. Parameters describing transfer function models are estimated by minimizing the error between the model output and recorded output in the discrete time domain using least squared techniques. The transfer function surface can be estimated by minimizing cumulative error for the entire time history (Safak, 1991), or by recursively minimizing error for each time step using a window of time immediately preceding that time step (Safak, 1988).

The evaluation of vibration frequencies and damping ratios from transmissibility functions can be problematic (especially for damping), because the shape of the functions is dependent on details associated with the computation of the spectral density functions such as the number of points in the Fast Fourier Transform and the windowing procedures used (Pandit, 1991). Parametric procedures provide a relatively rigorous modeling of system response, because the transfer function for a given set of time histories is only dependent on two user-defined parameters: the delay between the input and output and the number of modes used in the analyses (i.e. the order of the model). When these parameters are selected judiciously, the modal frequencies and damping ratios can be reliably evaluated for linear structures. Hence, parametric identification techniques were used here for the evaluation of modal vibration parameters. Further details on the identification procedures are provided in Stewart et al. (1998).

Evaluation of Modal Parameters for Various Base Fixity Conditions

Three cases of base fixity are of interest in analyses of SSI: (1) fixed-base, representing only the flexibility of the structure, (2) flexible-base, representing the combined flexibility of the complete soil-structure system, and (3) pseudo flexible-base, representing flexibility in the structure and rocking in the foundation. Pseudo flexible-base parameters are of interest because they can sometimes be used to approximate flexible-base parameters or to estimate either fixed- or flexible-base parameters.

Stewart et al. (1998) evaluated the types of input and output strong motion recordings that are necessary to evaluate fixed-, flexible- and pseudo flexible-base vibration parameters of structures with parametric identification procedures. While roof translations are always used as output, the input motions for various base fixity conditions vary as indicated in Fig. 3. Recordings of free-field, foundation, and roof level translations, as well as base rocking, are needed to evaluate directly both fixed- and flexible-base modal parameters of a structure.

Instrumented buildings often lack sensors for recording base rocking or free-field translations. For such cases either fixed-base parameters (missing base rocking) or flexible-base parameters (missing free-field translations) cannot be evaluated directly from system identification analyses. Stewart et al. (1998) derived expressions to estimate either flexible- or fixed-base parameters using "known" modal parameters for the two other cases of base fixity. The estimation procedures operate on the premise that differences between known parameters can be used to calibrate the foundation impedance at the structure's period; the calibrated impedance can then be used to estimate the unknown parameters. These estimation procedures extend significantly the number of sites for which SSI effects can be empirically evaluated.

DATABASE

Two classes of sites are used in this study: Class 'A' sites, which have a free-field accelerograph and a structure instrumented to record base and roof translations (and in some cases, base rocking as well), and Class 'B' sites, which have structures instrumented to record base rocking as well as base and roof translations, but have no free-field accelerographs. This section presents criteria employed for the selection of 'A' sites. The 'B' sites are simply those with the stated structural instrumentation.

Each 'A' site was reviewed for the following: (1) the free-field instrument is not so close to the structure as to be significantly affected by structural vibrations, and (2) the free-field instrument is not so far from the structure that free-field and foundation-level motions exhibit significant incoherence.

The check for contamination of free-field motion by structural vibrations is made by examining power spectral density and coherency functions for the free-field and foundation motions. High coherencies between the two motions at modal frequencies, or spectral peaks in free-field motions at modal frequencies, indicate potential contamination. Results for all sites considered in this study can be found in Stewart and Stewart (1997). Significant contamination of free-field data was only found at two sites, and in both cases arose from vibrations of structures other than the subject structure that were near the free-field seismograph.

The incoherence between foundation-level and free-field motions is assumed to follow the empirical models developed using data from the Lotung, Taiwan LSST array (Abrahamson et al., 1991) and SMART1 array (Abrahamson, 1988). A minimum coherency of 0.8 was enforced, yielding maximum free-field/structure separations of about 800 m for 1 Hz structures, 450 m for 2 Hz structures, and 150 m for 4 Hz structures.

Suitable free-field instruments were sought for virtually all instrumented structures in California, and 44 sites were identified (plus one additional structure in Taiwan). An additional 13 structures in California were considered in this study as 'B' sites. The 'A' and 'B' sites are listed in Table 1. For the 57 sites, 74 processed data sets are available as a result of multiple earthquake recordings at 13 sites.

Fifteen California earthquakes contributed data to this study with magnitudes ranging from 4.8 to 7.3. Moderate to low level shaking (pga < 0.1 to 0.2g) is well represented in the database (50 data sets), while a moderate amount of data (24 data sets) is available for more intense shaking (pga > 0.2g).

The foundation conditions at the sites include 23 buildings with piles or piers, and 34 with footings, mats, or grade beams. Most buildings are not embedded (36) or have shallow single-level basements (14). Only seven buildings have multi-level basements. The buildings range from single story warehouses to high-rise office buildings. Lateral force resisting systems include shear walls, frames, and base isolation.

EMPIRICAL EVALUATION OF INTERACTION EFFECTS

Comparison of Free-Field and Foundation-Level Structural Motions

A simple investigation of kinematic and inertial interaction effects can be made by comparing indices of free-field and foundation motions. Shown in Fig. 4 for free-field and foundation-level motions at 'A' sites are (a) peak horizontal accelerations and (b) 5%-damped spectral accelerations at the flexible-base period of the structure ($\tilde{T}$). The $\tilde{T}$ values were established from system identification analyses. Second order polynomials are fit to the data in Fig. 4 using linear regression.

The data in Fig. 4 indicate that peak foundation-level accelerations are de-amplified relative to the free-field, especially in embedded structures. Earlier studies utilizing smaller databases had similar findings (e.g. Poland et al., 1993). Conversely, spectral accelerations at $\tilde{T}$ for foundation motions are generally negligibly de-amplified for surface foundations (open circles in Fig. 4), and only modestly de-amplified for embedded foundations (solid dots in Fig. 4). These different de-amplification levels at different spectral periods can be attributed to frequency dependent kinematic de-amplification effects which are maximized at low periods (i.e. T=0), coupled with potential contributions of inertial interaction to foundation motions for periods near $\tilde{T}$. As it is the spectral acceleration at $\tilde{T}$ that best simply describes the ground motion controlling structural response, for design purposes, there appears to be little useful ground motion de-amplification on surface foundations relative to the free-field, and only modest de-amplification on most embedded foundations (average reduction of 20%). However, as indicated in Fig. 4(b), significant reductions on the order of 40% can occur in individual cases (typically deeply embedded foundations).

Although significant further study is needed to more fully evaluate kinematic interaction effects, the data in Fig. 4 suggest that for purposes of engineering design, free-field and foundation-level motions are often comparable in amplitude. Hence, a more significant SSI effect would appear to be the modification of structural response associated with the flexibility of foundation support. These inertial interaction effects are examined in the remainder of this paper through evaluations of period lengthening ratios and foundation damping factors.

Period Lengthening and Foundation Damping

System identification analyses were performed for the 57 sites considered in this study using procedures outlined in Stewart et al. (1998). Modal vibration periods and damping ratios were evaluated for the fixed-base (T,ζ) and flexible-base ($\tilde{T},\tilde{\zeta}$) cases. These parameters are listed in Table 1, along with the calculated period lengthening ratio $\tilde{T}/T$, foundation damping factor $\tilde{\zeta}_0 = \tilde{\zeta} - \zeta/(\tilde{T}/T)^3$, and dimensionless structure-to-soil stiffness ratio $1/\sigma = h/(V_S \cdot T)$, where h = effective structure height and V_S = effective soil shear wave velocity.

Each site was assigned a confidence level based on the quality of available geotechnical data and the accuracy/uncertainty associated with the identification. These confidence levels are indicated in Table 1, with "A" indicating acceptable confidence, "L" indicating low confidence, and "U" indicating unacceptable confidence. Unacceptable confidence is associated with one of the following situations:

- U1: Reliable flexible-base parameters could not be developed due to significant incoherence between foundation and free-field motions.
- U2: The structure was so stiff that the roof and foundation level motions were essentially identical, and hence the response could not be established by system identification.
- U3: Fixed-base ('A' sites) or flexible-base ('B' sites) parameters could neither be estimated nor obtained directly from system identification.
- U4: Reliable parametric models of structural response could not be developed for unknown reasons.

Presented in Fig. 5 are the variations of $\tilde{T}/T$ and $\tilde{\zeta}_0$ with $1/\sigma$ for sites where there is an "acceptable" or "low" confidence level in the modal parameters. Also shown are second-order polynomials fit to the acceptable confidence data by regression analysis, and analytical results by Veletsos and Nair (1975) for h/r = 1 and 2. Both $\tilde{T}/T$ and $\tilde{\zeta}_0$ are seen to increase with $1/\sigma$, and the best fit lines through the data are similar to the Veletsos and Nair curves.

There is significant scatter in the data in Fig. 5, although much of this results from systematic variations in $\tilde{T}/T$ and $\tilde{\zeta}_0$ associated with factors such as structure aspect ratio, embedment, foundation type, and foundation shape and flexibility effects. In addition, $\tilde{\zeta}_0$ is influenced by the hysteretic soil damping (β), which varies with soil type.

Results from several sites help to illustrate the strong influence of $1/\sigma$ on inertial interaction effects. The most significant inertial interaction occurred at site A46 ($\tilde{T}/T \approx 4$ and $\tilde{\zeta}_0 \approx 30\%$), which has a stiff ($T \approx 0.1$ sec) cylindrical concrete structure (h=14.3 m, r= 4.9 m) and relatively soft soils ($V_S \approx 85$ m/s), giving a large $1/\sigma$ of about 1.5. Conversely, the inertial interaction effects are negligible at site A21 ($\tilde{T}/T \approx 1$ and $\tilde{\zeta}_0 \approx 0\%$), which has a relatively flexible ($T \approx 0.8$-1.0 sec) base-isolated structure (h=6.7 m, r_u=21.6 m) that is founded on rock ($V_S \approx 300$ m/s), giving a much smaller $1/\sigma$ value of 0.02-0.03. These two sites represent the extremes of inertial interaction. More typical SSI effects occur at sites B14 ($\tilde{T}/T = 1.14$ and $\tilde{\zeta}_0 \approx 3.4\%$) and A1-tr ($\tilde{T}/T = 1.57$ and $\tilde{\zeta}_0 \approx 15.4\%$). The structures at both sites are shear wall buildings with periods of T = 0.49 and 0.15 sec, respectively, and are founded on medium-stiff soils (V_S = 256 and 213 m/s), combining to give $1/\sigma \approx 0.12$ at B14 and $1/\sigma \approx 0.29$ at A1-tr. The results from these four sites illustrate that both $\tilde{T}/T$ and $\tilde{\zeta}_0$ increase with increasing $1/\sigma$.

To examine the influence of parameters other than $1/\sigma$ on SSI effects, the data in Fig. 5 were sorted according to aspect ratio (h/r_θ), foundation type (piles or piers vs. shallow foundations), embedment ratio (e/r), and lateral force resisting system by Stewart et al. (1998). The trends

resulting from these regressions are relatively weak, as the influence of the respective parameters could not be readily isolated from each other given the limited scope of the database. Nonetheless, some dependence on aspect ratio was found, with larger period lengthening and smaller damping for structures with $h/r_\theta > 1$ than for structures with $h/r_\theta < 1$. This is consistent with trends from the analytical models. Well-defined trends in data sorted according to the other parameters were not identified.

CALIBRATION OF SIMPLIFIED ANALYSIS PROCEDURES FOR INERTIAL INTERACTION

Period lengthening ratios and foundation damping factors were evaluated by the Modified Veletsos (MV) procedure for each data set in Table 1. These factors were also evaluated by the Modified Bielak (MB) procedure for embedded structures.

Modified Veletsos (MV) Formulation

Deviations in MV predictions of $\tilde{T}/T$ and $\tilde{\zeta}_0$ relative to empirical values are shown in Fig. 6 for sites with acceptable and low confidence designations. Also plotted are best fit second-order polynomials established from regression analyses on data from acceptable confidence sites. For most sites, the predictions are accurate to within absolute errors of about ± 0.1 in $\tilde{T}/T$ and $\pm 3\%$ damping in $\tilde{\zeta}_0$ for $1/\sigma = 0$ to 0.4. The regression curves indicate no significant systematic bias in predictions of either $\tilde{T}/T$ or $\tilde{\zeta}_0$ up to $1/\sigma = 0.4$. However, there is a downward trend in the best fit curve for damping for $1/\sigma > 0.5$ (beyond the range on Fig. 6) due to a significant underprediction of $\tilde{\zeta}_0$ at site A46 ($1/\sigma = 1.5$) which results from a pronounced embedment effect at this site that is not fully captured by the MV formulation.

The results from several sites help illustrate the general findings of Fig. 6. The minimal inertial interaction effects at site A21 ($1/\sigma = 0.02$ to 0.03, $\tilde{T}/T \approx 1$ and $\tilde{\zeta}_0 \approx 0\%$) are well predicted by the MV analyses, as is typical for sites with $1/\sigma < 0.1$. The predictions are also generally satisfactory for sites with intermediate $1/\sigma$ values such as B14 and A1-tr ($1/\sigma = 0.12$, $1/\sigma = 0.29$). At these sites, period lengthenings of 1.14 and 1.57 are over- and under-predicted by absolute differences of about 0.11 and 0.06, respectively, while foundation damping factors of 3.4 and 15.4% are underpredicted by absolute differences of 2.3 and 4.8%, respectively. The large inertial interaction effects at site A46 ($1/\sigma = 1.5$, $\tilde{T}/T \approx 4.0$ and $\tilde{\zeta}_0 \approx 30\%$) are predicted to within an absolute difference of about 0.4 for period lengthening, but damping is underpredicted by an absolute difference of about 14%. With the exception of the damping

results at site A46 (where there is a significant embedment effect), these results indicate that predictions of $\tilde{T}/T$ and $\tilde{\zeta}_0$ by the MV procedure are reasonably good considering the breadth of conditions represented in the database.

There are several noteworthy outliers in Fig. 6. When the residuals in Fig. 6 are considered with respect to the magnitude of the observed SSI effect, the most significant outliers for period lengthening are seen to be site A34 and several long period structures (A4, B3). The unusual results at site A34 may be associated with erroneously high shear wave velocity measurements (Stewart et al., 1998). The long period structures at sites A4 and B3 are founded on soft Bay Mud soils in the San Francisco Bay Area, and were subject to negligible period lengthening (a common system identification result for all long-period structures). The soft soils at sites A4 and B3 lead to overpredictions of period lengthening, suggesting an error in the model. It appears from these data that the simple single-degree-of-freedom models on which the MV and MB formulations are based are incapable of adequately modeling SSI effects in long period structures with significant higher mode responses.

Effect of Embedment: Comparison of "Modified Veletsos" and "Modified Bielak" Predictions

Plotted in Fig. 7 are deviations between analytical and empirical results for three data sets, (1) MV predictions for buildings with surface foundations, (2) MV predictions for buildings with embedded foundations, and (3) MB predictions for buildings with embedded foundations. As before, the best fit curves are second-order polynomials established from regression analyses.

The regression curves in Fig. 7 indicate that $\tilde{T}/T$ is slightly over-predicted for embedded structures (by either MV or MB), and more accurately predicted for surface structures. The differences between MV and MB predictions are generally minor (e.g. absolute differences of about 0.02 at A20-tr, 0.02 at A23) for typical values of $1/\sigma$ (i.e. < 0.4). At site A46 ($1/\sigma = 1.5$), the absolute difference between the predictions is about 1.2, which is modest compared to the empirical value of $\tilde{T}/T \approx 4.0$.

The accuracy of $\tilde{\zeta}_0$ predictions by the MV methodology are comparable for surface and embedded structures. However, there are disparities between the MB and MV $\tilde{\zeta}_0$ predictions for embedded structures which increase with $1/\sigma$ (e.g. absolute differences of 0.7% at A23, $1/\sigma = 0.11$; 2.7% at A20-tr, $1/\sigma = 0.17$; 10% at A46, $1/\sigma = 1.5$). The regression curves are primarily controlled by the shallowly embedded foundations ($e/r < 0.5$), which are the most numerous in the database. For such cases, MV predictions are typically more accurate than MB predictions, as shown by the regression curves in Fig. 7, and as illustrated by sites A20 ($e/r = 0.27$) and A26

(e/r = 0.41). However, there are systematic errors in MV predictions for more deeply embedded foundations. These errors are not surprising because only the MB formulation incorporates dynamic basement wall/soil interaction effects into the foundation impedance function. As shown by individual labeled sites in Fig. 7, MV predictions of $\tilde{\zeta}_0$ are generally too low for relatively deeply embedded structures with continuous basement walls around the building perimeter such as A46 (e/r = 0.92) as well as A9, B12, and A16-L (e/r > 0.5). Other structures in the database with e/r > 0.5 had negligible foundation damping (i.e. $\tilde{\zeta}_0 < 1\%$) which was overestimated by both MV and MB predictions (i.e. A16-tr and B13). Hence, it appears that MB predictions of $\tilde{\zeta}_0$ are generally more accurate than MV predictions for structures with e/r > 0.5 and significant SSI effects. These differences are most pronounced at site A46, where the MB and MV predictions of $\tilde{\zeta}_0$=27 and 17% can be compared to the empirical value of 30%.

In summary, the accuracy of period lengthening predictions by the MV methodology are reasonably good for surface and shallowly embedded structures, and differences between the MV and MB predictions are generally minor for $1/\sigma$ values of common engineering interest ($1/\sigma <$ 0.4). Accuracies of MV damping predictions are generally acceptable for surface and shallowly embedded structures (e/r < 0.5). For deeper embedment (e/r > 0.5), MB damping predictions are generally more accurate. These results suggest that the dynamic basement-wall/soil interaction modeled by the MB procedure can be important for deeply embedded foundations.

Other Effects

The adequacy of the MV/MB analysis procedures to capture the influence of factors such as structural aspect ratio, foundation type, structure type, foundation shape, and foundation flexibility were investigated by Stewart et al. (1998). The influence of aspect ratio and structure type were adequately captured by the analyses.

Foundation type was found to have a minor influence on prediction accuracy, indicating that the shallow disk foundation models provided reasonable evaluations of SSI for many structures with pile or caisson foundations. However, many of the deep foundation sites for which this trend was established have fairly stiff surficial soils and no marked increase in stiffness across the depth of the foundation elements. For such cases, it is reasonable that dynamic foundation performance would be strongly influenced by the interaction of surface foundation elements (e.g. pile caps, base mats, footings) with soil. Conversely, for several sites with pile foundations and soft soils, the shallow foundation models were found to underpredict foundation damping.

Foundation shape effects were generally found to be minor for the structures in the database. That is, the exclusion of correction factors by Dobry and Gazetas (1986) for shape effects did not adversely effect the accuracy of damping predictions. Foundation flexibility effects were found

to be significant for the only structure in the database with a stiff central core of shear walls and a integral connection between the foundation for the walls the foundation for the remainder of the structure. For this site (B2), corrections to the impedance function adapted from the results of Iguchi and Luco (1982) substantially improved predictions of period lengthening.

CONCLUSIONS AND RECOMMENDATIONS

Summary of Findings

Available strong motion data suggests that foundation-level and free-field spectral accelerations at the period of principal interest in structural design (i.e. the first-mode flexible-base period, $\tilde{T}$) are similar for structures with surface foundations, and that foundation-level spectral accelerations are generally only modestly de-amplified (averaging about 20%) for embedded foundations. Since the free-field and foundation level ground motions therefore appear to be comparable, this study has focused principally on evaluating the effects of inertial interaction on structural response.

Inertial interaction effects for buildings are expressed in terms of the lengthening of first-mode period ($\tilde{T}/T$) and the damping associated with soil-foundation interaction ($\tilde{\zeta}_0$). Simplified analytical procedures for predicting $\tilde{T}/T$ and $\tilde{\zeta}_0$ include Modified Veletsos (MV) and Modified Bielak (MB) approaches that can be adapted for a wide range of conditions.

Based on the database of 57 sites compiled for this study, the factor with the greatest influence on $\tilde{T}/T$ and $\tilde{\zeta}_0$ is the ratio of structure-to-soil stiffness as quantified by the parameter $1/\sigma = h/(V_S \cdot T)$. When $1/\sigma$ is nearly zero, $\tilde{T}/T$ and $\tilde{\zeta}_0$ values are about unity and zero, respectively, whereas at the maximum observed value of $1/\sigma = 1.5$ at site A46, interaction effects dominated the structural response ($\tilde{T}/T \approx 4$ and $\tilde{\zeta}_0 \approx 30\%$). Additional factors which can significantly affect inertial interaction include the structure's aspect ratio (h/r_θ) and foundation embedment and flexibility. For the majority of sites in the database, other factors such as the type of structural lateral force resisting system as well as foundation type and shape, were found to have a relatively small influence on SSI.

Recommendations

Inertial SSI effects can be expressed by a period lengthening ratio ($\tilde{T}/T$) and foundation damping factor ($\tilde{\zeta}_0$). These factors are used to estimate flexible-base fundamental-mode parameters, which in turn are used in response spectrum based approaches for evaluating base

shear forces and deformations in structures (e.g. Fig. 2). A key finding of this research is that these inertial interaction effects can generally be reliably predicted by the MV analysis procedure. However, several caveats apply to this basic recommendation:

1. Inertial interaction effects were generally observed to be small for $1/\sigma < 0.1$ (i.e. $\tilde{T}/T < 1.1$ and $\tilde{\zeta}_0 < 4\%$), and for practical purposes could be neglected in such cases.
2. For structures with embedment ratios greater than 0.5, the MB methodology should be used in lieu of MV to appropriately model the extra radiation damping contributed by dynamic soil/basement-wall interaction.
3. Damping results for pile supported structures on soft foundation soils ($V_S < 500$ fps) should be interpreted with caution, as the damping is likely to exceed the values predicted from simplified analyses (which assume shallow foundations) due to soil-pile interaction effects.
4. Period lengthening for long-period ($T > 2$ sec.) structures with significant higher-mode responses is negligible and can be neglected.
5. Corrections to rocking damping values for foundation shape effects are generally small and can be neglected without introducing significant errors.

ACKNOWLEDGMENTS

Support for this project was provided by the U.S. Geological Survey, Department of the Interior (USGS award number 1434-HQ-97-GR-02995) and the National Science Foundation. The views and conclusions contained in this document are those of the authors and should not be interpreted as necessarily representing the official policies, either expressed or implied, of the U.S. Government.

REFERENCES

Abrahamson, N.A. (1988). "Empirical models of spatial coherency of strong ground motion," *Proc. 2nd Workshop on Strong Motion Arrays*, Taipei, Taiwan, 65-92.

Abrahamson, N.A., Schneider, J.F., and Stepp, J.C. (1991). "Empirical spatial coherency functions for application to soil-structure interaction analyses," *Eq. Spectra*, EERI, 7(1),1-27

Bechtel Power Corporation (1991). "A synthesis of predictions and correlation studies of the Lotung soil-structure interaction experiment," *Rpt. No. EPRI NP-7307-M*, EPRI, October.

Bielak, J. (1975). "Dynamic behavior of structures with embedded foundations," *J. Eq. Engrg. Struct. Dynamics*, 3(3), 259-274.

Borja, R.I., Smith, H.A., Wu, W-H., and Amies, A.P. (1992). "A methodology for nonlinear soil-structure interaction effects using time-domain analysis techniques," *Rpt. No. 101*, Blume Earthquake Engrg. Ctr., Stanford Univ., June.

Building Seismic Safety Council, BSSC (1995). "NEHRP Recommended provisions for seismic regulations for new buildings, Part 1, Provisions and Part 2, Commentary" *Rpt. No. FEMA 222A*, Federal Emergency Management Agency, Washington D.C.

Dobry, R. and Gazetas, G (1986). "Dynamic response of arbitrarily shaped foundations," *J. Geotech. Engrg.*, ASCE, 112(2), 109-135.

Elsabee, F. and Morray, J.P. (1977). "Dynamic behavior of embedded foundations," *Rpt. No. R77-33*, Dept. of Civil Engrg., Massachusetts Inst. Technology.

Fenves, G.L. and DesRoches, R. (1994). "Response of the northwest connector in the Landers and Big Bear Earthquakes," *Rpt No. UCB/EERC-94/12*, Earthquake Engrg Research Ctr., Univ. of California.

Iguchi, M. and Luco, J.E. (1982). "Vibration of flexible plate on viscoelastic medium," *J. Engrg. Mech.*, ASCE, 108(6), 1103-1120.

Kausel, E. (1974). "Forced vibrations of circular foundations on layered media," *Rpt. No. R74-11*, Dept. of Civil Engrg., Massachusetts Inst. Technology.

Liou, G.-S. and Huang, P.-H. (1994). "Effect of flexibility on impedance functions for circular foundations," *J. Engrg. Mech.*, ASCE, 120(7), 1429-1446.

Ljung, L. (1995). *System Identification Toolbox, Users Guide*, The Math Works, Inc.

Pandit, S.M. (1991). *Modal and Spectrum Analysis*, John Wiley, New York, NY.

Poland, C.D., Soulages, J.R., Sun, J., and Mejia, L.H. (1994). "Quantifying the effect of soil-structure interaction for use in building design," *SMIP-93, Seminar on Seism. & Engrg. Aspects of Recent Strong Motion Data*, CDMG, 43-54.

Roesset, J.M. (1980). "A review of soil-structure interaction," *in* Soil-structure interaction: the status of current analysis methods and research, J.J. Johnson, ed., *Rpt. No. NUREG/CR-1780 and UCRL-53011*, U.S. Nuclear Regulatory Com. and Lawrence Livermore Lab.

Riggs, H.R. and Waas, G. (1985). "Influence of foundation flexibility on soil-structure interaction," *J. Eq. Engrg. Struct. Dynamics*, 13(5), 597-615.

Safak, E. (1988). "Analysis of recordings in structural engineering: adaptive filtering, prediction, and control," *Open File Rpt. 88-647*, U.S. Geological Survey, October.

Safak, E. (1991). "Identification of linear structures using discrete-time filters," *J. Struct. Engrg.*, ASCE, 117(10), 3064-3085.

Stewart, J.P., Seed, R.B., and Fenves, G.L. (1998). "Empirical evaluation of soil-structure interaction effects," *Rpt. No. PEER-98/??*, Pacific Earthquake Engineering Research Center, Richmond, CA (in press).

Stewart, J.P. and Stewart, A.F. (1997). "Analysis of soil-structure interaction effects on building response from earthquake strong motion recordings at 58 sites," *Rpt. No. UCB/EERC 97/01*, Earthquake Engineering Research Ctr., Univ. of California.

Valera, J.E., Seed, H.B., Tsai, C.F., and Lysmer, J. (1977). "Soil structure interaction effects at the Humboldt Bay Power Plant in the Ferndale Earthquake of June 7, 1975," *Rpt. No. UCB/EERC 77/02*, Earthquake Engrg. Research Ctr., Univ. of California, Berkeley.

Veletsos, A.S. and Nair V.V. (1975). "Seismic interaction of structures on hysteretic foundations," *J. Struct. Engrg.*, ASCE 101(1), 109-129.

Veletsos, A.S. and Verbic, B. (1973). "Vibration of viscoelastic foundations," *J. Eq. Engrg. Struct. Dynamics*, 2(1), 87-102.

Table 1: Compilation of first-mode parameters for 'A' and 'B' sites

Site	Station	Eqk.	MHA (g)	h (ft)	e (ft)	Vs (fps)	β(%)	Transverse									Longitudinal									Conf.
								r_u (ft.)	r_θ (ft.)	$\tilde{T}$ (sec.)	T (sec.)	$\tilde{\zeta}$ (%)	ζ (%)	$\frac{1}{\sigma}$	$\tilde{T}/T$	$\tilde{\zeta}_0$	r_u (ft.)	r_θ (ft.)	$\tilde{T}$ (sec.)	T (sec.)	$\tilde{\zeta}$ (%)	ζ (%)	$\frac{1}{\sigma}$	$\tilde{T}/T$	$\tilde{\zeta}_0$	
'A' Sites																										
1	Eureka Apts.	PT	0.18	31	0	701	5.1	57	42	0.24	0.15	19.6	15.9	0.29	1.57	15.4	57	77	0.25	0.22	12.8	5.5	0.20	1.09	8.6	A
2	Fortuna Market	PT	0.12	22	0	772	5.6	115	112	0.37	0.36	34.0	26.0	0.08	1.04	11.2	115	122	0.31	0.29	39.4	18.0	0.10	1.08	25.1	L
		PTA	0.19			786	5.8			0.35	0.34	17.2	15.0	0.08	1.05	4.1			0.29	0.28	25.6	17.6	0.10	1.03	9.6	L
4	Emeryville PPP	LP	0.25	218	0	448	6.8	87	94	2.50	2.45	13.0	7.4	0.20	1.02	6.1	87	94	2.58	2.65	12.6	5.9	0.18	1.00	8.9	A
5	Hayward City Hall	LP	0.05	84	0	2210	0.8	66	54	1.16	1.11	3.6	3.5	0.03	1.04	0.7	66	82	0.87	0.85	3.2	4.2	0.04	1.03	0.0	A
6	Hayward 13-St.	LP	0.09	141	0			63	64	U3	U3	U3	U3	U3	U3	U3	63	64	U3	U3	U3	U3	U3	U3	U3	
7	Hollister 1-St.	LP	0.36	30	0	502	7.7	97	75	0.73	0.71	26.9	19.0	0.08	1.03	9.3	97	130	U2	U2	U2	U2	U2	U2	U2	A
8	Piedmont Jr. HS	LP	0.08	25	0	1820	1.3	52	46	0.18	0.16	4.8	2.2	0.09	1.16	3.4	52	59	0.17	0.17	7.0	5.1	0.08	1.00	2.0	A
9	PVPP	CGA	0.21	48	32	970	3.2	53	37	0.53	0.53	8.2	5.2	0.09	1.00	3.0	53	77	U2	U2	U2	U2	U2	U2	U2	L
10	Richmond CH	LP	0.13	33	10	768	3.7	75	54	0.30	0.28	9.2	3.9	0.16	1.08	6.1	75	106	0.27	0.26	14.4	1.4	0.16	1.03	13.1	A
11	San Jose 3-St.	LP	0.27	35	0	2642	0.9	86	68	0.64	0.67	20.6	24.8	0.02	1.00	0.0	86	111	0.80	0.66	20.3	23.6	0.02	1.00	0.0	A
12	El Centro Bldg.	IMP	0.24	54	0	484	6.6	61	55	0.74	0.50	16.0	23.4	0.23	1.47	8.8	61	69	1.23	1.25	33.9	36.6	0.09	1.00	0.0	A
13	Indio 4-St.	LD	0.09	56	15.5	695	4.1	69	58	0.71	0.67	10.3	7.5	0.12	1.05	3.8	69	85	0.66	0.64	10.9	10.9	0.13	1.03	1.0	A
14	Lancaster 3-St.	WT	0.07	26	0	908	2.1	54	47	0.20	0.20	13.4	12.4	0.14	1.00	1.1	54	63	U2	U2	U2	U2	U2	U2	U2	A
15	Lancaster 5-St.	NR	0.07	40	0	1001	2.5	99	83	0.73	0.69	10.0	7.5	0.06	1.06	3.6	99	121	0.72	0.71	8.2	9.1	0.06	1.02	0.0	A
16	Lancaster Airfield	NR	0.08	45	6	953	1.7	11.9	11.9	0.34	0.27	9.9	24.5	0.18	1.28	0.0	11.9	11.9	0.33	0.24	8.9	13.6	0.20	1.34	3.3	L
17	Loma Linda VA	NR	0.06	50	0	1415	3.4	246	248	0.29	0.25	15.0	5.8	0.14	1.17	11.3	246	250	0.32	0.29	10.1	5.6	0.12	1.09	5.7	A
18	Long Beach 7-St.	WT	0.07	58	0	615	3.5	49	46	U3	U3	U3	U3	U3	U3	U3	49	53	1.12	1.14	5.5	6.5	0.08	1.00	0.0	A
20	Long Beach VA	NR	0.07	98	23	1143	2.9	84	83	0.58	0.51	3.1	4.6	0.17	1.13	0.0	84	87	0.58	0.55	4.5	4.1	0.16	1.05	1.0	A
21	LA 2-St. FCCB	SM	0.11	22	0	1006	1.3	71	59	0.79	0.79	9.4	13.3	0.03	1.01	0.0	71	88	0.79	0.82	21.5	17.7	0.03	1.00	3.9	L
		LD	0.05			1010	1.2			0.97	0.98	14.2	14.9	0.02	1.00	0.0			0.90	0.90	18.4	18.9	0.02	1.00	0.0	L
		NR	0.32			981	1.7			0.92	0.95	34.4	40.1	0.02	1.00	0.0			0.83	0.84	33.4	39.5	0.03	1.00	0.0	L
22	LA 3-St. Bldg.	NR	0.28	46	22.5	980	5.9	130	128	U1	U1	U1	U1	U1	U1	U1	130	134	U1	U1	U1	U1	U1	U1	U1	L
23	LA 6-St. Bldg.	NR	0.25	56	14	630	5.2	21.4	20.6	0.89	0.82	5.5	6.9	0.11	1.08	0.0	21.4	22.7	U3	U3	U3	U3	U3	U3	U3	A
24	LA 6-St. Garage	NR	0.22	40	0	870 (tr) 640 (L)	7.3 (tr) 6.2 (L)	159	154	0.52	0.51	6.6	6.1	0.09	1.04	1.1	54	47	0.44	0.28	6.1	6.5	0.23	1.60	4.5	A
25	LA 7-St. Hos.	LD	0.04	68	0	1148	1.2	110	110	1.14	1.18	11.6	12.1	0.05	1.00	0.0	110	110	1.09	1.11	10.1	13.1	0.05	1.00	0.0	A
		NR	0.49			1065	2.5			1.19	1.27	27.1	29.3	0.05	1.00	0.0			1.21	1.19	21.1	28.0	0.05	1.01	0.0	A
26	LA 7-St. Bldg.	NR	0.47	66	13.5	548	7.6	33	30	0.66	0.63	9.2	16.1	0.19	1.04	0.0	33	37	1.04	1.09	7.0	11.5	0.11	1.00	0.0	L
27	LA 15-St. Bldg.	LD	0.03	174	0	1161	1.2	131	110	3.15	3.20	3.9	3.0	0.05	1.00	1.0	131	161	3.09	3.10	2.1	1.8	0.05	1.00	0.3	A
		NR	0.19			1120	2.0			3.12	3.20	8.5	2.8	0.05	1.00	5.6			3.07	3.09	8.8	2.0	0.05	1.00	6.8	A
28	LA 19-St. Bldg.	NR	0.28	220	38	980	5.9	92	76	3.24	3.45	U1	U1	0.07	1.00	U1	92	113	3.72	3.89	U1	U1	0.06	1.00	U1	A
29	LA Hollywood SB	WT	0.21	96	9	930	2.8	59	42	1.80	1.77	9.1	5.4	0.06	1.01	3.9	59	86	U4	U4	U4	U4	U4	U4	U4	L
		NR	0.39			879	4.4			2.10	2.05	18.3	15.4	0.05	1.02	3.9			0.80	0.75	8.0	8.5	0.15	1.06	0.9	L
30	LA Wadsworth	NR	0.25	78	17	981	6.3	189	199	1.00	0.92	9.3	9.3	0.09	1.08	1.9	189	199	U3	U3	U3	U3	U3	U3	U3	A
31	Newport Beach	LD	0.04	94	0	1009	2.3	61	52	0.84	0.70	4.7	2.9	0.13	1.19	3.0	61	74								A
		NR	0.11			969	3.2			0.86	0.75	3.2	8.5	0.13	1.16	0.0			0.77	0.67	3.9	4.4	0.14	1.14	0.9	A
32	Norwalk 12400	WT	0.23	70	13.5	730	6.8	93	83	U3	U3	U3	U3	U3	U3	U3	93	106	1.48	1.54	9.6	8.5	0.06	1.00	1.1	A

33	Norwalk 12440	WT	0.23	72	15	794	7.3	142	105	1.32	1.32	2.0	1.8	0.07	1.00	0.2	142	195	1.20	1.22	3.5	3.0	0.07	1.00	0.5	A
		NR	0.08			906	4.0			1.28	1.30	6.3	4.9	0.06	1.00	1.4			1.20	1.22	4.6	3.4	0.07	1.00	1.2	A
34	Palmdale 4-St.	NR	0.08	24	0	1575	1.7	69	49	0.20	0.12	18.5	24.1	0.12	1.66	13.1	69	100	0.20	0.16	12.4	4.9	0.09	1.22	9.7	A
35	Pomona 2-St.	WT	0.06	28	10.5	1246	1.6	59	57	0.26	0.25	8.7	5.5	0.09	1.02	3.6	59	63	0.27	0.26	5.8	8.6	0.09	1.02	0.0	A
		UP	0.21			1178	3.2			0.29	0.29	9.2	4.9	0.08	1.01	4.4			0.30	0.30	11.2	12.1	0.08	1.00	0.0	A
36	Pomona 6-St.	UP	0.21	53	12.5	1148	3.1	50	43	U1	U1	U1	U1	U1	U1	U1	50	59	U1	U1	U1	U1	U1	U1	U1	L
		LD	0.07			1188	2.2			1.26	1.07	9.3	13.4	0.04	1.17	1.0			1.20	0.87	9.8	9.5	0.05	1.39	6.2	L
37	Rancho Cuc. LJC	RD	0.04	56	14	1172	1.4	120	87	0.60	0.59	4.3	3.7	0.08	1.03	0.9	120	170	0.60	0.60	5.6	4.2	0.08	1.00	1.4	A
		WT	0.06			1157	1.7			0.65	0.63	4.4	5.0	0.08	1.02	0.0			0.66	0.65	8.4	6.1	0.07	1.01	2.5	A
		UP	0.24			1060	4.5			0.76	0.77	4.7	7.8	0.07	1.00	0.0			0.75	0.77	6.0	6.7	0.07	1.00	0.0	A
		LD	0.11			1039	4.4			0.87	0.85	11.2	12.5	0.06	1.01	0.0			0.89	0.87	17.2	17.4	0.06	1.02	0.9	A
		NR	0.07			1114	2.8			0.76	0.75	4.6	6.9	0.07	1.02	0.0			0.81	0.79	7.5	8.9	0.06	1.02	0.0	A
38	San Bern. 3-St.	LD	0.09	29	0	883	3.8	78	77	0.56	0.52	6.2	7.2	0.06	1.07	0.4	78	80	0.57	0.55	7.6	10.9	0.06	1.03	0.0	L
39	San Bern. 5-St.	NR	0.07	52	13	1233	2.6	95	86	0.63	0.65	9.1	5.2	0.06	1.00	3.9	95	107	0.50	0.51	7.5	6.2	0.08	1.00	1.3	L
40	San Bern. 9-St.	LD	0.10	74	0	848	3.4	55	52	2.01	2.01	5.0	6.8	0.04	1.00	0.0	55	59	2.05	2.08	7.4	6.0	0.04	1.00	1.3	A
41	San Bern. CGC	NR	0.04	38	0	1011	2.4	114	114	0.51	0.51	2.6	3.4	0.07	1.01	0.0	114	114	0.93	0.91	4.5	4.0	0.04	1.02	0.7	A
42	Santa Susana	NR	0.28	91	0	4460	1.0	23.5	20.5	0.54	0.53	19.1	15.1	0.04	1.02	4.9	23.5	27.6	0.54	0.55	11.4	8.3	0.04	1.00	3.1	L
43	Seal Beach 8-St.	LD	0.05	83	16	933	2.6	103	90	1.28	1.26	11.5	13.2	0.07	1.02	0.0	103	121	1.16	1.12	13.7	16.2	0.08	1.04	0.0	A
		NR	0.08			911	3.3			1.21	1.18	6.6	7.1	0.08	1.03	0.0			1.09	1.06	9.1	8.7	0.09	1.03	1.1	A
44	Sylmar Hos.	WT	0.05	63	0	1506	1.9	126	132	0.30	0.27	9.1	9.9	0.16	1.10	1.7	126	132	0.29	0.25	9.5	8.6	0.17	1.17	4.1	A
		NR	0.84			1119	9.1			0.38	0.37	18.9	19.4	0.15	1.04	1.7			0.34	0.26	23.4	17.5	0.21	1.29	15.2	A
45	Ventura 12-St.	NR	0.06	69	0	886	2.8	62	47	0.71	0.53	4.0	5.7	0.15	1.34	1.6	62	83								A
46	Lotung Reactor	L07	0.11	47	15	275	9.7	16.3	18.3	0.49	0.12	30.6	3.0	1.45	4.14	30.6	16.3	16.3	0.45	0.11	31.0	3.0	1.54	4.01	31.0	A
'B' Sites																											
1	Milpitas 2-St.	LP	0.14	26	0	649	4.1	6.4	10.9	0.25	0.24	15.3	21.9	0.17	1.06	0.0										A
2	San Bruno 9-St.	LP	0.11	66	0	916	3.6	72	59	1.10	0.97	12.5	11.4	0.07	1.13	4.7										A
3	San Fran. 47-St.	LP	0.16	414	27	478	4.3	86	80	5.16	5.03	U4	U4	0.17	1.03	U4										A
4	San Fran. Trans.	LP	0.12	475	51	801	5.9	98	99	U3	U3	U3	U3	U3	U3	U3										A
5	San Jose 10-St.	LP	0.12	61	0	768	4.1	65	49	0.48	0.29	6.7	18.6	0.27	1.64	2.5										A
6	San Jose 13-St.	LP	0.10	109	13.5	725	3.5	83	84	2.16	2.13	1.0	1.3	0.07	1.01	0.0	83	84	2.19	2.17	2.8	2.2	0.07	1.01	0.6	A
7	Walnut Crk 10-St	LP	0.10	89	14	1405	1.2	32	26	0.77	0.66	6.6	13.3	0.10	1.17	0.0										A
9	El Segundo 14-St.	NR	0.13	114	0	899	4.1	69	64	U3	U3	U3	U3	U3	U3	U3										A
10	LA 9-St.	NR	0.16	89	13	878	3.7	50	38	1.25	1.25	10.3	7.8	0.08	1.00	2.5	65	67	1.06	1.04	11.5	13.0	0.10	1.03	0.0	A
11	LA 17-St.	LD	0.04	91	0	1190	0.9	76	35.2	0.96	0.85	4.1	3.4	0.09	1.13	1.7										A
		NR	0.26			1140	1.4			1.05	0.90	4.9	3.9	0.09	1.17	2.5										A
12	LA 32-St.	NR	0.11	300	54	1339	1.2	93	91	1.94	1.84	7.6	7.1	0.12	1.06	1.7	93	97	U3	U3	U3	U3	U3	U3	U3	A
13	LA 54-St.	NR	0.14	414	57.5	1317	3.4	96	87	5.81	5.70	7.7	15.0	0.06	1.02	0.0										A
14	Whittier 8-St.	NR	0.17	48	0	842	3.2	64	28.5	0.56	0.49	12.1	12.9	0.12	1.14	3.4										A

h= effective structure height ≈ 0.7 · full height

e= embedment depth

Vs= soil shear wave velocity

β = soil hysteretic damping

Vs and β evaluated from soil profiles in Stewart (1997)

U1-U4 denote unacceptably low confidence results that are unreported

A, L denote acceptable and low confidence in results, respectively

blank entries = insuffiencient strong motion data to evaluate modal parameters

r_u, r_θ =foundation radii matching area and moment of inertia of actual foundation

$1/\sigma = h / (V_s \cdot T)$

* Lateral force resisting systems:
SW = shear wall, masonry or conc.
DWF = dual wall/frame system
CF = concrete frame
SF = steel frame
BI = base isolated

Earthquakes: CGA=Coalinga Aftershock, IMP=Imperial Valley, LD=Landers, LP=Loma Prieta, L07=Lotung Event 7, NR=Northridge, PT=Petrolia, PTA=Petrolia Aftershock, RD=Redlands, SM=Sierra Madre, UP=Upland, WT=Whittier

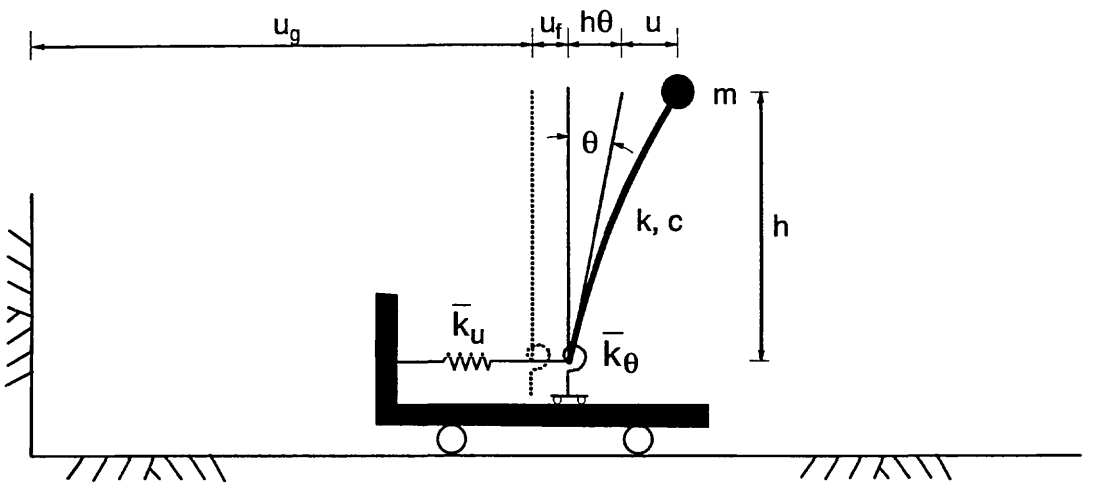

Fig. 1: Simplified model for analysis of inertial interaction

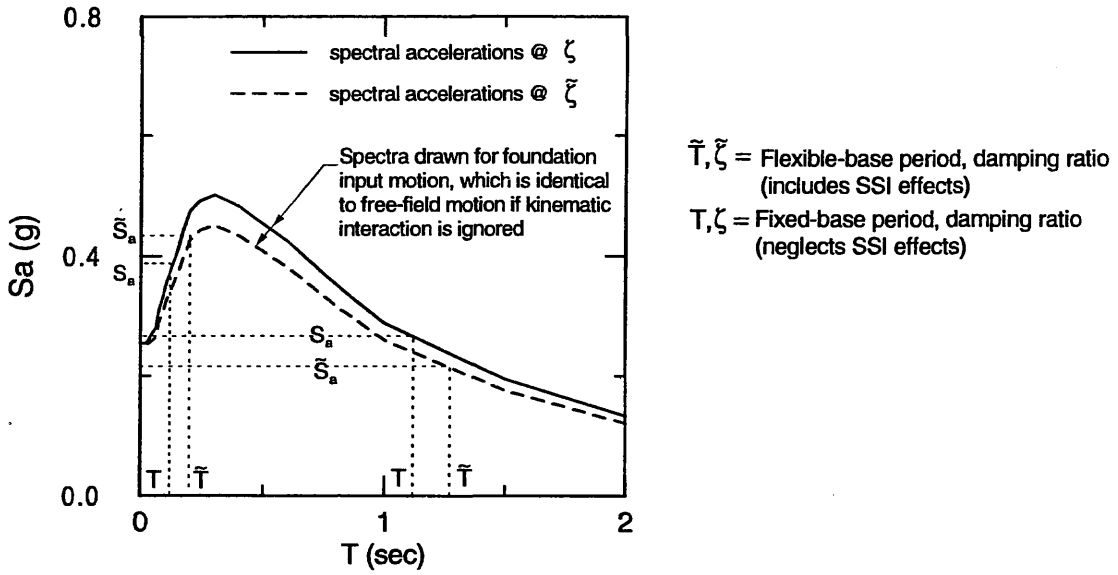

Fig. 2: Schematic showing effects of period lengthening and foundation damping on design spectral acceleration using smoothed spectral shape. Sa can increase or decrease due to SSI.

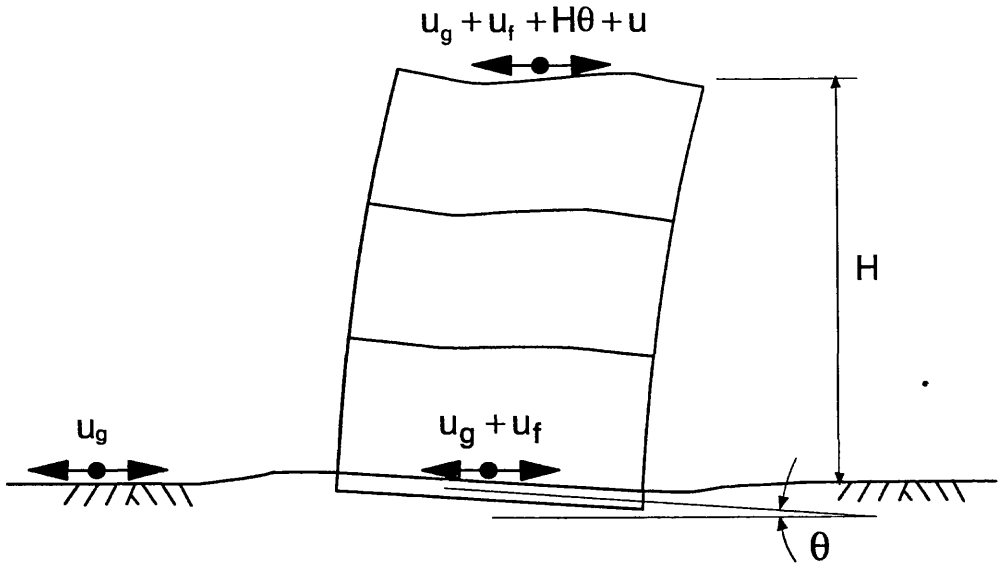

	Input	Output
Flexible-Base	u_g	$u_g + u_f + H\theta + u$
Pseudo Flexible-Base	$u_g + u_f$	$u_g + u_f + H\theta + u$
Fixed-Base	$u_g + u_f + H\theta$	$u_g + u_f + H\theta + u$

Fig. 3: Motions used as inputs and outputs for system identification of structures

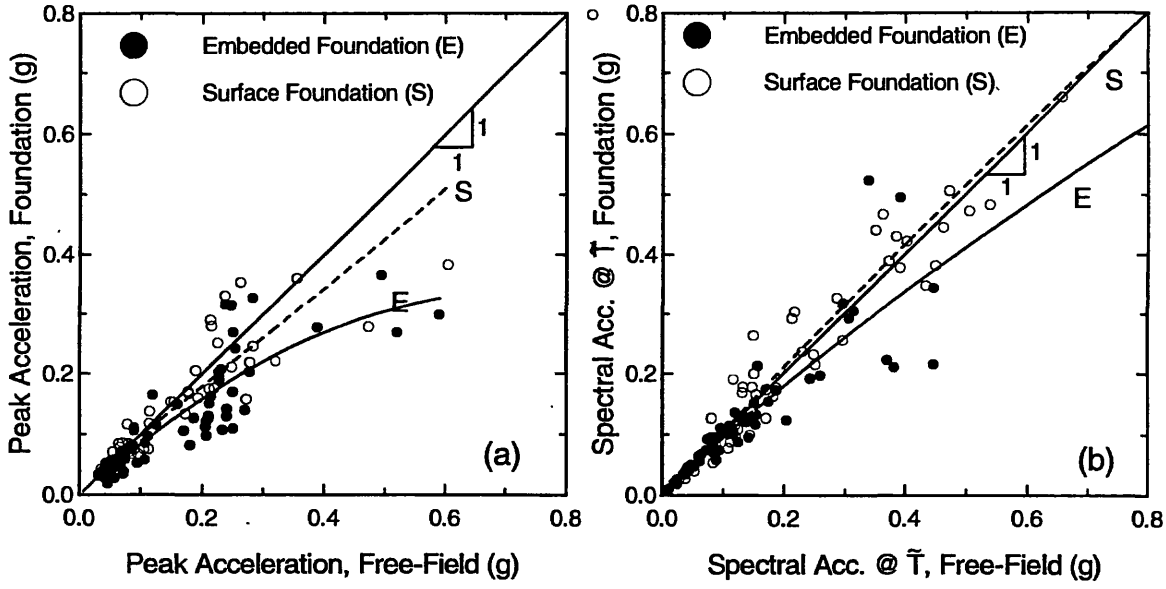

Fig. 4: Comparison of free-field and foundation-level structural motions: (a) peak acceleration data, and (b) 5%-damped spectral accelerations at $\tilde{T}$

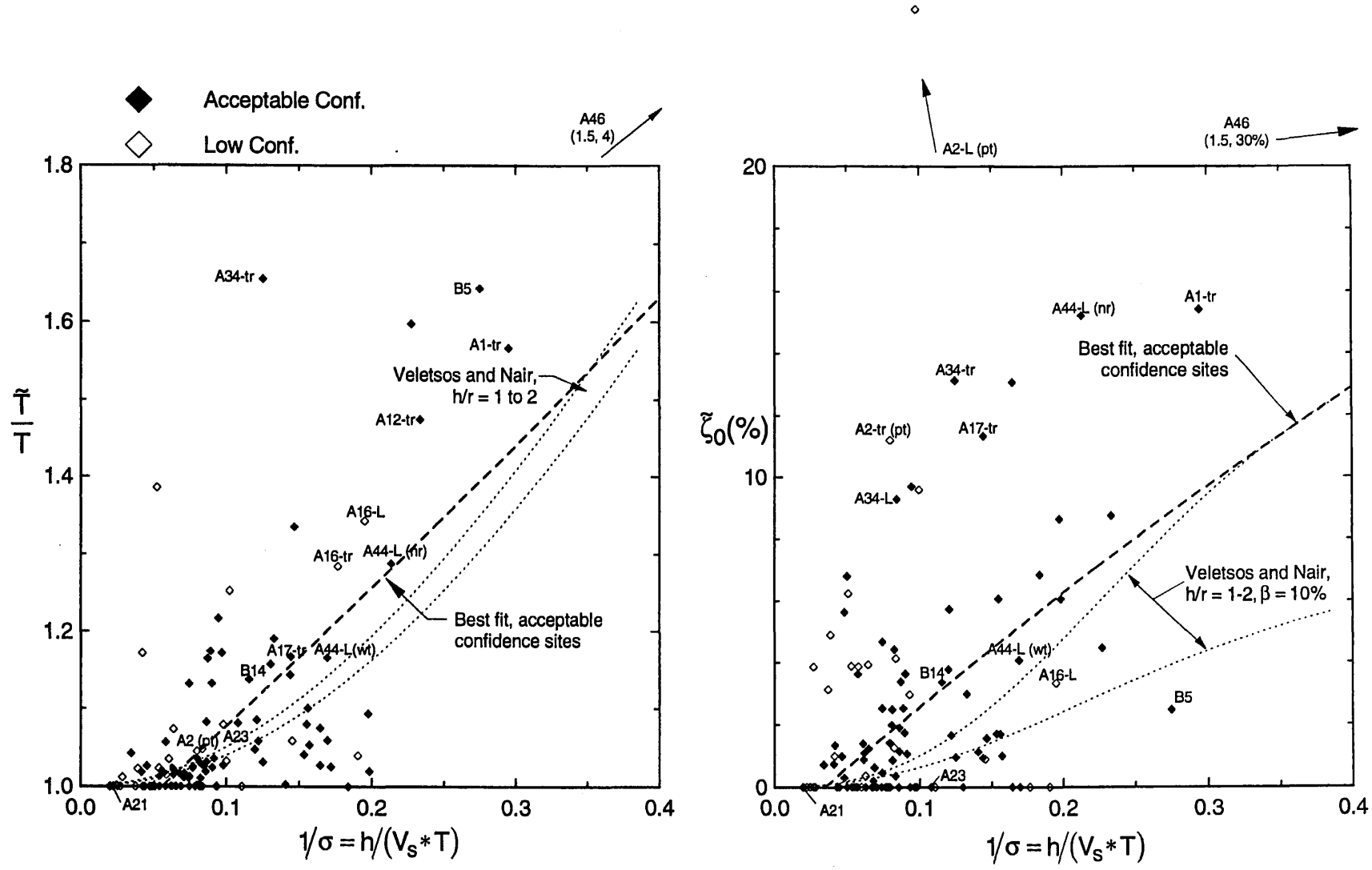

Fig. 5: Period lengthening ratio and foundation damping factor for sites sorted by confidence level, and analytical results from Veletsos and Nair (1975). (tr=transverse, L=longitudinal direction)

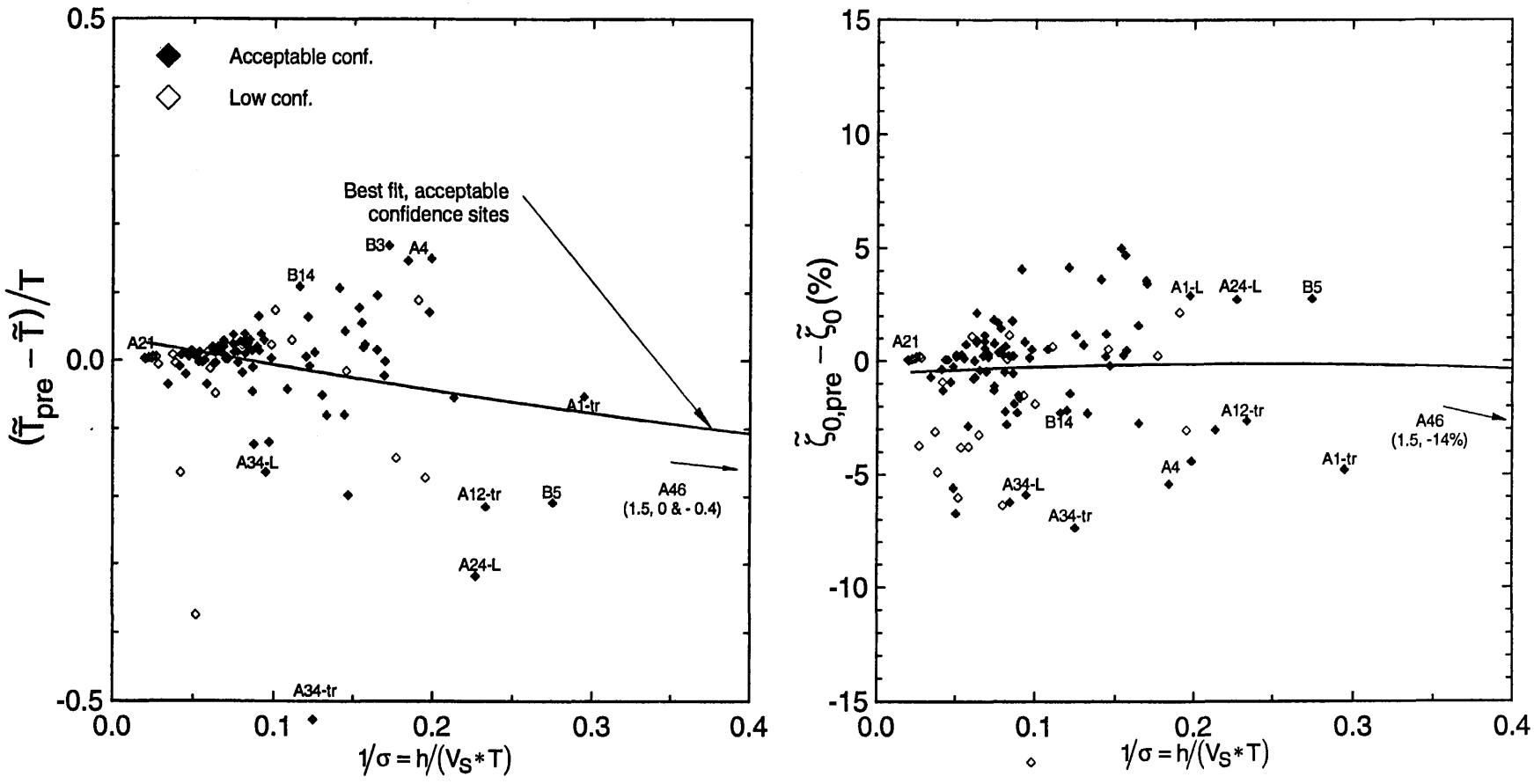

Fig. 6: Errors in "modified Veletsos" formulation for sites sorted by confidence level (tr=transverse, L=longitudinal direction)

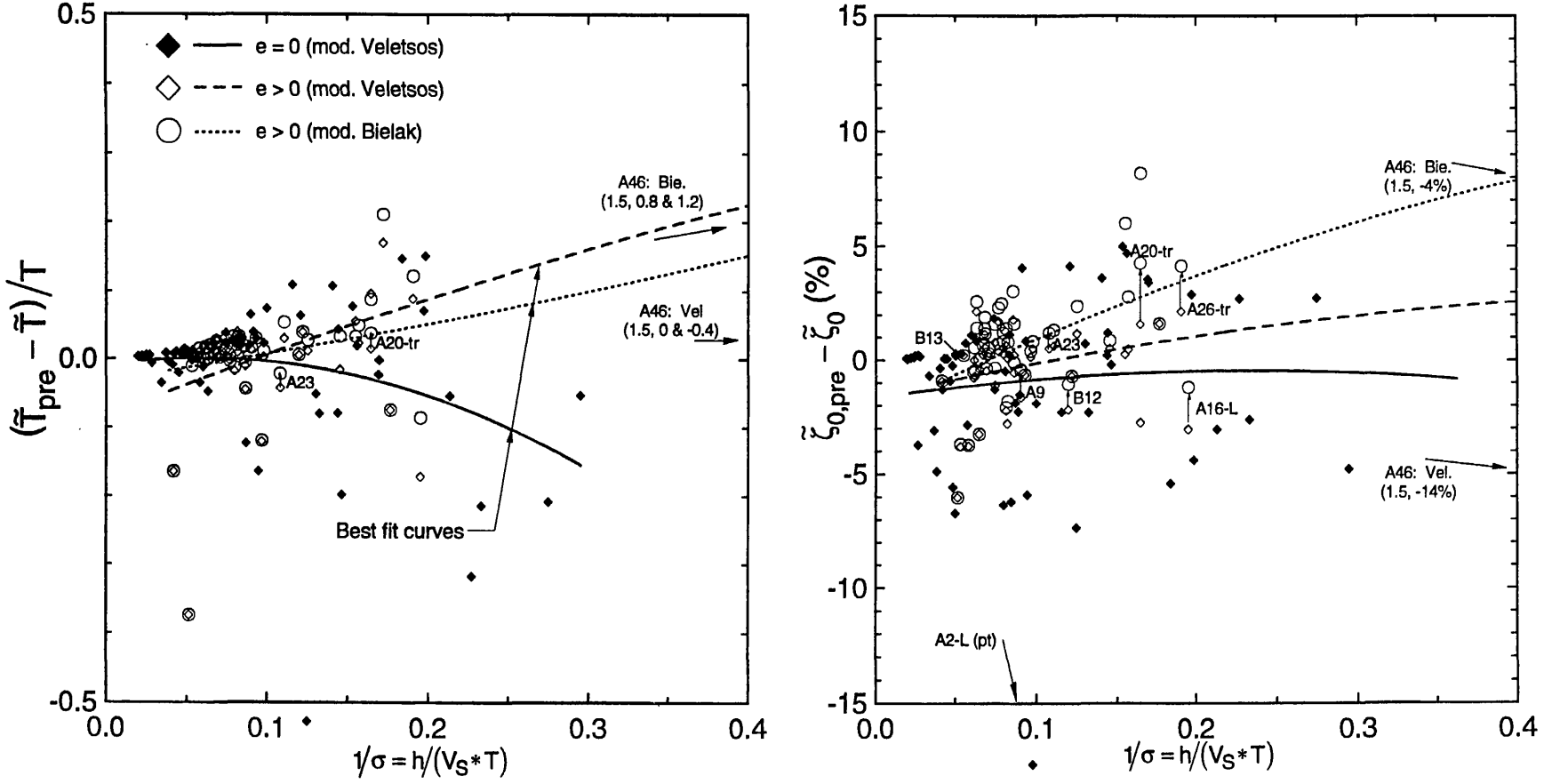

Fig. 7: Errors in "modified Veletsos" and "modified Bielak" formulations for surface and embedded structures

DYNAMIC RESPONSE OF SOIL-PILE-BUILDING INTERACTION SYSTEM IN LARGE STRAIN LEVELS OF SOILS

By Shin'ichiro Tamori[1], Masanori Iiba[2] and Yoshikazu Kitagawa[3]

ABSTRACT: A series of shaking-table tests of a scaled soil-pile-building model were performed in order to study the effects of the plastic deformation of soil on dynamic characteristics of the soil-pile-building interaction system. Results showed the natural frequency and amplification factor decreased by 40% and 60%, respectively, when shear strain of soil was 4.2×10^{-2}. Dynamic response analyses, which combined the Sway-Rocking model and an equivalent linearization method, were done. The maximum acceleration of the building was underestimated when amplitude of input motion was 600 cm/s^2, because the amplification factor of the rocking motion were overestimated in this case. This facts was caused by underestimation of the damping effects for the rocking motion of the foundation.

INTRODUCTION

When designing a building, it is important to evaluate earthquake performance of a building including non-linear soil-building interaction effects during an earthquake. Many method(Novak and Sheta 1980; Darbe and Wolf 1988; Motosaka et. al.1992, etc.) have been proposed to evaluate the effects, but they are too complex for a practical design process. In the practical designing of a building, analytical methods should be simple so that , for example, an equivalent linearization method, like SHAKE(Schnabel et. al. 1972), have been used frequently to evaluate ground response. But, in the case of the non-linear soil-building interaction system, the accuracy of the method had not been tested enough.

In this study, a series of shaking table tests were done in order to evaluate the effect of plastic deformation of soils on dynamic characteristics of soil-pile-building interaction system. Dynamic response analyses, which combined Sway-Rocking model and an equivalent linearization method, of the tests were also done to evaluate the accuracy of this analytical method.

PLASTIC MATERIAL FOR GROUND MODEL

Plastic material for the artificial ground model used in this study was made of Plasticine and oil. Plasticine , being a mixture of calcium-carbonate and oil, has been used as a model material for plastic deformation processing of steel, since it has restoring force curves similar to high-temperature steel(Cook 1953).

Fig. 1 shows the soil characteristics, strain-shear modulus and strain-damping factor relationships for actual clayey soils and Plasticine, which is the plastic soil material used in this shaking table tests.

The initial shear modulus, G_t (strain being 1.0×10^{-5}), shear modulus at large strain levels, G_s, and damping factors, h_g, were obtained by tri-axial compression tests in which ambient stress were kept at 1.0 kg/cm^2 and exciting frequency was 1.0Hz. The shear modulus and damping factor of the plastic soil material, Plasticine, has strain dependency similar to those of actual clayey soils.

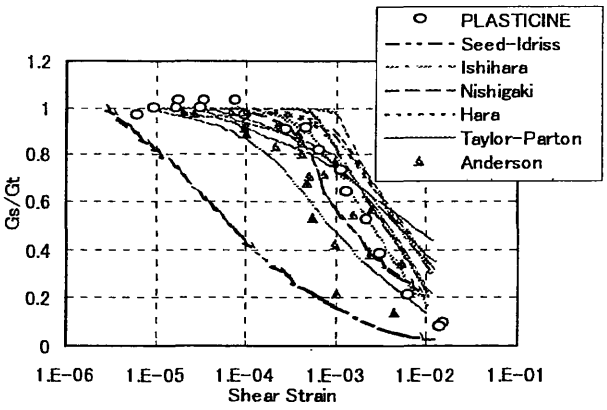

(a) Shear modulus ratios versus shear strain

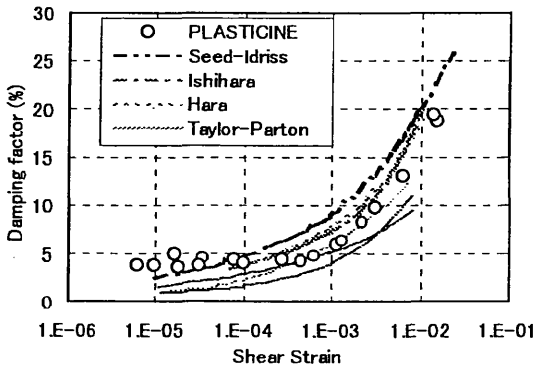

(b) Damping factor versus shear strain

Fig.1 Soil characteristics

[1] Associate Prof. , Department of Architecture and Civil Engineering., Faculty of Engineering., Shinshu University, Nagano, Japan.

[2] Head, Geotechnical Div., Structural Department., Building Research Institute, Ministry of Construction, Tsukuba, Japan.

[3] Professor, Department of Structural Engineering., Cluster IV Faculty of Engineering., Hiroshima University, Higashi Hiroshima, Japan.

OUTLINE OF SHAKING TABLE TESTS

The similarity which proposed by Buckingham was used in modeling the building and the ground soils. The scale factors calculated from this formula are summarized in Table 1.

This similarity is applicable to non-linear soil dynamics when the soil model material has a shear modulus-strain and a damping factor-strain relations similar to those of the prototype(Kagawa 1987). Under these conditions the ratio of shear forces in the model and the prototype were kept approximately equal to that of the damping forces for wide strain levels of soil.

Fig. 2 shows a outline of the building and the ground model together with the location of the measurement apparatus. Two dwelling units of 11-story buildings were modeled in the transverse direction. Table 2 shows the natural frequency and damping factor of the building model. The building model was made of steel weight and it's columns were made of steel plates. The building foundation was made of aluminum and acryl plates. Four cylinder-shaped(ϕ 38mm, length is 487mm) pile models were made of steel plate attached with rubber, they were set at the corners of the foundation.

The ground model has a block shape and its size is 2x1.46x0.6m. Stainless plates were set at both side ends in transverse direction of the ground to prevent vertical motion of the ground. The central part(ϕ 800mm, depth is 387mm) of the ground model was made from Plasticine and oil. The remaining portions of the model were composed of polyacrylamid and bentnite, and remained elastic throughout the tests. Table 3 shows characteristics of the ground. Damping factors were obtained by a free torsional vibration test and shear wave velocity was obtained by the P-S wave propagation tests.

Two earthquake records in which the time length was corrected according to the similarity were used for the input ground motion: 1968 Hachinohe EW and 1940 El Centro NS. Maximum acceleration of the input motions were set as 100, 300 and 600 cm/s^2 on the shaking table.

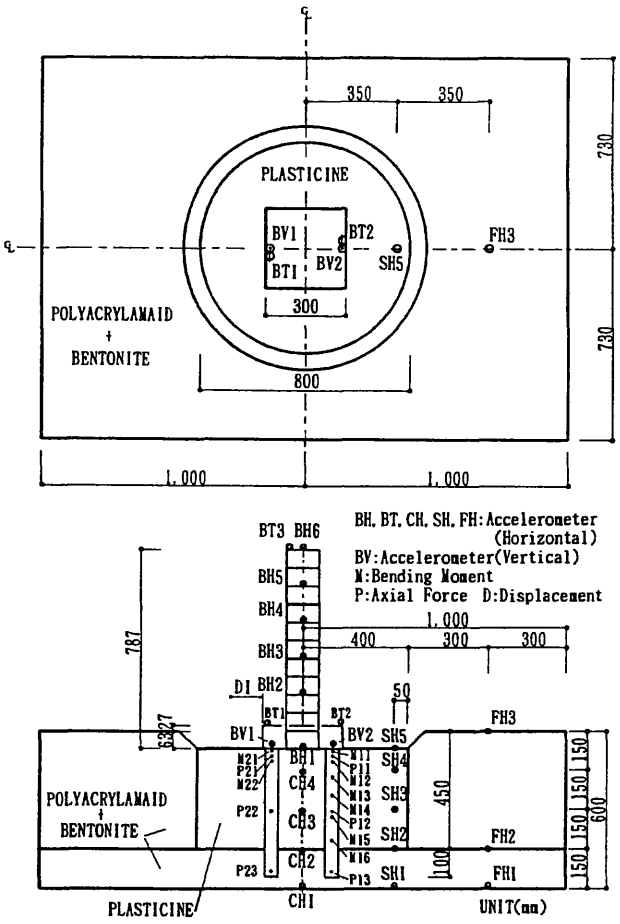

Fig.2 Building and ground model

Table 1 Similitude ratios

Item		Ratio(Model/Prototype)	
Soil Density	kgf/cm^3	$1/\eta$	1
Length	cm	$1/\lambda$	1/40
Acceleration	cm/s^2	1	1
Displacement	cm	$1/\lambda$	1/40
Mass	kgf.s^2/cm	$1/\eta\,\lambda^3$	$1/6.4\times10^4$
Shear Modulus	kgf/cm^2	$1/\eta\,\lambda$	1/40
Frequency	1/s	$\sqrt{\lambda}$	6.325
Velocity	cm/s	$1/\sqrt{\lambda}$	1/6.325
Stress	kgf/s^2	$1/\eta\,\lambda$	1/40
Strain		1	1

Table 2 Characteristics of building model

Foundation		Building		Characteristics of fixed base building	
Size (cm)	Weight (kgf)	Height (cm)	Weight (kgf)	Natural Freq. (Hz)	Damping Factor (%)
30 x 30	6.79	78.7	28.4	18.8	0.22

Table 3 Characteristics of ground model

Item	Upper layer (GL~GL-45cm)		Lower layer (GL-45~60cm)
	Center	Edge	
Vs(m/s)	23.7	18.4	36.0
Damping factor(%)*	6.63*	5.57	6.05
Density(gf/cm^3)	1.57	1.17	1.41

*Strain level is 3.6×10^{-4}

RESULTS OF THE TESTS

Fig. 3 shows first natural frequency estimated by spectral ratios of BH6/SH5 (see Fig. 2) . The shear strain shown in Fig. 3 is maximum strain that calculated from displacement at BH1, CH3 and CH4.

Fig. 4 shows the amplitude of the spectral ratio at the natural frequency. The natural frequency was decreased by 40% and the amplitude of spectral ratio was 60% at most when the shear strain of soil was 4.20×10^{-2}.

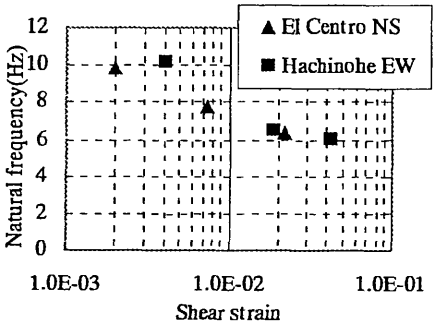

Fig. 3 Natural frequency versus shear strain of soil

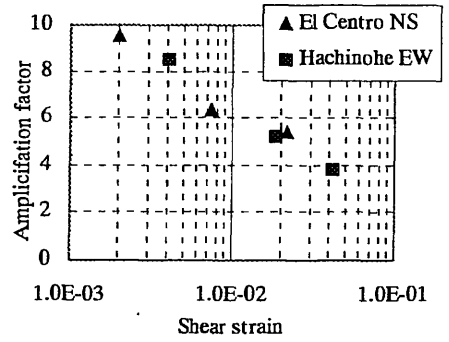

Fig. 4 Amplification factors versus shear strain of soil

THEORETICAL MODEL

The theoretical model employed in this study was the Sway-Rocking(S-R) model, and an equivalent linearization method was used for dynamic response analyses. Dynamic stiffness and the damping factor for sway and rocking motion were calculated as follows:

(1) Dynamic stiffness and damping factor of piles for horizontal and rocking motion proposed by Novak and Nogami (1977) were employed.

(2) Dynamic stiffness and damping factor of piles for vertical motion were calculated by the D.G.C.(Kobori et. al. 1970) of the rigid plate, which has same cross section of the pile. Vertical stiffness of a end bearing pile, which was obtained by a wave propagation theory(Nogami and Novak 1976), was significantly larger than those obtained by the D.G.C., so that we neglected the stiffness of the end bearing pile.

(3) Dynamic stiffness and damping factor of the bottom of the foundation was calculated by the D.G.C.

In this study, the dynamic stiffness of the soil-pile-foundation system was calculated by the sum of the dynamic stiffness of the piles and that of the bottom of the foundation.

The equivalent linearization method was employed in order to consider plastic deformation of soils. Soil stiffness, damping factor and strain of soil were determined as follows:

Shear modulus, G_s, and damping factor, h_g, of the soil were determined by the tri-axial compression tests according to the following equation modified by the Hardin-Drnevich model(Hardin and Drnevich 1972):

$$\frac{G_s}{G_t} = \frac{1.01}{1 + 0.96\,(r_s / 0.002072\ )^{1.258}} \qquad (1)$$

$$h_g = 0.035 + 0.145(1 - G_s / G_t) \qquad (2)$$

Where G_t is the initial shear modulus and γ_s is shear strain of the soil.

Strain of the soil caused by wave propagation, γ_{wave} was estimated by displacement at SH3, SH4 and SH5. Soil strain caused by the foundation was estimated from the maximum relative displacement of the foundation, $u_{b,max}$, as follows:

Displacement of soil at depth z, $u_b(z)$, was assumed to be determined by eq. (3).

$$u_b(z) = \frac{B_1}{B_1 + z / \sqrt{bc}} u_{b,\max} \qquad (3)$$

where B_1 is a constant, b and c are the width of half the foundation in the vibration and transverse direction, respectively.

This formula was proposed by Kobori et. al.(1972)

By averaging the strain from z = 0 to H, considering energy caused by the displacement, $u_b(s)$, the equivalent maximum strain of the soil caused by displacement of the foundation, γ_{base}, becomes ,

$$\gamma_{base} = \sqrt{\int_0^H \frac{1}{H} \left(\frac{du_b(z)}{dz}\right)^2 dz} \qquad (4)$$

where H = b .

Equivalent shear strain of the soil, γ_{eq}, which has determined soil stiffness and damping factor, is

$$\gamma_{eq} = 0.7 \text{ or } 1.0(\ \gamma_{base} + \gamma_{wave}) \qquad (5)$$

RESULTS OF ANALYSES

Figs. 5, 6 and 7 show spectral ratios , where input motion was Hachinohe EW. In these figures, UR is rocking motion at the top of the building and UH is relative deformation of the building. Ratio of the equivalent strain divided by maximum strain was set to 0.7 in this case(see. eq.(5).) Fig. 8a shows the first natural frequencies detected form spectral ratio of BH6/SH5 (see Fig. 2) and 8b shows amplification factors, which are the amplitude of the spectral ratio at the first natural frequency. Fig. 8c shows maximum acceleration and 8d shows maximum shear strain of the soil beneath the foundation.

As shown in Figs.8a~8d, difference in natural frequencies by the test and by the analyses were within about 20%. For amplification factor and maximum acceleration, the difference became 30%. When the maximum input acceleration was 100 cm/s^2, the amplification factor was overestimated(see Fig. 5a also). Figs. 5a ~5d show that transfer function of rocking motion was overestimated. When the maximum input motion became 600 cm/s^2 , the amplification factor and maximum acceleration at BH6 were underestimated by the analysis. From Fig. 7b , this fact was caused by underestimation of the amplification factor of the rocking motion.

So when maximum acceleration of the input motion was 100 cm/s^2, the damping effects of the rocking motion were underestimated and when the maximum acceleration was 600 cm/s^2 , the effects were overestimated.

Figs. 9a~9c show comparisons of maximum acceleration at the model building by the tests and analyses. When maximum acceleration of input motion was 600 cm/s^2, the maximum acceleration at the upper part of the building was underestimated by the analysis.

Figs. 10~13 show results, where input motion was El Centro NS. In this case, ratio of the equivalent strain divided by maximum strain was set to 1.0. We have done tests by using Hachinohe EW first, and then by using El Centro NS. So, this ratio may be affected by the order of the test. As shown in Figs. 3 and 4, the maximum shear strains beneath the foundation for Hachinohe EW is as twice as those for El Centro NS. So, In the case of El Centro NS, the soil had already experienced strain level lager than that occurred during the test.

As shown in Figs. 13a and 13b, difference of natural frequency, according to the tests and the analyses were within 10% and, for amplification factors, the differences were within 25%. Results of maximum acceleration of BH6 and of maximum shear strain by the analyses were in agreement with those of the test. The amplification factor was overestimated when maximum input motion was 100 cm/s^2(see Fig. 10a) and was underestimated when maximum input motion was 600 cm/s^2 (see Fig. 12a). This was caused by the difference of damping effects of rocking motion by the analyses and those by the tests also in this case (see Figs. 10b and 12b).

Fig. 14 shows a comparison of maximum acceleration of the building by the tests and analyses. In this case, results by the tests and the analyses agree well.

CONCLUSION

This study involved performing shaking table tests on elasto-plastic soil material to investigate the soil-pile-building interaction system in large strain levels of soils. Dynamic analyses of the test, which incorporated Novak's and Kobori's method and an equivalent linearization method were used to determine dynamic stiffness of foundation and piles.

Results of the analyses were as follows;

(1) Ratio of equivalent strain divided by maximum strain was set from 0.7 to 1.0. It must be changed by the order of the tests or character of input motion. Difference in natural frequency obtained by the analyses were within 20% and those of maximum acceleration were within 30%.

(2) Transfer functions for the rocking motion at the natural frequency was overestimated when maximum acceleration of input motion was 100 cm/s^2 and those were underestimated when maximum acceleration of input motion was 600 cm/s^2. In conclusion, the method used to evaluate the damping effects of the rocking motion should be reconsidered in order to improve the accuracy of the analyses.

REFERENCES

Cook, P. M. (1953). "Forging research - use of Plasticine models." Metal Treatment and Drop Forging 20: 534.

Darbre, G. R. and Wolf, J.P. (1988). "Criterion of stability and implementation issues of hybrid frequency-time-domain procedure for non-linear dynamic analysis," Earthquake Engineering and Structural Dynamics, 16, 569-581.

Hardin, B. O. and Drnevich, V. P. (1972). "Shear modulus and damping in soils, Design equation and curves," Journal of Soil Mech. and Foundation, Div. ASCE, 98(SM7), 667-692.

Kagawa, T. (1987). "On the similitude in model vibration tests on earthquakes." Proc. Of Japan Society of Civil Engineering, 275: 69-77

Kobori, T. and Suzuki, T. (1970). "Foundation vibration on a viscoelastic multi-layered medium," Proc. of the 3rd Japanese Earthquake Engineering Symposium: 493-500.

Kobori, T., Soji, Y., Minai, R., Suzuki, T. and Yuwakasaki, Y. T. (1972). "Effects of soil and geological conditions on structural response in Osaka area," Proc. of International Conf. on Microzonation for Safer Construction, Research and Application, 719-734.

Motosaka, M., Wolf, J. P. and Nagano, M. (1991) "Application of recursive evaluation of convolution integral in nonlinear dynamics based on transfer function of linear system in frequency domain,", Proc. of IV-ICCCBE, 243-250.

Nogami, T. and Novak, M. (1996). "Soil-pile interaction in vertical vibration," Earthquake Engineering and Structural Dynamics, 4, 263-281.

Novak, M. and Nogami, T. (1977). "Soil-pile interaction in horizontal vibration," Earthquake Engineering and Structural Dynamics, 5, 263-281.

Novak, M. and Sheta, M. (1980). "Approximate approach to contact effects of piles," Proc. of Session on Dyn. Response of Pile Foundation: Analytical Aspects, ASCE National Conv., 53-79.

Schabel P. B., Laysmer, J. and Seed H. B.(1972). "A computer program of earthquake response analysis of horizontally layered sites," Report No. EERC 72-12, College of Engineering, University of California Berkeley.

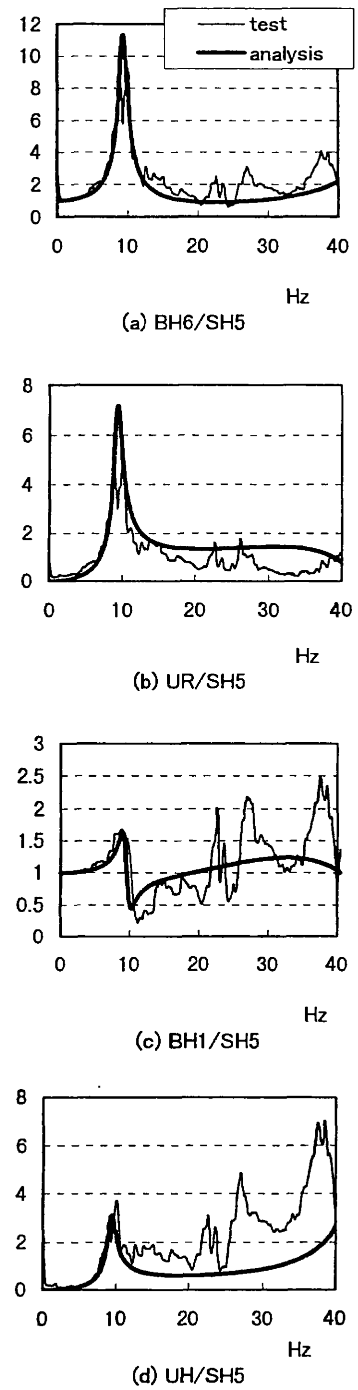

Fig. 5 Spectral ratios (Hachinohe 1968 EW, 100cm/s/s)

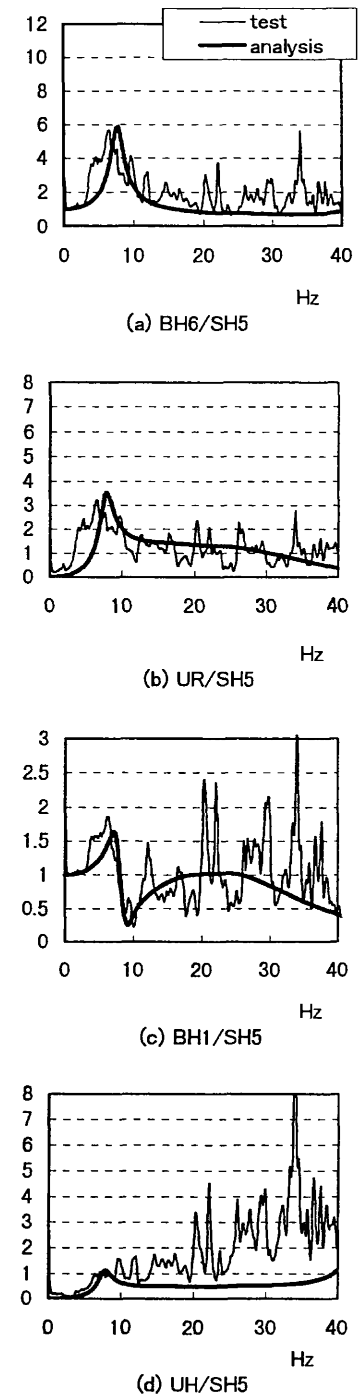

Fig. 6 Spectral ratios (Hachinohe 1968 EW, 300cm/s/s)

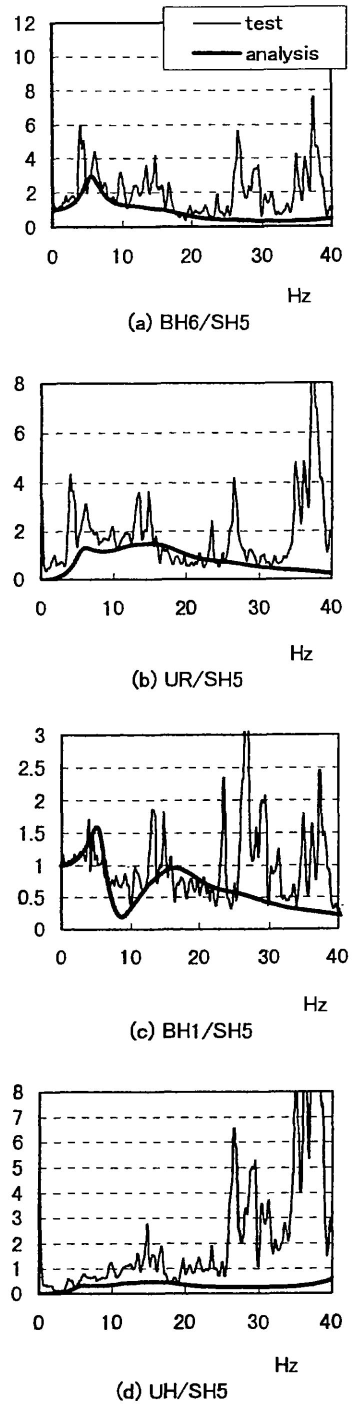

Fig. 7 Spectral ratios (Hachinohe 1968 EW, 600cm/s/s)

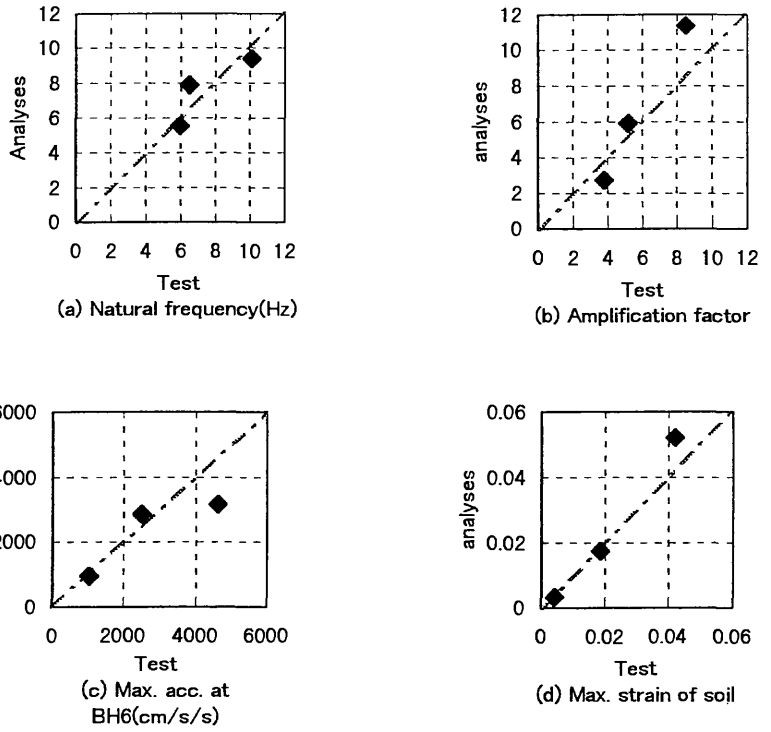

Fig.8 Comparison results of tests and analyses (Hachinohe EW)

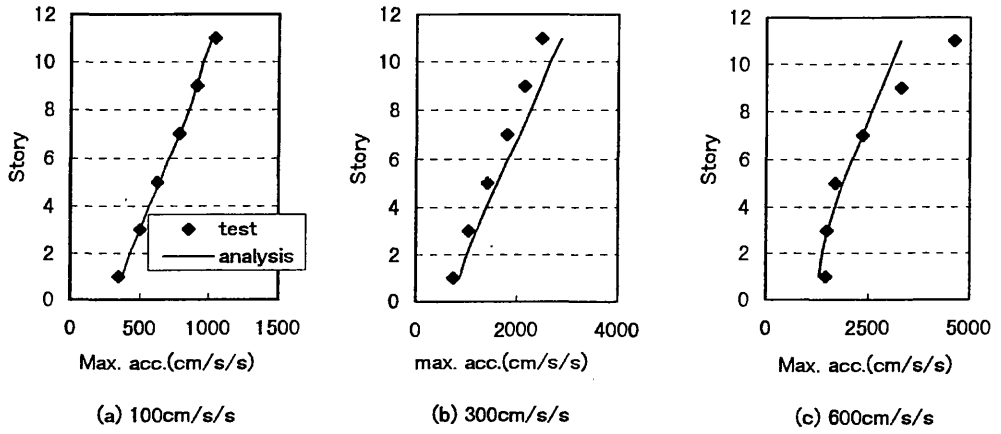

Fig. 9 Maximum acceleration at building (Hachinohe EW)

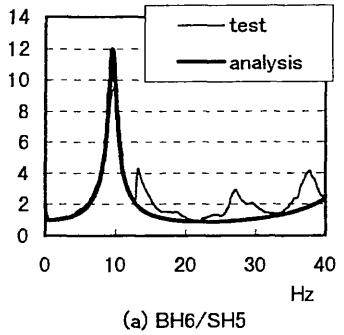

(a) BH6/SH5

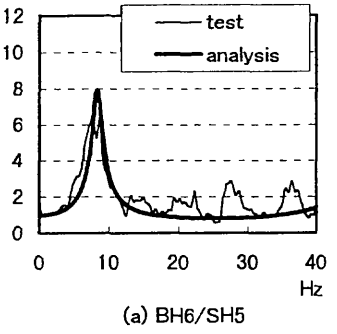

(a) BH6/SH5

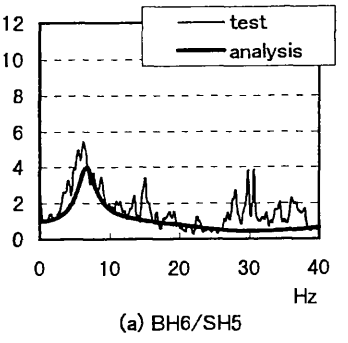

(a) BH6/SH5

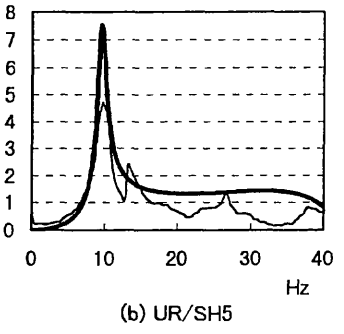

(b) UR/SH5

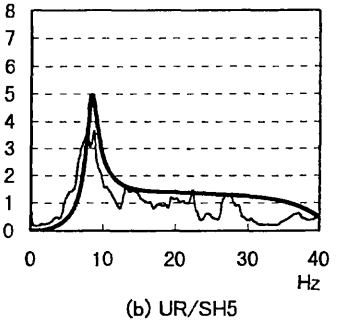

(b) UR/SH5

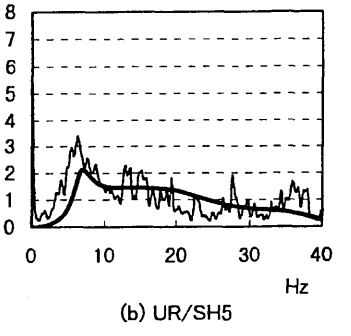

(b) UR/SH5

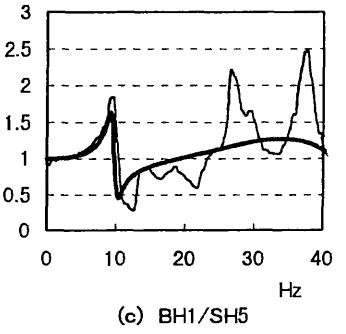

(c) BH1/SH5

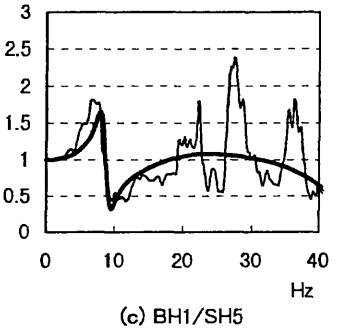

(c) BH1/SH5

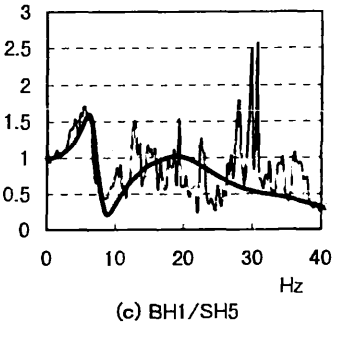

(c) BH1/SH5

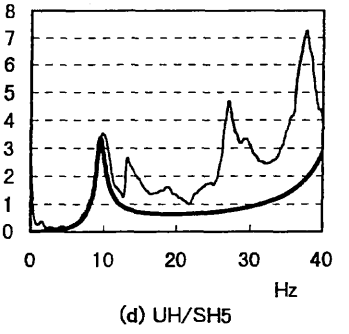

(d) UH/SH5

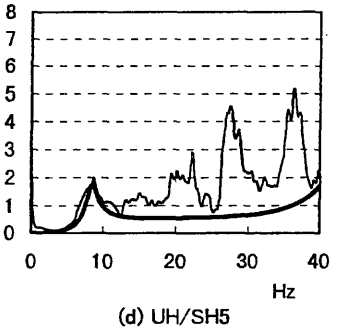

(d) UH/SH5

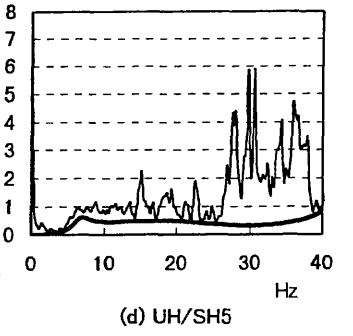

(d) UH/SH5

Fig. 10 Spectral ratios (El Centro 1940 NS, 100cm/s/s)

Fig. 11 Spectral ratios (EL Centro 1940 NS, 300cm/s/s)

Fig. 12 Spectral ratios (EL Centro 1940 NS, 600cm/s/s)

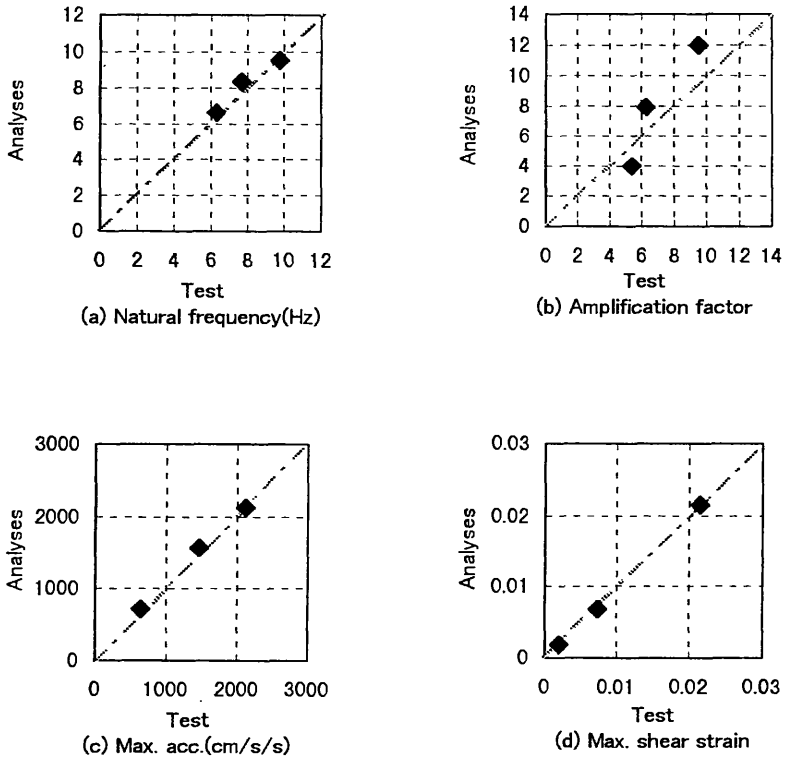

Fig.13 Comparison results of tests and analyses (El Centro NS)

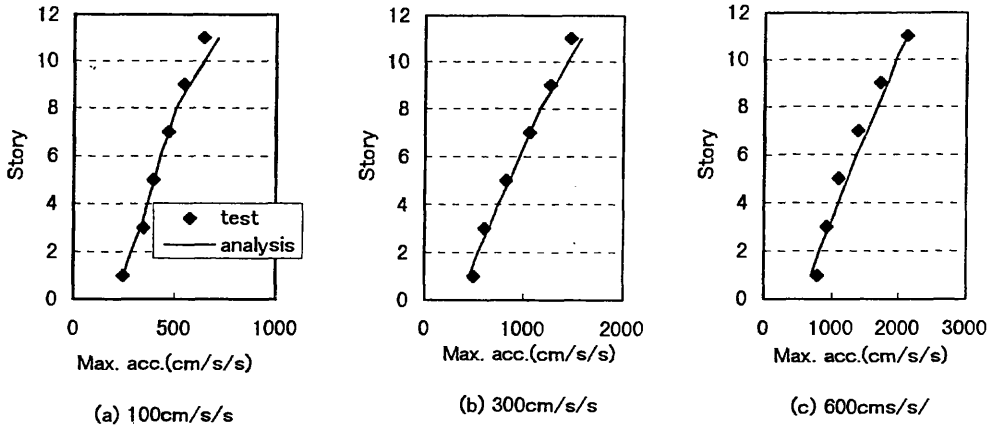

Fig. 14 Maximum acceleration at building (El Centro NS)

Nonlinear SSI analysis

by
Ronaldo I. Borja, Heng-Yih Chao and Chao-Hua Lin
Department of Civil & Environmental Engineering
Stanford University, Stanford, CA 94305-4020, USA

Abstract

Accurate representation of soil-structure interaction (SSI) effects is a crucial part of earthquake engineering analysis. The SSI model must be robust enough to capture nonlinear 3D effects, as well as accommodate the spectrum of frequencies of interest to the analyst. This paper investigates the potential of standard nonlinear finite element (FE) procedures for 3D analysis of SSI systems. The analysis uses the Lotung Large-Scale Seismic Test (LSST) problem as a case study. Nonlinear ground response is a ubiquitous feature of the soil behavior in Lotung; thus the analysis utilizes a direct method in which the entire soil-foundation-structure system is modeled and analyzed in a single step.

1. Introduction

Ground motions are generally influenced by the presence of structures, and structural motions are in turn influenced by the compliance of the supporting subsoils. These coupling phenomena are due to soil-structure interaction (SSI) effects, which are absent when the structure is founded on solid rock with extremely high stiffness. Dynamic analysis of SSI effects requires varying levels of rigor depending on the type of analysis (linear or nonlinear) and geometrical contraints (2D or 3D). In general, the computational challenge lies in modeling nonlinear effects in a general three-dimensional setting. This paper discusses the performance of a standard nonlinear finite element (FE) program, called SPECTRA, for 3D analysis of SSI systems.

Inclusion of nonlinear effects in SSI analysis eliminates the convenience offered by the principle of superposition, which allows a separate treatment of inertial and kinematic interactions before obtaining the combined response. Instead, nonlinear analyses are best carried out by direct method, which entails modeling and analysis of the entire soil-structure system in a single step. Section 2 describes some computational issues and challenges relevant to a faithful modeling of SSI effects, as well as discusses some aspects necessary for selecting a sound framework for nonlinear FE analysis by direct method.

In Section 3 we report the performance of a standard (implicit) nonlinear FE program, SPECTRA, for estimating the ground response in Lotung incorporating SSI effects. The type of analysis pursued is based on elastoplastic modeling with deviatoric plasticity under the assumption of infinitesimal deformation. The solution is based on a total stress formulation in which the soil solid and fluid are assumed to move as one body (undrained condition). The Lotung Large-Scale Seismic Test (LSST) problem has been selected as a prototype case study because of the relevance of its design to the goals of accurate SSI modeling.

2. Framework for nonlinear SSI analysis

We consider an analytical platform for nonlinear SSI analysis embodied in a time-domain FE model. The global iterative solution strategy is Newton-Raphson iteration with line

search, but the technique should also be able to accommodate quasi-Newton, modified Newton, and even PCG-based equation solving techniques (each technique has its own strengths and limitations). The specific platforms for each of the model components are outlined and described below.

2.1. Constitutive model and stress-point algorithm. We seek a constitutive model that best describes the material response. Models based on plasticity theory are on top of the author's hierarchical list. The stress-point integration algorithm must be at least first-order accurate and unconditionally stable. This is achieved with the use of standard implicit return-mapping algorithm in computational plasticity. Explicit stress-point integration algorithms for elastoplasticity are unacceptable---they simply create unnecessary stability problems and are not accurate enough for large load steps. Hypoplasticity models rank next on the author's list of hierarchical models. Unconditionally stable stress-point algorithms are also available for this class of model and must be utilized whenever possible. Regardless of the type of model, the stress-point integration algorithm must be linearized consistently as there is so much efficiency to be gained by using the consistent tangent operator.

2.2. Finite deformation model. A finite deformation theory based on multiplicative plasticity and implemented using product formula algorithm is on top of the author's hierarchical list. This formulation has considerable advantage over the conventional hypoelastic formulation. In the first place, there is no question as to what objective stress rate must be used (Jaumann rate, Green-Naghdi rate, etc.), and so problems associated with the use of the Jaumann stress rate, for example, do not exist. Furthermore, the model has a hyperelastic basis which imposes no restriction on the elastic strains (unlike the hypoelastic formulation which requires that the elastic strains be small). Finally, the product formula algorithm can accommodate the standard return maps of infinitesimal plasticity without loss of objectivity under rigid-body rotations. Quite recently, the author has implemented the proposed technique in a nonlinear consolidation FE code, and the results are very encouraging (Borja et al. 1998).

2.3. Time-integration algorithm. The classical Newmark family of algorithms has become the backbone feature of many structural dynamics FE codes over the years, and has indeed performed quite successfully in the geometrically linear case. Quite recently, this algorithm has been found to fail to conserve energy and total angular momentum for the geometrically nonlinear case. This result has a profound impact on the development of robust mathematical models since conservation laws play a central role in classical mechanics; in particular, conservation of angular momentum is crucial in motions with significant rigid-body rotation, such as structures undergoing rocking motion. The impact of this discovery on SSI research remains largely unexplored. Simo et al. (1992) have suggested time-stepping algorithms that conserve energy and total angular momentum for general nonlinear Hamiltonian systems, but this class of algorithms remains untested for earthquake engineering analysis applications.

2.4. Liquefaction model. The problem of lateral flows and liquefaction-induced large ground movement of saturated soils during and following an earthquake is a subject of considerable importance in SSI modeling. Models based on Biot's two-phase mixture theory and cast within the finite deformation model are possible, as described in Sec. 2.2. The constitutive model should be capable of replicating hysteretic volume change behavior to allow pore pressure buildup. Pore pressure buildup and the attendant liquefaction phenomena have profound impacts on the responses of soil-structure systems.

2.5. Strain localization model. A problem not typically covered by the standard finite element approximation is strain localization, particularly in the soil medium. Strain

localization effects are particularly important in simulating cracking of concrete, shear banding in geomaterials, and structural collapse. Traditionally, cracking and softening were treated as a constitutive response, although strictly speaking, they are a structural response (see review by Read and Hegemier 1984). The SSI model should be robust enough to accommodate strain localization as a structural response, and to allow modeling of damage, limit states, and collapse.

An ideal FE analysis code must accommodate the above features, among others, or a faithful simulation of the SSI phenomena is not possible. Although developing a package with all of the above features is difficult, it is possible to include at least some of the most important SSI aspects in the analysis. To illustrate the rigors of a 3D nonlinear FE analysis of SSI phenomena, the next section describes a FE modeling of a soil-structure system in Lotung, Taiwan, as it responded to the earthquake of May 20, 1986.

3. SSI analysis of Lotung LSST problem

Lotung is a seismically active region in northeastern Taiwan, and was the site of two scaled-down nuclear containment structures (1/4-scale and 1/12-scale models) constructed by the Electric Power Research Institute, in cooperation with Taiwan Power Company, for SSI research (Tang et al. 1990). The local geology at the test site has been established from shear wave velocity and field boring tests. On May 20, 1986, a strong earthquake, denoted as the LSST7 event, with magnitude 6.5, epicentral distance of 66 km, and focal depth of 15.8 km shook the test site. Two downhole arrays located approximately at 3 m and 49 m from the edge of the 1/4-scale model, herein called DHA and DHB arrays, respectively, recorded the downhole motions at depths of 0, 6, 11, 17, and 47 m (Fig. 1). In this paper, we will analyze the downhole motions recorded by both arrays using a nonlinear FE code SPECTRA.

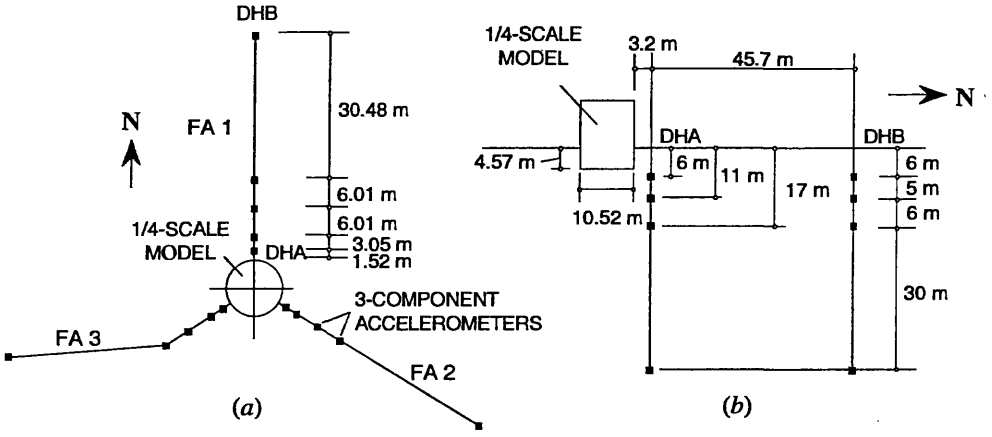

Figure 1. Location of surface and downhole instrumentation, LSST site: (a) plan; (b) elevation.

For purposes of 3D analysis, a full-scale FE model for the 1/4-scale structure and foundation is shown in Fig. 2. Array DHB is located at the edge of the mesh, while array DHA is located approximately 3 m from the edge of the structure. Both arrays are located along the northern arm, as indicated in the figure (see also Fig. 1). The mesh consists of 4,320 eight-noded trilinear brick elements, with a total of over 13,000 degrees of freedom.

Free-field motions are applied at the bottom and side boundaries. Before a full SSI analysis can be carried out, it is necessary that the input free-field motions be first determined. In the following we describe a numerical model for generating the input free-field ground motion consistent with the SSI model for the Lotung problem.

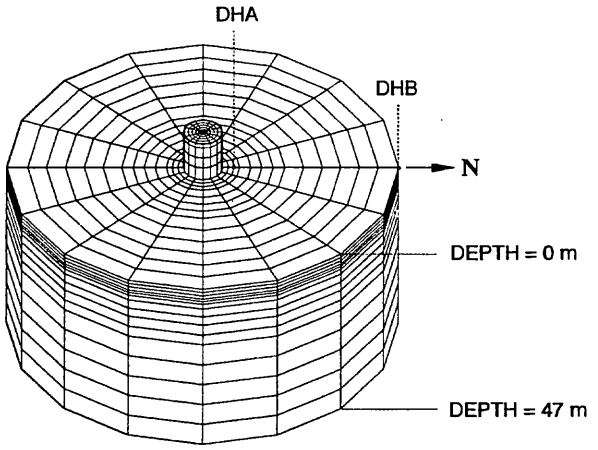

Figure 2. FE mesh for Lotung LSST case study.

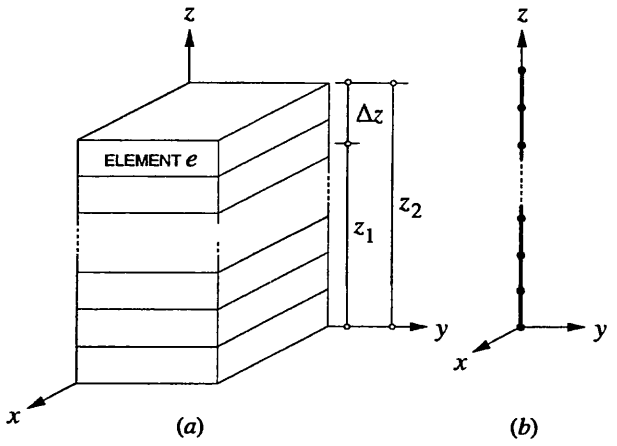

Figure 3. FE mesh for nonlinear ground response analysis: (a) soil column model; (b) stick FE mesh.

The input free-field motions are generated by the same FE code assuming the case of vertically propagating waves. Fig. 3 shows a FE mesh consisting of column and stick elements representing the 47-m deep soil column. The special element shown in Fig. 3(b) has been included in the library of the code SPECTRA specifically for nonlinear ground response analysis. The vertical discretization of the soil layer is consistent with the full 3D mesh of Fig. 2. Each stick element contains 3 DOFs at the nodes: two horizontal and one vertical. The constraints imposed by the condition of vertically propagating waves are that

the two normal horizontal strains as well as the shear strain on the horizontal plane must be equal to zero, and that for the general nonlinear case the three kinematical components of motion must be coupled. Previous studies suggest that the angle of incidence of the seismic waves during the May 20, 1986 event is only around 6 degrees relative to the vertical direction (Chang et al. 1990), which justifies the simplifying assumption of vertically propagating waves.

The soil in Lotung is modeled using bounding surface plasticity theory with a vanishing elastic region in which the hardening modulus is interpolated by an exponential hardening function (Borja and Amies 1984). The material parameters for this soil include the elastic bulk and shear moduli as well as the exponential hardening parameters, which have been determined for the Lotung soil from shear and compressional wave velocity profiles as well as from moduli ratio degradation curves available for the LSST site. Details of how the model parameters have been determined for the LSST site are described by Borja et al. (1998) and Borja and Lin (1998).

Figures 4, 5 and 6 show respective east-west (EW), north-south (NS) and up-down (UD) free-field motions predicted by the program SPECTRA using the stick FE model of Fig. 3, superimposed with the free-field motions recorded by downhole array DHB (the assumption that array DHB is sufficiently far from the structure and that it recorded basically free-field motion is crucial for the rest of the analysis to be meaningful). Calculations were carried out on a 266-MHz Pentium II PC. The close agreement between the recorded and predicted responses is noteworthy, which implies that it is possible to generate reasonably accurate free-field motions with a soil column model that allows for a full kinematical coupling of all three components of motion. Computer runtimes are in the order of 2 minutes on the PC for a time-domain analysis consisting of about 1000 time steps and 4-5 iterations per time step.

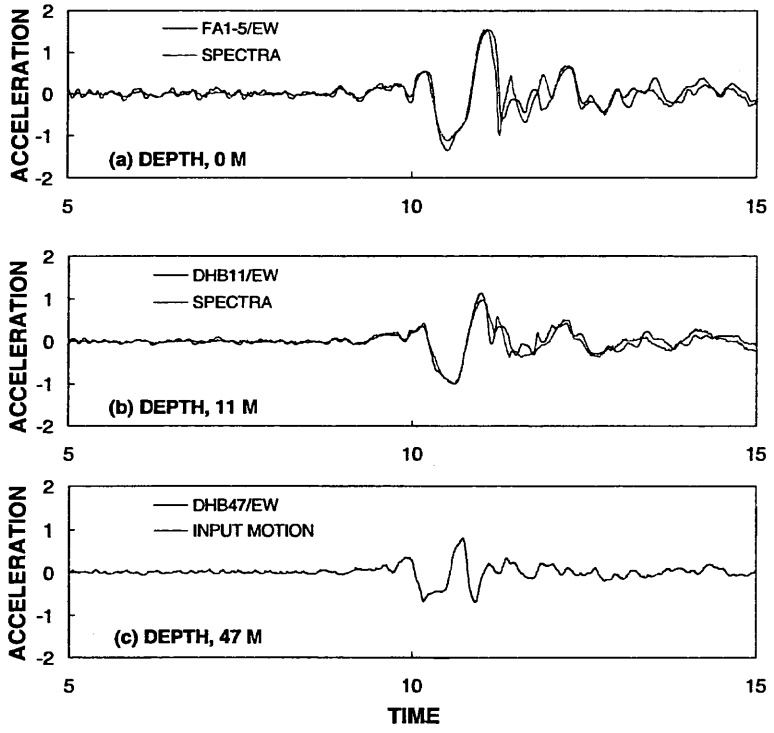

Figure 4. EW free-field acceleration (m/sec^2)-time (sec) history: Lotung LSST7 case study.

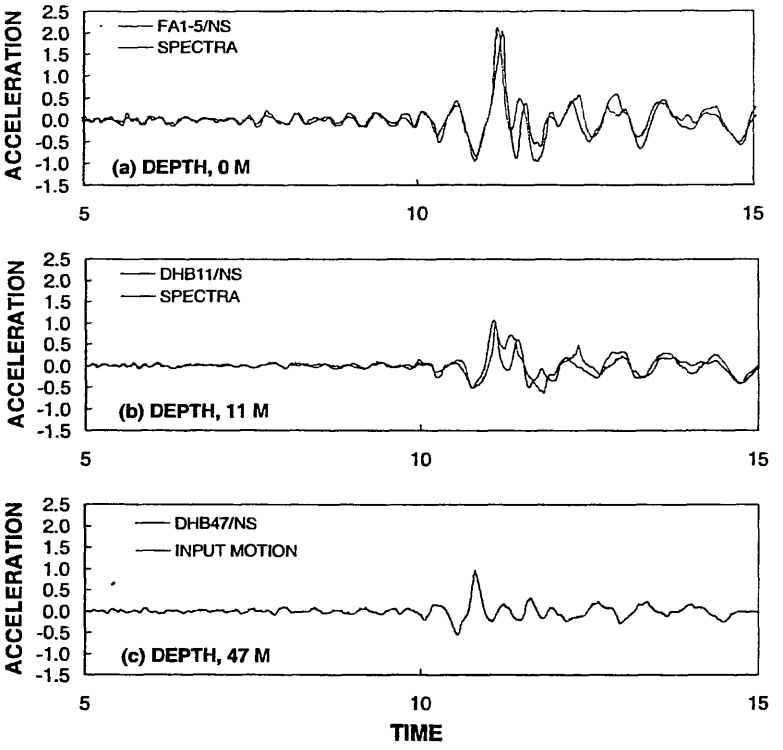

Figure 5. NS free-field acceleration (m/sec^2)-time (sec) history: Lotung LSST7 case study.

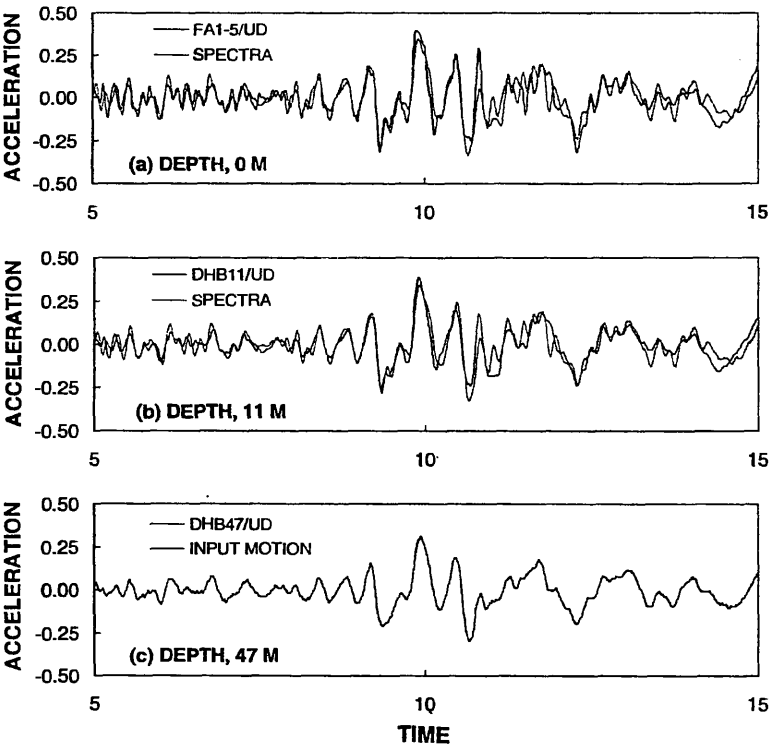

Figure 6. UD free-field acceleration (m/sec^2)-time (sec) history: Lotung LSST7 case study.

Assuming that array DHB recorded truly free-field responses and that the soil profiles and the input seismic motions are essentially the same for arrays DHA and DHB, the effect of SSI can be inferred by comparing the motions recorded by the two arrays. Figures 7, 8 and 9 compare the EW, NS and UD motions recorded by arrays DHA and DHB. Note that the recorded motions at depth of 47 m are essentially the same, but the responses are quite different at shallower depths. Considering that DHA is only 3 m away from the structure, we can postulate that this difference is due to SSI effects. We will follow this idea and proceed with the nonlinear SSI analysis of the Lotung problem.

SSI effects are now investigated using the program SPECTRA along with the full 3D FE mesh shown in Fig. 2. Calculations were carried out on CRAY C90 supercomputer at San Diego Supercomputer Center (SDSC). The 3D mesh of Fig. 2 was the biggest that the authors could construct for this problem at the time of the analysis, given the limited CRAY storage and CPU time made available by SDSC. There is certainly more room for improvement in so far as refining the mesh is concerned, since this mesh is admittedly too coarsely discretized on the horizontal plane compared to the much finer mesh discretization of the soil layers in the vertical direction. However, for ground motions dominated by horizontal sidesway action, this mesh has a resolution comparable to that of the stick model used for nonlinear ground response analysis.

The 1/4-scale nuclear plant structure is modeled as a hollow cylindrical tank made of elastic trilinear brick elements and integrated using the standard 8-point Gauss integration rule. The dimensions of the model and properties of the material are similar to those of the prototype structure. The soil is modeled as elastoplastic brick elements integrated using the B-bar method to alleviate mesh locking in the nearly incompressible regime

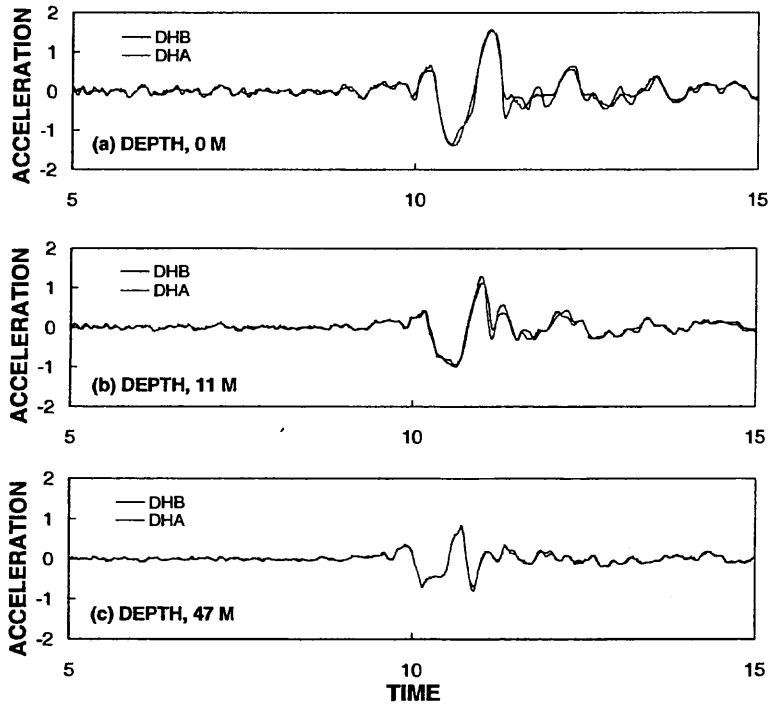

Figure 7. EW acceleration (m/sec^2)-time (sec) history: comparison between DHA and DHB.

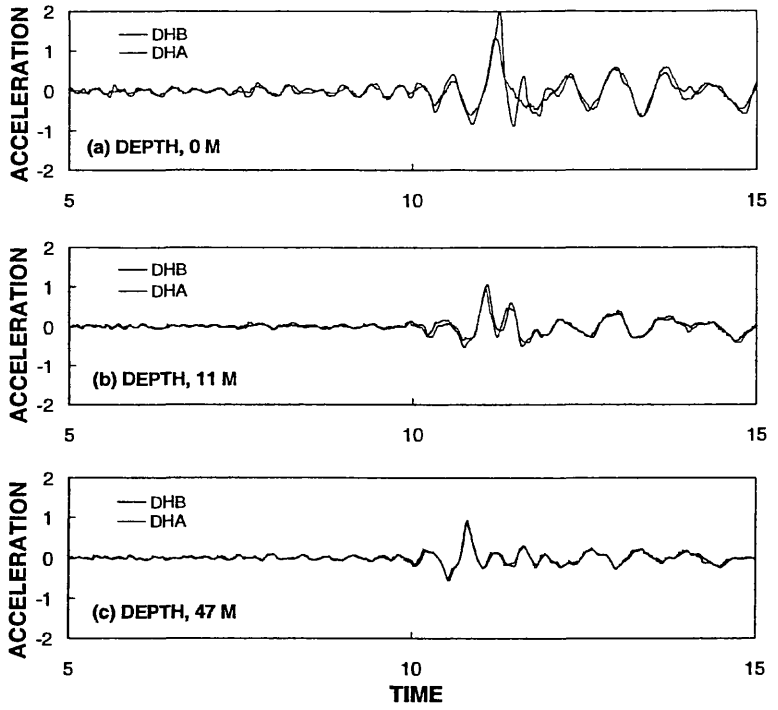

Figure 8. NS acceleration (m/sec^2)-time (sec) history: comparison between DHA and DHB.

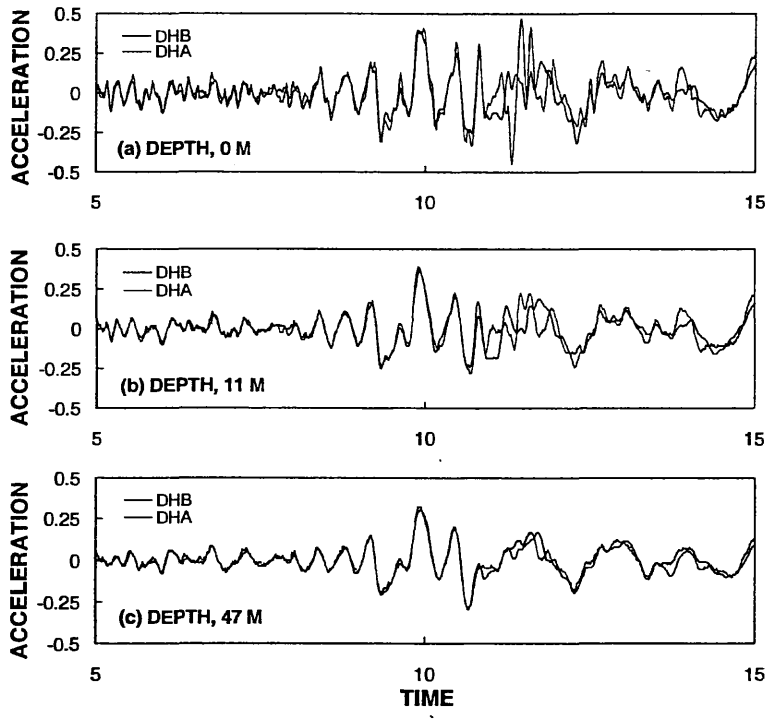

Figure 9. UD acceleration (m/sec^2)-time (sec) history: comparison between DHA and DHB.

The solution procedure goes as follows. Free-field motions are computed from the nonlinear ground response analysis described previously. Then, the computed motions are applied at the base and side boundaries of the mesh in Fig.2 for SSI analysis. Iterations are performed at each time step via a composite Newton-PCG iteration algorithm, in which Newton's method is applied globally at each time step to solve the nonlinear problem and the PCG iteration is applied locally to solve the linearized problem. For purposes of executing the PCG algorithm, a global elastic tangent operator is employed as the preconditioner. The solutions generally converged in 4-5 iterations based on a maximum residual error norm of 0.001%.

Results of the analysis are shown in Figs. 10, 11 and 12. In these figures, the computed motions are shown with and without SSI effects. The latter results (no SSI) were obtained from the nonlinear ground response analysis discussed previously (cf. Figs. 4, 5 and 6). Note that SSI effects are again seen to be more evident at shallower depths, consistent with the results of comparisons between the motions recorded by DHA and DHB as shown in Figs. 7, 8 and 9. That the difference between the results of Figs. 10, 11 and 12 may indeed be attributed to SSI effects is explainable as follows: if the structure in Fig. 2 were removed and the 3D mesh were still used in the SSI analysis, the computed motions on DHA would be *identical* to the free-field motion applied on DHB.

Implicit 3D nonlinear analyses are computer-intensive as affirmed by the following statistics: for a 3D mesh with about 4.5K elements, 5K nodes, and 13K DOFs similar to that shown in Fig. 2, a time-domain analysis composed of 1,000 time steps and 4 to 5 iterations per time step would require about 4 CPU-days on the CRAY C90 supercomputer utilizing one processor.

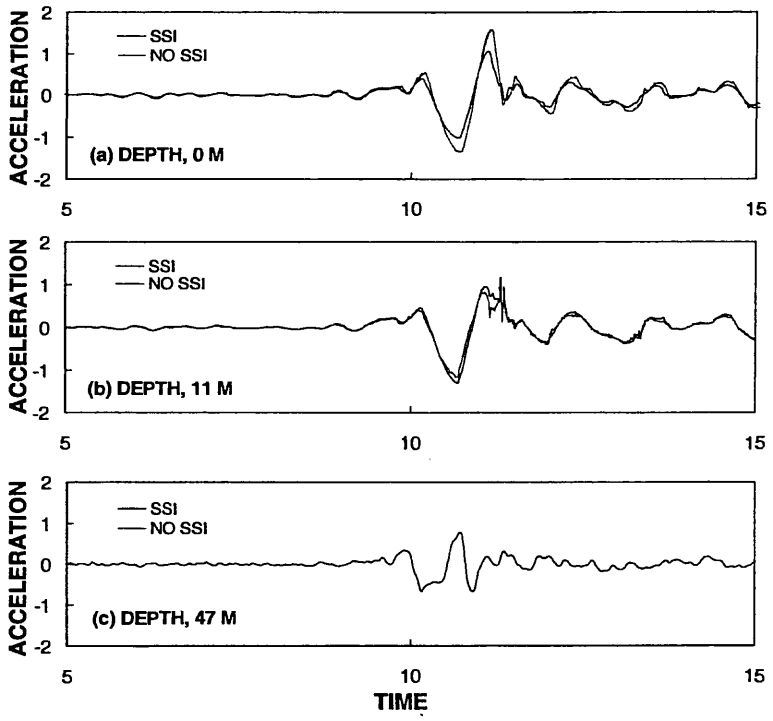

Figure 10. EW acceleration (m/sec^2)-time (sec) history with and without SSI: Lotung LSST7 case study.

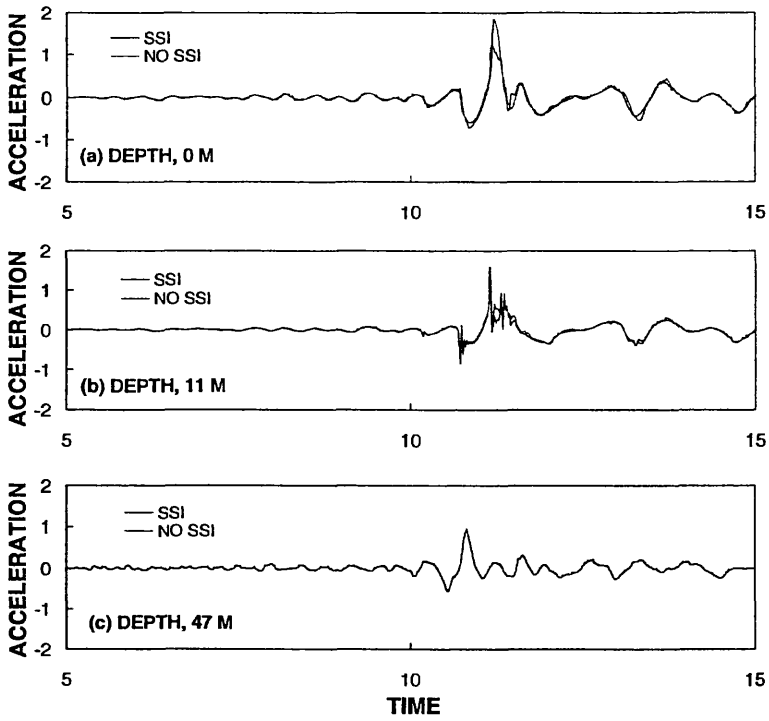

Figure 11. NS acceleration (m/sec^2)-time (sec) history with and without SSI: Lotung LSST7 case study.

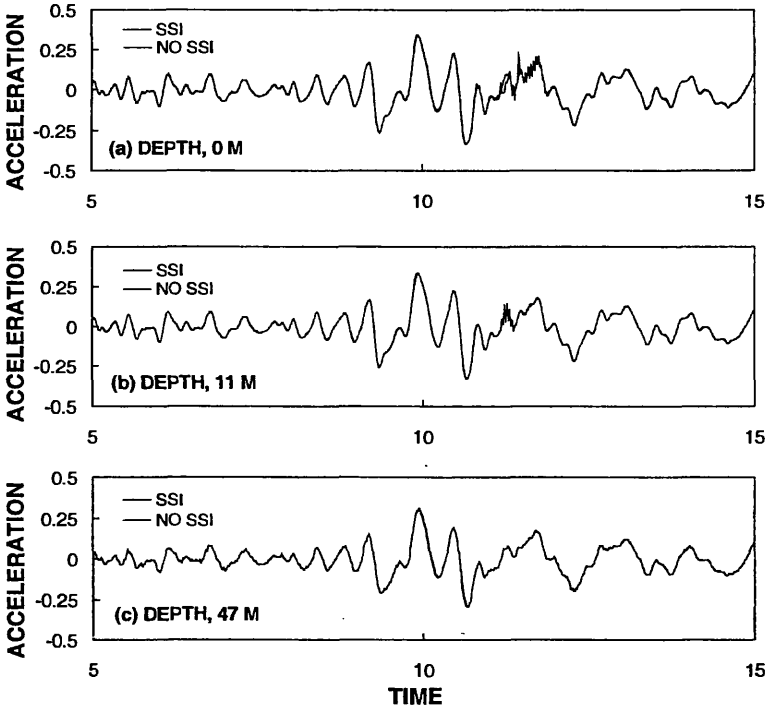

Figure 12. UD acceleration (m/sec^2)-time (sec) history with and without SSI: Lotung LSST7 case study.

These above statistics look astounding, although it is somewhat comforting to see that at least this task is now feasible. The new parallel vector 14-processor CRAY T90 supercomputer available in SDSC is similar to the CRAY C90 systems but each processor is about 1.7 times faster (24 Gflops peak speed). Thus, we can expect a similar improvement in the computer runtime with this faster machine.

4. Closure

Implicit 3D nonlinear FE analyses are computer-intensive but can provide detailed information on the effects of SSI without undue simplifications of the geometrical configurations and the boundary conditions. Advances in the computer hardware will enhance the accuracy of the simulations and must be accompanied by parallel developments of more advanced analytical platforms for nonlinear SSI analysis.

Acknowledgments

Financial support for this research was provided by the Earthquake Hazard Mitigation Division of National Science Foundation under contract Nos. CMS-9114869 and CMS-9613906 through the direction of Dr. C.J. Astill. The writers would like to thank Dr. H.T. Tang and Electric Power Research Institute for making the digitized data for the LSST7 event available.

References

Borja, R.I. and Amies, A.P. (1994). Multiaxial cyclic plasticity model for clays, J. Geotech. Engrg., ASCE 120, 1051-1070 (1994).

Borja, R.I., Tamagnini, C., and Alarcón, E. (1998). Finite strain elastoplastic consolidation, Part 2: Finite element implementation and numerical examples, Comput. Methods Appl. Mech. Engrg., 159, 103-122.

Borja, R.I., Chao, H.Y., Montáns, F., and Lin, C.H. (1998). Nonlinear ground response at Lotung LSST site, J. Geotech. and Geoenvironmental Engrg., ASCE, in review.

Borja, R.I. and Lin, C.H. (1998). Modeling nonlinear ground response of nonliquefiable soils, Earthquake Engrg. Struc. Dyn., in review.

Chang, C.Y., Mok, C.M., Power, M.S., Tang, Y.K., Tang, H.T., and Stepp, J.C. (1990). Equivalent linear and nonlinear ground response analyses at Lotung seismic experiment site, Proc. 4th U.S. Nat. Conf. Earthquake Engrg, Palm Springs, California, 1, 327-336.

Chao, H.Y. and Borja, R.I. (1998), Nonlinear dynamic soil-structure interaction analysis and application to Lotung problem, John A. Blume Earthquake Engineering Report, preprint.

Read, H.E. and Hegemier, G.A. (1984). Strain softening of rock, soil, and concrete-A review article, Mech. Mater., 3, 271-294.

Simo, J.C., Tarnow, N. and Wong, K.K. (1992). Exact energy-momentum conserving algorithms and symplectic schemes for nonlinear dynamics, Comput. Methods Appl. Mech. Engrg. 100, 63-116.

Tang, H.T., Tang, Y.K., and Stepp, J.C. (1990). Lotung large-scale seismic experiment and soil-structure interaction method validation, Nuclear Engrg. Des., 123, 197-412.

THREE DIMENSIONAL SEISMIC RESPONSE OF BUILDING-FOUNDATION SYSTEMS

By E. Bazán-Zurita[1], N. C. Bazán-Arias[2] and J. Bielak[3]

[1]GAI Consultants, Inc.,
Pittsburgh, PA
[2]Department of Civil and Environmental Engineering, University of Pittsburgh
Pittsburgh, PA
[3]Department of Civil and Environmental Engineering, Carnegie-Mellon University
Pittsburgh, PA

ABSTRACT

This paper provides means for quantifying the importance of three-dimensional soil-structure interaction (SSI) during earthquakes on elastic building-foundation systems localized on sites where SSI effects can be significant. The building is modeled as an elastic one-story three-dimensional structure resting on an embedded foundation. A parametric study is conducted to assess the effects of the foundation impedance, building eccentricity, and excitation characteristics on the seismic response. The results indicate that it is often not conservative to ignore SSI in the seismic analysis of torsionally eccentric structures.

INTRODUCTION

The seismic design of buildings, according to current building codes, is based on static or dynamic analyses that consider elastic behavior. Effects of inelastic behavior during strong earthquakes are taken into consideration by reducing by a global factor the forces obtained in the elastic analysis. Such a factor is derived from comparisons of the response of simple elastic and inelastic models, and is justified in practice on the basis of the overall performance of different types of buildings during actual earthquakes. Elastic analysis remains, therefore, the most widely used approach for the seismic design of building-foundation systems.

The objective of this study is to evaluate the impact of three-dimensional soil-structure interaction (SSI) on the elastic response of building-foundation systems under earthquake excitation. In pursuing this objective, we have conducted a parametric analysis of an idealized single-story three-dimensional model, meant to represent the first two translational and the first torsional modal response of actual buildings, using two prototype foundation conditions: one very stiff (fixed base) and the other simulating soft soil conditions. We focus our attention on the two

response quantities that are most important in seismic design of three-dimensional systems, namely base shear force and dynamic torsional eccentricities.

FORMULATION

The system under investigation is shown in Figure 1. It consists of an elastic viscously damped structure with mass m_1 and three degrees of freedom (two horizontal perpendicular translations along the X, Y axes and one rotation around the vertical axis, Z). The structure's properties represent the three (two translational and one torsional) "fundamental modes" of a multistory building with floors stiff enough in their own plane to be considered as infinitely rigid horizontal diaphragms. This structure rests on a rigid foundation with mass m_0, embedded in a flexible soil, and with no slippage allowed between the base and the soil. The soil flexibility allows translational and rotational displacements related to the X and Y axes and torsional rotations around the Z axis. Formulated thus, the system has eight significant degrees of freedom, namely, two horizontal translations and one torsional rotation at the top mass, m_1, and two horizontal translations, two rocking rotations and one torsional rotation at the base mass, m_0. The position of the lumped masses m_1 and m_0 (center of masses of the diaphragms) can be eccentric in both the X and Y directions. The seismic input motion occurs in the X direction. This SSI system was modeled by a three-dimensional two-story column whose first story represents the foundation and its second the structure. The program ETABS (Wilson et al., 1975) was used to perform the numerical calculations.

PLANAR SYSTEMS

To establish a basis of comparison for three dimensional behavior, we have studied planar SSI systems with no torsional eccentricities and masses moving only along the X horizontal axis. In this case only three degrees of freedom remain active: horizontal translation of the top mass in the X axis, horizontal translation of the base mass relative to free field motion, and rotation of the system in the X-Z plane. If there is no interaction, the relevant dynamic properties of the superstructure are the fixed-base period, T_1, and the damping ratio, ζ_1. When SSI is significant, the most relevant foundation parameters are its mass, m_0, the SSI translational (horizontal) and rocking stiffness coefficients, k_v, and k_ϕ, and the corresponding SSI damping ratios, ζ_v and ζ_ϕ.

To examine design situations, we have used the response spectrum method to analyze planar SSI systems considering two types of input spectra: 1) a constant design acceleration for all periods, and 2) a hyperbolic spectrum with design acceleration that decreases inversely with the period. The two spectra are depicted on Figure 2. m_0 has been taken to be 0.2 m_1 throughout this paper. We have assumed that the translational and rocking SSI stiffness are $k_v = \alpha\ (5\ k_1)$ and $k_\phi = \alpha\ (k_1\ H^2)$ varying α such that T'/T_1 varies from 1.0 (α very large) to 1.33 ($\alpha = 1$). T' is the fundamental SSI period. SSI damping usually increases the damping ratio of the fundamental mode of a building foundation system. This effect could be included by modifying the design spectra. However, we opted to ignore it since our interest is focused in the changes of seismic

response attributed to differences in modes and periods of vibration when SSI is included. In any event, beneficial SSI damping effects should be carefully evaluated in practice since soil layering, separation of the foundation from the surrounding soil, and the presence of adjacent structures could decrease them significantly.

Table 1 summarizes the resulting dynamic base shear normalized by the product of m_1 times the spectral acceleration, S', corresponding to T'. Since the values in the table are very close to unity, it is concluded that the seismic shear forces can be accurately calculated as $m_1 S'$. The errors are smaller than 3.0 percent and are well covered by the factors of safety included in design spectra and regulations. However, it is clearly important to calculate accurately the fundamental SSI period to determine the correct value of S'.

TABLE 1
NORMALIZED BASE SHEAR FORCE, $V/(m_1 S')$ FOR PLANAR SYSTEMS

Factor α	T'/T_1	Flat Spectrum	Hyperbolic Spectrum
10000	1.000	1.000	1.000
10	1.037	1.004	1.005
3	1.120	1.010	1.012
1	1.329	1.020	1.027

DYNAMIC PROPERTIES OF 3-D SYSTEMS

We have considered two types of three-dimensional systems. Firstly, it has been assumed that the masses m_1 and m_0 both have the same eccentricity along the Y axis, i.e., in the direction perpendicular to the input motion, and no eccentricity along the X axis. The floor and the foundation mat of the model are both taken to be square, with side dimension b and torsional radius of gyration $b/\sqrt{6}$. We have also considered that the structure has the same translational stiffness k_1 in the X and Y directions, and that the SSI translational and rocking SSI stiffnesses are respectively the same in both horizontal directions.

The torsional stiffness of the structure has been varied such that the ratio of the fixed-base uncoupled torsional period, T_θ, to the fundamental uncoupled fixed-base translational period, T_1, equals 0.6, 0.8 and 1.0. These values represent, respectively, buildings where the lateral stiffness is concentrated in the exterior portions of its plan, distributed more or less uniformly in plan, or concentrated at the central part of the building's plan (see Figure 3). For the base case studied herein, we have set $k_v = 5k_1$ and $k_\phi = k_1 H^2$ resulting in $T'/T_1 = 1.33$ for symmetric systems. The torsional SSI stiffness, k_θ, was taken as 1.5 k_ϕ, which represents a mat foundation embedded in a viscoelastic halfspace. For a second basic SSI case, the values of k_v and k_ϕ remained the same but k_θ was reduced to 0.15 k_ϕ. This could correspond, for instance, to structures founded in a soil

layer underlain by bedrock or with flexible foundation. To examine systematically systems where torsion is relevant, the static eccentricity has been varied from zero to 0.3 times the building's plan dimension, b.

For this type of torsionally eccentric systems, the first and third modes of vibration exhibit coupled translations and rotations. The second mode is uncoupled, with displacements only in the Y direction, and has the same period as the corresponding planar system. Figure 4 shows the first and the third natural periods of these SSI systems. All values have been normalized by the fundamental fixed-base period of the corresponding symmetric system. It is noted that the first period ratio of eccentric systems is always larger than unity, in agreement with the known result that torsional eccentricities amplify the fundamental period of the associated symmetric structure. The increase of the fundamental period with the eccentricity is greater when T_θ/T_1 approaches unity, for both fixed base and SSI systems. Conversely, the normalized third periods are always smaller than the corresponding ratio T_θ/T_1. In all cases incorporation of SSI results in longer periods. The effects of SSI on the first period are always more significant, showing increasing factors greater than 1.33, since the SSI parameters were set to amplify the translational period by 33 percent when there is no eccentricity. The SSI effects on the third period are small when k_θ was taken as 1.5 k_ϕ, but more noticeable when k_θ was reduced to 0.15 k_ϕ.

To examine cases with eccentricities in two directions, systems for which the two masses m_1 and m_0 have the same static eccentricity, e_{st}, along both the X and Y axes have been analyzed. The properties of these systems are the same as those for the cases with eccentricity in only one direction. The difference is the additional eccentricity in the Y direction. The first and third modes of vibration are again coupled. The second mode has no torsional component and has the same period as the corresponding planar system. Figure 5 shows the first and the third natural periods of these doubly eccentric SSI systems, normalized by the fundamental fixed-base period of the corresponding symmetric system. The trends of these periods are the same as those for systems eccentric in only one direction. However, the increasing and decreasing amounts are always more pronounced. Again, the SSI effects are more noticeable when k_θ assumes the reduced value of 0.15 k_ϕ, and the impact of torsional eccentricities is more noticeable as T_θ/T_1 approaches unity.

RESPONSE OF 3-D SYSTEMS WITH ECCENTRICITY IN ONE DIRECTION

The three-dimensional systems with eccentricity in only one direction described in the previous section have been analyzed with the response spectrum method, including all modes of vibration in the calculations. The seismic input consists of two simplified design spectra: flat and decreasing with period. Since these systems have natural periods with very close values, a complete quadratic combination rule was used to combine modal responses. The base shear forces obtained using a flat spectrum for $T_\theta/T_1 = 0.6$, 0.8 and 1.0 are presented in Figure 6. The forces have been divided by the product of the mass m_1 times the spectral acceleration, S' (in this case constant). In all cases, whether with or without SSI, an increase in the eccentricity decreases the shear force, with reductions as large as 25 percent for fixed bases systems with $T_\theta/T_1 = 1$. The reductions are

considerably smaller when SSI effects are significant. This clearly indicates that ignoring SSI will not necessarily lead to conservative results in the dynamic elastic analysis of eccentric structures.

The dynamic eccentricities resulting from a flat spectrum are presented in Figure 7. These eccentricities have been normalized by the corresponding static eccentricity, thus illustrating the dynamic amplification factors of static torsional moments. Such factors increase significantly when the uncoupled torsional period of the structure approaches the uncoupled translational period (i.e., when T_θ/T_1 approaches unity). Values as high as 5.5 occur in fixed-base systems with small eccentricities, indicating that in practice torsional moments can be significant even in buildings that are almost symmetric. SSI always reduces the dynamic amplifications of the eccentricities; but, again, if the SSI torsional stiffness becomes small, these reductions also become appreciably smaller or even negligible for systems with large eccentricities. As a rule, the beneficial effects of SSI decrease as the static eccentricity increases, particularly when the uncoupled translational and torsional periods are close to each other. Sound design recommendations aim at preventing the tuning of translational and torsional uncoupled periods on the basis of this observation.

The normalized shear forces and dynamic eccentricities corresponding to the hyperbolic spectrum are presented in Figures 8 and 9. The variations of shear force with dynamic properties and SSI parameters are very similar to those shown in Figures 6 and 7 for a flat spectrum. The maximum differences are approximately 10 percent. This indicates that by dividing the shear forces by the spectral ordinate the normalized response becomes almost independent of the type of spectrum. On the other hand, it highlights again the importance of calculating accurately the SSI periods of vibration since the seismic response is almost directly proportional to spectral accelerations.

The comparison of Figures 7 and 9 shows that the ratio of the dynamic eccentricity, e_{dyn}, to the static eccentricity, e_{st}, is in most cases greater for the hyperbolic spectrum (Figure 9) than for the flat spectrum (Figure 7). The differences are the result of different relative participations of the various modes of vibration of the system in the calculation of shear forces and torsional moments. This emphasizes the importance of calculating accurately higher modes of vibration that exhibit significant torsional rotations.

RESPONSE OF 3-D SYSTEMS ECCENTRIC IN TWO DIRECTIONS

To examine three-dimensional cases with eccentricities in two directions, systems for which the two masses m_1 and m_0 have the same static eccentricity, e_{st}, along both the X and Y axes have been analyzed. The properties of these systems have been selected to be the same as those in the previous section with the exception of the additional eccentricity in the Y direction. The input spectrum is flat. Table 2 presents the normalized shear forces in the horizontal X and Y directions and the dynamic torsional eccentricity as a function of the static eccentricity, e_{st},. It is immediately apparent that all these response quantities are significantly affected by the eccentricity. While the shear in the direction of the ground motion, V_x, decreases with increasing values of e_{st}, the opposite occurs for the torsional moments and the shear in the perpendicular direction, V_y, which

now is not nil as a result of the coupling of displacement in the modal shapes. The effects of SSI and of the eccentricity on V_x and on the dynamic eccentricity follow the same trends as in systems with eccentricity in only one direction, but are always numerically higher.

TABLE 2
SEISMIC RESPONSE OF SYSTEMS
ECCENTRIC IN TWO DIRECTIONS. FLAT SPECTRUM

	Shear Force in X, $V_x/(m_1S')$			Shear Force in Y, $V_y/(m_1S')$			Dynamic Eccentricity, e_{dyn}/e_{st}		
T_θ / T_1	0.6	0.8	1.0	0.6	0.8	1.0	0.6	0.8	1.0
FIXED BASE									
e = 0.00	1.000	1.000	1.000	0.000	0.000	0.000	NA	NA	NA
0.05	0.994	0.958	0.832	0.058	0.164	0.348	1.62	2.73	4.40
0.10	0.963	0.843	0.716	0.210	0.412	0.513	1.58	2.40	3.04
0.15	0.897	0.752	0.672	0.381	0.537	0.568	1.59	2.19	2.43
0.20	0.825	0.706	0.655	0.503	0.587	0.593	1.62	2.01	2.11
0.30	0.738	0.676	0.649	0.609	0.626	0.620	1.63	1.78	1.80
SSI, $K_\theta = 1.5\ K_\phi$									
e = 0.00	1.020	1.020	1.020	0.000	0.000	0.000	NA	NA	NA
0.05	1.019	1.013	0.990	0.030	0.064	0.138	1.30	1.67	2.44
0.10	1.009	0.977	0.891	0.117	0.229	0.383	1.30	1.63	2.22
0.15	0.982	0.904	0.792	0.242	0.406	0.529	1.30	1.63	2.08
0.20	0.935	0.829	0.736	0.373	0.525	0.592	1.33	1.65	1.96
0.30	0.831	0.744	0.696	0.553	0.624	0.696	1.42	1.64	1.76
SSI, $K_\theta = 0.15\ K_\phi$									
e = 0.00	1.020	1.020	1.020	0.000	0.000	0.000	NA	NA	NA
0.05	1.014	1.000	0.948	0.062	0.114	0.223	1.63	2.18	3.26
0.10	0.980	0.919	0.813	0.224	0.345	0.468	1.59	2.03	2.67
0.15	0.911	0.821	0.735	0.401	0.508	0.566	1.60	1.96	2.31
0.20	0.837	0.758	0.701	0.523	0.585	0.605	1.63	1.89	2.07
0.30	0.751	0.709	0.681	0.627	0.640	0.638	1.65	1.75	1.80

Table 3 presents similar results for the hyperbolic spectrum. Note that the normalized shear force in the horizontal X direction is in all cases higher than for the flat spectrum. This reflects a larger contribution of higher modes of vibration (with smaller periods) when the spectrum increases for decreasing periods. For the same reason, the normalized shear force in the Y direction is also higher than for the flat spectrum. On the other hand, for most cases, the ratio of the dynamic torsional eccentricity to the static eccentricity is smaller than the ratio corresponding to the flat spectrum. The explanation is that in the calculation of the dynamic eccentricity the dynamic torsional moment is divided by a relatively larger dynamic shear force. Again, all these response

quantities are appreciably affected by the eccentricity, following the same trends as in the case of the flat spectrum.

TABLE 3
SEISMIC RESPONSE OF SYSTEMS
ECCENTRIC IN TWO DIRECTIONS. HYPERBOLIC SPECTRUM

	Shear Force in X, $V_x/(m_1 S')$			Shear Force in Y, $V_y/(m_1 S')$			Dynamic Eccentricity, e_{dyn}/e_{st}		
T_θ / T_1	0.6	0.8	1.0	0.6	0.8	1.0	0.6	0.8	1.0
FIXED BASE									
e = 0.00	1.000	1.000	1.000	0.000	0.000	0.000	NA	NA	NA
0.05	0.998	0.972	0.906	0.059	0.169	0.379	1.76	2.91	4.29
0.10	0.980	0.888	0.845	0.216	0.441	0.603	1.69	2.49	2.81
0.15	0.931	0.832	0.853	0.400	0.602	0.719	1.66	2.16	2.10
0.20	0.879	0.826	0.890	0.542	0.694	0.804	1.64	1.87	1.68
0.30	0.840	0.882	0.997	0.699	0.822	0.951	1.52	1.45	1.24
SSI, $K_\theta = 1.5\ K_\phi$									
e = 0.00	1.027	1.027	1.027	0.000	0.000	0.000	NA	NA	NA
0.05	1.027	1.024	1.007	0.037	0.069	0.144	1.41	1.82	2.62
0.10	1.023	1.000	0.933	0.128	0.242	0.410	1.39	1.75	2.32
0.15	1.005	0.946	0.867	0.256	0.433	0.589	1.37	1.71	2.09
0.20	0.970	0.892	0.849	0.394	0.574	0.691	1.38	1.67	1.85
0.30	0.896	0.861	0.892	0.603	0.730	0.822	1.40	1.52	1.46
SSI, $K_\theta = 0.15\ K_\phi$									
e = 0.00	1.027	1.027	1.027	0.000	0.000	0.000	NA	NA	NA
0.05	1.025	1.015	0.976	0.065	0.118	0.233	1.80	2.35	3.39
0.10	1.003	0.956	0.879	0.234	0.365	0.513	1.74	2.15	2.70
0.15	0.950	0.945	0.845	0.425	0.594	0.656	1.71	2.00	2.21
0.20	0.897	0.854	0.855	0.568	0.666	0.744	1.69	1.84	1.85
0.30	0.861	0.877	0.931	0.725	0.798	0.876	1.58	1.53	1.41

CONCLUSIONS

The results presented in this paper show that the seismic response of a building-foundation system including soil structure interaction can be significantly different from that calculated with a fixed-base model. Simple single-story models have been used for rapid evaluation of SSI effects showing that changes of tens of percent occur in the shear force on the structure and on the torsional moments. The SSI effects are mainly the result of the increase in the fundamental period, which leads to a different spectral ordinate. However, in three-dimensional eccentric structures

SSI also produces appreciable changes in higher natural periods and modes of vibration, affecting significantly dynamic eccentricities and shear forces in the direction perpendicular to the seismic input.

For the three-dimensional fixed-base eccentric systems examined in this paper, an increase in eccentricity reduces the shear force up to 35 percent when the static eccentricity is 0.3 times the building plan dimension and the ratio T_θ/T_1 is equal to 1.0. These reductions are appreciably offset when SSI is significant. SSI also leads to even greater reduction in the dynamic amplifications of static eccentricities as compared to the associated fixed-base systems. The reductions are, however, much smaller when the torsional SSI stiffness is small compared to the rocking SSI impedance. In general, the beneficial effects of SSI diminish as the static eccentricity increases, particularly when the uncoupled translational and torsional periods are close to each other.

The above results point out to the convenience of incorporating SSI in the elastic dynamic analysis to avoid unconservative calculations of the seismic response. While simple formulas such as the one proposed by Jennings and Bielak (1973) provide rapid and accurate estimates of the SSI uncoupled fundamental translational period, the torsional SSI parameter should also be carefully evaluated and incorporated in the dynamic modal analysis of three-dimensional structures. Special attention should be paid to factors such as layering, proximity to other structures, stiffness of the foundation members, and embedment. It is pertinent to recall that torsional moments are favorable or detrimental to the vertical frames or walls of a building depending on their location in plan, and that a smaller moment is not favorable in every instance. This highlights the importance of estimating torsional eccentricities as accurately as possible.

The findings of this study reinforce design recommendations oriented to increase the torsional stiffness of a building to prevent tuning of translational and torsional uncoupled periods as well as to avoid excessive eccentricities. This can be achieved by properly locating in plan the vertical systems that resist the seismic forces. With the help of modern computer programs, effects of torsion and of SSI can be expeditiously incorporated in a three-dimensional dynamic analyses. Significant changes in the periods and modes of vibration with respect to the fixed-base uncoupled properties may indicate the need for reviewing the basic structural and foundation layout.

REFERENCES

Jennings, P.C., and J. Bielak. "Dynamics of Building-Soil Interaction." *Bull. Seism. Soc. Am.*, 1973 63 (1), 9-48.

Wilson, E.L., Holings, J.P. and Dovey, H.H., "Three Dimensional Analysis of Building Systems (extended version)", Report No. UCB/EERC 75-13, Earthquake Engineering Research Center, University of California, Berkeley, California, 1975.

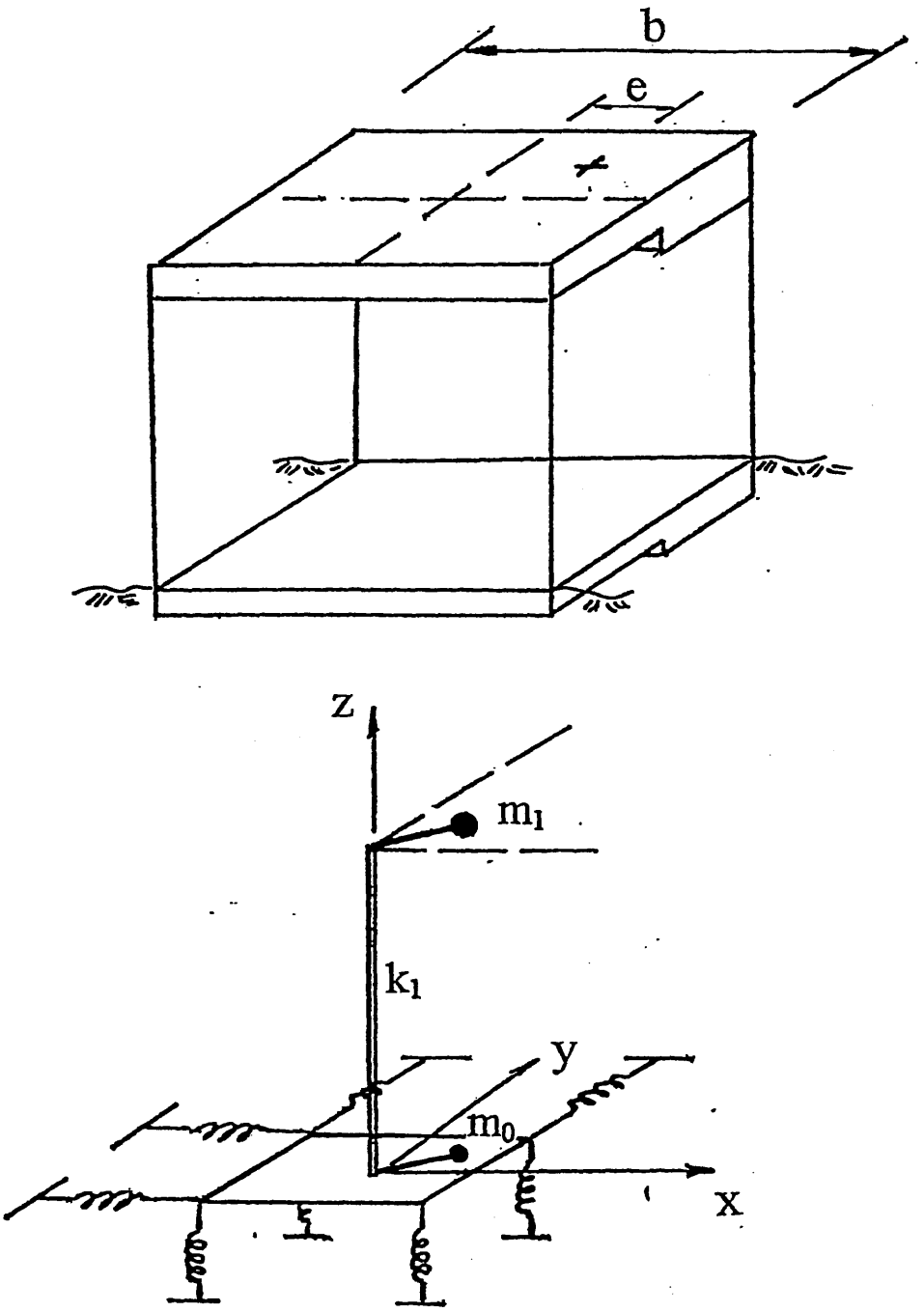

Figure 1. Three-Dimensional SSI System

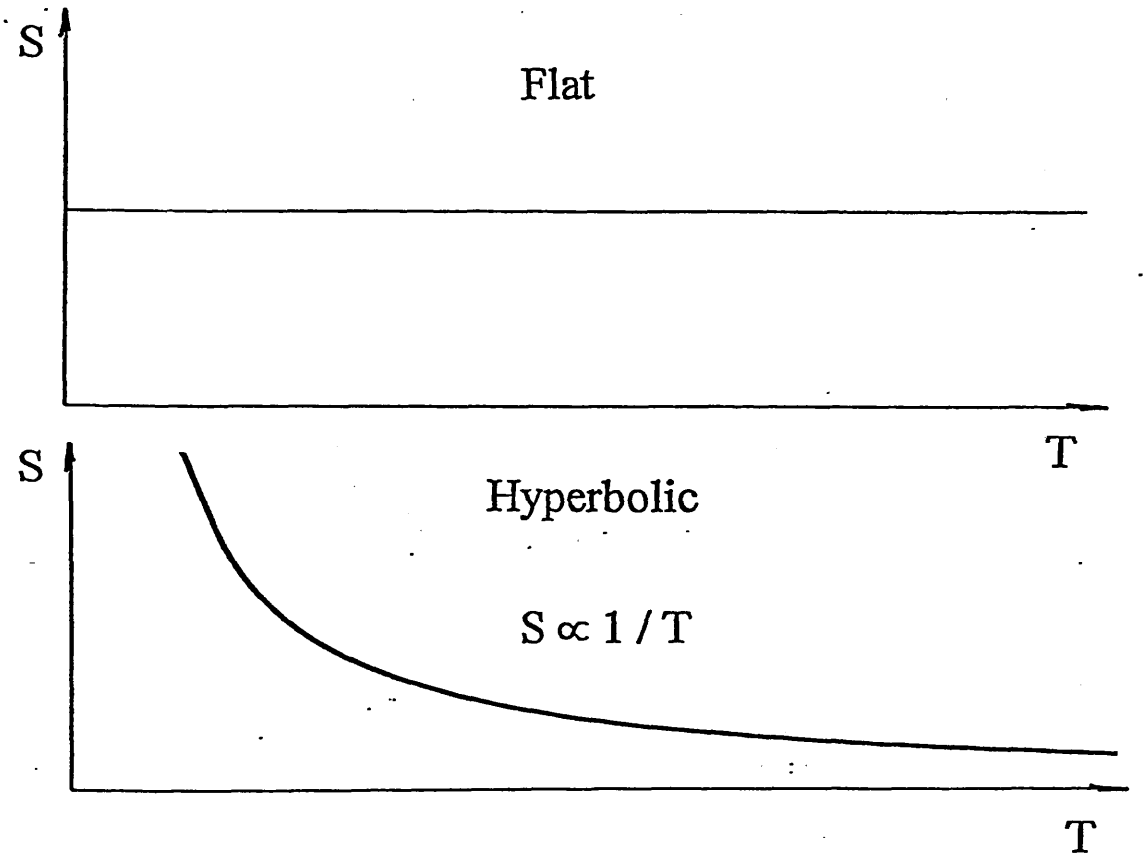

Figure 2. Flat and Hyperbolic Design Spectra

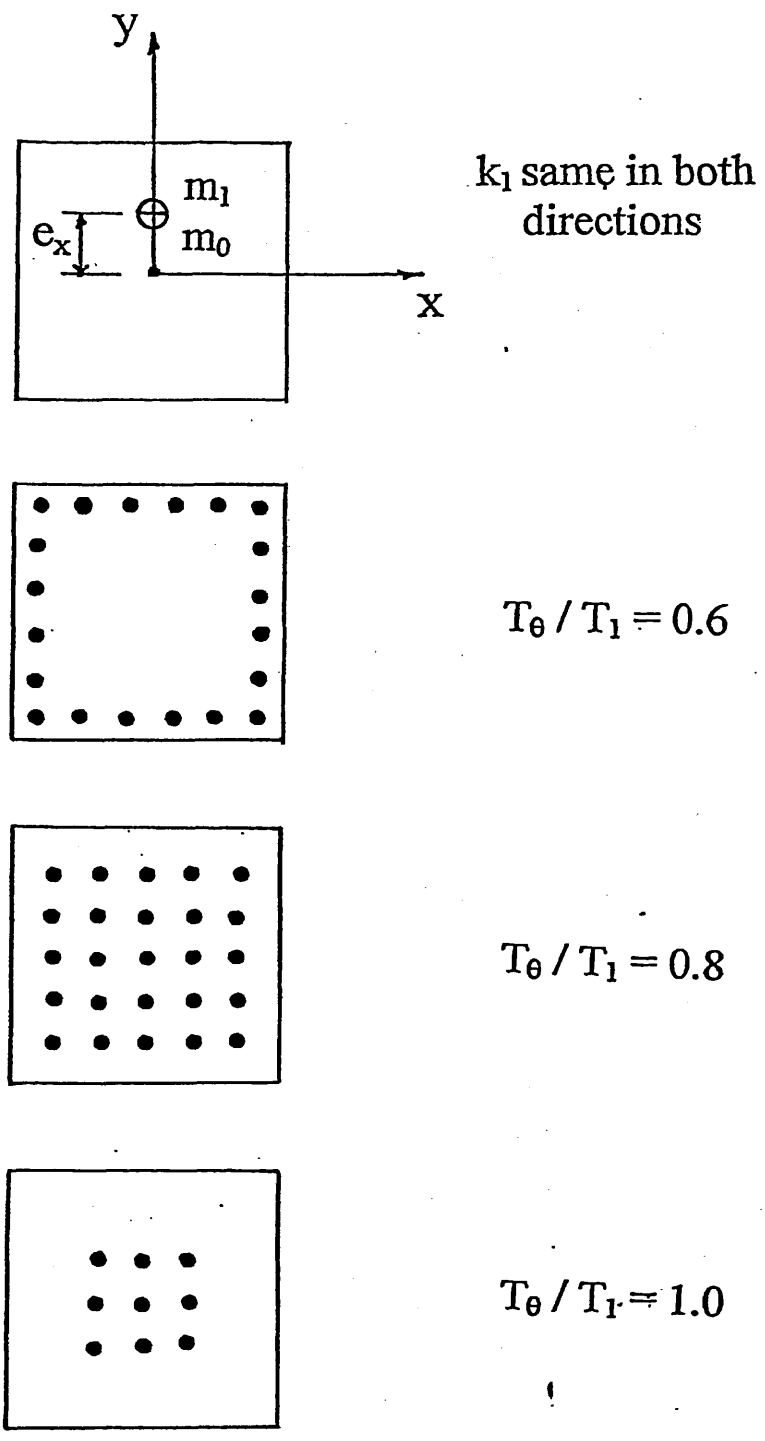

Figure 3. Plan View of Three-Dimensional Systems

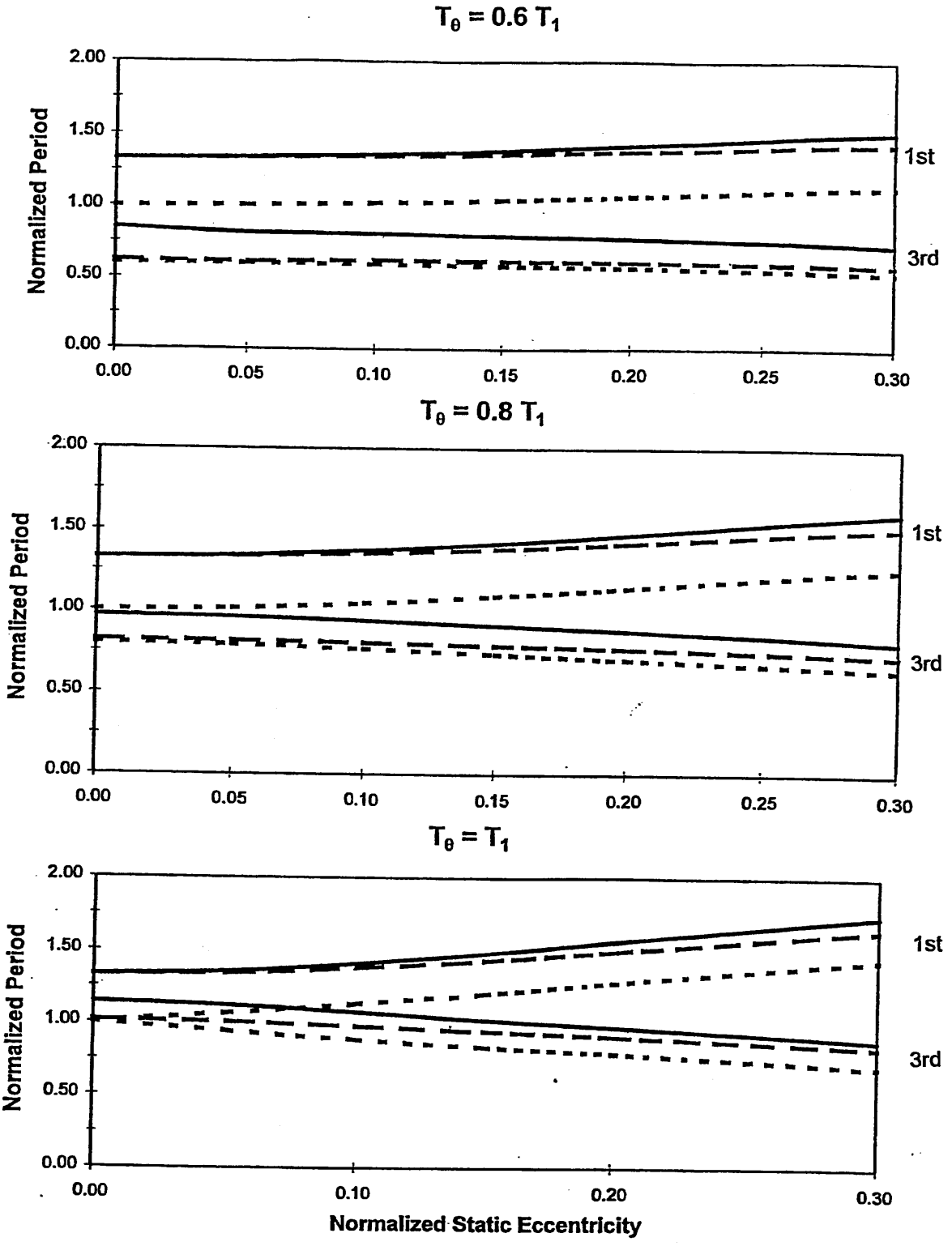

Figure 4. First and Third Natural Periods of Vibration, Systems Eccentric in One Direction

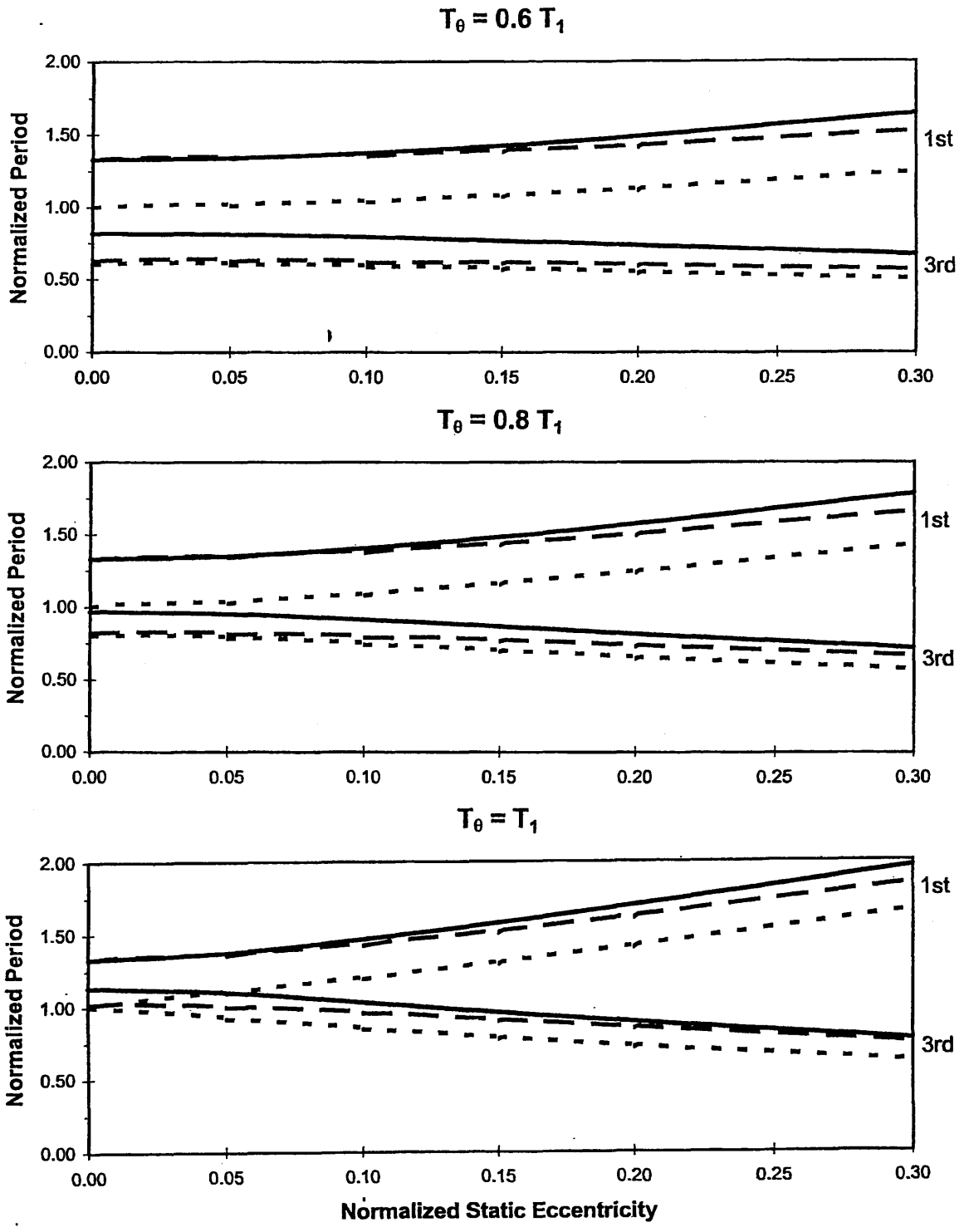

– – – No SSI, — — $K_\theta = 1.5K_\phi$, ——— $K_\theta = 1.5K_\phi$

Figure 5. First and Third Natural Periods of Vibration, Systems Eccentric in Two Directions

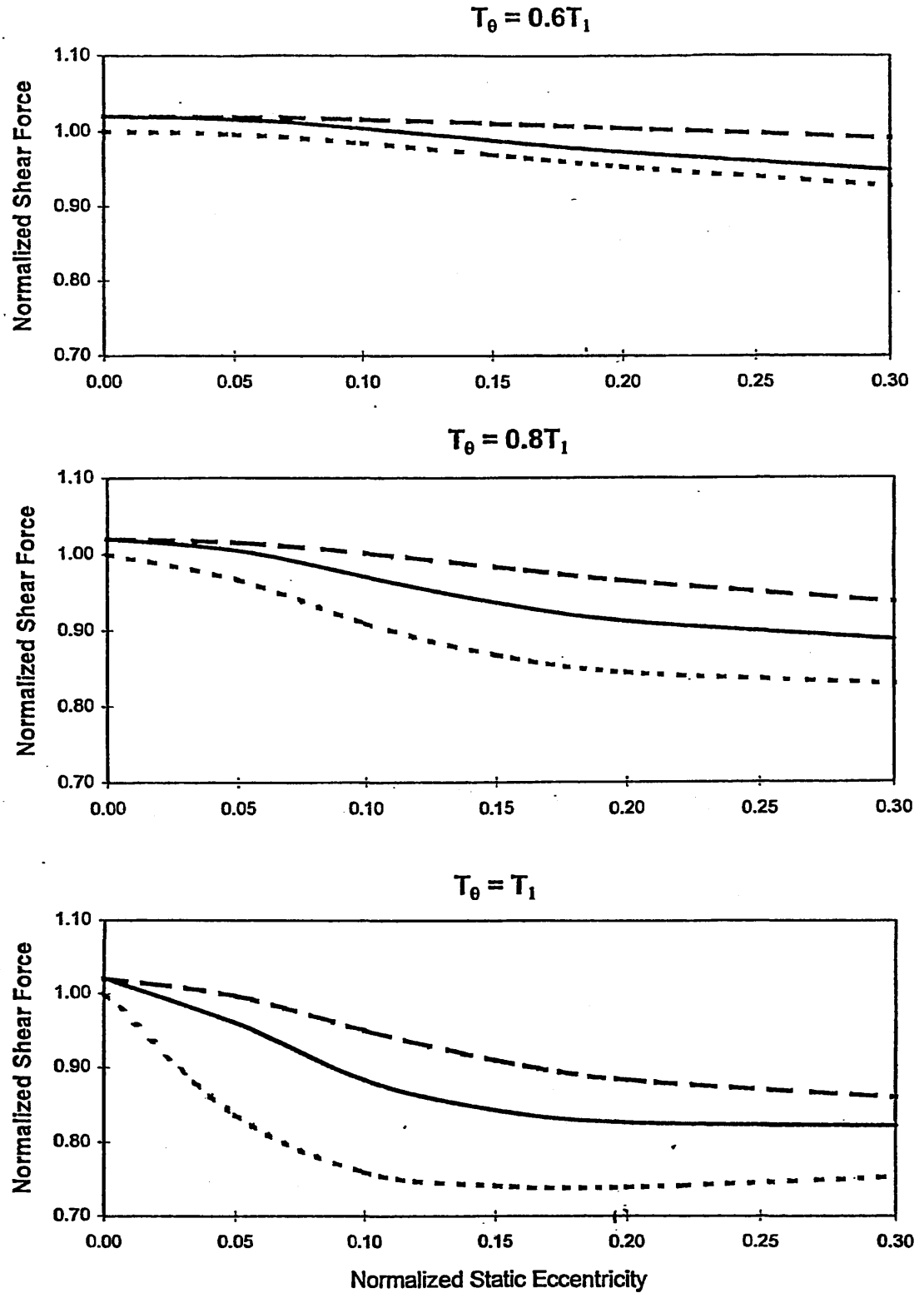

Figure 6. Normalized Base Shear Force along X Axis, Flat Spectrum

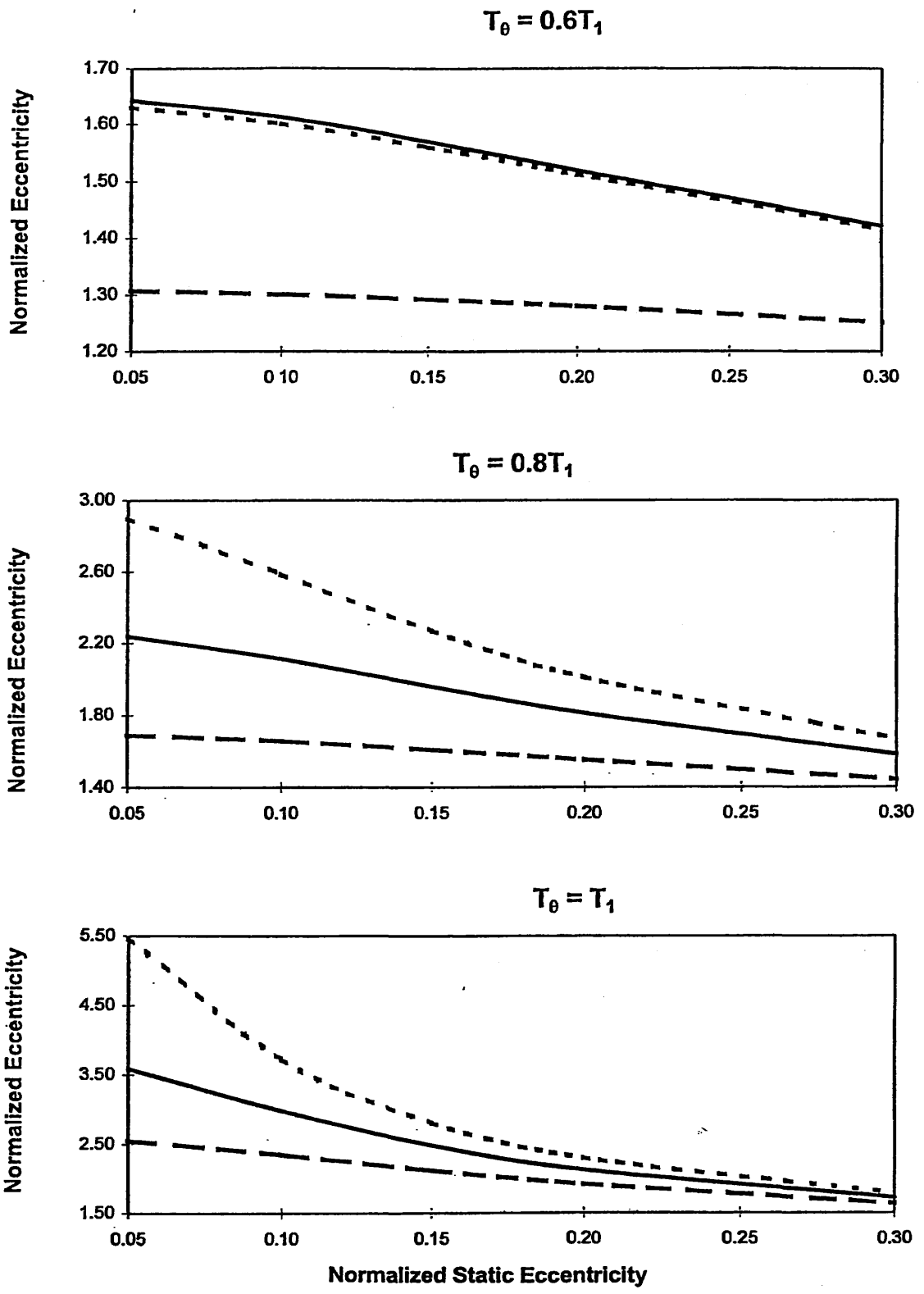

Figure 7. Normalized Dynamic Eccentricity Perpendicular to the X Axis, Flat Spectrum

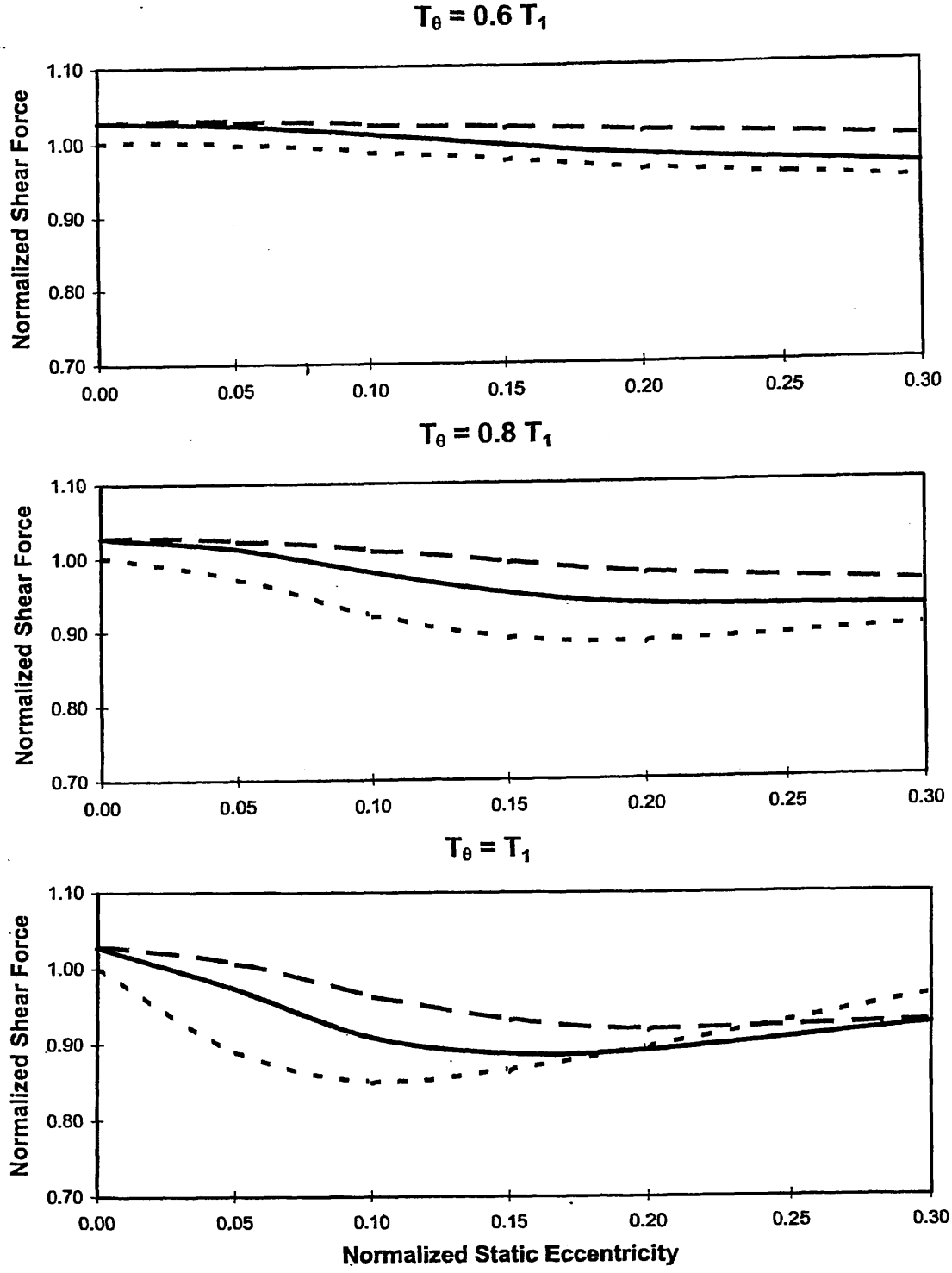

– – – No SSI, — — $K_\theta = 1.5K_\phi$, ——— $K_\theta = 1.5K_\phi$

Figure 8. Normalized Base Shear Force along X Axis, Hyperbolic Spectrum

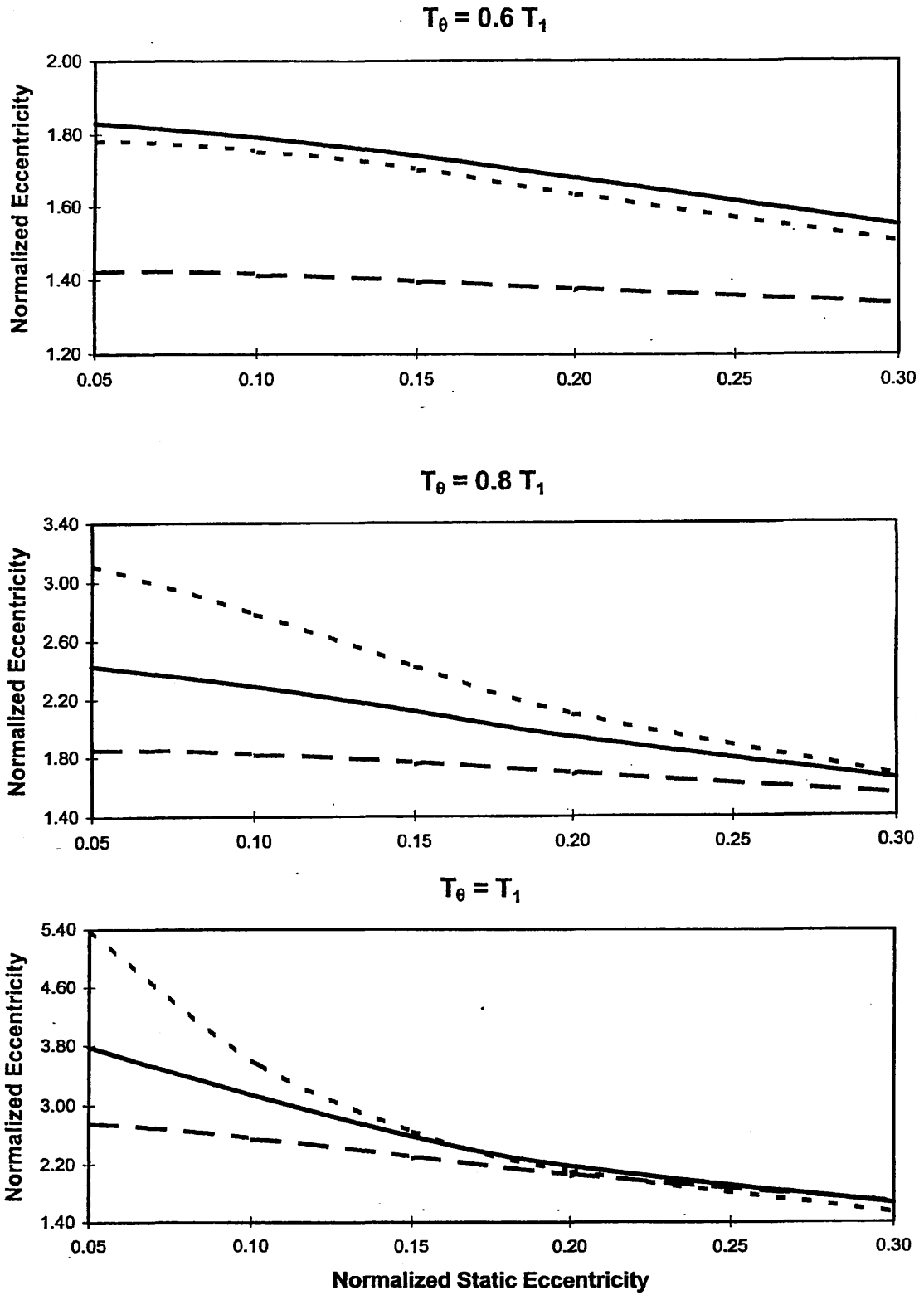

– – – No SSI, — — $K_\theta = 1.5K_\phi$, ——— $K_\theta = 1.5K_\phi$

Figure 9. Normalized Dynamic Eccentricity Perpendicular to the X Axis, Hyperbolic Spectrum

A Statistical Measure of Fit for Analytical Models Conditioned on Experimental Results

Roger Ghanem
The Johns Hopkins University
Baltimore, MD 21218

Introduction

The general question this paper tries to answer can be phrased as follows: Given data for some response quantity associated with an soil-structure-interaction (SSI) experiment, with what level of confidence can any particular mathematical model be claimed to represent the physics of the experiment ?

Mathematical models of physical phenomena usually attempt to address a very well defined aspect in isolation of the other aspects involved. This is necessitated by the complexity of nature and the restriction of our methods of inquiry to certain forms of logical statements. These isolated aspects of nature usually represent the behavior of a given system in a particular and isolated mode of operation. Since it is generally not possible to isolate and examine a physical system in this way, it should be expected that predictions from mathematical models would generally disagree with the observed behavior of the systems they purporte to model. By generalization and analogy, however, models permit us, starting from an observed fact, to follow a certain chain of logic in order to deduce and predict a number of additional facts. It should be remembered, though, that only the first fact is certain, and all the others are merely probable. As noted by Poincaré [4], however, it is far better to predict with certainty than to never have predicted at all.

In addition to uncertainties regarding the applicability of a certain model to a given situation, which is typically associated with the model having captured the physical mechanisms known to be at play, uncertainties are also present in identifying the parameters to be used in that model. These parameters are usually obtained through some fitting procedure. Were the model perfect, some set of parameters would produce a perfect fit between the predictions of the model and the observed data. Given the approximate nature of the model, however, fitting errors will necessarily be incurred in the estimated values of these parameters. The question identified at the beginning of the paper can then be restated as one of deducing the confidence to be attached to the model given the observed scatter, or uncertainty, in its parameters. Implicit here is the assumption that these parameters are the parameters that produce a best fit for the predictions of the model against experimental data. A closely related and equally important question is that of specifying the maximum level of uncertainty to be tolerated in the data if a decision about accepting or rejecting a particular model is desired with a specified confidence.

General Formulation

In trying to model physical phenomena, certain intrinsic principles have to be satisfied by any mathematical model attempting to rationalize observed behavior. Such principles may consist of some equilibrium or conservation laws whose applicability is not questioned within the confines of the problem at hand. Consider the set of models, denoted by $\mathcal{S}$, consisting of all models that satisfy such consistency requirements. Further, consider a model $\mathcal{M}(\theta_1, \ldots, \theta_p) \in \mathcal{S}$ parametrized by the set $(\theta_1, \ldots, \theta_p)$, and denote by $\mathcal{M}_s$, the model whose parameter set is equal to a specific set $\boldsymbol{\theta}_s$ indexed by s. Moreover, let $q_{\mathcal{M}_s} \equiv q(\mathcal{M}_s)$ symbolize the functional dependence of some predictable of the model on the parameter set $\boldsymbol{\theta}$. The symbol q_s will also be used when the specific model $\mathcal{M}$ is clear from the context. The quantity q_s could, for instance, represent the stress, or acceleration predicted by the model $\mathcal{M}_s$ at some point in the domain of interest. Finally, the symbol $\hat{q}$ will be used to denote the observed value of the physical quantity q_s attempts to predict. Although the parameter set for a given model is uncertain (i.e. can be viewed as having a probability measure induced on it), the relationship between this set and the predictables, q_s, is deterministic, and is completely specified through the functional $\mathcal{M}$. Thus, once the confidence in $\boldsymbol{\theta}_s$ has been quantified, the confidence in q_s is uniquely determined. A probabilistic framework will be used to represent the uncertainty in the problem. Probabilistic inquiries of the form, $P(Q \in \mathcal{Q})$ will be posed, where a capital letter will be used to denote a random variable and a calligraphic letter will be used to denote a set to which the random variable may belong; whenever this set consists of an interval on the real line, then lower case letter will be used to delineate the interval. Given the above definitions, the following equality holds,

$$P_Q(\mathcal{Q}) \equiv P(Q \in \mathcal{Q}) = P(Q(\mathcal{M}(\theta)) \in q) = P(\Theta \in \mathcal{T}) \ , \tag{1}$$

where $\mathcal{T}$ denotes a subset of the of the set of possible parameters. The probability statement on the right hand side can be deduced following the curve fitting of the observations to the predictions of the model. The statement to the left of the equality describes the probability of the prediction falling in the set $\mathcal{Q}$ when the parameters are in the set $\mathcal{T}$. Although conceptually straightforward, evaluating the probabilistic characterization of Q requires a significant computational effort, and is typically performed using a Monte Carlo simulation procedure. In the next section, the spectral stochastic finite element procedure will be implemented as a more efficient way of computing the transformation from probability measures on the parameters to probability measures on the predictions. It should be noted, before proceeding, that the transformation between the two probability measures is uniquely defined by the model $\mathcal{M}$ and can therefore be perceived as a characteristic of the model, in the same way that a transfer function is a characteristic of a dynamical system. Once the expression on the left hand side of equation (1) has been evaluated for all relevant sets $\mathcal{Q}$, however, hypothesis testing for the model given the observations can be readily performed. Thus, let the set $\mathcal{Q}_\alpha$ with confidence level α be specified in the sense that

$$P(Q \in \mathcal{Q}_\alpha) = 1 - \alpha \ . \tag{2}$$

Then an observation $\hat{q}$ within this set would corroborate the mathematical model with a confidence of at least $1 - \alpha$. Clearly, the largest such α is of most value in the present

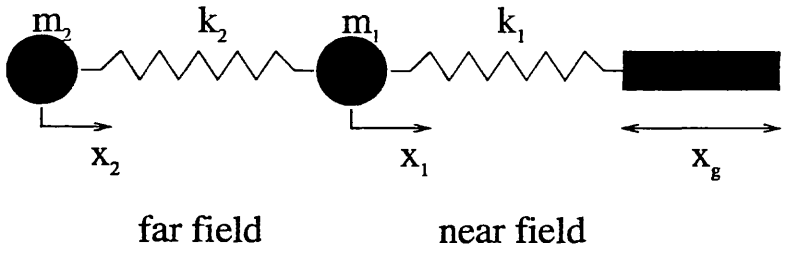

Figure 1: Two-Degree-of-Freedom Model for Foundation-Soil Interaction.

context, and can be used to define the confidence in the model provided by the data.

Physical Model

An often used model for soil-structure interaction consists of an elastic structure supported by an elastic foundation of Winkler type. Particularly in the case of pile foundations, and in an effort to provide for different soil behavior in near and far field regions, each spring in the Winkler reaction model is sometimes replaced by a two layer model, consisting of three masses connected by two springs. This model features the mass of the pile, that of the near field soil, and the far field soil. The springs connecting these masses represent the different elastic reactions that characterize the near and far field regions. Considering the pile-soil system to be part of a shaking table experiment, whereby the base of the pile is fixed to the shaking table, each section of the pile, along its length, oscillates with some amplitude. Considering a slice through the soil-pile system, and neglecting interactions between this layer and neighboring layers, the three-mass model for that layer can be perceived as being subjected to a base excitation due to the oscillation of the pile. Referring all motion to a coordinate system fixed on the pile at that layer, a two-degree-of freedom system is obtained as shown in Figure (1). Assume damping, of various sources, to be negligible. Although an oversimplification, the present model will serve the purpose of introducing the concepts set forth in the present paper.

Approximation of the Uncertainty in the Predictions

The stochastic finite element method presents a general heading under which a host of procedures have been developed for propagating the uncertainty from the model parameters to the model predictions. In particular, the spectral formulation will be used herein [2]. A typical equation of motion for a linear system, neglecting various damping agents, can be formulated in the frequency domain as,

$$\left[\mathbf{K} - \omega^2 \mathbf{M}\right] \mathbf{X} = \mathbf{U} \tag{3}$$

where $\mathbf{K}$, $\mathbf{M}$, $\mathbf{X}$, and $\mathbf{U}$ denote respectively, the stiffness matrix, the mass matrices, the Fourier amplitude vector of the displacement and that of the excitation. In the case of a base excitation, the input motion consists of a vector of **M.1**, multiplied by the Fourier

amplitude of the base acceleration. In that case, the motion $\mathbf{X}$ refers to the relative motion of the various masses with respect to the base motion. Clearly, equation (3) is a representation of a mathematical model $\mathcal{M}$ that attempts to represent the pile-structure interaction. This model depends on a set of variables $\boldsymbol{\theta} = (m_1, m_2, k_1, k_2)$. Assume that the masses and stiffnesses are modeled as random variables with a known mean and variance. In order to completely characterize the probabilistic structure of these parameters, higher order statistics or a closed form expression for their probability distribution function would normally be required. A Gaussian distribution will be assumed here in order simplify the presentation. The mass and stiffness matrices can thus be rewritten as,

$$\mathbf{M} = \bar{\mathbf{M}} + \sum_{i=1}^{2} \xi_i \mathbf{M}_i = \sum_{i=0}^{2} \xi_i \mathbf{M}_i \tag{4}$$

and

$$\mathbf{K} = \bar{\mathbf{K}} + \sum_{i=1}^{2} \eta_i \mathbf{K}_i = \sum_{i=0}^{2} \eta_i \mathbf{K}_i \ , \tag{5}$$

where an overbar denotes an average quantity, and ξ_i and η_i denote normalized uncorrelated random variables,

$$\xi_0 = \eta_0 \equiv 1 \qquad <\xi_i \xi_j> = <\eta_i \eta_j> = \delta_{ij}, \qquad <\xi_i^2> = <\eta_i^2> = 1 \qquad <\eta_i \xi_j> = 0 \ . \tag{6}$$

Next, the solution process $\mathbf{X}$ is expanded as a polynomial in the random variables describing the material properties resulting in,

$$\mathbf{X} = \bar{\mathbf{X}} + \sum_{i=1}^{P} \psi_i \mathbf{X}_i = \sum_{i=0}^{P} \psi_i \mathbf{X}_i \ , \tag{7}$$

where the set $\{\psi_i\}$ denotes orthogonal polynomials in the variables ξ_i and η_i, the first few of which are given as,

$$\{\psi_i\} = \{1, \xi_1, \xi_2, \eta_1, \eta_2, \xi_1^2 - 1, \xi_1\xi_2, \xi_1\eta_1, \xi_1\eta_2, \xi_1^2 - 1, \xi_2\eta_1, \xi_2\eta_2, \eta_1^2 - 1, \eta_1\eta_2, \eta_2^2 - 1, \ldots\} \ . \tag{8}$$

The orthogonality of these polynomial is interpreted to mean that they are uncorrelated,

$$<\psi_i> = 0, \quad i > 1 \ , \qquad <\psi_i \psi_j> = <\psi_i^2> \delta_{ij} \qquad \forall i, j. \tag{9}$$

Substituting the above expansions into the transformed equation of motion results in the equation,

$$\left[-\omega^2 (\bar{\mathbf{M}} + \xi_i \mathbf{M_i}) + (\bar{\mathbf{K}} + \xi_i \mathbf{K_i})\right] \left(\bar{\mathbf{X}} + \sum_{i=1}^{P} \psi_i \mathbf{X}_i\right) = \left(\bar{\mathbf{M}} + \sum_{i=1}^{2} \xi_i \mathbf{M}_i\right) \mathbf{U} \ . \tag{10}$$

Equality in this last equation is construed to be in the weak sense. Thus projecting the equation on each of the ψ_i used to approximate the solution and averaging, results in,

$$\left(\bar{\mathbf{K}} - \omega^2\bar{\mathbf{M}}_i\right) <\psi_k^2>\mathbf{X}_k \quad + \quad \left(\sum_{j=0}^{P}\sum_{i=1}^{2} <\eta_i\psi_j\psi_k>\mathbf{K}_i - \omega^2\sum_{j=0}^{P}\sum_{i=1}^{2} <\xi_i\psi_j\psi_k>\mathbf{M}_i\right)\mathbf{X}_j$$

$$= \quad \bar{\mathbf{M}}\mathbf{U}<\psi_k> + \sum_{i=1}^{2} <\xi_i\psi_k>\mathbf{M_i}\ , \quad k = 0,\ldots,P\ . \qquad (11)$$

These are P sets of equations, each with as many degrees of freedom as the physical set-up has. These equations can be solved for the deterministic coefficients $\mathbf{X}_i$. Once these have been computed, statistical realizations of the solution process can be readily computed by synthesizing the polynomial expansion of the solution process. From these, probability of various events can be easily computed. Alternatively, if less probabilistic information is enough for the problem at hand, the mean vector and the covariance matrix of $\mathbf{X}$ can be obtained as,

$$\bar{\mathbf{X}} = \mathbf{X}_0\ , \qquad (12)$$

and

$$\mathrm{Cov}(\mathbf{X},\mathbf{X}) = <(\mathbf{X}-\mathbf{X}_0)(\mathbf{X}-\mathbf{X}_0)^T> = \sum_{i=1}^{P} <\psi_i^2>\mathbf{X}_i\mathbf{X}_i^T\ , \qquad (13)$$

respectively.

Probabilistic measures of Closeness

Consider the quantities X_1 and X_2 in the above problem to constitute the set of relevant predictables. Thus the random variable Q is a 2-dimensional vector representing the motion of the near-field and field masses. Given the probabilistic characterization of Q, confidence intervals and tests of hypothesis regarding the closeness of the model predictions to the observations can be readily conducted. Thus assume that a number of experiments are conducted and a set of n observations of Q has been made. Let the mean of the observed set and its standard deviation be denoted, respectively, as $\bar{q}$ and s_q. The standard deviation of the model prediction is assumed known and can be computed according to the procedure described in the previous section. Given the mean and standard deviation of the predictions, and assuming they are Gaussian, a confidence interval can be constructed at some α significance level for the mean and variance of the observations. If the measured statistics of the observations fall within their respective intervals, then the observations are consistent, at the specified level of significance, with the model predictions. Otherwise, they are not.

Clearly, these confidence intervals depend on the level of uncertainty in the parameters of the model. Thus, if a perfect fit has been achieved for the parameters, resulting in a variance of zero, the corresponding variance of the model prediction is also zero, and the only observation that will corroborate the model is the observation that coincides with the

prediction. This, however, is highly unlikely as the model, not being perfect, will necessarily result in parameters that have a finite non-zero scatter around their nominal values. The larger this scatter is, the more tolerant the model is of non-matching observations. Clearly, a good model should be characterized by a narrow scatter in the computed values of its parameters, but it is ultimately the statistical scatter in the predicted values that controls the suitability of the model at the specified level of significance. Confidence interval estimates usually relate the number of observations, to the level of significance and the acceptable error. In their simplest form, these estimates can be developed as closed form expressions between the various quantities involved. This, however, is usually true for predicted quantities having a Gaussian probability distribution, which is rarely the case for most mathematical models. In such more realistic situations, Monte Carlo simulation procedures must be relied upon to delineate the boundaries of the confidence domain. As indicated above, the spectral stochastic finite element procedure is ideal for such situations as it greatly expedites the simulation process.

Numerical Example

In the numerical example, the following numerical values were assumed for the physical parameters involved,

$$\bar{k}_1 = 2\bar{k}_2 = 7339500\text{N/m}^2 \tag{14}$$

$$\bar{k}_2 = E_s = 3669750\text{N/m}^2 \tag{15}$$

$$\bar{m}_1 = 1281\text{kg} \tag{16}$$

$$\bar{m}_2 = 12810\text{kg} \tag{17}$$

where E_s denotes the elastic Young's modulus for the soil. These numerical values correspond roughly to the properties of Ottawa standard medium sand with shear wave velocity of about 30m/s. The mass of the near field is taken to correspond to the mass of a disk of radius 0.5m around the pile. The scatter in all these material properties is well documented [3]. In particular, shear wave velocities are known to vary with depth, frequency, level of compaction, and to be polluted by reflections and scatter. Figure (2) shows the shear wave velocity measured in a shaking table experiment, at various sections throughout the depth of the soil [5]. Accelerometers were placed at 5 different depths in the sand box, the shear wave velocity as obtained from processing the data from all the pairs of sensors was computed, and is shown in the Figure as a function of frequency. It is clear that estimated value for V_s depends to a great extent on which two sensors are used.

Figure (3) shows the mean frequency domain response associated with four different sets of the coefficients of variation. Figures (4) shows the coefficient of variation of the predictions associated with these same two cases. On each of these two figures are shown, on the same plot, the coefficients of variation obtained from first order approximation for the solution process, along with a second order approximation. As expected, the effect of the higher order approximation on the statistics of the solution decreases with the coefficient of variation in the parameters. This figure indicates the level of variability in the model

predictions that would be consistent with the level of variability observed in the model parameters. As expected, the variation in the coefficients of variation of X_1 and X_2 as a function of frequency follows closely that of their mean values. It is worth noting that the tolerated error in the neighborhood of the resonant frequencies is significantly larger than that at other frequencies. This indicates that, given the present model, while the magnitude of the response amplitude at resonant frequencies can be afforded to deviate significantly from their observed values, the location of these peaks along the frequency axis have a lower margin of tolerance. Clearly, these observations are only valid for the very approximate model used herein. Analogous conclusions regarding other models would involve producing similar curves associated with that model.

0.0.1 Conclusions

The paper emphasized the availability, as an intrinsic part of any mathematical model ofa physical system, of statistical diagnostic tools for assessing the closeness between observed data and the model. It is recommended that an effort be made to develop "neighborhood spheres" for various mathematical models currently in use for SSI.

References

[1] Fares, N., and Maloof, R. (1997), "Probabilistic framework for detecting and identifying anomalies," *Probabilistic Engineering Mechanics,* Vol. 12, No. 2, pp 63-73.

[2] Ghanem, R., and Spanos, P. (1991), *Stochastic Finite Elements: A Spectral Approach,* Springer-Verlag.

[3] Lamb, T. and Whitman, R. (1969), *Soil Mechanics,* John Wiley.

[4] Poincaré, H., (1905) *Science et Hypothèse,*

[5] Tazoh, T., and Shimizu, K., "Nonlinear seismic behavior of pile foundation structure systems," *Proceedings of the 10th World Conference on Earthquake Engineering,* Madrid, Spain, 1992, pp. 1807-1810.

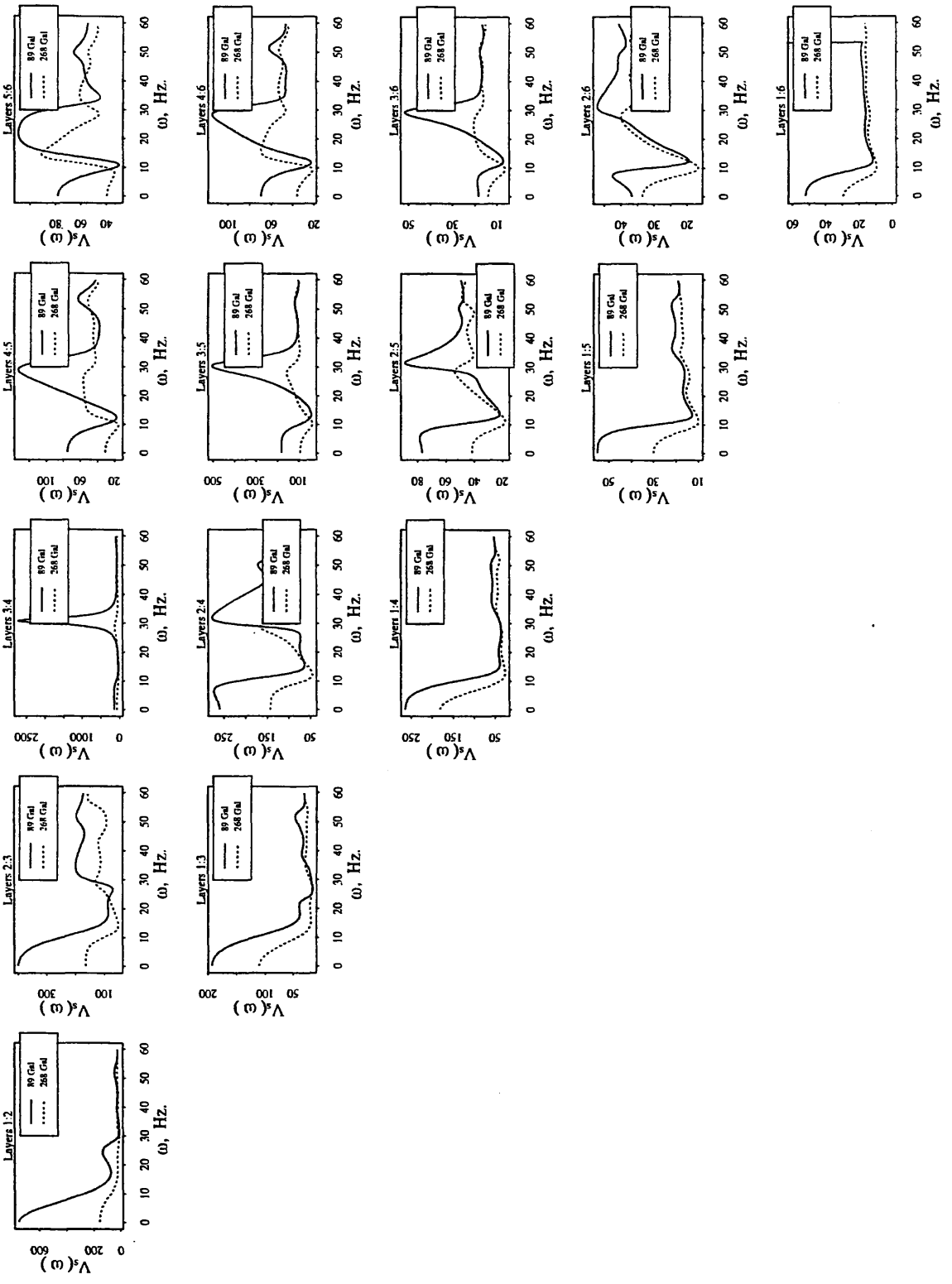

Figure 2: Typical Shear Wave Velocities Based on Experimental Data.

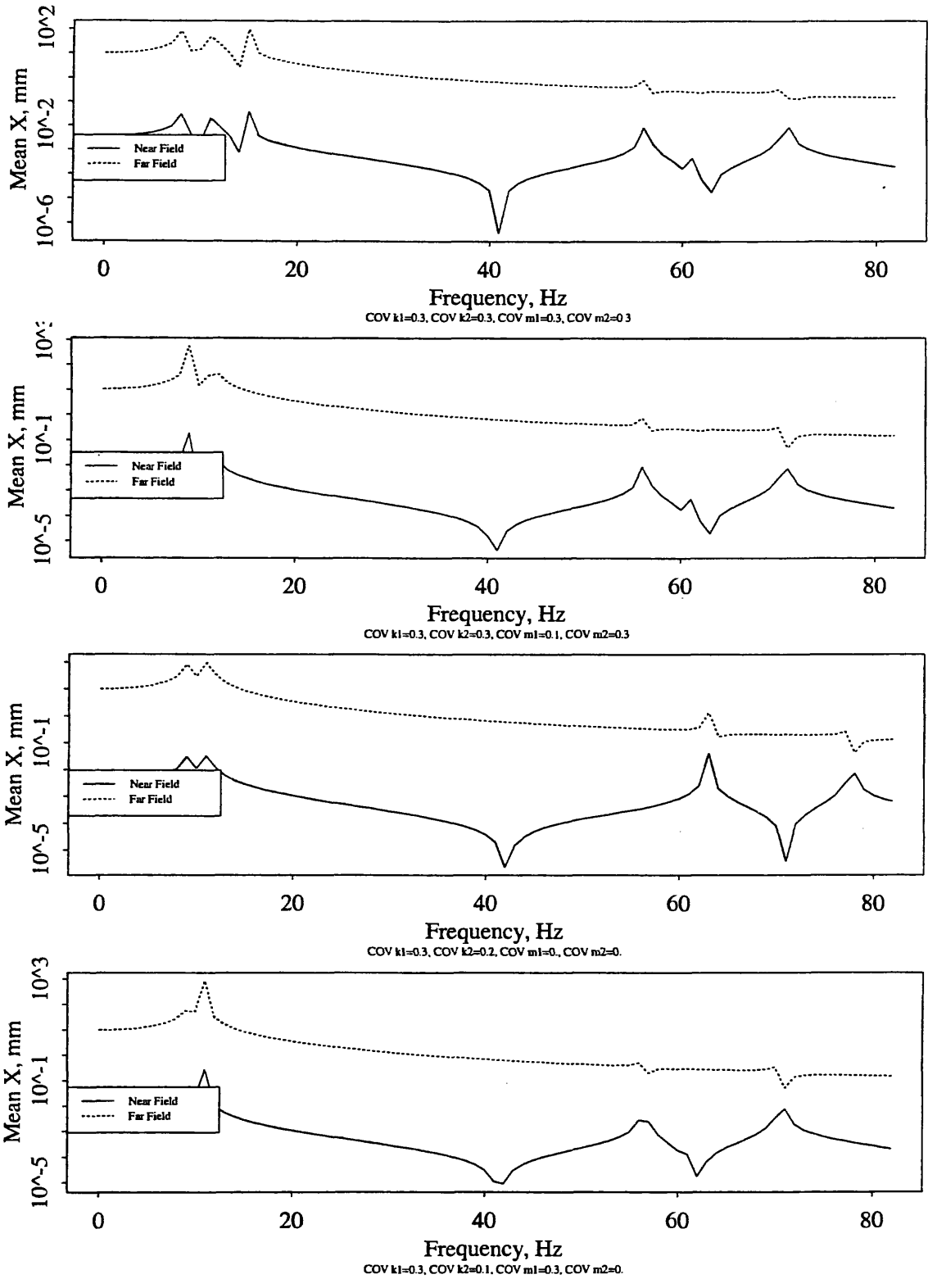

Figure 3: Mean Value of the Frequency Domain Response.

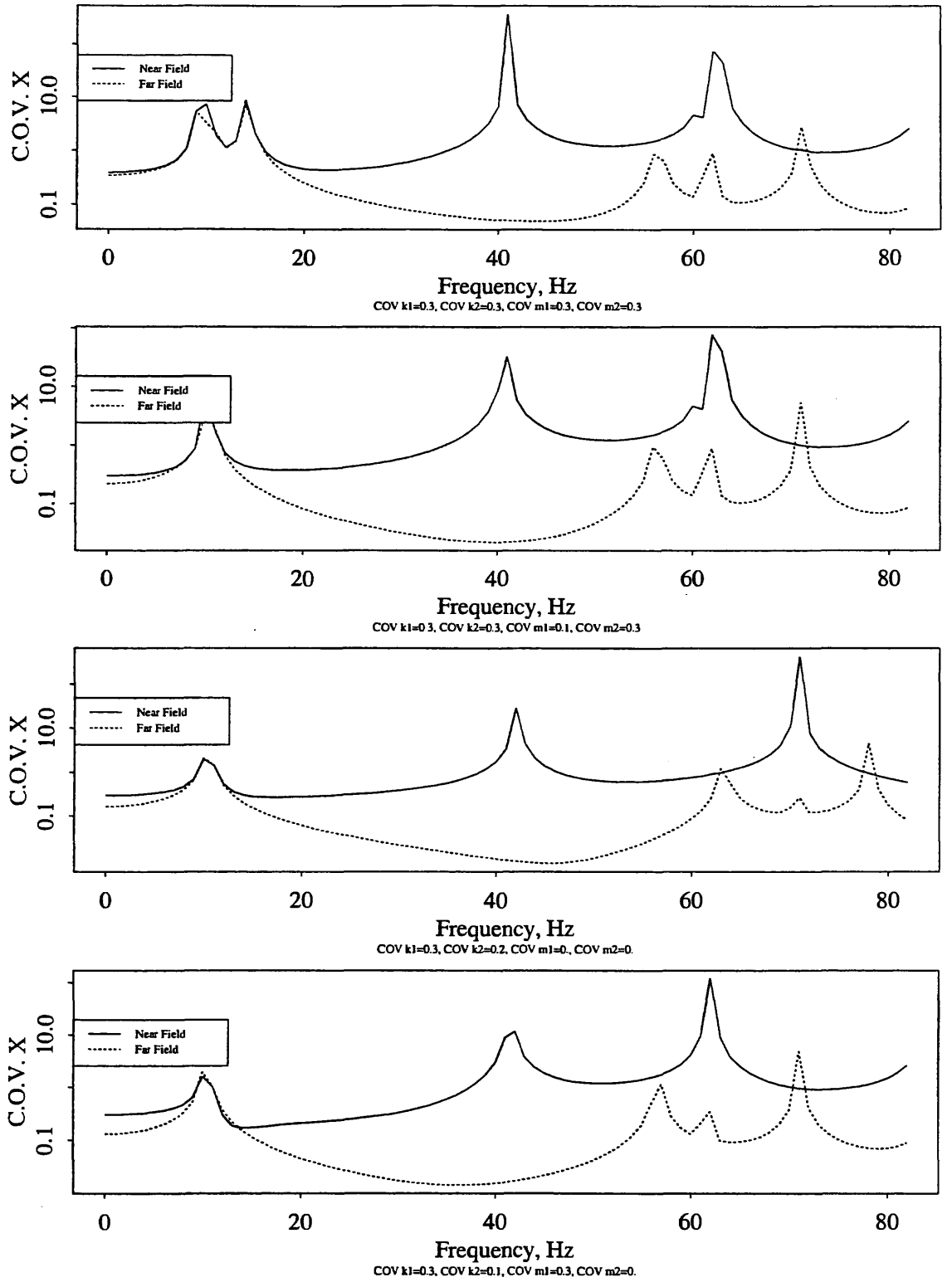

Figure 4: Mean Value of the Frequency Domain Response.

Uncertainties of Seismic Soil-Structure Interaction Analysis: Significance, Modeling and Examples

D. M. Ghiocel, Ph.D.
STI Technologies, Inc., Rochester, NY 14623

ABSTRACT: The aim of this paper is to (i) discuss the significance of different uncertainty sources on seismic soil-structure interaction (SSI), (ii) review the engineering current practice for assessing SSI uncertainty effects using probabilistic models and finally (iii) propose a new procedure for an accurate probabilistic SSI analysis. The intention of the paper is not to address all significant SSI aspects, but only few of these which based on author's opinion are not consistently reflected by the current state-of-engineering practice. Several shortcomings of the current engineering practice for assessing structural risks for critical facilities are pointed out. The proposed procedure uses for the idealization of seismic input and soil properties stochastic field models. Its implementation offers a significant advancement for performing probabilistic seismic SSI analyses.

INTRODUCTION

The factors influencing SSI are a myriad. This is due to the complexity of seismic SSI phenomenon. A short list of major factors influencing SSI may include:

Wave propagation:

- control motion, including intensity, directionality, frequency content
- wave composition, including internal waves, P and S, with surface waves, Rayleigh
- and Love, and other wave types
- spatial variation of ground motion with depth and distance, including motion
- incoherency and wave passage effects
- soil nonlinear behavior as a function of shear strain in soil, soil stability

Soil-structure interaction:

- wave scattering effects or kinematic interaction
- dynamic characteristics of structure-foundation-soil ensemble, including
- embedment effects on system stiffness and vibration energy radiation
- structure nonlinear behavior, which may be more ductile or brittler, including
- stiffness degradations and damping increase
- local contact interface nonlinearities between soil and foundation

SSI response depends drastically on both the seismic environment and structure-foundation-soil ensemble dynamic characteristics.

The seismic SSI uncertainties are usually divided in two major source types of uncertainties, namely: (i) uncertainties due to inherent randomness in natural phenomena induced by earthquakes and in material properties, and (ii) uncertainties due to modeling uncertainties in SSI models and assumptions.

To illustrate the contributions of the two types of uncertainty sources, the probabilistic seismic response of a nuclear power plant (NPP) is considered (Ghiocel et al., 1994). Figure 1 shows the simulated in-structure spectra for the Reactor Building (RB), at the basemat and the top of the

containment, and for the Auxiliary Building (AB), at the roof level. The SSI effects are larger for the RB than for AB. The random variability in the spectral response is higher at the top elevations than for the basemat. This indicates that the SSI uncertainties are mostly propagated through the rocking motion than through the horizontal motion. The contributions of two types of uncertainty on seismic response of the two NPP buildings are quantified in Figure 2. The two spectral curves correspond to coefficient of variation curves which were computed assuming that the uncertainties are due to inherent randomness in the input motion frequency content and soil properties, and that the uncertainties are due to both the inherent randomness and the modeling uncertainties, respectively. The final results of the seismic probabilistic risk assessment (SPRA) calculations for the investigated NPP are shown in Table 1. The results indicate that the two uncertainty sources, i.e. randomness and modeling, contribute almost equally to the total seismic response uncertainty. They are typical for NPPs founded on soil sites and consistent with the present state-of-the-engineering knowledge and practice. The paper focus is limited to SSI modeling uncertainties.

There are two major avenues for improving SSI modeling uncertainties: (i) improve deterministic SSI prediction models and (ii) improve probabilistic models. These two avenues are discussed in the next two sections.

DETERMINISTIC PREDICTION MODELS

There are many significant SSI aspects with significant impact on accuracy of seismic structural predictions which are not appropriately considered by the present state-of-engineering practice. Herein, only few of these aspects, subjectively selected, are addressed.

Table 1. Structural Fragility Analysis Results for the investigated NPP

Building	β_R	β_U	β_C	Median Capacity	HCLPF Capacity
Reactor Building (Basemat Failure)	0.43	0.32	0.54	2.31g	0.70g
Auxiliary Building (Steel Columns)	0.33	0.29	0.44	2.50g	0.90g
Penetration Area (Concrete Wall)	0.32	0.27	0.42	1.19g	0.45g
Intake Structure	0.31	0.26	0.40	1.40g	0.55g
Diesel Gen. Building (Concrete Slab)	0.32	0.25	0.41	1.24g	0.49g

One major aspect which is a significant barrier against SSI modeling accuracy is the limitation of currently available computational tools for performing efficiently rigorous nonlinear SSI analyses, including both wave propagation aspects and soil/structure nonlinear behavior aspects. Using the most currently applied computer programs such as SASSI, CLASSI, DRAIN, ADINA, ANSYS, ABAQUS, etc. there are strong limitations for rigorous nonlinear SSI analyses. The limitations are due to the computational effort, program capability and professional qualification and effort associated with the use of different computer programs. As a consequence of this situation, the SSI practical procedures include significant conservatism to cover the simplified assumptions made. On the

other side, simplified investigations may generate an uneconomical design due to higher stresses in structures. One may think more seriously to the potential savings coming from applying a more refined SSI analysis while designing or retrofitting a concrete highway bridge within the US. Any simplified conservative assumption on modeling of SSI effects, including structural/soil nonlinear behavior and local wave propagation/scattering effects, may induce additional cost of millions of dollars.

Other significant SSI aspects which need more attention and more adequate consideration in the future engineering practice are related to the evaluation of (i) torsional effects induced in structures with mass eccentricities and large size foundations due to motion incoherency, including wave passage effects, and structure-soil-structure interaction effects between neighboring structures, especially for massive, deeply embedded or buried structures. An important modeling SSI uncertainty is related to the computation of seismic pressures on embedded walls and deep foundations. Other aspect which in practice sometime is of a great interest is the local soil instability effects, especially liquefaction, on SSI response. To highlight the SSI aspects selected case study results are briefly discussed as shown Figures 3 through 10.

Figure 3 shows the in-structure spectra computed in an axisymmetric model of a Reactor Building founded on a soft soil, i.e. shear wave velocity of 1000 fps, at the basemat at the edge due to torsional accelerations and at the top of internal structure due to horizontal translational accelerations. The motion incoherency was idealized using a Luco-Wong model (Luco and Wong, 1986) with a coherence parameter of 0.30, which corresponds to an upperbound of incoherency. For this value, the computed peak acceleration due to torsional motion is 30% of the peak acceleration due to horizontal translation. The SSI calculations were done with the ACS SASSI/PC computer program (Ghiocel, 1997). This computer program is based on the original SASSI program, but has significant additional capabilities, including motion incoherency and multiple excitation options. Torsional motions induced by incoherency can have a severe effect on nonsymmetric structures with large mass eccentricities.

Figure 4 shows the seismic pressure computed on the lateral wall of a typical, flexible buried waste storage tank (WST) filled with liquid, using a Beredugo-Novak lumped parameter SSI model (Miller and Costantino, 1994) and a SASSI model. The computed pressure distribution has different shapes for the two SSI models. Further, Figure 5 shows the effect of SSI by comparing the seismic response of an isolated WST with that of two WST model. The two WST are identical and separated by a short horizontal distance, being coupled through the soil medium. The surface input excitation is the same for both comparative cases. The wave shadow effect (Xu et al., 1994) is visible in high frequency range. For the two WST coupled model there is a significant drop in the high frequency components from the bottom tank level to the surface due to the wave shadow effect. However for the bending moments in the tank shell the wave shadow effects appears to be less significant.

Figures 6 through 8 illustrates the results computed for a Reactor Building (RB) on a pile foundation in a relatively soft and liquefiable sand deposit (Ghiocel et al, 1996). Figure 6 shows the SASSI model of the RB including the pile foundation. Figure 7 shows the free-field liquefaction analysis results computed using an effective-stress computer program, LASS (Ghabousi and Dikmen, 1977-1984), and assuming the water table located just below ground surface. The liquefaction analyses indicated that there is a potential liquefiable sand layer between 1m and 6m depths. SSI analysis was performed using the equivalent soil properties computed from the free-field analysis assuming that limited liquefaction takes place between 1m and 6m depths. It was assumed that liquefaction starts at the beginning of the earthquake, and that it surrounds the pile foundation in all horizontal directions. The assumption is very drastic, so that the corresponding results represent an upper bound of the pile foundation response. As expected, the effect of liquefaction on pile forces was severe as illustrated in Figure 8. There is a major redistribution in the seismic forces and moments in the piles due to

liquefaction, which shows a large increase in the upper part of the piles, underneath basemat, where liquefaction occurred. It should be noted that the variability in the pile axial forces is larger than in the pile bending moments.

PROBABILISTIC PREDICTION MODELS

Most of probabilistic seismic SSI analyses currently applied in practice, usually for critical facilities, use a lognormal format and base on simple technical guidelines such as those for the SPRA for NPP (Reed and Kennedy, 1994). These guidelines are a sort of modeling "recipes", in which the effects of different SSI uncertainties are generically quantified. The bad part of such a simple approach is that the probabilistic modeling may be crude and that the quantified uncertainty effects given in guidelines are based on limited research investigations and measurements; so that may not reflect the particularity of a SSI problem. Because of this, such types of modeling "recipes" may impact sometimes negatively on the quality of a SSI prediction, especially when the particularity of the problem is significant. It should be understood that such simplified probabilistic approaches with questionable modeling simplifications, which were considered as feasible and versatile for practitioner engineers of the '80s, when the computational resources were low and probabilistic modeling was in infancy, should be replaced in the next future. Desirably, a probabilistic SSI analysis has to accurately determine, by itself, the effects of different uncertainties for a specific SSI problem and not to assume them. Several criticisms of the actual state-of-engineering practice are discussed in this section. Before doing this, a brief review of the lognormal format is presented (Kennedy el., 1980).

Lognormal Format

Lognormal format has been used extensively in the past two decades for developing seismic structural fragilities for critical facilities including SSI effects. At this time the lognormal format is the most popular probabilistic format in engineering practice. One of the main reasons for using lognormal format for SPRA reviews is its mathematical simplicity for implementation. The lognormal distribution format is based on a mathematical expedience by combining subjective inputs with a multiplication scheme for fragility evaluation.

Using the lognormal format approach (Kennedy et al., 1980), a structural fragility curve which is a function of hazard parameter, A, is defined in terms of the median capacity, $\breve{A}$, times the product of two random factors, ε_R and ε_U, representing the inherent randomness about the median value and the uncertainty in the median value as follows:

$$A = \breve{A}\varepsilon_R\varepsilon_U \qquad (1)$$

The two random factors are assumed to be lognormal random variables with median of unity and logarithmic standard deviation β_R and β_U, respectively. If there is no modeling uncertainty (only randomness) failure of probability as a function of hazard parameter is computed using the standard normal cumulative function $\Phi(.)$ by

$$P_f = \Phi[\frac{\ln(A/\breve{A})}{\beta_R}] \qquad (2)$$

If the modeling uncertainty is included then

$$P\,[p_f > p\,|A] = \Phi(\frac{\ln(A/A\exp[\beta\Phi^{-1}(p)])}{\beta_U}) \qquad (3)$$

which computes the probability for which the failure probability p_f exceeds p given hazard parameter value A (Kennedy et al.,1980). Using the lognormal format, the probabilistic dynamic structural response for a hazard parameter reference level and probabilistic structural capacities are expressed as products of different factors (Kennedy et al., 1980, Reed and Kennedy, 1994). The basic two properties of lognormal model are (i) the median of a product of lognormal distributed random variables is equal to the product of the medians and (ii) the logarithmic standard deviation

of a product is the square root of sum of squares of the individual logarithmic standard deviations.

In the early '80s, it has been considered by engineering experts that the accuracy of the probabilistic distribution in the region of fragility curve tails is not essential for a SPRA. Unfortunately, this is true only if the major risk contributors correspond to hazard parameter values far away from probability distribution tails, especially from the lower tail (Kennedy et al., 1980). More recently, comparative studies have indicated that the lognormal assumption for probability distribution applied in conjunction with multiplicative models for structural response and structural capacity may produce crude results for risk assessments (Hwang et al., 1987). In conjunction with the lognormal format, the use of a single reference level of the hazard parameter (assumed to be representative for the median structural capacity) for performing the SSI analysis, which has been applied in practice for expediency, may introduce significant inaccuracies. This is especially true when significant risk contributors come from random events defined by hazard parameters sensibly lower than reference level. A significant drawback of lognormal model is that the median capacity is insensitive to modeling uncertainty (Ellingwood, 1994).

One criticism of the lognormal format and its application based on the SPRA guidelines is related to probabilistic definition of seismic motion frequency content. As suggested by SPRA guidelines, the coefficient of variation of the spectral shape of a Uniform Hazard Spectrum (UHS) varies in the range of 0.25-0.30, which is typical for the Newmark-Hall spectrum type for the WUS, but less appropriate for the UHS type for the EUS. Figure 9 illustrate a typical UHS of a EUS NPP. It should be noted from this figure that the coefficient of variation of spectral shape varies in the range of 0.80-1.00, which is far larger than that recommended by the SPRA guidelines.

Another criticism is related to typical applications of the lognormal format in conjunction with SPRA guidelines for computing in-structure response spectra using the so-called "median output to median input" rule. This rule largely expedites the probabilistic SSI analysis, but introduces a significant modeling uncertainty due to the highly nonlinear relationship between in-structure spectral peaks and the soil stiffness. This nonlinear relationship is shown in Figure 10. The use of a single deterministic SSI analysis for computing the median response for the reference level earthquake (other questionable concept for simplifying the probabilistic analysis) may introduce artificially high spectral peaks.

The last criticism discussed herein is related to the computation of the structural capacity using the lognormal format and the SPRA guidelines when significant SSI effects are present. The use of inelastic energy absorption factors computed using the methods suggested in the SPRA guidelines is drastically unconservative. Those methods are calibrated for fixed-base structure without SSI effects. If the fixed-base inelastic factors are combined with SSI results the overall safety margin is incorrectly estimated, as the inelastic absorption and SSI effects are not independent and their combination must take into account their dependencies. Otherwise, a double-counted margin is introduced. This should be avoided when the Newmark modified spectra method or the spectral averaging method derived for fixed-base structures are combined with SSI effects. The changes in natural frequencies and structural damping due to structural nonlinear effects have considerably less impact on a structural system having a large effective damping (including SSI energy radiation phenomenon), than on a fixed-base structure with low damping which is very sensitive to changes in its frequency and damping. Kennedy et al., 1985, based on a limited number of cases, gives two different expressions for the median inelastic factor, F_μ:

$$F_\mu \approx \sqrt{0.6(\mu_S - 1) + 1} \quad \text{for fixed-base structures} \qquad (4)$$

$$F_\mu \approx \sqrt{0.2(\mu_S - 1) + 1} \quad \text{including SSI (valid for a stiff soil)} \qquad (5)$$

where μ_S is the story drift ductility factor. For example, for a story ductility factor μ_S=5.0 the

inelastic absorbtion factor is 1.8 for fixed-base cases and only 1.3 for SSI cases. For a NPP structure founded on a softer soil the difference is obviously larger. Further research on this important aspect is needed.

The above criticisms are only a few of the many possible criticisms and, probably not the severest ones against the current state-of-engineering practice for probabilistic SSI analysis, more specific for NPP practice. These methodological deficiencies can be improved if the lognormal format is applied in conjunction with extensive simulations using random sampling techniques. This implies significant higher costs of probabilistic SSI analysis due to larger computational and human effort. It also requires highly qualified engineers on both SSI modeling and probabilistic modeling. A cost-effective alternative is to use specialized computer programs with user friendly interface for performing probabilistic SSI. In this idea, a probabilistic approach is proposed in this section (Ghiocel and Ghanem, 1999). This approach was recently implemented and applied in conjunction with SASSI models for SSI computations.

The above discussions suggest the need of a case-by-case type of probabilistic SSI methodology and compuational tool, capable of including the particularity of a SSI problem. Specifically, SSI effects coming from deep embedment, structure-soil-structure interaction, motion incoherency for large size foundations, local soil instability should be more carefully considered in engineering practice. As shown in this paper each of these effects may significantly affect seismic SSI response.

Proposed Approach

The most extensive studies performed in the past on probabilistic (seismic) SSI, which were supported by Nuclear Regulatory Commission (NRC), are those performed by Lawrence Livermore National Laboratory (LLNL, Shieh et al., 1985) and by Brookhaven National Laboratory (BNL, Pires et al., 1985). The LLNL study was based on a large number of case studies with the aim of identifying the most significant variables for seismic SSI effects and their influence on structural response variability. However, the LLNL study did not involve any probabilistic methodology. The BNL study focused on nuclear containment structures using linear random vibration theory to calculate limit state probabilities under random seismic loads. The BNL departed from the current format suggested by the SPRA guidelines for NPP (Reed and Kennedy, 1994). However, the BNL methodology is restricted to superficial rigid circular foundations on a visco-elastic half-space. For realistic situations including arbitrary shaped and/or flexible foundations, partially embedded or buried structures, oblique seismic waves, non-uniform soil layering the BNL methodology is not directly applicable. The proposed probabilistic approach rigorously addresses these aspects.

A significant advantage of the proposed probabilistic approach is that the loads and system parameters can be more accurately described by random fields (time-space variability) rather than random variables (point variability) as assumed in the current SPRA reviews. Earthquake motion and soil properties are properly represented by random fields (Ghiocel, 1996, Ghiocel et. al 1996).

The key idea of the proposed approach is to provide a global complete description of the stochastic system response surface. The proposed approach has two implementation steps. The first step involves an expeditious condensation of the basic random processes via the KL expansion. The second step evaluates the coefficients of a stochastic orthogonal polynomial expansion of system response. After the coefficients of polynomial expansion are obtained, simulation of points on the system response surface can be obtained. Finally, probabilistic structural risks can be directly evaluated once the expansion of stochastic response surface is calculated.

Using Karhunen-Loeve (KL) expansion (Loeve, 1977, Ghanem and Spanos, 1991) a continuous random property field, $p(\mathbf{x},\theta)$, is expanded according to equation

$$p(\mathbf{x},\theta) = \sum_i \xi_i(\theta) p_i(\mathbf{x}) \qquad (6)$$

where θ denotes the random dimension, p_i represents a certain scale of fluctuation of the field p

while ξ_i represents its random magnitude and hence the random contribution of that particular scale to the overall property field. Both the property field and its various scales are global quantities and depend on the spatial position $\mathbf{x}$, they can also be multi-variate quantities. In the case where the material property in question is a random variable, the above sum is reduced to a single term.

The KL expansion of a stochastic process $e(\mathbf{x},\theta)$, is based on the spectral expansion of its covariance function $R_{ee}(\mathbf{x},\mathbf{y})$. Here, $\mathbf{x}$ and $\mathbf{y}$ are used to denote spatial coordinates, while the argument θ indicates the random nature of the corresponding quantity. The covariance function being symmetrical and positive definite, by definition, has all its eigenfunctions mutually orthogonal, and they form a complete set spanning the function space to which $e(\mathbf{x},\theta)$ belongs. It can be shown that if this deterministic set is used to represent the process $e(\mathbf{x},\theta)$, then the random coefficients used in the expansion are also orthogonal. The expansion then takes the following form

$$e(\mathbf{x},\theta) = \bar{e}(\mathbf{x}) + \sum_{i=1}^{\infty} \sqrt{\lambda_i}\,\xi_i(\theta)\phi_i(\mathbf{x}) \qquad (7)$$

where $\bar{e}(\mathbf{x})$ denotes the mean of the stochastic process, and $\{\xi_i(\theta)\}$ form a set of orthogonal random variables. Furthermore, $\{\phi_i(\mathbf{x})\}$ are the eigenfunctions and $\{\lambda_i\}$ are the eigenvalues, of the covariance kernel, and can be evaluated as the solution to the following integral equation

$$\int_{\Delta} R_{ee}(\mathbf{x},\mathbf{y})\phi_i(\mathbf{y})d\mathbf{y} = \lambda_i\phi_i(\mathbf{x}) \qquad (8)$$

where Δ denotes the spatial domain over which the process $e(\mathbf{x},\theta)$ is defined. The most important aspect of this spectral representation is that the spatial random fluctuations have been decomposed into a set of deterministic functions in the spatial variables multiplying random coefficients that are independent of these variables. The closer a process is to white noise, the more terms are required in its expansion, while at the other limit, a random variable can be represented by a single term. In physical systems, it can be expected that material properties vary smoothly at the scales of interest in most applications, and therefore only a few terms in the KL expansion can capture most of the uncertainty in the process. It should be noted that in comparison with other series representations, the KL expansion has the minimum number of terms, or in other words the minimum number of random variables for random field decomposition.

For seismic SSI problems, of a particular interest are positive random fields, such as the amplitude of as a function of frequency or soil stiffness and hysteretic damping profiles as functions of depth, which are positive quantities. Thus, a new development consisting of a transformed space KL expansion was used for representing the positive non-normal random fields. The basis of this development is to find a mapping between the positive non-normal random field and an associated normal random field (Grigoriu, 1997). In particular, the treatment of lognormal processes is particularly expeditious given a number of analytic expressions that are available regarding it.

For SSI response, the covariance function is not known apriori, and hence the KL expansion cannot be used to represent it. Since the SSI solution process is a function of the material properties and seismic input, the entries of the nodal response vector $\hat{\mathbf{c}}$ can be formally expressed as a nonlinear functional of a set $\{\xi_i(\theta)\}$ used to represent the material and seismic input stochasticity. It has been shown that this functional dependence can be expanded in terms of polynomials in gaussian random variables, referred to as Homogeneous (or Polynomial) Chaoses (Cameron, 1947).

The expansion of SSI response takes on the following form (Ghanem and Spanos, 1991):

$$u(\mathbf{x},t,\theta) = a_0(\mathbf{x},t)\Gamma_0 + \sum_{i_1=1}^{\infty} a_{i_1}(\mathbf{x},t)\Gamma_1(\xi_{i_1}(\theta)) + \sum_{i_1=1}^{\infty}\sum_{i_2=1}^{i_1} a_{i_1 i_2}(\mathbf{x},t)\Gamma_2(\xi_{i_1}(\theta),\xi_{i_2}(\theta)) + \ldots \qquad (9)$$

In equation 9, the symbol $\Gamma_n(\xi_{i_1},\ldots,\xi_{i_n})$ denotes the Homogeneous (or Polynomial) Chaos

(Kallianpur, 1980, Wiener, 1938) of order n in the variables $(\xi_{i_1},...,\xi_{i_n})$. Introducing a one-to-one mapping to a set with ordered indices denoted by $\{\psi_i(\theta)\}$ and truncating the Homogeneous (or Polynomial) Chaos expansion after the p^{th} term, equation 10 can be rewritten as

$$u(\mathbf{x},t,\theta) = \sum_{j=0}^{p} u_j(\mathbf{x},t)\psi_j(\theta) \qquad (10)$$

These polynomials are orthogonal in the sense that their inner product $<\psi_j\psi_k>$, which is defined as the statistical average of their product, is equal to zero for $j \neq k$. A complete probabilistic characterization of the solution process $u(\mathbf{x},t,\theta)$ is obtained once the deterministic coefficients $u_j(\mathbf{x},t)$ have been calculated. A given truncated series can be refined along the random dimension either by adding more random variables to the set $\{\xi_i\}$ or by increasing the maximum order of polynomials included in the Homogeneous (or Polynomial) Chaos expansion. The first refinement takes into account higher frequency random fluctuations of the underlying stochastic process, while the second refinement captures strong non-linear dependence of the solution process on this underlying process (Ghanem and Spanos, 1991).

Using the orthogonality property of polynomials, the coefficients of the Homogeneous Chaos of the solution process can be computed by

$$u_k = \frac{<\psi_k u>}{<\psi_k^2>} \text{ for } k = 1,... K \qquad (11)$$

One of the key factors for obtaining an efficient numerical implementation of the stochastic approach based on Homogeneous Chaos expansion is related to the computation of the inner products or averages $<\psi_k u>$ in equation 11. This can be rewritten in an explicit integral form

$$<\psi_k u> = \int_{-\infty}^{\infty} \psi_k(\xi)u(\xi)\exp(\frac{1}{2}\xi^T\xi)d\xi \qquad (12)$$

Polynomial Chaoses are orthogonal with respect to the Gaussian probability measure, which makes them identical with the corresponding multidimensional Hermite polynomials (Grad, 1949). From the above equation it is obvious that the integration domains spans a large multidimensional space, the dimensionality being given by the number of elementary standard normal random variables defining the set $\{\xi_i\}$. The multidimensional integral given in equation (11) can be computed using various integration procedures including Gauss-Hermite quadrature or efficient simulation techniques. For actual integration an innovative stratified sampling technique was employed. An alternate approach using advanced stochastic finite element concepts is described elsewhere (Ghiocel and Ghanem, 1999).

For getting a faster convergence in the case of non-normal processes, a transformed space representation of non-normal processes was used. Therefore, a logarithmic transformation was applied at the level of the extreme responses before expanding it in a Homogeneous Chaos. Then the expansion was performed in a transformed space for which the corresponding process is closer to a normal process. Finally, the non-normal process was determined using an inverse transformation, specifically an exponential transformation. This transformation is expressed mathematically by

$$u = \exp(\sum_{i=1}^{n} \frac{<\ln(u)\psi_i>}{<\psi_i^2>}\Psi_i) \qquad (13)$$

This significantly has speeded up the convergence and has improved the accuracy of the computed series expansions for extreme-value responses.

Earthquake Motion Description

Earthquake ground acceleration was represented by a segment of a (non)stationary random process (nonstationarity was introduced by using a deterministic intensity shape function) with zero mean, known frequency content and spatial correlation structure. This stochastic representation is conditional to the given zero-period peak ground

acceleration (ZPGA) level. For evaluation of the overall seismic structural risk all the ZPGA levels, i.e. the seismic hazard curve at the site, should be considered. For each ZPGA level, the frequency content of earthquake motion is described locally, in a point at ground surface, by either a acceleration probabilistic response or a power spectral density function. The three earthquake motion components were assumed to be statistically independent. The spatial correlation structure of ground motion field, which is a function of frequency, was defined by a coherency spectrum matrix.

Local (Point) Description: Typically in engineering practice probabilistic site-specific ground response spectra were defined for hazardous facilities (LLNL, 1993, EPRI, 1991). The probabilistic ground spectra are usually described by three digitized spectral response curves computed for 15%, 50% and 85% non-exceedance probability assuming a lognormal distribution of amplitudes. Herein, the probabilistic ground spectrum was assumed as an one-dimensional lognormal random field in frequency domain with certain bandwidth characteristics given by the soil deposit behavior as a second-order linear filter for incoming seismic waves. The spectral amplitude field was modeled by a lognormal random field using a transformed KL expansion. As an alternate of local description of earthquake ground motion, the power spectral density may be input instead of a probabilistic spectra. Four analytical expressions were considered for the power spectral density (Pires et al., 1985):

(i) Kanai-Tajimi spectrum (spectral shape similar to the acceleration transfer function of single degree of freedom subjected to a base excitation)

$$S(\omega) = \frac{1 + 4\xi_f^{\,2}(\omega/\omega_f)^2}{[1-(\omega/\omega)^2]^2 + 4\xi_f^2(\omega/\omega_f)^2} \qquad (14)$$

(ii) Ruiz-Penzien spectrum

$$S(\omega) = \frac{1 + 4\xi_f^{\,2}(\omega/\omega_f)^2}{[1-(\omega/\omega_f)^2]^2 + 4\xi_f^2(\omega/\omega_f)^2}$$

$$\frac{(\omega/\omega_p)^4}{[1-(\omega/\omega_p)^2]^2 + 4\xi(\omega/\omega_p)^2} \qquad (15)$$

(iii) Ruiz-Penzien spectrum multiplied by a low-pass first-order filter and

$$S(\omega) = \frac{1 + 4\xi_f^{\,2}(\omega/\omega_f)^2}{[1-(\omega/\omega_f)^2]^2 + 4\xi_f^2(\omega/\omega_f)^2} \frac{(\omega/\omega_p)^4}{[1-(\omega/\omega_p)^2]^2 + 4\xi(\omega/\omega_p)^2} \frac{1}{1+L^2\omega_q^{\,2}} \qquad (16)$$

(iv) Brookhaven National Lab (BNL) spectrum

$$S(\omega) = S_0 \sum_{j=1}^{2} P_j \frac{(1+4\xi_j^{\,2})[1-\exp(\omega^4/\omega_j^{\,4})]}{[1-(\omega/\omega_j)^2]^2 + 4\xi_j^2(\omega/\omega_j)^2} \qquad (17)$$

where ω_f, ω_p and ξ_f, ξ_p are the frequency and bandwidth of the filters.

These analytical forms are widely accepted by the earthquake engineering community, being the most popular ones. The Kanai-Tajimi spectrum, (i), was the first of the above expression to be proposed. The Ruiz-Penzien spectrum, (ii), was intended to adjust the low frequency content of Kanai-Tajimi spectrum at frequency equal to zero. The improved Ruiz-Penzien spectrum, (iii), reduces the high frequency content of the Kanai-Tajimi spectrum. The BNL spectrum, (iv), has a lower high frequency content than the Kanai-Tajimi spectrum removes the singularity of the displacement spectral power density at zero frequency (Pires et al., 1985).

Spatial Variation (Incoherency): For an incoherent wave field the unlagged coherence for two point motions i and k can be defined as (Abrahamson et al, 1990):

$$Coh_{U_{i,k}}(\omega) = Coh_{i,k}(\omega)\, A(i\omega, X_i - X_k) \exp[i\omega(X_{Di} - X_{Dk})/V_{XDi-XDk}] \qquad (18)$$

where $A(i\omega, X_i - X_k)$ is a decaying function of frequency starting from unit value which gives the relative power of the wave field described by a plane wave at all frequencies. The term $\exp[i\omega(X_{Di} - X_{Dk})/V_{XDi-XDk}]$ in equation 18

represents in the frequency domain the phase angle between the two point motions due to the wave passage effect along the direction D. Parameter $V_{XDi-XDk}$ is the apparent seismic wave velocity defined by the projected distance between the two points along the direction D. If the wave field is perfectly described by a single plane wave, the function $A(i\omega, X_i - X_k)$ is equal to unity.

For two one-dimensional random time series representing an unidirectional seismic motion components in two arbitrary points of the soil deposit, j and k, the (narrow band) coherence is defined by a complex function of frequency

$$Coh_{j,k}(\omega) = \frac{S_{j,k}(\omega)}{[S_{j,j}(\omega)S_{k,k}(\omega)]^{1/2}} \qquad (19)$$

where $S_{j,k}(\omega)$ is the cross-spectral density function for two points j and k, and $S_{j,j}(\omega)$ is the auto-spectral density for point j (similar for point k). The coherence describes the similarity of the two point motions. Generally, in engineering applications, the so-called "lagged" coherency spectrum or "lagged " coherence are used (Abrahamson et al., 1990). The lagged coherency includes only the amplitude randomness and removes the wave-passage randomness. From physical point of view, the lagged coherence represents the fraction of the total power of seismic motion which can be idealized by a single deterministic plane wave motion called the coherent motion. Usually in the current earthquake engineering language, the lagged coherence is called simply coherence. More generally than the "lagged" coherence, the "unlagged" coherence includes the wave-passage random effects.

Based on the experimental evidence of different records of past earthquakes, the following analytical forms for the coherence function were considered:

(i) Luco-Wong model (Luco and Wong, 1986), defined by

$$Coh_{i,k}(\omega) = C\,oh(|X_i - X_k|, \omega) = \exp[-(\gamma|X_i - X_k|/V_s)^2] \qquad (20)$$

in which γ is the coherence parameter and V_s is the shear wave velocity in the soil. The above analytical expression compared with others given in the technical literature based on experiment fitting (Hoshiya and Ishii, 1983, Harichandran and Vanmarcke, 1986, etc.) has the advantage of a theoretical support based on the analytical formulation of shear wave propagation in random media (Uscinski, 1977). Luco and Wong, 1986, suggested that the coherence parameter has generic values in the range of 0.10 to 0.30.

(ii) Abrahamson model (Abrahamson, 1991, 1993), defined by

$$Coh_{i,k}(\omega) = Coh(|X_i - X_k|, \omega) = Tanh\{(a1 + a2|X_i - X_k|)[\exp[-(b1 + b2|X_i - X_k|)\frac{\omega}{2\pi}] + \frac{1}{3}(\frac{\omega}{2\pi})^{-c}] + k\} \qquad (21)$$

where a1, a2, b1, b2 and c are model parameters. These parameters can be introduced by the user, otherwise by default the values (Abrahamson, 1990) are used, i.e. a1=2.55, a2=-0.012, b1=0.115, b2=0.00084, c=0.878 and k=0.35. These parameters may be defined as random variables.

Assuming that the seismic wave field can be modeled by a plane wave, an element of the cross-spectral density matrix of multidimensional motion random field can be derived analytically

$$S_{i,k}(\omega) = [S_{i,i}(\omega)S_{k,k}(\omega)]^{1/2} Coh(|X_i - X_k|, \omega) \exp[i\omega(X_{Di} - X_{Dk})/V_{Xi-Xk}] \qquad (22)$$

for each pair i,k of point motions.

To implement the random field model of incoherent soil motion, the coherence matrix is decomposed via KL expansion. The motion incoherency effects are are larger for higher frequency components than for lower frequency components. Usually, the effect of incoherency is to

reduce translational motion and rocking motion and increase torsional motion.

Soil Property Description

Soil properties were assumed to be homogeneous in a horizontal plane and therefore they were idealized as one-dimensional random fields, i.e. random varying profiles with depth. Specifically, the randomness in soil dynamic properties was considered by variabilities in shear modulus, hysteretic damping and Poisson ratio. First, the soil deposit was discretized in a geometric layering with varying properties. Soil shear modulus at low strains, G_{max}, was idealized as an one-dimensional lognormal random field in the vertical direction having a non-stationary mean and an assumed correlation length for same material type.

This idealization is considered to be significantly more realistic and less conservative than the assumption of perfect correlation currently applied for parametric deterministic SSI studies. For soil layering including different materials, a set of multiple random fields may be considered. The shape (nondimensional variation) of the shear modulus - shear strain curve, $G(\gamma)/G_{max} - \gamma$ was modeled by a random field along the shear strain axis with a non-stationary mean. The mean curve was assumed to have an arbitrary shape which is either introduced by the user or by default stored in the program database. The same modeling assumption used for the shear modulus curve was considered for the hysteretic damping - shear strain curve, $D(\gamma)$.

For implementation, the soil property fields were decomposed via KL expansion. The statistics of the soil property field models, including correlation length parameters, were derived by calibrating the mathematical models with experimental data available.

Structural Properties

Structure damping and stiffness parameters were assumed to be random variables. This assumption is based on the fact that the random variation of these parameters within the superstructure are appropriately a set of independent random variables, than by a continuous random field with a well-established correlation structure expandable in a KL series.

Example Application

The proposed approach was applied to a typical Reactor Building (RB) subjected to earthquake motion. The probabilistic SSI response was compared with a deterministic SSI response computed using the current practice for NPP. The finite element model used for seismic soil-structure interaction analysis is shown in Figure 11 (Lysmer et al., 1988). This SSI computational model represents a typical SASSI model for seismic design basis calculations of a reactor building. The superstructure is modeled by beam elements and the basemat is modeled by solid elements. Rigid links are introduced to transmit the rocking motion from the superstructure stick to the basemat. The ACS SASSI computer program (Ghiocel, 1997) was used for both the free-field analysis and the SSI analysis, performed either probabilistically or deterministically.

Deterministic analysis was done for a seismic input defined by the design ground spectrum associated to a 84% probability of nonexceedance. A spectrum compatible accelerogram was generated for SSI analyses. As shown in Figure 12 the computed response spectra of the generated accelerogram slightly envelopes the given design spectrum. Soil properties were be the best-estimate values (median). In accordance to the current seismic design requirements, two additional extreme bounds, 0.50 times best-estimate and 2.00 times best-estimate values were considered. The final results of the deterministic analysis are obtained by enveloping the results for the three soil-structure interaction analysis for the three set of values of soil parameters.

For probabilistic analysis, the earthquake input was defined by a probabilistic response ground spectrum as shown in Figure 13. The four spectral curves corresponds to mean, median and 16% and 85% nonexceedance probability estimates. The probability distribution was assumed to be

lognormal. The lognormal spectral amplitude field was represented using a transformed KL expansion. The correlation length along frequency axis was selected depending on the desired bandwidth of simulated spectra (function of damping). The number of frequency steps to describe the spectral shape was 100. The smaller the correlation length is, the narrower the spectral peaks are. Figure 14 illustrates the ensemble statistics (for nonexceedance probabilities of 15%, 50%, 85% and mean) of the probabilistic model of ground response spectrum for a set of 100 realizations. Few simulated realizations are shown in Figure 15.For probabilistic soil-structure interaction analysis the effect of motion incoherency was considered using a Luco-Wong model with a γ parameter of 0.20. The resulted spatial variation of motion amplitude for different frequencies is plotted in Figure 16.

Soil properties were defined assuming that the low strain soil shear modulus and hysteretic damping profiles (variation with depth) are lognormal random fields. Figure 17 shows the probabilistic shear modulus profile (statistically estimated profiles are included). Plotted curves correspond to mean, median and 16% and 84% nonexceedance probability. A transformed space KL expansion was used to represent these lognormal positive fields. The variation of nondimensional shear modulus and hysteretic damping versus shear strain were modeled as normal random fields decomposable directly in original space in KL expansion. Simulated variations are shown in Figure 19.

Structural properties are described using random variables. Specifically, the Young elastic modulus and the material damping ratio were assumed to be normal random variables with a coefficient of variation of 0.25. The means were assumed to be 0.80 of the linear elastic modulus and 8%, respectively.

A comparison of probabilistic response computed using the proposed approach (using 100 solutions) and a Monte Carlo simulation (using 500 solutions) is shown in Figure 20.

Figure 21 shows the coefficients of the transformed Homogeneous Chaos expansion using 72 basic random variables. Between 1 and 72 are the coefficients of the first-order polynomials, and between 73 and 144 are the coefficients of the second-order polynomials (without coupling). It is to be noted that only less than half of the number of basic random variables have significant contributions. Larger contributions come from linear terms than from nonlinear terms. However, it is very difficult for the complex soil-structure problem to preliminary establish with are the most significant variables. There is a need to get more insights on this aspect in the future.

Figure 22 shows a comparison between deterministic and probabilistic analysis results, both in terms of in-structure response spectra. Deterministic estimates corresponds to very low nonexceedance probability levels. Having in mind the additional conservatism introduced in the overall seismic evaluation by the seismic hazard definition and the evaluation of structural elements or equipment capacities, it appears that the current deterministic SSI analysis procedure is overly conservative.

CONCLUDING REMARKS

The paper addresses the effects of SSI modeling uncertainty on seismic response, discusses shortcomings of current state-of-engineering practice on probabilistic SSI for hazardous facilities, and proposes a new accurate procedure for performing probabilistic SSI analysis. SSI modeling uncertainty effects are illustrated using the results from different case studies. The proposed procedure represents a significant advancement for performing probabilistic seismic SSI analyses of hazardous facilities.

The proposed approach based on a stochastic series representation of SSI response offers accuracy, efficiency and significant modeling advantages in comparison with the currently SPRA approaches. The proposed approach addresses efficiently large number of variables problems such as dynamic SSI problems and handles random field models, useful for idealization of dynamic loading and system parameters. In addition, the proposed approach is capable of handling large variability and highly nonlinear problems.

ACKNOWLEDGEMENTS

The paper is partially based upon work supported by the National Science Foundation under a SBIR project with the Award Number DMI-9660321.

SELECTED REFERENCES

Abrahamson, N. A. et al. (1990). Spatial Variation of Strong Ground Motion for Use in Soil-Structure Interaction Analyses, *4th U.S. National Conference on Earthquake Engineering, Palm, Springs, Vol.1.*

Cameron, R. and Martin W (1947). The Development of Nonlinear Fuctionals in Series of Fourier-Hermite Functionals, *Ann. Math., 48,* 385-392.

EPRI (1989). Probabilistic Seismic Hazard Evaluation at Nuclear Plant Sites in the Central and Eastern United States: Resolution of Charleston Issue, *Report NP-6395-D.*

Ghaboussi, J. and Dikmen, S.U (1977). LASS II - Computer Program for Analysis of Seismic Response and Liquefaction of Horizontally Layered Sands, *Report UILU-ENG-79-2010.*

Ghanem, R., Ghiocel, D.M.(1996). A Comparative Analysis of FORM/SORM and Polynomial Chaos Expansion for Highly Nonlinear Systems *ASCE/EMD Speciality Conference, Ft. Lauderdale.*

Ghanem, R., and Spanos, P. (1991). Stochastic Finite Elements: A Spectral Approach, *Springer-Verlag.*

Ghiocel, D. M. and Ghanem, R. (1999). A Stochastic Finite Element Approach for Seismic Soil-Structure Interaction, Journal of Earthquake Engineering and Structural Dynamics, *ASCE (submitted).*

Ghiocel, D.M. and Ghanem, R. (1998). Stochastic Seismic SSI Using Homogeneous Chaos Expansion, the *12th ASCE Engineering Mechanics Speciality Conference, San Diego, May.*

Ghiocel, D.M. (1996) Seismic Motion Incoherency Effects on Dynamic Response, 7th ASCE EMD/STD Joint Speciality Conference on Probabilistic *Mechanics and Structural Reliability, Worcester, MA, August.*

Ghiocel, D.M. et al. (1996) Probabilistic Seismic Analysis Including Soil-Structure Interaction, *7th ASCE MD/STD Joint Speciality Conference on Probabilistic Mechanics and Structural Reliability, Worcester, MA, August.*

Ghiocel, D. M. (1997) ACS SASSI/PC - An Advanced Computational Software for System Analysis of Soil-Structure Interaction on Personal Computers, *ACS Report, Cleveland, Ohio.*

Ghiocel, D. M., Wilson, P., Stevenson, J. D., (1995). Evaluation of Probabilistic Seismic FRS Including SSI Effects, *the 13th SMIRT Conference, Invited Paper, Vol. M, Porto Alegre.*

Ghiocel, D.M., et al., (1990) "Evaluation of SSI and SSSI Effects on Seismic Response of Nuclear Heavy Buildings by Different Approaches", the *10th European Conference on Earthquake Engineering, Moscow.*

Ghiocel, D. M., et al.,(1987) "Structural Reliability of Prestressed Concrete Nuclear Containment Under Combined Loads", *the 9th SMIRT, Vol. M, Laussan.e*

Ghiocel, D. M.,(1986) "Probabilistic Seismic Soil-Structure Interaction Analysis", 8th ECEE Conference, Lisbon

Hwang et al. (1987). Seismic Probabilistic Risk Assessment for Nuclear Power Plants, *NCEER-BNL-Report 87-0011.*

Kallianpur, G. (1980). Stochastic Filtering Theory, *Springer Verlag.*

Kennedy, R.P, Cornell, C.A., Campbell, R.D., Kaplan,S., Perla, H.F. (1980). Probabilistic Seismic Safety Study of An Existing Nuclear Power Plant. *Nuclear Eng. & Des., Vol. 59.*

Kennedy, R.P., Kincaid, R.H., Short, S.A. (1985) . Engineering Characterization of Ground Motion. Task II, *NUREG/CR-3805, Vol. 2.*

LLNL (1993) Eastern US Seismic Hazard Characterization Update, *Lawrence Livermore National Laboratory Report UCRL-ID-115111*

Loeve, M.,(1948) Probability Theory, *McGraw-Hill.*

Lysmer, J.,Tabatabaie-Raissi, Tajirian, F.Vahdani, S., and Ostadan, F.(1988), SASSI - A System

for Analysis of Soil - Structure Interaction, Report UCB 1988, *Geotechnical Engineering, University of California, Berkeley.*

Luco, J. and Wong, H. L. (1986). Response of a Rigid Foundation to a Spatially Random Ground Motion, *Earthquake Engineering & Structural Dynamics.*

Miller, C.A. and Costantino, C.J. (1994). " Seismic Induced Pressures in Buried Vaults", Natural Hazard Phenomena and Mitigation, *ASME, PVP-Vol.217,* p. 3-11.

Pires, J., Hwang, H., and Reich, M., (1985). Reliability Evaluation of Containments Including Soil-Structure *Interaction, USNRC Report NUREG/CR-4329, BNL-NUREG-5190.6*

Reed , J.W, Kennedy, R.P. 1994. Methodology for Developing Seismic *Fragilities.*

Shieh, L.C., et al. 1985. Simplified Seismic PRA: Procedures and Limitation, *NUREG/4331, UCID-20468.*

Xu, J., Bandyopadhyay, K., Miller, C.A., Costantino, C.J. (1994) "Spacing Effects on Seismic Responses of Underground Waste Storage Tanks", Natural Hazard Phenomena and Miitigation, *ASME, PVP-Vol. 217,* p. 13-18.

Wiener, N (1938). The Homogeneous Chaos, *Amer. J. Math., 60,* p. 897-936.

DMG:jah
D:\ghiocel\ssiawk98.doc

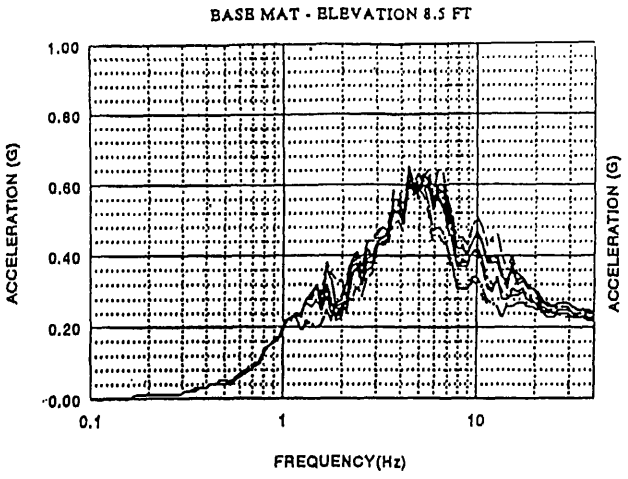

a) RB, basemat

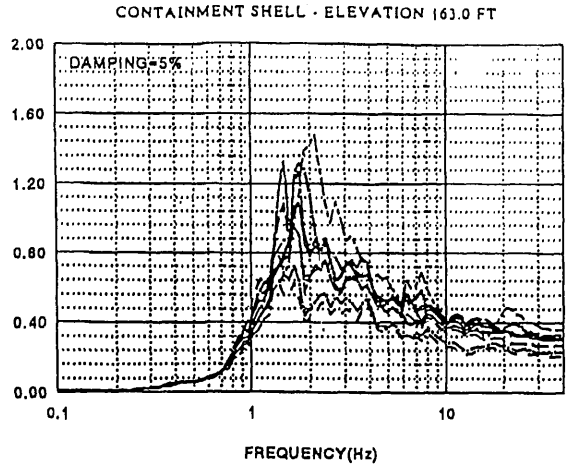

b) RB, top on containment

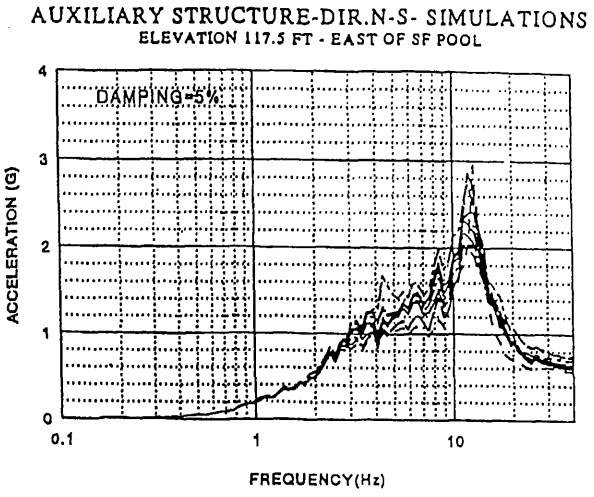

c) AB, roof level

Figure 1. In-structure spectra in the RB and AB

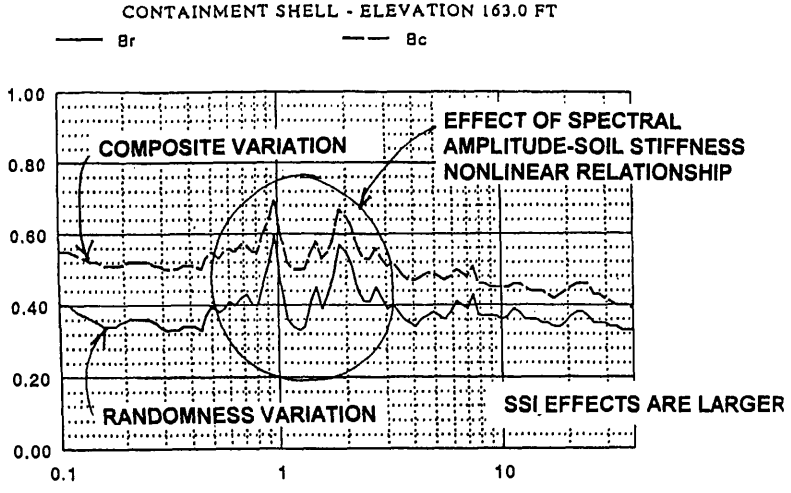

a) RB, top of containment

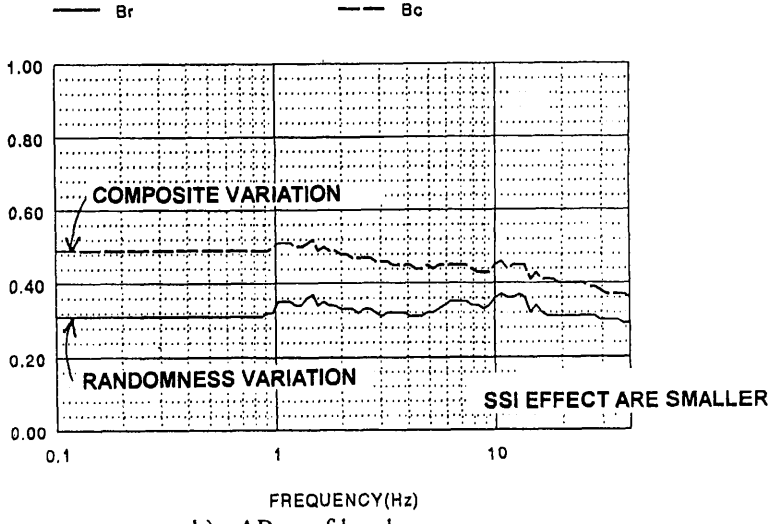

b) AB, roof level

Figure 2. Coefficients of variation for the in-structure spectra

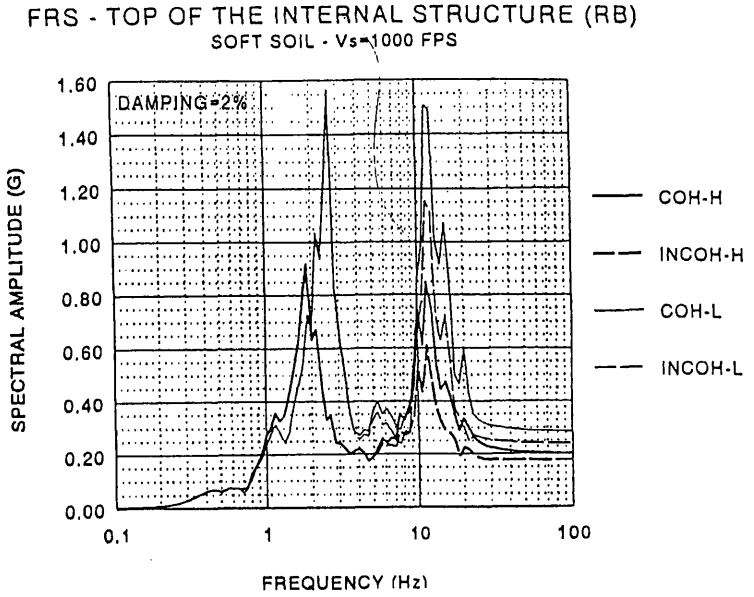

a) Top of internal structure, horizontal motion

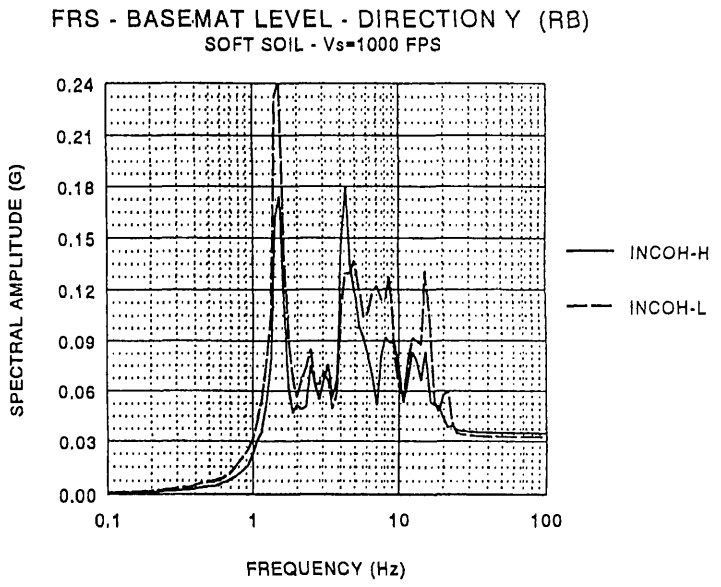

b) Basemat, torsional motion

Figure 3. Effect of incoherency on in-structure spectra

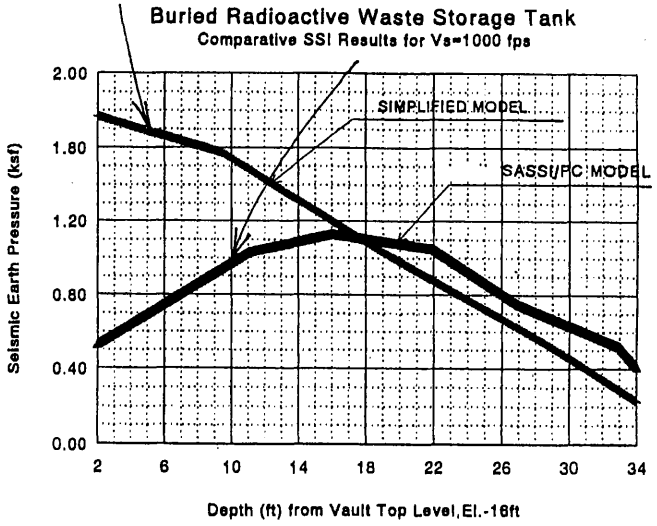

Figure 4. Seismic pressure on WST wall

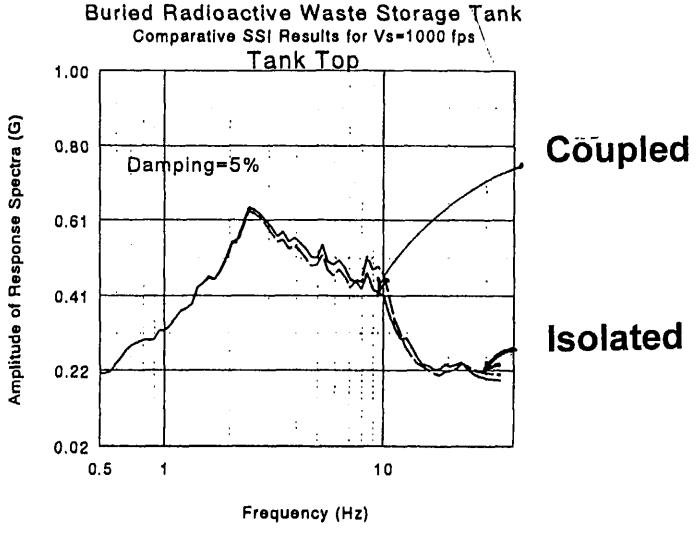

a) Surface motions

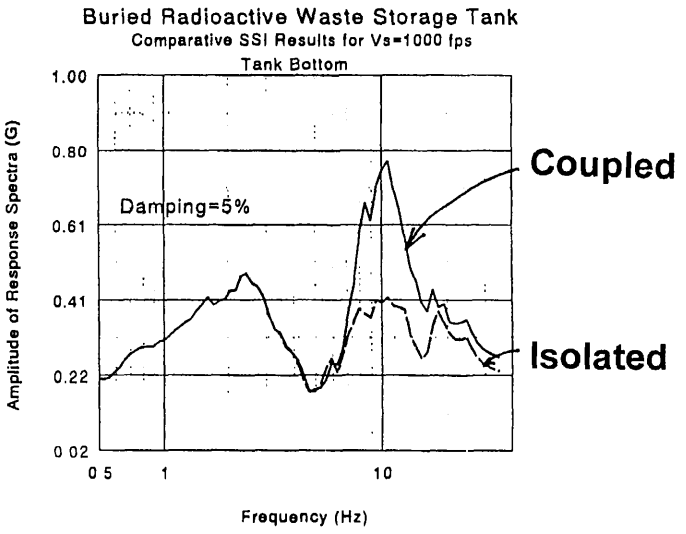

b) Bottom tank motions

Figure 5. Response spectra for the WST model

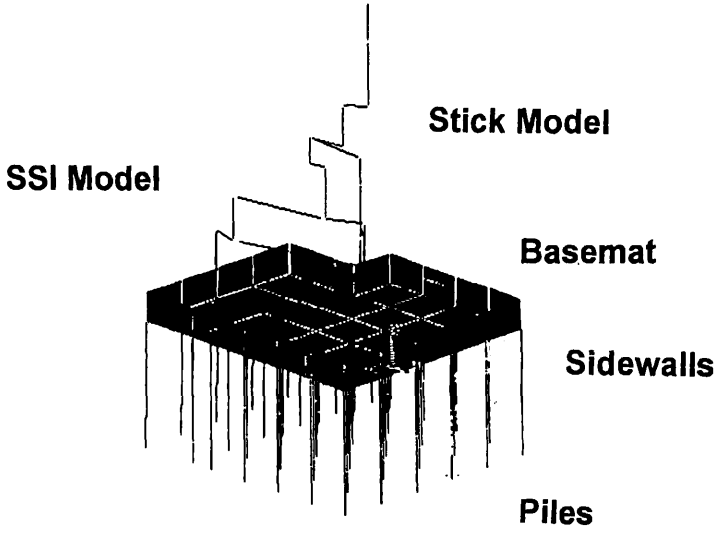

Figure 6. Structure-pile foundation SSI model

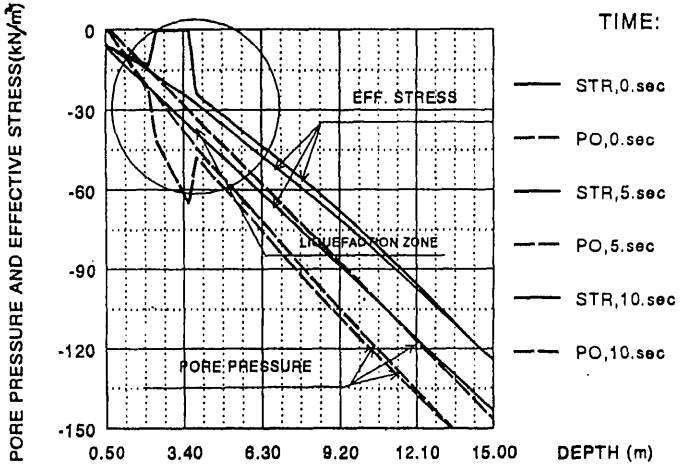

Figure 7. Pore pressure and effective stresses in soil

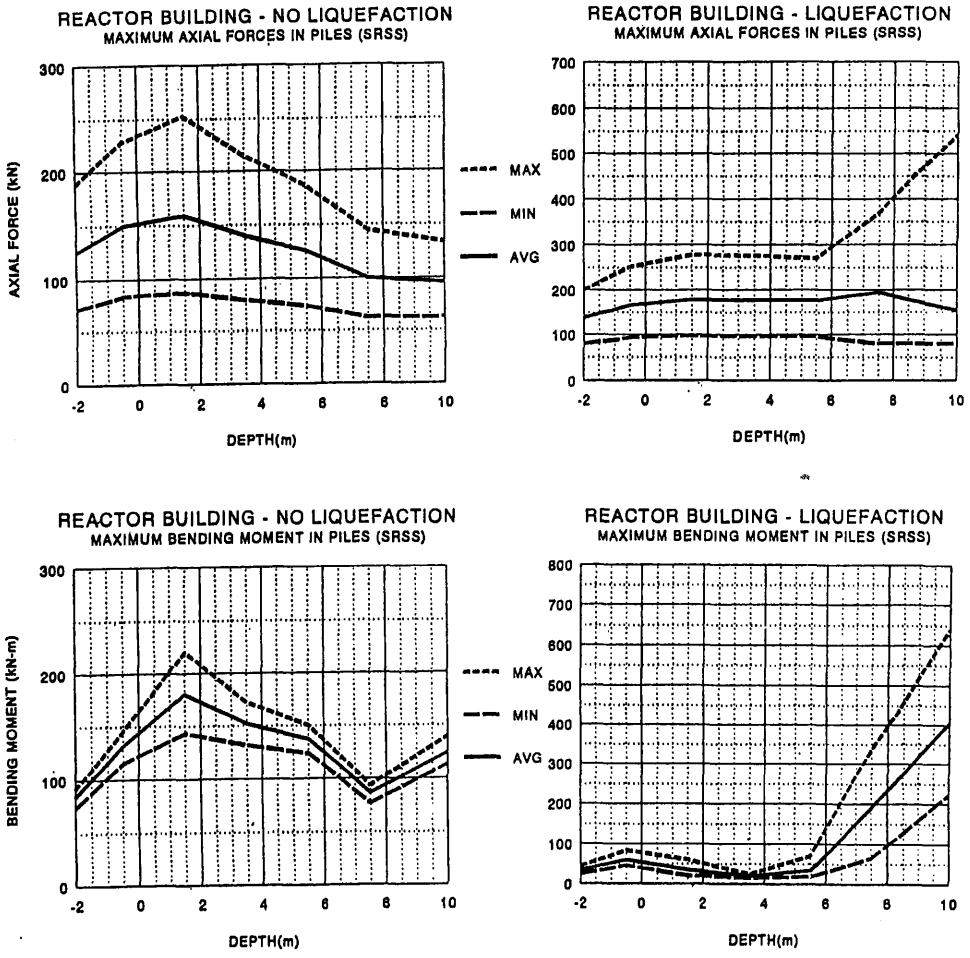

Figure 8. Forces and moments in piles

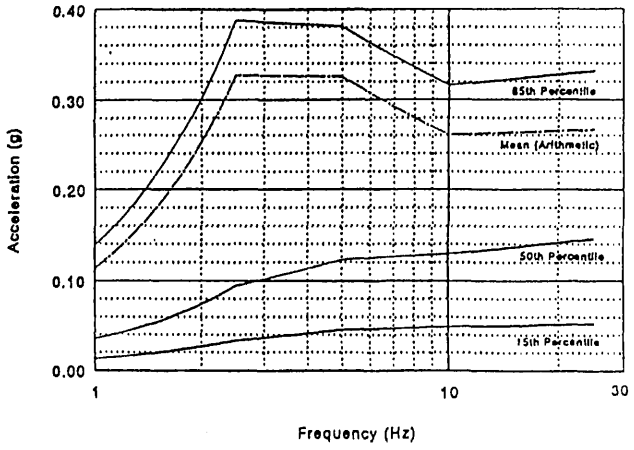

Figure 9. Typical UHS for a EUS NPP site

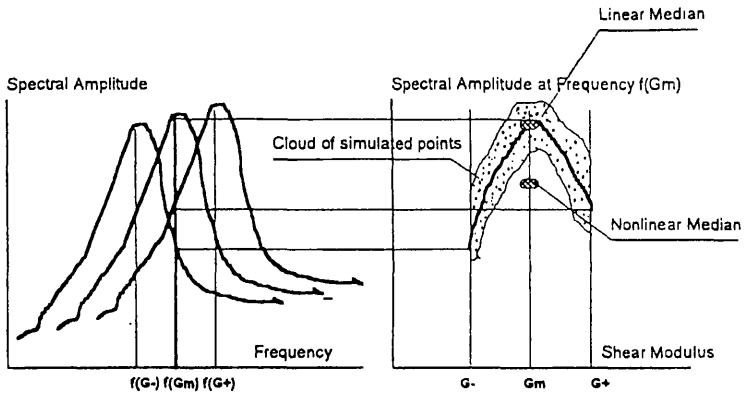

Figure 10. Highly nonlinear relationship between spectral peaks and soil stiffness

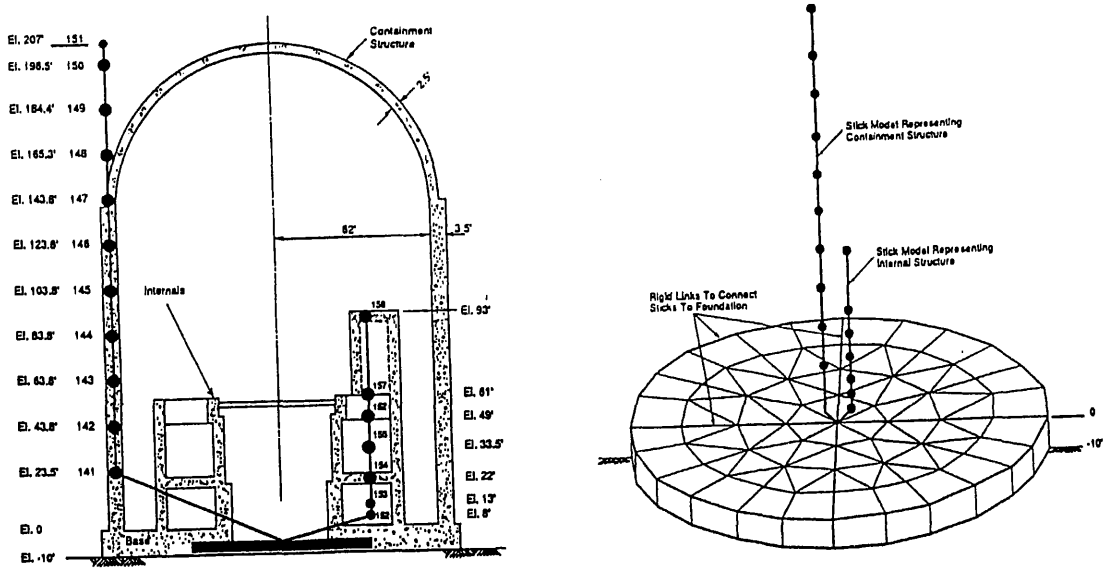

Figure 11. RB SSI model (after Lysmer et al., 1988)

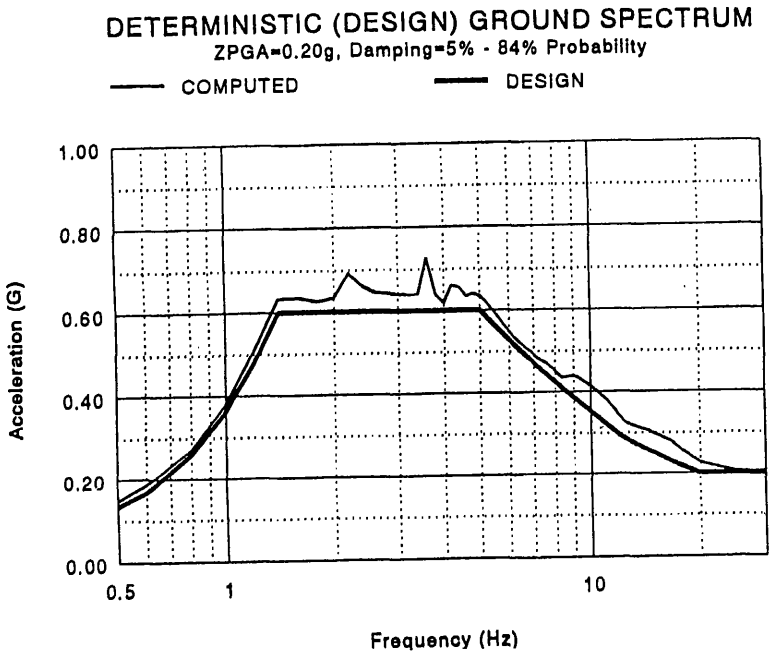

Figure 12. Deterministic ground response spectra

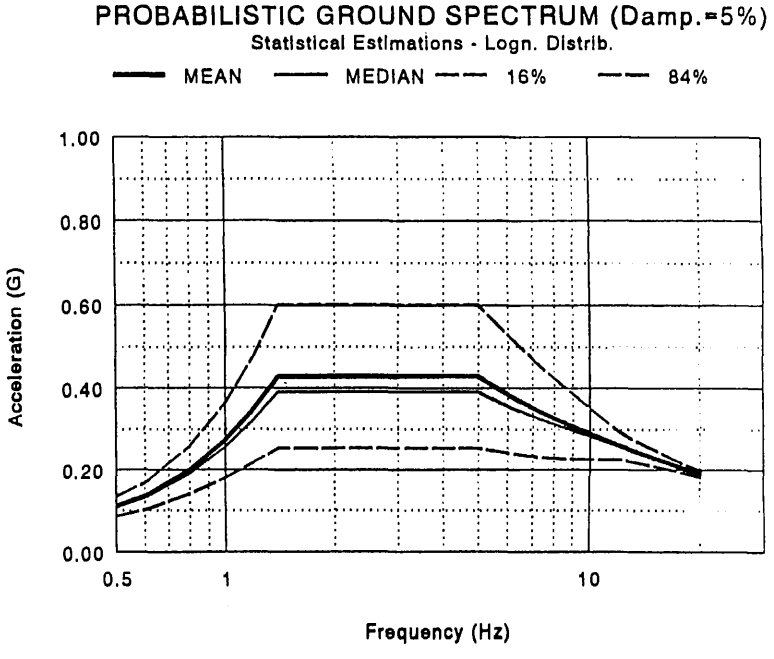

Figure 13. Probabilistic ground response spectra

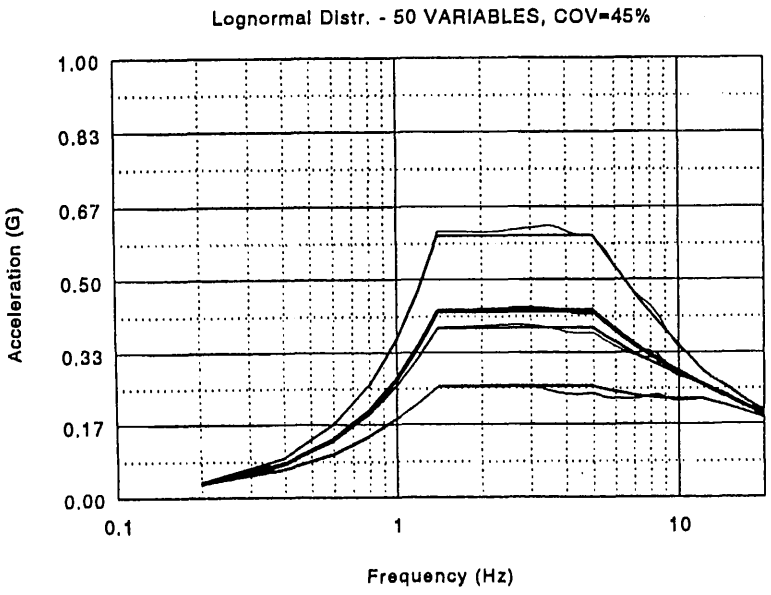

Figure 14. Statistical estimate of probabilistic spectra

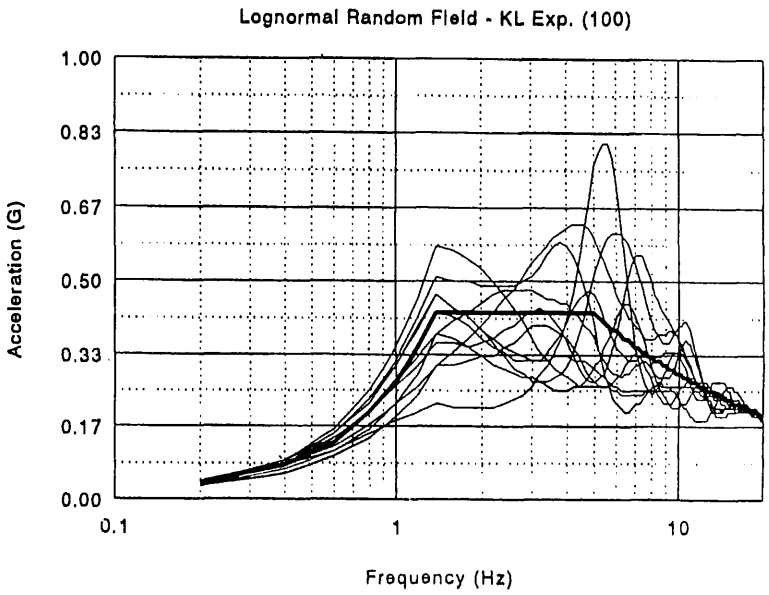

Figure 15. Simulated ground ground spectra

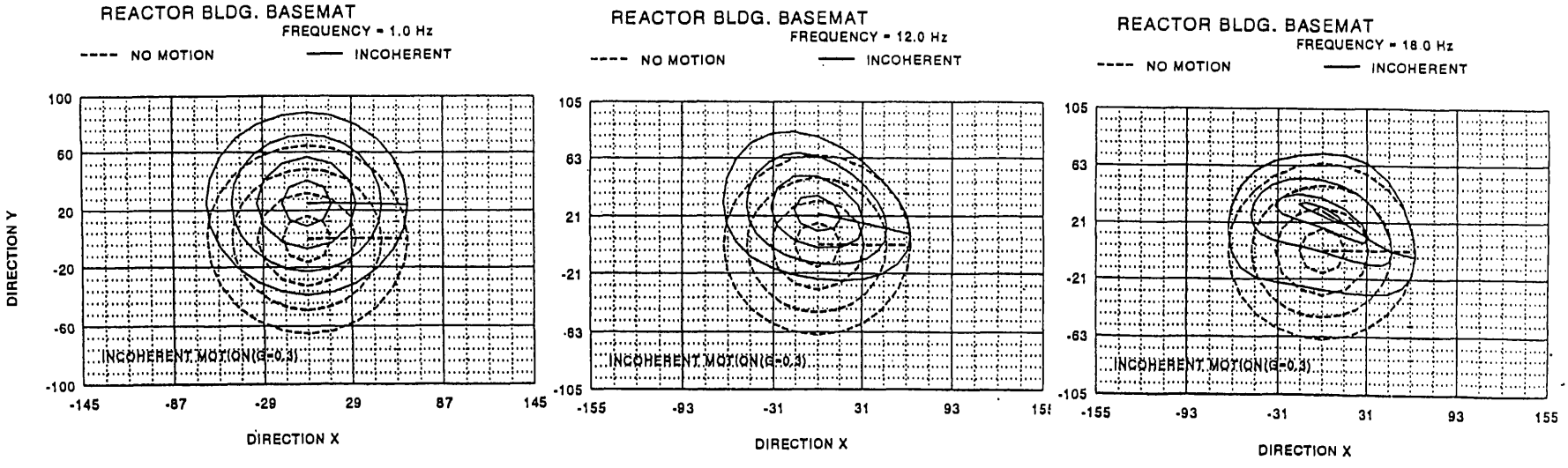

Figure 16. Motion incoherency effects on input

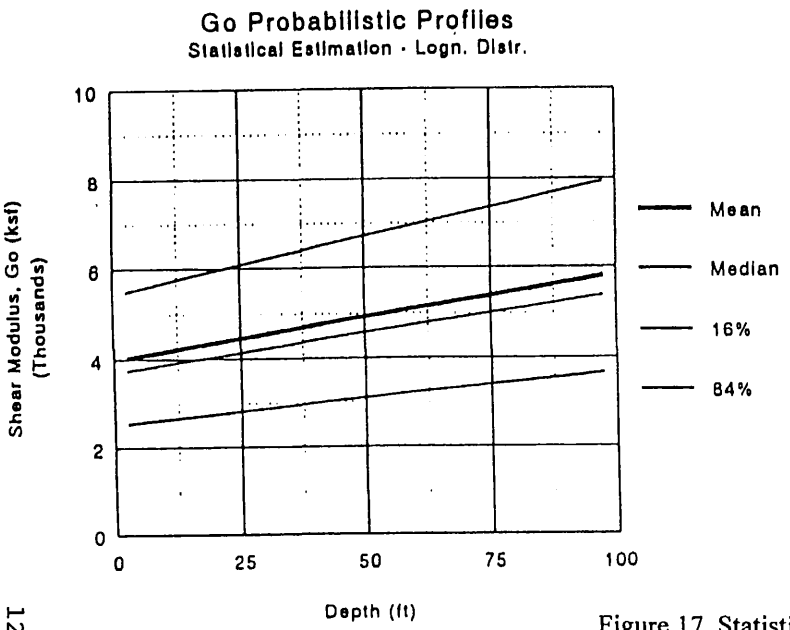

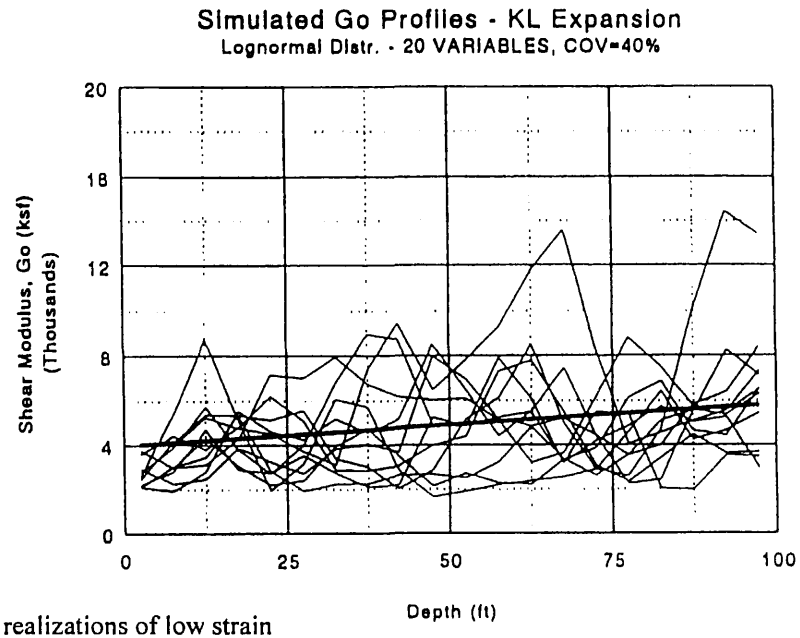

Figure 17. Statistics and realizations of low strain shear modulus profile

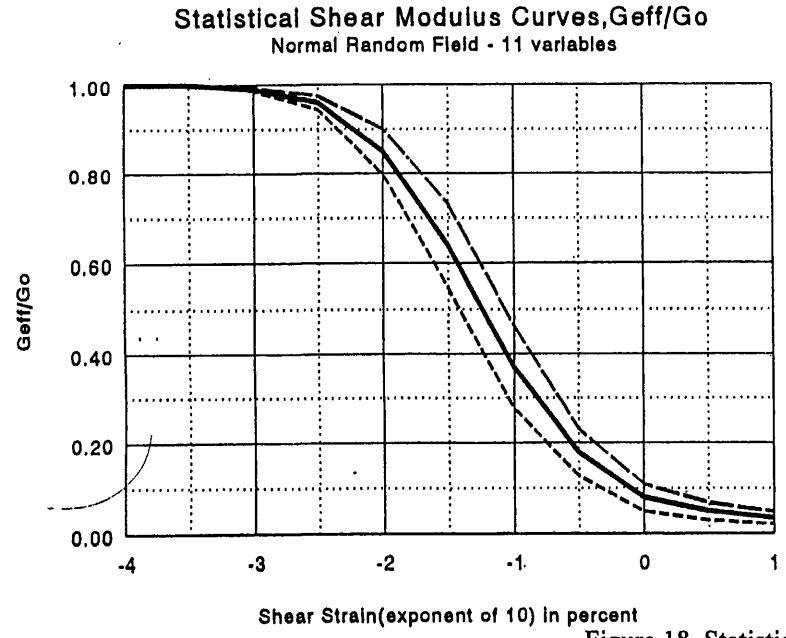

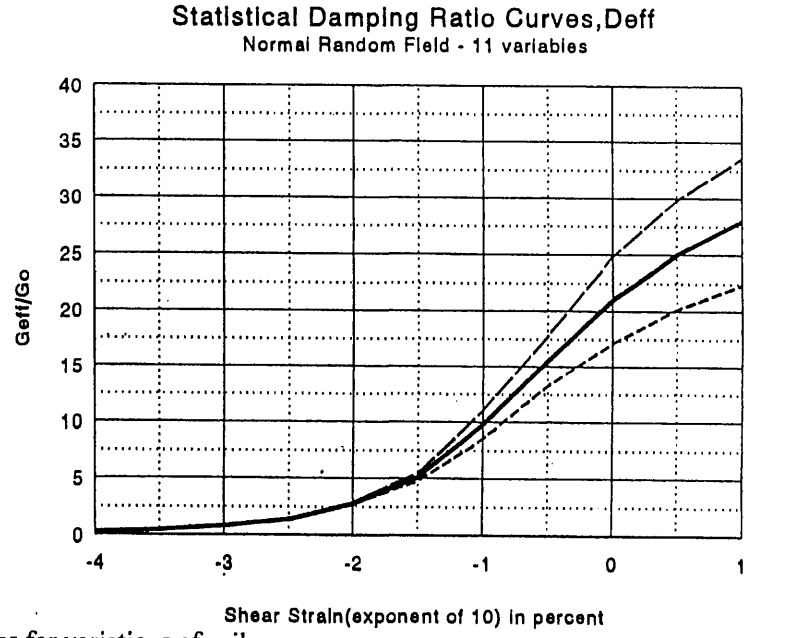

Figure 18. Statistical curves for variations of soil properties with shear strain

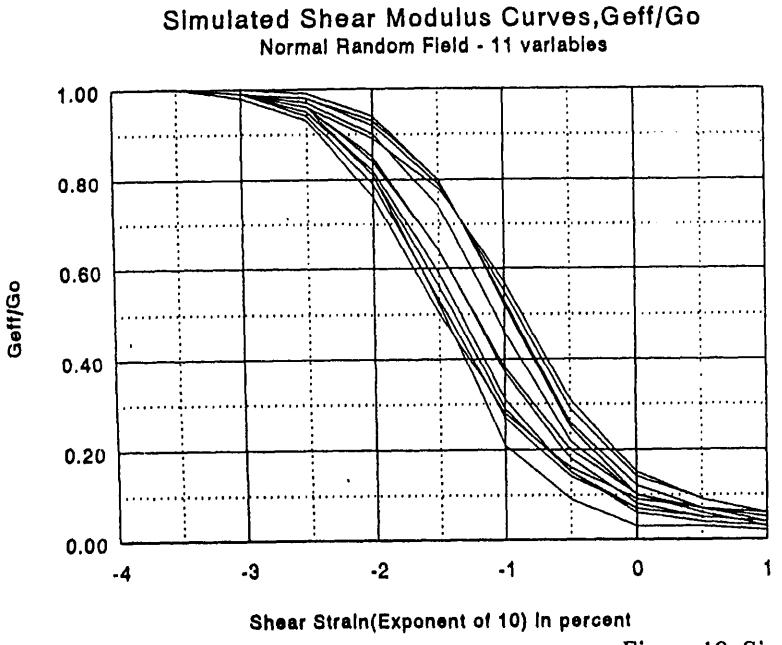

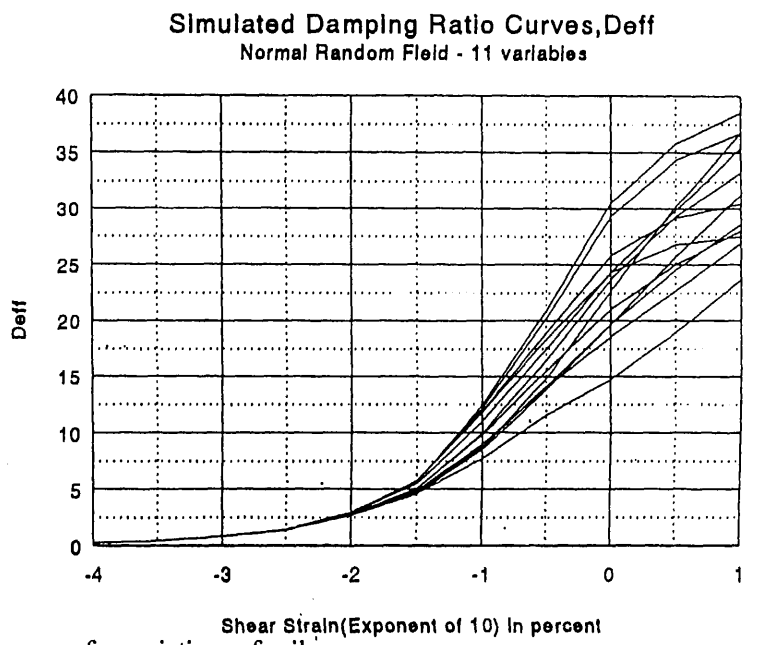

Figure 19. Simulated curves for variations of soil properties with shear strain

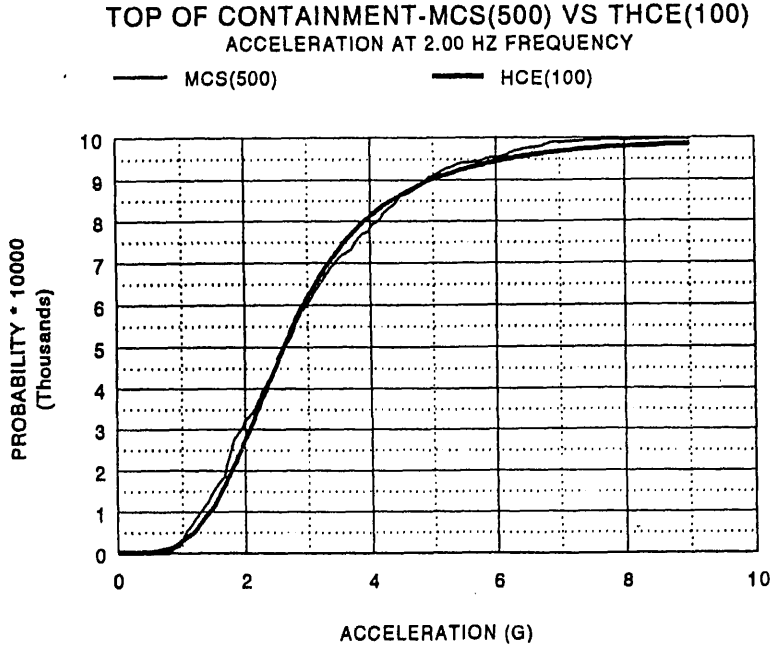

Figure 20. Comparison of probabilistic results

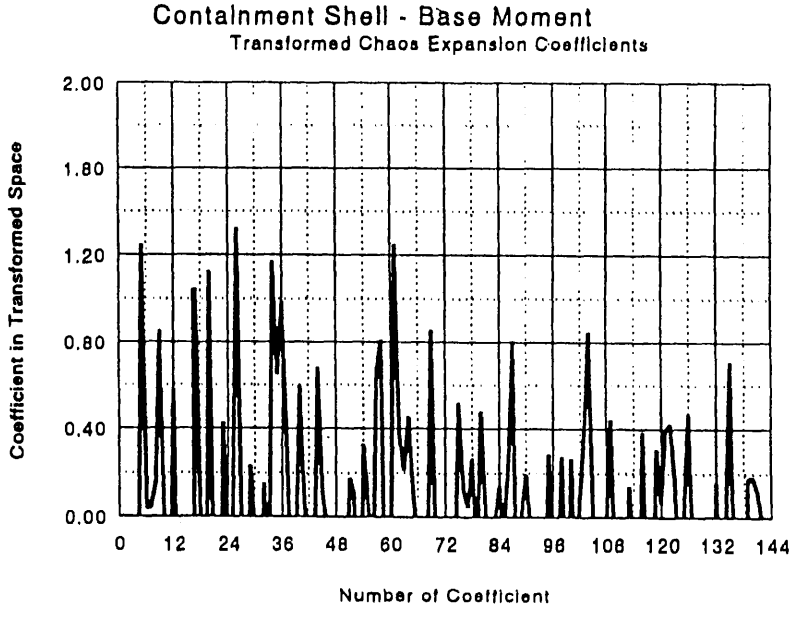

Figure 21. Coefficient of chaos expansion

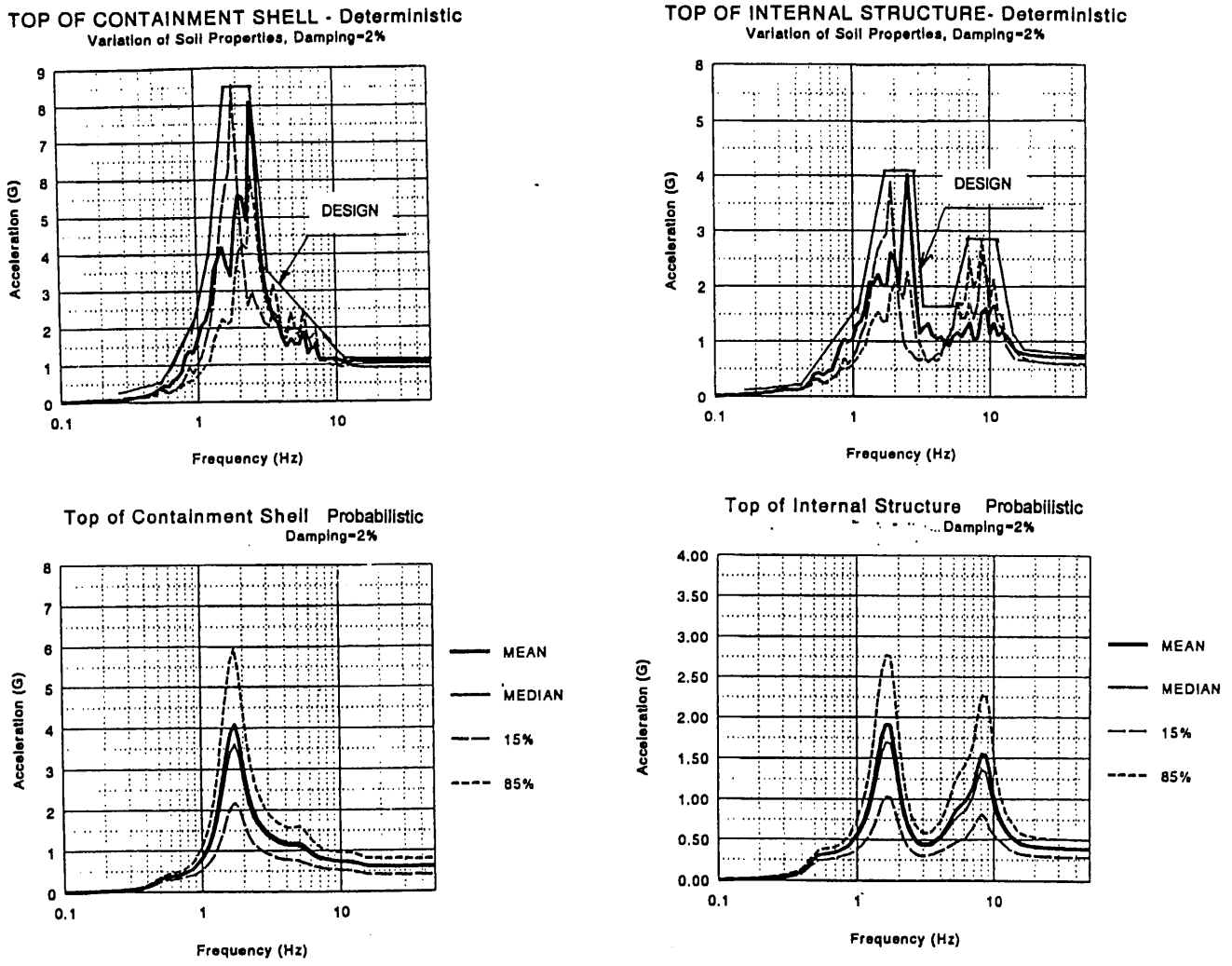

Figure 22. Probabilistic vs. deterministic in-structure response spectra

SEISMIC SOIL-FOUNDATION-STRUCTURE INTERACTION IN BRIDGES

By Wen S. Tseng[1] and Joseph Penzien[1]

ABSTRACT: Discussed herein are state-of-the-art methodologies used in assessing soil-foundation-structure interaction (SFSI) in bridges during seismic events, including (1) generating free-field ground-motion inputs, (2) determining foundation impedances and "scattered" input motions, (3) conducting global demand analyses of the complete soil-foundation-structure system, and (4) performing foundation capacity analyses for assessing foundation system performance.

INTRODUCTION

Prior to the 1971 San Fernando, California earthquake, nearly all damages to bridges during earthquakes were caused by ground failures, such as liquefaction, differential settlement, slides, and/or spreading; little damage was caused by seismically induced vibrations. Vibratory response considerations had been limited primarily to wind excitations of large bridges, the great importance of which was made apparent by failure of the Tacoma Narrows suspension bridge in the early 1940s, and to moving-loads and impact excitations of smaller bridges.

The importance of designing bridges to withstand the vibratory response produced during earthquakes was revealed by the 1971 San Fernando earthquake, during which many bridge structures collapsed. Similar bridge failures occurred during the 1989 Loma Prieta and 1994 Northridge, California earthquakes, and the 1995 Kobe, Japan earthquake. As a result of these experiences, much has been done recently to improve provisions in seismic design codes, advance modelling and analysis procedures, and develop more effective detail designs, all aimed at insuring that newly designed and retrofitted bridges will perform satisfactorily during future earthquakes.

Unfortunately, many of the existing older bridges in the U.S.A. and other countries, which are located in regions of moderate to high seismic intensity, have serious deficiencies which threaten life safety during future earthquakes. Because of this threat, aggressive actions have been taken in California, and elsewhere, to retrofit such unsafe bridges so as to bring their expected performances during future earthquakes to an acceptable level. To meet this goal, retrofit measures have been applied to the bridge superstructures, piers, abutments, and foundations.

[1]Principal and Senior Principal, International Civil Engineering Consultants, Inc., 1995 University Avenue. Suite 119, Berkeley, CA 94704, USA

It is because of this most recent experience that the importance of coupled soil-foundation-structure interaction (SFSI) on the dynamic response of bridge structures during earthquakes has been fully realized. In treating this problem, two different methods have been used (1) the so-called "elasto-dynamic" method developed and practiced in the nuclear power industry for large foundations, and (2) the so-called "empirical p-y" method developed and practiced in the offshore oil industry for pile foundations. Each method has its own strong and weak characteristics, which generally are opposite to those of the other, thus restricting their proper use to different types of bridge foundation. By combining the models of these two methods in series form, a hybrid method has been developed by Tseng and Penzien (1998) which makes use of the strong features of both methods, while minimizing their weak features. While this hybrid method may need some further development and validation at this time, it is fundamentally sound; thus, it is expected to eventually become a standard procedure in treating seismic SFSI of large bridges supported on different types of foundation.

FREE-FIELD SEISMIC GROUND MOTIONS

The first step in conducting a seismic performance evaluation of a bridge structure is to define the seismic input to the coupled soil-foundation-structure system. In a design situation, this input is defined in terms of the expected free-field motions in the soil region surrounding each bridge foundation. It is evident that to precisely characterize such motions is practically unachievable within the present-state-of-knowledge of seismic ground motions. Therefore, it is necessary to use a rather simplistic approach in generating such motions for design purposes. The procedure most commonly used for designing a large bridge is to (1) generate a three-component (two horizontal and vertical) set of accelerograms representing the free-field ground motion at a "control point" selected for the bridge site, and (2) characterize the spatial variations of

the free-field motions within each soil region of interest relative to the control motions.

The control point is usually selected at the surface of bedrock (or surface of a firm soil stratum in case of a deep soil site), referred to herein as "rock outcrop", at the location of a selected reference pier; and the free-field seismic wave environment within the local soil region of each foundation is assumed to be composed of vertically propagating plane shear (S) waves for the horizontal motions and vertically propagating plane compression (P) waves for the vertical motions. For a bridge site consisting of relatively soft top soil deposits overlying competent soil strata or rock, the assumption of vertically propagating plane waves over the depth of the foundations is reasonably valid as confirmed by actual field downhole array recordings.

The design ground motion for a bridge is normally specified in terms of a set of parameter values developed for the selected control point which include a set of target acceleration response spectra (ARS) and a set of associated ground motion parameters for the design earthquake, namely (a) magnitude, (b) source-to-site distance, (c) peak ground (rock-outcrop) acceleration (PGA), velocity (PGV), and displacement (PGD), and (d) duration of strong shaking. For large important bridges, these parameter values are usually established through regional seismic investigations coupled with site-specific seismic hazard and ground motion studies; whereas, for small bridges, it is customary to establish these values based on generic seismic study results such as contours of regional PGA values and standard ARS curves for different general classes of site soil conditions.

For a long bridge supported on multiple piers which are in turn supported on multiple foundations spaced relatively far apart, the spatial variations of ground motions among the local soil regions of the foundations need also be defined in the seismic input. Based on the results of analyses using actual earthquake ground motion recordings obtained from strong motion instrument arrays, such as the El Centro differential array in California and the SMART-1 array in Taiwan, the spatial variations of free-field seismic motions have been characterized using two parameters, namely, (a) apparent horizontal wave propagation velocity (speed and direction) which controls the first-order spatial variations of ground motion due to the seismic wave passage effect and (b) a set of horizontal and vertical ground-motion "coherency functions" which quantifies the second-order ground-motion variations due to scattering and complex three-dimensional wave propagation (Abrahamson, 1992). Thus, in addition to the design ground motion parameter values specified for the control motion, characterizing the design seismic inputs to long bridges needs to include the two additional parameters mentioned above, namely, (a) apparent horizontal wave velocity and (b) ground motion coherency functions; therefore, the seismic input motions developed for the various pier-foundation locations need to be compatible with the values specified for these two additional parameters.

Having specified the design seismic ground-motion parameters, the steps required in establishing the pier-foundation location-specific seismic input motions for a particular bridge are: (1) develop a three-component (two horizontal and vertical) set of free-field rock-outcrop motion time-histories which are compatible with the design target ARS and associated design ground motion parameters applicable at a selected single control-point location at the bridge site (these motions are referred to herein simply as the "response-spectrum-compatible" time-histories of control motion), (2) generate response-spectrum-compatible time-histories of free-field rock-outcrop motions at each bridge pier-support location such that their coherencies relative to the corresponding components of the response-spectrum-compatible motions at the control-point and at other pier-support locations are compatible with the wave passage parameters and the coherency functions specified for the site (these motions are referred to herein as "response-spectrum-and-coherency-compatible" rock-outcrop motions), and (3) carry out free-field site response analyses for each pier-support location to obtain the time-histories of free-field soil motions at specified discrete elevations over the full depth of each foundation using the corresponding response-spectrum-and-coherency-compatible free-field rock-outcrop motions as inputs.

Rock-Outcrop Motions At Control-Point Location

Given a prescribed set of target acceleration response spectra (ARS) and a set of associated design ground motion parameters for a bridge site as described previously, the objective herein is to develop a three-component set of time-histories of control motion that (1) provides a reasonable match to the corresponding target ARS and (2) has time-history characteristics reasonably compatible with the other specified associated ground motion parameter values. In the past, several different methods have been used for developing rock-outcrop time histories of motion compatible with a prescribed set of target ARS, including (1) the response-spectrum compatibility time-history adjustment method, (2) the source-to-site numerical model time-history simulation method, (3) the multiple actual recorded time-history scaling method, and (4) the connecting accelerogram segments method. At the present time, the first of these four methods is considered most suitable and

practical for bridge engineering applications, particularly the method developed by Lilhanand and Tseng (1988) which is based on earlier work by Kaul (1978). In this case, small local perturbations are added in a systematic manner to the initial or starting acceleration time history at those times corresponding to the occurrences of the response spectral values. As a result, the phasing characteristics (wave sequence or pattern) in the initial, or starting, time history are largely maintained. It is important therefore that the initial time history be selected carefully.

Each three-component set of starting accelerograms for a given bridge site should preferably be a set recorded during a past seismic event that has (1) a source mechanism similar to that of the controlling design earthquake, (2) a magnitude within about ±0.5 of the target controlling earthquake magnitude, and (3) a closest source-to-site distance within 10 km of the target source-to-site distance. The selected recorded accelerograms should have their PGA, PGV, and PGD values and their strong shaking durations within a range of ±25% of the target values specified for the bridge site and they should represent free-field surface recordings on rock, rock-like, or a stiff soil site; no recordings on a soft site should be used. For a close-in controlling seismic event, e.g. within about 10 km of the site, the selected accelerograms should contain a definite velocity pulse or the so-called "fling". When such recordings are not available, Method (2) described previously can be used to generate a starting set of time histories having an appropriate fling or to modify the starting set of recorded motions to include the desired directional velocity pulse.

Having selected a three-component set of starting time histories, the horizontal components should be transformed into their principal components and the corresponding principal directions should be evaluated (Penzien and Watabe, 1975). These principal components should then be made response-spectrum compatible using the time-domain adjustment procedure described above or the standard frequency-domain adjustment procedure (Hao, Oliviera, and Penzien, 1989; Silva and Lee, 1987; and Bolt and Gregor, 1993). Using the latter procedure, only the Fourier amplitude spectrum, not the phase spectrum, is adjusted iteratively.

Rock-Outcrop Motions At Bridge Support Locations

Characterization of the spatial variations of rock-outcrop motions for engineering purposes is based on a set of wave passage parameters and ground motion coherency functions. The wave passage parameters currently used are the apparent horizontal seismic wave speed, V, and its direction angle relative to an axis normal to the longitudinal axis of the bridge. Studies of strong- and weak-motion array data including those in California, Taiwan, and Japan show that the apparent horizontal speed of S-waves in the direction of propagation is typically in the 2-3 km/sec range (Chang et al., 1986 and Abrahamson, 1992). In applications, the apparent wave-velocity vector showing speed and direction must be projected along the bridge axis giving the apparent wave speed in that direction. To be realistic, when becomes small, a minimum angle for θ, say 30 degrees, should be used in order to account for waves arriving in directions different from the specified direction.

The spatial coherency of the free-field components of motion in a single direction at various locations on the ground surface has been parameterized by a complex coherency function defined by the relation

$$\Gamma_{ij}(i\omega) = \frac{S_{ij}(i\omega)}{\sqrt{S_{ii}(\omega)}\sqrt{S_{jj}(\omega)}} \quad i,j = 1, 2, ..., n \text{ locations} \quad (1)$$

in which $S_{ij}(i\omega)$ is the smoothed complex cross-power spectral density function and $S_{ii}(\omega)$ and $S_{jj}(\omega)$ are the smoothed real power-spectral density (PSD) functions of the components of motion at locations i and j. The notation $i\omega$ in the above equation is used to indicate that the coefficients $S_{ij}(i\omega)$ are complex-valued (contain both real and imaginary parts) and are dependent upon excitation frequency ω. Based on analyses of strong motion array data, a set of generic coherency functions for the horizontal and vertical ground motions has been developed (Abrahamson, et al., 1991).

Given a three-component set of response-spectrum-compatible time histories of rock-outcrop motions developed for the selected control-point location and a specified set of wave-passage parameters and "target" coherency functions as described above, response-spectrum-compatible and coherency-compatible multiple-support rock-outcrop motions applicable to each pier-support location of the bridge can be generated using the "marching method" developed by Hao, Oliveira, and Penzien (1989) and extended later by Tseng, Lilhanand, and Yang (1993).

For a long bridge located close-in to the controlling seismic source, attenuation of motion with distance away from the control-pier location should be considered. This can be achieved by scaling the generated motions at various pier locations by appropriate scaling factors determined from an appropriate ground motion attenuation relation. The acceleration time histories generated for all pier

locations should be integrated to obtain their corresponding velocity and displacement time histories, which should be checked to ensure against having numerically-generated baseline drifts. Relative displacement time-histories between the control-pier location and successive pier locations should also be checked to ensure that they are reasonable. The rock outcrop motions finally obtained should then be used in appropriate site response analyses to develop the corresponding free-field soil motions required in conducting the SFSI analyses for each pier location.

Soil Motions at Bridge Support Locations

The seismic inputs to large bridges are defined in terms of the expected free-field soil motions at discrete elevations over the entire depth of each foundation. Such motions must be evaluated through location-specific site-response analyses using the corresponding previously-described rock-outcrop free-field motions as inputs to appropriately-defined soil/bedrock models. Usually, these models are based on the assumption that the horizontal and vertical free-field soil motions are produced by upward/downward propagation of one-dimensional shear and compression waves, respectively, as caused by the upward propagation of incident waves in the underlying rock or firm soil formation. Consistent with these types of motion, it is assumed that the local soil medium surrounding each foundation consists of uniform horizontal layers of infinite lateral extent. Wave reflections and refractions will occur at all interfaces of adjacent layers, including the soil/bedrock interface, and reflections of the waves will occur at the soil surface. Computer program SHAKE (Schnabel et al., 1972, Idriss and Sun, 1991) is most commonly used to carry out the above-described one-dimensional type of site-response analysis. For a long bridge having a widely varying soil profile from end to end, such site response analyses must be repeated for different soil columns representative of the changing profile.

The cyclic free-field soil deformations produced at a particular bridge site by a maximum expected earthquake are usually of the nonlinear hysteretic form. Since the SHAKE computer program treats a linear system, the soil column being analyzed must be modelled in an equivalent linearized manner. To obtain the equivalent linearized form, the soil parameters in the model are modified after each consecutive linear time-history response analysis is complete, which continues until convergence to strain-compatible parameters are reached. In generating horizontal free-field motions produced by vertically propagating shear waves, the needed equivalent-linear soil parameters are the shear modulus G and the hysteretic damping ratio β. These parameters, as functions of shear strain γ have been published by Vucetic and Dobry (1991) for clay and by Sun, Golesorkhi and Seed (1988), and the Electric Power Research Institute (EPRI) for sand. The shear modulus is given in its nondimensional form G/G_{max} where G_{max} is the in-situ shear modulus at very low strains ($\gamma \leq 10^{-4}\%$). The shear modulus G must be obtained from cyclic shear tests, while G_{max} can be obtained using $G_{max} = \rho V_s^2$ in which ρ is mass density of the soil and V_s is the in-situ shear wave velocity obtained by field measurement.

For generating vertical free-field motions produced by vertically propagating compression waves, the needed soil parameters are the low-strain constrained elastic modulus, $E_p = \rho V_p^2$, where V_p is the compression wave velocity, and the corresponding damping ratio. The variations of these soil parameters with compressive strain have not as yet been well established. At the present time, vertical site response analyses have generally been carried out using the low-strain constrained elastic moduli, E_p, directly and the strain-compatible damping ratios obtained from the horizontal response analyses, but limited to a maximum value of 10%, without any further strain-compatibility iterations. For soils submerged in water, the value of E_p should not be less than the compression wave velocity of water.

Having generated acceleration free-field time histories of motion using the SHAKE computer program, the corresponding velocity and displacement time histories should be obtained through single and double integrations of the acceleration time histories. Should unrealistic drifts appear in the displacement time histories, appropriate corrections should be applied. Should such drifts appear in a straight line fashion, it usually indicates that the durations specified for Fourier transforming the recorded accelerograms are too short; thus, increasing these durations will usually correct the problem. If the baseline drifts depart significantly from a simple straight line, this tends to indicate that the analysis results may be unreliable, in which case, they should be carefully checked before being used. Time histories of free-field relative displacement between pairs of pier locations should also be generated and then be checked to judge the reasonableness of the results obtained.

SOIL-FOUNDATION INTERACTION

Basic to solving the seismic SFSI problem for a bridge is the interaction between the combined structure-foundation system and its supporting soil medium, which, for analysis purposes, can be considered to be a full half-space. The fundamental step in solving this problem is to characterize the constitutive relations between the dynamic forces acting on each foundation of the bridge at its interface

boundary with the soil and the corresponding foundation motions, expressed in terms of the displacements, velocities, and accelerations. Such forces are called herein the "soil-foundation interaction forces". For a bridge subjected to externally applied static and/or dynamic loadings, such as dead, live, wind, and wave loadings, these soil-foundation interaction forces are functions of the foundation motions only; however, for a bridge subjected to seismic conditions, they are functions of the free-field soil motions as well.

Let h be the total number of degrees-of-freedom (DOF) of the bridge's foundations as defined at their soil/foundation interface boundaries; $\boldsymbol{u}_h(t)$, $\dot{\boldsymbol{u}}_h(t)$ and $\ddot{\boldsymbol{u}}_h(t)$ be the corresponding foundation displacement, velocity, and acceleration vectors, respectively; and $\bar{\boldsymbol{u}}_h(t)$, $\dot{\bar{\boldsymbol{u}}}_h(t)$ and $\ddot{\bar{\boldsymbol{u}}}_h(t)$ be the free-field soil displacement, velocity, and acceleration vectors in the h DOF, respectively; and let $\boldsymbol{f}_h(t)$ be the corresponding soil-foundation interaction force vector. Using these notations, characterization of the soil-foundation interaction forces under seismic conditions is usually expressed in linear (or equivalent linear) form as shown by the matrix equation

$$\boldsymbol{f}_h(i\omega) = \boldsymbol{G}_{hh}(i\omega)\{\boldsymbol{u}_h(i\omega) - \bar{\boldsymbol{u}}_h(i\omega)\} \qquad (2)$$

in which matrix $\boldsymbol{G}_{hh}(i\omega)$ is a complex, frequency-dependent coefficient matrix called herein the "soil impedance matrix". Depending upon the type of foundation, this matrix and the associated free-field soil input motion vector $\bar{\boldsymbol{u}}_h(i\omega)$ to be used for seismic demand analysis purposes can be established utilizing different soil models as described below.

Elasto-Dynamic Model

For a large bridge foundation such as a large spread footing, caisson, or single or multiple shafts having very large diameters, for which the nonlinearities occurring in the local soil region immediately adjacent to the foundation are small, the soil impedance matrix $\boldsymbol{G}_{hh}(i\omega)$ can be evaluated utilizing the dynamic Green's functions (dynamic displacements of the soil medium due to harmonic point-load excitations) obtained from the solution of a dynamic boundary-value problem of a linear damped-elastic half-space soil medium subjected to harmonic point-loads applied at each of the h DOF on the soil/foundation interface boundaries. Such solutions have been obtained in analytical form for a linear damped-elastic continuum half-space soil medium by Apsel (1979). Because of complexities in the analytical solution, dynamic Green's functions have only been obtained for foundations having relatively simple soil/foundation interface geometries, e.g. rectangular, cylindrical, or spherical soil/foundation interface geometries, supported in simple soil media. In practical applications, the dynamic Green's functions are often obtained in numerical forms based on a finite element discretization of the half-space soil medium and a corresponding discretization of the soil/foundation interface boundaries using a computer program such as SASSI (Lysmer et al. 1981), which has the capability of properly simulating the wave radiation boundary conditions at the far-field of the half-space soil medium. The use of finite element soil models to evaluate the dynamic Green's functions in numerical form has the advantage that foundations having arbitrary soil/foundation interface geometries can be easily handled; it, however, suffers from the disadvantage that the highest frequency, i.e. cut-off frequency, of motion for which a reliable solution can be obtained is limited by size of finite element used for modelling the soil medium.

Having evaluated the dynamic Green's functions using the procedure described above, the desired soil impedance matrix can then be obtained by inverting, frequency-by-frequency, the "soil compliance matrix", which is the matrix of Green's function values evaluated for each specified frequency ω. Because the dynamic Green's functions are complex-valued and frequency-dependent, the coefficients of the resulting soil impedance matrix are also complex-valued and frequency-dependent. The real parts of the soil-impedance coefficients represent the dynamic stiffnesses of the soil medium which also incorporate the soil inertia effects; the imaginary parts of the coefficients represent the energy losses resulting from both soil material damping and radiation of stress waves into the far-field soil medium. Thus, the soil impedance matrix as developed reflects the overall dynamic characteristics of the soil medium as related to the motion of the foundation at the soil/foundation interfaces.

Because of the presence of the foundation excavation cavities in the soil medium , the vector of free-field soil motions $\bar{\boldsymbol{u}}_h(i\omega)$ prescribed at the soil/foundation interface boundaries has to be derived from the seismic input motions of the free-field soil medium without the foundation excavation cavities. The derivation of the motion vector $\bar{\boldsymbol{u}}_h(i\omega)$ requires the solution of a dynamic boundary-value problem for the free-field half-space soil medium having foundation excavation cavities subjected to a specified seismic wave input such that the resulting solution satisfies the stress-free conditions at the surfaces of the foundation excavation cavities. Thus, the resulting seismic response motions, $\bar{\boldsymbol{u}}_h(i\omega)$, reflect the effects of seismic

wave scattering due to the presence of the cavities. This scattering effect is much more important for a large bridge foundation, such as a large caisson or a group of very-large diameter shafts, than it is for a foundation having small characteristic dimensions, such as a slender-pile group; and, it is more significant for foundations supported in soft soil sites than in stiff soil sites.

The characterization of the soil impedance matrix utilizing the elasto-dynamic model of the soil medium as described above requires soil material characterization constants which include (a) mass density, ρ, (b) shear and constrained elastic moduli, G and E_p (or shear and compression wave velocities, V_s and V_p), (c) and constant-hysteresis damping ratio, β. As mentioned previously, the soil shear modulus decreases, while the soil hysteresis damping ratio increases as functions of soil shear strain induced in the free-field soil medium due to the seismic input motions. The effects of these so-called "global soil nonlinearities" can be easily incorporated into the soil impedance matrix based on an elasto-dynamic model by using the free-field-motion-induced strain-compatible soil shear moduli and damping ratios as the soil material constants in the evaluation of the dynamic Green's functions. For convenience of later discussions, the soil impedance matrix, $\boldsymbol{G}_{hh}(i\omega)$, characterized using an elasto-dynamic model will be denoted by the symbol $\boldsymbol{G}^{e}_{hh}(i\omega)$.

Empirical "p-y" Model

For a slender-pile group foundation for which soil nonlinearities occurring in the local soil regions immediately adjacent to the piles dominate the behavior of the foundation under loadings, the characterization of the soil resistances to pile deflections has often relied on empirically derived "p-y" curves for lateral resistance and "t-z" and "Q-d" curves for axial resistance. For such a foundation, the characterization of the soil impedance matrix needed for demand analysis purposes can be made by using the secant moduli derived from the commonly used nonlinear "p-y", "t-z," and "Q-d" curves. Since the development of these empirical curves has been based upon static or pseudo-static test results, it does not incorporate the soil inertia and material damping effects. Thus, the resulting soil impedance matrix developed from the secant moduli of the "p-y", "t-z," and "Q-d" curves reflects only the static soil stiffnesses but not the soil inertia and soil material damping characteristics. Hence, the soil impedance matrix so obtained is a real-valued constant coefficient matrix applicable at the zero frequency ($\omega = 0$); it, however, is a function of the foundation displacement amplitude. This matrix is designated herein as $\boldsymbol{G}^{s}_{hh}(0)$ to differentiate it from the soil impedance matrix $\boldsymbol{G}^{e}_{hh}(i\omega)$ defined previously.

The construction of the "p-y", "t-z," and "Q-d" curves depends only on the strength parameters but not the stiffness parameters of the soil medium; thus, the effects of global soil nonlinearities on the dynamic stiffnesses of the soil medium, as caused by soil-shear-modulus decrease and soil-damping increase as functions of free-field-motion-induced soil shear strains, can not be incorporated into the soil impedance matrix developed from these curves. Furthermore, since these curves are developed on the basis of results from field tests in which there are no free-field ground-motion-induced soil deformations, the effects of such global soil nonlinearities on the soil strength characterization parameters and hence the "p-y", "t-z," and "Q-d" curves can not be incorporated.

Because of the small cross-sectional dimensions of slender piles, the seismic wave scattering effect due to the presence of pile cavities is usually negligible; thus, the scattered free-field soil input motions $\bar{\boldsymbol{u}}_h(i\omega)$ in this case are often taken to be the same as the free-field soil motions when the cavities are not present.

Hybrid Model

From the discussions in the above two sections, it is clear that characterization of the soil-foundation interaction forces for demand analysis purposes can be achieved using either an elasto-dynamic model or an empirical "p-y" model for the soil medium, each of which has its own merits and deficiencies. The elasto-dynamic model is capable of incorporating soil inertia, damping (material and radiation), and stiffness characteristics; and, it can incorporate the effects of global soil nonlinearities induced by the free-field soil motions in an equivalent linearized manner. However, it suffers from the deficiency that it does not allow for easy incorporation of the effects of local soil nonlinearities. On the contrary, the empirical "p-y" model can properly capture the effects of local soil nonlinearities in an equivalent linearized form; but, it suffers from the deficiencies of not being able to properly simulate soil inertia and damping effects, and it can not treat the effects of global soil nonlinearities. Since the capabilities of the two models are mutually complimentary, it is logical to combine the elasto-dynamic model with the empirical "p-y" model in a series form such that the combined model has the desired capabilities of both models. This combined "hybrid" model is presented in more detail in the publication by Tseng and Penzien (1998).

DEMAND ANALYSIS PROCEDURE

The seismic response of a complete bridge system involves interactions between the structure and its supporting foundations and between the foundations and their surrounding soil media. To develop the equations of motion governing the response of this system in discrete (finite element) form, let s denote the number of degrees-of-freedom (DOF) in the structure, excluding its f DOF at the structure/foundation interface locations, and let g denote the number of DOF in the foundations, also excluding the f DOF but including the h DOF at all soil/foundation interfaces as defined previously. Corresponding with those DOF, let vectors $\boldsymbol{u}_s(t)$, $\boldsymbol{u}_f(t)$, and $\boldsymbol{u}_g(t)$ contain the total-displacement time histories of motion at the DOF s, f, and g, respectively.

Linear Modelling

Since the soil medium surrounding all foundations is continuous and of infinite extent, a rigorous model of a complete bridge system must contain stiffness and damping coefficients which are dependent upon the excitation (or response) frequencies. Such being the case, the corresponding equations of motion of the complete system having n DOF ($n = s + f + g$) must rigorously be represented in the frequency domain.

Considering the coupled structure-foundation system as a free-free (no boundary constraints) system having externally applied forces $-\boldsymbol{f}_h(t)$ acting in the h DOF, its equations of motion can be expressed in the frequency-domain form

$$\begin{bmatrix} \boldsymbol{D}_{ss}(i\omega) & \boldsymbol{D}_{sf}(i\omega) & \boldsymbol{0} \\ \boldsymbol{D}_{sf}^{T}(i\omega) & \boldsymbol{D}_{ff}(i\omega) & \boldsymbol{D}_{fg}(i\omega) \\ \boldsymbol{0} & \boldsymbol{D}_{fg}^{T}(i\omega) & \boldsymbol{D}_{gg}(i\omega) \end{bmatrix} \begin{Bmatrix} \boldsymbol{u}_s(i\omega) \\ \boldsymbol{u}_f(i\omega) \\ \boldsymbol{u}_g(i\omega) \end{Bmatrix} = \begin{Bmatrix} \boldsymbol{0} \\ \boldsymbol{0} \\ \boldsymbol{f}_g(i\omega) \end{Bmatrix} \quad (3)$$

in which $\boldsymbol{u}_s(i\omega)$, $\boldsymbol{u}_f(i\omega)$, $\boldsymbol{u}_g(i\omega)$, and $\boldsymbol{f}_g(i\omega)$ are the Fourier transforms of vectors $\boldsymbol{u}_s(t)$, $\boldsymbol{u}_f(t)$, $\boldsymbol{u}_g(t)$, and $\boldsymbol{f}_g(t)$, respectively; and matrices $\boldsymbol{D}_{ij}(i\omega)$, $i,j = s, f, g$, are the corresponding impedance (dynamic stiffness) matrices. The g components in vectors $\boldsymbol{u}_g(i\omega)$ and $\boldsymbol{f}_g(i\omega)$ are ordered such that their last h components make up vectors $\boldsymbol{u}_h(i\omega)$ and $-\boldsymbol{f}_h(i\omega)$, respectively, with all other components being equal to zero.

For a viscously-damped linear structure-foundation system, the impedance matrices $\boldsymbol{D}_{ij}(i\omega)$ are of the form

$$\boldsymbol{D}_{ij}(i\omega) = \boldsymbol{K}_{ij} + i\omega\boldsymbol{C}_{ij} - \omega^2\boldsymbol{M}_{ij} \qquad i,j = s,f,g \quad (4)$$

in which $\boldsymbol{K}_{ij}$, $\boldsymbol{C}_{ij}$, and $\boldsymbol{M}_{ij}$ are the standard stiffness, damping, and mass matrices, respectively, which would appear in the system's equations of motion if expressed in the time domain. For a constant-hysteresis-damped linear system, the impedance matrices are given by

$$\boldsymbol{D}_{ij}(i\omega) = \boldsymbol{K}_{ij}^{*} - \omega^2\boldsymbol{M}_{ij} \qquad i,j = s,f,g \quad (5)$$

in which $\boldsymbol{K}_{ij}^{*}$ is a complex stiffness matrix obtained by assembling individual finite-element matrices $\boldsymbol{K}^{*(m)}$ of the form

$$\boldsymbol{K}^{*(m)} \equiv \left\{1 - 2(\beta^{(m)})^2 + 2i\beta^{(m)}\sqrt{1-(\beta^{(m)})^2}\right\}\boldsymbol{K}^{(m)} \doteq (1 + 2i\beta^{(m)})\,\boldsymbol{K}^{(m)} \quad (6)$$

where $\boldsymbol{K}^{(m)}$ denotes the standard elastic stiffness matrix for finite element m as used in the assembly process to obtain matrix $\boldsymbol{K}_{ij}$ and $\beta^{(m)}$ is a damping ratio specified appropriately for the material used in finite element m (Clough and Penzien, 1993).

The hysteretic form of damping represented in Eq. (5) is the more appropriate form to use for two reasons (1) it is easy to accommodate different damping ratios for the different materials used in the system, and (2) the resulting modal damping is independent of excitation (or response) frequency ω, consistent with test evidence showing that real damping is indeed essentially independent of this frequency. As noted by the form of Eq. (4), viscous damping is dependent upon frequency ω, contrary to test results; thus, preference should definitely be given to the use of hysteretic damping for linear systems which can be solved in the frequency domain. Hysteretic damping is unfortunately incompatible with solutions in the time domain.

Vector $-\boldsymbol{f}_h(i\omega)$, which makes up the last h components in force vector $\boldsymbol{f}_g(i\omega)$ appearing in Eq. (3), represents, as defined previously, the internal soil-foundation interaction forces at the soil/foundation interfaces when the entire coupled soil-foundation-structure system is responding to the free-field soil input motions. Therefore, to solve the SFSI problem, this vector must be characterized in terms of the foundation displacement vector $\boldsymbol{u}_h(i\omega)$ and the free-field soil displacement vector $\bar{\boldsymbol{u}}_h(i\omega)$. As discussed previously, for demand analysis purposes, this vector can be linearized to the form

$$-\boldsymbol{f}_h(i\omega) = \boldsymbol{G}_{hh}(i\omega)\{\bar{\boldsymbol{u}}_h(i\omega) - \boldsymbol{u}_h(i\omega)\} \quad (7)$$

in which $-f_h(i\omega)$ represents the force vector acting on the foundations from the soil medium and $G_{hh}(i\omega)$ is the soil impedance matrix which is complex-valued and frequency-dependent.

Substituting Eq. (7) into Eq. (3), the equations of motion of the complete bridge system become

$$\begin{bmatrix} D_{ss}(i\omega) & D_{sf}(i\omega) & 0 \\ D_{sf}^T(i\omega) & D_{ff}(i\omega) & D_{fg}(i\omega) \\ 0 & D_{fg}^T(i\omega) & [D_{gg}(i\omega)+G_{gg}(i\omega)] \end{bmatrix} \begin{Bmatrix} u_s(i\omega) \\ u_f(i\omega) \\ u_g(i\omega) \end{Bmatrix} = \begin{Bmatrix} 0 \\ 0 \\ \bar{f}_g(i\omega) \end{Bmatrix} \quad (8)$$

in which

$$G_{gg}(i\omega) = \begin{bmatrix} 0 & 0 \\ 0 & G_{hh}(i\omega) \end{bmatrix} \; ; \; \bar{f}_g(i\omega) = \begin{Bmatrix} 0 \\ G_{hh}(i\omega)\,\bar{u}_h(i\omega) \end{Bmatrix} \quad (9)$$

Vector $G_h(i\omega)\bar{u}_h(i\omega)$ is the free-field soil "seismic driving force" vector, in which the free-field soil displacements in vector $\bar{u}_h(i\omega)$ result from scattering of incident seismic waves propagating to the bridge site as explained previously.

Nonlinear Modelling

When large nonlinearities develop in the structure-foundation subsystem during a seismic event, evaluation of its performance requires nonlinear modelling and analysis in the time domain. In this case, the standard linear equations of motion of the complete system as expressed by

$$\begin{bmatrix} M_{ss} & M_{sf} & 0 \\ M_{sf}^T & M_{ff} & M_{fg} \\ 0 & M_{fg}^T & M_{gg} \end{bmatrix} \begin{Bmatrix} \ddot{u}_s(t) \\ \ddot{u}_f(t) \\ \ddot{u}_g(t) \end{Bmatrix} + \begin{bmatrix} C_{ss} & C_{sf} & 0 \\ C_{sf}^T & C_{ff} & C_{fg} \\ 0 & C_{fg}^T & C_{gg} \end{bmatrix} \begin{Bmatrix} \dot{u}_s(t) \\ \dot{u}_f(t) \\ \dot{u}_g(t) \end{Bmatrix} + \quad (10)$$

$$\begin{bmatrix} K_{ss} & K_{sf} & 0 \\ K_{sf}^T & K_{ff} & K_{fg} \\ 0 & K_{fg}^T & K_{gg} \end{bmatrix} \begin{Bmatrix} u_s(t) \\ u_f(t) \\ u_g(t) \end{Bmatrix} = \begin{Bmatrix} 0 \\ 0 \\ f_g(t) \end{Bmatrix}$$

must be modified appropriately to characterize the nonlinearities for use in a step-by-step numerical solution. Usually, it is the third term on the left-hand side of this equation which must be modified to represent the nonlinear-hysteric force-deformation behavior taking place in the individual finite elements of the system. The second term in this equation, representing viscous damping forces, is usually retained in its linear form with the full viscous damping matrix C being expressed in the Rayleigh form

$$C = \alpha_R M + \beta_R K \quad (11)$$

in which M and K are the full mass and elastic-stiffness matrices shown in Eq. (10) and α_R and β_R are constants assigned numerical values which will limit the modal damping ratios to levels within acceptable bounds over a range of modal frequencies dominating the seismic response.

For a time-domain solution of Eq. (10) in its modified nonlinear form, all parameters in the equation must be real (no imaginary parts) and frequency independent. It remains therefore to modify the soil impedance matrix $G_{hh}(i\omega)$ so that when introduced into Eq. (7), the inverse Fourier transform of $-f_h(i\omega)$ to the time domain will yield a vector $-f_h(t)$ having no frequency dependent parameters. To accomplish this objective, separate $G_{hh}(i\omega)$ into its real and imaginary parts in accordance with

$$G_{hh}(i\omega) = G_{hh}^R(\omega) + iG_{hh}^I(\omega) \quad (12)$$

in which $G_{hh}^R(\omega)$ and $G_{hh}^I(\omega)$ are real functions of ω. Then approximate these functions using the relations

$$G_{hh}^R(\omega) \doteq \bar{K}_{hh} - \omega^2 \bar{M}_{hh} \; ; \; G_{hh}^I(\omega) \doteq \omega \bar{C}_{hh} \quad (13)$$

where the real constants in matrices $\bar{K}_{hh}$, $\bar{M}_{hh}$, and $\bar{C}_{hh}$ are assigned numerical values to provide best fits to the individual frequency-dependent functions in matrices $G_{hh}^R(\omega)$ and $G_{hh}^I(\omega)$ over the frequency range of major influence on seismic response. Typically, applying these best fits to the range $0 < \omega < 4$ radians/second, corresponding to the range $0 < f < 2$ Hz, where $f = \omega/2\pi$, is adequate for most large bridges. In this fitting process, it is sufficient to treat $\bar{M}_{hh}$ as a diagonal matrix, thus affecting only the diagonal functions in matrix $G_{hh}^R(\omega)$. The reason for selecting the particular frequency-dependent forms of Eqs. (13) is that when they are substituted into Eq. (12), which in turn is substituted into Eq. (7), the resulting expression for $f_h(i\omega)$ can be Fourier transformed to the time domain yielding

$$-f_h(t) = \bar{K}_{hh}\{\bar{u}_h(t) - u_h(t)\} + \bar{C}_{hh}\{\dot{\bar{u}}_h(t) - \dot{u}_h(t)\} + \bar{M}_{hh}\{\ddot{\bar{u}}_h(t) - \ddot{u}_h(t)\} \quad (14)$$

Substituting $-f_h(t)$ given by this equation for the last h components in vector $f_g(t)$, with all other components

in $f_g(t)$ being equal to zero, and then substituting the resulting vector $f_g(t)$ into Eq. (10) gives

$$\begin{bmatrix} M_{ss} & M_{sf} & 0 \\ M_{sf}^T & M_{ff} & M_{fg} \\ 0 & M_{fg}^T & [M_{gg}+\bar{M}_{gg}] \end{bmatrix} \begin{Bmatrix} \ddot{u}_s(t) \\ \ddot{u}_f(t) \\ \ddot{u}_g(t) \end{Bmatrix} + \begin{bmatrix} C_{ss} & C_{sf} & 0 \\ C_{sf}^T & C_{ff} & C_{fg} \\ 0 & C_{fg}^T & [C_{gg}+\bar{C}_{gg}] \end{bmatrix} \begin{Bmatrix} \dot{u}_s(t) \\ \dot{u}_f(t) \\ \dot{u}_g(t) \end{Bmatrix} + \tag{15}$$

$$\begin{bmatrix} K_{ss} & K_{sf} & 0 \\ K_{sf}^T & K_{ff} & K_{fg} \\ 0 & K_{fg}^T & [K_{gg}+\bar{K}_{gg}] \end{bmatrix} \begin{Bmatrix} u_s(t) \\ u_f(t) \\ u_g(t) \end{Bmatrix} = \begin{Bmatrix} 0 \\ 0 \\ \bar{K}_{gg}\bar{u}_g(t)+\bar{C}_{gg}\dot{\bar{u}}_g(t)+\bar{M}_{gg}\ddot{\bar{u}}_g(t) \end{Bmatrix}$$

in which

$$\bar{M}_{gg} = \begin{bmatrix} 0 & 0 \\ 0 & \bar{M}_{hh} \end{bmatrix}; \quad \bar{K}_{gg} = \begin{bmatrix} 0 & 0 \\ 0 & \bar{K}_{hh} \end{bmatrix}; \quad \bar{C}_{gg} = \begin{bmatrix} 0 & 0 \\ 0 & \bar{C}_{hh} \end{bmatrix} \tag{16}$$

showing that no frequency-dependent parameters remain in the equations of motion, thus allowing the standard time-domain solution procedure to be used for solving them. Usually, the terms $\bar{C}_{gg}\dot{\bar{u}}_g(t)$ and $\bar{M}_{gg}\ddot{\bar{u}}_g(t)$ on the right-hand side of Eq. (15) have small effects on the solution of this equation; however, the importance of their contributions should be checked. Having modified the third term on the left-hand side of Eq. (15) to its nonlinear hysteretic form, the complete set of coupled equations can be solved for displacements $u_s(t)$, $u_f(t)$, $u_g(t)$ using standard step-by-step numerical integration procedures.

SOLUTION PROCEDURES

One-Step Direct Approach

In this approach, the equations of motion are solved directly in their coupled form. If the system is treated as being fully linear (or equivalent linear), the solution can be carried out in the frequency domain using Eq. (8). In doing so, the complete set of complex algebraic equations are solved separately for discrete values of ω over the frequency range of interest yielding the corresponding sets of displacement vectors $u_s(i\omega)$, $u_f(i\omega)$, and $u_g(i\omega)$. Having obtained these vectors for the discrete values of ω, they are inverse Fourier transformed to the time domain giving vectors $u_s(t)$, $u_f(t)$, $u_g(t)$. The corresponding time histories of internal forces and/or deformations in the system can then be obtained directly using standard finite-element procedures.

If the structure-foundation subsystem is modelled as a nonlinear system, the solution can be carried out in the time domain using Eq. (15). In this case, the coupled nonlinear equations of motion are solved using standard step-by-step numerical integration procedures.

This one-step direct approach is simple and straight forward to implement for a structural system supported on a single foundation, such as a building. However, for a long multiple-span bridge supported on many independent foundations, a very large system of equations and an associated very large number of seismic free-field inputs in vector $\bar{u}_g(i\omega)$ result, making the solution computationally impractical, especially when large nonlinearities are present in the equations of motion. In this case, it is desirable to simplify the problem by finding separate solutions to a set of smaller problems and then combine the solutions in steps so as to achieve the desired end result. The multiple-step substructuring approach described subsequently is ideally suited for this purpose.

Multiple-Step Substructuring Approach

For long bridges supported on multiple foundations, the support-separation distances are sufficiently large so that each foundation subsystem can be treated as being independent of the others; therefore, the soil impedance matrix for each foundation will be uncoupled from those of the other foundations. In this case, to simplify the overall problem, each foundation subsystem can be analyzed separately to obtain a boundary impedance matrix called the "foundation impedance matrix" and a consistent boundary force vector called the "foundation driving-force vector", both of which are associated with the DOF at its structure/foundation interface. Having obtained the foundation impedance matrix and associated driving force vector for each foundation subsystem, all such matrices and vectors can be combined into the equations of motion for the total structure as a free-free system, resulting in $(s+f)$ DOF present in the structure-foundation subsystem rather than the $(s+f+g)$ DOF present in the complete soil-structure-foundation system. This reduced set of equations having $(s+f)$ DOF can be solved much more efficiently than solving the equations for the complete system having $(s+f+g)$ DOF as required by the one-step direct approach.

CAPACITY EVALUATIONS

The objective of the capacity evaluation is to determine the most probable levels of seismic resistance of the various elements, components, and subsystems of the bridge. The resistance capacities provided by this evaluation, along with the corresponding demands, provide the basis for judging seismic performance of the complete bridge system

during future earthquakes. In the domain of SFSI as discussed here, the capacity evaluation focuses on soil-foundation systems.

For a bridge subjected to static loadings, the soil-foundation capacities of interest are the load resistances and the associated foundation deflections and settlements. Their evaluation constitutes the bulk of the traditional foundation design problem. When the bridge is subjected to oscillatory dynamic loadings, including seismic, the static capacities mentioned above are, alone, insufficient in the process of judging soil-foundation performance. In this case, it is necessary to assess entire load-deflection relationships, including their cyclic energy dissipation characteristics, up to load and/or deformation limits approaching failure conditions in the soil-foundation system. Because of the complexity of this assessment, the capacity evaluation must be simplified in order to make it practical. This is usually done by treating each soil-foundation system independently and by subjecting it to simplified pseudo-static monotonic and/or cyclic deformation-controlled step-by-step patterns of loading, commonly referred to as the "push-over" analysis.

ACKNOWLEDGEMENT

For a more comprehensive treatment of soil-foundation-structure interaction, including example solutions, the reader is referred to Ref. 1 by W. S. Tseng and J. Penzien, upon which this condensed paper is based.

REFERENCES

1. Tseng, W. S. and Penzien, J., "Soil-Foundation-Structure Interaction," Chapt. 42 of "*Handbook of Bridge Engineering*," W. F. Chen and L. Duan, Editors, CRC Press LLC, Cat. No. 74-34.

2. Abrahamson, N. A., "Spatial Variation of Earthquake Ground Motion for Application to Soil-Structure Interaction," Report No. TR-100463, Electric Power Research Institute, March 1992.

3. Lilhanand, K. and Tseng, W. S., "Development and Application of Realistic Earthquake Time Histories Compatible with Multiple-Damping Design Response Spectra," *Proc. 9th World Conference of Earthquake Engineers*, Tokyo-Kyoto, Japan, August 2-9, 1988.

4. Kaul, M. K., "Spectrum-Consistent Time-History Generation", *J. of Eng. Mech. Div.*, ASCE, Vol. 104, No. EM4, 781, 1978.

5. Penzien, J. and Watabe, M., "Simulation of 3-Dimensional Earthquake Ground Motions", *J. of Earthquake Eng. & Str. Dyn.*, Vol. 3, No. 4, 1975.

6. Hao, H., Oliviera, C. S., and Penzien, J., "Multiple-Station Ground Motion Processing and Simulation Based on SMART-1 Array Data," *Nuc. Eng. and Des.*, Vol. III, No. 6, 2229-2244, 1989.

7. Silva, W. J. and Lee, K., "WES RASCAL Code for Synthesizing Earthquake Ground Motions," State-of-the-Art for Assessing Earthquake Hazards in United States, Report 24, Army Engineers Waterway Experimental Station, Miscellaneous Paper 5-73-1, 1987.

8. Bolt, B. A. and Gregor, N. J., "Synthesized Strong Ground Motions for the Seismic Condition Assessment of Eastern Portion of the San Francisco Bay Bridge", Report No. EERC 93-12, Earthquake Engineering Research Center, University of California, Berkeley, 1993.

9. Chang, C. Y., Power, M. S., Idriss, I. M., Sommerville, P. G., Silva, W. and Chen, P. C., "Engineering Characterization of Ground Motion, Task II; Observation Data on Spatial Variations of Earthquake ground Motion", NUREG/CR-3805, Vol. 3, U.S. Nuclear Regulatory Commission, Washington, D.C., 1986.

10. Tseng, W. S., Lilhanand, K., and Yang, M. S., "Generation of Multiple-Station Response-Spectra-and-Coherency-Compatible Earthquake Ground Motions for Engineering Applications", *Proc. 12th Int. Conference on Struct. Mech. in Reactor Technology*, Paper No. K01/3, Stuttgard, Germany, August 15-20, 1993.

11. Schnabel, P. B., Lysmer, J., and Seed, H. B., "SHAKE - A Computer Program for Earthquake Response Analysis of Horizontally Layered Sites," Report No. EERC 72-12, Earthquake Engineering Research Center, University of California, Berkeley, 1972.

12. Idriss, I. M. and Sun, J. I., "User's Manual for SHAKE 91," Center for Geotechnical Modeling, University of California, Davis, 1992.

13. Vucetic, M. and Dobry, R., "Effects of Soil Plasticity on Cyclic Response", *J. of Geotech. Eng.*, ASCE, Vol. 117, No. 1, 89-107, 1991.

14. Sun, J. I., Golesorkhi, R., and Seed, H. B., "Dynamic Moduli and Damping Ratios for Cohesive Soils", Report No. UBC/EERC-88/15, Earthquake Engineer Research Center, University of California, Berkeley, 1988.

15. Apsel, R. J., "Dynamic Green's Function for Layered Media and Applications to Boundary Value Problems", Ph.D. Thesis, University of California, San Diego, 1979

16. Lysmer, J., Tabatabaie-Raissai, M., Tajirian, F., Vahdani, S., Ostadan, F., "SASSI-A System for Analysis of Soil-Structure Interaction", Report No. UCB/GT/81-02, Department of Civil Engineering, University of California, Berkeley, 1981.

17. Clough R. W. and Penzien, J., "*Dynamics of Structures*," Second Edition, McGraw-Hill, Inc. 1993.

ANALYTICAL AND EXPERIMENTAL STUDIES ON THE EFFECT OF SOIL-STRUCTURE INTERACTION ON DAMPING, NATURAL FREQUENCY AND EFFECTIVE INPUT MOTION OF BUILDINGS

Nobuo Fukuwa[1], M. Ali Ghannad[2], Jun Tobita[3] and Riei Nishizaka[4]

ABSTRACT: The effect of Soil-Structure Interaction on the dynamic response of buildings is studied through analytical and experimental approaches. As the analytical approach, simplified models with different levels of simplicity are employed in order to study the SSI effect on the natural period and damping of buildings. Parametric studies are conducted for the cases of structures located on the surface of either a homogeneous half-space or a layered half-space soil medium. The results are then compared with current seismic code provisions. The general trends learnt from the analytical study are compared with experimental results on real buildings through both microtremor measurements and seismic observations.

1. INTRODUCTION

It has been known for many years that the flexibility of soil under structures affects the structural response to dynamic loads. The effect of Soil-Structure Interaction (SSI), thus, has been considered in the design of massive and critical facilities such as nuclear power plants. However, the SSI effect on dynamic behavior of ordinary building type structures has not attracted much attention. Also, the experimental studies on dynamic behavior of such buildings are rare in contrast to the large number of such studies on high-rise buildings and nuclear facilities. This may be due to the fact that the experimental evaluation of dynamic characteristics of short and squatty buildings can be quite difficult. Additionally, the final results can be subjective and may render different values, depending on the techniques used and the personal judgement applied.

The most significant event intervention in this regard has been the 1978 inclusion of SSI in the tentative provisions ofATC3-06 in the United States (ATC 1978). The seismic codes of other countries including Japan, however, continue to have no provisions addressing SSI (Earthquake Resistant Regulations 1988). In fact, it seems that even in the United States the beneficial use of SSI have not been sufficiently exploited. Also, the regulations have remained unchanged since their first appearance in 1978 (NEHRP 1994). On the other hand, studies have indicated that the level of damages caused by recent earthquakes, particularly in case of short and stiff buildings, has been predominantly related to the effects of SSI (Celebi 1997; Hayashi et al. 1998; Wallace and Moehle 1990; Yasui and Tokimatsu 1998). Hence, there is much opportunity in further analytical and experimental studies on this matter.

The key factors in the seismic design of buildings are the natural period, damping ratio and the effective input motion and all of which are affected by SSI phenomenon. Therefore, it is necessary to examine the variation of these factors due to the change in the soil and the structure's physical characteristics. However, it is impossible to develop an exact deterministic solution for the soil-structure system due to the complexity of soil material properties, involved geometry of building foundation and the complicated nature of earthquake ground motions. Thus, for the sake of simplification, it is necessary to make numerous assumptions so that the problem at hand is amenable to solution; and it is the art of engineering to make models as simple as possible. To this end, it is necessary to confirm the achieved analytical results through comparison with the results of experimental studies. In this paper, simplified models for the soil-structure system, with different levels of simplicity, are employed in order to study the SSI effect on the natural period and damping of buildings. Parametric studies are conducted for the cases of structures located on the surface of either a homogeneous half-space or a layered half-space soil medium. The general trends learnt from the analytical study are then compared with experimental results on real buildings through both microtremor measurements and seismic observations.

2. ANALYTICAL STUDY

2.1 ANALYSIS MODEL

Figure 1 shows the conventional soil-structure model where the structure is simply modeled as a shear building model with lumped mass and mass moment of inertia in each story and the soil is replaced by the sway and rocking springs and dashpots, i.e., k_s, k_r, c_s and c_r. Here, as a further simplification, the same mass, m, mass moment of inertia, j, height, h, and stiffness, k, are considered for all stories and it is believed that such a simple structure model is quite adequate for the purpose of this study. The other substructure, the unbounded soil, however, should be treated more carefully. The soil model should consider the unboundedness of the soil and should satisfy the radiation condition in the soil. It also must be simple enough to allow the required parametric studies to be carried. In this regard, the concept of cone models based on one-dimensional wave propagation theory is used. The cone models, in spite of their simplicity, are able to capture most of the basic and important

1, Prof., Center for Cooperative Research in Advanced Science & Technology, Nagoya University, Japan, Dr. Eng.
2, Former Graduate Student at Nagoya University, Japan, Dr. Eng.
3, Assoc. Prof., School of Engineering, Nagoya University, Japan, Dr. Eng.
4, Research Associate, Graduate School of Engineering, Nagoya University, Japan, Dr. Eng.

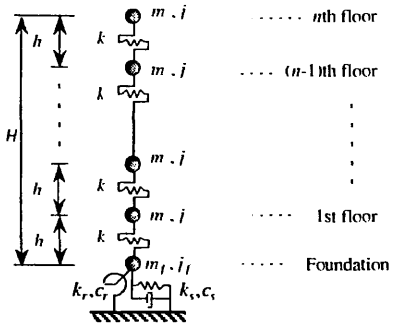

FIG. 1. The soil-structure model

concepts of more rigorous solutions (Wolf 1994).

2.2 TRANSFER MATRIX METHOD

The simplified structural model of Fig.1 may be considered as a periodic structure with slight modifications. Thus, the transfer function for the structure itself may be calculated by transfer matrix method which is a powerful method for dealing with periodic structures. The transfer function for the soil-structure system can then be constructed readily by introducing the effect of soil related degrees of freedom. It can be shown that the transfer function for the jth storey of the sway-permitted model will be as follows (Fukuwa et al. 1995)

$$U_j = \frac{\kappa_s^* \cos\frac{(2n-2j+1)}{2}\psi}{(\kappa_s^*-1)\cos\frac{(2n+1)\psi}{2}+\cos\frac{(2n+3)\psi}{2}} \qquad (1)$$

where

$$\kappa_s^* = \frac{k_s + i\omega c_s}{k^*} \;,\; k^* = k(1+2\xi_{str.}\,i) \;,\; \psi = \mathrm{Cos}^{-1}\left[1-\frac{\varpi^2}{2k^*/m}\right] \qquad (2)$$

and n is the number of stories and $i=\sqrt{-1}$. Also, ϖ and $\xi_{str.}$ are the circular frequency of excitation and the hysteretic damping ratio in the structure, respectively.

2.3 COFACTOR EXPANSION METHOD

It is well-known that standard eigenvalue analysis methods are not applicable to soil-structure systems due to nonproportionality of the damping matrix. Although there are well-established techniques for handling even nonclassical damped systems, they are not applicable when the frequency dependency of soil stiffness is also considered. Also, the application of such techniques is limited to cases with real stiffness matrices where the use of complex damping for modeling the material damping in the soil or structure is not applicable (Hurty and Rubinstein 1964). That's while the results of experimental studies on structures show more compatibility with the concept of complex damping model (hysteretic damping) than the commonly used viscous form of damping. The hysteretic damping model has also been proposed as the best possibility for modeling the material damping in the soil (Kausel and Roesset 1974). As an alternative method capable to deal with above mentioned problems, explicit presentation of the determinant of the system's stiffness matrix is introduced here. The uniform distribution of mass and stiffness in the structural model allows the determinant of its stiffness matrix in the fixed-base state can be presented explicitly by polynomials through direct cofactor expansion method (Fukuwa and Ghannad 1996). Having the determinant of the stiffness matrix for the fixed base structure, the related expression for the case of the structure located on the sway and rocking springs and dashpots can be expressed by polynomials readily. The complex eigenvalues of the soil-structure model can then be calculated by solving the respective polynomials. The equations, however, would be nonlinear due to the frequency dependency of the soil representative springs and dashpots' coefficients. Special techniques such as searching in the complex plane thus should be employed in this regard. Once having the eigenvalues of the system, the damped natural frequencies, ω_j, and the modal damping ratios, ξ, can be calculated. The detailed discussion on the method as well as related formulations can be found in (Fukuwa et al. 1995).

2.4 APPROXIMATION THROUGH A SIMPLIFIED 3DOF MODEL

Figure 2 shows the simplified 3-degree of freedom (3DOF) model where the superstructure -building- is replaced by its modal effective mass, $m_{str.}$, and modal effective stiffness, $k_{str.}$, providing the same modal frequency as the original multi degree of freedom (MDOF) model of Fig.1. Also, $\hat{H}$ represents the modified effective height of the structure defined as follows

$$\hat{H} = \mu_H \cdot \overline{H} \qquad (3a)$$

where

$$\mu_H = \sqrt{1+\frac{1}{4\left(\overline{H}/r\right)^2}} \qquad (3b)$$

and $\overline{H}$ is the effective height of the structure. Also, r is the radius of the (equivalent) circular foundation. It is shown that μ_H introduces the effect of floor's mass moment of inertia, j, into the model implicitly (Ghannad 1998). The effect may be considerable for the case of short and squatty buildings. The foundation is replaced by mass m_f and the soil is replaced by complex sway and rocking springs, K_s and K_r. The dynamic properties of the system are then evaluated through parametric eigenvalue analysis. It can be shown that the first complex eigenfrequency of the system will be (Ghannad et al. 1998)

$$\omega = \omega_{fix}\sqrt{\frac{2\gamma}{\zeta+\sqrt{\zeta^2-4\alpha\beta\gamma(1+\gamma)}}} \qquad (4)$$

where ω_{fix} is the natural circular frequency of the structure in the

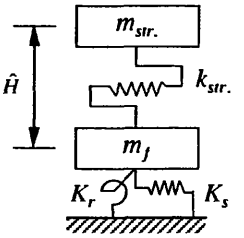

FIG. 2. The simplified 3DOF model

fixed-base state. Also,

$$\alpha = \frac{m_f}{m_{str.}} \quad , \quad \beta = \frac{k_{str.}}{K_s} \quad , \quad \gamma = \frac{K_r}{k_{str.} \cdot \bar{H}^2} \qquad (5a)$$

$$\zeta = 1 + \gamma + \beta\gamma + \alpha\beta\gamma \qquad (5b)$$

The material damping in the soil and structure may also be included in the formulations as the hysteretic form of damping by using the correspondence principle. Using compatible values for the effective mass, effective stiffness and effective height of building with those of MDOF model, the results would be in full agreement for the two models (Ghannad et al. 1998). The 3DOF model, however, needs much less effort to be solved.

2.5 TRANSFER FUNCTIONS

In order to clarify the importance of damping model in SSI studies, the transfer function of soil-structure systems with different damping models are compared to each other As a representative example, an ordinary reinforced concrete building with different number of stories located on a square 35x35 meters foundation is studied. The shear wave velocity in soil under the foundations considered to be V_s=200m/s. As the damping mechanism in the soil-structure system, three different models are examined as follows: (1) Only material damping in the soil and structure, modeled as 1% complex damping (hysteretic damping), (2) Complex material damping in the soil and structure (1%) and radiation damping in the soil based on the concept of cone models and (3) Stiffness proportional damping as the material damping in the soil and structure (1% at the first mode of vibration) and radiation damping in the soil based on the concept of cone models. The first damping model leads to a proportional damping matrix for the system, which can be diagonalized by the same transformation that uncouples the undamped system, whereas the two other models result to nonproportional damping matrices. Transfer functions for the three mentioned cases are drawn in Fig.3 in comparison to those of the fixed-base structure model. The transfer functions are computed based on the response of the top story in comparison to the soil surface. The results are shown for three different building models with different number of stories. As shown, the effect of SSI on the eigenfrequencies of the system (the frequencies related to peak values) is overestimated for the first model with proportional damping matrix. The same conclusion is applicable to any other damping model which leads to real eigenvalues (Ghannad 1998). Additionally, the peak values related to the second and higher modes are obviously underestimated for the case of stiffness proportional damping model. It is because the stiffness proportional damping model leads to high damping ratios for higher modes of vibration which are in fact much larger than the actual damping in the system. These effects are seen more clearly for short and moderate height buildings.

From another point of view, Fig.4 shows the response of model (2) at different story levels. The results are shown for the first, the last and the middle story of three different building models with different number of stories. The results show a clear phase difference in the vibration of different parts of the structure for all three cases. In the other words, the mode shapes would be complex, whose elements differing in phase as well as in amplitude. This means that models which lead to real eigenvalue analysis and real mode shapes, such as those with proportional damping models, can not be a suitable choice.

2.6. STRUCTURES ON THE SURFACE OF A HOMOGENEOUS HALF-SPACE

The effect of SSI on the natural frequencies and the damping ratios of buildings located on the surface of a homogeneous half-space soil medium is studied in this section through the

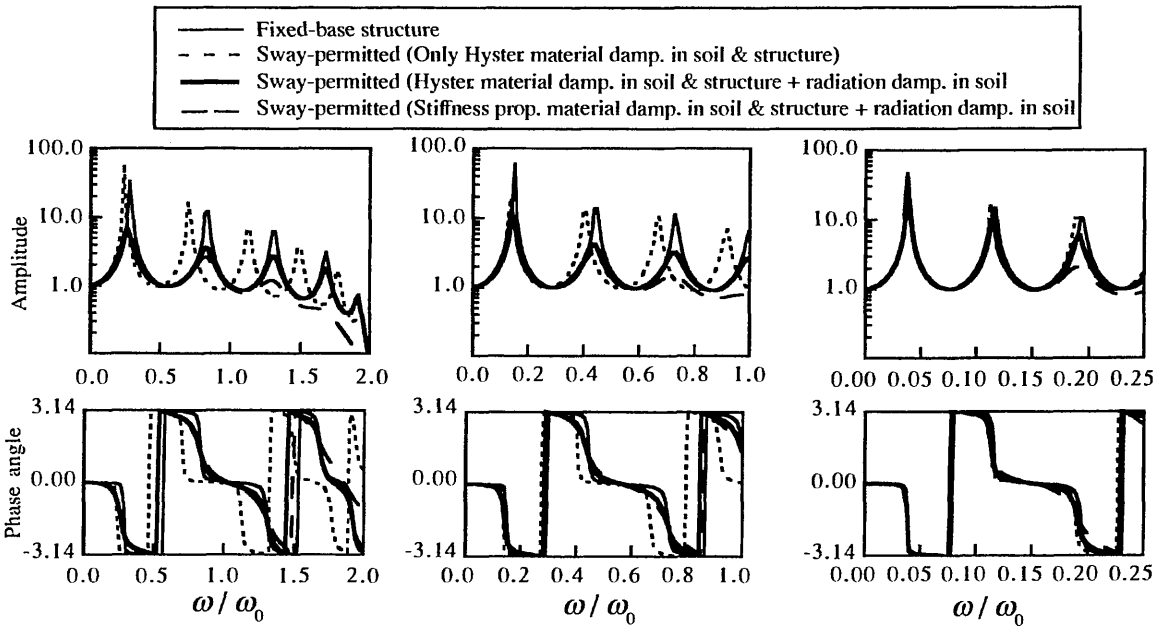

FIG. 3. Transfer functions for systems with different damping models

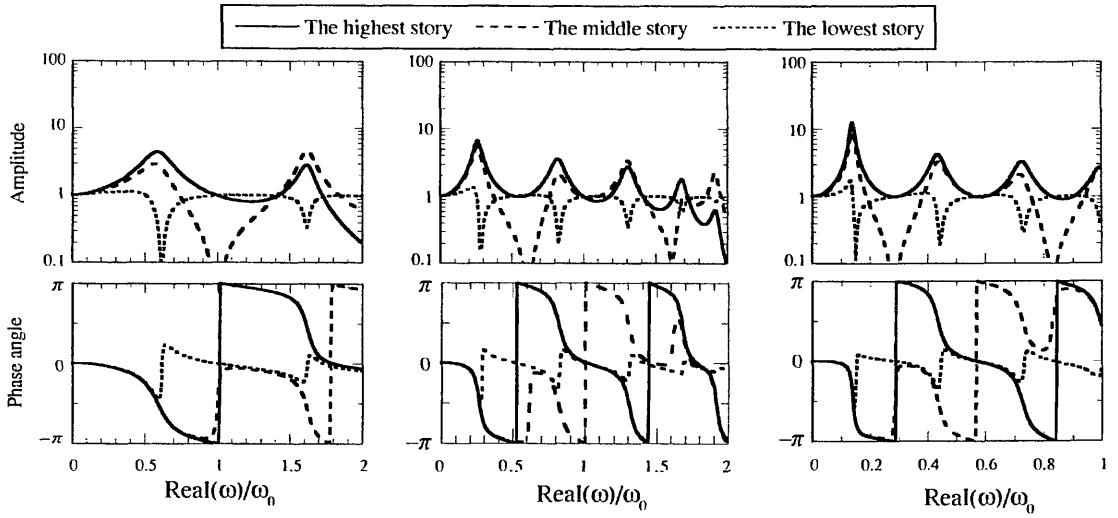

(a) 2-story building (b) 5-story building (c) 10-story building

FIG. 4. Transfer functions for different parts of the building (Sway-permitted model)

application of cofactor expansion method. The effective aspect ratio of the building, $\overline{H}/r$, and the dimensionless frequency

$$(a_0)_{fix} = \frac{r \cdot \omega_{fix}}{V_s} \qquad (6)$$

are considered as the key parameters whereas the other soil and structure parameters are set to some typical values. In (6), ω_{fix} is the circular frequency of the fixed-base building model and V_s is the shear wave velocity in soil. Figure 5 shows the results of parametric studies where a damping ratio ξ_{soil}=3% is assigned to the material damping for low strain levels in the soil (Kokusho 1980; AIJ 1996). No material damping, however, is addressed for the structure. The results apparently show more dramatic interaction effect for higher values of $(a_0)_{fix}$ in all cases as would be expected. Consequently, drastic change in the first natural period, and also very high damping ratios are seen for stiff structures located on soft soils. It should be mentioned that the practical range of interest for $(a_0)_{fix}$ is different for buildings with different aspect ratios. For example, $(a_0)_{fix}$ would hardly exceed 0.5 for ordinary buildings with $\overline{H}/r = 5$. The limit value may be considered about 1.5 and 2.0 for buildings with the effective aspect ratios 2 and 1.5, respectively. The results also point to severe effect on the natural period of slender buildings due to rocking effect. However, the SSI effect on the damping ratios are more important for squatty buildings. The results of Fig. 5 are independent of the number of stories and also are in full agreement with the results of 3DOF model. The results of Fig.5 may be presented in a new fashion as the variation the system's damping ratio with the change in the natural period of the

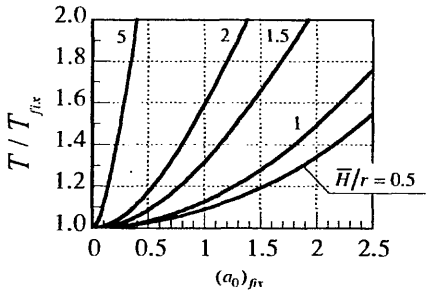

(a) The first natural period

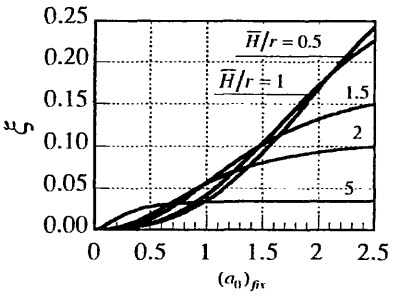

(b) The soil induced damping ratio (ξ_{soil}=0.03)

FIG. 5. The effect of soil on the dynamic properties of system

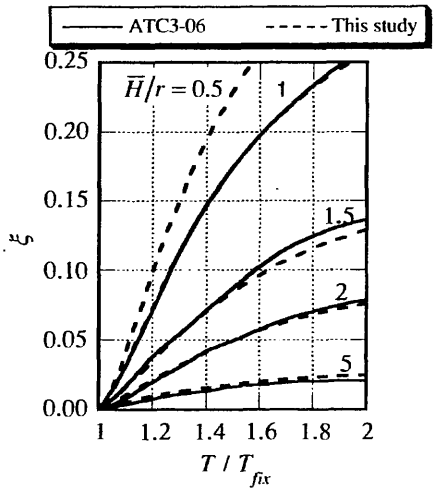

FIG. 6. Damping ratio as a function of the change in the natural period of the building.

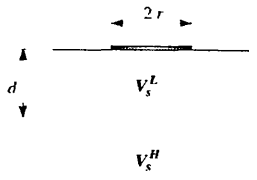

FIG. 7. The layered half-space soil model

building. This format is generally more desirable in practical structural design. Figure 6 shows the results in this new format in comparison to the ATC3-06 regulations. As shown, the results of this study are in a good agreement with the graphs suggested by ATC3-06. It is also shown that the results of the two studies are in a good agreement even for higher levels of strain in soil (Ghannad 1998). Although no material damping is addressed for the structure in this study, it should be kept in mind that the internal damping of structures is also subject to change due to SSI (Novak 1975). The change in the structural damping has been approximated by some researchers as follows (Veletsos 1977; AIJ 1996)

$$\bar{\xi}_{str.} = \xi_{str.}\left(\frac{T_{fix}}{T}\right)^3 \qquad (7)$$

in which $\xi_{str.}$ and $\bar{\xi}_{str.}$ are the internal damping ratio of the structure in the fixed-base state and when located on flexible soil, respectively. The same approximation has been also used by ATC3-06. Equation (7) is valid for systems with viscous type of material damping in the structure. The assumption of hysteretic type of damping for the structure, as adopted here, however, leads to an exponent 2 (instead of 3) in the right-hand side of (7) (Wolf 1985; Ghannad et al. 1998).

2.7 STRUCTURE ON THE SURFACE OF A LAYERED HALF-SPACE SOIL MEDIUM

Figure 7 shows the layered half-space soil model which consists of a soil layer located on surface of a homogeneous soil half-space. The mass density and Poisson's ratio are considered to be the same for the materials of the two media. However, the shear wave velocity is different for them. As the stiffness of underlain half-space increases, the reflection of waves at the interface of two media results to lower damping for the soil-structure system. Additionally, for the limit state of a soil layer on rigid rock a cutoff frequency equal to the fundamental natural frequency of the layer exists below which no radiation occurs. Using the latter concept, the ratio of the fundamental period of layer, T_{layer}, to that of the soil-structure system, T, is introduced as *radiation index*, I_r, for verification of existence or absence of radiation in soil.

$$I_r = \frac{T_{layer}}{T} = \frac{4d}{V_s^L T} \qquad (8)$$

The same concept has been used by ATC3-06 regarding buildings located on a stratum of a soft soil underlain by a much stiffer soil. According to ATC3-06, the soil induced damping ratios related to the half-space case shall be scaled down by the factor of square value of radiation index, i.e., I_r^2. Equation (8) may be rewritten in the following format.

$$I_r = \frac{T_{layer}}{T} = \frac{2}{\pi} \cdot \frac{(a_0)_{fix}}{T/T_{fix}} \cdot \frac{d}{r} \qquad (9)$$

This thus allows to study the variation of radiation index as a function of $(a_0)_{fix}$ for any specific soil-structure system. Figure 8 shows the results of such studies for different cases. The graphs have been drawn for a range of $(a_0)_{fix}$ which is practically important for buildings with each specific aspect ratio. As shown, the radiation index for slender buildings ($\bar{H}/r = 5$) would be much less than 1.0 even for sites with deep layers. Therefore, for different sites with different depths of the layer, slender system would be in "no radiation" zone and consequently, depth of the layer doesn't play any important role. On the other hand, for the case of squat buildings, the radiation index may be below or above the radiation limit depending on depth of the layer. Consequently, the *depth index*, d/r, would be an important factor for the case of buildings with moderate or low aspect ratios. Another factor which plays an important role in the level of soil induced damping ratio is the difference between the stiffness of the layer's material and that of the underlain half-space, i.e., the *stiffness contrast index* which has not been addressed by ATC3-06. As a result, different systems with the same radiation index may have quite different levels of damping ratio due to difference in the stiffness contrast index. Consequently, the radiation index

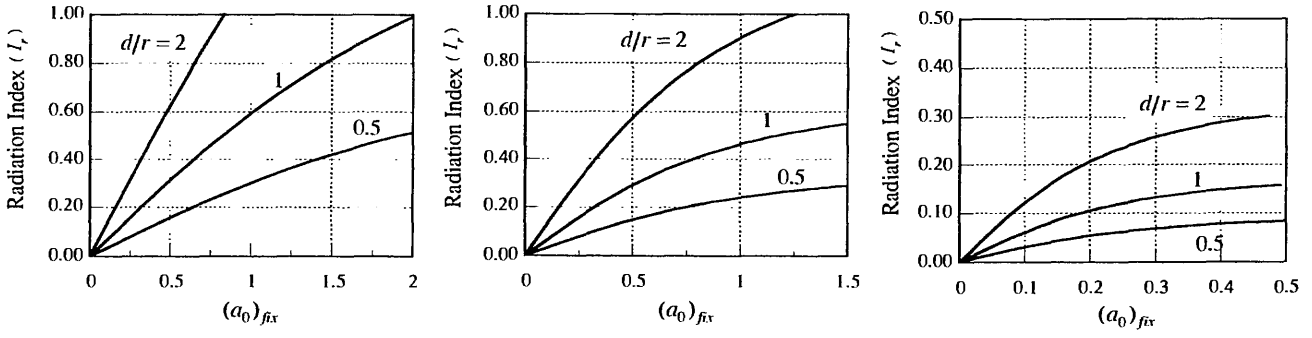

FIG. 8. Variation of radiation index, I_r ($V_s^H/V_s^L = 2$)

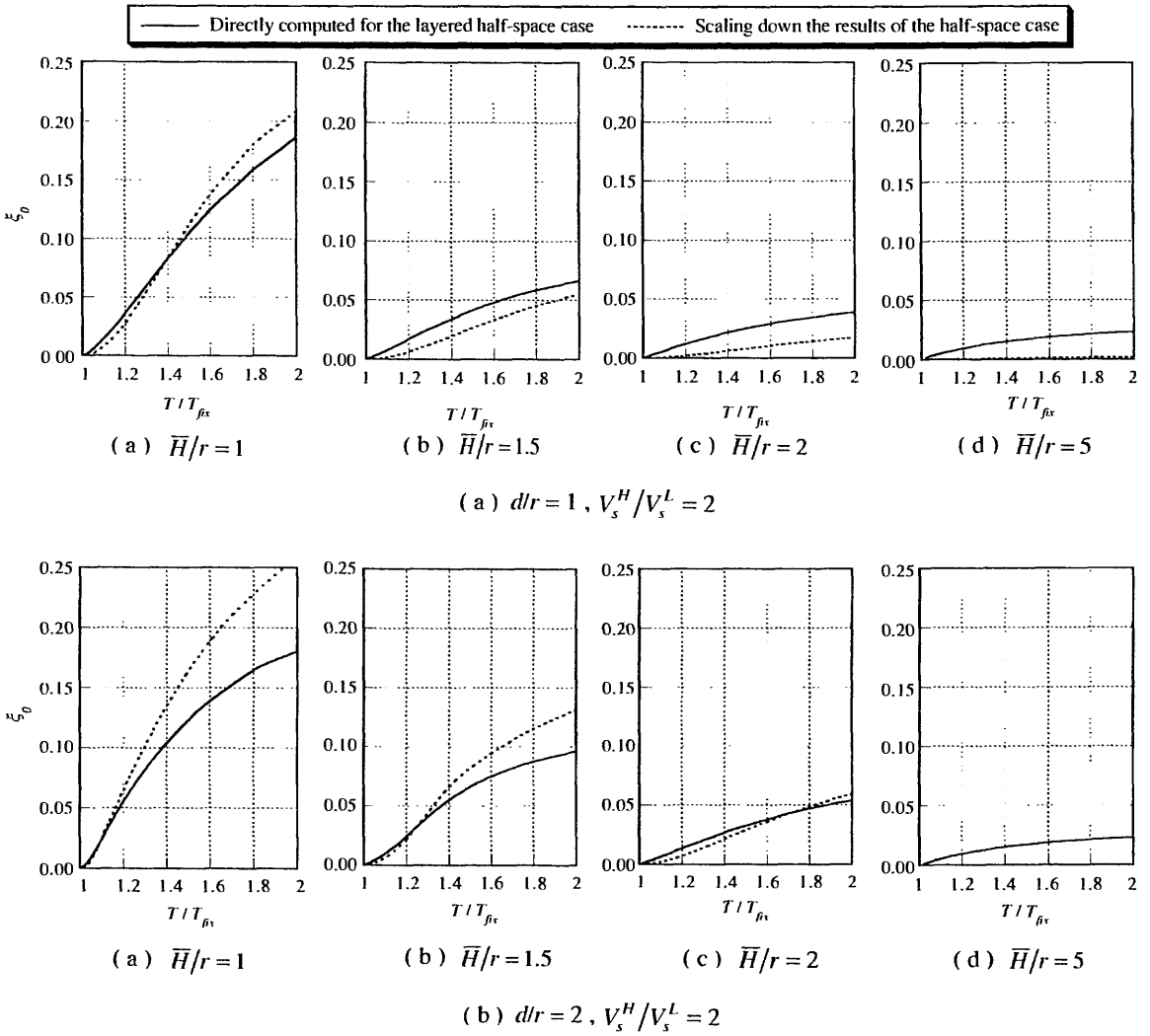

FIG. 9. Verification of ATC3-06 suggested approach for calculation of soil induced damping ratio in the layered half-space case

alone can not be used as a suitable criteria for estimation of damping capacity in soil. On the other hand, considering the effect of stiffness contrast index does complicate the method and makes it far from a code suited approach. So, for the sake of simplicity it may be desirable to set the stiffness contrast index to a practically conservative value, say $V_s^H/V_s^L=4$, compatible with the qualitative description of layered half-space sites by ATC3-06. However, even doing so, it is necessary that the effect of the two other key factors, the depth index and the effective aspect ratio of the building, be included in the construction of the scaling factor more explicitly. Figure 9 shows the resulted soil induced damping ratios for different circumstances. In each figure, the obtained values for damping ratio of the system by scaling down the half-space case results are compared with those directly achieved through the complex eigenvalue analysis. The results are related to a typical stiffness contrast index $V_s^H/V_s^L=2$. According to results, damping ratios obtained by application of ATC3-06 recommendation tend to become overestimated by increase in depth index value and by decrease in the effective aspect ratio of the structure. This is mainly because ATC3-06 doesn't consider any reduction in the damping of systems with natural frequencies above the cutoff frequency limit. On the other hand, the results for very slender structures, such as those with $\overline{H}/r=5$, would be underestimated in all cases (almost no damping). Although this conservatism involved inATC3-06 for tall buildings is partly compensated by the requirement that system's damping ratio, with or without considering the SSI effect, be no less than 5%, there is no justification for overestimation of damping ratios for short and moderate height buildings which is not in the safe side!

3. EXPERIMENTAL STUDIES BASED ON MICROTREMOR MEASUREMENTS

Ambient vibration measurements have always been a fast and efficient way of determining the dynamic properties of existing buildings. Recently, even more reliable results have been achieved through the use of high precision measurement devices, more accurate techniques and high speed computers. Here, also, the method is employed to study the effect of the size of buildings and the flexibility of the underlain soil on the dynamic characteristics of soil-structure systems.

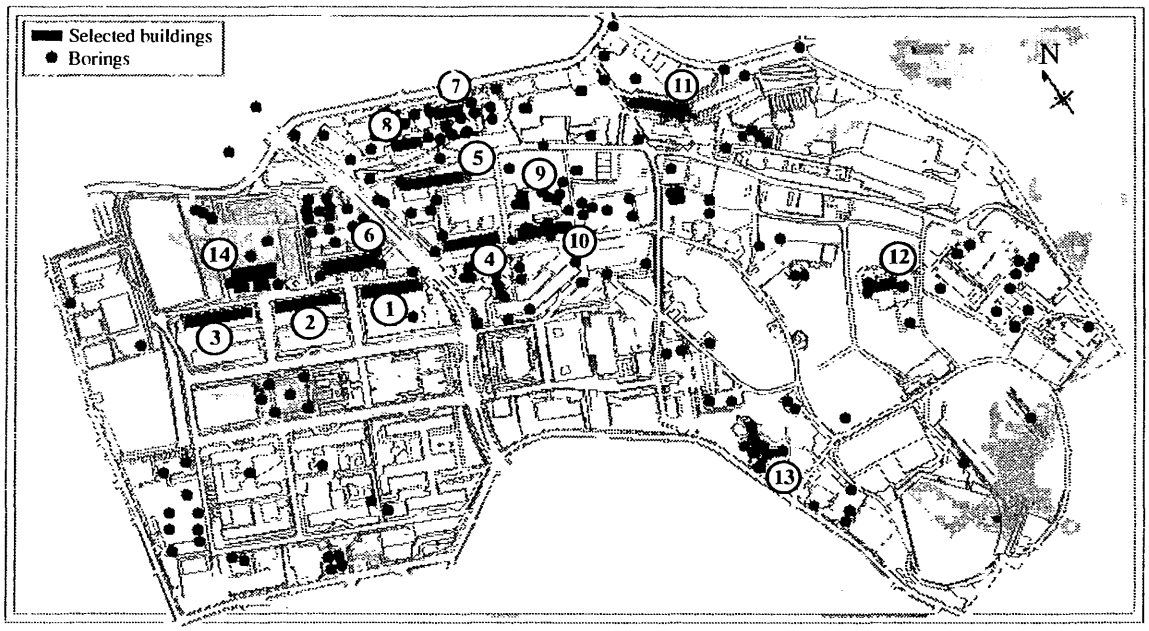

FIG.10. The location of selected buildings in the campus

TABLE 1. The selected buildings' information

No.	Building	Ref. name	No. of Stories	Height (m)	Struc. System	Pile length (m)	Embe-dment (m)	Construc. Year	Average N-value
1	Faculty of Eng. No.1	Eng1	3+1	15.3	RC	-	1.2	1951-70	14.6
2	Faculty of Eng. No.2	Eng2	3+1	15	RC	-	1.1	1954-65	10.8
3	Faculty of Eng. No.3	Eng3	4	15.8	RC	5 - 16	1.5	1962-70	12.5
4	Faculty of Eng. No.4	Eng4	4	14.75	RC	6	1.25	1964-70	17.2
5	Faculty of Eng. No.5	Eng5	6	22.17	RC	5 - 33	1.7	1967-69	14.4
6	Faculty of Eng. No.7	Eng7	4	15.2	RC	20	1.2	1971-89	16
7	Faculty of Eng. No.8	Eng8	4	16	RC	9 - 10	2.8	1987	28.9
8	Faculty of Eng. No.9	Eng9	6	22.2	RC	12	2.3	1982-93	22.9
9	Faculty of Science_A2	Sc.A2	5	18.1	RC	9	1.5	1979	17.2
10	Faculty of Science_E	Sc.E	5+1	19.7	RC	8	1.7	1967-85	21.6
11	Faculty of Agriculture	Agr.	6	21	RC	-	2	1966	23.1
12	Inst. for Hydrospher.	Hyd.	5	18.8	RC	9	1.6	1971	30.2
13	International Residence	Res.	8	33.2	RC	15	2	1981-88	27.8
14	Faculty of Eng. No.1(new)	Eng1_N	10	39.3	SRC	45	8.05	1995	11.6

3.1 BUILDINGS IN NAGOYA UNIVERSITY

3.1.1 OUTLINE OF BUILDINGS AND SOIL CONDITIONS

Microtremor tests were conducted on fourteen buildings in the Higashiyama campus of Nagoya University. It should be mentioned that because of heavy earthworks during the years, the topography of the campus has been drastically changed from the original situation. Therefore, the different parts of the campus have different soil conditions. On the other hand, most of the selected buildings have almost a typical plan of educational type buildings, i.e. a slender rectangular with almost the same width. So, the effect of soil condition on the eigenproperties of buildings can be studied well. Figure 10 shows the Higashiyama campus and the location of the selected buildings. The numbers on the figure refer to the order number of buildings in the first column of Table 1 where the information of the selected buildings have been summarized. The change of topography of the campus due to heavy earthworks from 1936 to 1991 is shown in the background where darker shades indicate an increase in filling depth. Although only the groundfilled parts are shown in the figure, it is interesting to say that the difference between the level of the excavated and filled areas reaches up to 50 meters in some parts. Generally speaking, the northwestern and northeastern parts of the campus are the earthfilled areas and consequently have looser soil. The other areas, especially the central part of the campus have been mainly excavated and better soil condition is expected in these areas. The buildings were selected among the existing RC buildings considering some parameters which are of interest, e.g. the number of stories, plan's shape and size, soil condition and also the availability of boring data. It should be mentioned that totally, there are 202 boring data available in the campus which are mainly related to the northern and central parts of the campus as it can be seen in Fig.10.

3.1.2 MEASUREMENTS AND ANALYSIS METHODS

The microtremor measurements were performed for NS and EW directions which are related to the transverse and longitudinal dimensions of buildings, respectively. The responses were

measured at the first floor and top of the buildings as well as on the ground surface. The measurements on the ground surface were done at a distance from the building which are not affected by the building's vibration. In the case of the Eng1_N building, the test was repeated for different stages of construction, i.e. after completion of each story.

The moving coil type seismometers with natural period of 1.0 second were used to measure the responses simultaneously at the above mentioned locations and the velocity was measured in all cases. The signals, after amplification and low pass filtering (f_c =30 Hz) are digitized at the rate of 100 samples per second. In all cases, the measurements were conducted three times in ten-minute intervals, providing the total length of 30 minutes. The Fast Fourier Transform was computed for every 2048 points leading to a total of 87 specimens which were used for ensemble averaging.

For the parameter estimation methods, two techniques are used: 1, Transfer function fitting method and 2, Random Decrement (RD) method. In the former method, the dynamic properties of the building are estimated by finding a known system whose transfer function can be matched well with the observed one (Tobita 1996) whereas the latter technique is based on the extraction of the free vibration motion from the recorded data by superimposing a sequence of intervals with the same phase (Jeary 1986; Tamura et al. 1996).

3.1.3 RESULTS AND DISCUSSION

The estimated values for the period and damping ratios in the NS direction of the examined buildings have been summarized in Table 2. Three sets of results presented for each building are related to the following cases respectively: 1) Using the transfer function fitting method by considering the responses at the ground as the input for calculating the observed transfer functions, 2) The same as case #1 but using the responses of the first floor as input, 3) Using the RD method. It is believed that the results of the second case can be considered as a quasi-fixed base model because the sway effect is not included. Although the results are not generally compatible with this quasi-fixed base idea, there are some cases where this idea works well. For example, the effect of SSI can be studied well in the well-performed case of Eng1_N building by comparing the 6th and 10th columns of Table 2. The higher effect for the lower number of stories can also be seen clearly. Also, the results show higher damping ratios for the longitudinal direction (EW) which is compatible with the results of the analytical study.

The results using the RD method are drawn in Fig.11 for both of NS and EW directions. The figure represents a general tendency of lower damping ratios for taller buildings which may be interpreted as the effect of SSI. Although the site's soil condition is not the same for all buildings, generally one may conclude that the SSI effect is higher for shorter buildings. More specifically, the results of the Eng1_N building, which are related to the different number of stories but the same soil condition, clearly lead to the same conclusion. From another point of view the results show higher dispersion in the left hand side of the graph, i.e., for shorter buildings. This can be partly explained by SSI effect. For evaluation of the effect of soil condition on the dynamic properties of the building, the natural periods and damping ratios are plotted versus the average N-value of the soil over the first 10 meters from the ground surface. Since the height of the building affects the severity of SSI effect, the buildings are divided into two categories according to their height: 1) Short buildings including 3 and 4-story buildings and 2) Moderate height buildings including 5 and 6-story buildings. The results of the transfer function fitting method for the second category are shown in Fig.12. Although the number of data is not so large, a general trend of lower damping ratios and shorter periods for buildings located on stiffer soils can be observed. However, the results for the shorter buildings (the first category) dont show any clear trend and thus are not presented here. More detailed discussion can be found in (Ghannad et al. 1997a, 1997b).

3.2 LOW-RISE R.C. SCHOOL BUILDINGS IN NAGOYA CITY

3.2.1 OUTLINE OF BUILDINGS AND SOIL CONDITIONS

Totally sixty seven 3-story elementary school buildings were examined in Nagoya city (Yagi et al. 1998). All the buildings have almost a typical plan of educational buildings, i.e., a slender rectangular with the same width. The structural system is also the same for all buildings which is consisted of 2-span reinforced concrete frames with shear walls and multi-span frames with few walls in the transverse and longitudinal directions, respectively. However, the foundation type and soil condition are different for them. Figure 13 shows the location of the buildings in Nagoya city. As shown, almost half of buildings are located on alluvium deposits. Also, almost half of them have pile foundations.

3.2.2 MEASUREMENTS AND ANALYSIS METHODS

Almost the same devices and methodology as described in Sec. 3.1.2 are also used here. However, for the parameter estimation, only the transfer function fitting method is used. As mentioned before, the evaluation of dynamic characteristics of low-rise buildings would be difficult through conduction of microtremor tests. It is because a well-shaped transfer function can not be achieved except under very well-controlled conditions due to the low amplitude of vibrations and due to the remarkable effect of soil under buildings. Figure 14 and 15 show the results of two cases which have been selected as the representatives for well and poor estimations. Using the same classification for all cases, Fig.16 shows the statistical results based on the soil type, the type of foundation and the examined direction of buildings. Generally speaking, better performance is seen for the cases of spread foundations on stiffer soils. On the other hand, comparison of the Fourier amplitudes at the three mentioned levels in Fig.14 reveals that the effect of SSI is much lower for the well-performed case of Building Y. Thus, the effect of SSI may be considered as one of the parameters responsible for the distortion of transfer functions.

3.2.3 RESULTS AND DISCUSSIONS

Using the idea of quasi-fixed base model introduced in Sec.3.1.3, the results for the frequency of the superstructure are drawn versus the frequency of the soil-structure system in Fig.17. Only the results of well-performed cases are shown. The results

TABLE 2. The estimated parameters for NS direction

Ref. name	Average rms (m.kine)		Transfer Function Fitting Method								RD Method	
			Top / 1st floor				Top / Ground					
	@ ground	@ top	freq (Hz)	ξ	ξ/β	Error	freq (Hz)	ξ	ξ/β	Error	freq (Hz)	ξ
Eng1	0.213	0.397	5.13	0.134	0.102	1.82%	4.82	0.146	0.081	2.57%	5.08	0.117
Eng2	0.170	0.244	5.82	0.137	0.094	0.67%	5.51	0.134	0.093	0.86%	5.47	0.128
Eng3	0.098	0.196	-	-	-	-	5.25	0.310	0.142	2.29%	5.08	0.137
Eng4	0.380	0.486	6.93	0.243	0.113	3.42%	6.34	0.113	0.115	1.02%	6.64	0.132
Eng5	0.638	1.347	3.30	0.119	0.089	0.85%	3.06	0.057	0.048	1.50%	2.93	0.075
Eng7	0.374	0.273	6.64	0.184	0.115	0.45%	5.22	0.204	0.225	2.49%	5.08	0.161
Eng8	0.264	0.278	5.54	0.107	0.051	0.85%	5.15	0.093	0.057	1.46%	5.08	0.095
Eng9	0.277	0.406	4.72	0.156	0.076	1.43%	4.05	0.103	0.066	1.37%	3.71	0.089
Sc.A2	0.339	0.897	5.04	0.220	0.068	0.80%	4.48	0.096	0.040	2.70%	4.49	0.088
Sc.E	0.212	0.697	4.08	0.272	0.158	0.27%	3.48	0.055	0.031	1.43%	3.52	0.096
Hyd.	0.362	0.814	5.93	0.177	0.077	0.87%	5.36	0.122	0.060	3.57%	5.47	0.093
Agr.	0.152	0.251	3.70	0.189	0.080	3.70%	3.59	0.117	0.038	5.22%	3.32	0.114
Res.	0.235	0.809	3.37	0.054	0.018	1.41%	3.33	0.022	0.021	3.08%	3.32	0.056
Eng1_N (3)	0.190	0.240	7.56	0.224	0.137	0.94%	9.10	0.150	0.261	0.96%	9.38	0.120
Eng1_N (4)	0.196	0.305	5.67	0.194	0.093	0.66%	5.71	0.450	0.270	0.93%	4.30	0.203
Eng1_N (5)	0.200	0.414	4.78	0.126	0.074	2.30%	4.60	0.217	0.177	1.61%	5.08	0.084
Eng1_N (6)	0.208	0.483	3.05	0.086	0.076	5.55%	2.90	0.107	0.097	4.64%	2.73	0.101
Eng1_N (7)	0.166	0.484	2.93	0.070	0.045	0.98%	2.74	0.065	0.056	11.60%	2.73	0.079
Eng1_N (8)	0.167	0.528	2.67	0.071	0.039	0.56%	2.46	0.072	0.053	1.72%	2.54	0.104
Eng1_N (9)	0.190	0.628	2.35	0.057	0.034	0.71%	2.23	0.059	0.043	1.00%	2.15	0.079
Eng1_N (10)	0.204	0.715	2.09	0.051	0.030	0.54%	2.00	0.031	0.018	1.82%	2.06	0.042

β : Participation factor

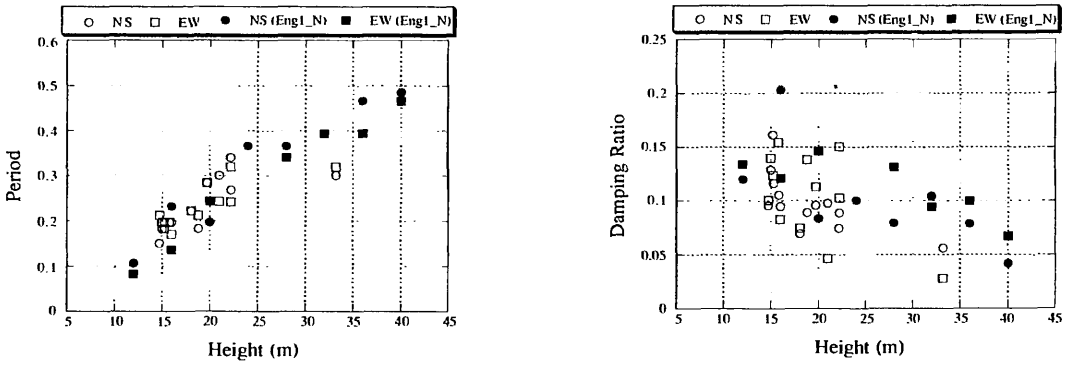

(a) Period of vibration (b) Damping ratio

FIG. 11. Distribution of period and damping ratio with the height of buildings (RD method)

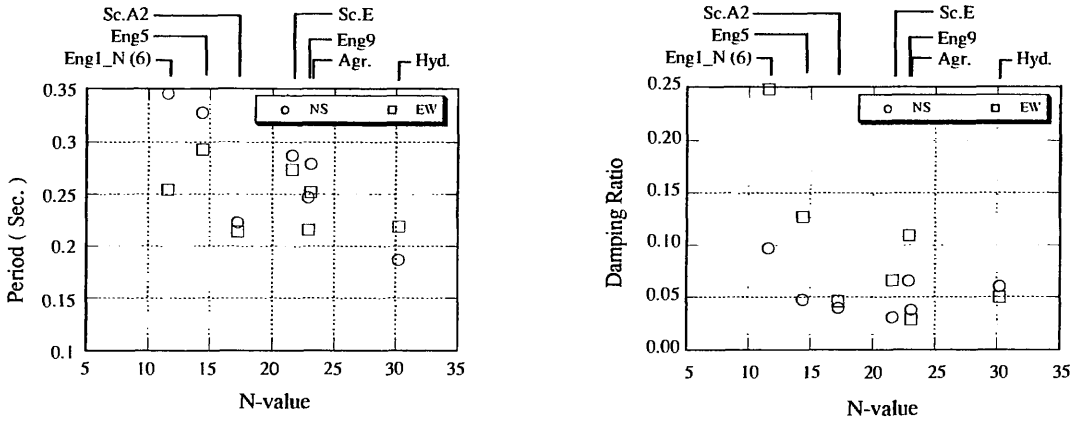

(a) Period of vibration (b) Damping ratio

FIG. 12. The results of transfer function fitting method for moderate height buildings

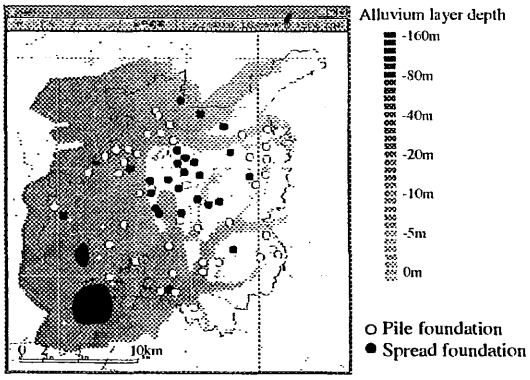

FIG. 13. Soil condition in Nagoya city and the location of investigated buildings

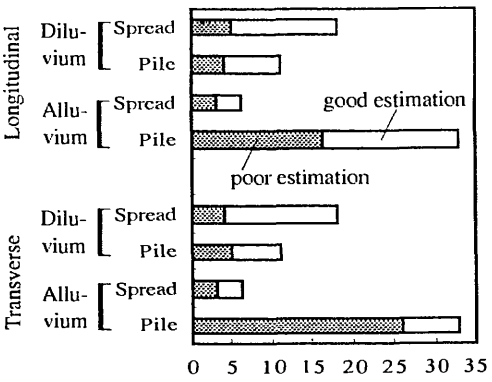

FIG. 16. The quality of transfer function estimation for different conditions

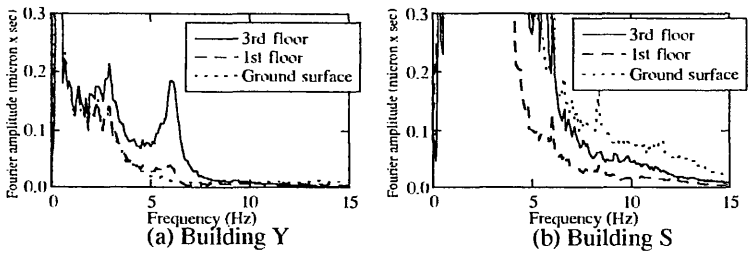

FIG. 14. Examples of Fourier spectra for two representative buildings

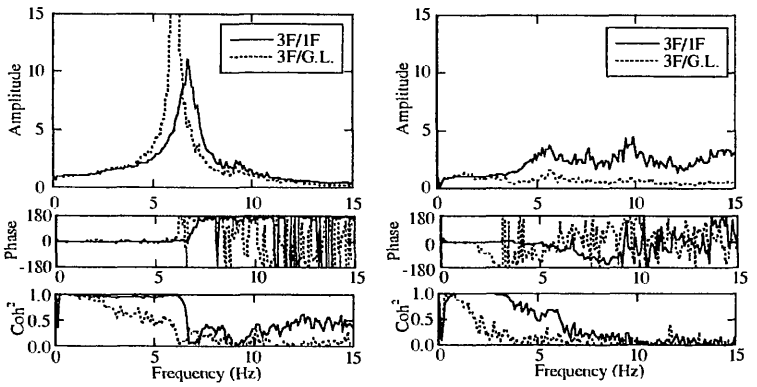

FIG. 15. Good and poor estimations of transfer function and coherence

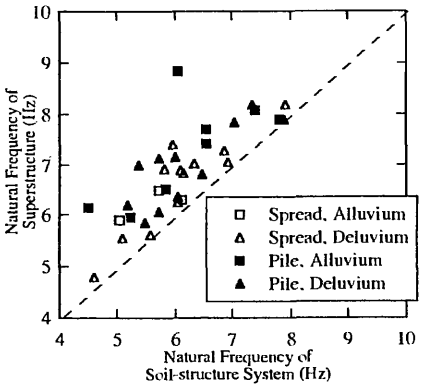

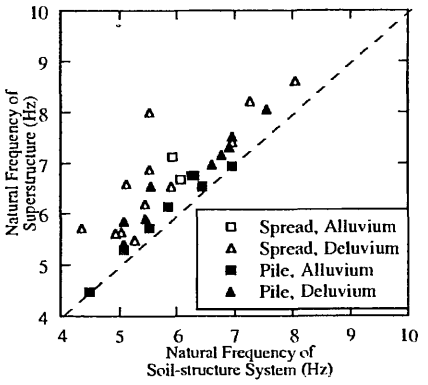

FIG. 17. Natural frequencies of superstructure compared with those of soil-structure systems

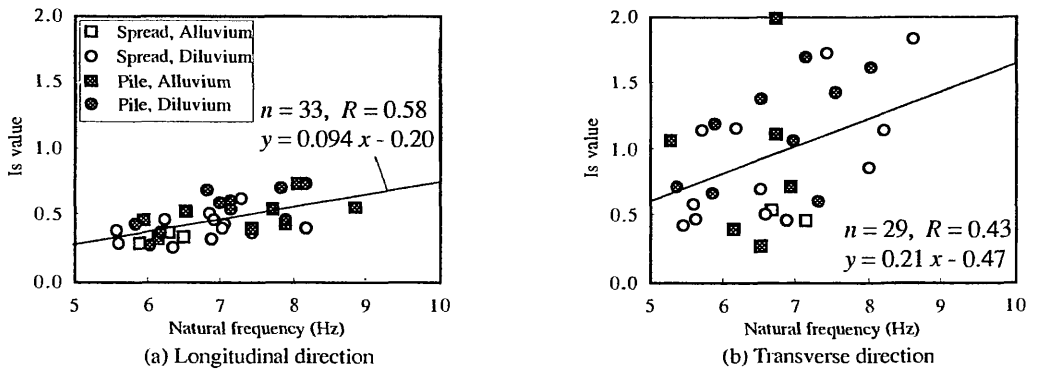

FIG. 18. Correlation between the aseismic performance index (Is) and the natural frequency of the superstructure

clearly show lower natural frequencies for soil-structure systems which is an explicit consequence of SSI effect.

From another point of view, Fig.18 shows a correlation between the observed natural frequencies of buildings and their aseismic performance index, I_s. This in turn points to the possibility of easy and rapid evaluation of the aseismic performance of buildings through microtremor measurements.

4. SEISMIC OBSERVATION IN NAGOYA UNIVERSITY

The vibration data from six instrumented buildings in the Higashiyama campus of Nagoya University were collected during three weak and moderate earthquakes (Tobita et al. 1998a). The collected data were then analyzed in order to study the effect of SSI on the dynamic characteristics of buildings as well as on the effective input motions. Figure 19 shows the outline of investigated buildings which are numbered in descending order of their area. Also shown are the locations of seismometers. The information of the investigated buildings are summarized in Table 3. It should be mentioned that the buildings #1, #3 and #4 in this table are, respectively, the same buildings #14, #4 and #8 in Table 1 which were studied in Sec.3.1. More detailed results on building #1, i.e., the 10-story building will be discussed in Sec.5.

Figure 20 shows the acceleration response of the buildings at roof, 1st floor and ground levels. Also shown are the Fourier spectral ratios for the two cases of top/1st floor and top/ground. It is believed that the former case may be considered as a representative for the fixed-base structure whereas the latter case includes the SSI effect too. The results thus show a clear change in the natural frequency of the system due to SSI for the 6-story and the 4-story buildings. Regarding the vertical vibration of buildings, remarkable difference is seen among the response of the three buildings.

The peak acceleration and velocity at the ground level and the first floor of all buildings have been summarized in Table 4 for the case of Mar. 16,1997 earthquake. Investigating the results reveals that there is more input motion loss for buildings with larger foundations. The loss of effective input motion is also studied through construction of Fourier spectral ratio graphs in Fig.21. The results are drawn versus nondimensional frequencies. The loss of input motion is seen clearly in the results, especially for the range of higher frequencies.

The results of natural frequencies and damping ratios for the superstructure are drawn versus the corresponding values of the soil-structure system in Fig.22. The results for natural frequencies clearly show lower values for soil-structure systems which can be interpreted as SSI effect. Also, the effect is more drastic for larger earthquakes (EQ2>EQ3>EQ1). Regarding the damping ratios, the results for building #3 are compatible with the general expectation of higher damping ratios for soil-structure systems. However, the results of building #4 show a different trend which may be due to the effect of neighboring building's vibration through structure-soil-structure interaction. An example of the curve fitting process for the building #1 is shown in Fig.23.

Finally, Fig.24 shows the amplitude dependency of the results. The estimated natural frequencies and damping ratios for different cases with various levels of vibration amplitude are drawn in the same figure versus the peak acceleration values at top of buildings. A clear trend of lower natural frequencies for higher levels of vibration is observed. However, the results for damping ratios are almost inconclusive.

5. DYNAMIC BEHAVIOR OF A 10-STORY BUILDING IN NAGOYA UNIVERSITY

The building #1 studied in Sec.4 is studied in more detail in this section (Tobita et al. 1997, 1998b). The building as shown in Fig.25 is a 10-story Steel Reinforced Concrete (SRC) structure with irregular plan. The building is located on deep soft soil deposits (building No.14 in Fig.14) and consequently has pile foundation with long piles up to 45 meters. The dynamic behavior of the building was studied through precise microtremor measurements. The observation points are also shown in Fig.25.

The translational and torsional mode shapes of the building are drawn in Fig.26 where the effect of building's irregularity is seen clearly. Table 6 shows the sway and rocking ratios computed based on displacements at the top story for different points of the plan. Rocking ratios even up to 50% is observed for the building at the eastern side. The ratio is 26% at the western side where the foundation width is bigger. But even at the western side, the rocking ratio is much larger than would be expected for buildings supported by pile foundations. Such large values of rocking ratio may be considered as a result of long piles and of softness of the underlain soil.

The spatial vibration shape of the building at the top floor are also presented in Fig.27 in a different style. Deformation of the first floor slab is shown in Fig.28. An obvious out-of-plane deformation is observed which is mainly due to different rocking motion in the two sides of the building. This complex behavior is among parameters which complicate the study of SSI effect on this building.

6. CONCLUDING REMARKS

The effect of SSI on the dynamic properties of structures was studied analytically and experimentally. As a result, the dominant effect of SSI for the cases of low and medium-rise buildings was clearly recognized. The main concluding remarks are as follows:

- Simplified methods were adapted for estimation of frequency and damping ratio of soil-structure systems which may be used for the design of ordinary buildings. The results were then compared with currently available provisions.

- The natural frequency and damping ratio of a few low and medium-rise buildings were evaluated through microtremor measurements. The effect of size of building on the severity of SSI effect was then studied through comparison of the results. Also, microtremor tests were conducted on several buildings with the same size but located on different soil conditions. It was concluded that identification of dynamic characteristics of buildings can be quite difficult for cases in which SSI is dominant.

- The dynamic behavior of three buildings was studied during three low and medium size earthquakes. The loss in the effective input motion was clearly observed, especially for buildings with large foundations. Also studied was the amplitude dependency of the results which leads to lower frequencies and larger damping ratios for more severe excitations.

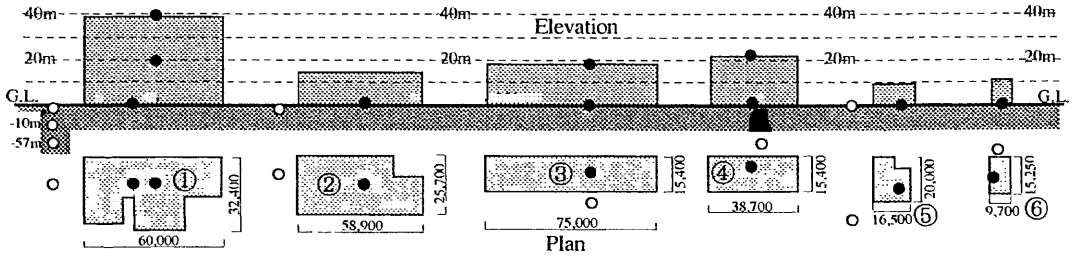

FIG. 19. Plan and elevation of investigated buildings and pickup points (○ :ground, ● :structure).

TABLE 3. Outline of investigated buildings

No.	Structure	Floor	Height(m)	Area(m2)	Foundation type	Av. Vs (m/s)
①	SRC	10	39.3	1,541	Pile (45m)	202
②	RC	3	(12)	1,370	R.C. Pile	(315)
③	RC	4	17.9	1,155	Pile (6m)	288
④	RC	6	22.3	604	P.C. Pile (12m)	303
⑤	RC	2	(9)	290	Spread and R.C. Pile (5m)	291
⑥	RC	1	(15)	150	R.C. Pile (7m)	305

TABLE 4. Maximum acceleration and velocity values during Mar. 16, 1997 earthquake

	Max. Acce. (gal)						Max. Vel. (kine)					
	NS		EW		UD		NS		EW		UD	
	G.L.	1F	G.L.	1F	G.L.	1F	G.L.	1F	G.L.	1F	G.L.	1F
①	72.1	48.4	97.2	60.6	37.0	18.1	3.95	3.85	5.81	5.42	1.80	1.59
②	54.0	52.7	63.2	49.8	34.7	37.9	2.49	4.04	4.58	3.28	1.58	1.61
③	50.3	57.3	73.5	50.0	31.4	24.1	2.87	4.02	4.51	4.05	1.81	1.93
④	44.2	42.7	55.9	58.7	38.8	20.5	2.83	3.69	4.69	4.40	1.91	1.88
⑤	61.2	49.1	69.7	61.3	37.5	31.1	3.79	4.40	4.50	3.86	1.73	1.63
⑥	54.5	61.3	74.0	80.4	57.6	51.6	3.19	4.32	5.26	4.84	1.96	1.90

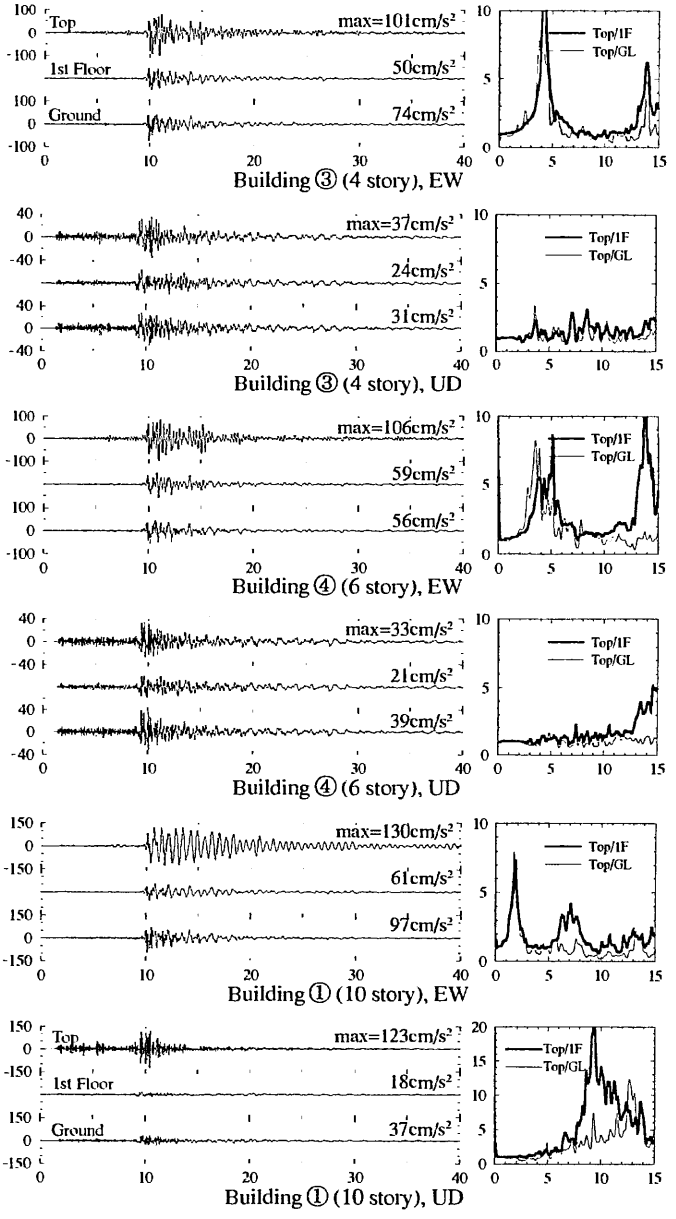

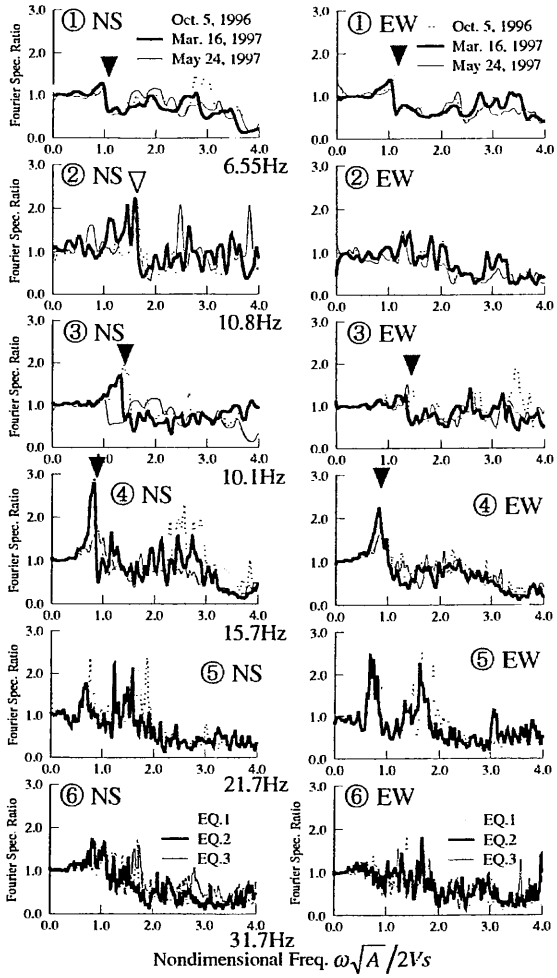

FIG. 21. Fourier spectral ratio (1st floor / ground) plotted versus nondimensional frequency

←

FIG. 20. Response acceleration (cm/s²) during Mar. 16, 1997 earthquake, and Fourier spectral ratios (top/1st floor, top/ground)

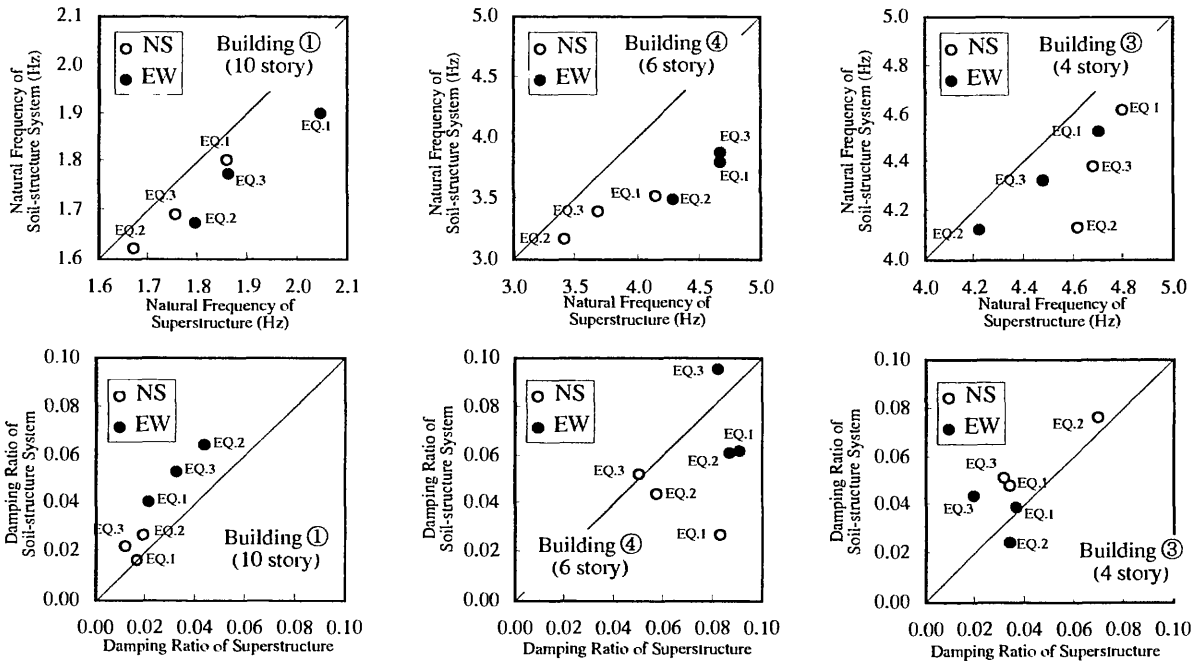

FIG. 22. Correlation between estimated parameters of superstructure and those of the soil-structure system

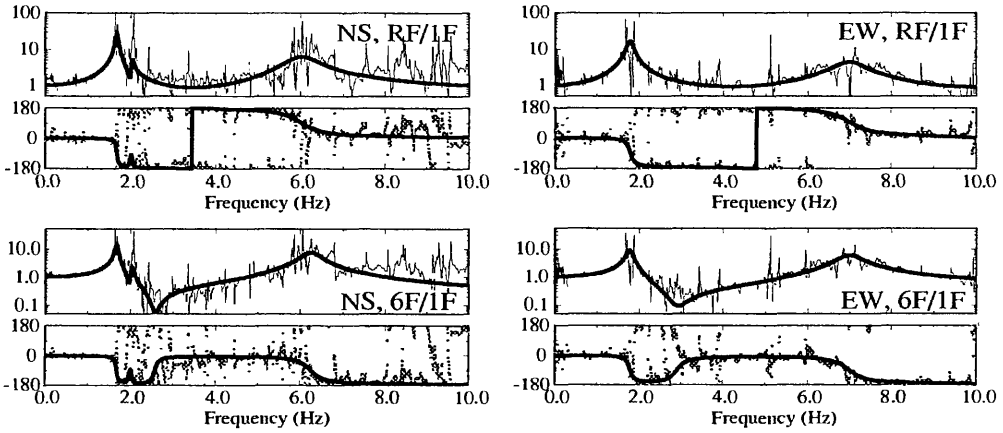

FIG. 23. Transfer functions fitting for building #1 (Mar. 16, 1997 earthquake)

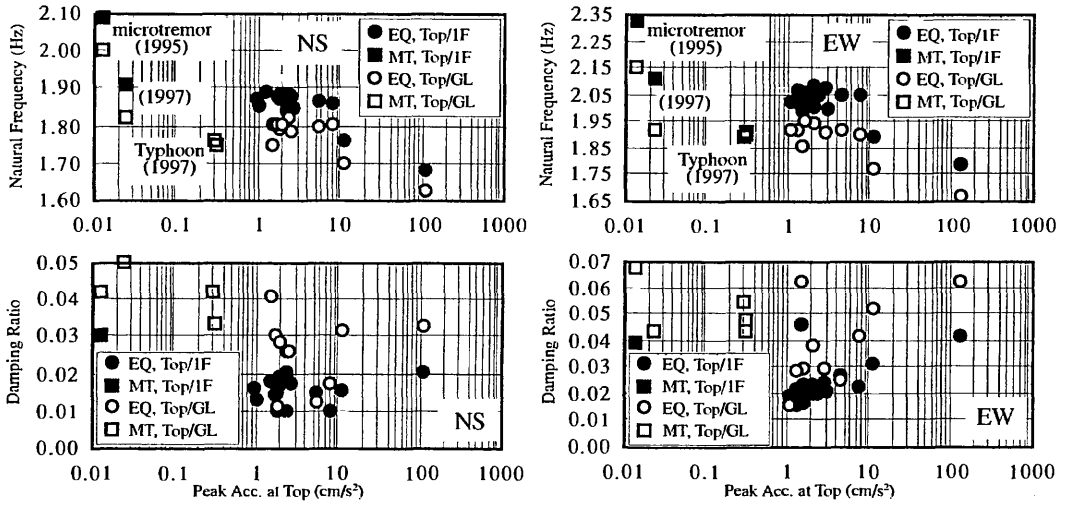

FIG. 24. Amplitude-dependency of natural frequencies and damping ratios for building #1

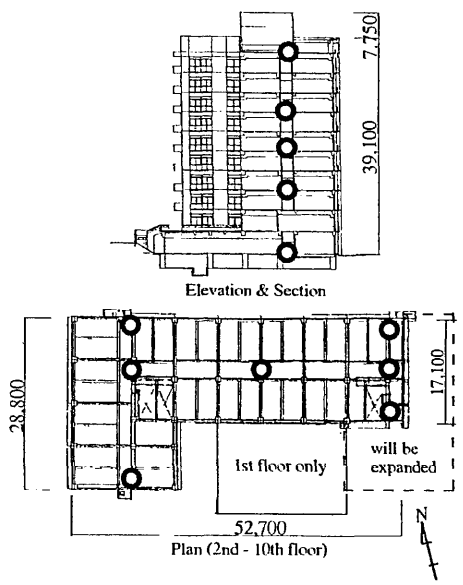

FIG. 25. Outline of the building and microtremor observation points

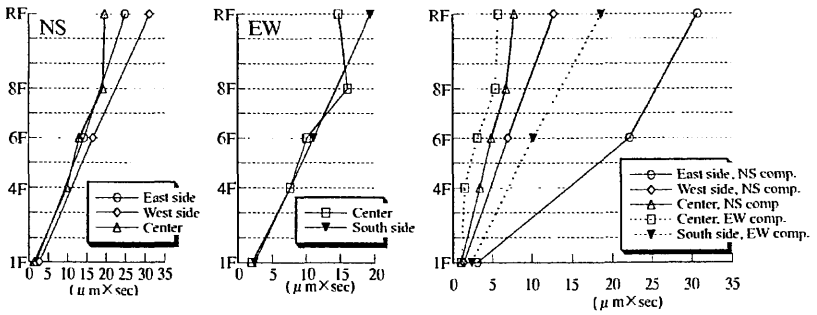

FIG. 26. Mode shapes of translational and torsinal modes estimated by the amplitude of displacement

TABLE 5. Sway and rocking ratios for NS and EW directions

	West, NS comp.		Center, NS comp.		East, NS comp.		Center, EW comp.	
	Ratio (%)	Amp. (μm×sec)	Ratio (%)	Amp. (μm×sec)	Ratio (%)	Amp. (μm×sec)	Ratio (%)	Amp. (μm×sec)
Total Top Disp.	100	31.5	100	19.7	100	24.6	100	14.6
Rocking	26	8.2			50	12.3	22	3.2
Sway	8	2.5	7	1.4	8	2.0	13	1.9
Elastic Deform.	66	20.8			48	11.8	69	10.1
Ground	2	0.6	3	0.6	3	0.6	5	0.7

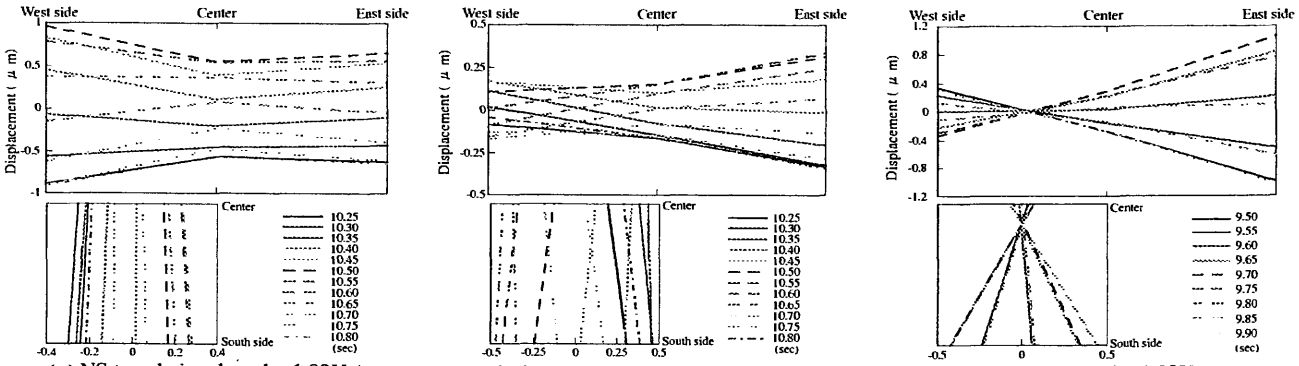

(a) NS translational mode (1.82Hz) (b) EW translational mode (1.92Hz) (c) torsional mode (1.82Hz)

FIG. 27. Horizontal vibration shapes of the top floor of translational and torsional modes

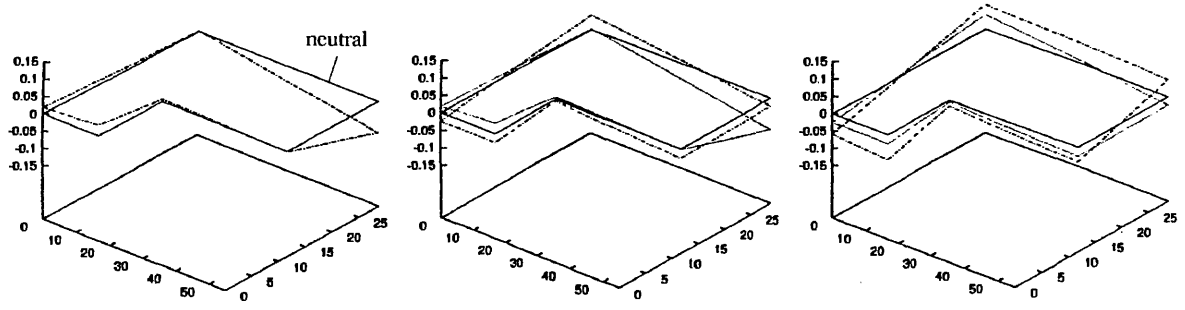

T=79.00 sec T=79.05 sec T=79.10 sec

FIG. 28. Out-of-Plain deformation of the 1st floor (NS Translational Mode, 1.82Hz)

- The dynamic behavior of a 10-story building was studied precisely through dense microtremor measurements. Large rocking motions were observed for the building in spite of existence of pile foundation. Different levels of rocking motion were observed for the two sides of the building due to change in the size of foundation. This leads to out of plane deformation of floors which, in turn, complicates the experimental evaluation of dynamic characteristics of the building.

Finally, the need to improve the reliability of simplified formulations was pointed out which may be achieved by increasing the quality and quantity of experimental studies on ordinary buildings.

REFERENCES

Architectural Institute of Japan (AIJ) (1996).*An Introduction to Dynamic Soil-Structure Interaction* (In Japanese)

Applied Technology Council (1978). *Tentative Provisions for the Development of Seismic Regulations for Buildings, ATC Publications, ATC3-06*

Celebi, M. (1997). "Response of Olive View Hospital to Northridge and Whittier earthquakes",*J. Struc. Engng., ASCE,* Vol.123, No.4, 389-396

Earthquake Resistant Regulations -A World List (1988). International Association for Earthquake Engineering,Tsukuba, Japan

Fukuwa, N., Ghannad, M.A. &Yagi, S. (1995). "A study on the effect of soil-structure interaction on the eigenproperty of structure",*J. Struct. Constr. Engng.,* Transactions of Arch. Inst. of Japan (AIJ), No.475, 35-44, (In Japanese)

Fukuwa, N. and Gahnnad, M.A. (1996). "Soil-structure interaction efect on the eigenproperties of structure",*Proc. 11WCEE,* Acapulco, Mexico, Paper No. 949

Ghannad, M.A., Tobita, J., Fukuwa, N., Nishizaka, R. and Koide, E. (1997a). "A study on the effect of soil-structure interaction on the dynamic properties of RC structures based on the microtremor records", *J. Structural Engng.,* Architectural Inst. of Japan (AIJ), Vol.43B, 441-450

Ghannad, M. Ali, Fukuwa, N. andTobita, J. (1997b), "The effect of soil-structure interaction on the damping of structure",*Proc. 7th International Conf. on Structural Safety and Reliability (ICOSSAR'97)* Kyoto, Japan, Paper No. WeB1-01

Ghannad, M.A., Fukuwa, N. and Nishizaka, R. (1998). "A study on the frequency and damping of soil-structure systems using a simplified model",*J. Structural Engng.,* Architectural Inst. of Japan (AIJ),Vol.44B, 85-93

Ghannad, M.A. (1998).*A Study on the Effect of Soil-Structure Interaction on the Dynamic Properties of Structures Using Simplified Methods,* Thesis presented to Graduate School of Engineering, Nagoya Univin partial fulfillment of the requirements for the degree of Doctor of Engineering

Hayashi, Y. , Yasui, Y. and Yoshida, N.(1998). "Effects of soil-structure interaction in heavily damaged zone during Hyogo-ken Nanbu Earthquake", *Proceeding of the 5th Symposium on Dynamic Soil-Structure Interaction Effect,* Sponsored by Architectural Institute of Japan (AIJ), Tokyo, Japan, 13-24

Hurty, W.C. and Rubinstein, M.F (1964) *Dynamics of Structures,* Prentice-Hall Inc.

Kausel, E. & Roesset, J. (1974). "Dynamic stiffness of circular foundations",*Engng. Mech. Div., ASCE,* Vol.101, 771-785

Kokusho, T. (1980). "Cyclic triaxial test of dynamic soil properties for wide strain range",*Soil and Foundations,* Vol.20, 45-60

NEHRP Recommended provisions for the development of seismic regulations for new buildings (1994). The Building Seismic Safety Council for the Federal Emergency Management Agency

Novak, M. (1975). "Additional note on the efect of soil on structural response",*Earthq. Engng. Struct. Dynam.,* Vol.3, 312-315

Tobita, J. (1996). "Evaluation of nonstationary damping characteristics of structures under earthquake excitations",*Journal of Wind Engineering and Industrial Aerodynamics,* Vol.59, Nos.2,3, 283-298

Tobita, J., Fukuwa, N., Nishizaka, R. and Nishiyama,T. (1997). "Evaluation of damping properties of structures based on high density earthquake observation in Nagoya University Higashiyama Campus", *D&D '97 Symposium, JSME,* 41-44, (in Japanese with English abstract).

Tobita, J., Nishiyama, T. and Fukuwa, N. (1998a). "Observed soil-structure response characteristics of low- and middle-rise reinforced concrete buildings",*5th Symposium on Soil Structure Interaction, AIJ,* 131-136, (in Japanese).

Tobita, J., Nishiyama,T., Fukuwa, N., Nishizaka, R. and Murahashi, R. (1998b). "Three-dimensional vibration characteristics of a 10-story SRC building observed by microtremor test",*10th JEES,* (in Japanese with English abstract), (will be published).

Veletsos, A.S. (1977). "Dynamic of structure-foundation systems", *Structural and Geotechnical Mechanics,* A Volume Honoring N.M. Newmark (Editor: W.J. Hall), Prentice-Hall, Inc. Englewood Cliffs, N.J., 333-361

Wallace, J.W. and Moehle, J.P(1990). "Evaluation ofATC requirements for soil-structure interaction using data for the 3 March 1985 Chile earthquake", Earthquake Spectra, Vol.6, No.3, 593-611

Wolf, J.P. (1985). *Dynamic Soil-Structure Interaction,* Prentice-Hall, Englewood Cliffs, N.J.

Wolf, J.P. (1994). *Foundation Vibration Analysis Using Simplified Physical Models,* Prentice-Hall, Englewood Cliffs, N.J.

Yagi, S., Tobita, J., Fukuwa, N. and Nishizaka, R. (1998). "Estimation of dynamic characteristics and effect of soil-structure interaction at R.C. buildings based on the microtremor tests",*5th Symposium on Soil Structure Interaction, AIJ,* 125-130 (in Japanese).

Yasui, Y. and Tokimatsu, K. (1998). "Outline of damage to buildings and foundations during the Hyogo-ken Nanbu Earthquake of 1995", *Proceeding of the 5th Symposium on Dynamic Soil-Structure Interaction Effect,* Sponsored by Architectural Institute of Japan (AIJ),Tokyo, Japan, 3-12

SOIL-STRUCTURE INTERACTION ANALYSIS VIA FIXED-BASE SYSTEM SUBJECTED TO A MODIFIED GROUND MOTION

M.Nuray Aydınoğlu[1], Ş.Şeref Polat[2] and Kemal Beyen[3]

ABSTRACT : Analysis of seismic soil-structure interaction is reformulated to define an equivalent (modified) ground motion and an equivalent pseudo acceleration for the first mode response of a given fixed-base structure under a given earthquake. Equivalent ground acceleration corresponds to the total acceleration of the "rigid" structure defined at the centre of modal inertia forces developed in the first vibration mode of the fixed-base structure. A typical example dealing with an extremely stiff and stocky building actually constructed in the city of Dinar (Turkey) after 1995 Dinar earthquake on relatively soft soil conditions exhibited a considerable amplification in terms of equivalent (modified) earthquake ground acceleration. Set of numerical results also presented in this contribution deals with the generation of modified pseudo-acceleration response spectra under the same earthquake (Dinar 1995) for typical shear wall buildings. Such buildings are selected to represent those constructed by the so-called "*tunnel formwork*" system in Turkey during the last decade for mass-construction of multi-storey residential buildings. Response spectra ordinates which are calculated and plotted by varying the soil stiffness and the building aspect ratio, clearly demonstrate the expected effects of soil-structure interaction particularly on stiff, short-period buildings.

INTRODUCTION

The idea behind the present paper has originated from the observation of extensive use of the so-called "*tunnel formwork*" system in Turkey during the last decade for mass-construction of multi-storey residential buildings. Such buildings are made of merely reinforced concrete walls and slabs resulting in extremely stiff structural systems (Fig.1). When they are supported through raft foundations on relatively soft soils, almost ideal conditions are created for the pronounced effects of seismic soil-structure interaction.

Contrary to traditional engineering approach and the established seismic code procedure of soil-structure interaction analysis based on the appropriate modification of fundamental period and the effective damping of the structure (BSSC 1995), the present study attempts for the determination of a fictitious "*equivalent input ground motion*" to be applied to fixed-base structure system in the fundamental mode without necessarily modifying its dynamic properties. Thus, this alternate approach makes it possible to develop "*modified response spectra*" applicable to first mode response of soil-structure systems. Although such output requires the full analysis of SSI systems, it may be justified if the systems under consideration can be standardised, as in the case of above mentioned uniform shear wall building structures which may be characterised by few independent parameters only.

The present paper does not have any claim in terms of originality of research except that SSI effects are demonstrated in a different fashion. It is anticipated that practical engineers who, in part, still experience some difficulty in understanding the favourable and/or unfavourable effects of soil-structure interaction, may find it more interesting to observe how SSI affects the building response as the effect is directly read from the familiar pseudo-acceleration response spectra.

[1] Professor, [2] Graduate student, [3] Dr.Eng., Boğaziçi University, Kandilli Observatory and Earthquake Research Institute, Department of Earthquake Engineering, 81220 Çengelköy, Istanbul - Turkey

EQUIVALENT GROUND MOTION AND PSEUDO-ACCELERATION

A systematic formulation of soil-structure interaction for building type structures is presented in the Appendix. The following derivation, on the other hand, aims only to give the definition of "*equivalent ground motion*" and that of the "*equivalent pseudo-acceleration*". Reference is made to the Appendix as necessary.

Referring to the soil-structure system shown in Fig.2, equations of motion of the structural part of the system can be expressed in the frequency domain as,

$$([K_{ss}]+ i\omega[C_{ss}] - \omega^2 [M_{ss}])\{\delta_s\} = -[M_{ss}]\,[T_{so}]\{\ddot{u}^t_o\} \qquad (1)$$

Being the first row of equation of motion of the soil-structure system given by **Eq.A1** of the Appendix, in the above expression ω denotes excitation frequency, $[K_{ss}]$, $[C_{ss}]$, $[M_{ss}]$ represent structural property matrices and $\{\delta_s\}$ refers to structure's horizontal displacement vector relative to the rigid foundation. Total acceleration vector of the rigid foundation, $\{\ddot{u}^t_o\}$, includes sway and rocking degrees of freedom only, as indicated in Fig.2:

$$\{\ddot{u}^t_o\} = <\ddot{u}^t_x \qquad \ddot{\theta}>^T \qquad (2)$$

In Eq.1, $[T_{so}]$ is as given by **Eq.A4** of the Appendix and represents the kinematic transfer matrix for transmitting total motion of the rigid foundation to the structure.

Referring to the Appendix, relative structural displacements, $\{\delta_s\}$, appearing in **Eq.1** can be expressed in terms of modal coordinates of the fixed base structure. Resulting modal equation of motion written for an r'th mode is as follows:

$$(\Omega_r^2 - \omega^2 + 2i\,\omega\,\xi_r\Omega_r)\,Y_{sr} = -\{\Phi_r\}^T[M_{ss}]\,[T_{so}]\{\ddot{u}^t_o\} \qquad (3)$$

Since soil-structure interaction effect is dominantly pronounced in the first vibration mode only, by considering **Eq.2** above expression can be written for the first mode as,

$$(\Omega_1^2 - \omega^2 + 2i\,\omega\,\xi_1\Omega_1)\,Y_{s1} = -<L_{x1} \qquad h_1 L_{x1}><\ddot{u}^t_x \qquad \ddot{\theta}>^T \qquad (4)$$

where L_{x1} represents the participation factor in the first mode (**Eq.A20**) and h_1 refers to the centre of the effective seismic forces in the first mode of the fixed-base structure measured from the level of soil-foundation interface (**Eq.A21**). By using variables γ_1 and $\ddot{u}_\theta$ defined in **Eq.A25** and **Eq.A30** of the Appendix, respectively, **Eq.4** can be rewritten as (Fig.2),

$$(\Omega_1^2 - \omega^2 + 2i\,\omega\,\xi_1\Omega_1)\,Y_{s1} = -L_{x1}\,(\ddot{u}^t_x + \gamma_1\,\ddot{u}_\theta) \qquad (5)$$

Thus, "*equivalent horizontal ground acceleration*" defined for the first mode of the fixed-base structure to replace the horizontal component of the effective foundation input acceleration, $\ddot{u}^g_x$, is determined as,

$$\ddot{u}^g_{x,eq} = \ddot{u}^t_x + \gamma_1\,\ddot{u}_\theta \qquad (6)$$

By the above definition, it can be stated that equivalent horizontal ground acceleration corresponds to the total horizontal acceleration of the "rigid" structure defined at the

centre of modal inertia forces developed in the first vibration mode of the fixed-base structure.

Under the above defined equivalent horizontal ground acceleration, equation of motion of a single degree of freedom system with natural frequency of Ω_1 is expressed in the frequency domain as,

$$(\Omega_1^2 - \omega^2 + 2i\,\omega\,\xi_1\,\Omega_1)\,u_s = -\ddot{u}^g_{x,eq} = -(\ddot{u}^t_x + \gamma_1\,\ddot{u}_\theta) \qquad (7)$$

"*Equivalent pseudo-acceleration*", a_{ps1} , is then determined in the frequency domain as,

$$a_{ps1} = \Omega_1^2\,u_s = -(D_1 / \beta_1^2)\,(\ddot{u}^t_x + \gamma_1\,\ddot{u}_\theta) \qquad (8)$$

where $\beta_1 = \omega / \Omega_1$ and D_1 is as defined in the Appendix (**Eq.A16b**).

In practical applications it is appropriate to obtain the required response quantities first in terms of transfer functions in the frequency domain. Since condensed equations of motion given in **Eq.A31** of the Appendix are also valid for accelerations, i.e., $\{\ddot{u}^t_o\}$ and $\{\ddot{u}^g_o\}$, in lieu of displacements, transfer functions $\ddot{U}^g_{x,eq}$ and A_{ps1} corresponding to equivalent horizontal ground acceleration and pseudo-acceleration, respectively, can be obtained from **Eq.A34** of the Appendix by imposing unit amplitude to the effective foundation input acceleration, i.e., $\ddot{u}^g_x = 1$ and utilising **Eqs.6,8** given above. Pseudo-spectral acceleration for the first mode is then obtained in the time domain as,

$$S_{pa,1} = [IFT\,(A_{ps1} \times FT\,(\ddot{u}^g_x))]_{max} \qquad (9)$$

where abbreviations **FT** and **IFT** denote Fourier Transform and Inverse Fourier Transform operations, respectively, for which well known Fast Fourier Transform algorithm is ideally suited. In the following examples complex, frequency dependent stiffness influence coefficients of rigid surface foundations given in (Veletsos, Wei 1971) are utilised where equivalent radii are calculated for the sway and rocking motions of the rectangular surface foundation considered in this study.

Condensed equations of motion in terms of rigid foundation degrees of freedom are given in detail by **Eqs.A31, A32, A33** and **A34** of the Appendix. Nondimensional parameters are, $\eta_{x\theta}=\eta_{\theta x}$, $\eta_{\theta\theta}$ (defined by **Eq.A9**), ε (defined by **Eq.A6**), λ_1 (defined by **Eq.A24**), γ_1 (defined by **Eq.A25**) and three independent, nondimensional SSI parameters defined by **Eqs.A27**. However in dealing with the above mentioned uniform shear wall structures, it may be more appropriate to use the following independent, nondimensional SSI parameters in lieu of those defined in **Eqs.A27**.

$$\delta_A = M_s / (\rho_s\,A\,B\,H_n) \qquad (10a)$$

$$T_g = 4\,H_n / V_{sg} \qquad (10b)$$

$$\alpha_A = H_n / A \qquad (10c)$$

where $A = 2a$ and $B = 2b$ are the plan dimensions of the rectangular raft foundation in the earthquake direction and in perpendicular direction, respectively. ρ_s represents the mass density of the superstructure material. (For reinforced concrete, $\rho_s \approx 1.35\,\rho_g$ may be assumed). Parameter δ_A defined by **Eq.10a** above may be taken nearly constant

for certain range of shear wall buildings. Parameters given in **Eqs.A27** and **Eqs.10** are interrelated as follows:

$$\alpha = 2\,\alpha_A \tag{11a}$$

$$\delta = (8\,\kappa\,\alpha_A\,\rho_s / \rho_g)\,\delta_A \tag{11b}$$

$$s = (\pi / 2)\,(T_g / T_1) \tag{11c}$$

where T_1 refers to the first natural vibration period of the superstructure ($T_1 = 2\pi / \Omega_1$) and κ is defined as

$$\kappa = B / A = b / a \tag{12}$$

NUMERICAL RESULTS

a) Equivalent ground acceleration applicable to first mode response

As an example of the above explained procedure, a five storey shear wall building is analysed for Dinar Earthquake of October 1, 1995 (M_s = 6.0) by considering EW component of a near-field strong motion record. Actually such buildings have been built after the damaging earthquake occurred in the town of Dinar in western Turkey for those people whose houses were either collapsed or demolished due to irreparable heavy damage. Interestingly, buildings were built on relatively soft soil conditions with mat foundations such that pronounced effects of soil-structure interaction can be expected. A typical storey plan and vertical cross section of the building are shown in Fig.1. Wall and slab thickness throughout the building are 0.15 m and 0.14 m, respectively, whereas mat foundation is 0.40 m thick. SSI parameters defined in this paper are calculated as, α_A=**0.728**, κ=**0.927** (**A=19.71**m, **B=18.27**m, H_n=**14.35**m), $\eta_{x\theta}=\eta_{\theta x}$=**0.568**, $\eta_{\theta\theta}$=**0.403**, ε=**0.271**, δ_A=**0.1285**, γ_1=**0.6859**, λ_1=**0.8813**. Fundamental period of the fixed-base building is calculated as T_1=**0.052** s, and average shear wave velocity of the site is assumed to be V_{sg} = **200** m/s, leading to above defined fictitious soil period of T_g=**0.287** s. Fig.3 shows acceleration time histories of actual and equivalent (modified) ground motions applicable to fixed base structure in its first vibration mode, respectively, which clearly demonstrate the pronounced response amplification in such an extremely stiff building due to SSI effect. Contrary to the beneficial effect of SSI which is usually the case in practice, this example shows that constructing stiff, stocky buildings on soft soils may result in substantially higher seismic response.

b) Modified response spectra applicable to first mode response

By inspection on above mentioned stiff buildings constructed by "tunnel formwork" system, it can be concluded that parameters κ, $\eta_{x\theta} = \eta_{\theta x}$, $\eta_{\theta\theta}$, ε and δ_A may not vary considerably in practice, whereas first-mode mass parameters λ_1 and γ_1 can be reasonably estimated by considering the nearly uniform mass distribution of such buildings. Thus, by choosing building aspect ratio α_A and fictitious soil period T_g as independent variables, sets of "*equivalent pseudo-acceleration response spectra*" for the first mode response of the fixed-base structure can be generated in accordance with

Eq.9. Such response spectra shown in Fig.4 and Fig.6 are calculated for Dinar (1995) earthquake EW component with the following constant parameters: κ=**1**, $\eta_{x\theta}=\eta_{\theta x}$=**0.5**, $\eta_{\theta\theta}$=**0.33**, ε=**0.175**, δ_A=**0.15**, λ_1=**0.75**, γ_1=**0.75**. The first independent parameter, i.e., fictitious soil period starts from T_g=**0** (representing infinitely stiff soil) and increases up to **1.40 s** with **0.20 s** increments. On the other hand, building aspect ratio ($\alpha_A = H_n / A$) is taken as **0.75** and **1.50**, respectively. In order to show the significance of SSI effect, equivalent pseudo-acceleration response spectra amplitudes given in Figs.4,6 are normalised with respect to those obtained for infinitely rigid soil and presented in Fig.5 and Fig.7, respectively. Curves shown in those figures effectively correspond to the first mode amplification (or de-amplification) spectra due to SSI effect.

Figs.4 through 7 clearly demonstrates favourable and/or unfavourable effects of SSI for certain type of structures under a typical earthquake motion recorded on relatively soft soil conditions. It is observed that peaks of the response spectra of the modified ground motion generally shift to shorter periods with respect to no SSI situation. Thus, as expected, response spectrum amplitudes for periods shorter than peak response period tend to amplify, while those for periods longer than peak response period de-amplify, indicating the well known effective period increase in the actual soil-structure system. As a result of this trend substantial amplification occurs in very short-period buildings, especially those with higher aspect ratios. In order to show the effect of building aspect ratio, response spectra are presented in Figs. 8,9 for constant fictitious soil periods of T_g = **0.4 s** and T_g =**0.6 s**, respectively, under Dinar earthquake EW component. In each case, building aspect ratio ($\alpha_A = H_n / A$) is varied from **0.75** to **1.75** with increments of **0.25**. Very high amplifications for short period buildings with high aspect ratios are clearly observed. However amplifications are relatively less pronounced as the soil softens.

CONCLUSIONS

Analysis of seismic soil-structure interaction is reformulated to result in an equivalent ground motion and equivalent pseudo spectral acceleration for the first mode response of a given fixed-base structure under a given earthquake. Equivalent ground acceleration corresponds to the total acceleration of the "rigid" structure defined at the centre of modal inertia forces developed in the first vibration mode of the fixed-base structure. Expressions for equivalent ground motion and pseudo spectral acceleration are obtained in the frequency domain in the form of transfer functions. In order to obtain the desired output quantities in the time domain, convolution is applied to the transfer function involved and Fourier transform of the earthquake input ground motion through inverse Fourier transform. The well-known Fast Fourier Transform Algorithm is efficiently used for the transform operations.

The first example dealing with an extremely stiff and stocky building actually constructed in the city of Dinar (Turkey) after 1995 Dinar earthquake on relatively soft soil conditions exhibited a considerable amplification in terms of equivalent (modified) earthquake ground acceleration applicable to the first mode response of the building in its fixed base condition. The second set of numerical results deals with the generation of modified pseudo-acceleration response spectra under the same earthquake (Dinar 1995) for typical shear wall buildings for which certain parameters may be taken to be constant. Response spectra ordinates are calculated and plotted by varying the soil stiffness and the building aspect ratio, which clearly demonstrated the expected effects of soil-structure interaction particularly on stiff, short-period buildings.

REFERENCES

Aydınoğlu, M.N. (1980), *Unified Formulations for Soil-Structure Interaction*, Proc. 7th World Conference on Earthquake Engineering, Vol.6, pp.121-128, Istanbul.

BSSC-Building Seismic Safety Council (1995), *NEHRP Recommended Provisions for Seismic Regulations for new Buildings, 1994 Edition, Part 1: Provisions and Part 2: Commentary*, Federal Emergency Management Agency, Washington, D.C.

Veletsos, A.S. and Y.T.Wei (1971), *Lateral and Rocking Vibration of Footings*, ASCE, Journal of Soil Mechanics and Foundations, Vol.97, No.SM9, pp.1227-1248.

Wolf, J, P. (1985), *Dynamic Soil-Structure Interaction*, Prentice-Hall, Englewood Cliffs, N.J.

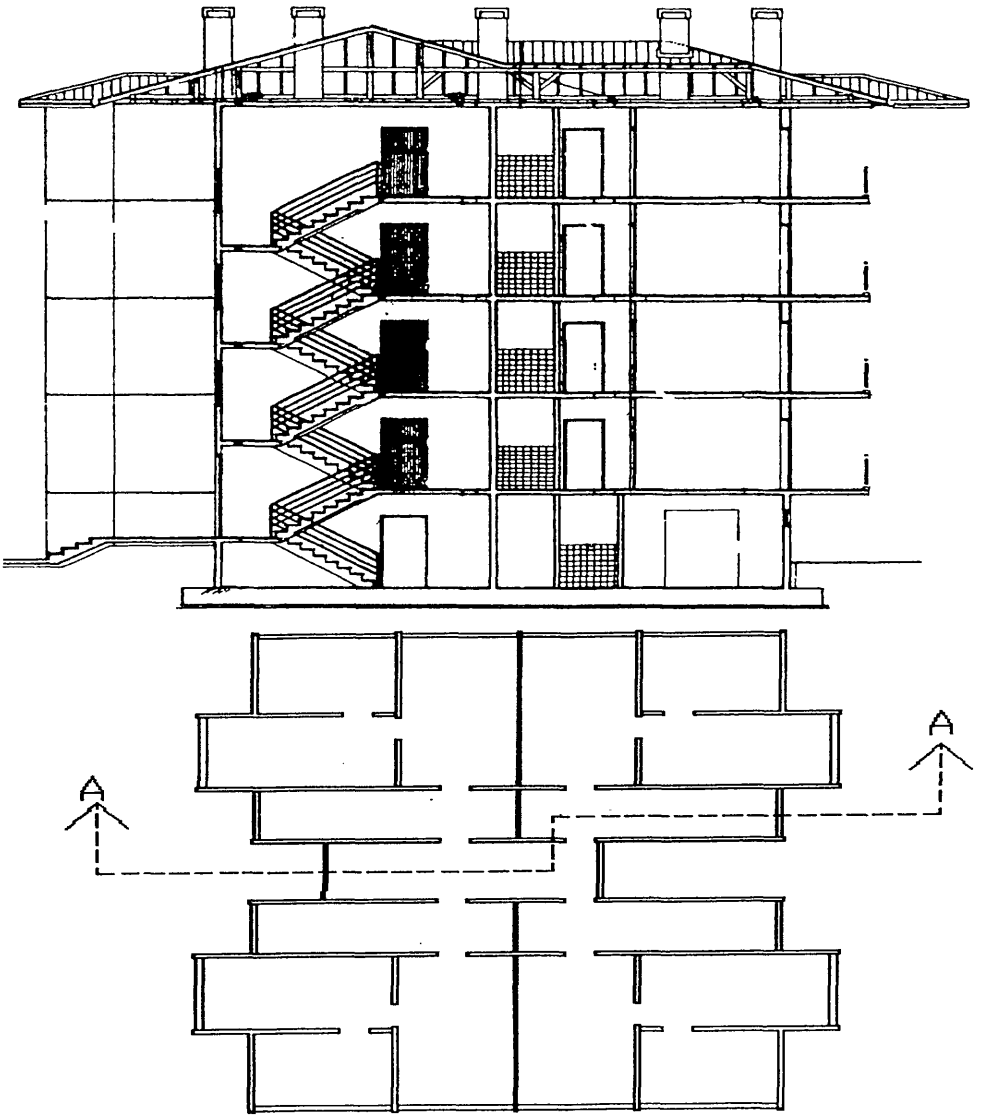

Figure 1. Plan and profile of the typical building

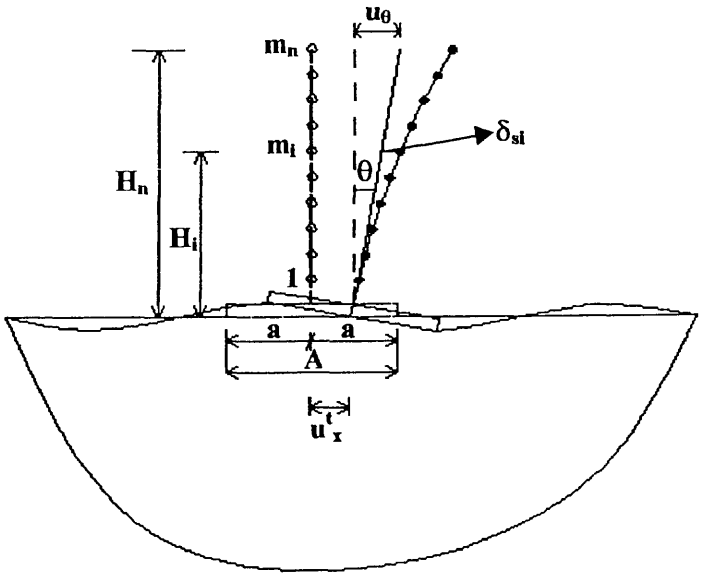

Figure 2. Soil-structure system considered

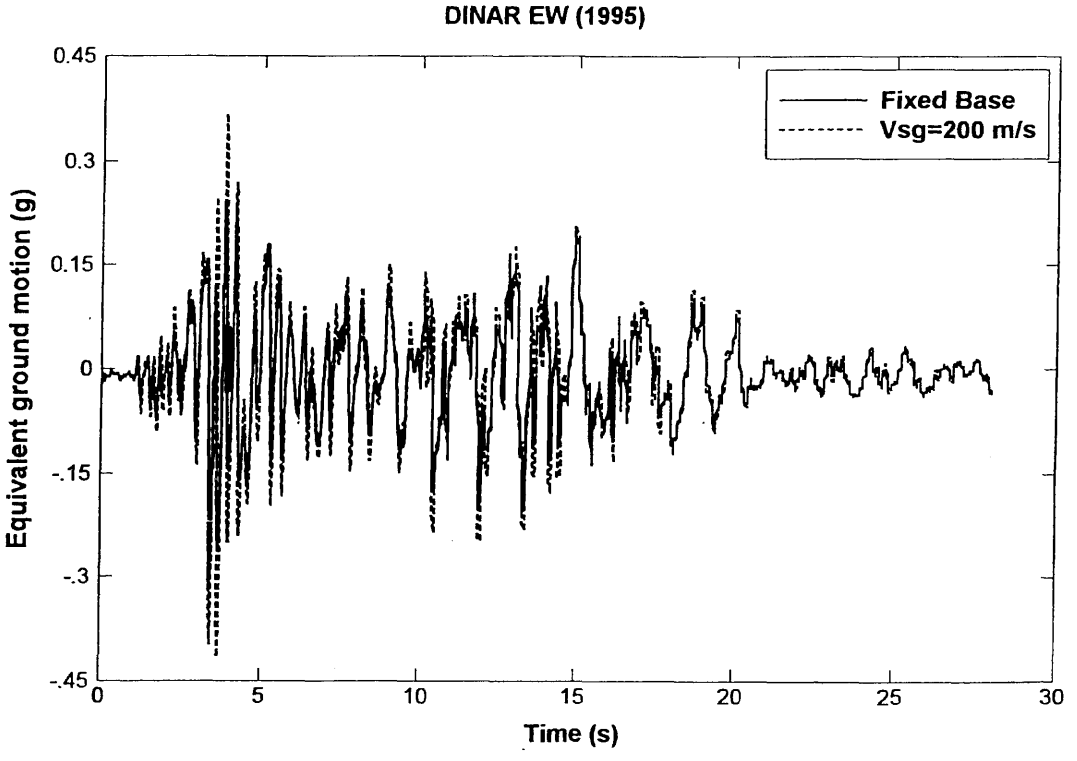

Figure 3. Equivalent (modified) earthquake ground acceleration for the typical building to replace recorded ground acceleration in Dinar (1995) earthquake, EW component

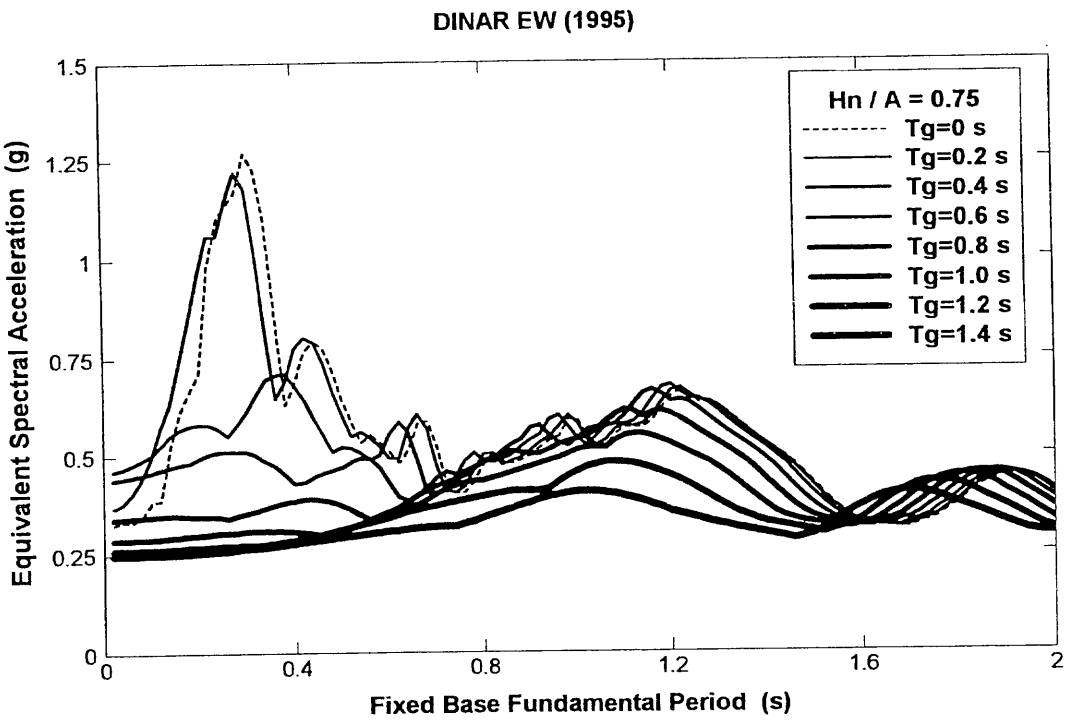

Figure 4. Equivalent (modified) pseudo-acceleration spectra under Dinar Earthquake (1995) EW component for $H_n / A = 0.75$ and varying fictitious soil period

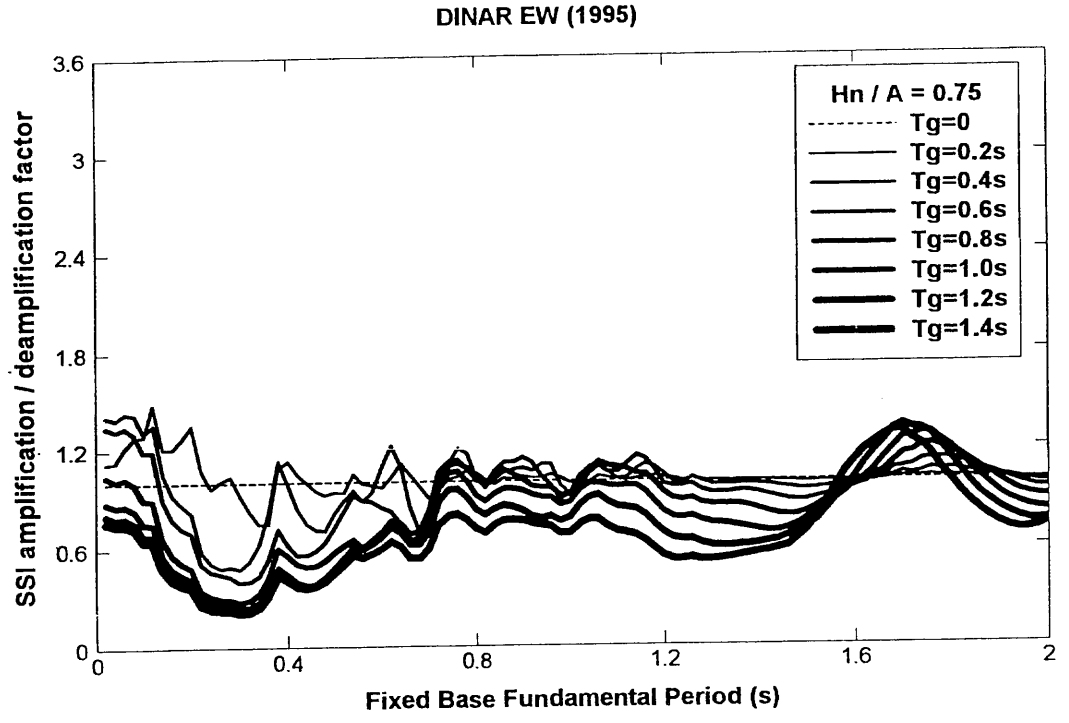

Figure 5. Spectra for SSI amplification / deamplification factor under Dinar Earthquake (1995) EW component for $H_n / A = 0.75$ and varying fictitious soil period

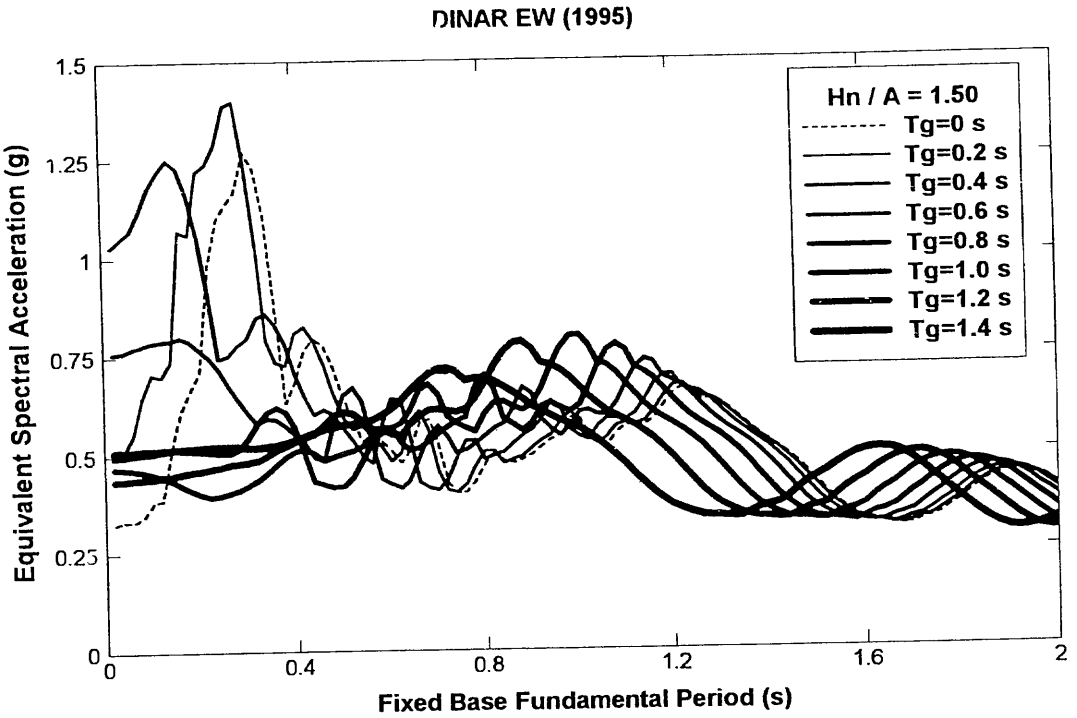

Figure 6. Equivalent (modified) pseudo-acceleration spectra under Dinar Earthquake (1995) EW component for H_n / A = 1.50 and varying fictitious soil period

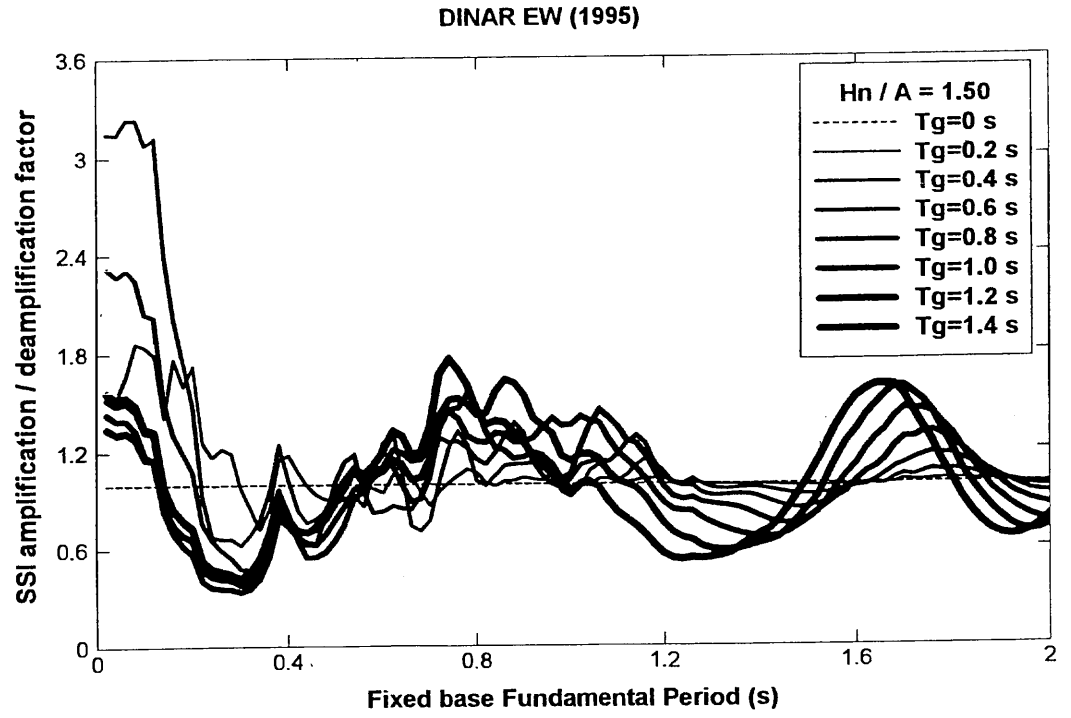

Figure 7. Spectra for SSI amplification / deamplification factor under Dinar Earthquake (1995) EW component for H_n / A = 1.50 and varying fictitious soil period

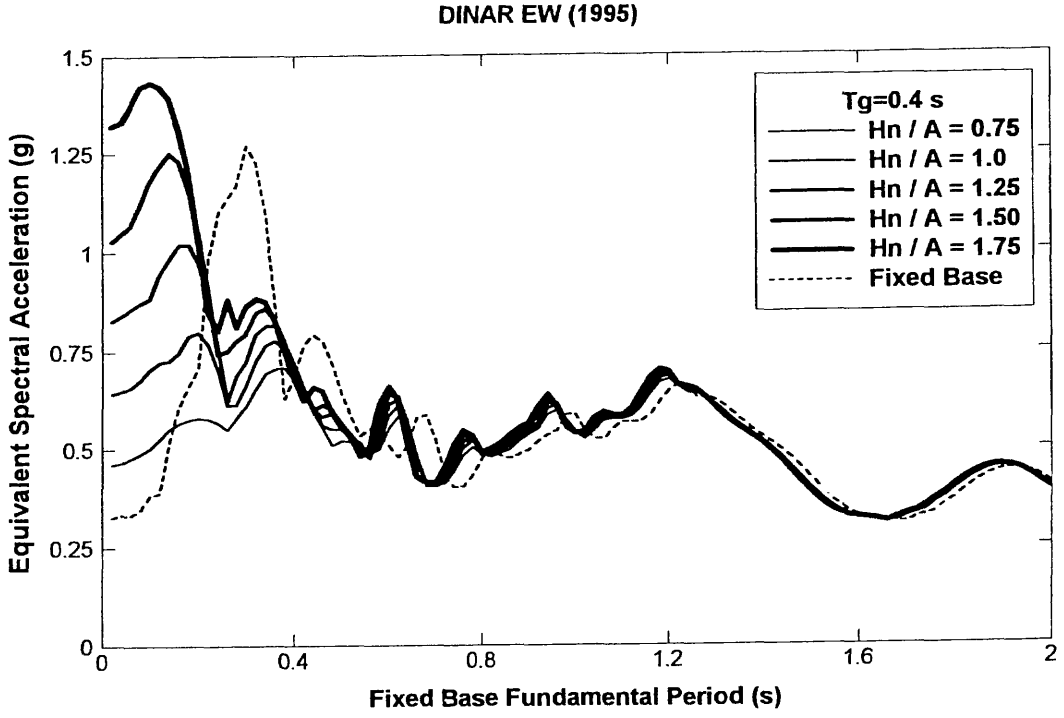

Figure 8. Equivalent (modified) pseudo-acceleration spectra under Dinar Earthquake (1995) EW component for fictitious soil period of $T_g = 0.4$ s and varying aspect ratio

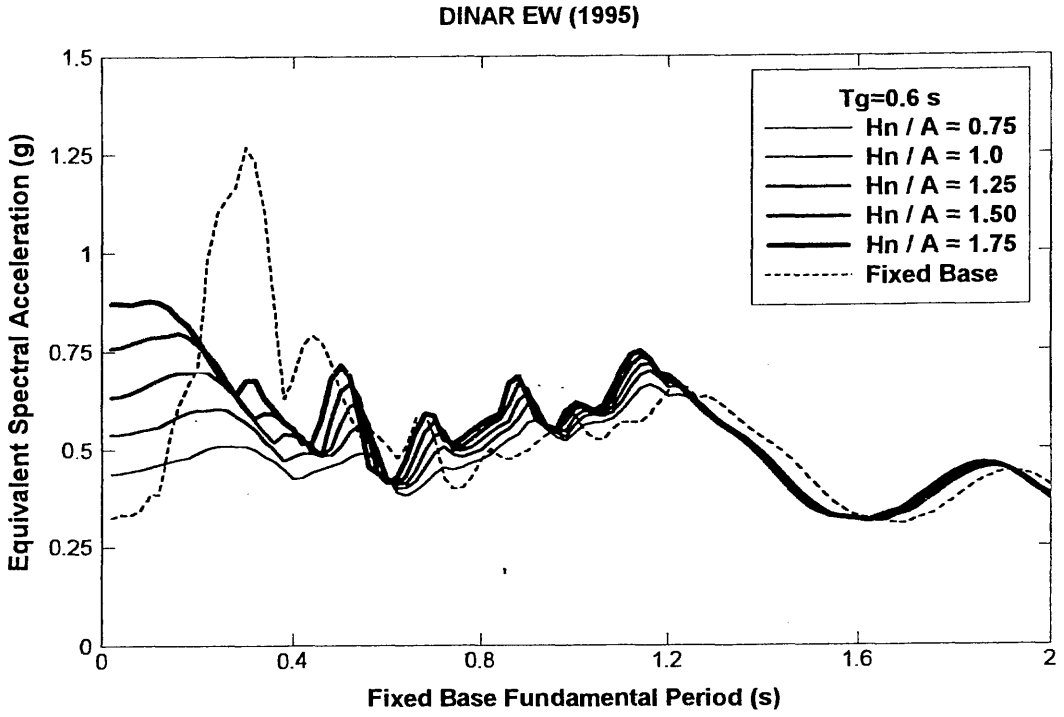

Figure 9. Equivalent (modified) pseudo-acceleration spectra under Dinar Earthquake (1995) EW component for fictitious soil period of $T_g = 0.6$ s and varying aspect ratio

APPENDIX : FORMULATION OF SOIL-STRUCTURE INTERACTION FOR BUILDINGS

Referring to Fig.1, equations of motion of a building system with a rigid foundation can be expressed in the frequency domain as (Aydınoğlu 1980, Wolf 1985),

$$[K]\{u\} = \{P\} \tag{A1a}$$

where,

$$\{u\}^T = <\{\delta_s\}^T \quad \{u^t_o\}^T> \tag{A1b}$$

$$[K] = \begin{bmatrix} ([K_{ss}] + i\omega[C_{ss}] - \omega^2[M_{ss}]) & -\omega^2[M_{ss}][T_{so}] \\ -\omega^2[T_{so}]^T[M_{ss}] & ([S^g_{oo}] - \omega^2[M_{oo}]) \end{bmatrix} \tag{A1c}$$

$$\{P\}^T = <\{0\}^T \quad \{P_o\}^T> \quad ; \quad \{P_o\} = [S^g_{oo}]\{u^g_o\} \tag{A1d}$$

in which ω denotes excitation frequency, $[K_{ss}]$, $[C_{ss}]$, $[M_{ss}]$ represent structural property matrices, $\{u^g_o\}$ refers to the effective foundation input motion and $\{\delta_s\}$ represents the structure's horizontal displacement vector relative to the rigid foundation (Fig.1). Since 2-D response of the soil-structure system is considered to exclude vertical and torsional response, total displacement vector of the rigid foundation, $\{u^t_o\}$, includes horizontal and rocking degrees of freedom only, as indicated in Fig.1:

$$\{u^t_o\}^T = <u^t_x \quad \theta> \tag{A2}$$

Dynamic stiffness matrix of the rigid foundation, $[S^g_{oo}]$, is expressed as,

$$[S^g_{oo}] = G_g a \begin{bmatrix} S_{xx} & aS_{x\theta} \\ aS_{\theta x} & a^2S_{\theta\theta} \end{bmatrix} \tag{A3}$$

where G_g refers to shear modulus of the soil (ground) material, **a** denotes the half length (or radius) of the rigid rectangular (or circular) raft foundation in the direction of earthquake excitation, and S_{xx}, $S_{x\theta}=S_{\theta x}$, $S_{\theta\theta}$ are complex, frequency dependent, nondimensional stiffness coefficients.

In Eq.A1, $[T_{so}]$ represents kinematic transfer matrix relating the rigid part of the total motion of superstructure to the degrees of freedom of the foundation which can be expressed as (Fig.1),

$$[T_{so}]^T = \begin{bmatrix} 1 & 1 & . & . & 1 & . & . & 1 \\ H_1 & H_2 & . & . & H_i & . & . & H_n \end{bmatrix} \tag{A4}$$

where H_i refers to the height of the i'th storey measured from the level soil-foundation interface. Further in **In Eq.A1**, total foundation mass matrix, $[M_{oo}]$, is expressed as,

$$[M_{oo}] = [M^f_{oo}] + [T_{so}]^T[M_{ss}][T_{so}] \tag{A5}$$

in which $[M^f_{oo}]$ denotes the mass matrix of the foundation itself:

$$[M^f_{oo}] = \varepsilon M_s \begin{bmatrix} 1 & 0 \\ 0 & a^2/3 \end{bmatrix} \quad \text{(A6)}$$

where thickness of the raft foundation is neglected and ε denotes the ratio of the foundation mass to the total mass of the superstructure, M_s. The latter is expressed as,

$$M_s = \sum_{i=1}^{n} m_i \quad \text{(A7)}$$

in which m_i represents typical storey mass (Fig.1). By taking $[M_{ss}]$ as a diagonal (lumped) mass matrix, the second term of **Eq.A5** can be written in an open form as,

$$[T_{so}]^T [M_{ss}] [T_{so}] = \begin{bmatrix} \sum_{i=1}^{n} m_i & \sum_{i=1}^{n} (m_i H_i) \\ \sum_{i=1}^{n} (m_i H_i) & \sum_{i=1}^{n} (m_i H_i^2) \end{bmatrix} \quad \text{(A8)}$$

or above expression can be simplified as,

$$[T_{so}]^T [M_{ss}] [T_{so}] = M_s \begin{bmatrix} 1 & \eta_{x\theta} H_n \\ \eta_{\theta x} H_n & \eta_{\theta\theta} H_n^2 \end{bmatrix} \quad \text{(A9)}$$

It is obvious that for a single storey building with total mass concentrated at the top $\eta_{x\theta} = \eta_{\theta x} = \eta_{\theta\theta} = 1$, and in the special case of uniformly distributed mass along the building height, $\eta_{x\theta} = \eta_{\theta x} = 1/2$ and $\eta_{\theta\theta} = 1/3$.

Transformation to Modal Coordinates

$\{\delta_s\}$ in **Eq.A.1** can be expressed in terms of modal coordinates of the fixed base structure as,

$$\{\delta_s\} = [\Phi]\{Y_s\} \quad \text{(A10)}$$

in which $\{Y_s\}$ refers to the vector of modal coordinates and $[\Phi]$ represents mass-normalised mode-shape matrix, i.e.,

$$[\Phi]^T [M_{ss}] [\Phi] = [I] \quad \text{(A11a)}$$

Thus for a typical r'th mode,

$$\{\Phi_r\}^T [K_{ss}] \{\Phi_r\} = \Omega_r^2 \quad \text{(A11b)}$$

$$\{\Phi_r\}^T [C_{ss}] \{\Phi_r\} = 2\xi_r \Omega_r \quad \text{(A11c)}$$

in which Ω_r and ξ_r denote r'th mode natural frequency and modal damping factor of the fixed base structure. Substituting **Eq.A10** into **Eq.A1** and premultiplying the first row by $[\Phi]^T$ yields the transformed equations of motion as follows:

$$[K_R]\{u_R\} = \{P\} \tag{A12a}$$

where force vector given by **Eq.A.1d** remains unchanged and the displacement vector takes the form,

$$\{u_R\}^T = <\{Y_s\}^T \quad \{u^t_o\}^T> \tag{A12b}$$

with transformed dynamic stiffness matrix as,

$$[K_R] = \begin{bmatrix} [R] & -\omega^2[L] \\ -\omega^2[L]^T & ([S^g_{oo}] - \omega^2[M_{oo}]) \end{bmatrix} \tag{A12c}$$

where [L] represents the "*modal participation matrix*" which is expressed as,

$$[L] = [\Phi]^T [M_{ss}] [T_{so}] \tag{A13}$$

and [R] is a diagonal matrix whose r'th mode element is,

$$R_r = \Omega_r^2 - \omega^2 + 2i\,\omega\,\xi_r\Omega_r \tag{A14}$$

Solving for $\{Y_s\}$ from the first row of **Eq.A12** yields;

$$\{Y_s\} = \omega^2[R]^{-1}[L]\{u^t_o\} = [D][L]\{u^t_o\} \tag{A15}$$

in which diagonal matrix [D] and its typical element corresponding to r'th mode are defined as,

$$[D] = \omega^2[R]^{-1} \tag{A16a}$$

$$D_r = \beta_r^2 / (1 - \beta_r^2 + 2i\,\xi_r\beta_r) \tag{A16b}$$

where normalised frequency β_r is defined as $\beta_r = \omega / \Omega_r$. Actually **Eq.A16b** represents the complex frequency response of a fixed-based single-degree-of-freedom system with natural frequency Ω_r subjected to a ground motion with unit displacement amplitude and frequency of ω.

Substituting **Eq.A15** into the second row of **Eq.A12** or in other words by condensing out the modal coordinates of the superstructure from **Eq.A12** yields;

$$[E_{oo}]\{u^t_o\} = [S^g_{oo}]\{u^g_o\} \tag{A17}$$

in which condensed dynamic stiffness matrix, $[E_{oo}]$, is expressed as,

$$[E_{oo}] = [S^g_{oo}] - \omega^2([M_{oo}] + [L]^T[D][L]) \tag{A18}$$

The term $[L]^T[D][L]$ included in above can be expressed in an open form as,

$$[L]^T[D][L] = \begin{bmatrix} \sum_{r=1}^{n} D_r L_{xr}^2 & \sum_{r=1}^{n} D_r L_{xr}^2 h_r \\ \sum_{r=1}^{n} D_r L_{xr}^2 h_r & \sum_{r=1}^{n} D_r L_{xr}^2 h_r^2 \end{bmatrix} \quad \text{(A19)}$$

in which L_{xr} represents the participation factor and L_{xr}^2 the participating mass of the fixed base structure for the r'th mode. The former can be expressed as,

$$L_{xr} = \sum_{i=1}^{n} (m_i \Phi_{ir}) \quad \text{(A20)}$$

In **Eq.A19**, h_r refers to the centre of effective seismic forces in the r'th mode of the fixed-based structure measured from the level of soil-foundation interface:

$$h_r = (1 / L_{xr}) \sum_{i=1}^{n} (m_i \Phi_{ir} H_i) \quad \text{(A21)}$$

After **Eq.A17** is solved for $\{u^t_o\}$, relative structural displacement vector can be determined by utilising **Eqs.A10** and **A15** as,

$$\{\delta_s\} = [\Phi][D][L]\{u^t_o\} \quad \text{(A22)}$$

First Mode Approximation

It is well known that soil-structure interaction effect is dominantly pronounced in the first vibration mode, and the higher modes can be taken into account without soil-structure interaction considered. In this case **Eq.A19** can be written as,

$$[L]^T[D][L] = D_1 L_{x1}^2 \begin{bmatrix} 1 & h_1 \\ h_1 & h_1^2 \end{bmatrix} \quad \text{(A23)}$$

Since participating mass of the structure in the first vibration mode is a fraction of the total mass, a new parameter λ_1 can be defined as:

$$L_{x1}^2 = \lambda_1 M_s \quad \text{(A24)}$$

On the other hand the location of the resultant of seismic forces in the first mode can be expressed in terms of a new parameter γ_1 as,

$$h_1 = \gamma_1 H_n \quad \text{(A25)}$$

Thus,

$$[L]^T[D][L] = D_1 \lambda_1 M_s \begin{bmatrix} 1 & \gamma_1 H_n \\ \gamma_1 H_n & \gamma_1^2 H_n^2 \end{bmatrix} \quad \text{(A26)}$$

SSI Parameters

In addition to above defined system parameters, the following are the well known independent, nondimensional parameters of soil-structure interaction:

$$\alpha = H_n / a \qquad \text{(A27a)}$$

$$\delta = M_s / (\rho_g a^3) \qquad \text{(A27b)}$$

$$s = \Omega_1 H_n / V_{sg} \qquad \text{(A27c)}$$

where ρ_g and V_{sg} represent the mass density and the shear wave velocity of the soil medium (ground), respectively ($G_g = \rho_g V^2_{sg}$). Nondimensional frequency parameter $a_o = \omega a / V_{sg}$ can now be expressed in terms of above defined parameters as,

$$a_o = \beta_1 s / \alpha \qquad \text{(A28)}$$

For the special case of surface foundations and vertically propagating shear waves, foundation input motion is expressed as,

$$\{u^g_o\}^T = < u^g_x \quad 0 > \qquad \text{(A29)}$$

By defining a new variable, u_θ, as

$$u_\theta = \theta H_n \qquad \text{(A30)}$$

Eq.A17 can now be modified as

$$[I_{oo}] < u^t_x \quad u_\theta >^T = \{Q_o\} \qquad \text{(A31)}$$

and the elements of $[I_{oo}]$ and $\{Q_o\}$ are then expressed in terms of the above defined independent, nondimensional parameters, as follows:

$$I_{xx} = S_{xx} - \delta a_o^2 (1 + \varepsilon + \lambda_1 D_1) \qquad \text{(A32a)}$$

$$I_{x\theta} = I_{\theta x} = S_{x\theta} / \alpha - \delta a_o^2 (\eta_{x\theta} + \gamma_1 \lambda_1 D_1) \qquad \text{(A32b)}$$

$$I_{\theta\theta} = S_{\theta\theta} / \alpha^2 - \delta a_o^2 [\eta_{\theta\theta} + \varepsilon / (3\alpha^2) + \gamma_1^2 \lambda_1 D_1] \qquad \text{(A32c)}$$

$$Q_x = S_{xx} u^g_x \qquad \text{(A33a)}$$

$$Q_\theta = (S_{\theta x} / \alpha) u^g_x \qquad \text{(A33b)}$$

For surface foundations, coupling term of the foundation stiffness matrix, $S_{\theta x}$, may be omitted and hence $Q_\theta = 0$. In this case, solution of **Eq.A31** yields;

$$u^t_x = S_{xx} I_{\theta\theta} / (I_{xx} I_{\theta\theta} - I_{x\theta}^2) u^g_x \qquad \text{(A34a)}$$

$$u_\theta = -S_{xx} I_{x\theta} / (I_{xx} I_{\theta\theta} - I_{x\theta}^2) u^g_x \qquad \text{(A34b)}$$

Study on Strong Ground Motions for the Application to Seismic Design of Structures -Semi-empirical Method for Ground Motion Estimation and Non-linear Response Spectra-

Keiichi Tamura[1], Yoshihiro Nakao[2] and Riki Honda[3]

Abstract: The extremely strong ground motion generated by the Hyogoken Nanbu (Kobe) Earthquake caused serious damage to many kinds of structures. The destructive ground motions in near field generated by the intra-plate inland earthquake were attributed to the damage.

Recently semi-empirical method has been noted as the method synthesizing ground motions including such strong motions in near field. Various earthquake source parameters have to be determined for this synthesis, however it is very difficult to evaluate them with sufficient accuracy. The effects of these parameters with expected variation on the estimated ground motions have to be evaluated for the application of semi-empirical method to seismic design. In this paper firstly studied are the effects of the source parameters on the estimated ground motions.

Under the extremely strong ground motions in near field such as generated by the Kobe Earthquake, structures behave inelastically. The ground motion characteristics which affect the inelastic response of structures should be considered when the seismic design force and input ground motion for seismic design are discussed. Secondary studied in this paper are the effects of ground motion characteristics on the inelastic response of structures.

1. Introduction

In the early morning of January 17, 1995, the Hyogoken-Nanbu(Kobe) Earthquake occurred causing serious damage to many kinds of structures. Although its magnitude was relatively moderate (Mj=7.2, Mj is Japan Meteorological Agency (JMA) Magnitude), extremely strong ground motions were generated. Its causative faults reached inland areas though the epicenter was located in the Akashi strait north of Awaji Island, which was unusual because most of the past large earthquakes in Japan were inter-plate earthquakes and therefor the causative faults were in the ocean areas. The destructiveness of the intra-plate inland earthquake was obviously attributed to its extremely strong ground motions in near field, and records from the earthquake proved it. Many records show large peak acceleration and large response spectra. One of such records was obtained at Kobe Maritime Observatory of JMA (hereinafter described as JMA Kobe), whose peak acceleration was larger than 800 cm/sec^2 and the peak of the acceleration response spectra (damping h=5%) of the horizontal components was no less than 2g.

Ground motions generated by intra-plate inland earthquakes such as the Kobe Earthquake are near field ground motions, which have different characteristics from those by inter-plate earthquakes in strengths and frequency characteristics. From the serious damage to many structures caused by extremely strong ground motions from the Kobe Earthquake, it was recognized that 1) Near field ground motion estimation techniques should be improved and 2) Inelastic behavior of structures under extremely strong ground motions should be considered for rational seismic design.

1) Ground motion estimation technique in near field

Semi-empirical method has been noted as an effective technique for synthesizing near field ground motions. Various earthquake source parameters such as fault length, width and dislocation rise time have to be determined for this synthesis, however it is very difficult to determine these parameters with sufficient accuracy. Effects of source parameters with expected variation on the estimated ground motions should be

1) Head, Ground Vibration Division, Public Works Research Institute, Ministry of Construction, Dr.Eng

2) Research Engineer, Ground Vibration Division, Public Works Research Institute, Ministry of Construction, M.Eng

3) Research Associate, Dynamics of Foundation Structures, Disaster Prevention Research Institute, Kyoto UNIV, M.Eng.

evaluated when the technique is applied to seismic design. In this paper the ground motion at JMA Kobe from the Kobe Earthquake is estimated using source models which have fault parameters varied within expected range, and the extent of the estimated ground motion variation is evaluated.

2) Seismic force and input ground motion for seismic design considering inelastic behavior of structures

There are limits to the extent to which simply strengthening structural members resists extremely strong ground motions. Energy absorption capacity should be improved by ensuring allowable appropriate displacement ductility.

Therefore it is important to study ground motion characteristics which have effects on nonlinear response of structures so that they can be incorporated into seismic design force and input ground motion for seismic design.

This paper presents the effects of ground motions on inelastic behavior of structures using strength reduction factor spectra and the ground motion characteristics which contributes to the effects.

2. Effects of variation of source parameters on estimated ground motions

(1) Ground motion synthesis method using earthquake source model

Ground motions in short and long period ranges are generated by semi-empirical and theoretical methods, respectively. Then, ground motions in short and long period ranges are integrated into a ground motion in wide period range.

(2) Semi-empirical method

In semi-empirical method ground motion records from small events such as foreshocks and aftershocks with their hypocenters near the fault area of a large event are utilized as Green's functions to estimate a ground motion from the large event (Fig. 1). The fault plane is divided into subfaults as large as the fault size of the small events. The Green's functions are summed up considering time delays due to fault ruptures from hypocenter to subfaults and wave traveling from each subfault to an estimation point. Semi-empirical method can estimate short period component of ground motion, which are strongly affected by delicate underground structures on wave propagation path, because the Green's functions include complex effects of the dynamic rupture process on the fault, heterogeneous structures around the source and an estimation point.

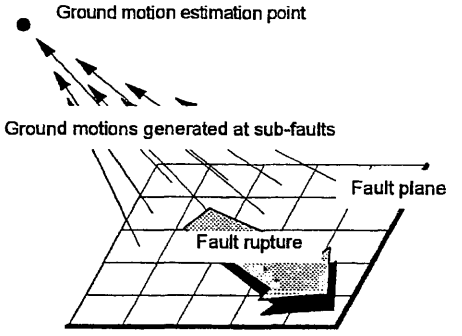

Fig. 1 Semi-empirical method

Temporal and spatial variations of dislocation are considered by utilizing proper function T_{mn} and weight function ω_{mn}, respectively (eqs. (1),(2)).

$$U(\omega)=\sum_{m=1}^{N}\sum_{n=1}^{N}\frac{R_0}{R_{mn}}T_{mn}(\omega)\omega_{mn}u_0(\omega)\exp(-i\omega\tau_{mn}) \quad (1)$$

where,

T_{mn} : Function representing the difference in source time function between small and large events.

ω_{mn} : Weight function representing spatial variation of dislocation

u_0 : Frequency component of ground motion from small event

R_{mn} : Radiation pattern coefficient of the ground motion generated at subfault

R_0 : Radiation pattern coefficient of the ground motion from a small event

τ_{mn} : Time delay due to fault rupture from hypocenter to subfaults and wave traveling from subfaults to the estimation point.

N : Number of subfaults

$$T_{mn}(\omega) = N \exp\left[-i\left(\frac{\omega\tau}{2} - \frac{\omega\tau}{2NN_1}\right)\right] \frac{\dfrac{\sin\dfrac{\omega\tau}{2}}{\dfrac{\omega\tau}{2}}}{\dfrac{\sin\dfrac{\omega\tau}{2NN_1}}{\dfrac{\omega\tau}{2NN_1}}}$$

$$+ N \sum_{k=1}^{N} \frac{d_k - d_{k-1}}{D} \exp\left[-i\omega(k-1)\frac{\tau}{NN_1}\right] \qquad (2)$$

D : Dislocation

d_k : Temporal valiation of dislocation at the time of $k\Delta\tau$ (Fig. 2)

N_1 : Coefficient to avoid the synthetically generated periodicity

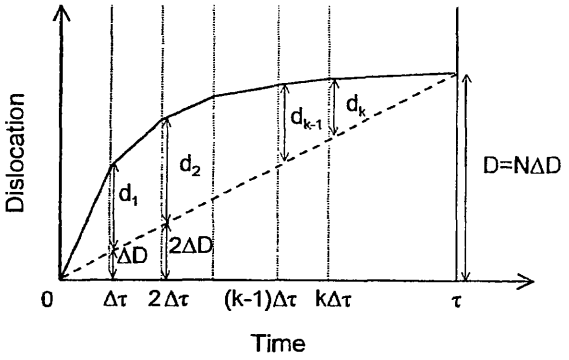

Fig. 2 Source time function

(3) Theoretical method

Long period component of a ground motion is estimated by theoretical method in which the solution for the elastdynamic Green's function in homogeneous, isotropic, unbounded medium is used as waves generated at subfaults. Ground motions from all subfaults are summed up considering time delay due to fault rupture from hypocenter to each subfault and wave traveling from each subfault to the estimation point.

(4) Combination of long period and short period components of ground motions

Ground motions estimated by semi-empirical and theoretical methods are combined by eq. (3), using high-pass and low-pass filters(Fig. 3).

$$u(\omega) = f_H(\omega) \cdot u_E(\omega) + f_L(\omega) \cdot u_T(\omega) \qquad (3)$$

where,

$$f_H(\omega) = \begin{cases} 0 & \cdots\cdots \omega < \dfrac{\omega 0}{n} \\ \dfrac{1}{2} + \dfrac{1}{2}\sin\left(\dfrac{\pi}{2} \cdot \dfrac{\ln(\omega) - \ln(\omega_0)}{\ln(n)}\right) & \cdots \dfrac{\omega 0}{n} \le \omega \le n\omega 0 \\ 1 & \cdots\cdots n\omega 0 < \omega \end{cases}$$

$$f_L(\omega) = \begin{cases} 1 & \cdots\cdots \omega < \dfrac{\omega 0}{n} \\ \dfrac{1}{2} - \dfrac{1}{2}\sin\left(\dfrac{\pi}{2} \cdot \dfrac{\ln(\omega) - \ln(\omega_0)}{\ln(n)}\right) & \cdots \dfrac{\omega 0}{n} \le \omega \le n\omega 0 \\ 0 & \cdots\cdots n\omega 0 < \omega \end{cases}$$

$f_H(\omega)$: High-pass filter

$f_L(\omega)$: Low-pass filter

$u_E(\omega)$: ω component of the ground motion by semi-empirical method

$u_T(\omega)$: ω component of the theoretical ground motion

$n, \omega 0$: Coefficients to determine the shape of filters

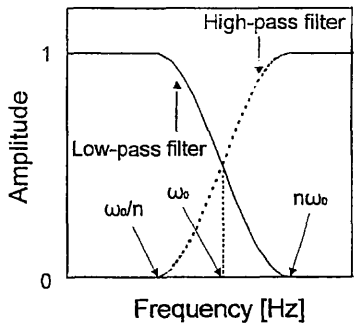

Fig. 3 Pass filters

(5) Target ground motion and earthquake source parameters

Ground motions at JMA Kobe from the Kobe Earthquake with Mj=7.2 are synthesized. Basic earthquake source parameters such the location, strike and dip angle of the event are determined on the basis of the source model proposed by Kikuchi (1995) for the Kobe Earthquake, which are shown in Fig. 4. Other source parameters such as fault length, width and dislocation rise time are determined by regressing the source parameters deduced for past earthquakes whose magnitudes(Mj) were 6 or greater, which occurred after the 1923 Kanto Earthquake. In the case that there are some source models deduced for an earthquake, the most credible source model is adopted to the regression analysis. Standard deviations are given to source parameters

as expected variation ranges. Fig. 5 shows relationship between magnitude and earthquake source parameters which were deduced for past earthquakes. Table 1 shows the source parameters determined for the Kobe Earthquake (Mj=7.2) by the regression analysis and standard deviations.

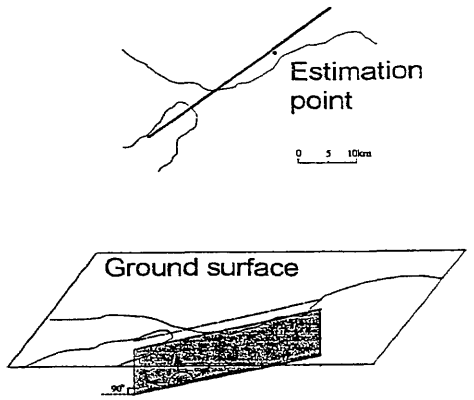

Fig. 4 Earthquake source model for the Kobe Earthquake

Table 1 Source parameters by regression analysis

Earthquake source parameter	Determined Parameter for Mj=7.2	Standard deviations	
		$+\sigma$	$-\sigma$
Fault length(km)	40.0	×1.68 (67.2)	×1/1.68 (23.8)
Fault width(km)	27.4	×1.71 (47.0)	×1/1.71 (16.0)
Dislocation(m)	1.56	×1.67 (2.60)	×1/1.67 (0.93)
Rise time(sec)	2.28	×1.75 (3.99)	×1/1.75 (1.30)
Fault rupture velocity (km/s)	3.22	×1.29 (4.15)	×1/1.29 (2.50)
Dislocation velocity(m/s)	—	×2.2	×1/2.2

Ground motions are computed with various source models shown in Table 2. Case1 is the basic case using source parameters determined for an earthquake with Mj=7.2 by regression analysis. In this case the source time function proposed by Irikura (1986) is assumed for semi-empirical method and the ramp function is assumed for theoretical method as its source time function(Fig. 6). Cases2 to 27 are cases in which source parameters are varied.

In contrast with Case1 in which radial rupture process from fault center is assumed, the focus and the rupture process are varied in Cases12 to 18.

Case19 is a source model which adds spatial variation of dislocation to Case1 on the basis of the

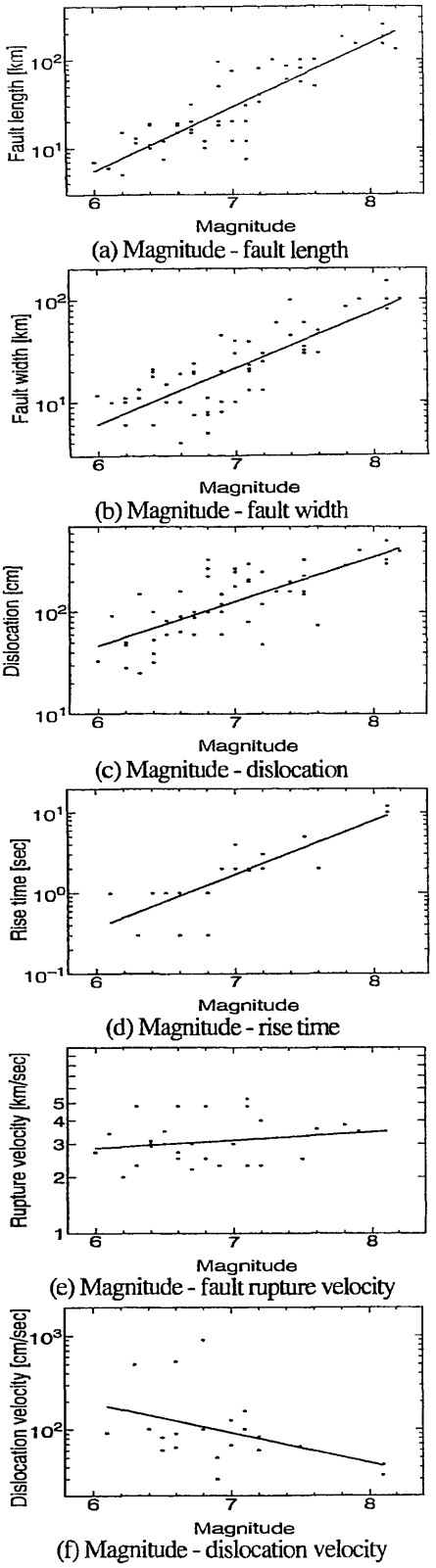

Fig. 5 Relationship between magnitude and various parameters

source model by Sekiguchi et al.(1996). Case20 employs the source time function proposed by Irikura(1986) for both semi-empirical and theoretical methods. Case21 and Case22 are derived from Case20 by changing the initial slope of the source time function by standard deviation of dislocation velocity (Table 1). Fig. 6 shows the initial slopes varied from the source time function by Irikura (1986). In Cases23 to 26 the fault plane is divided into A, B, C and D parts (Fig. 7). Temporal and spatial variations of dislocation shown in Fig. 8 are adopted in Cases23 to 26. In Case27 the ramp function is assumed for both semi-empirical and theoretical methods. Temporal variation of dislocation is not considered in Case27.

Table 2 Source model cases

Model name	Contents
Case1	Basic Case The ramp function is assumed for semi-empirical method (Fig. 6). The source time function by Irikura (1986) is assumed for theoretical method (Fig. 6). Radial fault rupture extends from the fault center.
Case2	Variation of Case1 in fault length by $+\sigma$
Case3	Variation of Case1 in fault length by $-\sigma$
Case4	Variation of Case1 in fault width by $+\sigma$
Case5	Variation of Case1 in fault width by $-\sigma$
Case6	Variation of Case1 in rise time by $+\sigma$
Case7	Variation of Case1 in rise time by $-\sigma$
Case8	Variation of Case1 in dislocation by $+\sigma$
Case9	Variation of Case1 in dislocation by $-\sigma$
Case10	Variation of Case1 in rupture velocity by $+\sigma$
Case11	Variation of Case1 in rupture velocity by $-\sigma$
Case12	Variation of Case1 in rupture start point. Radial rupture extends from southwest upper corner.
Case13	Variation of Case1 in rupture start point. Radial rupture extends from southwest lower corner.
Case14	Variation of Case1 in rupture start point. Radial rupture extends from northeast upper corner.
Case15	Variation of Case1 in rupture start point. Radial rupture extends from northeast lower corner.
Case16	Variation of Case1 in rupture process. Unilateral rupture extends from southwest.
Case17	Variation of Case1 in rupture process. Unilateral rupture extends from northeast.
Case18	Variation of Case1 in rupture process. Bilateral rupture extends from fault center.
Case19	Spatial variation of dislocation is given to Case1 on the basis of Sekiguchi model.
Case20	The source time function by Irikura(1986) is given to Case1 (Fig.6). The source time function is assumed for semi-empirical and theoretical methods.
Case21	$+\sigma$ dislocation velocity (Fig.6) is given to Case20.
Case22	$-\sigma$ dislocation velocity (Fig.6) is given to Case20.
Case23	$+\sigma$ and $-\sigma$ dislocations are given to A, D and B, C parts of Case 1 model, respectively.
Case24	$-\sigma$ and $+\sigma$ dislocations are given to A, D and B, C parts of Case 1 model, respectively.
Case25	$+\sigma$ and $-\sigma$ dislocation velocities(Fig.6) are given to A, D and B, C parts of Case 1 model, respectively.
Case26	$-\sigma$ and $+\sigma$ dislocation velocities(Fig.6) are given to A, D and B, C parts of Case 1 model, respectively
Case27	The ramp function (Fig.6) is given to Case20 as its source time function.

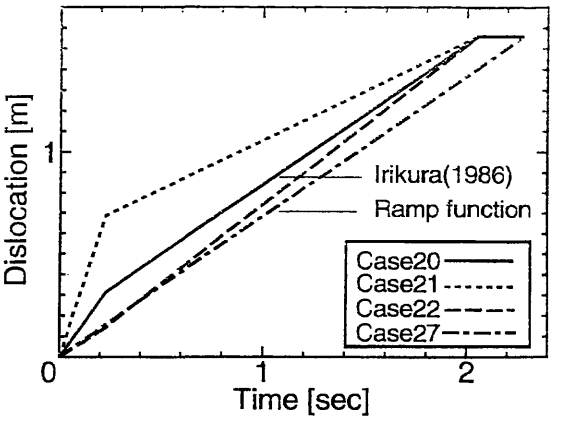

Fig. 6 Source time function

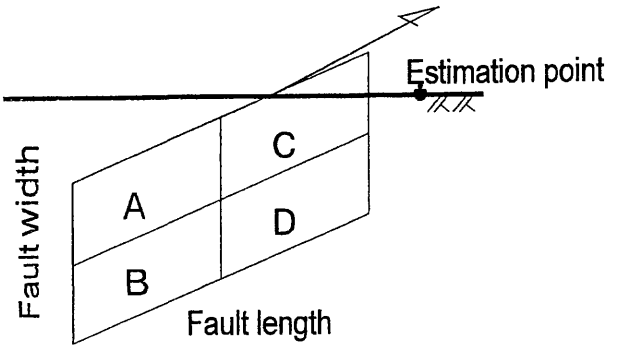

Fig. 7 A, B, C and D parts of the fault plane

A $+\sigma$ dislocation	C $-\sigma$ dislocation
B $-\sigma$ dislocation	D $+\sigma$ dislocation

(a)Case 23 (spatial variation of dislocation is considered)

Figs. 8(1) Cases 23 to 26

A $-\sigma$ dislocation	C $+\sigma$ dislocation
B $+\sigma$ dislocation	D $-\sigma$ dislocation

(b) Case 24 (spatial variation of dislocation is considered)

A $+\sigma$ dislocation velocity	C $-\sigma$ dislocation velocity
B $-\sigma$ dislocation velocity	D $+\sigma$ dislocation velocity

(c) Case 25 (temporal variation of dislocation is considered.)

A $-\sigma$ dislocation velocity	C $+\sigma$ dislocation velocity
B $+\sigma$ dislocation velocity	D $-\sigma$ dislocation velocity

(d) Case 26 (temporal variation of dislocation is considered.)

Figs. 8(2) Cases 23 to 26

(6) Effects of Source Parameters on estimated ground motion

An aftershock ground motion (Mj=5.2) of the Kobe Earthquake is used as a Green's function to synthesize a main shock motion. Fig. 9 shows acceleration response spectra (damping h=0.05) of estimated ground motions. To study the extent of estimated ground motion variation, Fig. 10 presents the ratio of the maximum spectral value to the minimum one for each natural period, in which source parameters are varied. The effects of source parameters on estimated ground motion are summarized as follows.

1) Fault length, width, rise time, dislocation, rupture velocity

The ground motion component longer than 0.6 sec decreases as fault length, width or rise time is increased by standard deviation, while it increases as dislocation is increased (Figs. 9(a)-(d)). Ground motion component longer than 0.6 sec is affected more than shorter period component by variation of fault length, rise time. dislocation and rupture velocity (Fig. 10(a), (c), (d), (e)). Fig. 10(c) shows that variation of rise time has less effects on estimated ground motion than another parameters.

2) Rupture process

In the cases that rupture extends unilaterally or bilaterally, or focus is located at an upper corner, acceleration response longer than 1.5 sec varies from 30 to 50 % of the another cases and long period component is affected more than short period component(Fig. 9(f)). Differences in rupture start points and rupture process have large effects on component longer than 0.7 sec(Fig. 10(f)).

3) Temporal and spatial variation of dislocation

In contrast to Case1, spatial variation of dislocation is assumed in Case 19, 23 and 24. Considering spatial variation of dislocation increases ground motion component longer than 0.7 sec(Fig. 9(g)). Spatial variation of dislocation has larger effects on ground motion component above 0.5 sec than component under 0.5 sec (Fig. 10(g)). The effects of spatial variation of dislocation on estimated ground motions are large as compared with fault length, width, rise time, dislocation and rupture velocity (Fig. 10(a)-(e),(g)).

Different temporal variations of dislocation are assumed in Cases1, 20, 21 and 22. Similar assumptions are adopted in Cases 25 and 26. Comparison of Case27, in which temporal variation of dislocation is not considered, and other Cases in Fig.9 (h) shows that temporal variation of dislocation increases ground motion component in wide period range, especially ground motion component shorter than 0.5 sec (Fig.10(h)). Note that the temporal variation is not assumed for the long period component of Case1. The source time function used in Case27 is not thought to be proper practically because of the small short period component of the estimated ground motion. Among Cases 20 to 22 ground motion increases when initial slope of source time function increases. Consideration of the temporal variation has greater effects on ground motion than the differences in initial slopes of source time function which are assumed in this paper (Fig.

9(h)).

(7) Conclusion

Ground motion at JMA Kobe from the Kobe Earthquake is estimated. Effects of variation of various parameters on the estimated ground motions are studied. The variation given to various parameters are determined by past earthquakes. Following conclusions may be deduced from the study.

1) Long period component of ground motion is affected more than short period component by variation of fault length, dislocation, rise time, rupture velocity and rupture process.
2) Spatial variation of dislocation has large effects on ground motion, especially on long period component, as compared with fault length, width, rise time and dislocation.
3) Temporal variation of dislocation increases ground motion in wide period range, especially short period component. When initial slope of source time function is increased, ground motion is also increased. Consideration of the temporal variation has greater effects on ground motion than the differences in initial slopes of source time function which are assumed in this paper.

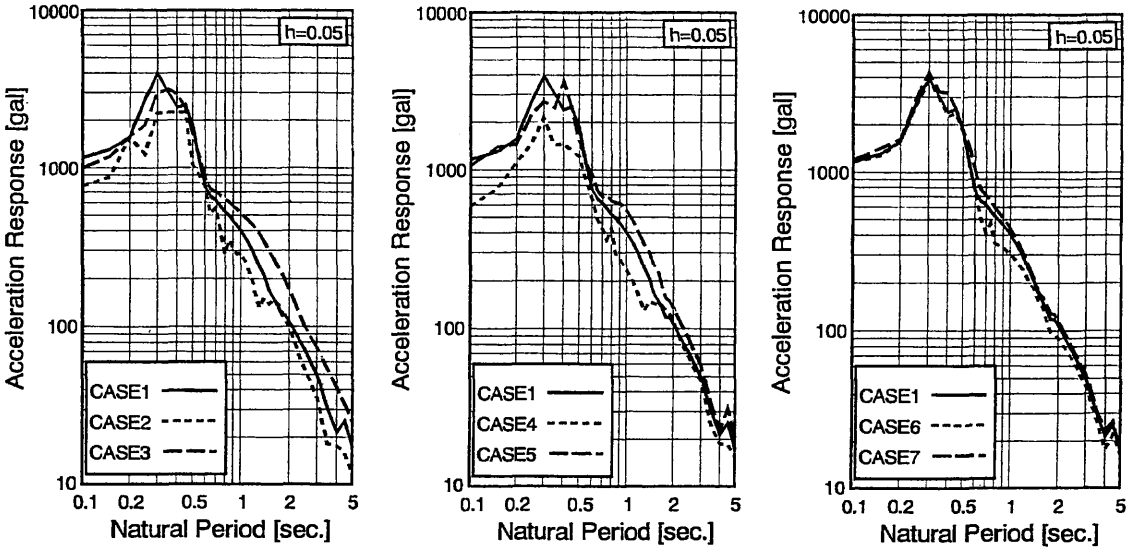

(a)Fault length (b)Fault width (c) Rise time

Fig. 9 (1) Acceleration Response Spectra

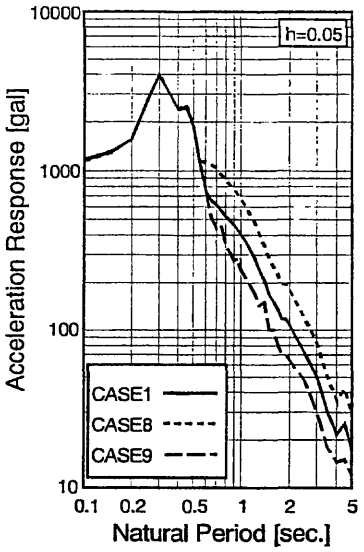

(d)Dislocation

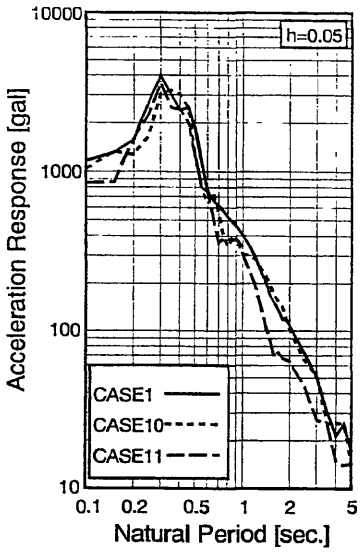

(e) Rupture velocity

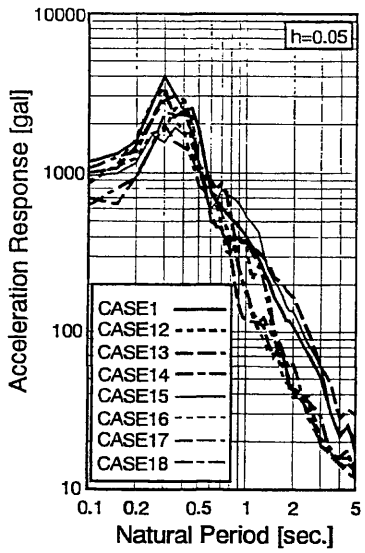

(f) Rupture process

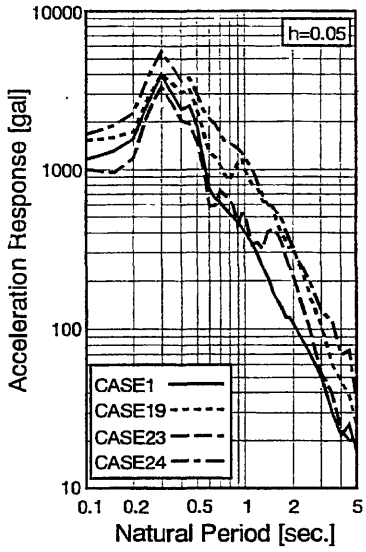

(g) Spatial Variation of Dislocation

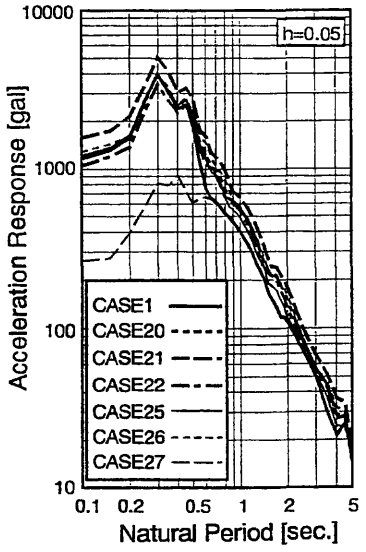

(h) Temporal Variation of Dislocation

Fig. 9 (2) Acceleration Response Spectra

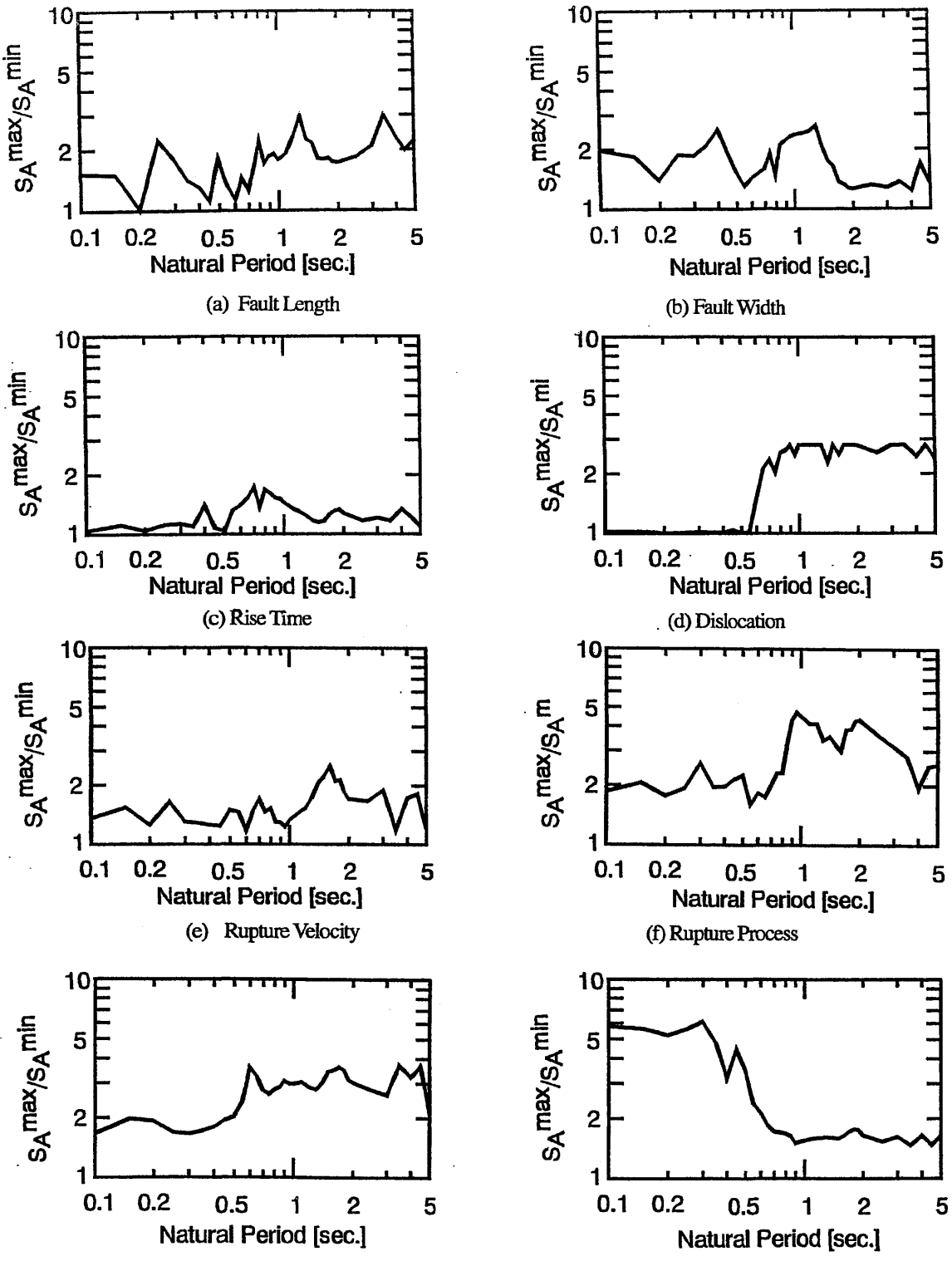

(a) Fault Length

(b) Fault Width

(c) Rise Time

(d) Dislocation

(e) Rupture Velocity

(f) Rupture Process

(g) Spatial Variation of Dislocation

(h) Temporal Variation of Dislocation

Fig. 10 Variation of Acceleration Response

3. The effects of ground motion characteristics on nonlinear response

(1) Evaluation of nonlinear response characteristics of structures

Extremely strong ground motion generated by the Kobe Earthquake, intra-plate inland earthquake, caused serious damage to various structures. Through the investigation of the damage it was realized that seismic design force as large as the ground motion from the Kobe earthquake should be introduced to seismic design. However there are still many unresolved points in the relation between ground motion characteristics and inelastic response of structures. In order to develop rational seismic design force and input ground motion, the effects of ground motion characteristics on inelastic response of structures should be made clear.

In this paper response of an inelastic single-degree-of-freedom(SDOF) system is calculated for ground motions from intra-plate and inter-plate earthquakes and the differences in inelastic response due to ground motion characteristics are discussed using nonlinear response spectra: Strength Reduction Factor Spectra.

(2) Strength Redaction Factor Spectra

In order to evaluate the differences in the inelastic behavior of structures due to ground motion characteristics, strength reduction factor $R\mu$ is calculated. $R\mu$ indicates the possible reduction of the strength of a structure when a certain displacement ductility is allowed, and it is defined as:

$$R\mu = \frac{F_{ye}}{F_{yp}(\mu)} \qquad (4)$$

where,

μ :Predetermined allowable displacement ductility, defined as $\mu = \delta_{max}/\delta_y$

δ_{max} :Peak response displacement of the inelastic system exposed to an imput motion.

δ_y :Yielding displacement of the inelastic system.

F_{ye} :Strength required to prevent the SDOF system from yielding. It corresponds to the force applied to the system when it behaves elastically.

$F_{yp}(\mu)$:Strength required to maintain the displacement ductility smaller or equal to the pre-determined allowable ductility μ.

$R\mu$ can be calculated for arbitrary natural period and therefore it makes spectrum, namely Strength Reduction Factor spectrum ($R\mu$ spectrum).

The concept of $R\mu$ is shown in Fig. 11 and according to energy constant rule it is approximated as:

$$R\mu = \sqrt{2\mu - 1} \qquad (5)$$

Eq. (5) is adopted in the Design Specifications for Highway Bridges in Japan.

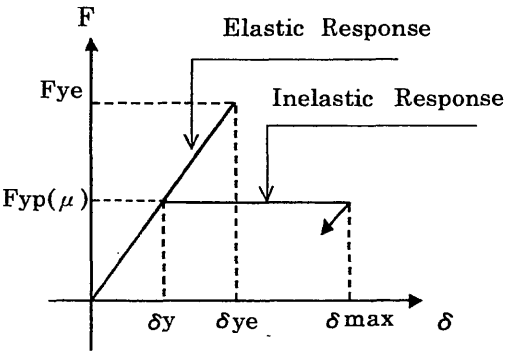

Fig. 11 Concept of $R\mu$

(3) Effects of ground motions from intra-plate and inter-plate earthquakes on inelastic response of structures

A bi-linear system with damping ratio h=5%, whose strength is assumed to be constant after yielding, is adopted for an inelastic single-degree-of-freedom(SDOF) system, and its natural period is evaluated from the initial stiffness.

Fig. 12 shows $R\mu$ spectra for Kaihoku Bridge record and JMA Kobe record. Kaihoku Bridge record is ground motion from the Miyagi-ken Oki Earthquake, inter-plate earthquake, and JMA Kobe record is ground motion from the Kobe Eartquake, intra-plate earthquake. Both records were obtained on the stiff ground.

Comparison of $R\mu$ spectra reveals that $R\mu$ of ground motion from the Kobe Earhquake is small and independent of the allowable ductility μ in relatively short period range and becomes large in the long period range especially for large μ. $R\mu$ spectra of ground motion from the Miyagi-ken Oki Earthquake shows large dependence on allowable ductility μ in the wide natural period range including long natural period range.

(4) Ground motion characteristics having effects on $R\mu$ spectra

1) Ground motion time history

One of the uniqueness of the ground motion characteristics of the Kobe Earthquake is that the motion contains a few relatively long-period spike shaped waves and it may be attributed to the differences mentioned in (3), because similar tendency is observed in the $R\mu$ spectra of a sinusoidal wave. $R\mu$ spectra of a single cycle of sinusoidal wave with a period of 1.0 sec are shown in Fig. 13. It is independent of allowable ductility μ in the short period range, and it becomes large in the long period range, converging $R\mu = \mu$.

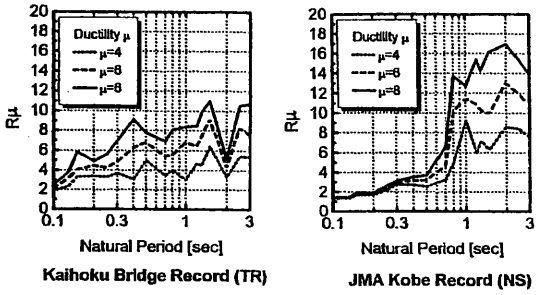

Fig. 12 Difference in $R\mu$ spectra

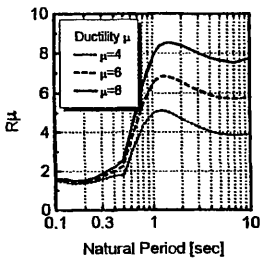

Fig. 13 A single cycle of wave with a period of 1.0 sec

2) Amplitude of ground motion

To study the effects of ground motion characteristics on $R\mu$ spectra, the amplitudes of various frequency components of JMA Kobe record and Kaihoku Bridge record are adjusted so that their 5% damped accelaration response spectra are close to the response spectra shown in Fig. 15. Fig. 16 shows the process of amplitude adjustment. in which phase characteristics are not changed. The spectra shown in Fig. 15 are changed so that long period components are increased in order of line number.

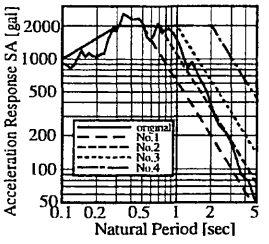

Fig. 15 Target acceleration response

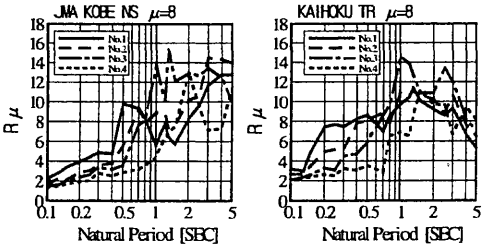

Fig. 17 Variation of $R\mu$ spectra due to long period component of ground motion

$R\mu$ spectra of these adjusted ground motions are shown in Fig. 17. It can be seen that $R\mu$ decleases in the component shorter than 0.7 sec in the order of line number. It indicates that when the long period component of ground motion is increased, $R\mu$ spectra are decreased in the short period range.

(5) Conclusion

Following knowledge is obtained from this study.

1) The effects of ground motion characteristics on inelastic response of structures are evaluated by $R\mu$ spectra.

2) Relatively long-period spike shaped waves in

wave form have effects on $R\mu$ spectrum characteristics.

3) Long period component of ground motion has effects on $R\mu$ spectra in short period range.

Although further research is required, the above-mentioned points should be taken into consideration as the ground motion characteristics which have effects on inelastic behavior of structures, when the seismic design force and input ground motion for seismic design are discussed.

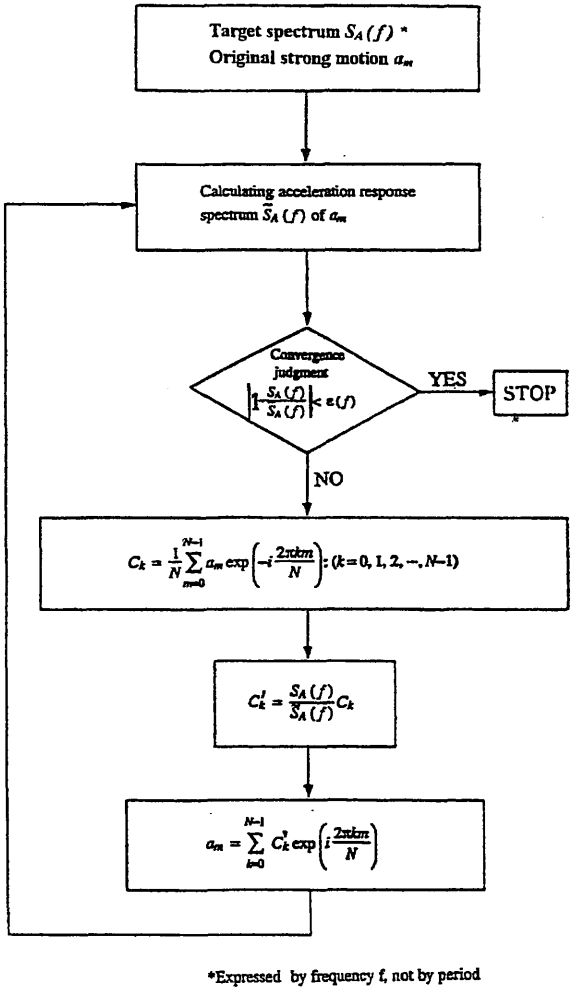

Fig. 16 Process of amplitude adjustment

Acknowledgments

The authors would like to express their gratitude to the personnel engaged in the ground motion data observation for their efforts.

Authors would also like to express their cordial appreciation to Dr. Shojiro Kataoka, Public Works Research Institute, for his informative discussions.

Referencese

1) Aki, K. and P. G. Richards, "Quantitative Seismology", theory and Methods, 1980, W.H. Freeman and Company
2) Irikura, K., "Prediction of strong acceleration motions using empirical Green's function", 1986, Proc. of 7th Japan Earthquake Engineering Symposium.
3) Kamae, K. et al., "A Technique for simulating Strong Ground Motion Using Hybrid Green's Function, 1998, Bulletin of Seismological Society of America
4) Kikuchi, M. , "Source Model For the Kobe Earthquake", 1995, Chishitsu (Geology) News Vol. 486
5) Sato, R., "Japanese Source Parameters Handbook", 1989, Kajima Institute Publishing Co.,Ltd.
6) Sekiguchi, H., "Minute locating of faulting beneath Kobe and the waveform inversion of the source process during the Kobe, Japan, earthquake using strong ground motion records", 1996, J. Phys. Earth, 44
7) Tamura, K. et al, 1997, "Ground Motion Characteristics of the Kobe Earthquake and Seismic Design Force for Highway Bridges", 1997,
8) Proc. of Second National Conference on Bridges and Highways

RELATIVE FLEXIBILITY OF A BUILDING FOUNDATION

by

M.D. Trifunac and M.I. Todorovska

Univ. of Southern California, Civil Eng. Dept., Los Angeles, CA 90089-2531

ABSTRACT

This paper analyzes deformations of the foundation in a seven-storey hotel building in Van Nuys, California, from measurements of ambient noise and strong motion recordings. This building has been instrumented by strong motion accelerographs, and has recorded several earthquakes, including the 1971 San Fernando, 1987 Whittier-Narrows, 1992 Landers, 1992 Big Bear, and 1994 Northridge earthquake and its aftershocks. It suffered minor structural damage in 1971 earthquake and extensive damage in 1994. Two detailed ambient vibration tests were performed following the Northridge earthquake, one before and the other one after the 20 March aftershock. These included measurements at a grid of points on the ground floor and in the parking lot surrounding the building, summarized and analyzed in this paper. The analysis shows that the foundation system, consisting of grade beams on friction piles, does not act as a "rigid body" but deforms during the passage of microtremor and therefore earthquake waves. For this geometrically and by design essentially symmetric building, the center of stiffness of the foundation system appears to have large eccentricity (this is seen both from the microtremor measurements and from the earthquake recordings). This eccentricity may have contributed to strong coupling of transverse and torsional responses, and to larger than expected torsional response, contributing to damage during the 1994 Northridge, earthquake.

INTRODUCTION

Earthquake resistant design of structures must be based on analyses of realistic models of the structure, foundation and soil system, considering wave propagation and all the aspects of nonlinear response. Such analyses require solution of a complicated and difficult to solve system of governing equations and boundary conditions. Hence, it has been necessary to make various simplifications. In doing so, it is important to evaluate the accuracy of the approximations and to define the range of the model parameters for which the approximations are valid. This is best accomplished by careful experimental verification using full scale tests of actual structures.

A common assumption in many models which consider soil-structure interaction effects is that the foundation is rigid. This reduces the number of degrees-of-freedom of the model, and gives good approximations for wavelengths long relative to the foundation dimensions (Lee, 1979). For short wavelengths, this assumption can result in non conservative estimates of the relative deformations in the structure and, in general, is expected to result in excessive estimates of scattering of the incident wave energy and in

excessive radiation damping (Todorovska and Trifunac 1990a; 1991; 1993). The extent to which this assumption is valid depends on the stiffness of the foundation system relative to that of the soil, and also on the overall rigidity of the structure. For a nine-storey reinforced concrete building, extensively tested during the 1970's, the foundation could be represented by a "rigid" slab for NS vibrations (because of stiffening effects of the end shear walls) but not for EW vibrations (Foutch et al. 1975; Luco et al. 1975; 1977; 1986; Moslem and Trifunac, 1986; Wong et al. 1987). The other extreme is to neglect the stiffness of the foundation system and to assume that the wave energy is transmitted from soil into the building according to the principles of wave propagation (Todorovska and Trifunac 1989; 1990a,b,c; Todorovska et al. 1988). This approximate approach underestimates the incident wave energy scattered by the foundation and overestimates the energy transmitted into the building. The reality is somewhere between these two approximations, and can be studied in detail only by means of numerical methods.

In this paper, an instrumented seven-storey hotel building in Van Nuys, California, is studied. Records of several earthquakes were available for the study, including the 1971 San Fernando (M_L=6.6, R=22 km), 1987 Whittier-Narrows (M_L=5.9, R=41 km), 1992 Landers (M_L=7.5, R=186 km), 1992 Big Bear (M_L=6.5, R=149 km), and 1994 Northridge (M_L=6.4, R=1.5 km) earthquake and two of its aftershocks (20 March: M_L=5.2, R=1.2 km; and 6 December, 1994: M_L=4.3, R=11 km). The building is supported by a friction pile foundation. The Northridge earthquake caused severe damage, and the building was declared unsafe. The damage was most severe at the fifth floor, where many columns were damaged, just below the spandrel beam. The specific aspects of the response, which caused this type of failure, have not been deciphered so far. One plausible group of causes can be sought in the large relative deformations of the foundation system (pile caps connected by grade beams), but the limited number of accelerographs, which recorded the main event, is not sufficient to verify this hypotheses (Trifunac 1997, Trifunac and Todorovska, 1997).

In this paper, a summary of ambient noise measurements in the parking lot and on the ground floor of this building is presented. The objective is to describe the deformations of the foundation system during the passage of ambient noise waves (mostly Rayleigh waves caused by surface traffic), and to speculate on how the foundation may have moved during the Northridge earthquake. Further details about this experiment can be found in Trifunac et al. (1998).

DESCRIPTION OF THE BUILDING

The building analyzed in this paper is a seven-storey reinforced concrete structure, in the city of Van Nuys (Los Angeles metropolitan area), near the intersection of Roscoe Ave. and I-405 (Fig. 1). It was designed in 1965 (Blume et al., 1973) and served as a hotel until 1994. Its plan dimensions are about 62 by 160 feet (Fig. 2a). The typical framing consists of columns spaced at 20 foot centers in the transverse direction and 19 foot centers in the longitudinal direction. Spandrel beams surround the perimeter of the structure. Lateral forces in each direction are resisted by the interior column-slab frames and exterior column spandrel beam frames. The added stiffness afforded the exterior

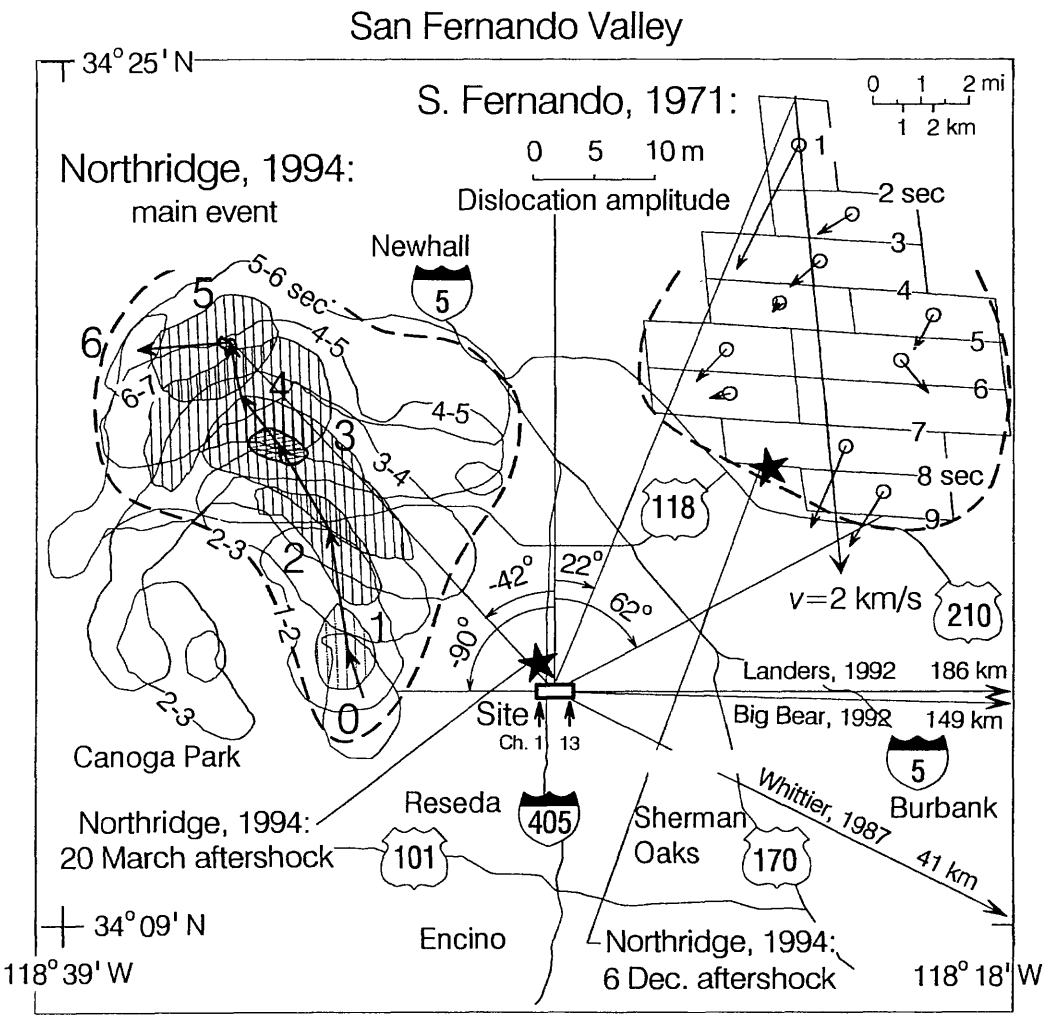

Fig. 1 Geometrical relationship of the building site to the earthquakes causing strong motion. Whittier, Landers and Big Bear earthquake are outside the limits of this figure, at epicentral distances 41, 186 and 199 km respectively.

frames by the spandrel beams, creates exterior frames that are roughly twice as stiff as interior frames. With the exception of some light framing members supporting the stairway and elevator openings, the structure is essentially symmetric. The contribution to the overall stiffness and mass from the nonstructural brick filler walls and some of the exterior cement plaster could cause some asymmetry for lateral motion in the longitudinal direction, which is expected to be minor.

The first floor is a slab on grade over about 2 feet of compacted fill. Except for two small areas at the ground floor, covered by one-storey canopies, the plan configurations of the floors, including the roof, are the same. The floor system is a reinforced concrete flat slab, 10 inches thick at the second floor, 8.5 inches thick at the third to seventh floors and 8 inches thick at the roof.

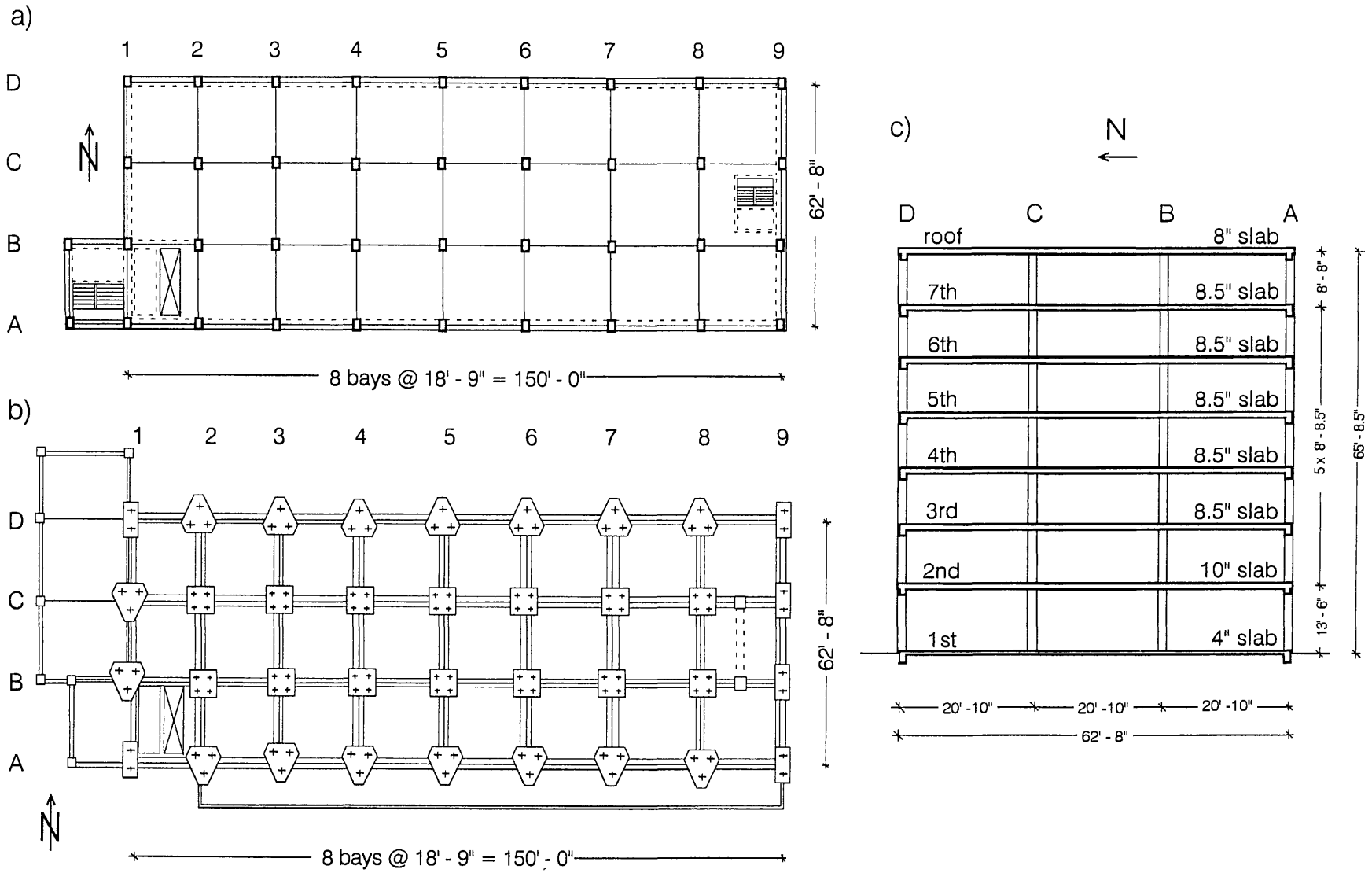

Fig. 2 (a) Typical floor plan. (b) Foundation plan. (c) Typical transverse section.

The site lies on recent alluvium. A typical boring log shows the underlying soil to be primarily fine sandy silts and silty fine sands. The average shear-wave velocity in the top 30 m is ~300 m/s. The foundation system (Fig. 2b) consists of 38 inch deep pile caps, supported by groups of two to four poured-in-place 24 inch diameter reinforced concrete friction piles. These are centered under the main building columns. All pile caps are connected by a grid of the beams. Each pile is roughly 40 feet long and has design capacity of over 100 kips vertical load and up to 20 kips lateral load. The structure is constructed of regular weight reinforced concrete (Blume et al., 1973).

The Feb. 9, 1971, San Fernando earthquake caused minor structural damage. Epoxy was used to repair the spalled concrete of the second floor beam column joints on the north side and east end of the building. The nonstructural damage, however, was extensive and about 80% of all repair cost was used to fix the drywall partitions, bathroom tiles and plumbing fixtures. The damage was most severe on the second and third floors and minimal at the sixth and seventh floors.

The building was severely damaged by the 17 January, 1994, Northridge earthquake, and was not in use on February 4, 1994, when we conducted the first ambient vibrations experiment. The structural damage was extensive in the exterior north (D) and south (A) frames, designed to take most of the lateral load in the longitudinal direction. Severe shear cracks occurred at the middle columns of frame A, near the contact with the spandrel beam of the fifth floor. Those cracks significantly decreased the axial, moment and shear capacity of the columns. The shear cracks which appeared in the north (D) frame on third and fourth floors, and the damage of columns D2, D3 and D4 on the first floor caused minor to moderate changes in the capacity of these structural elements. No major damage of the interior longitudinal (B and C) frames was noticed. There was no visible damage in the slabs and around foundations. The nonstructural damage was significant. Almost every guestroom suffered considerable damage. Severe cracks were noticed in the masonry brick walls, and in the exterior cement plaster.

EARTHQUAKE RECORDINGS

The first known recorded strong motion in the building is of the Feb. 9, 1971, San Fernando earthquake (Fig. 1). The sensors, three self-contained tri-axial AR-240 accelerographs, were located in the SE corner (near Chan. 14; Fig. 3), middle of the fourth floor, and on the roof (near present Chan. 2; Fig. 3). During this earthquake, the first strong motion waves started to arrive from N22°E, having originated at depth ~9 to 13 km below epicenter (Trifunac, 1974). With rupture propagating up towards south at about 2 km/s, the last direct waves were arriving from N 62°E, 9-10 s later. The 1987 Whittier-Narrows, 1992 Landers and 1992 Big Bear earthquakes occurred at epicentral distances of 41, 186 and 149 km respectively and caused strong motion arrivals from E 27°S, East, and E 1.5°S. During the 1994 Northridge earthquake, the first motions started to arrive from the West, with the last arrivals coming from N 42°W, about 7 to 10 s later (Fig. 1). These latter earthquakes were recorded by a CR-1 system; the sensor locations are shown in Fig. 3.

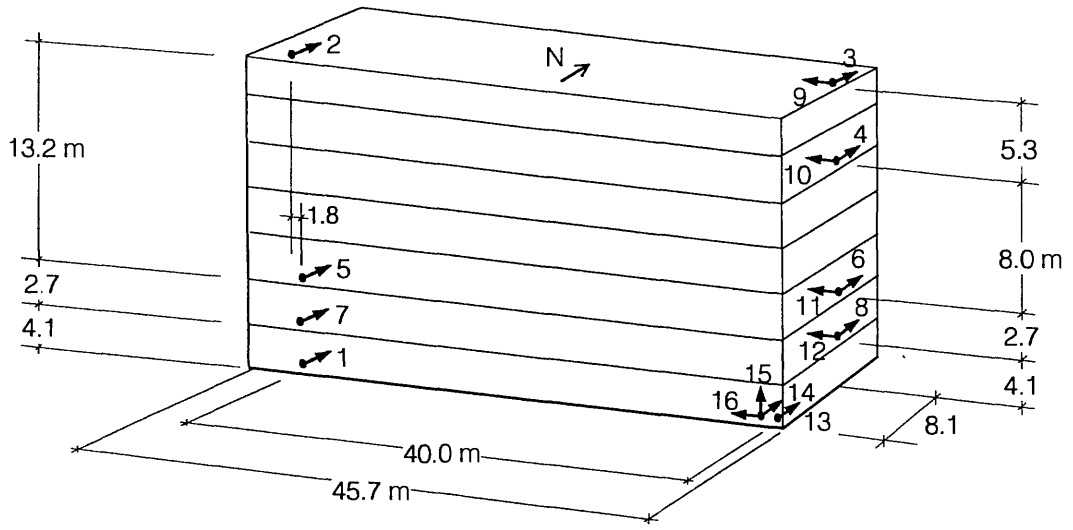

Fig. 3 Location and orientation of 13 sensitivity vectors of CR-1 recording system. Chan. 14, 15 and 16 belong to SMA-1 accelerograph.

Table 1 summarizes selected parameters of the above earthquakes and accelerograms. The San Fernando accelerogram was digitized manually, at a sampling rate of minimum 50 points per second. The accelerograms of the Whittier Narrows, Landers, Big Bear and Northridge earthquakes were processed by the California Division of Mines and Geology. Figure 4 shows the computed displacements for Chan. 1 (solid line) and 13 (dashed line) (see Fig. 3) during the Landers and Northridge earthquakes. The other earthquakes which triggered the instruments (Table 2) generally resulted in smaller displacement amplitudes (Trifunac et al., 1998) and are not presented here.

Table 1 Selected earthquake and accelerogram parameters describing the data used in this work

Earthquake	Magnitude M_L	Date	Epicentral distance km	Azimuth of Arriving strong motion waves	Peak horizontal acceleration (g)	Peak vertical acceleration (g)
San Fernando*	6.6	9 Feb., 71	22	22°-62°	0.25	0.17
Whittier	5.9	1 Oct., 87	41	117°	0.16	-
Landers	$M_s = 7.5$	28 Jun., 92	186	90°	0.041	0.007
Big Bear	6.5	28 Jun., 92	149	91.5°	0.01	0.007
Northridge	6.4	17 Jan., 94	1.5	240°–350°	0.44	0.27
Northridge aft.	5.2	20 Mar., 94	1.2	320°	0.27	0.10
Northridge aft.	4.3	6 Dec., 94	10.9	40°	0.06	0.03

* Not considered in this analysis; provided for general background only.

Table 2 Other earthquakes which have triggered the instruments in the 7-storey hotel*

Aftershock of Whittier-Narrows	4 Oct.1987	M=5.3	10:59:38 GMT
Pasadena Earthquake	3 Dec.1988	M=4.9	11:38:26 GMT
Malibu Earthquake	19 Jan.1989	M=5.0	06:53:28 GMT
Upland Earthquake	28 Feb.1990	M=5.2	23:43:37 GMT
Sierra Madre	28 June 1991	M=5.8	14:43:54 GMT

* V. Graizer, personal communication (1997).

Analyses of the displacement time histories for Chan. 1, 2, 3 and 13 (see Fig. 3) show that during the larger peaks of the relative response, the torsion within the building contributes 20 to 40% of the peak relative response, at the locations of Chan. 2, for example (Whittier-Narrows ~23%; Landers ~33%, Fig. 5 top; Big Bear ~42%; and Northridge ~22%, Fig. 5 bottom). Comparison of displacement time histories of Chan. 1 and 13 shows that at the site of Chan. 1, the peak displacements were up to 10 to 20% larger than at the site of Chan 13 (~20% during Landers earthquake, 30–35 s after trigger; ~10% during Northridge earthquake, 5 to 10 s after trigger, see Fig. 4). It is not likely that these differences were caused by the nature of incident waves. The motions arriving from the Landers earthquake had mainly long period surface waves, propagating from east to

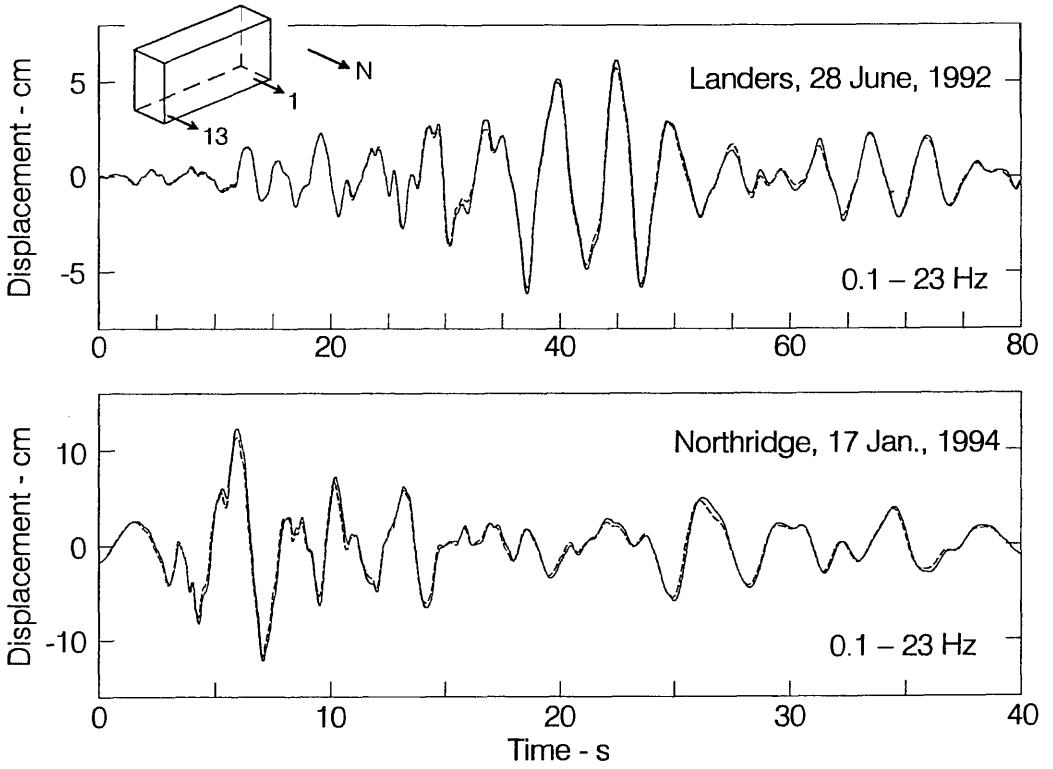

Fig. 4 Displacement time histories for Chan. 1 (solid lines) and 13 (dashed lines) located at ground floor, at the west and east ends of the building respectively for strong motion shaking during Landers, 1992, and Northridge, 1994, earthquakes.

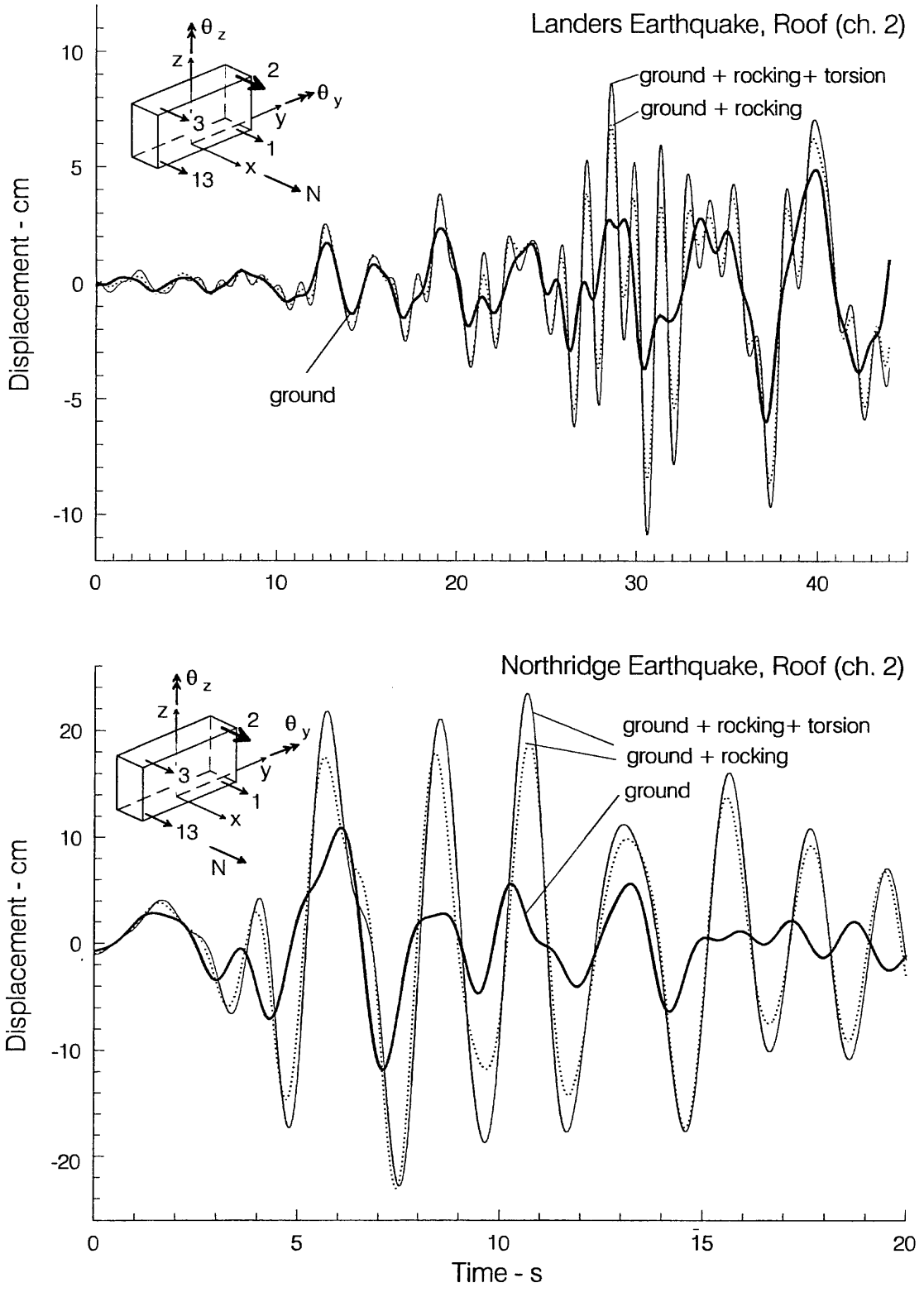

Fig. 5 Contributions from ground translation, rocking θ_y and torsion θ_z to computed displacement at the site of recording Chan. 2.

west (Fig. 1), while the waves generated by Northridge earthquake were mainly direct near-field arrivals, propagating predominantly from west to east, with high phase velocities associated with mostly vertical incidence, during the first 3 to 4 s of strongest motion (between 4 and 8 s in Fig. 4). The amplitudes of the observed differences depend somewhat on the choice of the band-pass filters (shown for each event in Fig. 4), but occur systematically only during large motions. Furthermore, the differences should be emphasized by EW wave arrivals, because the building is elongated in EW direction. If the observed differences result from separation and relative displacement between the soft soil surrounding the foundation and the piles, it is expected that these differences would be large during Landers and Northridge earthquakes, which both caused large motions at this site, and both arrived predominantly along EW direction. During two aftershocks of Northridge earthquake the waves arrived from North-West and North-East (Fig. 1), and so were less efficient in exciting the torsional response, but their motions were also small.

AMBIENT VIBRATION EXPERIMENTS

General Overview and Objectives

Two ambient vibration experiments were conducted in the building, one on Feb. 4-5 (about two and a half weeks after the Northridge main event) and the other one on April 19-20, 1994 (about three months after the main event and one month after one of the largest aftershocks, of March 20, $M = 5.2$). Between the two experiments, the building was temporarily restrained, as it was severely damaged by the main event.

The objective of the first experiment was to measure the dynamic characteristics of the damaged building and to see whether the changes in stiffness due to the extensive structural damage could be identified by small amplitude tests. The second experiment was much more detailed. Besides detecting changes in stiffness due to new damage from the 20 March aftershock, it also had as an objective to measure the motion of the ground around the building. This was planed to be done by a series of measurements at a dense grid of points in the parking lot of the building. Similar measurements were made during a three-dimensional forced vibration survey of a 9-storey reinforced concrete building in Pasadena (Foutch et al., 1975; Luco et al, 1975). The analysis of the amplitudes and phases of the recorded motion confirmed that soil deforms as predicted by theoretical models, and provided an experimental verification of various simplifying assumptions, which usually accompany soil-structure interaction models (e.g., the rigid foundation assumption, and the effects of embedment; Luco et al., 1986).

The aim of the parking lot measurements in the building was to detect ground deformations associated with at least the fundamental transverse and longitudinal modes of vibration. This would have been useful for characterization of soil-structure interaction involving a complex pile foundation. However, no peaks associated with rocking or translation at the apparent frequencies of the building-soil system could be found in the Fourier amplitude spectrum, above the noise level. Nevertheless, the results came out to be even more useful, revealing evidence of flexibility of the foundation and of wave propagation through the first floor slab and the surrounding soil.

For the analysis of this paper, the parking lot measurements of the second experiment are of interest, and are presented and analyzed. From the measurements in the building, only the results on the apparent modal frequencies for both experiments are summarized.

Instrumentation and Methods of Analysis–Second Experiment

Four Ranger SS-1 seismometers and two Earth Sciences Rangers were used (Ivanovic and Trifunac, 1995; Trifunac, 1972). The response was measured along frame C (Fig. 2a), at all columns and at each floor, for all three components of motion. Three of the SS-1 Ranger seismometers were used to record motion at various locations (the location and orientation were changed as required). The motion of the ground floor was measured at each column and in all three directions (N, E and vertical).

Three reference points were used for calculations of the transfer functions (marked by "R" in Fig. 6). Two of the Earth Sciences Ranger seismometers were placed on the ground floor, at reference locations A5 and D5. Their orientation was always up. The reference instrument for horizontal motions was at location B2 on the ground floor. It was oriented either along the longitudinal (east) or along the transverse (north) direction, depending on the measurement.

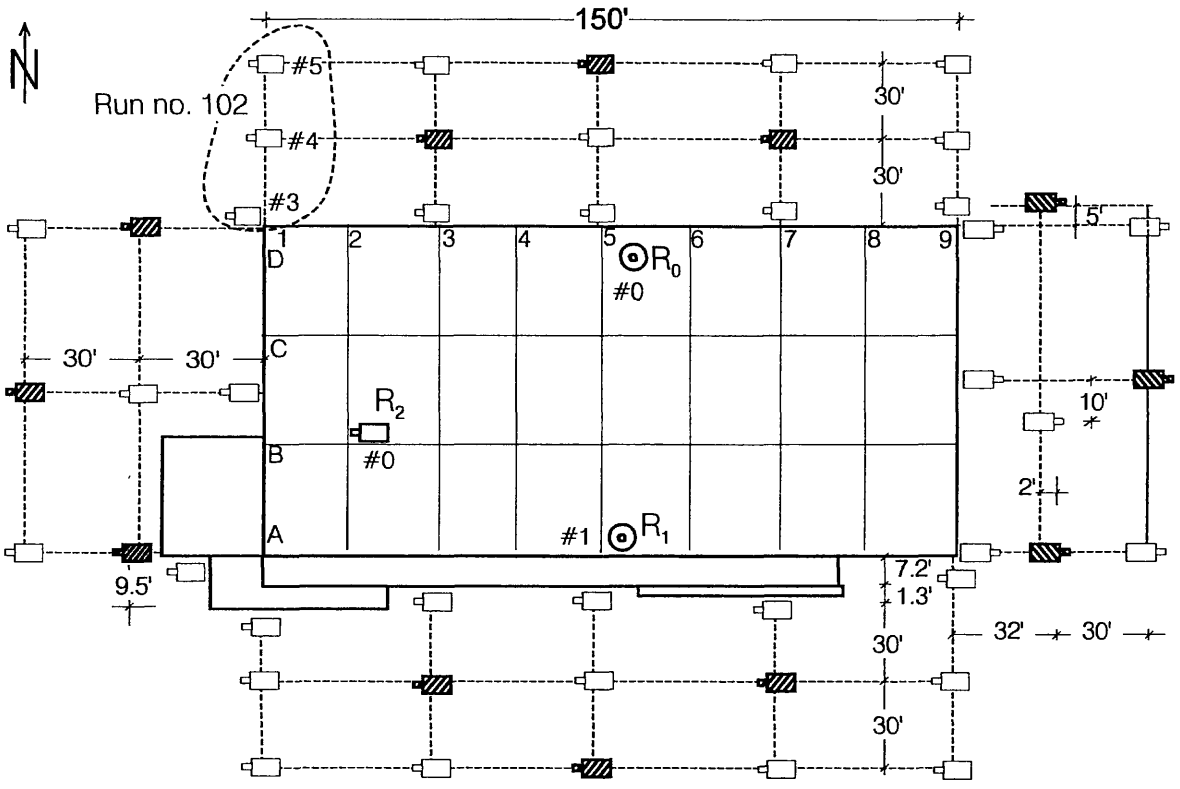

Fig. 6 Position of instruments during the recording of ambient noise in the parking lot of the building.

The measurements in parking lot were carried out at 46 locations within 15 to 20 m from the structure, and in three directions (north, east and up; Fig. 6). This was done during daytime, when high direct sun could have contributed to the noise in the soft asphalt surface. To abate this, the instruments were covered with towels. The experiment was carried out continuously from 12 noon of April 19 (Tuesday), until 9 p.m., April 20 (Wednesday) 1994. Those were quiet sunny days (temperature was in the range of 12 to 25°C). The building was not in use, and except for electricity, other facilities were not available (no elevators, air-conditioning, or running water...). Each of the measurements lasted about 3 minutes, and the sampling frequency was 400 points per second. The PC computer used to record was located on the ground floor. The instruments were placed either directly onto the concrete slab, ceramic tiles, or onto the asphalt, for the outside measurements. Two calibration tests were performed for both horizontal and vertical transducer orientation, one at the beginning and the other one at the end of the experiment.

To describe the overall nature of microtremors in the area surrounding the building, cross-correlation analyses were performed as follows. Measurements were performed by "new" Ranger seismometers (#3, 4 and 5; e.g., during run No. 102, see Fig. 6), while the reference instruments (#0, 1 and 2) were located inside the building at locations B2 (#2), D5 (#0) and A5 (#1, as shown in Fig. 6). Two "old" Ranger seismometers recorded vertical motion during all measurements, but only transducer #1 at A5 was used as reference for the analysis of vertical motions in the parking lot.

Results on Modal Frequencies

The results of the measurements in the building are summarized here only in terms of frequencies and mode shapes for horizontal motion. It was found that in the transverse (N-S) direction the soil-structure system vibrates with frequencies f = 1.4, 1.6, 4.2 and 4.9 Hz. In the longitudinal direction, the apparent frequencies were at f = 1.1, 3.7, 5.7 and 8.5 Hz. Detailed description of the mode shapes and of other aspects of the response is

Table 3 Mode shapes and apparent frequencies for EW and NS vibrations, measured during Experiments 1 and 2.

Mode shapes EW	f - Hz		Δf - %
	Expl. I Feb. 94	Expl. II Apr. 94	
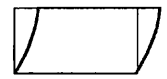	1.0	1.1	10
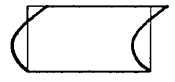	3.5	3.7	6
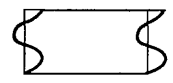	5.7	5.7	0
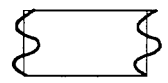	8.1	8.5	5

Mode shapes NS	f - Hz		Δf - %
	Expl. I Feb. 94	Expl. II Apr. 94	
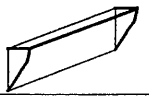	1.4	1.4	0
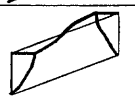	1.6	1.6	0
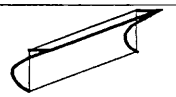	3.9	4.2	10
	4.9	4.9	0

outside the scope of this paper. Table 3 summarize the results on the apparent modal frequencies for both experiments, for the longitudinal (EW) and transverse (NS) directions, only to suggest the overall characteristics of the transfer functions for horizontal motions and to provide a general background for the analysis of the foundation response. It is seen that three out of the four identified frequencies in the longitudinal direction were larger during the second experiment, while one (f = 5.7 Hz), reminded the same. The increase in frequency most probably resulted from the wooden braces restraining the building, placed at the longitudinal frames between the two experiments. The frequency of the first longitudinal mode increased by 10%, and of the second and fourth longitudinal modes by 6 and 5%. Apparently the restrainers did not affect the third mode. It is also seen that the frequency of the first transverse mode and of the first torsional mode are the same (apparently, the braces located along the longitudinal frames, did not increase stiffness for those two modes), but of the frequency of the third transverse mode had frequency larger by 10% for the second experiment.

Results of Motion of the Ground Floor and of the Surrounding Soil

General Characteristics

Figure 7 shows average Fourier amplitude spectra of NS, EW and vertical components of motions in the parking lot (averaging was done to emphasize the predominant wave motion and to reduce the local noise). The average spectra were obtained from three runs at a group of three locations, located north, east, south and west of the building (i.e. total of 12 locations, highlighted in Fig. 6 by cross-hatched schematic representation of the recording instruments). It is seen that there are many large amplitude peaks in the spectra. In most cases, these do not coincide with identified apparent modal frequencies of the building (shown by solid, open and shaded bars in Fig. 7), and were created by strong periodic sources in San Fernando Valley (industrial sites with large moving machinery). The overall large amplitudes for frequencies centered near 4 Hz were caused by the NS traffic on I-405 (~150 m west of the building) and by EW traffic on Roscoe Blvd. (~50 m north of the building).

Cross-correlation Functions

The cross-correlation function, $R_{i,\,\mathrm{ref.}}(\tau)$, was computed for each location, defined by

$$R_{i,\,\mathrm{ref.}}(\tau) = \frac{1}{T}\int_{-T/2}^{T/2} f_i(t)\, f_{\mathrm{ref.}}(t+\tau)\mathrm{d}t \qquad (1)$$

where $f_i(t)$ is the motion at the i$^{\mathrm{th}}$ location and $f_{\mathrm{ref}}(t)$ is the simultaneous record at the reference point (B2 for EW and NS motions, and A5 for vertical motions, see Fig. 6) and T~3 min. Then, the spatial distribution of the peak amplitude, $R_{i,\mathrm{ref}}(\tau)_{\mathrm{max}}$, and corresponding time lag, τ, were plotted and analyzed. Figures 8–10 show contour plots of the peak amplitudes of $R_{i,\,\mathrm{ref.}}(\tau)$ (solid line) and of the relative delay τ (dotted lines). The amplitudes are on an arbitrary scale, but consistent for the NS, EW and vertical directions, and τ is in seconds. In Fig. 8, 30 feet (~ 10 m) west of the building, τ = 0.03 s. This corresponds to apparent horizontal phase velocity of about 300 m/s, consistent with

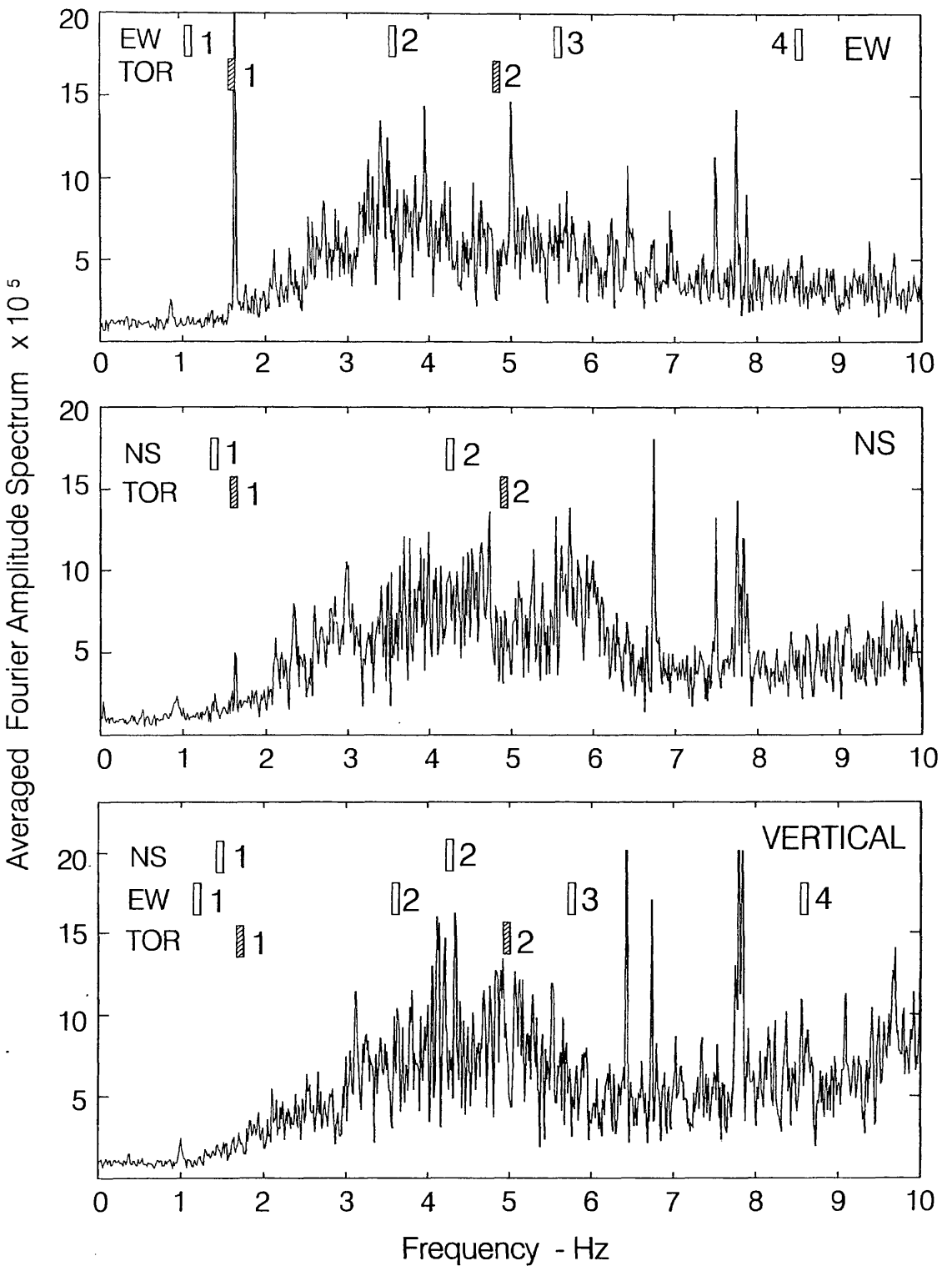

Fig. 7 Average (over time and space: four groups of three points, shaded in Fig. 6) of Fourier amplitude spectra of microtremor noise recorded in the parking of the building. Frequencies of apparent NS, EW and torsional modes of building vibration are shown.

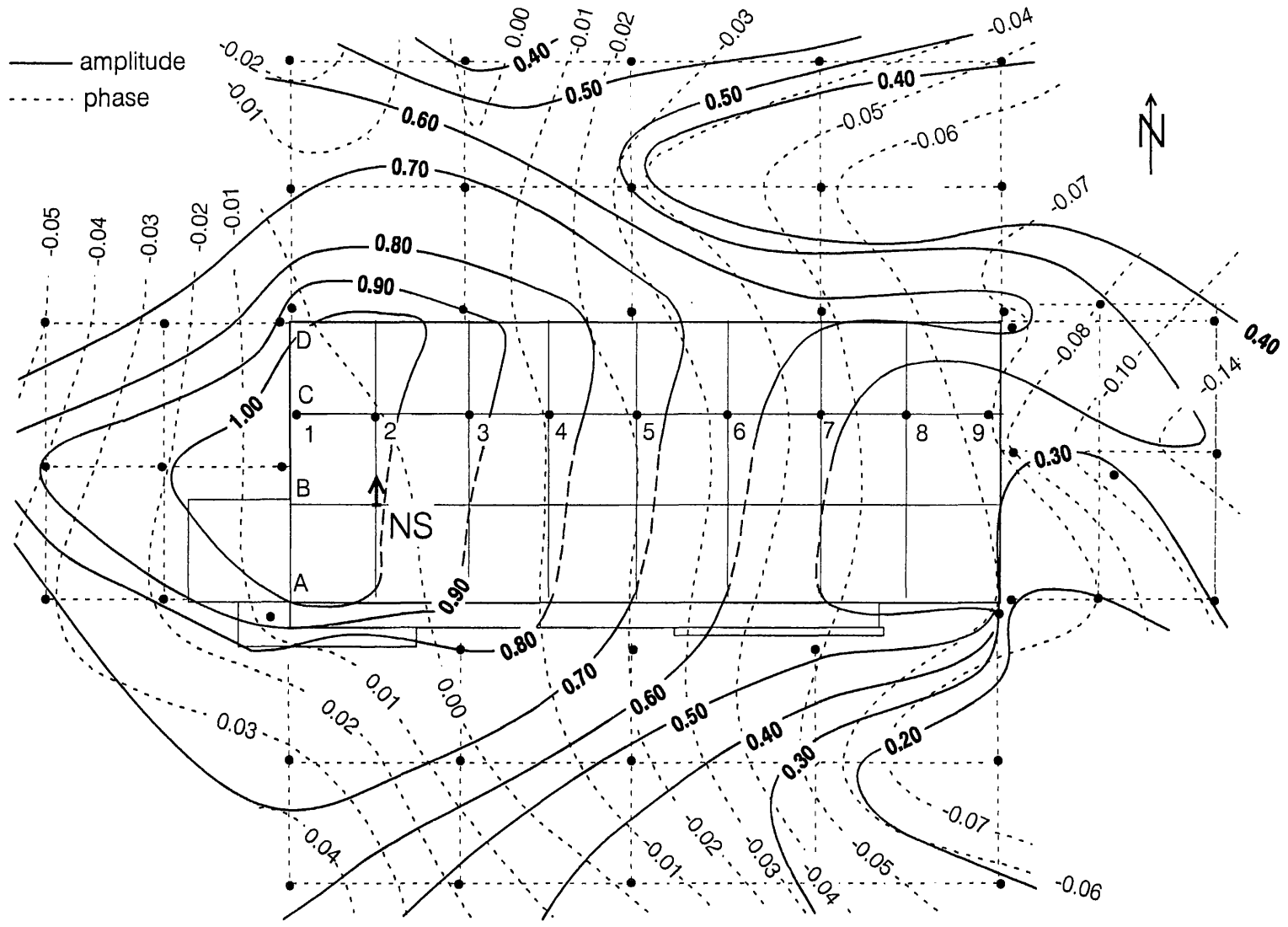

Fig. 8 Contours of $(R_{i,\,\mathrm{ref.}}(\tau))_{\max}$ for NS motion (arbitrary normalized amplitudes, shown by heavy lines), and (τ) (in seconds) of $(R_{i,\,\mathrm{ref.}}(\tau))_{\max}$ relative to the reference station at B2.

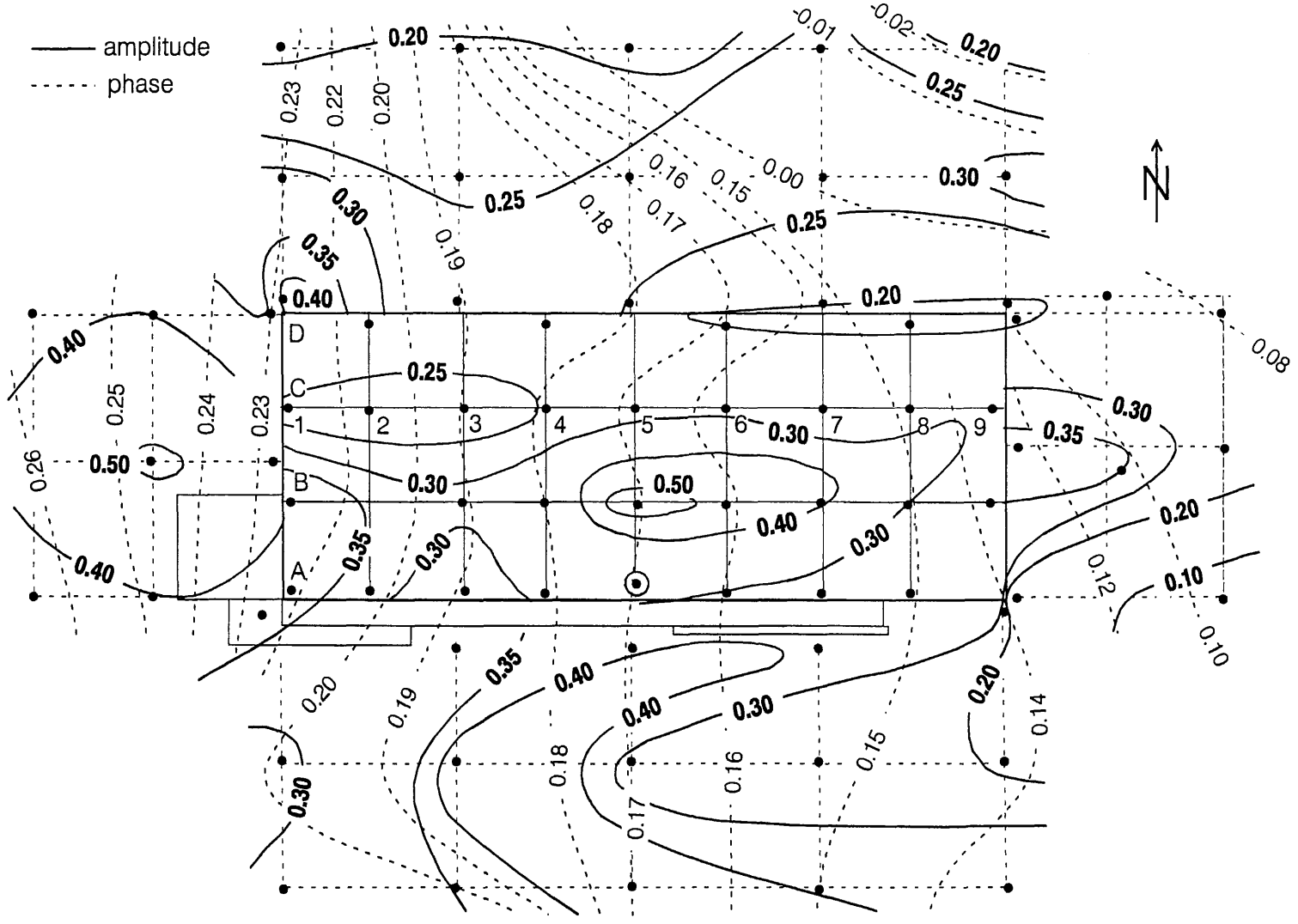

Fig. 9 Contours of $(R_{i,\text{ref.}}(\tau))_{\max}$ for vertical motion (arbitrary normalized amplitudes, shown by heavy lines), and (τ) (in seconds) of $(R_{i,\text{ref.}}(\tau))_{\max}$ relative to the reference station at A5.

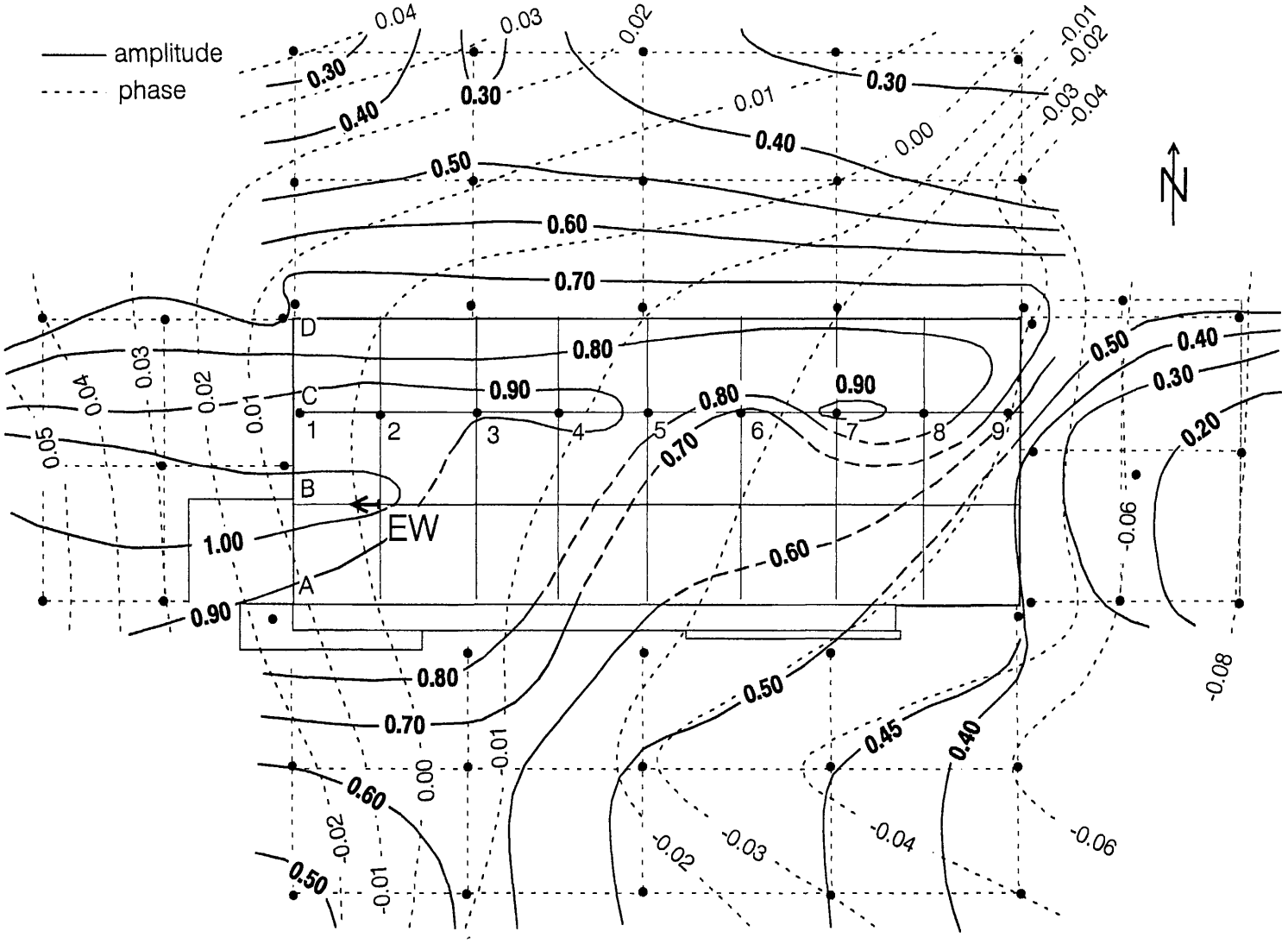

Fig. 10 Contours of $(R_{i,\,\mathrm{ref.}}(\tau))_{\max}$ for EW motion (arbitrary normalized amplitudes, shown by heavy lines), and (τ) (in seconds) of $(R_{i,\,\mathrm{ref.}}(\tau))_{\max}$ relative to the reference station at B2.

the interpretation that microtremors are high frequency Rayleigh waves propagating through shallow soil layers. The overall pattern of the time lag, τ, implies wave arrival from the west, and scattering and diffraction around the building foundation. The corresponding contours for vertical motion (Fig. 9) imply wave arrival from west and south-west, with apparent phase velocities between 250 and 300 m/s. The corresponding contours for the EW motions are shown in Fig. 10.

The results in Figs 8–10 have been evaluated using unfiltered recordings. As it can be seen from Fig. 7, this motion has most of its energy between 3 and 6 Hz, while the recorded signal is small between 1 and 1.5 Hz. This is inconvenient, because the motions of the soil driven by soil-structure interaction are expected to be seen at frequencies near the horizontal and vertical apparent frequencies of the building (~1.0 Hz for EW and ~ 1.4 Hz for NS and vertical motions). To analyze the motions near these frequencies, the signals were first band-pass filtered, using a "cosine bell" function centered at 1.0 Hz for EW motions and at 1.4 Hz for NS and vertical motions, and 0.6 Hz wide. The results were consistent with the overall propagation of energy from west to east, but difficult to interpret (Trifunac et al., 1998). The contours of the amplitudes of $R_{i,\,\mathrm{ref.}}\,(\tau)_{\max}$ implied strong warping of the building foundation and of the parking lot, different from slowly decaying motions with same relative phase, away from the building, as would be expected from soil-structure interaction effects based on rigid foundation modeling (Foutch et al., 1975, Luco et al., 1975).

To eliminate the consequences of amplitude variations of the ambient noise with the time of the day, the cross-correlation functions in Figs 8–10 were normalized by $R_{1,1}$ (0) or $R_{2,2}$ (0) for the unfiltered record and for band-pass filtered data, for all measurement runs (runs 79–143). The variations in amplitude and phase caused by fluctuations in the direction of approach of the ambient noise cannot easily be accounted for by simple normalization, and the associated effects were not corrected for in the presented results.

This experiment was carried out about three months after the earthquake and many of its aftershocks. Perhaps too soon after the earthquake for the "gaps" and "clearances" between the vertical walls of the building and soil, and piles and the surrounding soil to have been "recemented". It may be that what we see in the above measurements is the response of the "disturbed" foundation system, with "minute cracks" and "gaps" in the foundation soil, causing the wave motion in the parking lot to be so irregular. Of course, this is further complicated by apparent arrival of wave energy from different directions, though mainly from moving sources on a major freeway just 150 m west of the site (NS vehicular traffic on I-405).

DISCUSSION AND CONCLUSIONS

One of the more interesting results of this analysis is seen in Fig. 8, displaying normalized amplitudes of the cross-correlation function of NS velocities for the complete (unfiltered) recorded motions. It shows that during passage of microtremor waves, mainly from west to east, the foundation essentially rotates about a point close to the south-eastern corner of the building (near A9). The EW components of this motion, shown in Fig. 10, are consistent with this interpretation if one allows for some in-plane

deformation of the foundation system, in the north and west ends of the building. If present during strong motion, this would imply very large eccentricities of torsional stiffness of the overall foundation, and consequently strong coupling of the NS and torsional components of response.

We speculate that during very strong motion, the soil is pushed sideways by large relative response of the foundation and piles, in this case more along the west end of the building. The width of this separation probably closes partially during "dynamic compaction" effected by many small aftershocks. Therefore, the pattern of recorded ambient noise amplitudes, shown in Fig. 8, and our interpretation could also depend on the status of this separation during the time of our experiment.

The above described mechanism acts as a powerful passive energy absorption system, but analyses of its nonlinear, time dependent behavior and complex soil-structure interaction analyses would be very difficult. Evaluation of its effects on the dynamics of the system would require analyses in which the geometric characteristics experience large changes during the duration of the excitation. Analyses of such problems are possible, but it is helpful first to learn more about the expected nature of the changes with time from full scale observations during actual earthquakes.

The above observations could result from nonuniform soil properties below the foundation or from partial shear failure of several piles (probably as early as in 1971 during San Fernando earthquake), resulting in "softer" soil-pile system below the western end of the building. Such variations in stiffness must be included in the response analyses which should explicitly address the strong coupling between translation and torsion. Several repeated full scale tests of the as-built structure would have detected the range of actual variations of these centers of stiffness.

The measuring grid shown in Fig. 6 was not sufficiently dense to determine whether the side walls of the building and the soil moved as a continuum or independently. Most horizontal displacement contours are consistent with the assumption that these two are in contact. The contours of vertical motions, however, suggest that some separation may be present, for example, near the north-western corner of the building (Fig. 9).

All the contour plots of horizontal and vertical amplitudes of deformation of the ground floor show that the foundation of this building did not act as a rigid body, but it deformed with the passage of incident waves. The grade beams allowed differential vertical (Fig. 9) and horizontal motions (Fig. 8 and 10), which followed the deformation of the "body" of soil with piles. In this example this "body" is stiffer than the surrounding soil by a factor perhaps as large as two, because the velocity of NS displacements is roughly 40% higher over the ground floor than outside the building (see the dashed lines representing the relative phases of motion in Fig. 8). Consequently, in addition to the inertial forces, the differential motions of the first story columns would contribute additional moments and shears. The actual amplitudes of these additional effects can be calculated by numerical modeling, but conservative estimates of their upper bounds can be obtained by assuming that the soil-pile-foundation system has same stiffness as the surrounding soil,

and that there is no soil-structure interaction (Trifunac, 1997; Trifunac and Todorovska, 1997).

Albeit speculative and qualitative, the above considerations show that the state of the art of strong motion instrumentation of buildings is not adequate to address most of the aspects of the problems we considered. Additional recording channels on the ground floor would have provided invaluable information. Analyses of the damage in this building is outside the scope of this paper, but it could be shown that additional instruments were called for at the upper floors as well. Therefore, with limited resources, we should explore what is better: to instrument in more detail selected geometrically simple structures, or to continue with the present programs which instrument many buildings, but with limited instrumentation in each building. At present, while this decision is made, the emphasis should be placed on processing and dissemination of all recorded accelerations in structures, so that small (linear) and large nonlinear motions can be analyzed and compared. For identification of the soil-structure system, all recorded motions are valuable, even the very small ones, particularly when those contribute to the database of simple and symmetric buildings, for which most of our analysis tools should be applicable.

During the last 20 years, too much emphasis has been placed on laboratory experiments, while the full-scale tests of structures have been neglected. The best and truly informative experiments are the full-scale tests in actual buildings. In the laboratory, we mimic imperfectly our hypotheses and expectations. Only the full scale observations of the actual nature can unveil our misconceptions and occasionally provide a basis for better understanding and for creation of new theories and ideas.

REFERENCES

Blume, J.A. and Assoc. (1973). Holiday Inn, Chapter 29 in "San Fernando, California Earthquake of February 9, 1971," Volume I, Part A, *U.S. Dept. of Commerce*, National Oceanic and Atmospheric Administration, Washington, D.C.

Foutch, D.A., J.E. Luco, M.D. Trifunac and F.E. Udwadia (1975). Full scale three-dimensional tests of structural deformation during forced excitation of a nine-story reinforced concrete building, *Proceedings, U.S. National Conference on Earthquake Engineering*, Ann Arbor, Michigan, pp. 206-215.

Ivanovic, S. and M.D. Trifunac (1995). Ambient vibration survey of full scale structures using personal computers (with examples in Kaprielian Hall), *Dept. of Civil Eng. Report No. 95-05*, Univ. of Southern California, Los Angeles, California.

Lee, V.W. (1979). Investigation of three-dimensional soil-structure interaction, *Dept. of Civil Eng. Report No. 79-11*, Univ. of Southern California, Los Angeles, California.

Luco, J.E., H.L. Wong and M.D. Trifunac (1975). An experimental study of ground deformations caused by soil-structure interaction, *Proceedings, U.S. National Conference on Earthquake Engineering*, Ann Arbor, Michigan, pp. 136-145.

Luco, J.E., H.L. Wong and M.D. Trifunac (1977). Contact stresses and ground motion generated by soil-structure interaction, *Earthquake Eng. and Structural Dynamics*, **5**, 67-79.

Luco, J.E., H.L. Wong and M.D. Trifunac (1986). Soil-structure interaction effects on forced vibration tests, *Dept. of Civil Eng. Report No. 86-05*, Univ. of Southern California, Los Angeles, California.

Moslem, K. and M.D. Trifunac (1986). Effects of soil structure interaction on the response of buildings during strong earthquake ground motions, *Dept. of Civil Eng. Report No. 86-04*, Univ. of Southern California, Los Angeles, California.

Todorovska, M.I. and M.D. Trifunac (1989). Antiplane earthquake waves in long structures, *J. of Eng. Mech.*, ASCE, **115**, 2687-2708.

Todorovska, M.I. and M.D. Trifunac (1990a). A note on excitation of long structures by ground waves, *J. of Eng. Mech.*, ASCE, **116**, 952-964.

Todorovska, M.I. and M.D. Trifunac (1990b). Propagation of earthquake waves in buildings with soft first floor, *J. of Eng. Mech.*, ASCE, **116**, 892-900.

Todorovska, M.I. and M.D. Trifunac (1990c). Analytical model for the plane building-foundation-soil interaction: incident P-, SV-, and Rayleigh waves, *Dept. of Civil Eng. Report No. 90-01*, Univ. of Southern California, Los Angeles, California.

Todorovska, M.I. and M.D. Trifunac (1991). Radiation damping during two-dimensional in-plane building-soil interaction, *Dept. of Civil Eng. Report No. 91-01*, Univ. of Southern California, Los Angeles, California.

Todorovska, M.I. and M.D. Trifunac (1993). The effects of the wave passage on the response of base isolated buildings on rigid embedded foundations, Dept. of Civil Eng., *Report No. 93-10*, Univ. of Southern California, Los Angeles, California

Todorovska, M.I., V.W. Lee and M.D. Trifunac (1988). Investigation of earthquake response of long buildings, *Dept. of Civil Eng. Report No. 88-02*, Univ. of Southern Calif., of Los Angeles, California.

Trifunac, M.D. (1972). Comparison between ambient and forced vibration experiments, *Earthquake Eng. and Structural Dynamics*, **1**, 133-150.

Trifunac, M.D. (1974). A three-dimensional dislocation model for the San Fernando, California, Earthquake of February 9, 1971, *Bull. Seism. Soc. Amer.*, **64**, 149-172.

Trifunac, M.D. (1997). Differential earthquake motion of building foundations, *J of Structural Eng.*, ASCE, **123**, 414-422.

Trifunac, M.D. and M.I. Todorovska (1997). Response spectra and differential motion of columns, *Earthq. Eng. and Structural Dynamics*, **26**, 251-268.

Trifunac, M.D., S.S. Ivanovic and M.I. Todorovska (1998). Experimental evidence for flexibility of a building foundation supported by concrete friction piles, *Soil Dynam. and Earthquake Eng.*, (submitted for publication).

Wong, H.L., M.D. Trifunac and J.E. Luco (1987). A comparison of soil structure interaction calculations with results of full-scale forced vibration tests, *Soil Dynamics and Earthquake Eng.*, **7**, 22-31.

SOIL-STRUCTURE INTERACTION EFFECT ON AN NPP REACTOR BUILDING - ACTIVITIES OF NUPEC ; ACHIEVEMENTS AND THE CURRENT STATUS -

Yoshio Kitada[1], Masamitsu Kinoshita[2], Michio Iguchi[3], Nobuo Fukuwa[4]

ABSTRACT: This paper presents activities of Nuclear Power Engineering Corporation (NUPEC) in the field of the study on soil structure interaction (SSI). NUPEC had performed three projects related to the SSI study. These are "Model Tests on Dynamic Interaction Between Reactor Building and Soil", "Model Tests on Base-mat Uplift of Reactor Building", and "Model Test on Embedment Effect of Reactor Building". Through the tests, the adequacy of the analytical methods applied to the current aseismic design was confirmed. Nevertheless NUPEC is recognizing that the SSI phenomena is still problematic and there are many unresolved problems such as handling of uncertainty in detailed soil structure, the nonlinear behavior of soil, and structure-structure interaction etc. The dynamic cross interaction (DCI) between adjacent structures is one of the biggest problems of this kind. NUPEC then had planned the project to investigate the DCI effect in 1993. The project has started as "Model Tests on Dynamic Cross Interaction Effects of Adjacent Structures". The project consists of field and laboratory tests and starts in 1994 and will be completed in early 2002. In this paper we describe firstly a brief review of the results of the past three test projects on SSI performed by NUPEC. Secondly, we describe an outline and a summary of the current status of the on-going project, "Model Tests on Dynamic Cross Interaction Effects of Adjacent Structures".

1. INTRODUCTION

Nuclear Power Engineering Corporation (NUPEC) has conducted a series of research projects on soil structure interaction (SSI) under the entrustment of Ministry of International Trade and Industry (MITI) of Japan to ensure the adequacy of aseismic design methodologies used in a nuclear power plant (NPP) reactor building design. Up to the present, three projects have been completed. These are "Model Tests on Dynamic Interaction Between Reactor Building and Soil"(1980-1986), "Model Tests on Base-mat Uplift of Reactor Building"(1982-1987), and "Model Test on Embedment Effect of Reactor Building"(1986-1994). Through the tests, many fruitful test data including earthquake observation records and detailed information on the SSI phenomena have been obtained. As a consequence of detailed examination of the test data, the adequacy of the analytical methods applied to the current aseismic design was confirmed.

Nevertheless, to date, NUPEC has continued efforts to upgrade the methodology, because the SSI phenomena is still considered to be problematic and there are many unresolved problems such as handling of uncertainty in detailed soil structure, the nonlinear behavior of soil, and structure-structure interaction etc. The effect of adjacent structures on the earthquake response characteristics of the structure in consideration is one of the biggest problems of this kind. The effect is termed here as "dynamic cross interaction (DCI)" which is defined as the dynamic interaction through the soil between buildings during earthquakes. NUPEC had planned the project to investigate the DCI effect in 1993 after the preceding SSI investigation project, "Model Tests on Embedment Effect of Reactor Building". The project has started as "Model Tests on Dynamic Cross Interaction Effects of Adjacent Structures". The project consists of field and laboratory tests and starts in 1994 and will be completed in early 2002.

In this paper, we describe firstly a brief review of the results of the past three test projects on SSI performed by NUPEC. Secondly, we describe an outline and a summary of the current status of the on-going project, "Model Tests on Dynamic Cross Interaction Effects of Adjacent Structures".

1) Seismic Engineering Center, Nuclear Power Engineering Corporation, Dr.Eng.
2) Seismic Engineering Center, Nuclear Power Engineering Corporation.
3) Professor, Dept. Architectural Engineering, Science University of Tokyo, Dr.Eng.
4) Professor, Dept. Center for Cooperative Reserch in Advanced Science & Technology,Nagoya University, Dr.Eng.

2. BRIEF REVIEW OF THE RESULTS OF THE PAST TESTS ON SSI

NUPEC conducted three research projects on SSI phenomena from 1980 to 1994 to confirm the adequacy of aseismic design processes for NPP reactor buildings. These projects were "Model Tests on Dynamic Interaction between Reactor Building and Soil", "Model Tests on Base-mat Uplift of Reactor Buildings", and "Model Tests on Embedment Effect of Reactor Buildings". Numerous important results were obtained from these test projects. A brief review of each project follows.

2.1 MODEL TESTS ON DYNAMIC SOIL STRUCTURE INTERACTION

The project was started in 1980 and completed in 1986. In this test, three kinds of building model and two concrete block models were constructed in a field, representing an NPP site, to study basic phenomena related to SSI. Two types of reactor building model were used, namely BWR and PWR. A model building was also constructed adjacent to one of the BWR type reactor building as a control. These building

models consisted of a reinforced concrete foundation and a steel frame superstructure with reinforced concrete floors. Figures 1 and 2 show the layout of test models and outline of each model respectively. Figure 3 shows a typical snap shot of test models, a BWR type reactor building and its adjacent structure. The concrete block models, D_1 and D_2, were designed as cubic models with a side length of 4m.

The purposes of the models are to investigate the SSI effect on buildings, which have a low non-dimensional frequency. In addition, the block models are used to investigate the cross interaction through the soil between adjacent foundations.

Vibration tests using an exciter and earthquake observations were carried out using these models. These test results were summarized and presented at several international conferences. [1]-[6].

In the tests, many factors which affect SSI were studied using vibration test data and earthquake observation data, e.g., the relationship between soil spring and base-mat size, soil layer properties, soil contact pressure distributions at the bottom of the base-mat. The simulation analyses were performed using the so called Sway-Rocking (S-R) models based on a 3-D (Dimension) wave propagation theory, 2-D FEM models including out of plane viscous boundary and lattice type SSI analysis models.

Through these tests the following results were obtained:

(1) Interaction between the concrete foundation and soil

Through excitation tests using four foundation models, it was clarified that the spring characteristics of soil could be explained by the wave propagation theory.

(2) Interaction between the reactor building and soil

Basic dynamic interactions between the building and soil as well as between buildings were grasped through vibration tests and earthquake observation.

2.2 BASE-MAT UPLIFT TESTS OF REACTOR BUILDINGS

The project of "Base-mat Uplift Tests" was started in 1981 and was completed in 1987. The tests were planned and performed to confirm the base-mat uplift phenomena of an NPP reactor building, which is predicted through seismic response analyses of the building. We also evaluated the base-mat uplift effect on the earthquake response characteristics of the building. Laboratory and field tests were carried out for this purpose. Laboratory tests were carried out using artificial ground models made of silicon rubber and two types of structure models. One structure model, called a large-scale model, was made of concrete and the other model, called small-scale model, was made of steel. The large-scale model had dimensions of 1m square for the base and 2m in height, as shown in Fig.4. In the test, the structure models were placed on the ground models, which were fixed on a shaking table, and artificial motions were applied. The field tests were carried out using concrete blocks on two different actual fields representing NPP sites. External forces were applied to the blocks using an exciter. Figure 5 shows a typical snap shot of the field test site. The test results were presented on several papers at international conferences. [7],[8].

Typical test results obtained in the study were as follows:

(1) Laboratory tests

Relationships between contact ratio and input motion magnitude, and between contact ratio and response of structure were examined using shaking table test results. In addition, it was clarified that the influence of vertical input motion on the response of structure models is negligible. This result was obtained from the comparison of structural responses to the shaking table vibration test performed with and without vertical motion.

(2) Field tests

Relationships between contact ratio and distribution of soil contact pressure as well as stiffness of soil contact pressure were clarified.

We had obtained much valuable information on the phenomena related to the Base-mat uplift. These are relationships between overturning moment and rotational angle, between soil stiffness and the base-mat contact ratio, between soil damping and the base-mat contact ratio, between the dynamic structural response and base-mat uplift, and between the amplification in high frequency regions by base-mat uplift and vertical amplification induced by base-mat uplift. The simulation analyses were also performed using S-R models and 2-D FEM models. Simulation analysis using a method based on Green's function principle in the time domain was introduced as a detailed model.

2.3 TESTS ON EMBEDMENT EFFECT OF REACTOR BUILDINGS

The project was started in 1986 and completed in 1995. The objective of this project was to comprehend embedment effect on the SSI characteristics of reactor buildings, because it is known that the seismic response of embedded structures is greatly affected by the SSI phenomena. The backfill and surrounding soil resulting from the building embedment makes the phenomena more complicated. The project includes both laboratory tests and field tests. The laboratory tests were performed using a shaking table to investigate the spring characteristics of the soil along the side of a building and to estimate the motions applied to the building models. The test models used consisted of building models made of aluminum and a ground model made of silicone rubber. The building models were tested under different conditions with and without embedment in the ground model. The tests were also carried out by changing soil stiffness, embedment depth and applied input motion. The field tests were performed to investigate the spring characteristics of the actual soil layer and backfill soil around a structure by taking into account the actual soil conditions at NPP sites. Four reinforced concrete building models representing a BWR and a PWR reactor building were constructed on two different kinds of rock fields at the site. In order to investigate the embedment effect, each test building model was tested under conditions with and without embedment. Vibration tests and earthquake observation were carried out using these models. Figure 6 shows a typical snap shot of the building models, without embedment (model A) and with embedment (model B), used in the field test.

The data obtained from the vibration tests and earthquake observation were used to evaluate dynamic soil impedance, foundation input motions, responses of structures, and the

SSI characteristics of backfill and surrounding soils. The evaluated results were then compared using Axisymmetric FEM models. The test results were presented in several papers at many international conferences. [9]-[27].

Typical test results are summarized as follows;

(1). Increments in the real and imaginary parts of the dynamic soil impedance due to the embedment were observed. It was also observed that the dynamic characteristics became more complicated as the depth of the embedment increased.

(2). The resonance frequencies of soil-structure systems increase with the embedment, but the resonance amplitude decreases.

(3). The rocking component ratio decreases and the ratio of elastic deformation increases with embedment, but the sway component ratio is not influenced by embedment.

(4). The Fourier spectra of horizontal acceleration time histories obtained through earthquake observation of the test models show that the amplitude of the spectrum peaks due to SSI decrease and the predominant frequency becomes higher due to embedment. (Four typical examples of superimposed Fourier spectra of earthquake records obtained from models A(without embedment) and B(with embedment) are shown in Fig.7)

(5). In the vicinity of the natural frequency of the subsurface soil, the foundation input motions for the embedded structures were greater than those for non-embedded structures.

(6). Axisymmetric FEM models were confirmed as useful tools for investigating the dynamic interaction of embedded structures.

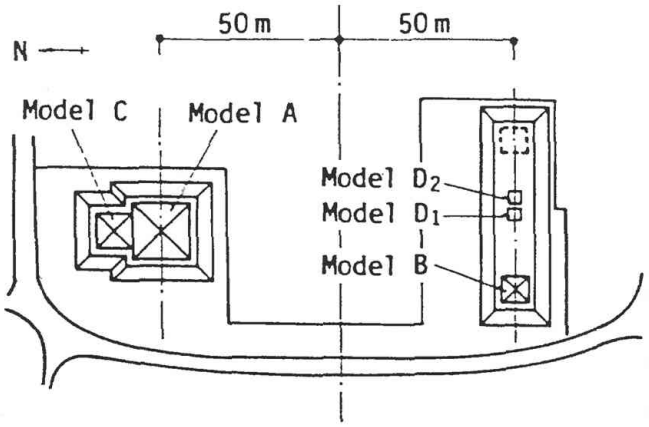

Fig.1
Layout of Building Models, A,B and C, and Block Foundation Models, D_1 and D_2.
(Model Tests on Dynamic Interaction Between Reactor Building and Soil)

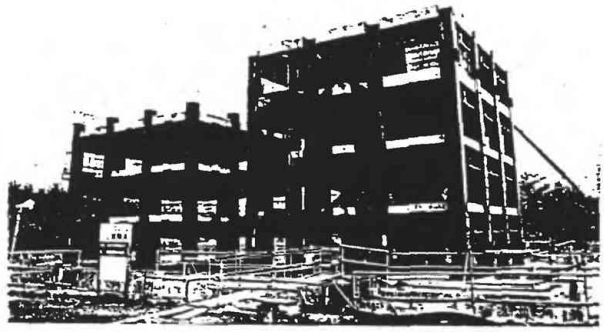

Fig.3 A Snap Shot of Building Models A and C
(Model Tests on Dynamic Interaction Between Reactor Building and Soil)

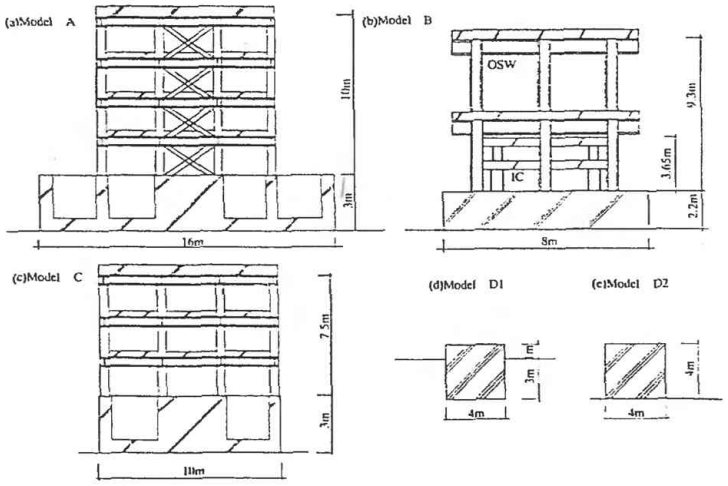

Fig.2 Outline of the Models Used in The Field Test
(Model Tests on Dynamic Interaction Between Reactor Building and Soil)

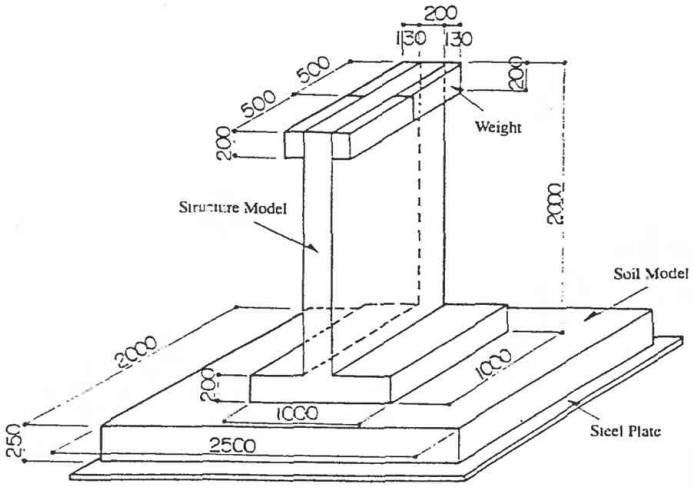

Fig.4 An Outline of Laboratory Test Models
(Model Tests on Base Mat Uplift of Reactor Building)

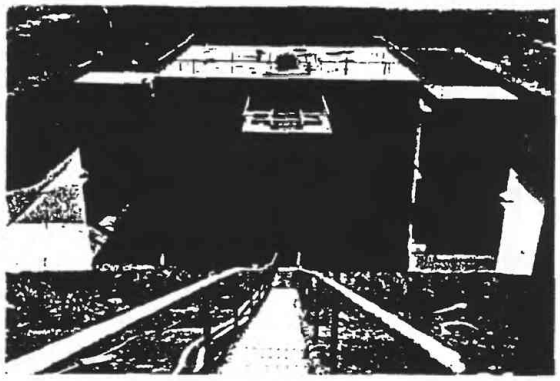

Fig.5 A Snap Shot of Field Test Models
(Model Tests on Base Mat Uplift of Reactor Building)

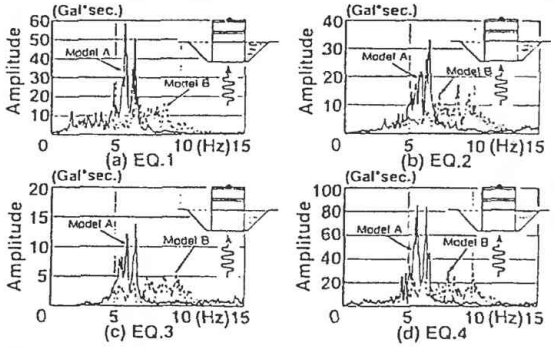

Fig7.
Comparison of Acceleration Fourier Spectra of Earthquake (EQ.) Responses Observed on RFs of buildings with and without embedment
(Model Test on Embedment Effect of Reactor Building)

Model A (Without Embedment)

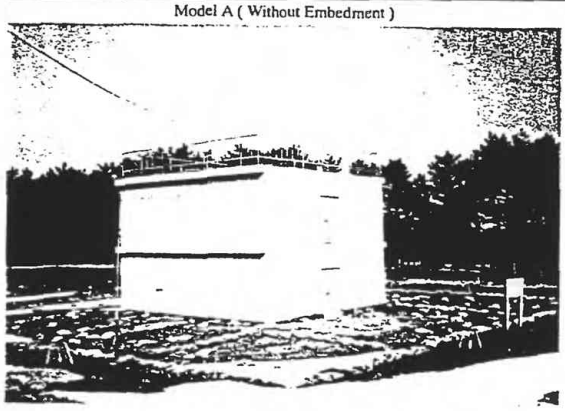

Model B (With Embedment)

Fig.6 A Snap Shot of Field Test Models
(Model Test on Embedment Effect of Reactor Building)

3. MODEL TEST ON DYNAMIC CROSS INTERACTION EFFECTS OF ADJACENT STRUCTURE

An overview of the generic NPPs shows that there are two aspects of the dynamic cross interaction (DCI) between adjacent buildings during earthquakes. One is the DCI effect between adjacent reactor buildings. The other is the DCI effect between reactor buildings and adjacent buildings such as turbine buildings. In either case, the dynamic behavior of reactor buildings during earthquakes is considered to differ from that of isolated single buildings, and this condition is assumed in the current earthquake response analyses for aseismic design of NPP reactor buildings. Thus, the DCI effect should be considered as one of the dynamic characteristics of NPP reactor buildings if the effect is too large to ignore. This is because the difference in dynamic characteristics of reactor buildings affects not only the aseismic performance of the reactor building itself but also the equipment related to NPP safety. At present the aseismic design of such equipment is performed using the evaluated earthquake responses of reactor buildings without considering DCI effects from adjacent structures. The following factors can be considered as a major cause of the effect: the dynamic impedance function, input motion to the foundation and the dynamic characteristics of the building. In order to evaluate this effect, NUPEC has been planning and carrying out field and laboratory tests under a commission from the Ministry of International Trade and Industry (MITI) of Japan using models of reactor buildings and adjacent structures. The field tests are being carried out to investigate the DCI effect under actual soil conditions. The field tests takes over the field and two building models from the preceding SSI research project, "Model Tests on Embedment Effect of Reactor Building". The site has soil conditions, which are approximately the same as those at actual nuclear power plant sites. The laboratory tests are being carried out to supplement the field tests using a ground model made of silicone rubber and building models made of aluminum. In these tests, building models are placed on the ground model, which is set up on a shaking table. Thus the models are subjected to excitations for detailed testing to evaluate the effect of the spaces between adjacent structures on the DCI effect among the building models. The tests are ongoing (started in April 1994 and will be completed in March 2002) and the results achieved to date are not sufficient to meet the final goal of this project. However, valuable test data has been accumulating gradually. This paper describes an outline and summary of the current status of this project.

3.1. BASIC CONCEPT

A system to investigate the SSI effect is shown in Fig.8. Figure 8(a) shows the method for single buiding and Fig.8 (b) shows that for adjacent structures.

The equation of motion for a single building as depicted in Fig.8 (a) is given as:

$$\begin{bmatrix} K_{BB} & K_{BF} \\ K^{T}_{BF} & K_{FF}+S^{(S)} \end{bmatrix} \begin{Bmatrix} U_B \\ U_F \end{Bmatrix} = \begin{Bmatrix} 0 \\ S^{(S)} \Delta^{(S)} \end{Bmatrix}$$

where, U_B and U_F are displacement vectors for the superstructure (B) and the foundation (F), respectively; K_{BB}, K_{BF}, and K_{FF}, are dynamic stiffness matrices of the superstructure and $S^{(C)}$ is the dynamic impedance function matrix involving the DCI effects, and $\Delta^{(C)}$ is the foundation input motion vector.

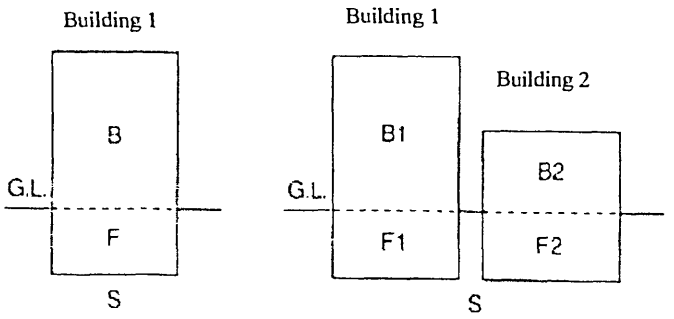

(a)Single Building (b)Adjacent Building

Fig.8 Soil-structure Interaction System

Similarly, the equation of motion for adjacent buildings (B1 and B2), as shown in Fig.8 (b), is described as:

$$\begin{bmatrix} K_{BB1} & 0 & K_{BF1} & 0 \\ 0 & K_{BB2} & 0 & K_{BF2} \\ K^T_{BF1} & 0 & K_{FF1}+S^{(C)}_{11} & S^{(C)}_{12} \\ 0 & K^T_{BF2} & S^{(C)T}_{12} & K_{FF2}+S^{(C)}_{22} \end{bmatrix} \begin{Bmatrix} U_{B1} \\ U_{B2} \\ U_{F1} \\ U_{F2} \end{Bmatrix} = \begin{bmatrix} 0 & 0 \\ 0 & 0 \\ S^{(C)}_{11} & S^{(C)}_{12} \\ S^{(C)T}_{12} & S^{(C)}_{22} \end{bmatrix} \begin{Bmatrix} \Delta^{(C)}_1 \\ \Delta^{(C)}_2 \end{Bmatrix}$$

where suffixes "1" and "2" represent buildings B1 and B2, respectively, $S^{(C)}_{ij}$ is the dynamic impedance function matrix involving the DCI effects, and $\Delta^{(C)}_i$ is the foundation input motion vector involving the DCI effects.

Equations (1) and (2), respectively, are the equations of motion for a single building and for adjacent buildings in which the DCI effect between two buildings is involved. In both cases, the dynamic interaction between the buildings and surrounding soil is evaluated from the dynamic impedance function and the foundation input motion. Thus, it is important in the present study to evaluate the dynamic impedance function of DCI in the building models and the input motion to their foundation through vibration tests and earthquake observations.

3.2. TEST PLAN

Field tests and laboratory tests are planned to investigate the DCI phenomena. Outlines of these tests are described in the following sections.

3.2.1 FIELD TESTS

Field tests are carried out at the same testing site as the field tests of the preceding test project, "Model Tests on Embedment Effect of Reactor Building". Two building models are used from the preceding test project.

Figure 9 shows an outline of the building models used in the field test. Three kinds of model conditions are introduced to investigate the effect of adjacent building on the SSI phenomena of the building in question, a single building model, two identical building models, and two different type buildings. The building models used in this project are models of reactor buildings (BWR) and a turbine building. The scale of these building models is about 1/10 of the actual buildings. The space between adjacent building models for the two different type buildings (reactor building and turbine building) was determined by referring to the closest example of these buildings, which was obtained by investigating actual plant construction conditions. The space between the identical building models was determined to facilitate observation of the dynamic interaction effect between the building models. The vibration tests of the building models using an exciter were carried out to evaluate accurate dynamic soil spring characteristics (dynamic impedance function and the foundation input motion) including the adjacent effect on SSI phenomena of the modeled buildings. Earthquake observation is also carried out to investigate the interactions between two adjacent building models under actual earthquake conditions. Furthermore, in order to comprehend embedment effect on the DCI of adjacent buildings, tests are carried out under different construction conditions, i.e., with and without embedment. Thus, the tests are divided into two parts. In the first part, vibration tests and earthquake observation is carried out without building embedment. In the second part, building models are embedded and vibration tests and earthquake observation are carried out.

3.2.2 LABORATORY TESTS

The laboratory tests are planned to supplement the field tests. Because the building models used in the field tests are too massive and heavy to move, some parameters, which have a strong influence on the DCI effect, are difficult to investigate in the field tests. The distance between adjacent buildings and/or the mutual adjacent effect between three closely constructed buildings are considered to be such items. In order to investigate such effects, small-scale model tests are planned as the laboratory tests.

Figure 10 shows a general outline of the laboratory tests. The test model consists of a ground model made of silicone rubber and building models made of aluminum. The building models are made to represent reactor buildings and a turbine building. The scale of the building models is about 1/260. These models are designed so that they have similar SSI characteristics to those of the building models used in the field tests. The ground models are fixed on a shaking table after placing building models on top. Several artificial earthquake ground motions are then applied to both the ground model and the building models to investigate the DCI effect in detail. The parameters in the test are adjacent building distance, building embedment depth and so on. Furthermore, one reactor building model has exciters at the top and base positions to apply eccentric centrifugal forces. The building models are used to simulate the vibration tests performed in the field tests, which are carried out using an exciter.

3.2.3 OVERALL TEST PLAN

The " Model Test on Dynamic Cross Interaction Effects of

Adjacent Structures" is being carrying out as an 8 year test project from fiscal 1994 to 2002. The test term can be divided into two parts at the end of fiscal 1997. In the first part, total planning and tests without building model embedment were carried out. These test results are currently being studied in detail. In the second part, which began in fiscal 1998, the building models are embedded to investigate the influence of the building embedment on the DCI effects of reactor buildings.

3.3. CURRENT STATUS OF TESTS

Because the tests are being carried out over rather a long time span, we feel that the current status of the tests should be reported to researchers in this field to gather many valuable comments on our project. Thus in the following section, we present the current status of the tests.

3.3.1 FIELD TEST

Figure 11 shows building model layout in the field tests. This figure represents our state of the art of the field test site in the end of fiscal 1997. Construction of all the building models has been completed and earthquake observation is on-going.

The site is located on a gentle hill. The building models are placed in three kind of conditions; single reactor building model (AA), closely constructed twin reactor building models (BAn and BAs), and two different type structures consisting of a reactor and a turbine building model (DA and DF respectively). The building models are made of reinforced concrete. Each building model is constructed on soil in a pit, which is excavated down to 4m from the surface level to prepare for the embedment of the buildings in the next stage of testing. The scale of these building models is about 1/10 of an actual BWR plant. Reactor building models all have the same dimensions of 8m×8m square in plan and 10.5m in height. The turbine building model has a rectangular plan of 6.4m in the north-south direction, 10m in the east-west direction and is 6.75m in height.

The building models, BAn and BAs, are installed on a soil layer of the same elevation. On the other hand, the building models, DA and DF are installed on different elevations in a pit reflecting actual plant conditions. The reactor building model, DA is installed on a lower ground level than that of the turbine building model by 1m as shown in Fig.12. Figure 13 shows a snap shot of the DA and DF building models. Up to the present, we have complete the construction of building models and vibration tests using an exciter for these building models under non-embedded conditions. Currently we are conducting earthquake observation with these test models.

The vibration tests were carried out in four steps. In the first step, the vibration characteristics of the reactor building model BAs was tested as a single structure before constructing the same type reactor building model BAn. Then after the construction of BAn, the BAs model was tested again together with newly constructed BAn as the second step in order to investigate the DCI effects of adjacent same type building models on their SSI characteristics. In the third step, The turbine building model DF was tested as a single structure before constructing the reactor building model DA. Then, after the construction of the DA model, the DF model was tested again together with DA as the final step in order to investigate the DCI effects of adjacent different type building models on their SSI characteristics.

In each vibration test, the buildings were excited in three directions, NS(north-south) direction, EW(east-west) direction and UD(up-down) direction independently. The vibration force was applied firstly to the top of the building using an exciter. Then the exciter was moved to the upper part of the base to apply force to the base of the building. Items measured during the test were the displacement in the major part of the buildings and soil pressure at the bottom of the foundation. Observed data was processed into resonance curves, and the soil pressure distribution and the data were used to evaluate vibration characteristics such as natural frequencies and damping.

Figure 14 shows superimposed resonance curves of the BAs model, which were obtained in the vibration test before and after the construction of the same type adjacent building model BAn as an example of the test results. Though the dominant frequency is nearly the same, the vibration peak after the construction of BAn forms two peaks and the peak height becomes slightly lower. Figures 15 and 16 show examples of the resonant curves of the turbine building model, DF, and one of the different two adjacent building models. Figure 15 shows the resonant curves obtained by excitation in the NS direction, the direction of the buildings in a line. The resonant curves of the building model DF, before and after the construction of the adjacent building DA, are superimposed. In addition, in Fig.16, two resonant curves obtained by excitation in the EW direction, perpendicular to the NS direction, are shown. In the figure, the resonant curves of the building model DF before and after the construction of the adjacent building model DA are superimposed. In Fig.15, reduction of the dominant natural frequency of SSI in the NS direction can be seen after the construction of adjacent building model DA. On the other hand in Fig.16, the natural frequency of SSI is nearly the same but a clear peak of 8.5Hz caused by the adjacent DA model is seen after the construction of the DA building model. The dominant frequency of the DA model of 8.5 Hz is slightly higher than that of BAs and BAn whose dominant frequencies are about 7.0Hz because of embedment of the base of DA model by 1m.

As has already been described in the previous section, earthquake observation of these building models has been carried out. Up to the present, acceleration records of nearly one hundred earthquakes have been observed including small acceleration records whose maximum acceleration is less than several Gal. Unfortunately these observed records were not necessarily obtained under the same structural conditions because the building were not constructed at the same time. Therefore, the systematic comparison of earthquake observation data for the evaluation of DCI effects of adjacent building models become possible from October 1997 when construction of

all building models was completed. As a typical example, we show an earthquake observation record of the earthquake of November 1997. Figure 17 shows tri-axial acceleration time histories observed in a free field. Earthquake observation in the free field is prepared at the site independently of the building models in order to estimate the actual input motion to the building models during earthquakes. The acceleration record shown in Fig.17 is observed at 3m below the ground surface level (GL-3.om). The record has a maximum acceleration of over 10Gal. in the NS direction.

Figure 18 shows Fourier spectra of earthquake acceleration time histories observed on top of the building models AA, BAs and BAn. Figure 18(a) shows the Fourier spectrum of the acceleration record of AA, a single structure model. Figure 18(b) shows superimposed two Fourier spectra observed in the acceleration records on BAs and Ban, the same type adjacent buildings. Although the Fourier spectra in Fig.18(b) show nearly the same spectral pattern, the Fourier spectrum in Fig.18(a) has a quite different pattern. The decrement of the dominant peak height in the Fourier spectra in Fig.18(b) was observed as compared with the Fourier spectrum in Fig.18(a). The cause of the difference might be pointed out immediately as the adjacent effects of building model composition, and differences between single and twin building compositions. However, because the detailed soil conditions under the building models are slightly different, so it should also be checked whether this difference is caused by the local soil conditions or not.

3.3.2 LABORATORY TESTS

For the laboratory tests, we manufactured a ground model made of silicone rubber and a reactor building model made of aluminum. We then performed shaking table vibration tests on the soil and building models. The ground model has dimensions of 2.8m in diameter and 1.0m in height. In order to avoid vertical transformation in the boundary of the ground model due to its own weight, 180 brass bars, each of which has a 3mm in diameter, were laid around the circumference of the ground model in the axial direction. In addition, to investigate the detailed ground model motion, accelerometers were laid inside the ground model at 13 points as shown in Fig.19. Thus we were able to measure 26 horizontal (13 cross directional components) and 5 vertical components of acceleration. The building model was made of aluminum with dimensions of 30cm×30cm in plan and 40 cm in height. Total weight of the model was 25 kgf. The model was designed to be similar to the reactor building model used in the field test.

In figures 20 and 21, we show the results of shaking table tests. The tests were performed by putting the building model on the ground model, which is installed on a shaking table, then swept sine motion and/or scaled earthquake motion were applied. Figure 20 shows a resonant curve obtained in the shaker test by applying swept sine motion using exciter installed in the building model. Figure 21 shows acceleration response spectra of 5% damping obtained by applying scaled earthquake motion in the shaking table test. In these figures, the dominant natural frequency of SSI is observed at 5.8Hz (0.17sec. in period). The response spectra in Fig.21 are seen to have nearly the same characteristics in despite of the differences in the excitation direction (cross directional direction). We then confirmed that the soil-structure model has no particular directional properties. Incidentally, the lower three natural frequencies of the ground model without the building model were observed at 2.4Hz, 7.3Hz and 13.0Hz. In addition, the natural frequency of the building model was observed at 140Hz in a hammering test.

From now on, the vibration test using exciters installed in a reactor building model, and the shaking table test by applying scaled earthquake motions, will be carried out together with other building models to be manufactured as adjacent building models. In particular, detailed investigation on the SSI effect under strong earthquake motions, which cannot be realized in the field tests, will be carried out systematically by taking into account the distance between the adjoining buildings as a parameter. The data obtained in the laboratory tests will be used to supplement the test results obtained in the field tests.

4. CONCLUDING REMARKS

The present paper describes the on-going study, "Model Test on Dynamic Cross Interaction Effect of Adjacent Structures" which is being carried out by NUPEC under a commission from the Ministry of International Trade and Industry. The purpose of the study is to evaluate the influence of buildings, which are constructed close to reactor buildings, on the earthquake response characteristics of the reactor building. The influence can be regarded as one of the soil structure interaction (SSI) phenomena which are still regarded as one of the most difficult problems in earthquake response simulation and/or design analysis of structures. Up to the present, many studies have been conducted to investigate the SSI phenomena. As the results of these studies, the effect of SSI on the earthquake response characteristics of structures has been found to be described in analytical models with the soil springs, which are assumed under the base of the buildings. However, SSI phenomena are still recognized as too complicate to allow proper analyses for earthquake response simulation and design of structures. Thus the success of the project will depend on ways to evaluate soil-spring characteristics, dynamic impedance function and the foundation input motion properly.

We are carrying out field tests using large-scale test building models on actual ground and a laboratory test using small-scale building models with an artificial ground model. At present, the test is on-going and there are not enough data for proper evaluation of the adjacent effect of the buildings. However, the tests without embedment have been completed and important basic test data are gradually accumulating. The embedment of the building models is scheduled for the latter half of fiscal 1998.

We will make much more effort hereafter to accumulate basic test data for evaluating the embedment effect on the dynamic cross interaction (DCI) among nearby buildings.

We will also conduct a detailed examination of the existing test data to establish an evaluation method for the DCI effect.

ACKNOWLEDGMENT

The project is being carried out through consultation with the sub-committee on "Model Test on Dynamic cross Interaction Effects of Adjacent Structure" (Chair person: Prof. Dr. M.Iguchi, Tokyo Science Univ., one of the authors). In addition, the annual test results have been being examined by the executive committee on "Verification Tests for Seismic Analysis Codes" (Chairperson: Prof. Dr. A.Shibata, Tohoku Univ.). The authors would like to express their thanks to everyone on the committee and the sub-committee for their hearty encouragement and advice on how to advanceing the project.

REFERENCES

1. Iguchi,M.,et al...: "Model Tests on Interaction of Reactor Building and Soil", Trans.9th SMiRT, vol.K1, pp.317-322, Lausanne, 1987.
2. Odajima,M.,et al..: "Analytical Study on Model Tests of Soil-structure Interaction", Trans.9th SMiRT, vol.K1, pp.311-316, Lausanne, 1987.
3. Iguchi,M., et al..,: "Large-Scale Model Tests on Soil-Structure Building Interaction – Part I : Forced Vibration Tests ", Proc.9th-WCEE, vol.III, pp.697-702, Tokyo, 1988.
4. Iguchi,M., et al..,: "Large-Scale Model Tests on Soil-Structure Building Interaction – Part II : Earthquake Observation", Proc.9th-WCEE, vol.VIII, pp.315-320, Tokyo, 1988.
5. Iguchi, M., et al..: "Model Test on Interaction of Reactor Building and Soil (Part 1: Cross Interaction Tests)". Trans.10th SMiRT, vol. K1: pp.211-216, Anaheim, 1989.
6. Iguchi, M., et al..: "Model Test on Interaction of Reactor Building and Soil (Part 2: Excitation by Earthquake)". Trans.10th SMiRT, vol. K1: pp.175-180, Anaheim, 1989.
7. Hangai,Y.,et al..: "Model Test of Base-mat Uplift of Nuclear Reactor Building (Part 1: Laboratory Test)". Trans.10th SMiRT, vol. K1: pp.169-174, Anaheim, 1989.
8. Onimaru,S.,et al..: "Model Test on Base-mat Uplift of Nuclear Reactor Building (Part 2: Field Tests on Actual Ground)". Trans.11th SMiRT, vol. K1, K08/2, pp.177-182, Tokyo,1991.
9. Nasuda,T.,et al..: "Embedment Effect Tests on Soil-structure Interaction", Trans.11th SMiRT, vol. K1, K06/1: pp.111-116,Tokyo,1991.
10. Shohara,R.,et al..: "Laboratory Model Tests with Silicone Rubber Ground Model (Embedment Effect Tests on Soil-structure Interaction)", Trans.11th SMiRT, vol. K1, K06/2: pp.117-122,Tokyo,1991.
11. Moriyama, K.,et al..: "Comparison between Tests and Analyses for Ground-Foundation Models (Embedment Effect Tests on Soil-structure Interaction)", Trans.11th SMiRT, vol. K1, K06/3: pp.123-1278,Tokyo,1991.
12. Kobayasi,T.,et al..: "Forced Vibration Test on Large Scale Model on Soft Rock Site (Embedment Effect Tests on Soil-structure Interaction)". Trans.11th SMiRT, vol. K1, K06/4: pp.129-134,Tokyo,1991.
13. Inukai,T.,et al..: "Forced Vibration Test on Large Scale Model on Hard Rock Site (Embedment Effect Tests on Soil-structure Interaction)". Trans.11th SMiRT, vol.K1, K06/5: pp.135-140,Tokyo,1991.
14. Fujimori,T.,et al..: "Experimental Study on Effects of Hardness of Supporting Ground Site (Embedment Effect Tests on Soil-structure Interaction)". Trans.11th SMiRT, vol.K1, K06/6: pp.141-146,Tokyo,1991.
15. Kurimoto,O.et al..: "Field Tests on Partial Embedment Effects (Embedment Effect Tests on Soil-Structure Interaction)", Trans.12th SMiRT, vol. K1, K02/2, pp.43-48, Stuttgart ,1993.
16. Fukuoka,A.,et al..: "Forced Vibration Tests on Three Types of Embedded Structures (Embedment Effect Tests on Soil-Structure Interaction)", Trans.12th SMiRT, vol. K1, K02/3, pp.49-54, Stuttgart ,1993.
17. Fujimori,T.,et al..: "Seismic Response of Embedded Structures (Embedment Effect Tests on Soil-Structure
18. Maeda,T.,: "Laboratory Tests on The Effect of Partial Interaction)", Trans.12th SMiRT, vol. K1, K02/3, pp. 55-60,Stuttgart ,1993.
19. Kurosawa,R.,: "Laboratory Tests on Soil — Structure Interaction with Backfill Soil Using Non-Linear Material Structures (Embedment Effect Tests on Soil-Structure Interaction)", Trans.12th SMiRT, vol. K1, K03/6, pp.97-102, Stuttgart ,1993.
20. Inukai.T.,et al..: "Dynamic Behavior of Embedded Structure on Hard Rock Site", Proc.10th-WCEE, vol.3, pp.1695-1700, Madrid, 1992.
21. Ohtsuka,Y.,: "Embedment Effects on Dynamic Soil-Structure Interaction", Proc.10th-WCEE, vol.3, pp.1707-1712, Madrid, 1992.
22. Fujimori,T.,: "Partial Embedment Effects on Soil-Structure Interaction", Proc.10th-WCEE, vol.3, pp.1713-1718, Madrid, 1992.
23. Shohara,R.,: "Tests on Dynamic Interaction Between Foundations", Proc.10th-WCEE, vol.3, pp.1879-1664, Madrid, 1992.
24. Moriyama,K.,et al..,: "Partial-Embedment Test on Soil-Foundation Interaction", Proc.10th-WCEE, vol.3, pp.1911-1916, Madrid, 1992.
25. Kurimoto,O.,: "Input Motions for Rigid Foundations to Observed Seismic Waves", Trans.13th SMiRT, vol.III, pp.13-18, Porto Alegre, 1995.
26. Fukuoka A.,: "Dynamic Soil-Structure Interaction of Embedded Structure", Trans.13th SMiRT, vol.III, pp.85-90, Porto Alegre, 1995.
27. Ohtsuka,Y.,: "Experimental Studiesy on Embedment Effects on Dynamic Soil-Structure Interaction", Proc.11th-WCEE, Paper No.59, Acapulco, 1996.

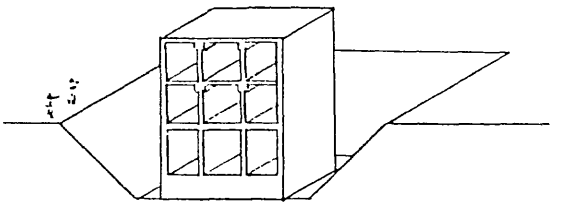

Single Reactor Building Model
(Without Embedment)

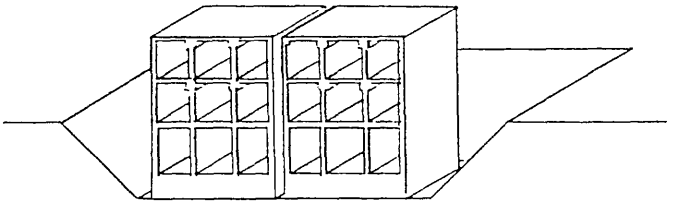

Two Identical Reactor Building Models
(Without Embedment)

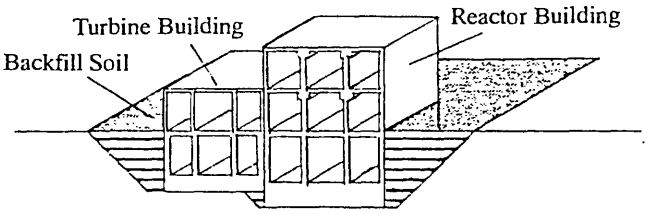

Two Different Building Models
(Reactor and Turbine Buildings With Embedment)

Fig.9 An Outline of the Field Test (Models and Test Conditions)

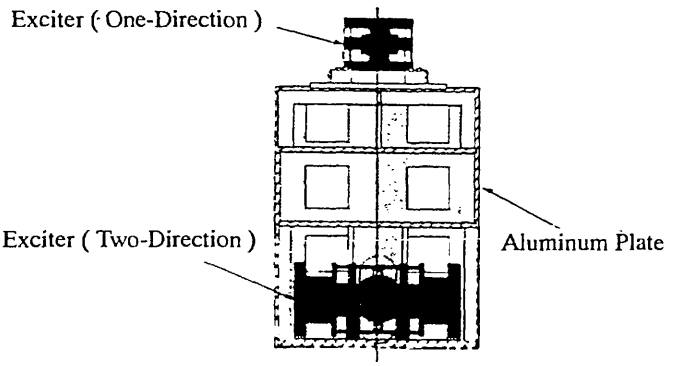

Reactor Building Model Detail

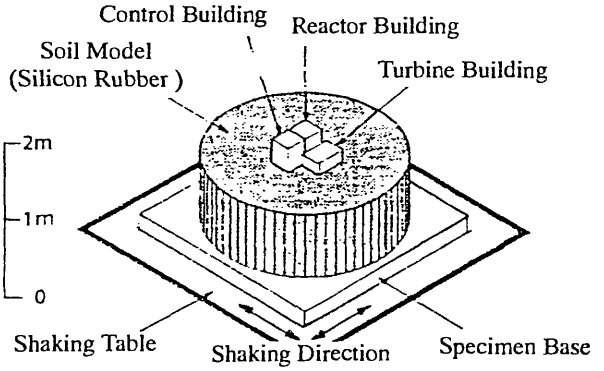

Laboratory Test

Fig.10 An Outline of the Laboratory Test

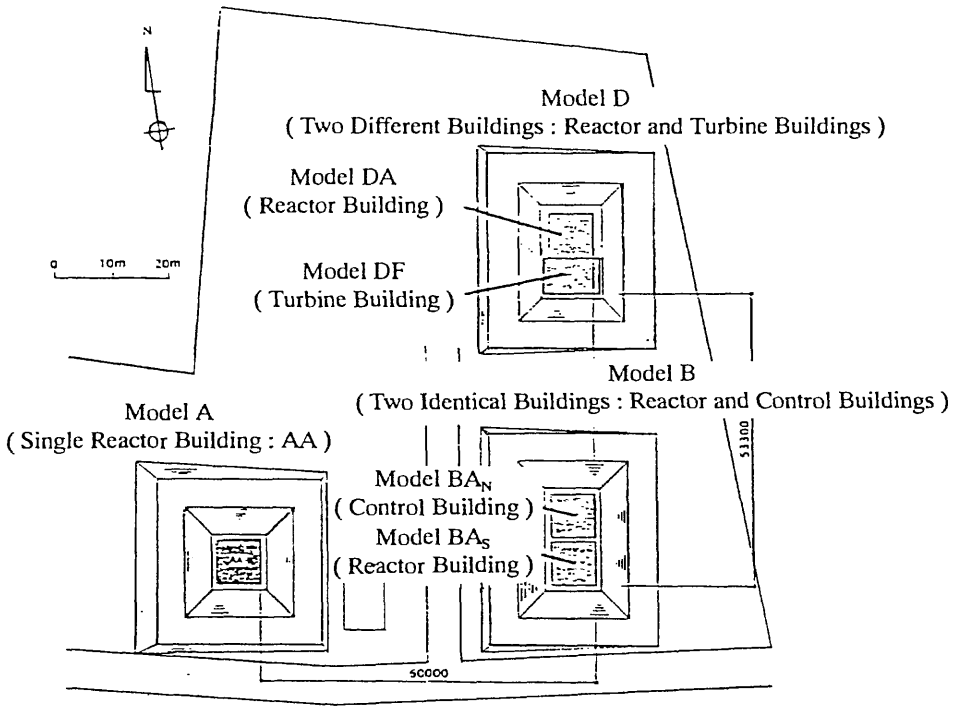

Fig.11 Layout of Test Building Models for the Field Test

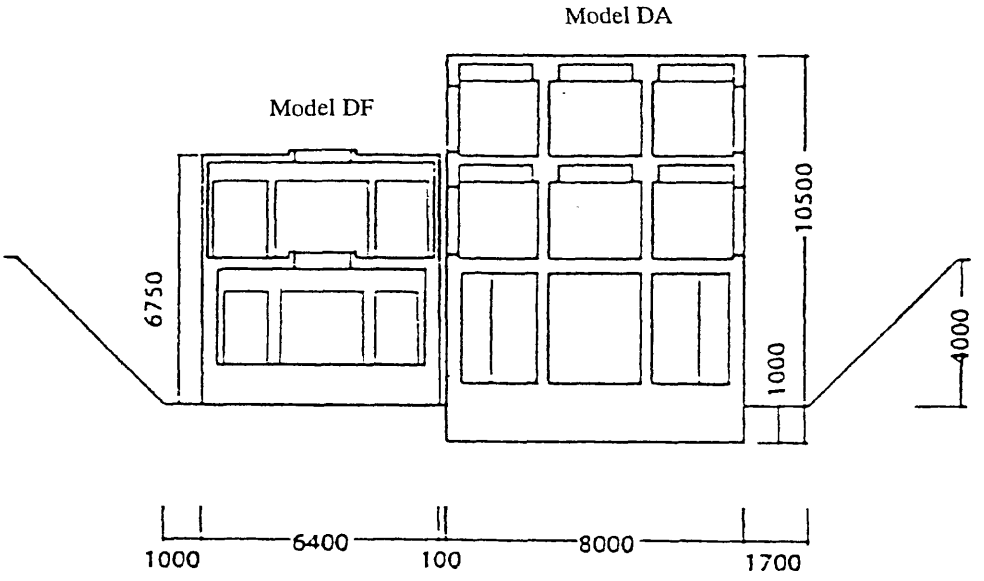

Fig.12 Cross Section of Building Models, DA(Reactor Bldg.) and DF(Turbine Bldg.) in The NS Direction.

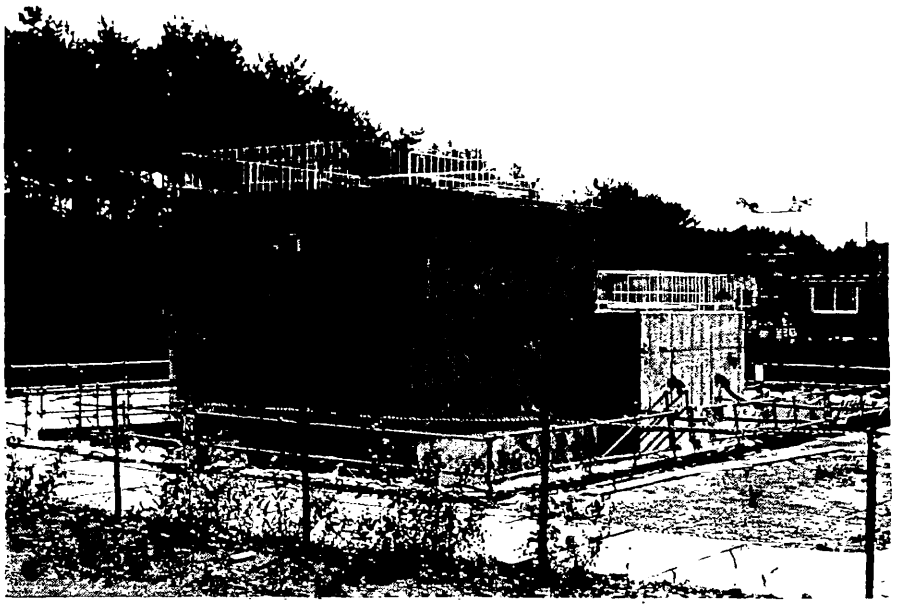

Fig.13 A Snap Shot of Building Models, DA(Reactor Bldg.) and DF(Turbine Bldg.)

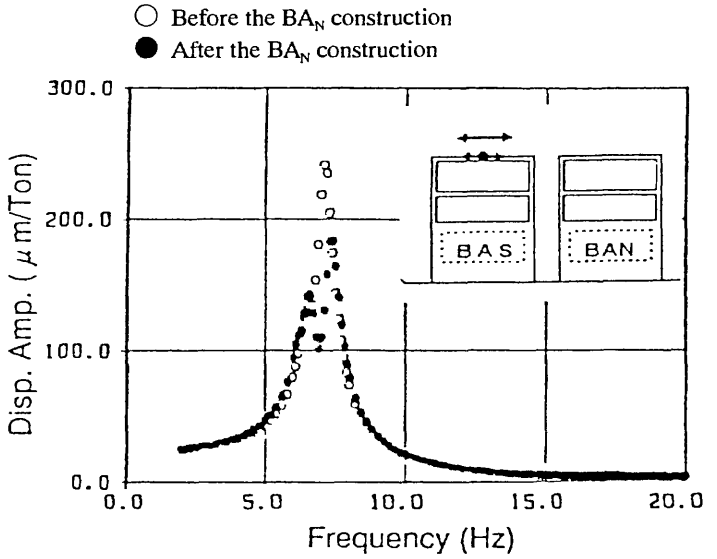

Fig.14 Resonance Curves Obtained by The Forced Vibration Test of BAs Bldg.
(NS Component due to Excitation in The NS Direction)

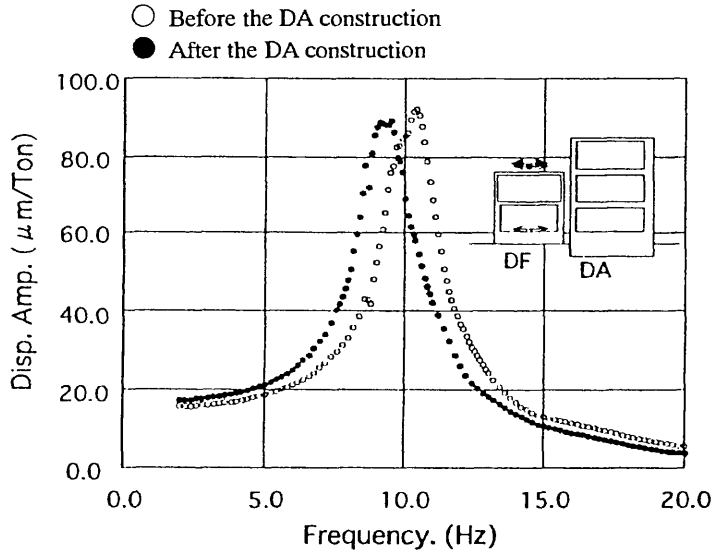

Fig.15 Resonance Curves Obtained by The Forced Vibration Test of DF Bldg.
(NS Component due to Excitation in The NS Direction)

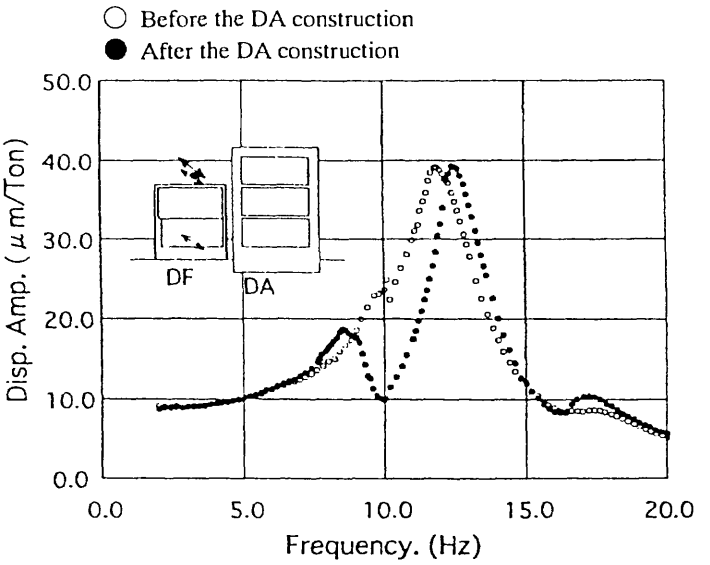

Fig.16 Resonance Curves Obtained by The Forced Vibration Test of DF Bldg.
(EW Component due to Excitation in The EW Direction)

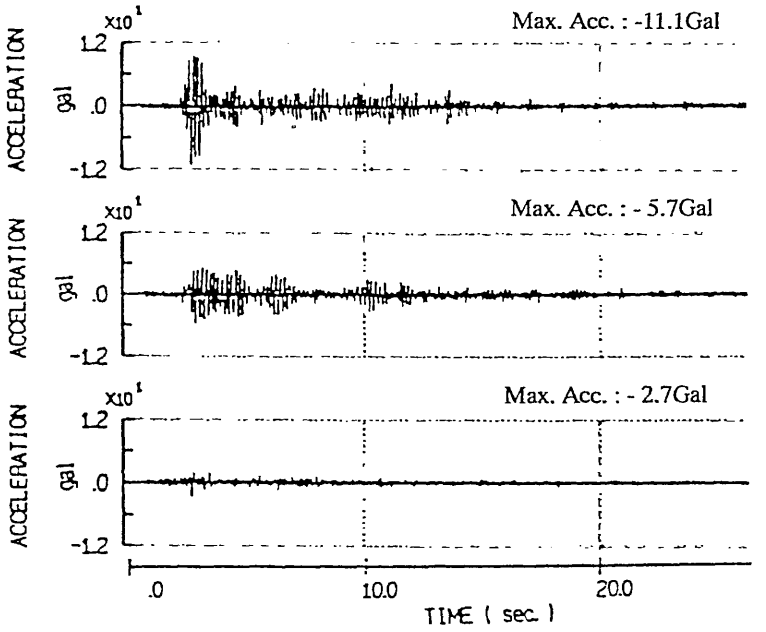

Fig.17 Observed Earthquake Record at Free Field of The Testing Site.(1997.11.20)

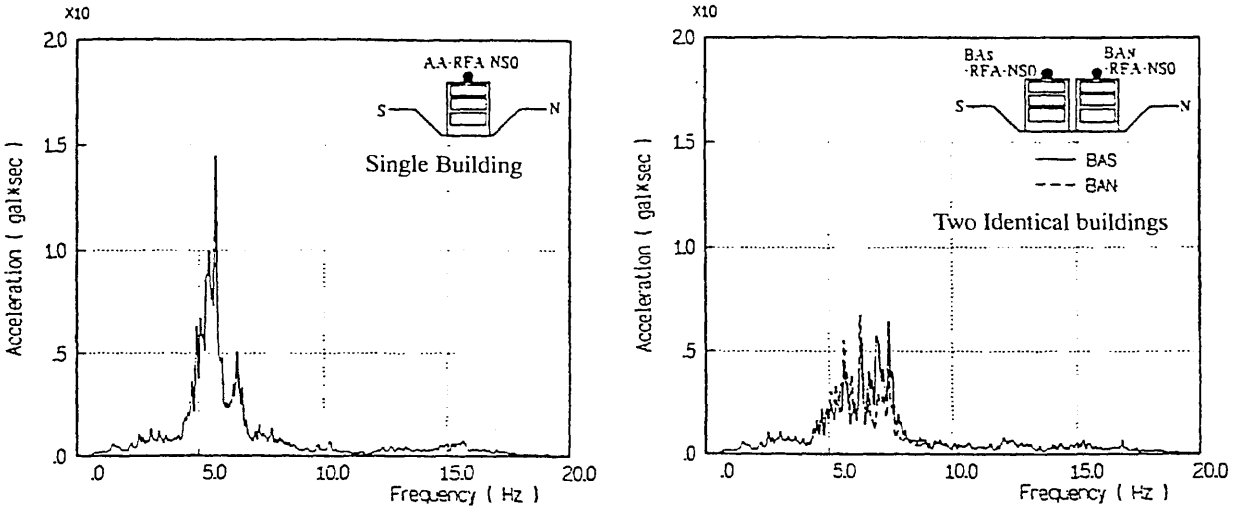

(a) Single Structure (b) Adjacent Structure

Fig.18 Fourier Spectra of Earthquake Acceleration Time Histories Observed at The Building Tops

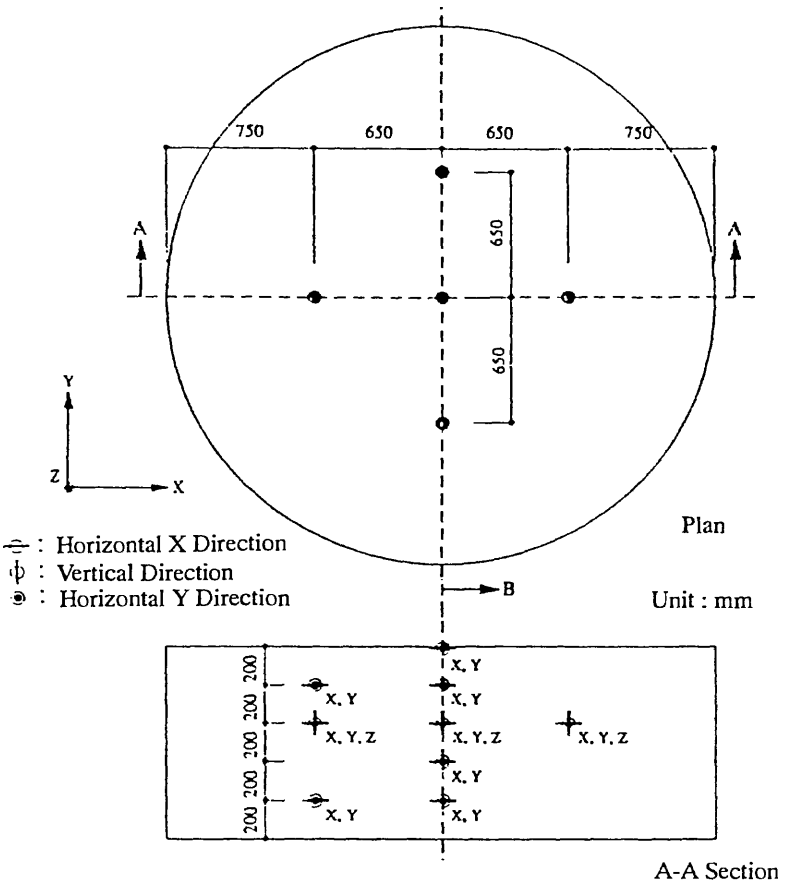

Fig.19 Location of Embedded Acceleration Sensors in The Soil Model

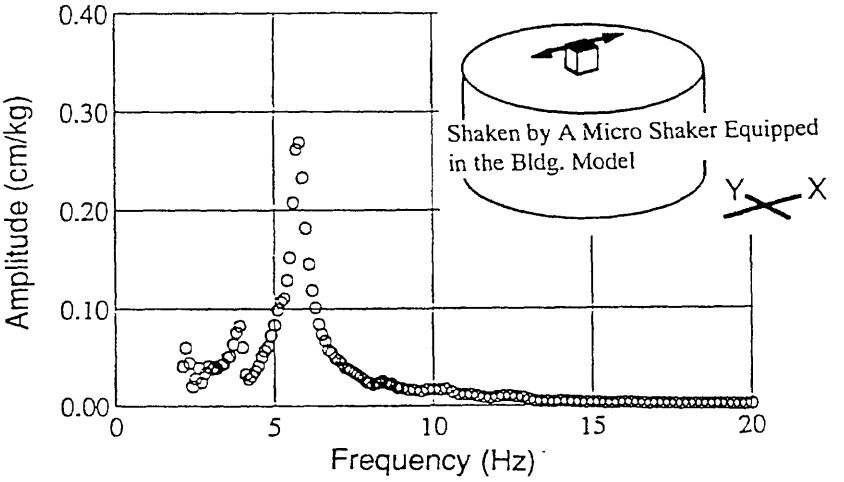

Fig.20 Resonant Curve of The Modeled Soil-Structure Obtained in the Shaker Test

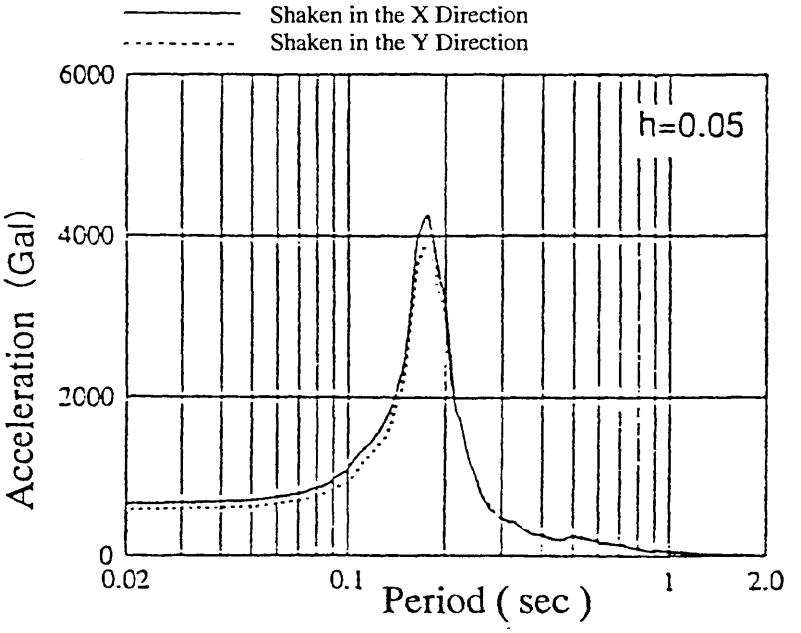

Fig.21 Acceleration Response Spectra at The Top of Building Model
(Shaking Table Test Results of Cross Directional Excitation)

DYNAMIC SOIL-FOUNDATION STRUCTURE INTERACTION ANALYSES OF LARGE CAISSONS

By Chin Man Mok[1], C.-Y. Chang[2], Randolph Settgast[3], Z.-L. Wang[1],

Helge M. Gonnermann[4], and C.-C. Chin[3]

ABSTRACT: A study was conducted to evaluate the important factors affecting the seismic response of large caissons. This paper presents the results of several equivalent linear and non-linear analyses performed for a typical case idealized based on the cellular caisson at Pier W3 of the West San Francisco Bay Bridge subject to longitudinal excitation with a peak rock acceleration of 0.6 g. This caisson is 127 ft long by 75 ft wide submerged in about 107 ft of water. It is embedded in 110 ft of soil deposits and is founded on rock. Equivalent linear 3-D analyses were conducted for the cases with and without the tower superstructure and suspension cables. The results indicate that superstructures have small effects on the seismic caisson response. The computed dynamic earth pressure and base stresses indicate that there will be soil-caisson gapping, rock-caisson base lifting, interface sliding, and soil yielding. The results from equivalent linear 2-D analyses in the direction of the short axis (longitudinal) are similar to those from the 3-D analyses. When the soil embedment is removed from the model, the dynamic stiffness and scattered motions at the caisson top only change slightly. However, the imaginary part of the foundation impedance functions is significantly smaller. Non-linear analyses were performed using a 2-D model. The results indicate that side gapping, base lifting, interface sliding, and soil yielding reduce the earth pressure, base and caisson stresses, and caisson motions. However, the frequency characteristics of the responses appear to be relatively unaffected.

[1] Senior Engineer, Geomatrix Consultants, Inc., 100 Pine Street, 10th Floor, San Francisco, CA 94111
[2] Principal Engineer, Geomatrix Consultants, Inc., 100 Pine Street, 10th Floor, San Francisco, CA 94111
[3] Staff Engineer, Geomatrix Consultants, Inc., 100 Pine Street, 10th Floor, San Francisco, CA 94111
[4] Project Engineer, Geomatrix Consultants, Inc., 100 Pine Street, 10th Floor, San Francisco, CA 94111

INTRODUCTION

Large caissons have been used as tower and pier foundations for many major long-span bridges (e.g., west and east spans of the San Francisco-Oakland Bay Bridge in San Francisco, California; the Bronx Whitestone Suspension Bridge in New York City; the Tacoma-Narrow Bridge in Seattle, Washington; and Benjamin Franklin Bridge in Philadelphia, Pennsylvania). Generally, these caissons are deeply embedded in soft soil deposits overlying rock or in rock-like materials. In relation to the seismic response and vulnerability evaluation of the bridges supported by large caisson foundations, an important concern is the effects of soil-foundation structure interaction (SFSI) on the superstructure response and the imposed load demands. Approaches used to model the SFSI for large caisson foundations differ substantially in methodology and degree of sophistication. There is little guidance for practitioners to follow in regard to choosing the appropriate approach to incorporate important factors under various situations in their analyses.

This study was part of a research project sponsored by the Federal Highway Administration and conducted by the National Center for Earthquake Engineering Research in Buffalo, New York to investigate the seismic vulnerability of existing highway construction. In this study, parametric sensitivity analyses were performed based on rigorous solution techniques to evaluate the important factors that affect the seismic response of caisson foundations. It includes an evaluation of soil yielding, gapping, slippage, sliding, and uplift in relation to potentially non-linear inelastic seismic response of the superstructure and caisson foundation. The results of this study will be used to develop guidelines on appropriate SFSI modeling requirements and analysis procedures for seismic analysis of caisson foundations. These modeling requirements include development of impedance functions (stiffness, mass, and damping matrices) to account for caisson response, and effective scattered motions for foundations (i.e., foundation input motions) for use in the response analysis of the superstructure using the substructuring approach.

This paper presents the results of dynamic equivalent linear and non-linear analyses performed to evaluate the SFSI effects on the seismic response of a typical caisson foundation. The analyzed example is based on the cellular caisson at Pier W3 of the West San Francisco Bay Bridge subject to longitudinal excitation with a peak acceleration of 0.6 g at rock outcrop. Equivalent linear finite element analyses were performed using the computer program SASSI (Lysmer et al., 1988). Three-dimensional analyses were performed for the cases with and without the superstructure to evaluate the effect of superstructure on the dynamic caisson response and to identify the potential for soil yielding, gapping, sliding, and foundation uplift. Two-dimensional equivalent linear analyses were performed to evaluate the appropriateness of using a 2-D model to approximate the dynamic caisson response along the short axis (longitudinal direction). Two-dimensional non-linear finite difference analyses were performed using the computer program FLAC (Itasca, 1993) to assess the effects of soil gapping, sliding, and uplift on the response of the caisson.

SUBSURFACE CONDITION

Figure 1 summaries the geologic condition at the site. It is interpreted based on the geotechnical data provided by the California Department of Transportation. The site is covered by about 110 ft of soil deposits overlying interbeds of weathered sandstone and mudstone. The mudline is

located at a depth of 107 ft. The top soil consists of about 20 ft of very soft Bay Mud underlain by about 30 ft of loose to medium dense sandy silt. Below these shallow soft layers is about 30 ft of medium dense to dense silty sand overlying about 10 ft of dense silty sand and gravel. In between these granular soil layers and the weathered bedrock is about 20 ft of hard sandy gravelly clay.

The measured shear- and compression-wave velocity profiles are also shown on Figure 1. The shear-wave velocity increases approximately from 600 ft/sec at 30 ft below mudline to about 1000 ft/sec at 100 ft below mudline. The compression-wave velocity in this depth range is almost constant at 5000 ft/sec. Below this depth range, the shear-wave velocity increases almost linearly to about 4500 ft/sec, while the compression-wave velocity increases to about 11000 ft/sec at 140 ft below mudline. Below this depth to about 200 ft below mudline, the shear- and compression-wave velocities of the rock are about 4500 ft/sec and 11000 ft/sec, respectively. There is no measurement in the top 30 ft of soil. The shear-wave velocity in the very soft Bay Mud is assumed to increase from 250 ft/sec to 300 ft/sec. The shear-wave velocity in the underlying loose sandy silt is assumed based on extrapolation from geophysical measurements. The compression-wave velocity in the top 30 ft of soil is assumed to be 5000 ft/sec.

DESIGN GROUND MOTIONS

The design rock motions were developed based on the ground motion study performed by Geomatrix. The acceleration, velocity, and displacement time histories of the longitudinal rock motion are shown on Figure 2. The corresponding 5% damped response spectrum is also shown on Figure 2. The predominant frequency of this motion is about 3 Hz.

FREE-FIELD SITE RESPONSE

Free-field site response analyses were performed using the computer program SHAKE based on an equivalent linear approach. The shear- and compression-wave velocity profiles used in the analyses were idealized based on the geophysical measurement shown on Figure 1. The shear-modulus reduction and damping ratio curves for clays were selected based on Vucetic and Dobry (1991). Those curves for sands were selected based on Seed and Idriss (1970). The acceleration, velocity, and displacement time histories of the computed longitudinal mudline motion are shown on Figure 3. The corresponding 5% damped response spectrum is also shown on Figure 3. The results indicate that the site frequency corresponding to the design ground motions is about 0.9 Hz. The strain-compatible shear-wave velocity and damping ratio obtained in the site response analyses were used to obtain the dynamic parameters for use in the SFSI analyses.

CAISSON FOUNDATION

The west bay spans of the San Francisco-Oakland Bridge consist of dual suspension bridges arranged back-to-back around a center anchorage. The general plan of Pier W3 is shown on Figure 4. The cellular concrete caisson is submerged in 107 ft of water and is embedded in 100 ft of soil deposit. The caisson and the underlying tremie concrete seal penetrate 14 ft into rock. The caisson is 127 ft long in the transverse direction and 75 ft wide in the longitudinal direction with twenty-eight (4 by 7) 15 ft diameter circular openings. The openings are filled with water

and extend to 30 ft above the caisson bottom. The top of the caisson is located at 25 ft above the water level.

THREE-DIMENSIONAL EQUIVALENT LINEAR ANALYSES

The analyses were performed using a quarter model to take advantage of the symmetry/anti-symmetry conditions. The SASSI 'structure' finite element mesh is shown on Figure 5. The mesh includes the caisson, superstructure tower, suspension cables, and two layers of soil/rock finite elements surrounding the caisson. Rigid links were added at the top of the caisson distribute the forces from the superstructure. The caisson is modeled by solid brick elements whose dynamic properties are selected based on smearing the composite flexural and shear rigidities of the caisson. The hydrodynamic masses accounting for the dynamic effects of water surrounding the caisson and inside the circular openings are included in the model (Goyal and Chopra, 1988). The hydrodynamic masses simulating the water in the internal openings are smeared in the model and the hydrodynamic masses simulating the external water surround the caisson are treated as lumped masses. The program SASSI was modified to include frequency dependent springs for modeling the suspension cables. The springs are connected to the superstructure on one end. Free-field rock outcrop excitation motions were prescribed at the other end of the springs.

To account for SFSI in the seismic analysis of a global superstructure model of a long span bridge, foundation impedance functions at the base of bridge piers or the top of caissons generally are required as input to the analysis. Also required are the input scattered motions incorporating the SFSI of the caissons at the same locations. To compute the foundation impedance functions and scattered motions at the top of the caisson, a foundation substructure model was created by removing the superstructure and cables from the mesh shown on Figure 5.

To study the effects of soil embedment on the seismic response of the impedance functions and scattered motions, another model was created by further removing the soil elements in the foundation substructure model.

Characteristics of Impedance Functions at Top of Caisson Foundation

The model shown on Figure 5 was analyzed using the dynamic finite element computer program SASSI (Lysmer et al., 1988). Figures 6 and 7 shows the real and imaginary parts of the impedance functions (6 x 6), respectively, at the top of the caisson at Pier 3 in the longitudinal direction. The impedance functions are frequency-dependent. To account for the frequency-dependent characteristics of the impedance functions (at least for the real parts) in the dynamic structural analysis using conventional codes, the following idealizations were made.

The impedance functions are defined as follows:

$$K_{ij}(\omega) = k_{ij}(\omega) + i\omega c_{ij}(\omega) \quad (i,j = 1,6) \tag{1}$$

where k_{ij} is the real part of the impedance, $T_{c_{ij}}$ is the imaginary part, and T is circular frequency. The impedance functions expressed by Equation 1 are a 6 x 6 symmetric matrix. The diagonal terms k_{ii}, $i = 1,3$ are associated with translations, and k_{ii}, $i = 4,6$ are associated with rotations. The

off-diagonal terms represent coupling between translations and rotations. For the piers analyzed, only the off-diagonal terms associated with the horizontal translation and rocking ($i=1, j=5$; and $i=2, j=4$) are significant; the remaining off-diagonal terms are negligible.

An attempt was made to fit a polynomial function through the real and imaginary parts of the computed impedance functions. The real parts of the impedance functions, k_{ij}, were fitted by:

$$k_{ij}(\omega) = (k_o)_{ij} - \omega^2 m_{ij} \qquad (2)$$

where $(k_o)_{ij}$ is the static stiffness and $(m)_{ij}$ is the equivalent mass or mass moment of inertia. For the imaginary parts, a third-order polynomial function was used to fit to the data.

$$\omega c_{ij} = A_{ij} + B_{ij}\omega + C_{ij}\omega^2 + D_{ij}\omega^3 \qquad (3)$$

The real part of the computed impedance was fitted reasonably well by Equation 2 (shown as solid lines on Figure 6), indicating that the frequency-dependent stiffness can be reasonably approximated by the use of a static stiffness and a mass (or mass moment of inertia) at frequencies up to about 2.5 to 4 Hz for the horizontal translations and rotations. The imaginary parts of the impedance functions shown on Figure 7 are strongly frequency-dependent, resulting in dashpot coefficients that also are frequency-dependent.

Scattered Motions at Top of Caisson Foundation

The response spectrum (5% damped) of the acceleration time history (i.e., foundation scattered motion) computed at the top of the caisson without the tower are shown on Figure 8. Also shown are the response spectra of the rock motion and the free-field mudline motion. Generally, the response spectra of the motions at the top of the caisson are amplified from the rock motion and are lower than the mudline motions at periods longer than 1 second for the longitudinal component, at periods longer than 0.8 second for the transverse component, and in the entire period range for the vertical component. Comparisons of the response spectra (5% damped) for the motions at the top of the caisson with and without the superstructure (tower) are shown on Figure 9. The two sets of motions are similar in frequency content and spectral values, indicating insignificant effects of the tower on the response of this caisson.

Effects of Soil Embedment on Impedance Functions and Foundations Scattered Motions

Because caisson foundations generally are embedded in soft soil deposits, it is desirable to examine effects of the upper soil deposits on the response of the caisson or specifically on the impedance functions and input foundation motions at the top of the caisson. Impedance functions and input motions were computed and compared for two caisson models at Pier W3, one with and the other without soil embedment.

The real and imaginary parts of the impedance functions computed at the top of the caisson in the longitudinal direction for the two cases (with and without soil embedment) are compared on Figure 10 (solid lines are for the case with soil embedment; dashed lines are for the case without

soil embedment). Generally, the real part of the impedance functions for the case with soil embedment is slightly higher than that for the case without soil embedment; the differences are generally less than a few percent. However, the imaginary part is significantly higher for the case with soil embedment than that for the case without soil embedment, reflecting greater radiation damping associated with soil embedment. The effect increases with frequency.

Figure 11 shows the response spectra (5% damped) of the acceleration time histories of the scattered motions for the two cases (with and without soil embedment). The frequency contents of these motions are similar.

Seismically Induced Soil Stresses Surrounding the Caisson

Dynamic stresses in the soils surrounding the caisson (along the base and side of the caisson) were calculated and compared with static hydrostatic stresses. The results indicated that dynamic stresses calculated from the SASSI analyses (based on equivalent linear techniques) are significantly higher than the static hydrostatic stresses, indicating a likelihood of separation (i.e., uplift along the base and gapping along the side of the caisson). Thus there is a need to perform nonlinear response analyses to examine the effects of potential uplift and gapping on the response of the caisson.

TWO-DIMENSIONAL EQUIVALENT LINEAR ANALYSES

A 2-D longitudinal model (short axis) was developed by considering a unit-width strip of the 3-D model described above without the superstructure and cables. The impedance functions and scattered motions obtained from the two-dimensional analyses were compared with the results from the three-dimensional analyses. The results from 2-D and 3-D analyses are similar, suggesting that a two-dimensional model can reasonably approximate the seismic response of the caisson in the longitudinal direction. Figure 12 shows the comparison of the response spectra of the scattered motions.

TWO-DIMENSIONAL NON-LINEAR ANALYSES

The primary objective of the non-linear analyses is to evaluate the significance of soil-caisson gapping, rock-caisson uplifting separation, and near-field soil softening on the seismic motions and stresses developed in the caisson. A visco-elastic constitutive model is used to represent the dynamic behavior of the soil and rock. The dynamic parameters of this model were calibrated to those used in the equivalent linear analyses. The analyses were performed in time domain. A Lagrangian approach is used to account for large-strain finite difference grid deformation. The finite difference grid used in the analyses is shown on Figure 13. Interfaces were added to model gapping, lifting, and sliding at the soil-caisson and rock-caisson contacts. It is developed based on the finite element mesh used in the equivalent linear analyses. The grid boundaries were extended sufficiently far away from the caisson to reduce the boundary effects on the caisson response. Viscous dashpots were attached to the boundaries to simulate the wave propagation through a semi-infinite medium. The input control motions are defined at the base and were obtained as interface motions at the appropriate depth from the free-field site response analyses.

The cases analyzed are presented in Table 1. These cases include various soil-caisson and rock-caisson interface properties as well as different levels of near-field soil softening.

Figure 14 shows the comparison of 5% damped response spectra of ground motions computed by the 2-D SASSI and FLAC analyses at the top of the caisson assuming no interface gapping, lifting, or sliding. The comparison of acceleration time histories at the center of the caisson at the top, mudline, and base levels are shown on Figure 15. The shear and bending moment time histories induced in the caisson at the mudline, above-tremie seal, and tremie seal levels are compared on Figures 16 and 17. These comparisons show that the results from these two programs are similar.

Figures 18 through 21 show similar comparisons of response spectra, acceleration time histories, and caisson shear and bending moment obtained for the cases of smooth interfaces, moderate interface strength, and glued interfaces (perfect contact). The results indicate that the seismic motions and stresses developed in the caisson are sensitive to the interface properties. A softer interface tends to reduce the peak response, but it does not significantly affect the frequency characteristics of the response. The predominant frequency appears to be relatively insensitive. It may be because a visco-elastic model was used to represent the dynamic rock behavior.

Similar comparisons of response spectra, acceleration time histories, and caisson shear and bending moment obtained for the cases of different near-field soil softening were performed. The results indicate that the responses are not sensitive to the properties of the soil because the resistance provided by soft soil is small. This behavior is similar to the results obtained by equivalent linear analyses without soil embedment. A comparison of the 5% response spectra of the motions computed at various caisson levels is shown on Figure 22.

CONCLUSIONS

The results of this study indicate that soil embedment has significant effects on the imaginary part of the impedance functions computed for the top of the caisson. However, the real part of the impedance functions only decreases slightly when the soil embedment is absent. The scattered motions at the top of the caisson are very similar for the cases with and without soil embedment.

The lateral earth pressure, base contact pressure, and soil stresses computed by the equivalent linear analyses indicate the possibility of soil-foundation separation (gapping and uplift). The results of non-linear analyses indicate that motions and stresses developed in the caisson are sensitive to the soil-caisson and rock-caisson interface properties. The peak responses are lower for softer interface strength. However, the frequency characteristics are less affected.

ACKNOWLEDGMENTS

The research on which this paper is based was supported by the National Center for Earthquake Engineering Research (NCEER), Highway Project No. 106, Seismic Vulnerability of Existing Highway Construction, under the sponsorship of the Federal Highway Administration (FHWA Contract No. DTFH61-92-C-00106).

APPENDIX I. REFERENCES

Itasca Consulting Group, Inc. (1993). "FLAC, fast Lagrangian analysis of continua, Version 3.2."

Lysmer, J., Ostadan, F., Tabatabaie, M., Vahdani, S., and Tajirian, F. (1988). "SASSI - A system for analysis of soil-structure interaction, user's manual", Geotechnical Engineering Division, Civil Engineering Department, University of California, Berkeley, and Bechtel Power Corporation.

Seed, H.B. and Idriss, I.M., (1970). "Soil Moduli and Damping Factors for Dynamic Response Analyses", Report No. EERC 70-10, Earthquake Engineering Research Center, University of California, Berkeley, California.

Vucetic, M and Dobry, R. (1991). "Effect of Soil Plasticity on Cyclic Response", Journal of Geotechnical Engineering, ASCE, Vol. 117, No.1, pp. 89-107.

Goyal, A. and Chopra, A.K. (1988), "Simplified Evaluation of Added Hydrodynamic Mass for Intake Towers", Journal of Engineering Mechanics, Vol. 115, No. 7.

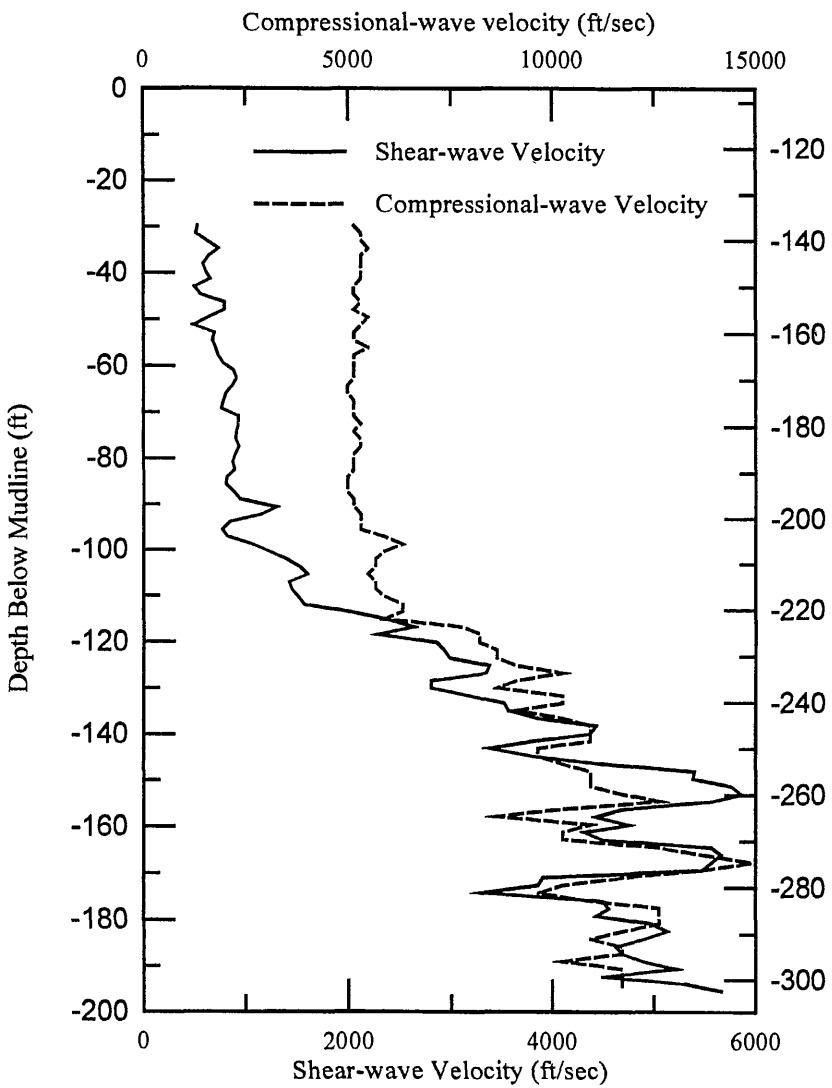

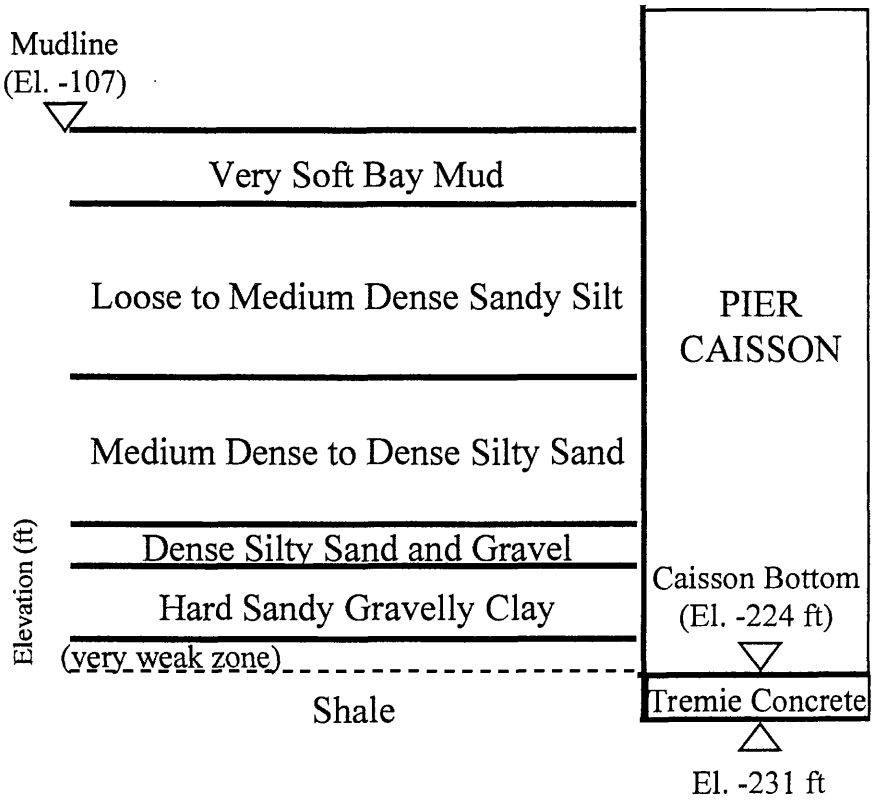

Figure 1: Idealized Geologic Profile

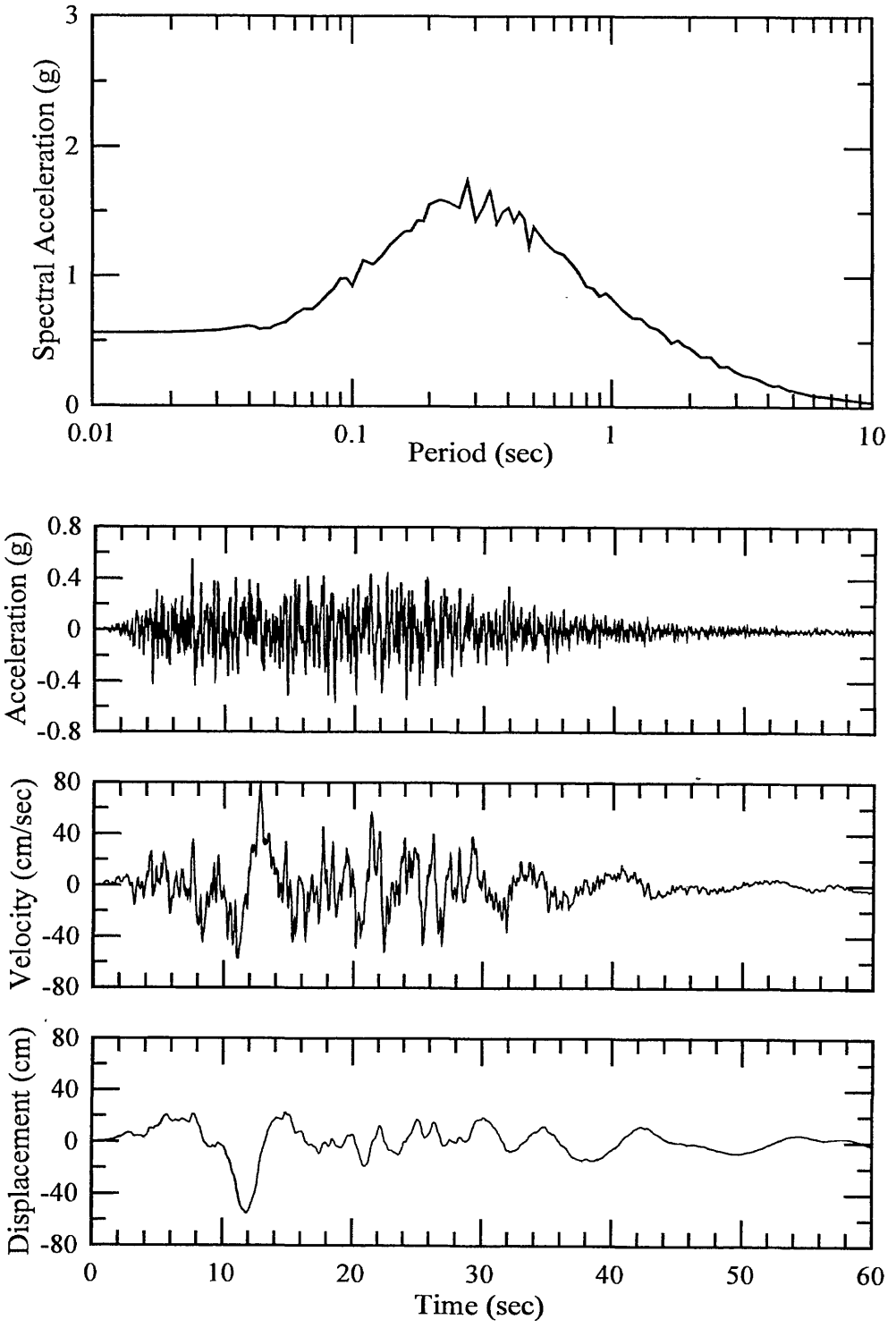

Figure 2: Longitudinal Input Rock Outcrop Motions

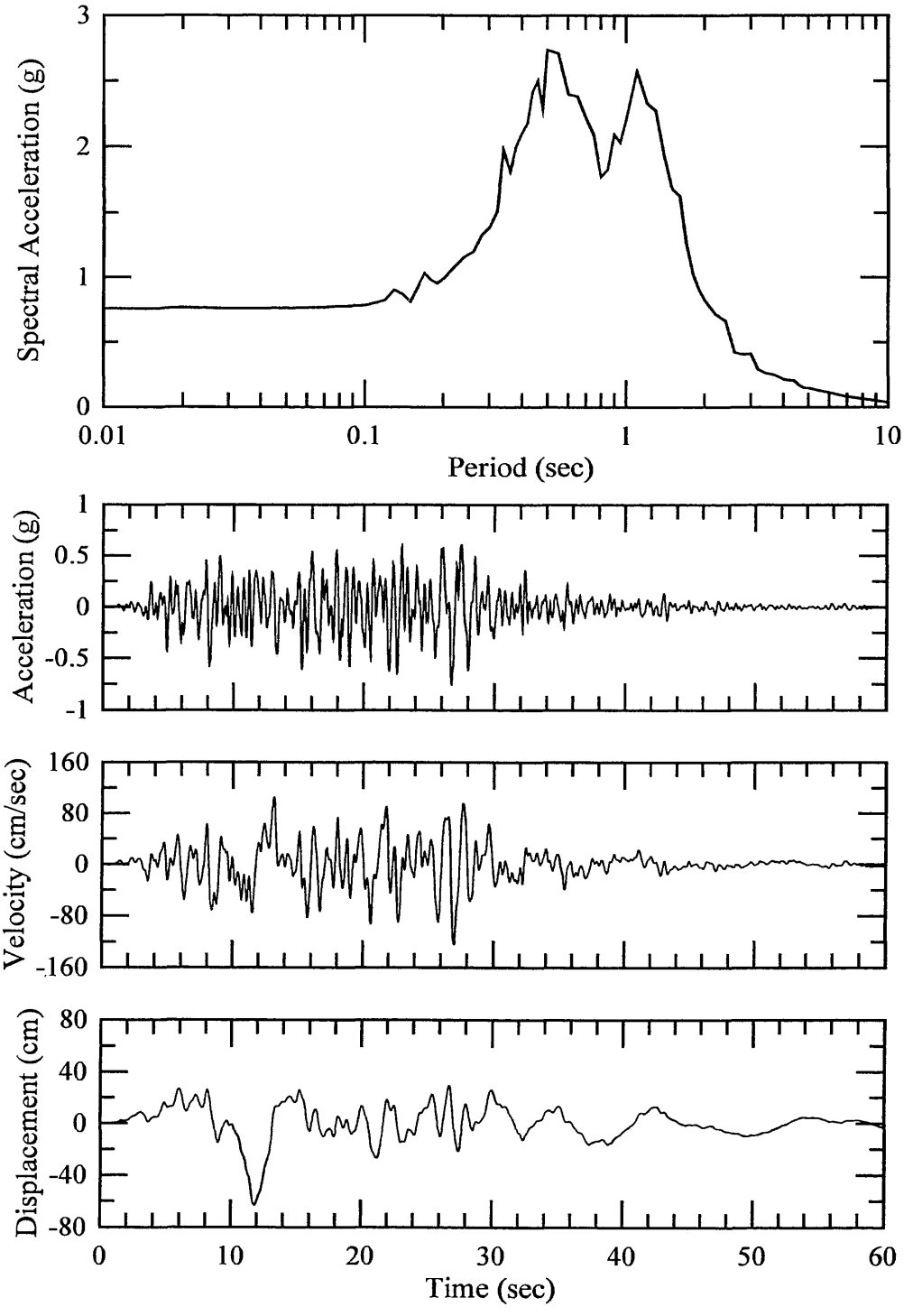

Figure 3: Computed Longitudinal Free-Field Mudline Motions

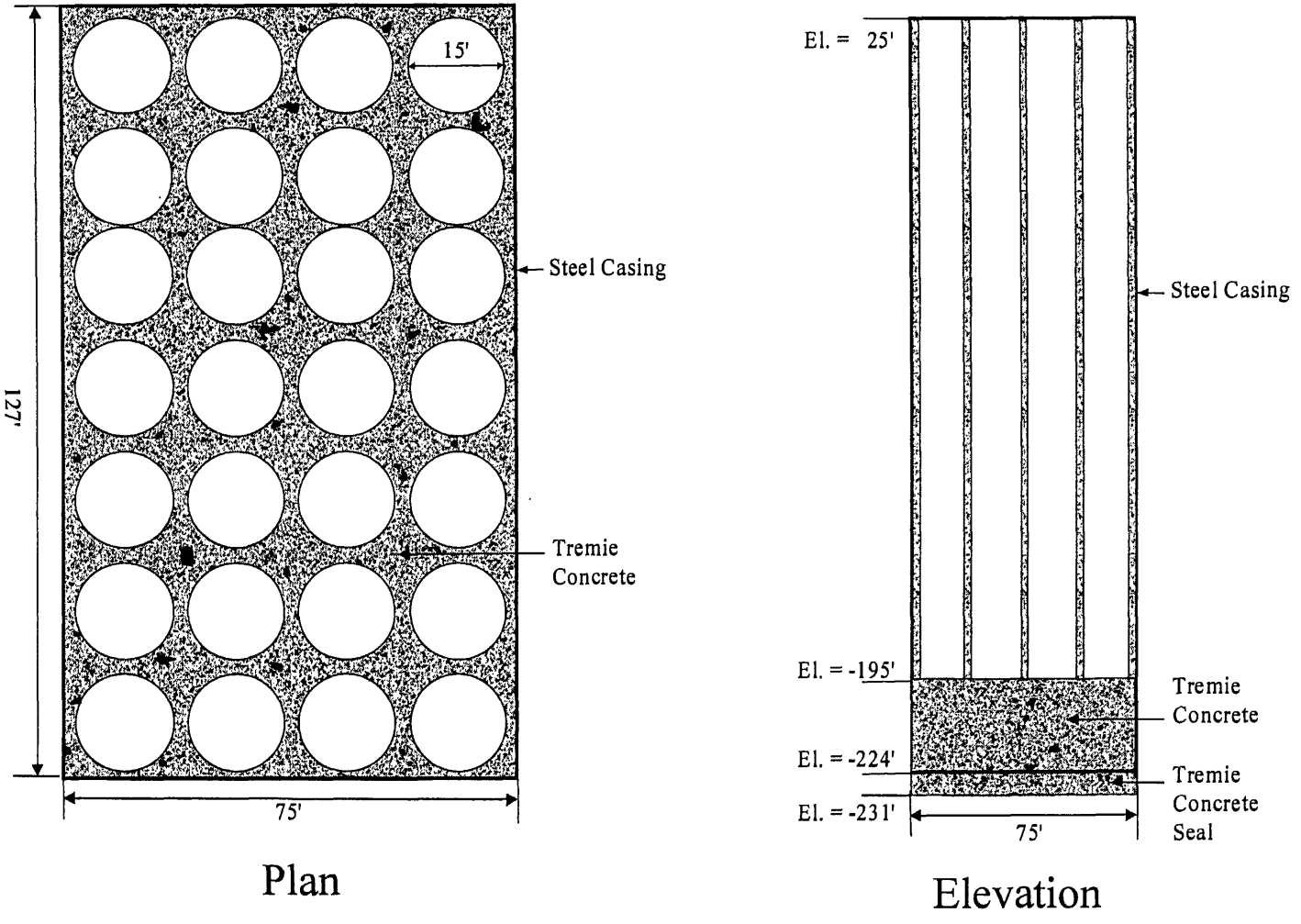

Figure 4: General Plan and Elevation

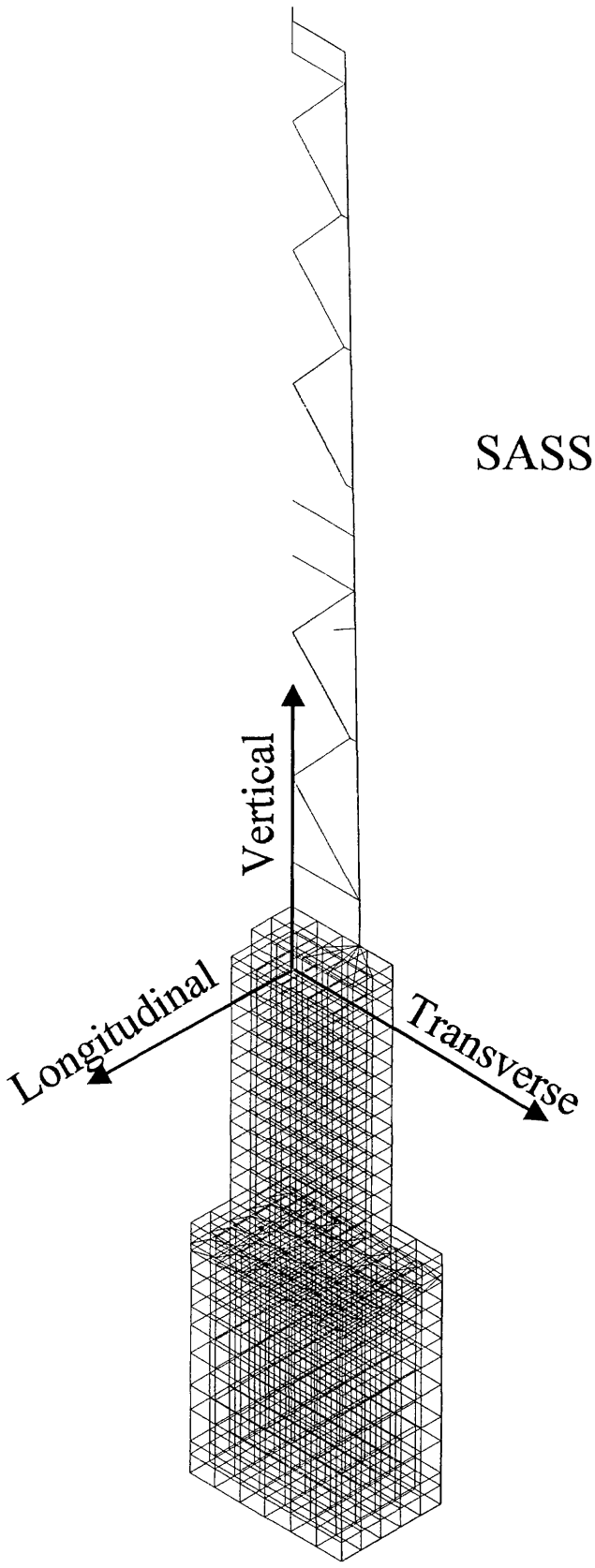

Figure 5:
SASSI Finite Element Quarter Model

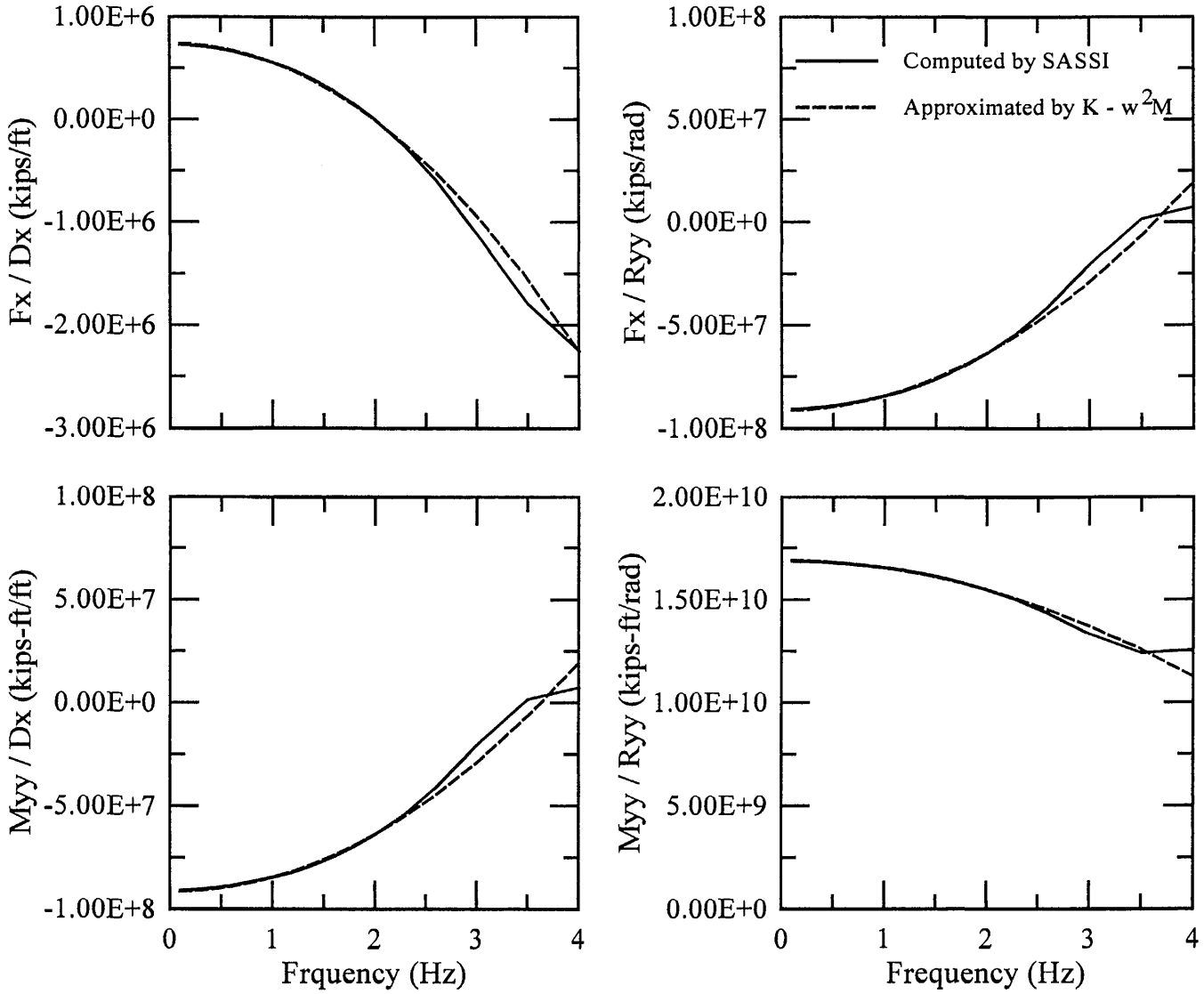

Figure 6: Real Part of Foundation Impedance Functions at Caisson Top

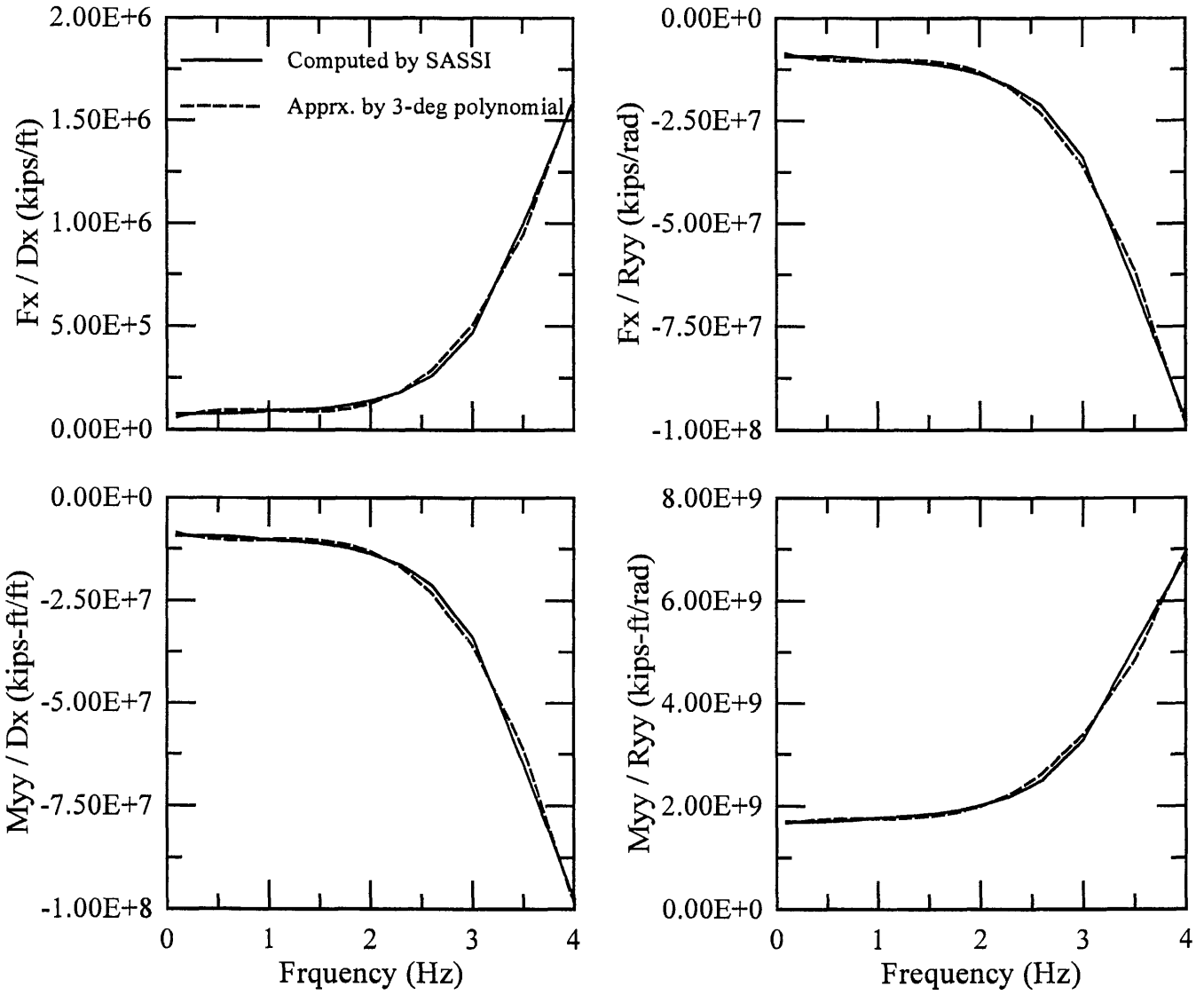

Figure 7: Imaginary Part of Longitudinal Foundation Impedance Functions at Caisson Top

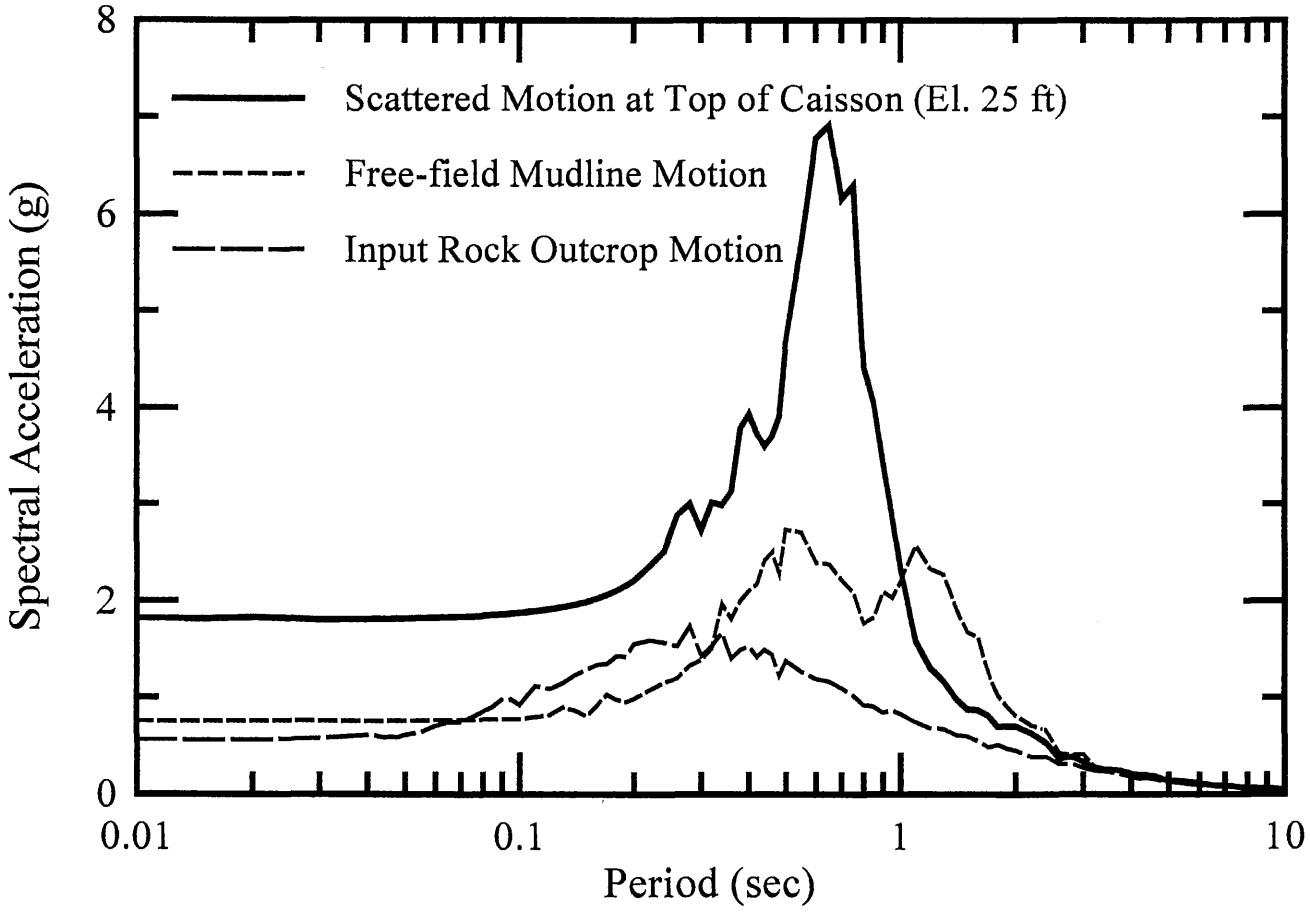

Figure 8: Comparison of 5% Damped Response Spectra of Substructure Scattered Motions with Computed Free-Field Mudline and Input Rock Outcrop Motions

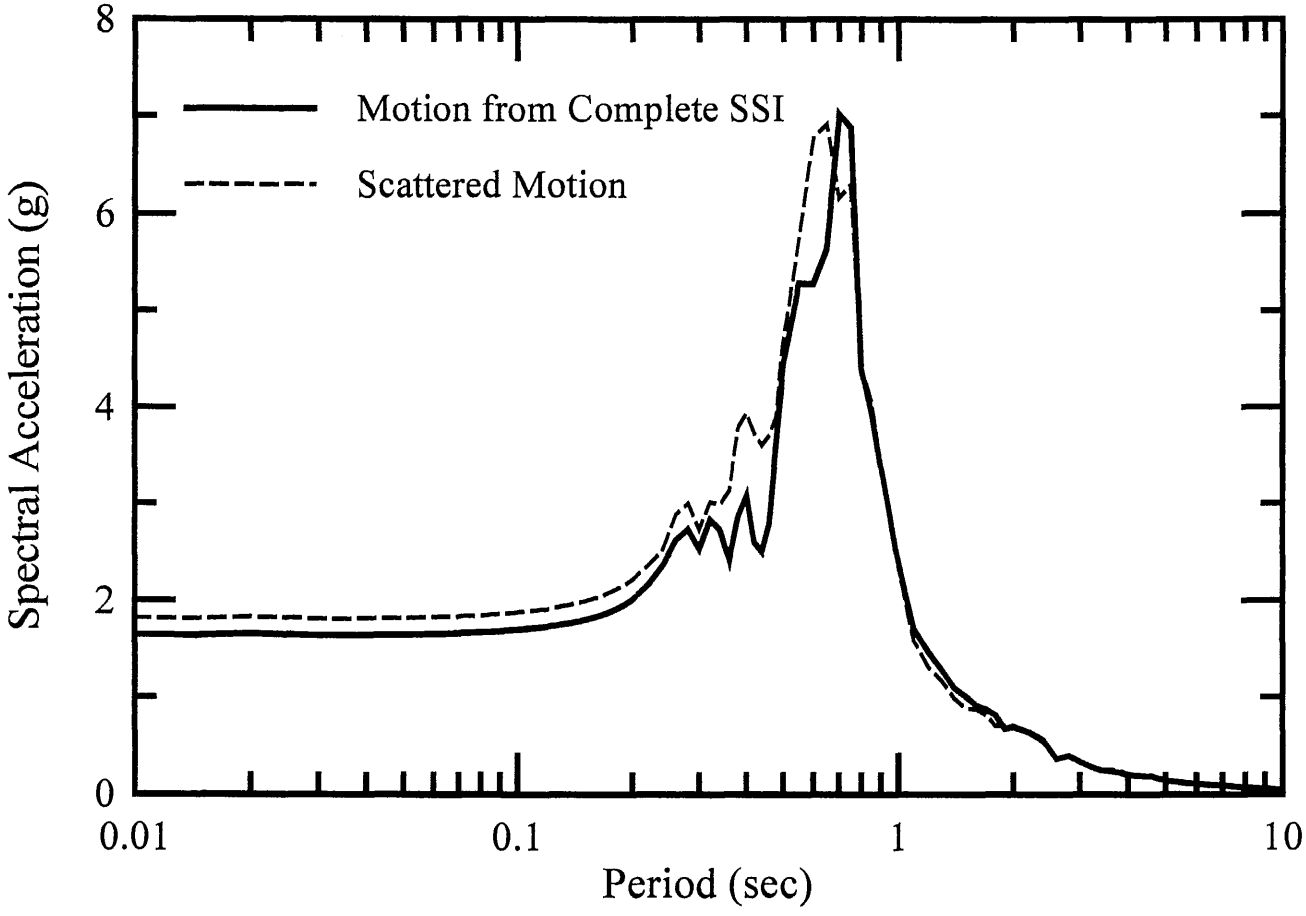

Figure 9: Comparison of 5% Damped Response Spectra of Substructure Scattered Motions with Motions at Caisson Top from Complete SSI Analyses

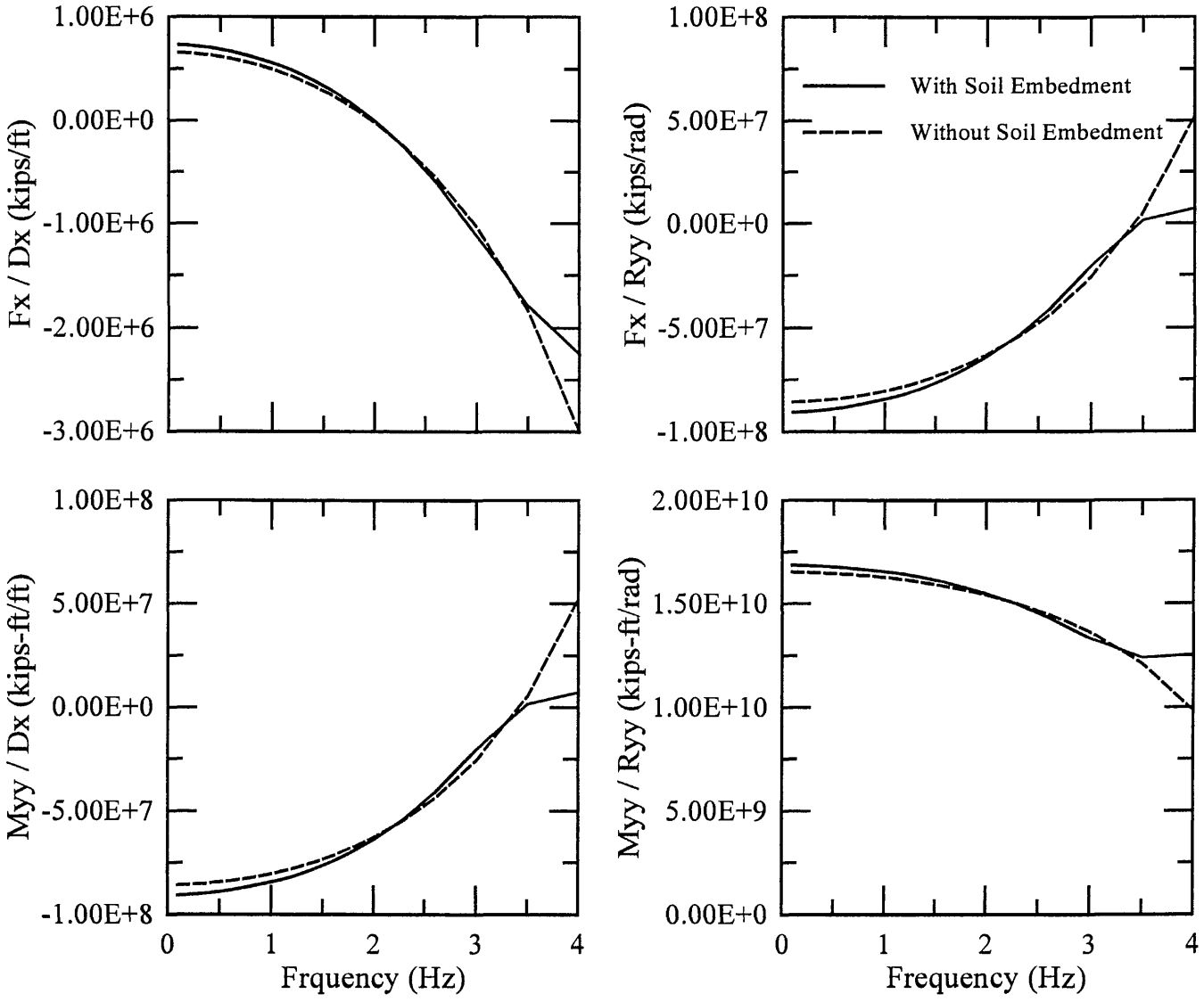

Figure 10: Comparison of Real Part of Foundation Impedance Functions for Cases With and Without Soil Embedment

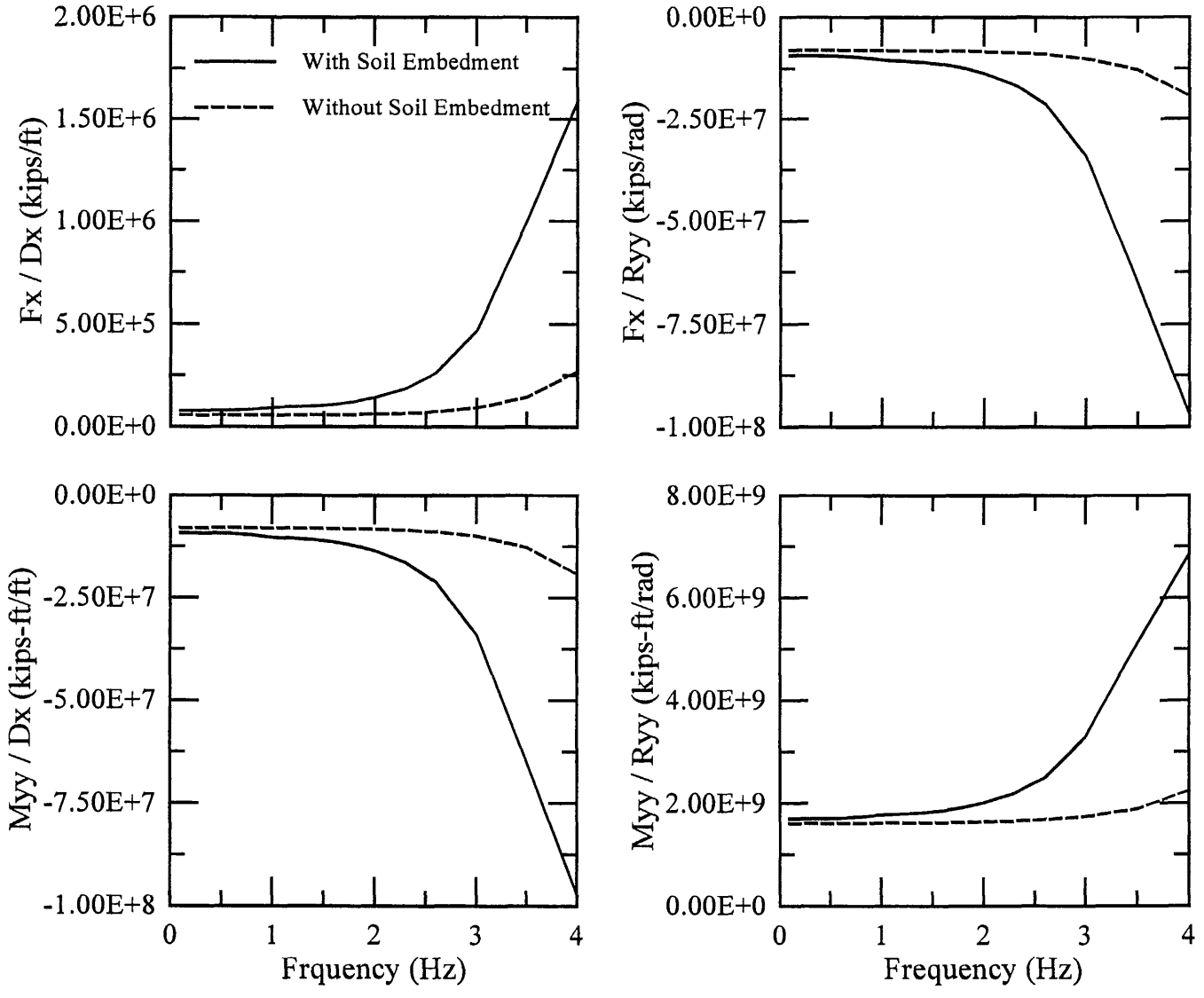

Figure 11: Comparison of Imaginary Part of Foundation Impedance Functions for Cases With and Without Soil Embedment

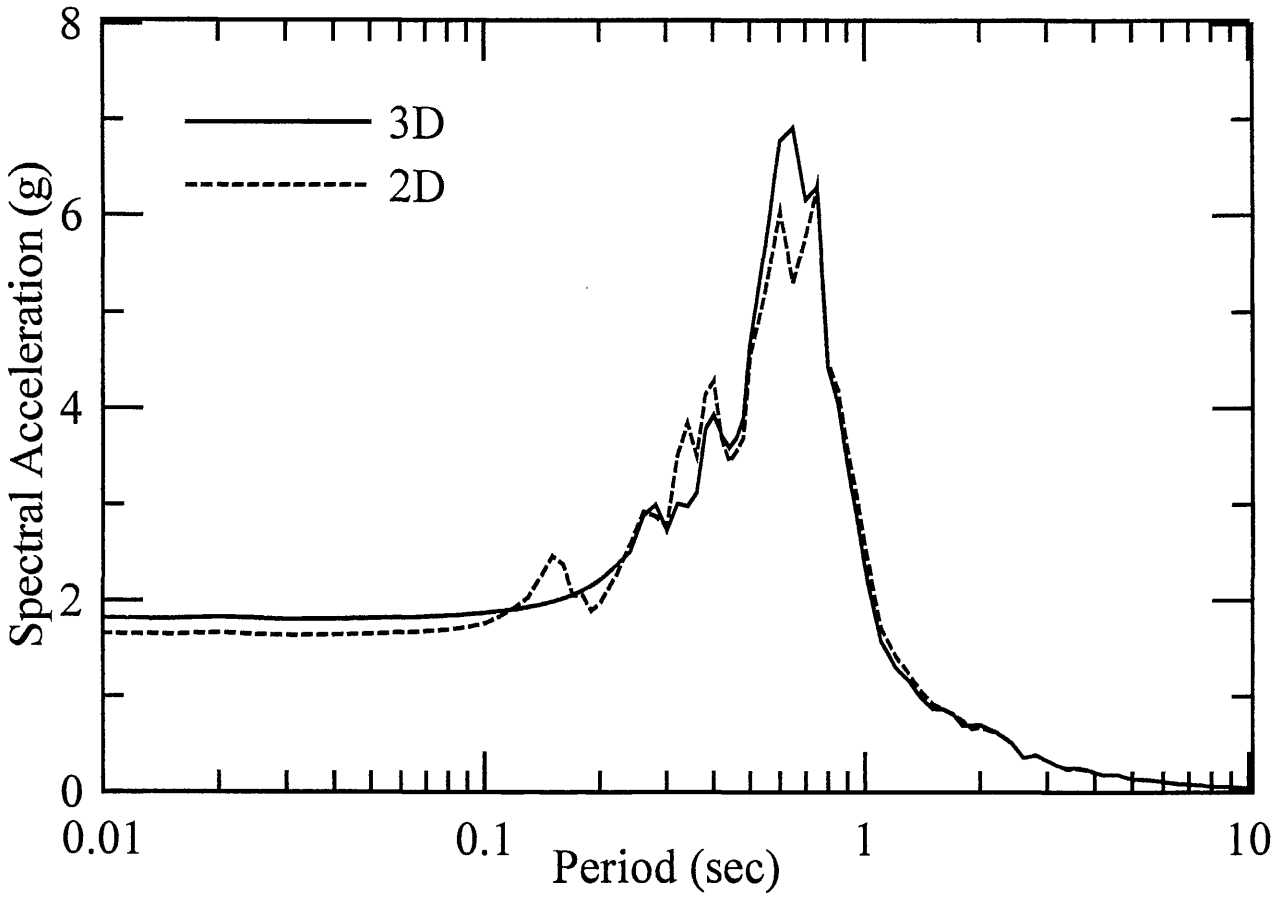

Figure 12: Comparison of 5% Damped Response Spectra of Longitudinal Scatter Motions for 3D and 2D SASSI models

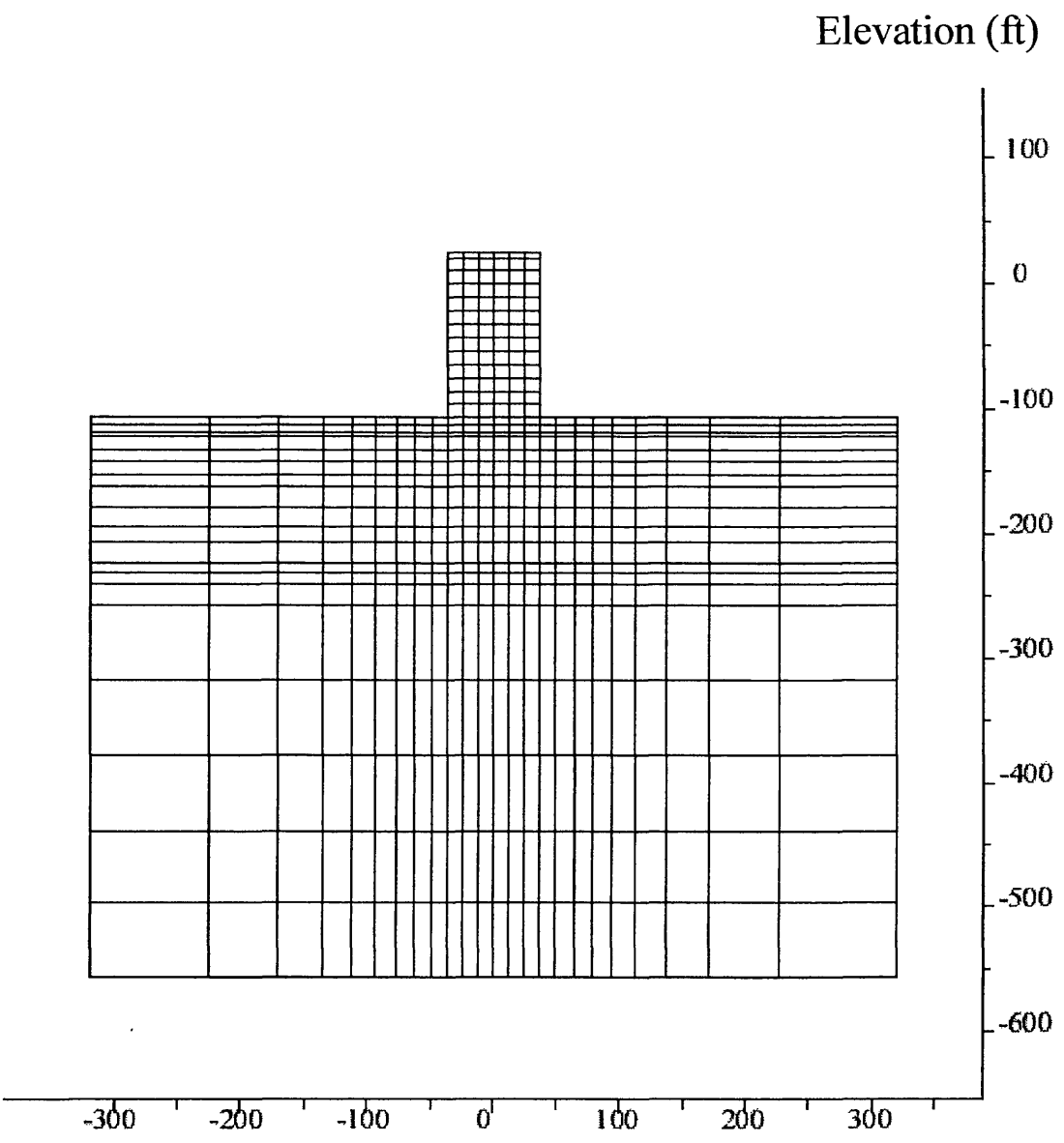

Figure 13: Finite Difference Grid

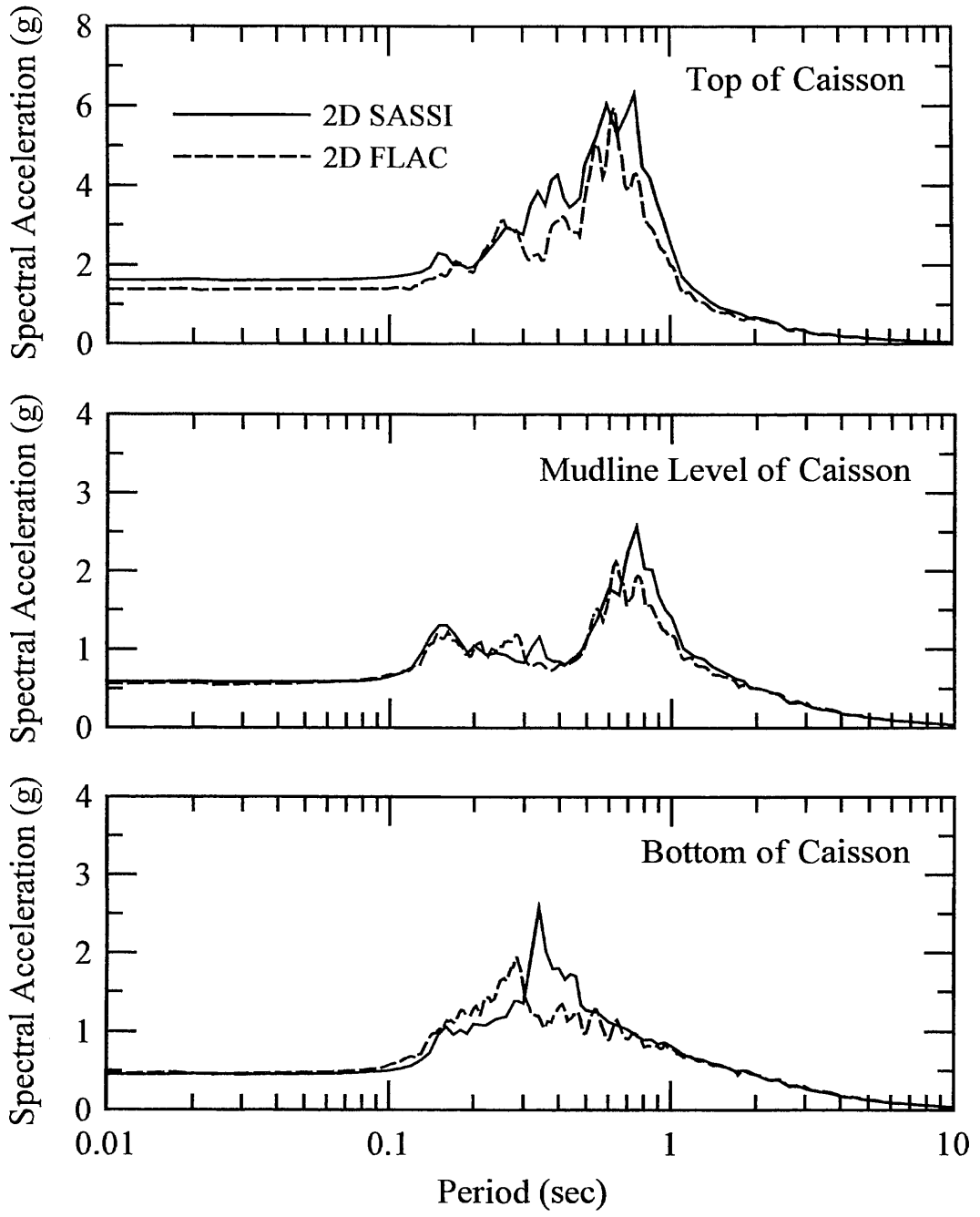

Figure 14: Comparison of 5% Damped Response Spectra of Longitudinal Motions Computed by 2-D SASSI and FLAC Models

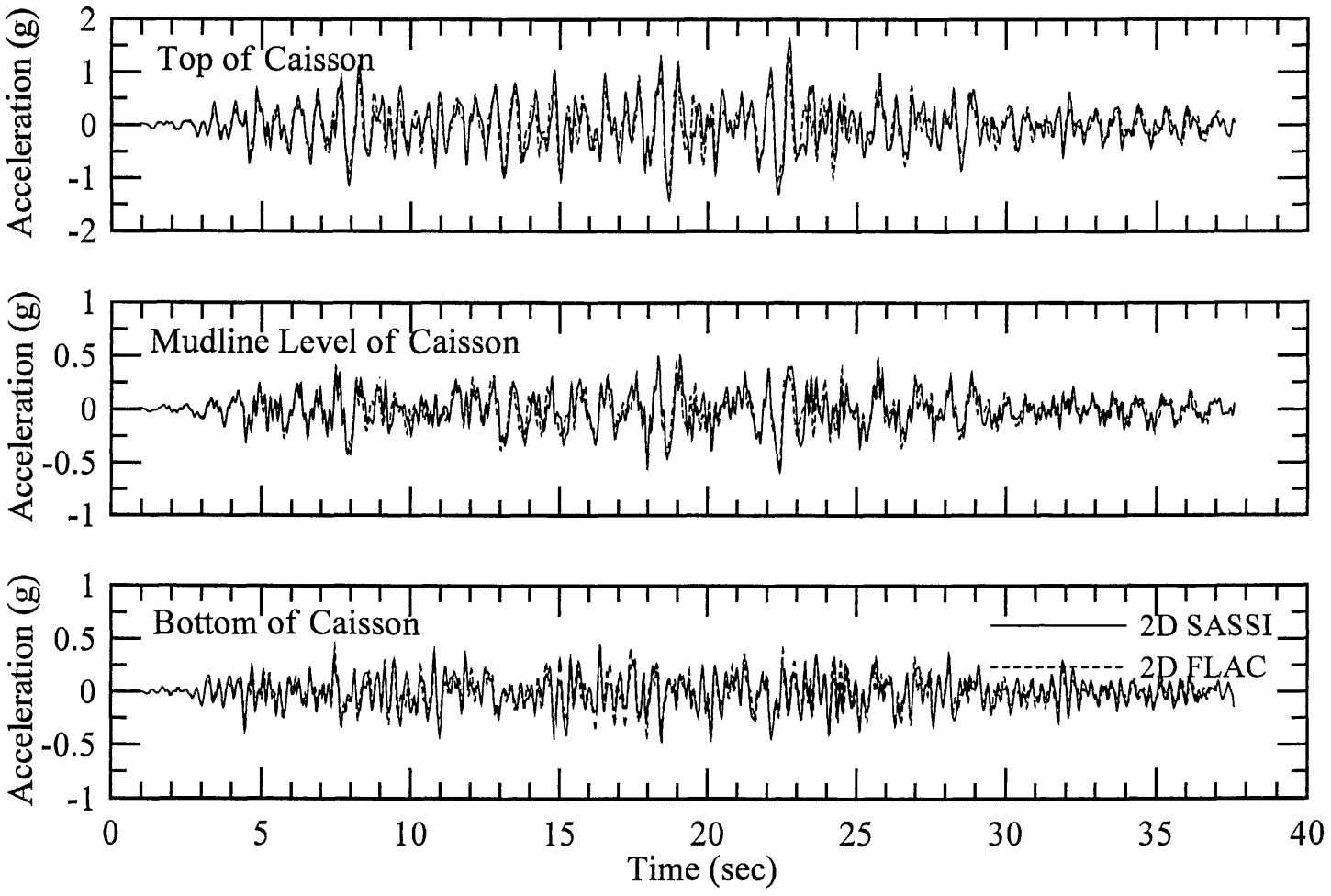

Figure 15: Comparison of Longitudinal Acceleration Time Histories from 2-D SASSI and FLAC Models

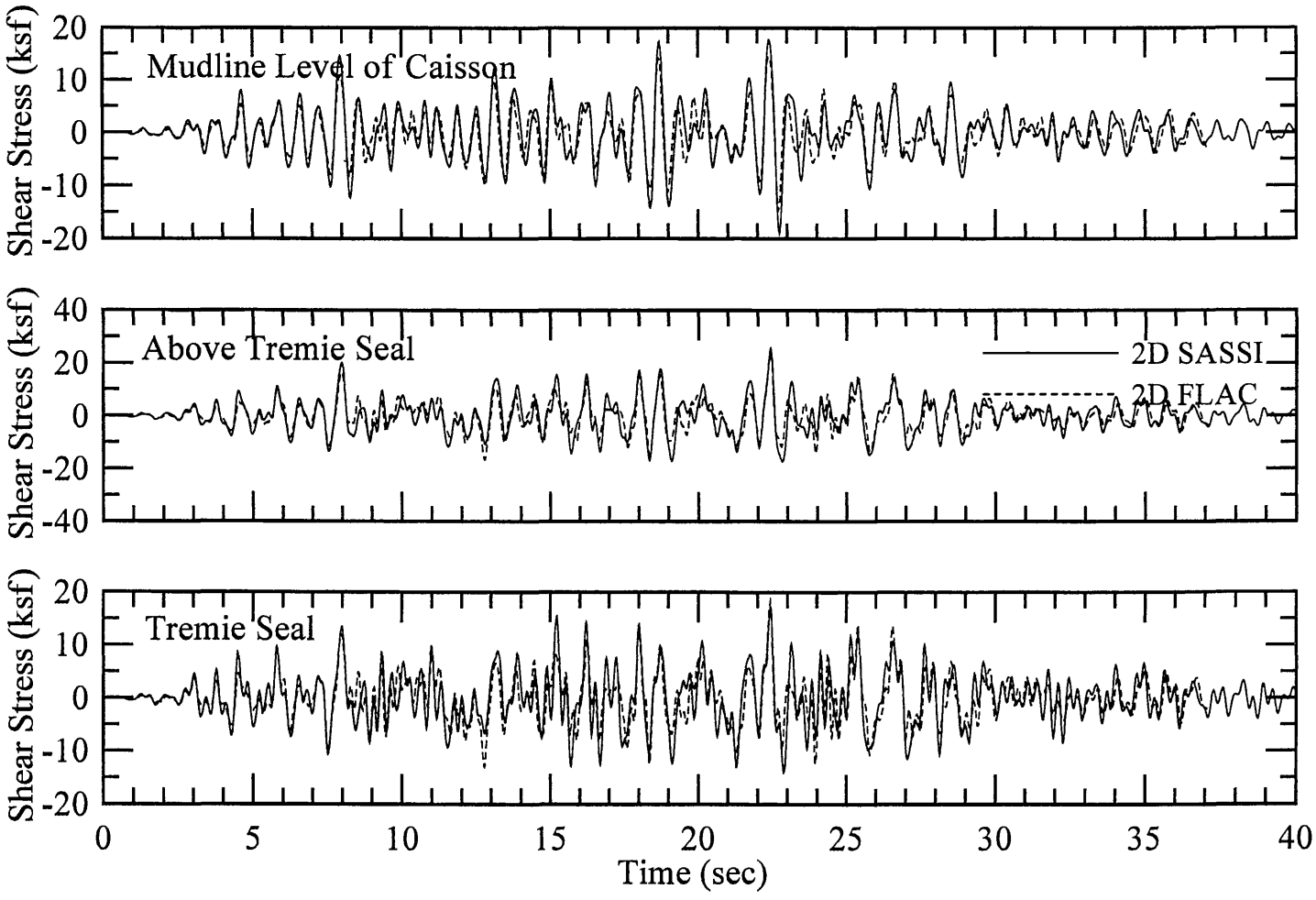

Figure 16: Comparison of Longitudinal Shear Stress Time Histories from 2-D SASSI and FLAC Models

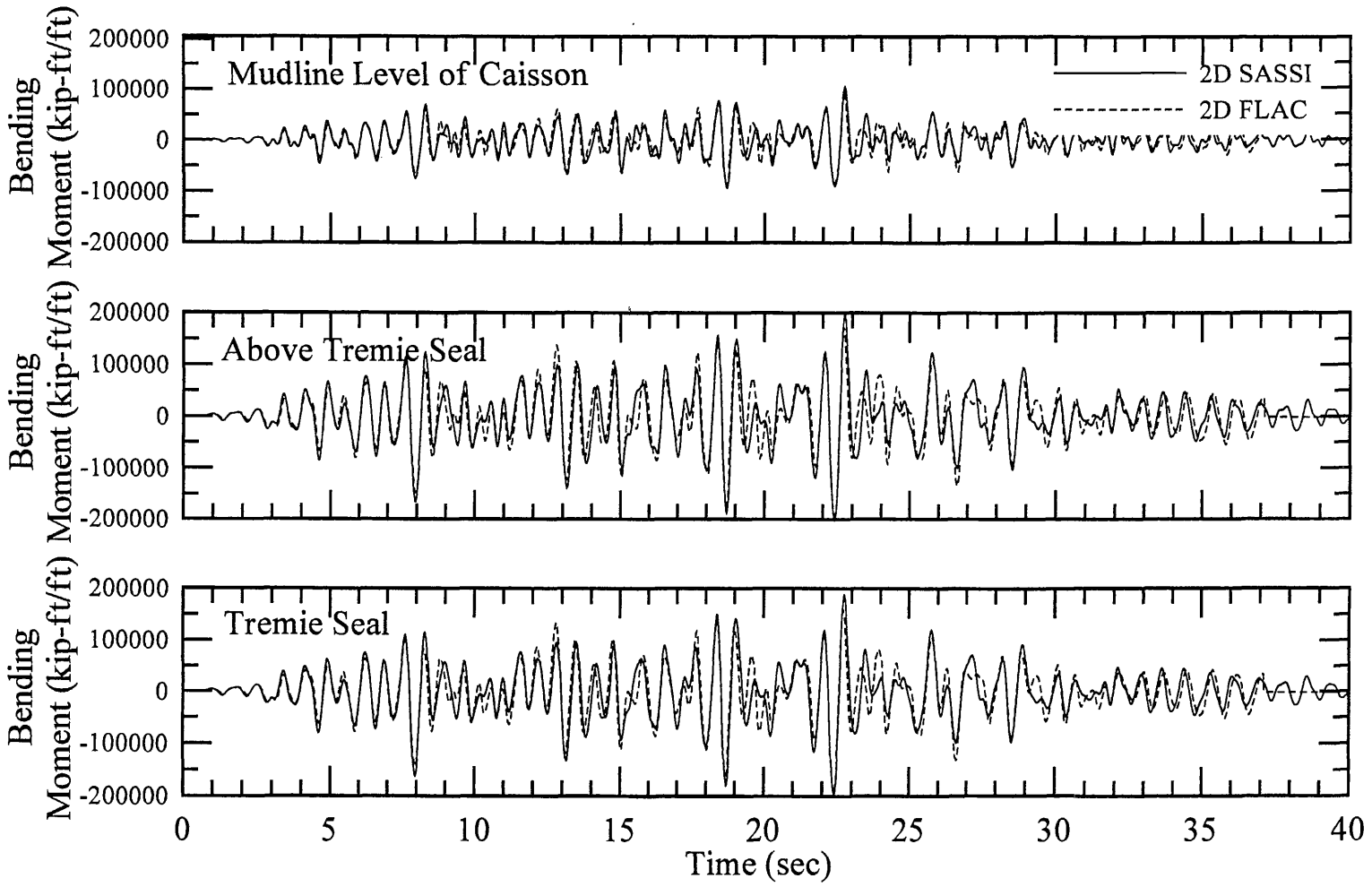

Figure 17: Comparison of Longitudinal Bending Moment Time Histories from 2-D SASSI and FLAC Models

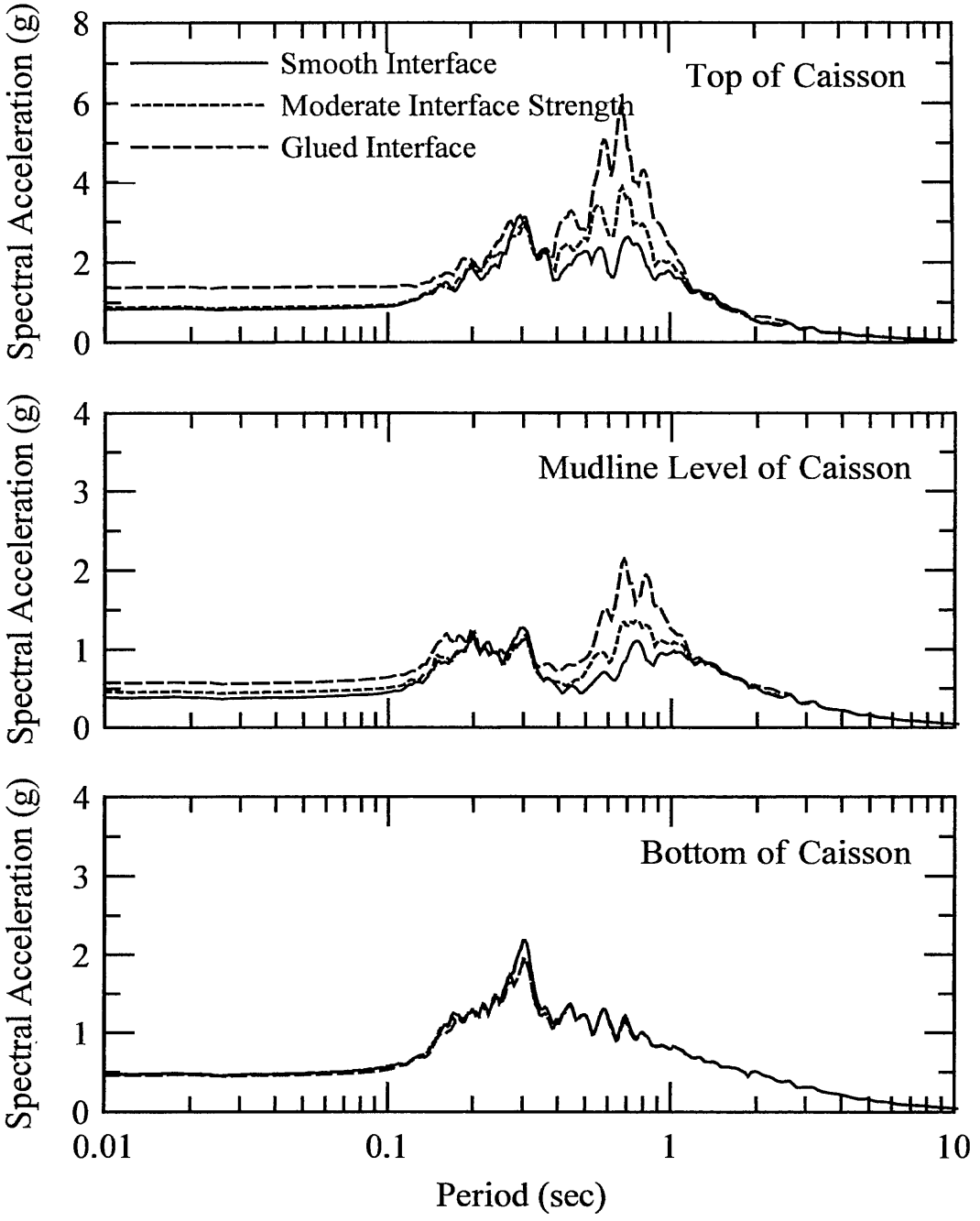

Figure 18: Comparison of 5% Damped Response Spectra of Longitudinal Motions Computed by FLAC Models with Various Interface Properties

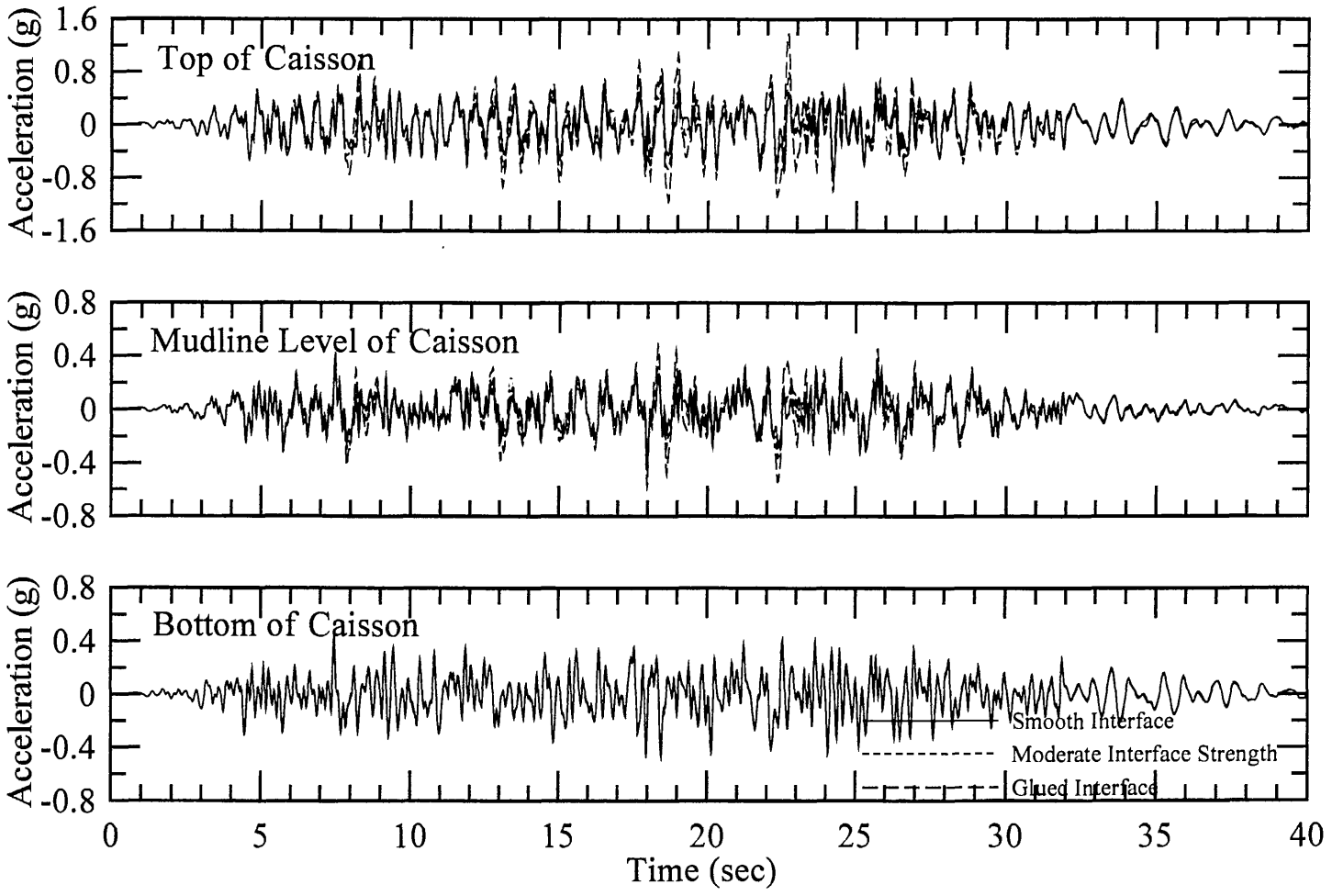

Figure 19: Comparison of Longitudinal Acceleration Time Histories from FLAC Models with Various Interface Properties

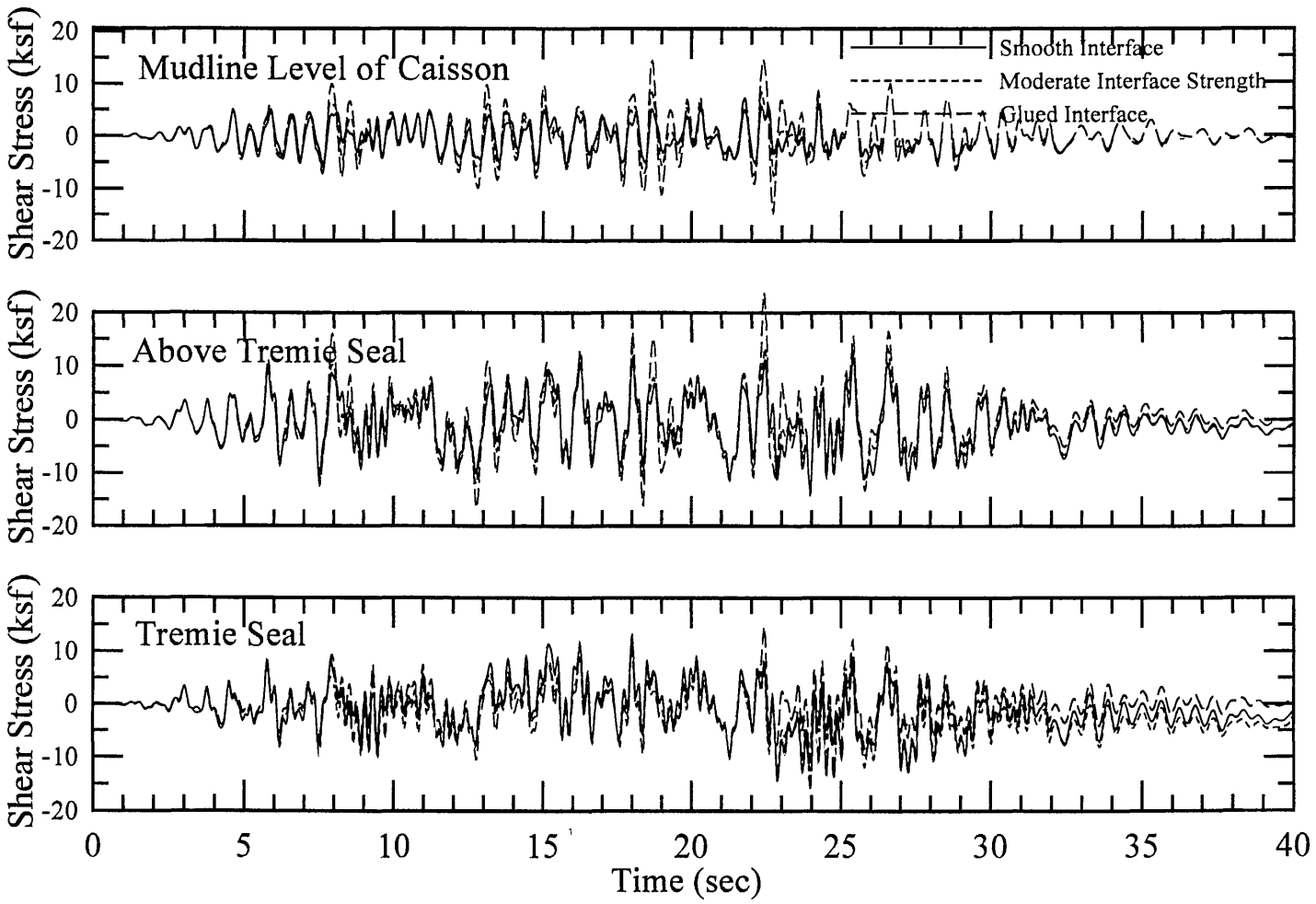

Figure 20: Comparison of Longitudinal Shear Stress Time Histories from FLAC Models with Various Interface Properties

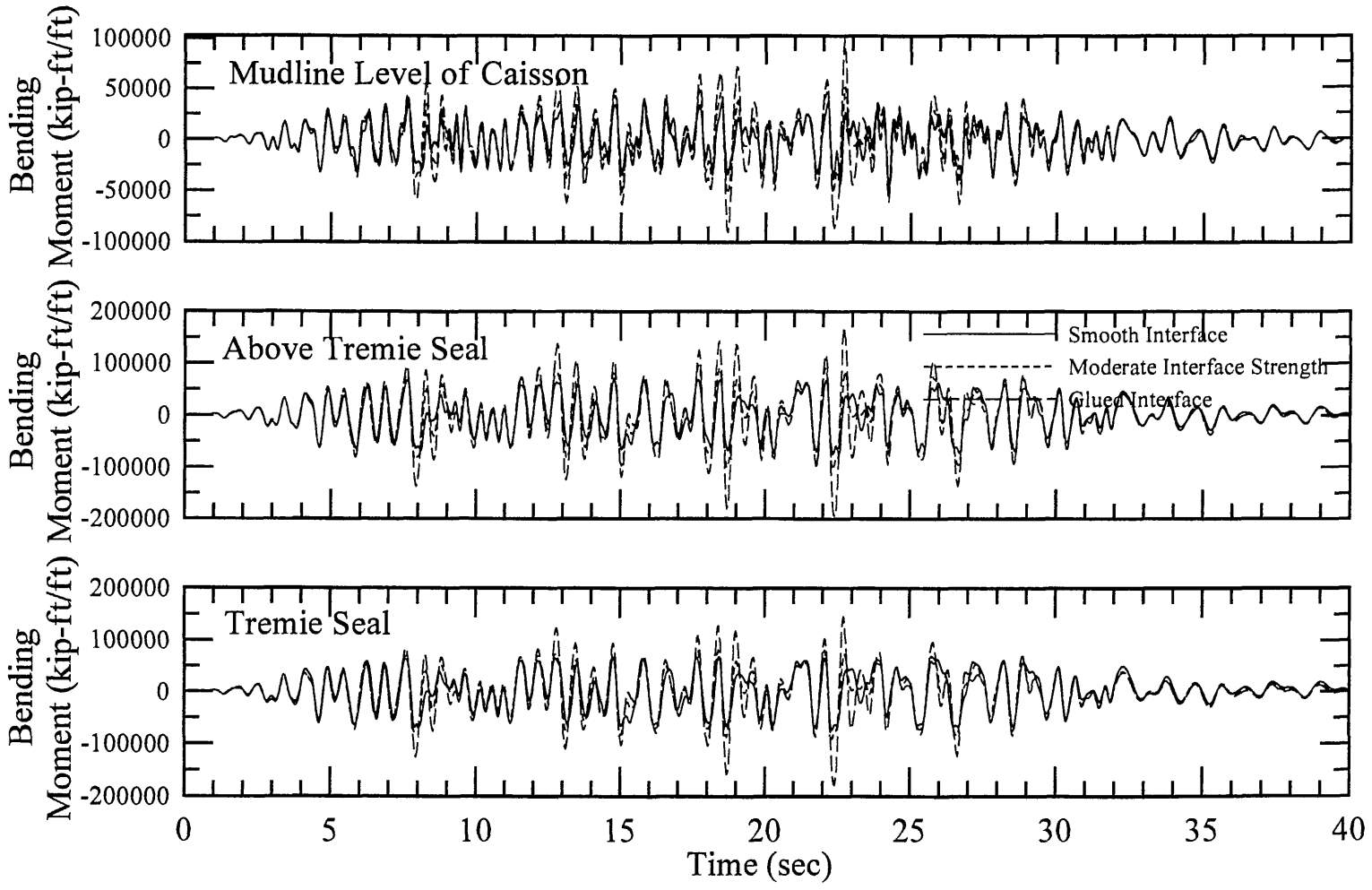

Figure 21: Comparison of Longitudinal Bending Moment Time Histories from FLAC Models with Various Interface Properties

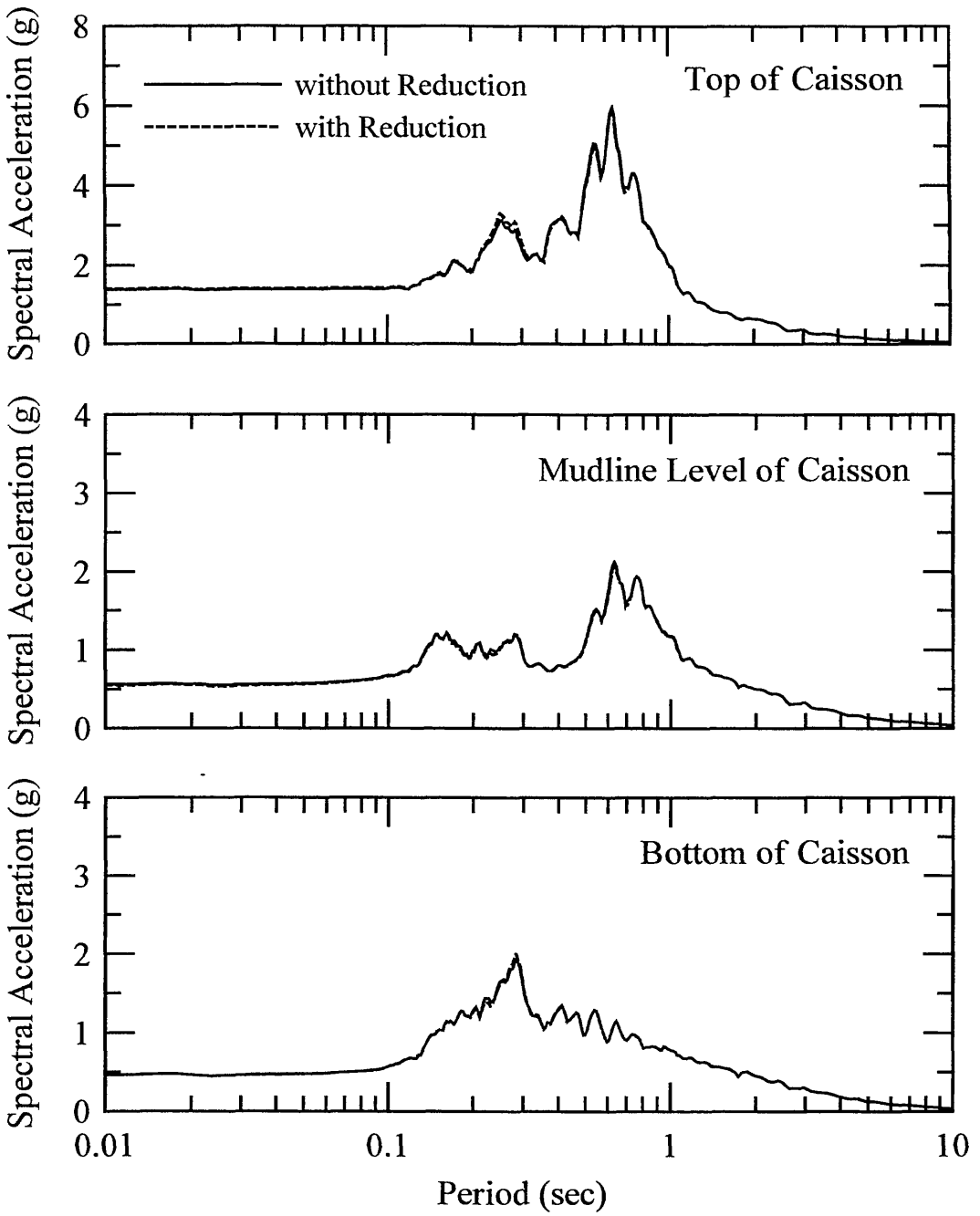

Figure 22: Comparison of 5% Damped Response Spectra of Longitudinal Motions Computed by FLAC Models with and without Soil Stiffness Reduction

SEISMIC DESIGN PROCEDURE OF BUILDING STRUCTURES INCLUDING SOIL-STRUCTURE INTERACTION EFFECT

BY

Yoshikazu KITAGAWA[1], Yutaka MATUSHIMA[2], Yutaka YAMAZAKI[3]

Soichi KAWAMURA[4], and Yoshio INOUE[5]

1) Department of Structural Engineering , Hiroshima University
2) Institute of Engineering Mechanics , University of Tsukuba
3) Building Research Institute , Ministry of Construction
4) Technology Research Center , Taisei Corporation
5) Housing and Urban Development Corporation(HUDC)

ABSTRACT

The objective of this paper is to present a procedure where design values of buildings are estimated by taking into account the dynamic soil-structure interaction produced during earthquakes. The building structure is represented by the mass-spring system having swaying and rocking springs and dashpots located at the foundation. The subsoil layers are transformed to the uniform medium with an equivalent shear wave velocity and Poisson's ratio. Generally, this is applied to the reinforced concrete and steel framed reinforced concrete building structures. The numerical results indicate the reasonable feature of the soil- structure interaction effect.

INTRODUCTION

Since the seismic design method for the building structures in Japan was amended in 1981, research focus has changed from static analysis to dynamic analysis. Dynamic analysis, as a technology aided by rapid progress, in recent year, in both theory and computers appears to be the most precise design method for the dynamic phenomenon of an earthquake. In the frequency domain, the response level at the structure roof is determined by the products of the following five characteristics; (1) epicentral characteristics, (2) seismic wave propagation characteristics, (3) ground characteristics surrounding the structure, (4) interaction characteristics between structure and surface layer, and (5) characteristics of structure.

On the other hand, building structures have been constructed on rather soft unstable soil, along with efficient uses of the land in Japan. In order to obtain more rational structures, it becomes all the more necessary to evaluate the seismic design for building, taking into consideration the characteristics of the soft-soil ground motion and the soil-pile-structure interactions. Taking into account these aspects above, we carried out this research for building structures of HUDC while considering dynamic soil-structure interaction effects theoretically, analytically, and experimentally. 1), 2) The main purpose was to set up the standards for evaluating seismic inputs for design.

On the premise of these conditions, this paper presents a

procedure where seismic design values of building structure are estimated by taking into account the soil-structure interaction and an example of numerical results obtained by applying the procedure to a real building.

MODELING OF BUILDING AND DESIGN PROCEDURE

The building structure is represented by the mass-spring system having swaying and rocking and dashpots located at the foundation as seen in Fig.1.

At that time, the subsoil layers are transformed to the uniform medium with an equivalent shear wave velocity and Poisson's ratio. Design procedure in the proposal is shown in Fig.2.

EVALUTION OF SPRING CONSTANTS

The static swaying and rocking spring constants of the soil, K_S, K_R are calculated according to the following equations:

$$K_S = \mu_S \cdot ({}_F K_S + {}_E K_S + {}_P K_S)$$
$$K_R = \mu_R \cdot ({}_F K_R + {}_E K_R + {}_P K_R) \quad (1)$$

where, μ_S, μ_R are coefficients for modification regarding cumulation of swaying and rocking constants of the soil and the pile. ${}_F K_S$, ${}_F K_R$ are calculated according to the equations below:

$${}_F K_S = \{8/(2-\nu_e)\} \cdot (\gamma_e / g) \cdot V_e^2 \cdot r_s$$
$${}_F K_R = [8/\{3(1-\nu_e)\}] \cdot (\gamma_e / g) \cdot V_e^2 \cdot r_R^3 \quad (2)$$

where, γ_e, ν_e, g, and V_e are, respectively, effective unit of the soil, effective Poisson's ratio of the soil, acceleration of gravity, and shear wave velocity of the soil. r_S, r_R are effective radii of the foundation swaying and rocking motions, respectively. ψ_S, ψ_R are coefficients for modification of the effective radii and calculated according to the equations below:

$$r_S = \Psi_S \cdot \sqrt{A/\pi}$$
$$r_R = \Psi_R \cdot \sqrt[4]{4I/\pi}$$
$$\Psi_S = 0.05 (\ell_{og_2} \lambda + 1.0)^2 + 0.95 \quad (3)$$

where, λ is ratio between the length and the width of the building (=2c/(2b)). 2c is the width of the building perpendicular to the direction of vibration and 2b is the width of the building of the direction of vibration. ${}_E K_S$, ${}_E K_R$ are swaying and rocking spring constants of the embedded part of the foundation and calculated according to the equations below:

$${}_E K_S = {}_F K_S \cdot (G_o/G_e) \cdot ({}_E H / r_S)$$
$${}_E K_R = 2.5 {}_F K_R \cdot (G_o/G_e) \cdot ({}_E H / r_R) \quad (4)$$

where, G_o, G_e are the average shear rigidity at the soil touching the side wall, and effective shear coefficients of the soil. $G_o/G_e = 1$, ${}_E H$ is the depth of the base foundation (bottom of the base beam) from the ground surface. However, when compression/settlement of the soil is expected, the settlement shall be subtracted. ${}_P K_S$, ${}_P K_R$ are swaying and rocking spring constants of the pile and calculated acceding to the equations below:

$${}_P K_S = \alpha_P \cdot N_P \cdot {}_P K_S$$
$${}_P K_R = \sum_j {}_P K_{y_j} y_j^2 \quad (5)$$

where, j is the serial number of the pile and y_j is the distance between the center line of the foundation and the center of the $j-th$ pile. α_P, the reduction coefficient of the swaying constant of piles due to the group-pile effects, is calculated according to the following equations:

$$\alpha_P = \exp\left\{-\left(\alpha_{P1}\sqrt{n_1 - 1} + \alpha_{P2}\sqrt{n_2 - 1}\right)\right\}$$
$$\alpha_{P1} = 0.5/\sqrt{S_1/B}$$
$$\alpha_{P2} = 0.3/\sqrt{S_2/B} \quad (6)$$

where, S_1 is the interval of piles in the vibration direction, S_2 is interval of piles perpendicular to the direction of vibration, B is the diameter of the pile and N_P is the

total number of piles (Fig.3). ${}_PK_S$ is the swaying spring constant of a single pile and in case pile-head is fixed, it is calculated as follows:

$$ {}_PK_S = 12_P \cdot I_P \cdot \beta_P^3 / \left\{ \left(1+\beta_{P\ell P}\right)^3 + 2 \right\} $$
$$ \beta_P = \sqrt[4]{K_h \cdot B / \left(4 \cdot E_P \cdot I_P\right)} \qquad (7) $$

where, E_P is Young's modulus of the pile. I_P is the 2nd inertial moment of the pile and K_h is horizontal reaction of the soil. ${}_PK_{V_j}$ is the spring constant of the $j-th$ single pile in the vertical direction and calculated according to the equation below:

$$ {}_PK_{V_j} = a \cdot A_P \cdot E_P / \ell \qquad (8) $$

where, A_P is the net area of the cross section of the pile, ℓ is the length of the pile and a is the coefficient for each of pile. In case of a supported pile which is reinforced concrete pile in site, it is calculated as follows:

$$ a = 0.022\left(\ell / B\right) - 0.05 \qquad (9) $$

where, μ_S, μ_R are calculated as follows:

$$ \mu_S = \left(1-\alpha_S\right)^{1.5} + \alpha_S{}^{1.5} $$
$$ \mu_R = 1.0 \qquad (10) $$

where, α_S is the ratio between the swaying spring constants of the pile and the total of swaying spring constants of the soil and pile and calculated as follows:

$$ \alpha_S = {}_PK_S / \left({}_FK_S + {}_EK_S + {}_PK_S\right) \qquad (11) $$

The natural period of the interaction-system is calculated by the use of weight of each story, spring constants, weight of the foundation and static soil swaying and rocking spring constants calculated in that step. The dynamic swaying and rocking spring constants of the soil, $\tilde{K}_S$, $\tilde{K}_R$ are respectively calculated according to the following equations:

$$ \tilde{K}_S = \tilde{\mu}_S \cdot \left({}_F\tilde{K}_S + {}_E\tilde{K}_S + {}_P\tilde{K}_S\right) $$
$$ \tilde{K}_R = \tilde{\mu}_R \cdot \left({}_F\tilde{K}_R + {}_E\tilde{K}_R + {}_P\tilde{K}_R\right) $$
$$ \tilde{\mu}_S = \mu_S $$
$$ \tilde{\mu}_R = \mu_R \left(= 1.0\right) $$
$$ {}_F\tilde{K}_S = {}_Sd_S \cdot {}_FK_S $$
$$ {}_E\tilde{K}_S = {}_Sd_S \cdot {}_EK_S $$
$$ {}_P\tilde{K}_S = {}_Pd_S \cdot {}_PK_S $$
$$ {}_F\tilde{K}_R = {}_Sd_R \cdot {}_FK_R $$
$$ {}_E\tilde{K}_R = {}_Sd_R \cdot {}_EK_R $$
$$ {}_P\tilde{K}_R = {}_Pd_R \cdot {}_PK_R \qquad (12) $$

where, ${}_Sd_S$, ${}_Pd_S$, ${}_Sd_R$, ${}_Pd_R$ are the ratio of dynamic rigidity reduction and calculated as follows:

$$ {}_Sd_R = \left(1-0.05a_{OR}\right)^2 \quad ; a_{OR} < 10 $$
$$ {}_Sd_R = 0.25 \quad ; a_{OR} \geq 10 $$
$$ {}_Sd_S = {}_Pd_S = {}_Pd_R = 1.0 \qquad (13) $$

where, a_{OR} is a non-dimensional frequency regarding the rocking spring and equal to $\Omega \cdot T_R / V_e$. Ω is the 1st natural circular frequency of the interaction system based on the static spring constant$\left(=2\pi/T_1\right)$. The $j-th$ natural period $\left(\tilde{T}_j\right)$ and the mode of the interaction system is calculated by and use of weight of each story, spring constants, weight of the foundation, and dynamic swaying and rocking spring constants.

EVALUATION OF DAMPING FACTOR

The damping factor of the $j-th$ mode $\left(h_{eq,j}\right)$ for calculating the response story base shear coefficient$\left({}_EC_i\right)$, is calculated by the following equation:

$$ h_{eq,j} = {}_B\gamma_j \cdot {}_Bh + {}_S\gamma_{S,j} \cdot {}_Sh_S' + {}_s\gamma_{R,j} \cdot {}_Sh_R' + {}_P\gamma_{S,j} \cdot {}_Ph_S' + {}_P\gamma_{R,j} \cdot {}_Ph_R' \qquad (14) $$

where, the damping factor of each part is weighted according to the strain energy. γ is the ratio between the associated strain energy and the whole strain energy of the vibration system at the $j-th$ vibration mode. ${}_Bh$ is the damping coefficient of the building and is normally 0.02. ${}_Sh_S'$, ${}_Sh_R'$ are damping coefficients of the soil for the swaying spring and rocking spring, respectively, modified according to the layered soil and calculated as follows:

$$ {}_Sh_S' = {}_S\delta_S \cdot {}_S\varepsilon_S \cdot {}_S\kappa_S \cdot {}_Sh_S + {}_Sh_I $$
$$ {}_Sh_R' = {}_S\delta_R \cdot {}_S\varepsilon_R \cdot {}_S\kappa_R \cdot {}_Sh_R + {}_Sh_I \qquad (15) $$

where, δ is the coefficient for modification of the damping of the soil due to the layered soil. ε is the coefficient for modification of the soil due to the embedment of the foundation. κ is the coefficient for modification of the soil due to the opening of the foundation and h is the damping coefficient of the half-space elastic soil replaced with the equivalent. ${}_{S}h_{I}$ is the constant of visco-damping of the soil and is normally 0.03. ${}_{S}\delta_{S}$, ${}_{S}\delta_{R}$ are coefficients for modification of the swaying spring and rocking spring of the soil, respectively, due to the embedment of the foundation and calculated as follows:

$$
\begin{aligned}
{}_{S}\delta_{S} &= \left\{0.1\left(V_{e2}/V_{e1}-1\right)^{3}\right\}+0.36 \Big/ \left\{\left(V_{e2}/V_{e1}-1\right)^{3}+0.36\right\} \\
&\quad ;\widetilde{a}_{OS} \le {}_{C}a_{OS} \\
{}_{S}\delta_{S} &= 1-\left[\left(1.2_{g}a_{OS}-\widetilde{a}_{OS}\right)\cdot 0.9\left(V_{e2}/V_{e1}-1\right)^{3}\right] \Big/ \\
&\quad \left[\left(1.2_{g}a_{OS}-{}_{C}a_{OS}\right)\cdot\left\{\left(V_{e2}/V_{e1}-1\right)^{3}+0.36\right\}\right] \\
&\quad ;{}_{C}a_{OS} < \widetilde{a}_{OS} \le 1.2_{g}a_{OS} \\
{}_{S}\delta_{S} &= 1.0 \qquad ;1.2_{g}a_{OS} \le \widetilde{a}_{OS} \le 1.2_{g}a_{OS} \\
{}_{S}\delta_{R} &= 0.05 \qquad ;\widetilde{a}_{OR} \le {}_{C}a_{OR} \\
{}_{S}\delta_{R} &= 0.05+0.95\left(\widetilde{a}_{OR}-{}_{C}a_{OR}\right)/\left(1.8_{g}a_{OR}-{}_{C}a_{OR}\right) \\
&\quad ;{}_{C}a_{OR} < \widetilde{a}_{OR} \le 1.8_{g}a_{OR} \\
{}_{S}\delta_{R} &= 1.0 \qquad ;1.8_{g}a_{OR} < \widetilde{a}_{OR}
\end{aligned}
\tag{16}
$$

where,

$$
\begin{aligned}
{}_{C}a_{OS} &= {}_{g}a_{OS}\left(1-1.8^{-\left(V_{e2}/V_{e1}-1\right)}\right) \\
{}_{C}a_{OR} &= 1.8_{g}a_{OR}\left(1-28^{-\left(V_{e2}/V_{e1}-1\right)}\right) \\
\widetilde{a}_{OS} &= \widetilde{\Omega}\cdot r_{S}/V_{e} \\
\widetilde{a}_{OR} &= \widetilde{\Omega}\cdot r_{R}/V_{e} \\
{}_{g}a_{OS} &= \pi\cdot r_{S}/\left(2H_{e}\right) \\
{}_{g}a_{OR} &= \pi\cdot r_{R}/\left(2H_{e}\right)
\end{aligned}
\tag{17}
$$

$\widetilde{\Omega}$ is the 1st natural circular frequency of the interaction system based on the dynamic soil spring constant and H_{e} is the thickness of the equivalent two layered soil's 1st layer. ${}_{S}\varepsilon_{S}$, ${}_{S}\varepsilon_{R}$, ${}_{S}\kappa_{S}$, ${}_{S}\kappa_{R}$ are calculated, respectively, as follows:

$$
\begin{aligned}
{}_{S}\varepsilon_{S} &= 1.0+\left(G_{o}/G_{e}\right)\cdot\left({}_{E}H/r_{S}\right) \\
{}_{S}\varepsilon_{R} &= 1.0 \\
{}_{S}\kappa_{S} &= \sqrt{1-A^{'}/\left(2A\right)} \\
{}_{S}\kappa_{R} &= 1.0
\end{aligned}
\tag{18}
$$

where, $A^{'}$ is area of the opening at the foundation and A is the area of the foundation (=2b*2c). ${}_{S}h_{S}$, ${}_{S}h_{R}$ are calculated respectively as follows:

$$
\begin{aligned}
{}_{S}h_{S} &= 0.30\cdot\widetilde{a}_{OS} \\
{}_{S}h_{R} &= 0.1\cdot\widetilde{a}_{OR}^{\,3} \qquad ;\widetilde{a}_{OR} < 1 \\
{}_{S}h_{R} &= 0.15\cdot\widetilde{a}_{OR}-0.05 \qquad ;1 \le a_{OR} < 5 \\
{}_{S}h_{R} &= 0.70 \qquad ;a_{OR} \ge 5
\end{aligned}
\tag{19}
$$

The damping coefficients of pile for the rocking spring, respectively, modified to the layered soil, ${}_{P}h_{S}^{'}$, ${}_{P}h_{R}^{'}$ are calculated as follows:

$$
\begin{aligned}
{}_{P}h_{S}^{'} &= {}_{P}\delta_{S}\cdot{}_{P}h_{S}+{}_{P}h_{I} \\
{}_{P}h_{R}^{'} &= {}_{P}\delta_{R}\cdot{}_{P}h_{R}+{}_{P}h_{I}
\end{aligned}
\tag{20}
$$

where, ${}_{P}h_{S}$, ${}_{P}h_{R}$ are respectively the damping coefficients for the swaying and rocking of pile located at the equivalent half-apace elastic soil and are normally 0.03. ${}_{P}h_{I}$ is damping coefficient due to the visco-damping of the pile and is normally 0. ${}_{P}\delta_{S}$, ${}_{P}\delta_{R}$ are coefficients for modification of the damping coefficient of the pile for the swaying and rocking due to the layered soil is 1, except in the case of special investigations.

RESPONSE STOREY SHEAR FORCE COEFFICIENT FOR DESIGN

The response story shear force coefficient for the design for the i-th story is calculated as follows:

$$
{}_{E}C_{i} = Z\cdot\lambda_{1}\cdot R_{t}\left(\widetilde{T}_{1}\right)\cdot\phi_{i}\cdot C_{O} \tag{21}
$$

where, Z, $R_{t}\left(\widetilde{T}_{1}\right)$, C_{O} are seismic hazard zoning coefficient, vibration property at the 1st natural period $\left(\widetilde{T}_{1}\right)$, standard layer shear force coefficient as given in the Building Standard Act, respectively. ϕ_{i} is the coefficient at the i-th story showing the vertical distribution of the response story shear force coefficient $\left(=\phi_{i}^{'}/\phi_{1}^{'}\right)$. λ_{1}

is the coefficient for modification of the spectrum at the 1st natural period and calculated as follows:

$$\lambda_1 = 1 - \left\{1 - 2.25/\left(1.75 + 10h_{eq,1}\right)\right\} \cdot t_1 \quad ; h_{eq\,1} \geq 0.05$$
$$\lambda_1 = 1 + \left\{1.5/\left(1.0 + 10h_{eq,1}\right) - 1\right\} \cdot t_1 \quad ; h_{eq.1} < 0.05 \qquad (22)$$

where, t_1 is unity in the usual range of the natural period $\left(\widetilde{T}_1\right)$ and is calculated by the use of $\widetilde{T}_1$ in accordance with the equations below:

$$t_1 = 0 \quad ; \widetilde{T}_1 \leq 0.05,\ \widetilde{T}_1 \geq 10.0$$
$$t_1 = \left(\ell_{og}\widetilde{T}_1 + 1.30\right)/0.3 \quad ; 0.05 < \widetilde{T}_1 < 0.1$$
$$t_1 = 1.0 \quad ; 0.1 \leq \widetilde{T}_1 \leq 2.5$$
$$t_1 = \left(1 - \ell_{og}T_1\right)/0.6 \quad ; 2.5 < \widetilde{T}_1 < 10.0 \qquad (23)$$

where, ϕ_i is the storied shear force coefficient for calculating at the $i-th$ story of the building and is calculated as follows:

$$\phi_i = \sqrt{\sum_{j=1}^{k}\left[\sum_{m=1}^{N}\left(W_m \cdot \beta_j \cdot u_{mj} \cdot \lambda_j \cdot R_t\left(\widetilde{T}_j\right)\right)\right]^2} \Big/ \sum_{m=1}^{N} W_m \qquad (24)$$

where, ${}_BN$ is the total number of stories above the foundation and W_m is the weight of the $m-th$ story. β_j U_{mj} is $j-th$ participation function of the $m-th$ story. λ_j is the coefficient for spectrum modification due to damping at the $j-th$ natural period and is calculated similarly by the equations for λ_j $R_t\left(\widetilde{T}_j\right)$ is the design spectrum coefficient at the $j-th$ natural period $\left(\widetilde{T}_j\right)$ as given in the Building Standard Act. k is the highest mode number to be considered to be more than 2. However, when the base shear force coefficient of the 1st story falls below the shear force coefficient $Z \cdot R_t \cdot C_o$ given in the Building Standard Act, its lower limit is 75% of $Z \cdot R_t \cdot C_o$, and the response story shear force coefficient for each story is modified at the same rate.

EXAMPLE OF APPLICATION FOR PROPOSAL

Various types of building structure founded on different grounds are analyzed by following this procedure. The building has fourteen stories and are made of reinforced concrete (Figs. 4 and 5). The underlying ground consists mainly of silty soil down to depth 18m from the ground surface (Fig. 6). The constants of the soil are shown in table1. The building is supported by reinforced concrete piles, 21m in length placed in site. The diameter of the piles is from 1.6m to 1.9m.The constants for analysis are shown in Table 1. In table 1, K_i is the spring constant of each story of the building and $\widetilde{K}_S$, $\widetilde{K}_R$ are dynamic soil spring constants of the swaying and the rocking, respectively. The design story shear force coefficients in a longitudinal direction of the building evaluated by this proposal is shown in Fig. 7. It is less than required by the code owing to the effect of soil-structure interaction.

CONCLUDING REMARKS

A procedure where seismic design values of building structure are estimated by taking into account the soil-structure interaction is presented. The numerical results obtained by applying the procedure to real buildings indicate the reasonable features of the soil-structure interaction effect.

ACKNOWLEGEMENTS

In order to execute this research, a research committee (chairman, the late Y Osawa, professor emeritus, University of Tokyo) was organized in the Japan Association for Building Research Promotion, and the scheme of the research and studying results were carried out. The authors wish to express there sincere thanks to members of the committee and persons concerned.

REFERENCES

1), 2) Inoue, Y. and Osawa, Y. et al.," Study on Seismic Input to Apartment Houses of HUDC (part-6,7,8) " , Proc. of Annual Meeting of AIJ, Oct. 1987 / " A Proposal for Seismic Design Procedure of Apartment Houses including Soil-Structure Interaction Effect " , Proc. of 9th WCEE, vol. VIII, PP.365-370, Aug. 1988

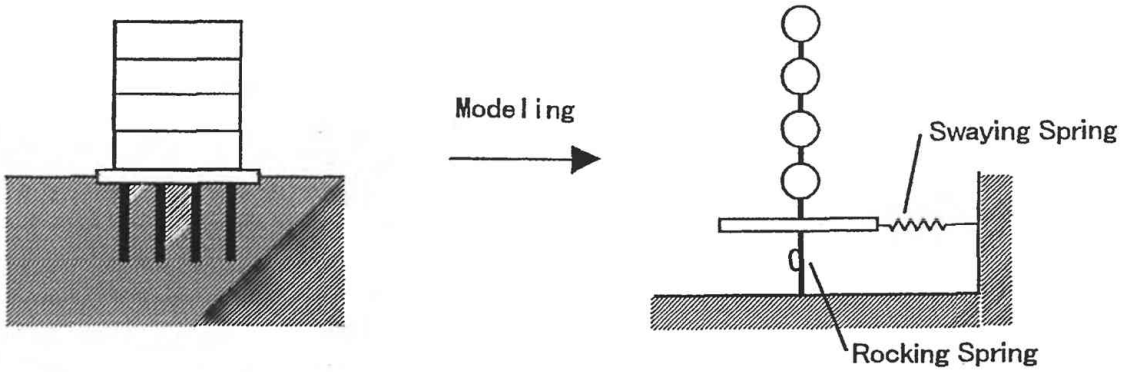

(a) Building,Foundation and Soil (b) Swaying-Rocking Model (SR Model)

Fig.1 Interaction System Model

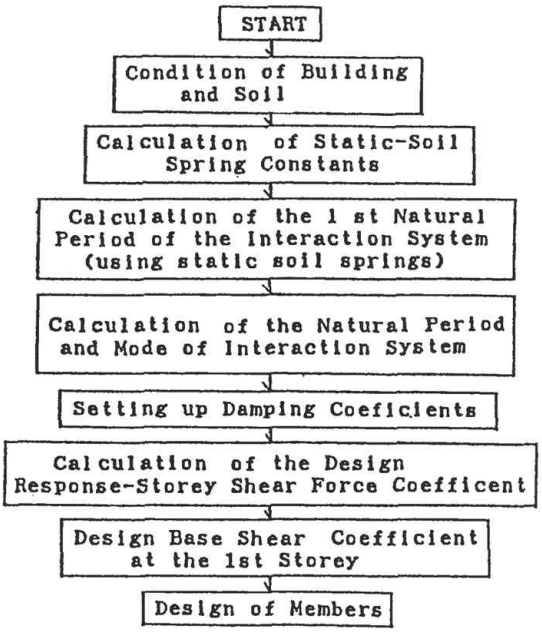

Fig.2 Design Procedure

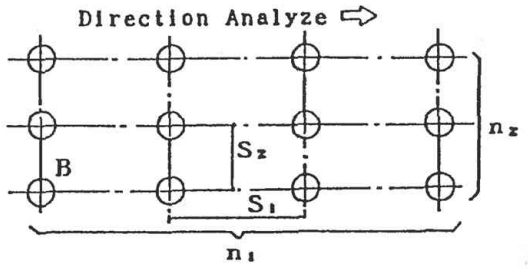

Fig.3 Total Number of Piles n_1,n_2

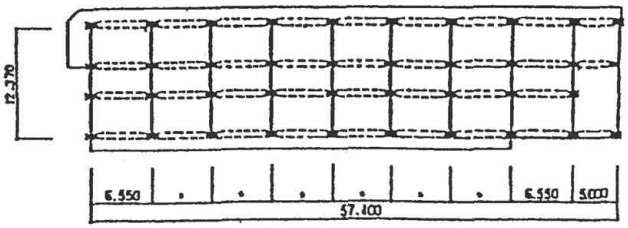

Fig.4 Plan of Building

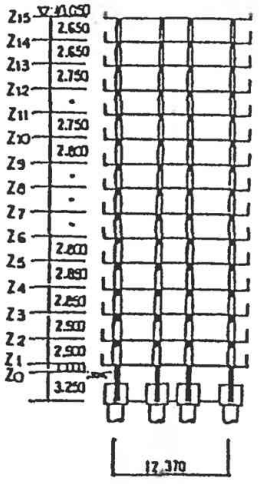

Fig.5 Section of Building

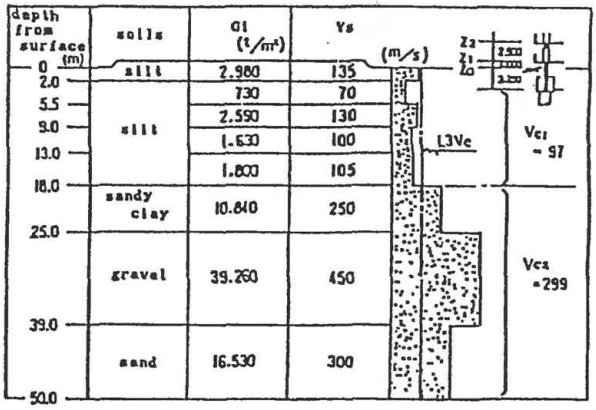

Fig.6 Constants of Soil

6

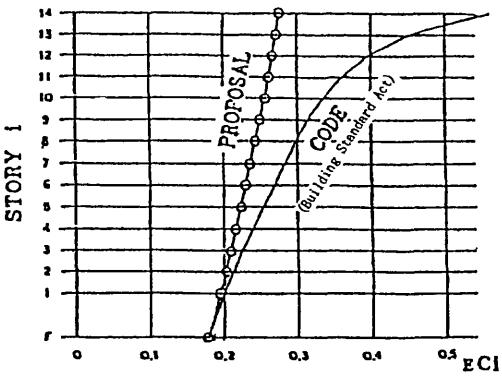

Fig.7 Design Story Sheer Force Coefficients, $_EC_i$

Tab.1 Constants $\tilde{K}_i, \tilde{K}_S, \tilde{K}_R$

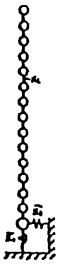

		longitudial	transverse
K_i (t/cm)	14	5.014	3.557
	13	6.298	5.320
	12	7.329	6.801
	11	7.949	8.299
	10	8.780	9.707
	9	9.708	11.385
	8	10.156	13.107
	7	10.897	15.368
	6	12.198	17.801
	5	13.132	20.679
	4	14.105	24.976
	3	15.503	30.513
	2	18.195	40.495
	1	28.177	43.865
$\tilde{K}_S$ (t/cm)		1.889	3.065
$\tilde{K}_R$ (t cm/r)		8.156×10^{10}	0.685×10^{10}

7

EXPERIMENTAL FACILITIES IN THE UNITED STATES FOR SOIL-STRUCTURE INTERACTION RESEARCH

By Scott A. Ashford[1]

ABSTRACT: This paper provides a brief summary of experimental facilities in the United States that can be used for Soil-Structure Interaction (SSI) research. The objective is to provide the participants of this US-Japan SSI Workshop with a description of existing and upcoming facilities in order to promote discussions on future collaborations at the workshop. The paper focuses on dynamic soil-structure interaction, though some facilities are included that are without dynamic capabilities. The first three sections discuss centrifuge testing, 1-g shake table testing, and full scale testing. A brief description of the National Geotechnical Experimental Site program is included within the full scale testing section. The final section introduces the NHPS concept in light of the review of existing facilities.

INTRODUCTION

The purpose of this paper is to provide a brief summary of experimental facilities in the United States that can be used for Soil-Structure Interaction (SSI) research. The objective is to provide the participants of this US-Japan SSI Workshop with a description of existing and upcoming facilities in order to promote discussions on future collaborations at the workshop. Contact information is provided for most facilities to direct the participants to further information if they are interested. Though I have tried to include most of the larger facilities, and a sampling of smaller facilities, I am certain that some valuable facilities have been inadvertently left out of this paper. Much of the information contained in this paper is the result of a request through the United States Universities for Geotechnical Engineering Research (USUGER) e-mail membership list. In addition, their have been several reviews of earthquake engineering research facilities in recent years, most notably the *Assessment of Earthquake Engineering Research and Testing Capabilities in the United States* (EERI, 1995) which is still available to interested workshop participants from EERI. This critical review of our existing capabilities has led to much discussion among the earthquake engineering community on the urgent need for a National Network of High Performance Seismic Simulation (NHPS), which will be discussed in more detail later in this paper.

This paper focuses on dynamic soil-structure interaction, though some facilities are included that are without dynamic capabilities. The paper is separated into 4 parts. The first three sections discuss centrifuge testing, 1-g shake table testing, and full scale testing. A brief description of the National Geotechnical Experimental Site program is included within the full scale testing section. The final section introduces the NHPS concept in light of the review of existing facilities.

CENTRIFUGE FACILITES

There are currently 14 geotechnical centrifuges located in the United States as shown in Table 1 (Dobry and Elgamal, 1989; Marcuson *et al.*, 1995). Eight of these have shakers that can be used for earthquake testing. The largest four have capacities an order of magnitude larger than the rest: the 1256 g-ton centrifuge at the US Army Corps of Engineers Waterways Experiment Station in Vicksburg, Mississippi; the 440 g-ton centrifuge at the University of Colorado, Boulder; the 400 g-ton centrifuge at the University of California, Davis, and the 100 g-ton centrifuge at Rensselaer Polytechnic Institute in Troy, New York. The other ten centrifuges located in the United States have a capacity of between 5 and 15 g-tons. The four medium and large centrifuges are discussed in more detail below.

TABLE 1. Description of US Centrifuges.

Location (1)	Max. Centrifugal Acceleration (g) (2)	Max. Payload (lbs/kg) (3)	Max. Capacity (g-ton) (4)
USACEWES	350	8800/4000	1256
CU, Boulder	200	4400/2000	440
UC, Davis	100	8000/3640	400
Boeing	600	400/180	120
RPI	200	1000/454	100
CU, Boulder	100	300/136	15
Tyndall AFB	100	300/136	15
U. of Maryland	200	150/68	15
MIT	200	150/68	15
UC, Davis	100	200/91	10
UC, San Diego	100	200/91	10
U. of Florida	120	125/57	7.5
Caltech	175	80/36	7.5
U. of Florida	100	100/45	5

The centrifuge at the US Army Corps of Engineers Waterways Experiment Station has the largest capacity of centrifuges in the United States. This new facility (opened in 1995) has a radius of 6.5m, a centrifugal acceleration range of

[1] Assistant Professor of Geotechnical Engineering, Division of Structural Engineering, University of California at San Diego, 9500 Gilman Drive, La Jolla, CA 92093-0085. Telephone: 619-822-0431. Fax: 619-822-2260. E-mail: sashford@ucsd.edu

10 to 350g's. The maximum capacity of 1256g-tons is reached at 143g's. Though primarily used for geotechnical research, it is also used extensively for coastal, cold region, environmental, hydraulics, and structural applications. In addition to modeling earthquake loading for soil-structure interaction experiments, it is also has the capability to model blast loading, frozen environments, and low pressure environments (even vacuums that would exist on other planets). More information can be obtained at the http://www.wes.army.mil/centrifuge.

The University of Colorado at Boulder has two centrifuges in their Geotechnical Engineering Laboratory, the largest being a 400 g-ton capacity Wyle centrifuge capable of dynamic simulation. This centrifuge is can carry a model 1m in dimension. More information can be obtained at http://bechtel.colorado.edu/Labs/Centrifuge.html.

The University of California, Davis, also has 2 centrifuges. The effort to install the largest of the two centrifuges started in 1978, with the centrifuge being operational at UC Davis in 1988. This centrifuge currently has a 9-m radius, a maximum payload of 4500 kg and an available bucket area of $4m^2$. This centrifuge is limited to 53g acceleration due to limited drive torque, but has the potential to nearly double it's capable acceleration. Currently 64 channels of data acquisition are available with sampling at 5000Hz. The shaker, installed in 1995, is capable of accelerating a rigid mass of 2700kg up to 14g's, but for flexible models accelerations up to 30g's can be obtained. For this shaker, 2 flexible shear beams and a rigid container are available with plan dimensions of well over 1 meter. A great deal of additional information can be found at http://www.engr.ucdavis.edu/%7Ecgm/FACILITIES.html, the website for UC Davis' Center for Geotechnical Modeling.

The 100 g-ton centrifuge at Rennesslaer Polytechnic Institute is the only medium sized centrifuge in the US, and is the largest on the eastern coast of the US. The nominal radius of the centrifuge is 2.5 m, and has a container of 0.8 m in plan dimension. A 0.5 ton payload can reach a centrifugal acceleration of 200g's and a 1 ton payload 100g's.

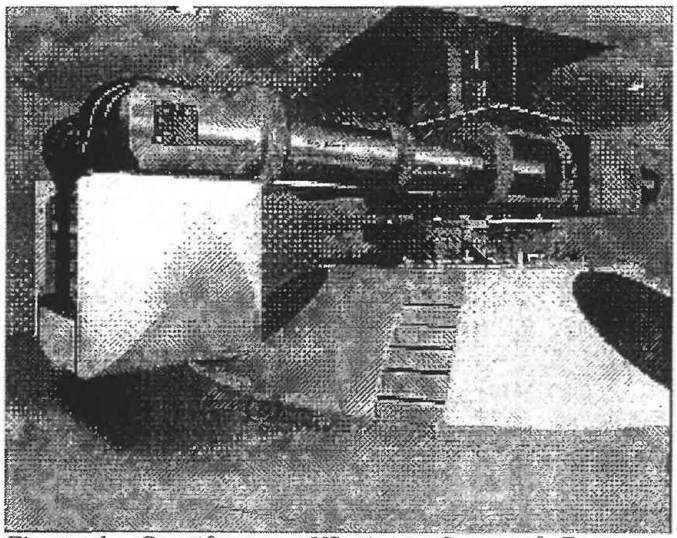

Figure 1: Centrifuge at US Army Corps of Engineers Waterways Experiment Station.

SHAKE TABLES

There are currently 6 "medium" size shake tables in operation in the United States, located at the University of California at Berkeley (6.0m x 6.0m), the State University of New York at Buffalo (3.7m x 3.7m), the University of Illinois at Urbana-Champaign (3.7m x 3.7m), the US Army Construction Engineering Research Laboratory (3.7m x 3.7m), the University of Nevada, Reno (3.7m x 3.7m), and the University of California, San Diego (4.9m x 3.0m). These are "medium" size table compared to Japanese standards, and have payload capacities ranging from 6,800 to 54,500kg. Two additional tables will be in operation shortly: the 3.7m x 3.7m table at the University of California, Irvine, and the 4.9m x 3.7m table associated with the Seismic Retrofit Modification Device (SRMD) testing system at the UC San Diego. The 6 degree-of-freedom SRMD table at UCSD will be one of the most powerful shake tables in the US, with a longitudinal force capacity of nearly 9,000kN, a longitudinal stroke of 1.2m, and a maximum velocity of 1.8m/s. In addition, there are over 10 additional small tables distributed around the US. Of the medium sized table, one has a flexible container for conducting soil-foundation-structure interaction experiments (UC Berkeley), and two have containers planned (UN Reno and UC San Diego).

The container at UC Berkeley was designed for soil-foundation-structure interaction experimentation in cohesive soils. The container consists of a thin-walled cylindrical rubber bag, reinforced with aramid fibers placed as horizontal hoops as well as in independent vertical strips. The container is approximately 2.4m in diameter and 2.1m high. The top and bottom of the bag are connected to rigid rings, supported by eight axial load-bearing columns with ball-and-socket joints at the rings. This container, when shaken on the UC Berkeley shake table can provide appropriately scaled response of up to 0.8g and can accommodate two-directional shaking (Reimer, 1996).

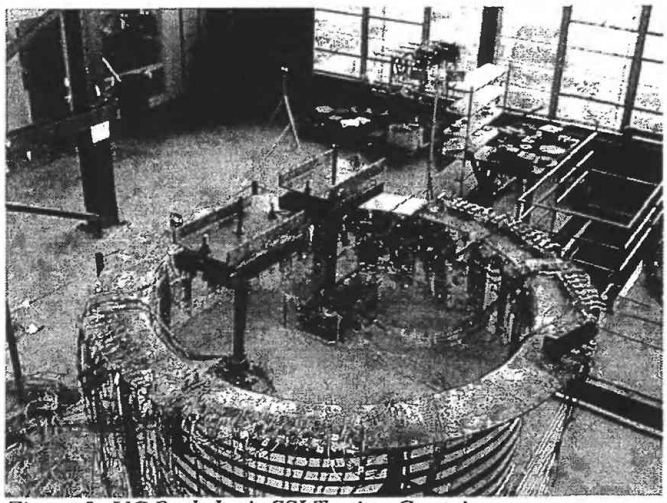

Figure 2: UC Berkeley's SSI Testing Container

The University of California, San Diego, is planning to construct a laminar soil box for soil-foundation-structure interaction testing of bridge columns. Though currently in the planning stages, this laminar box will be similar in design to the large laminar box at the NIED in Tskuba, Japan. It will be

used on both the medium-sized shake table at UC San Diego as well as the larger SRMD shaking table under construction.

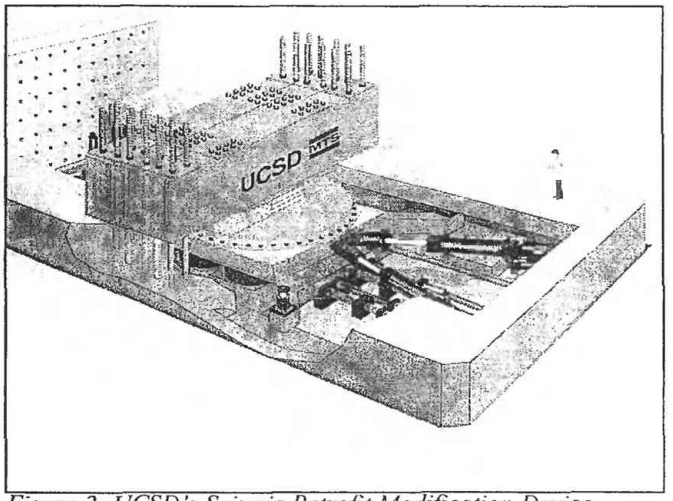

Figure 2: UCSD's Seismic Retrofit Modification Device

The University of Nevada, Reno, is currently constructing a laminar soil box for soil-foundation-structure interaction testing in sands. The box will have plan dimensions of 3.2m x 3.2m and a height of 1.9m. The walls of the box will be composed of alternating layers of aluminum and neoprene. In order to simulate overburden pressure in the granular soils to be tested, the laminar box is equipped with a sealable top plate to allow the box to be pressurized up to 30 psi (Sherif Elfass, personal communication).

FULL SCALE TESTING FACILITIES

There is a move in SSI research in the United States towards full scale testing and instrumentation of full scale structures in high seismic areas. Many of the full scale tests that take place are "one-of-a-kind" due to the high cost and space requirements. In this section, a few of the full scale test facilities that do have some opportunity for repeated use are discussed. In addition, special opportunities for cooperative full scale testing, including the National Geotechnical Experimentation Sites program, are presented.

The University of California, San Diego, is developing a Mobile Structures Testing Laboratory for conducting full scale lateral load testing of deep foundations. It will also be used for monitoring behavior of full scale bridge superstructures. The mobile laboratory will consist of a 196-channel high-speed data acquisition system capable of sampling rates of 500Hz, a 2000-kN hydraulic actuator with a portable hydraulic power supply capable of driving the actuator at velocities greater than 50 mm/sec, and a digital controller. The laboratory is being used in Fall of 1998 for conducting lateral load testing of drilled piers up to 2m in diameter at the UCSD campus, and also lateral load testing of drilled piers and driven pile groups sand liquefied by controlled blasting at the Treasure Island NGES. More information can be found in Ashford and Elgamal (1998).

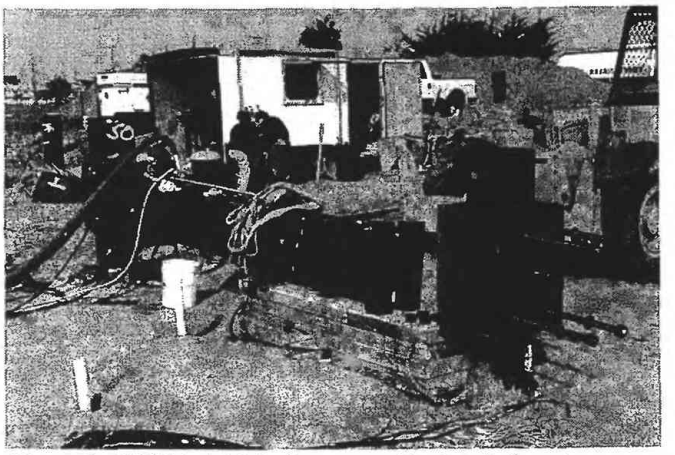

Figure 3: UCSD's Mobile Structures Testing Laboratory.

The University of California, Davis, has constructed an in-ground large diameter soil container for investigating plastic hinge formation in reinforced concrete piles. The corrugated steel container has a 6.7m diameter and is 5.5m deep. A large capacity concrete block (1.4m x1.5m x 6.1m) is used to provide lateral reaction for the test pile, and axial loads are provided by hydraulic jacks and tie rods connected to a strong beam at the base of the container. These features allow for the investigation of combined axial/lateral loading of the piles. More information can be found in Chai and Hutchinson (1998).

A full scale column/shaft is being installed for testing at the University of California, Los Angeles. The column/shaft, 2.4m in diameter, 21m deep and 15m high, is heavily instrumented with soil pressure meters, inclinometers, extensometers, strain gauges, displacement sensors, gamma ray sensors, as well as sensors for time domain reflectometry. The column/shaft will be subjected to a series of slow cyclic lateral load tests, with loads being applied to the top of the column through cables connected to ground reactions. More information can be found in Janoyan and Selna (1998).

Other examples of large scale testing facilities include a 6.7m diameter, infinitely deep sand box at the University of Michigan. The box is located adjacent to the structural engineering reaction wall to allow testing with a variety of hydraulic actuators and aboveground structures (R. Woods, personal communication). Another example is the Louisiana Transportation Research Center Test Wall at Louisiana State University (M. Tumay, personal communication). This 47m x 16m x 6m high embankment is being used to test 7 different types of slope reinforcement and retaining wall systems, including a large diameter culvert. On a smaller scale, Utah State University has developed a soil container for conducting lateral load testing of piles and pile groups in their geotechnical laboratory. The steel ribbed container measures over 3.05m long by 0.91m wide by 1.5m deep, and is being used to study cyclic loading of piles in soft clay (J. Caliendo, personal communication).

The NeTI Ground Motion Generation Project

An innovative SSI project is underway by the Nevada Testing Institute (NeTI), a non-profit Nevada corporation (P. Mote, personal communication). NeTI has developed a consortium of university and non-university research

institutions to design, test, and construct a ground motion test bed at the Nevada Test Site. The site will be used for large- and full scale soil-foundation-structure interaction testing under earthquake loading. Earthquake excitation for the site will utilize the Repeatable Earth Shaking by Controlled Underground Expansion (RESCUE) techniques. Using these techniques, ground motions are generated by rapidly expanding a buried neoprene rubber bladder using gasses generated by timed propellant ignitions.

Successful preliminary testing at a site in California was completed some time ago, and Phase 1 testing at the Nevada Test Site are ongoing. Tests have been completed on a 1.5m by 6m test bed, with source/soil test pressures on the order of 550 kPa. Ultimately, up to a 60m by 60m test bed is anticipated, with the capability to repeatably produce ground displacements of 500 mm and accelerations as high as 4g's. Universities participating in the initial testing include the University of Nevada, Las Vegas; University of Nevada, Reno; University of California, Irvine; as well as UC's Lawrence Livermore National Laboratory. More information can be obtained by contacting the Nevada Testing Institute by fax at (702) 895-0512.

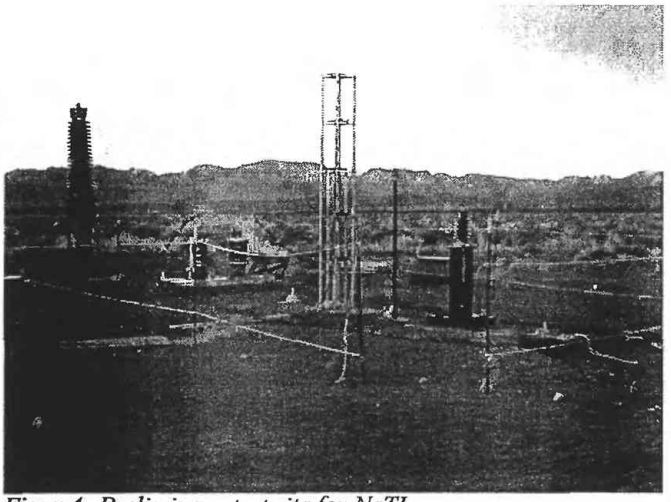

Figur 4: Preliminary test site for NeTI

National Geotechnical Experimentation Sites Program

The National Geotechnical Experimentation Sites (NGES) Program is a system of multiple user, well-documented geotechnical test sites with easy access. The NGES Program was funded by the National Science Foundation and the Federal Highways Administration. The NGES Program also has a central repository of geotechnical data collected at each NGES to promote exchange of information and reduce research costs.

In all, over 40 sites have been designated in the NGES Program. Of these, 5 have been classified as Level I and II sites; site that meet most or all of the research needs identified in national workshops, as well as having favorable site conditions. These site are Treasure Island Naval Station (San Francisco, California), Texas A&M University Riverside Campus (College Station, Texas), Northwestern University Lake Fill Site (Evanston, Illinois), University of Massachusetts-Amherst, Amherst, Massachusetts), and University of Houston Foundation Test Facility (Houston Texas).

The theme research areas that were deemed a priority for the NGES Program are geotechnical earthquake engineering (liquefaction, site amplification, and permanent deformations), calibration of new equipment, proof-testing of site improvement techniques, geo-environmental problems, expansive clay problems, and foundation prototype testing. Information for each of the Level I and II sites is available to potential users, including information on soil type, stratigraphy, previous test results, as well as results of previous research efforts conducted at the sites. Additional information can be obtained at the NGES website http://unhinfo.unh.edu/nges/.

NATIONAL NETWORK FOR HIGH PERFORMANCE SEISMIC SIMULATION

Over the last 25 years, there have been at least 8 assessments of the experimental facilities in the US for conducting earthquake engineering related research (EERI, 1995), the most recent being the *Assessment of Earthquake Engineering Research and Testing Capabilities in the United States* prepared by EERI in 1995 as required by law in the 1994 reauthorization of the National Earthquake Hazard Reduction Program (NEHRP). The assessment project was sponsored by NSF and the National Institute of Standards and Technology (NIST). This report concluded that the that the state of research and testing capabilities had not kept up with the needs of the greater community in reducing losses from earthquakes. Among the recommendations contained in the report were to upgrade existing experimental facilities, to develop new moderately-sized regional centers with unique and complementary facilities, to study the feasibility of a single national test facility, and to continue and expand programs where facilities and research results can shared among many users (including international users).

An outgrowth of this latest assessment is the proposed National Network for High Performance Seismic Simulation (NHPS). The NHPS has been proposed within NSF as a Major Research Equipment (MRE) initiative in order to develop integrated experimental research facilities to improve of fundamental understanding of earthquakes and help avoid catastrophes caused by lack of knowledge of the behavior engineering materials, soils, and construction during earthquakes. The intent of the NHPS is to develop a network of research facilities open to everyone that would provide a means for rapid exchange of ideas and information and offer immediate access to research data generated anywhere in the network.

A draft report from an NHPS workshop held in June 1998 at UC Davis (http://www.engr.ucdavis.edu/%7Ecgm/NHPS/) states that the NHPS would include three major categories of new and enhanced equipment:

1. Advanced-design earthquake simulation facilities including simulation systems for structural testing, geotechnical centrifuges with shakers, and wave generators for the study of tsunamis.
2. Large scale testing systems for testing structural elements, assemblies of elements, and response modification devices at full scale.

3. Field simulation and laboratories including field testing installations, mobile laboratory units for monitoring constructed facilities before, during and after an earthquake.

The NHPS would greatly enhance our ability to conduct SSI experimentation in the US. Some specific facilities in the NHPS include development of new instrumented field sites, development of high-energy mobile seismic wave forces, development of sites for ground motion simulation with high explosives, as well as the upgrading of existing centrifuge shaker capabilities. Much more detail on the development of the proposed NHPS is available at http://www.engr.ucdavis.edu/%7Ecgm/NHPS/.

REFERENCES

Chai, Y. H., and Hutchinson, T. C. (1998). "Revereved Cyclic Response of Reinforced Concrete Piles in Cohesionless Soil," *Proceedings, The 5th Caltrans Seismic Research Workshop,* June 16-18, Sacramento, CA.

Dobry, R. and Elgamal, A.-W. (1989). "The New RPI Geotechnical Centrifuge," *Geotechnical Centrifuge Newsletter,* Cambridge, England, April 1989.

EERI (1995). *Assessment of Earthquake Engineering Research and Testing Capabilities in the United States,* Earthquake Engineering Research Institute Publication No. WP-01, September 1995, 23 p.

Janoyan, K., and Selna, L. (1998). "Design and Construction of Large Scale Column/Shaft Test Project," *Proceedings, The 5th Caltrans Seismic Research Workshop,* June 16-18, Sacramento, CA.

Marcuson III, W. F., Ledbetter, R. H., Green, R. A., Steedman, R. S., Franklin, A. G., and Hynes, M. E. (1995). *Problems in Geotechnical Earthquake Engineering that Demand Experimental Test Facilities,* Commissioned Paper by EERI for *Assessment of Earthquake Engineering Research and Testing Capabilities in the United States.*

Reimer, M. (1996). "Physical Modeling of Seismic Soil-Pile Interaction," *EERC News,* Earthquake Engineering Research Center, University of California, Berkeley, 17(2), April 1996, pp. 1-3.

DENSE INSTRUMENTATION IN BRI BUILDING AND SURROUNDING GROUND

BY

IZURU OKAWA[1], TOSHIHIDE KASHIMA[2] AND SHIN KOYAMA[2]

ABSTRACT: The Building Research Institute (BRI) had conducted earthquake recordings mainly in buildings since 1957. Several recorded motions from our earthquake recording are used for seismic design of buildings. However, there had been regret that these motions recorded in buildings are contaminated with the vibratory characteristics of building itself. The consideration of the dynamic property of building is important when those motions are applied for other buildings. In the next step, we had started earthquake recording only in ground of Sendai area in the northern part of Japan focussing on the effect of surface soil conditions on seismic motions. Although we had obtained only records with small amplitudes, we recognized that the amplification characteristics are varied depending on site-specific nature of the recording sites. In 1993, we had a big earthquake in Hokkaido. Extremely large amplitude of 700 or 900 cm/s/s was obtained in the free field during the earthquake. However, damage to buildings was minor. Since then, we had kept in mind what the effective input motion to building is. The minor damage had been partly explained by the fact that most of the buildings in Hokkaido keep large foundation with deep embedment because of its cold weather in winter. We had devastating earthquake damage in Kobe. Considerable, not large, number of strong motion records had been obtained during this earthquake. Comparing free field motions with those from inside of buildings, it might be said that the former shows larger amplitudes than the latter. This difference might be partly caused by the soil-structure or soil-foundation-structure interaction. With these in background, we had started other earthquake recording systems after the Kobe earthquake. One is the strong motion seismograph array network deployed around the greater Tokyo metropolitan area. The other is the dense instrumentation in BRI campus. When we look the structural damage during the recent large earthquakes in Japan, the evaluation of effective input motion to buildings are very important. In this paper, our attempt on the earthquake recordings is introduce focussing in above matters.

INTRODUCTION

With rapid progress and advances in recording technology and reduction in cost for installing the instruments, tremendous number of strong motion records have been obtained and released with recent large earthquakes in Japan. Strong motion recordings were started with seismometers installed in structures. The Building Research Institute (BRI) published many epoch-making records such as the Kawagishi-cho apartment, for 1964 Niigata earthquake, recording the tilting of the apartment building due to soil liquefaction. This was the first recording of liquefaction phenomena in the world. After that, we had also obtained large earthquake record in the campus of Tohoku University, during 1978 Miyagiken-oki earthquake. The earthquake was recorded at the 1st and 9th floor of the building in the campus. The amplitude in the first floor was large at the time. Attention was drawn from many researchers that the 9th floor accelerogram showed amplitude more than 1G. We had also large amplitude records during 1993 Kushiro-oki earthquake, and 1994 Hokkaido Toho-oki earthquake and 1994 Sanriku Haruka-oki earthquake. Unfortunately, we had not installed seismographs in Kobe. Because Kobe had long been believed to be earthquake-free area by residents around there. We have instead obtained record in Osaka several tens km away from Kobe.

BRI seismograms had generally been installed in the buildings with some exceptions since its beginning. Considering the large amplitude recorded by the free field sites, we came up to bear idea in mind that the free field ground motion is not identical to the input motion to the structure. Here, we should define what is the input motion. That is the motion to be used for the analysis of superstructure with the assumption of fixed-base model. It might be appropriate to call it effective input motion to structure. With the terminology, it is said that we should seek for the effective motion or how to distinguish effective motion from recorded ones.

Recently we set up two kinds of earthquake recording systems. One is a system with 2 to 4 three component sensors in one site installing in first or basement floor, top floor and nearby free filed. We installed seismometers at 20 sites around Tokyo area. It is not easy; however, to find places for free field, since there are few free grounds with little influence of buildings. The other is the dense instrumentation to building and surrounding ground including deep boreholes.

1) Head, Building Engineering Division, International Institute of Seismology and Earthquake Engineering, Building Research Institute, Tatehara-1, Tsukuba-shi, Ibaraki-ken, 305-0802, Japan

2) Senior Research Engineer, International Institute of Seismology and Earthquake Engineering, Building Research Institute, Tatehara-1, Tsukuba-shi, Ibaraki-ken, 305-0802, Japan

We set up this system in newly constructed 8-story steel reinforced concrete (SRC) building next to the main building in our institute campus. Totally 66 channels record the event when certain level of motion is triggered. We hope the recording system of this kind will be very directly utilized for evaluating the SSI phenomena.

BRI EARTHQUAKE RECORDING ACTIVITIES

Nationwide Strong Motion Observation in Buildings

BRI has installed strong-motion instruments in major cities throughout Japan. There are now 47 observation sites in operation using the digital strong-motion instrument. The observation points are shown in Fig.1. The objects of observation are mainly buildings, and the measuring point is usually placed both on the top and in the foundations of the building. We are increasing the free field measuring points. However, the objective points had long been within the building. Most of the observation sites are connected to BRI via telephone line in order to reduce maintenance work and to retrieve data directly and promptly.

This observation network has obtained many noteworthy records. As was mentioned previously, the Kawagishi-cho apartment record for 1964 Niigata earthquake, in Fig.2 recording the tilting of the apartment building due to soil liquefaction. This was the first recording of liquefaction phenomena in the world. The earthquake record in the campus of Tohoku University, during 1978 Miyagiken-oki earthquake was also from BRI recording system. The earthquake was recorded at the 1st and 9th floor of the building in the campus as shown in Fig.3. The amplitude in the first floor was larger one at the time. Attention was drawn from many researchers that the 9th floor accelerogram showed amplitude more than 1G. There had been time with little significant ground motions. Then, we had also large amplitude records during 1993 Kushiro-oki earthquake, 1994 Hokkaido Toho-oki earthquake and 1994 Sanriku Haruka-oki earthquake. During the 1993 Kushiro-oki (Off Kushiro) Earthquake, 711 gal was recorded as the peak acceleration on the ground surface at Kushiro Local Meteorological Observatory. Whereas, JMA seismometer installed in the same observatory recorded 920 gal. After this earthquake, BRI installed additional seismometer under the ground of the site. These records are shown in Fig.4. In 1994 Hokkaido Toho-oki earthquake, simultaneous recordings in surface and underground were obtained. In the 1994 Sanriku-haruka-oki (Far off Sanriku) Earthquake, a large acceleration amplitude record was obtained in the building next to the severely damaged old Hachinohe municipal office building.

Strong-Motion Instrument Network in the Metropolitan Area

After 1995 Hyogoken-Nanbu (Kobe) earthquake, considerable number of strong motion seismographs were installed nationwide. Its typical example is the Kyoshin-Net (K-Net) by National Research Institute of Earth Science and Disaster Prevention, Science and Technology Agency (NIED). The Japan Meteorological Agency (JMA) and many local governments also deployed wide coverage of strong motion seismograph installation nationwide as well as the STA.

The 1995 Hyogo-ken-Nanbu Earthquake (Kobe Earthquake) awakened us again to the importance of disaster prevention measures for large-scale urban areas. It is important to predict the probability of a future earthquake and its impact, and make as many preparations as possible in anticipation of such an event. It is also very essential to grasp the damage condition immediately to put in effect the necessary countermeasures. BRI has established twenty new observation sites placed radially in the Tokyo metropolitan area. This project aims to investigate the characteristics of the seismic motion affecting the whole Kanto Plain through observation records. The system immediately collects information on the seismic intensity at the time of an earthquake occurrence. The site location is shown in Fig.5. We had tried to install seismometers both in the buildings and free field. However, it is very difficult to find free field point near the building especially densely populated Tokyo area. The recording sites in the suburbs have both, and therefore comparative data for SSI problem can be obtained.

Dense seismometer array earthquake recording in various soil conditions of Sendai

We also installed seismographs in grounds. Eleven recording stations are deployed around Sendai area, Japan as shown in Fig.6. The location and geology of observation sites are listed in Table 1. The recording stations were selected so that typical surface soil conditions of urban areas in Japan are contained. Sendai was severely damaged during the 1978 Miyagiken-oki earthquake. There is result of damage investigation. The damage distribution had clear correlation with the soil conditions. Therefore, we will get the difference of strong motion characteristics when large earthquake database is completed. Each station has three seismographs with three component sensors. They are installed from surface to so-called engineering bedrock. These records have provided data to evaluate the effect of surface geology on seismic motions. Unfortunately, earthquake data that are large enough to examine the effect of nonlinear behavior of soils are still very few in number. The specifications for recording instruments are listed in Table 2. In Table 3, the recorded earthquakes with moderate amplitudes are listed.

BRI DENSE SEISMOMETER ARRAY IN BUILDING AND GROUND

Geographical position of the instrumentation

Our institute (BRI) is located with approximately 60 kilometers to the northeast from downtown Tokyo. The site is situated 30 meter above sea level on the diluvial heights between Sakuragawa-river flowing into Kasumigaura Lake and Kokaigawa-river, a branch flow in the greater Tonegawa-river water system.

The external views are shown in Photos 1 and 2. As is shown, the new building is connected with the main building. The geological investigation shows that clay and fine sand are main contents up to 90 meters depth underground, inserting sandy gravel. We confirmed a sandy gravel layer at 88-meter depth. Its shear wave velocity, however, is not obtained. Transfer functions for shear waves between ground surface and depths of 42 meter, 68 meter and 88 meter are shown in Fig.7. We assume here that the shear wave velocity of the

layer beneath 88-meter depth is about 500 m/s. The figure shows common predominant periods of 3-5 Hz and 9 Hz. And the transfer function with up to 88-meter depths includes peak at 1 Hz. This might be the peak relevant to the fundamental frequency of the surface soils. In addition, the layer under 88 meter depth up to approximately 250 meter is called upper Kazusa formation group, the underlying layer is called lower Kazusa formation group, the Tertiary layers.

Building Characteristics

The outline of the building and ground is shown in Fig.8. The building for seismometer installation is a newly constructed as the Urban Disaster Prevention Research Center building completed in March 1998. The building has 8 stories with single basement floor. Total building area is approximately 5,000m^2 and supported by mat foundation on clayey layer of 8.2 meters underground.

Recording System and Observation

The sensors are installed with 11 locations (33 channels) in new building, 7 locations in surrounding ground, and 4 locations (12 channels) in main (older) building. Since the installation was very recent, the records obtained to date are very few. Here, a set of recorded motions of June 24th, 1998; Southwest of Ibaraki prefecture earthquake is introduced. The depth of hypocenter was about 70 km and its magnitude was estimated 5.1. In Fig.9, records of ground surface levels are compared. In Fig.10, the acceleration response spectra for these motions are shown. It is seen that free field ground surface records are larger than that for inside the building, in this case. In addition, comparisons are made between waveforms and response spectra for the records from underground. The results are shown in Figs.11 and 12.

CONCLUSIONS

The earthquake observation project with dense accelerometer array configuration has just started. High quality records will be accumulated year by year. We are ready to make these data open to the public via Internet, hoping the research of ground motion prediction becomes more active and the seismic design methodology for buildings is more upgraded in the future.

REFERENCES

1) Building Research Institute, "Report on the Damage by 1978 Off-Miyagi Prefecture Earthquake" (in Japanese), Research Report of BRI, No.86, pp.75-81, 1978.
2) T.Kashima et al., "Strong-Motion Observation Program in the Metropolitan Area", (in Japanese) Proceedings of the AIJ Annual Meeting, Vol.B-2, pp.275-276, Kinki, 1997
3) T.Kashima et.al., "Earthquake Motion Observation in and around 8-Story SRC Building", (in Japanese) Proceedings of the AIJ Annual Meeting, Vol.B-2, pp.213-214, Kyushu, 1998
4) I.Okawa et al., "Dense Array Observation and Analysis of Strong Ground Motions at Sites with Different Geological Conditions in Sendai", BRI Research Paper 139, 1994

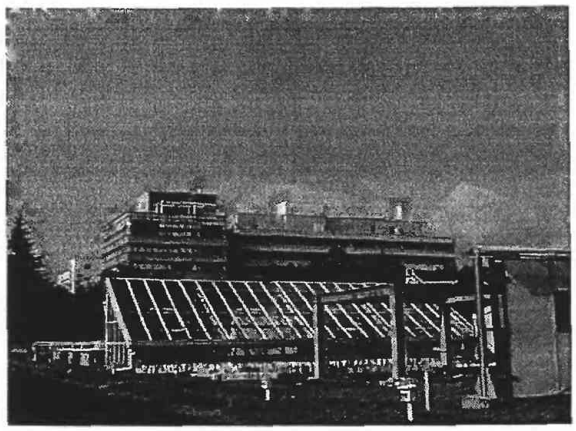

Photo 1. Distant View of the Earthquake Disaster Prevention Research Center Building with the Main Building of BRI in Tsukuba.

Photo 2 Front view of the building of Earthquake Recording

Table 1 Location and geology of observation sites and depths of accelerometers

Site name	Abr.	Latitude	Longitude	Soil type*	f_1 (Hz)	Year	V_S (m/s)	Depth (m)		
Miyagino	MIYA	38°15'24"N	140°55'16"E	2	2.40	1984	680	1	22	54
Nakano	NAKA	38°15'14"N	141°00'26"E	3	1.28	1985	720	1	30	61
Tamagawa	TAMA	38°19'03"N	141°00'34"E	1	7.50	1986	1400	2	11	33
Oridate	ORID	38°15'26"N	140°48'39"E	1**	2.06	1987	1050	1	57	76
Tsutsujigaoka	TSUT	38°15'30"N	140°53'36"E	2	2.08	1988	950	1	36	59
Tsurumaki	TRMA	38°15'38"N	140°58'15"E	3	1.26	1988	660	1	25	79
Okino	OKIN	38°13'26"N	140°55'05"E	3	2.14	1988	820	1	17	62
Shiromaru	SHIR	38°11'29"N	140°54'53"E	2	2.70	1988	830	1	20	76
Tsurugaya	TRGA	38°17'16"N	140°54'53"E	2	1.78	1988	1000	2	37	62
Nagamachi	NAGA	38°13'45"N	140°53'01"E	2	1.44	1989	700	1	29	81
Arahama	ARAH	38°13'11"N	140°59'00"E	3	1.22	1989	750	1	31	76

f_1: Theoretical first predominant frequency, V_S: Shear wave velocity of lowermost layer.

* Soil types according to Japan Building Standard. 1: hard, 2:medium, 3: soft.

** Although the soil condition for ORID site was presumed hard soil, it was confirmed by the soil survey that the surface soils were so heavily weathered that the soil condition type might be assigned to be the second classification.

Table 2 Specifications of the array observation system

Instrument	Specification	
Accelerometer	Type:	Tri-axial velocity-feedback type
	Frequency range:	0.05 to 30 Hz for 1G
Amplifier and AD Converter	Resolution:	16 bit
	Dynamic range:	96dB
	Sampling rate:	1/100 or 1/200 sec.
Pre-event Memory	Delay device:	IC memory
	Delay time:	5 sec.
Clock	Oscillator:	Quartz with accuracy of 10^{-7}, 10^{-8}
	Precision:	±0.01 sec.
	Calibration by:	NHK(JBC)
Digital Data Recorder	Medium:	Digital magnetic tape with 9 track, half-inch in width and 1600 BPI in recording density

Table 3 List of observed earthquakes

#	Date	Time	M	h (km)	Δ (km)	Max. Acc.	I
8608	1986/10/14	06:11	5.0	53	135	26.2 (NAKA)	3
8615	1986/12/01	5:15	6.0	51	108	29.6 (TAMA)	3
8701	1987/1/9	15:14	6.6	72	191	43.5 (NAKA)	4
8702	1987/1/14	20:04	7.0	119	505	11.1 (NAKA)	3
8704	1987/1/21	8:36	5.5	50	112	48.8 (NAKA)	3
8708	1987/2/06	21:24	6.4	30	178	47.4 (NAKA)	3
8709	1987/2/6	22:16	6.7	35	167	94.1 (NAKA)	4
8717	1987/3/10	12:24	5.6	29	166	15.7 (NAKA)	3
8719	1987/4/7	9:41	6.6	37	136	74.5 (NAKA)	4
8721	1987/4/17	4:23	6.1	45	151	45.3 (NAKA)	3
8724	1987/4/23	5:13	6.5	49	145	75.0 (NAKA)	3
8739	1987/9/4	13:55	5.8	42	185	25.4 (NAKA)	3
8740	1987/10/4	19:27	5.8	51	125	60.1 (NAKA)	3
8911	1989/4/28	0:27	4.9	53	98	29.0 (OKIN)	3
8915	1989/6/24	4:59	4.1	14	11	35.0 (TRMA)	3
8926	1989/11/02	3:26	7.1	0	256	22.8 (TRMA)	3
9217	1992/7/18	17:37	6.9	0	269	11.2 (TRMA)	3
9234	1992/12/18	1:21	5.9	34	160	41.0 (TRMA)	3
9305	1993/1/15	20:07	7.8	101	594	36.3 (TRMA)	3
9325	1993/11/11	9:06	5.5	36	154	18.5 (TRMA)	3
9327	1993/11/27	15:11	5.9	112	51	104.2 (NAKA)	4
9409	1994/8/14	18:06	6.0	42	136	45.3 (NAKA)	3
9410	1994/8/16	19:09	6.0	22	154	22.0 (ARAH)	3
9413	1994/10/4	22:24	8.1	23	806	59.7 (OKIN)	3
9414	1994/12/10	18:26	5.1	51	111	28.4 (NAKA)	3
9417	1994/12/28	21:20	7.5	0	343	35.3 (NAGA)	3
9502	1995/1/7	7:37	6.9	30	261	28.0 (OKIN)	3
9602	1996/2/17	0:23	6.5	6	178	106.4 (NAGA)	4
9604	1996/4/23	13:08	5.2	76	117	75.0 (OKIN)	3
9701	1997/2/20	5:22	5.3	88	99	46.7 (SHIR)	3

M: JMA (Japan Meteorological Agency) magnitude, h: focal depth, Δ: averaged epicentral distance, I: JMA seismic intensity at Sendai

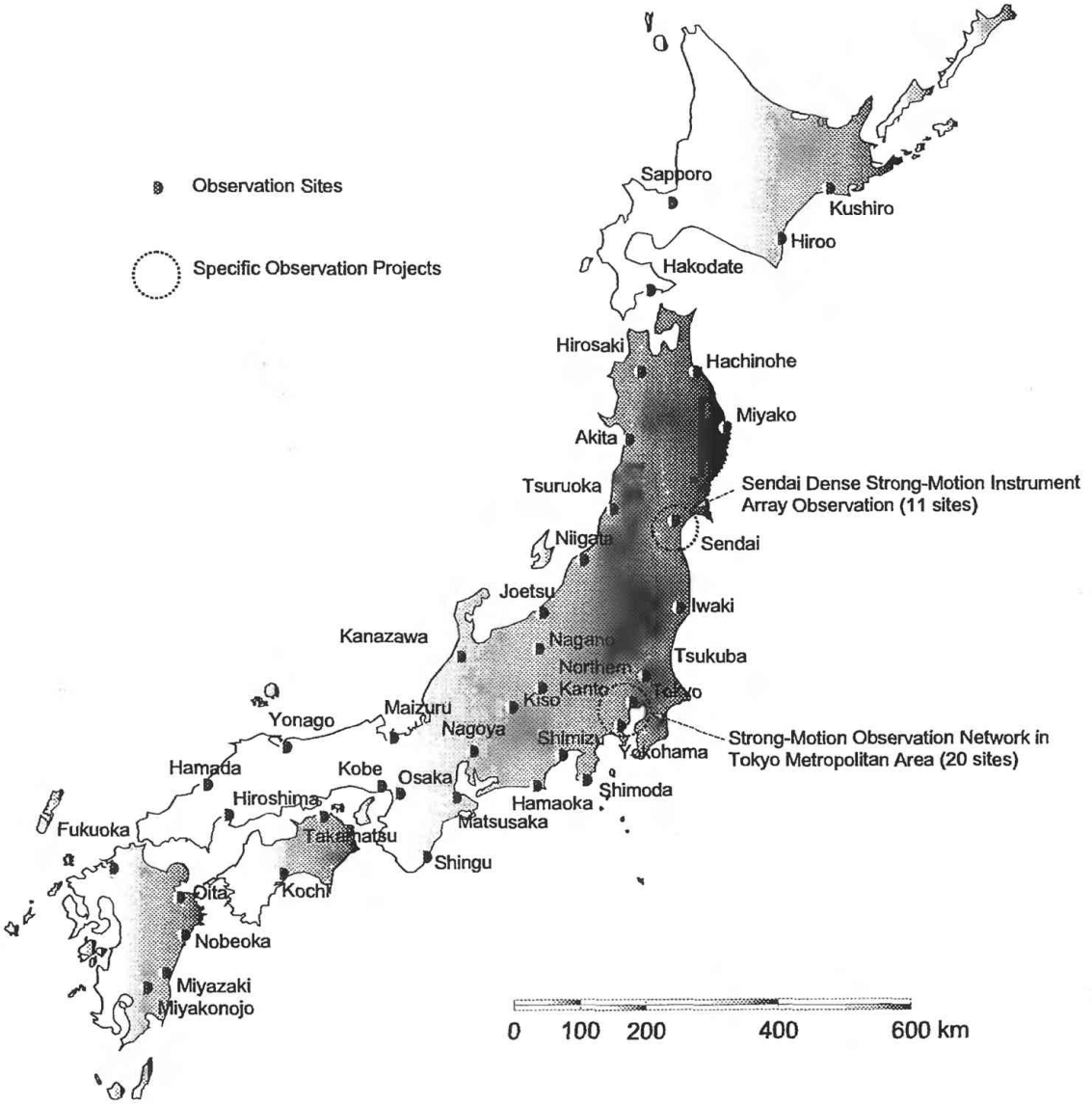

Fig. 1 Locations of Strong Motion Observation Network of Building Research Institute

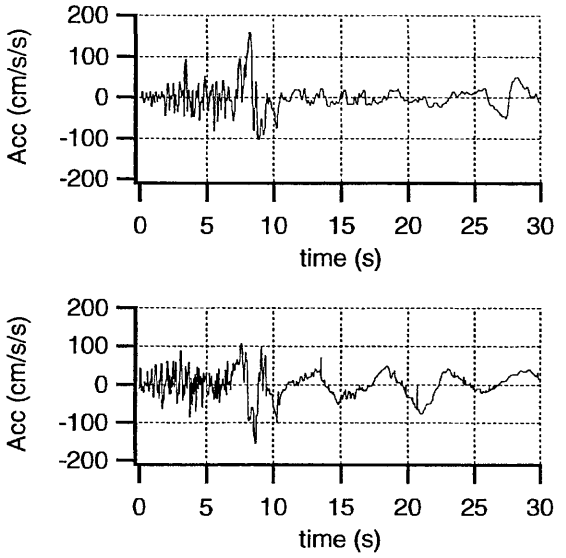

Fig.2 Recorded Motion in Kawagishi-cho Residential Apartment during 1964 Niigata Earthquake. The building was titled due to liquefaction.

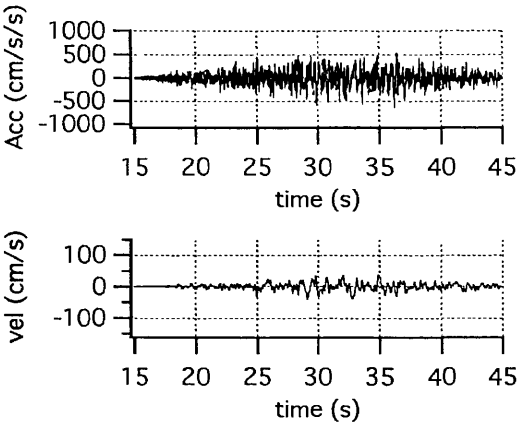

Fig.4 Recorded Motion on Ground at Kushiro BRI Recording Sit in Kushiro JMA Observatory during 1993 Kushiro-oki Earthquake

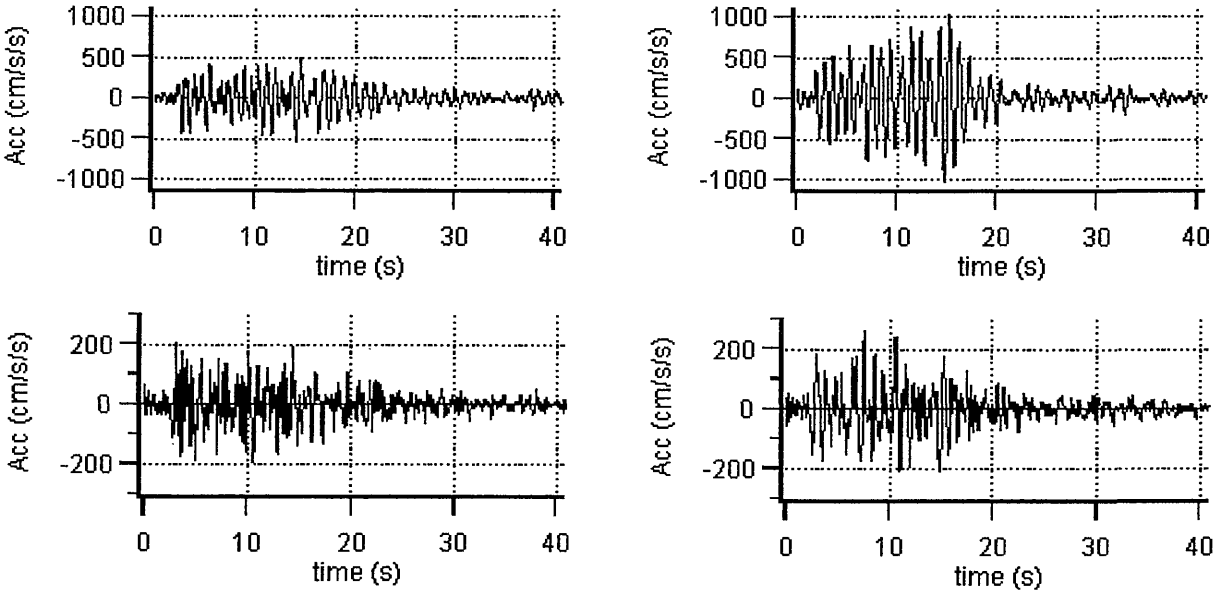

Fig.3 Accelerograms recorded in Tohoku Univ. building during 1978.6.12 Miyagiken-oki earthquake
Upper left: 9th floor, EW, Upper right: 9th floor, NS, Lower left: 1st floor, EW, Lower right: 1st floor, NS

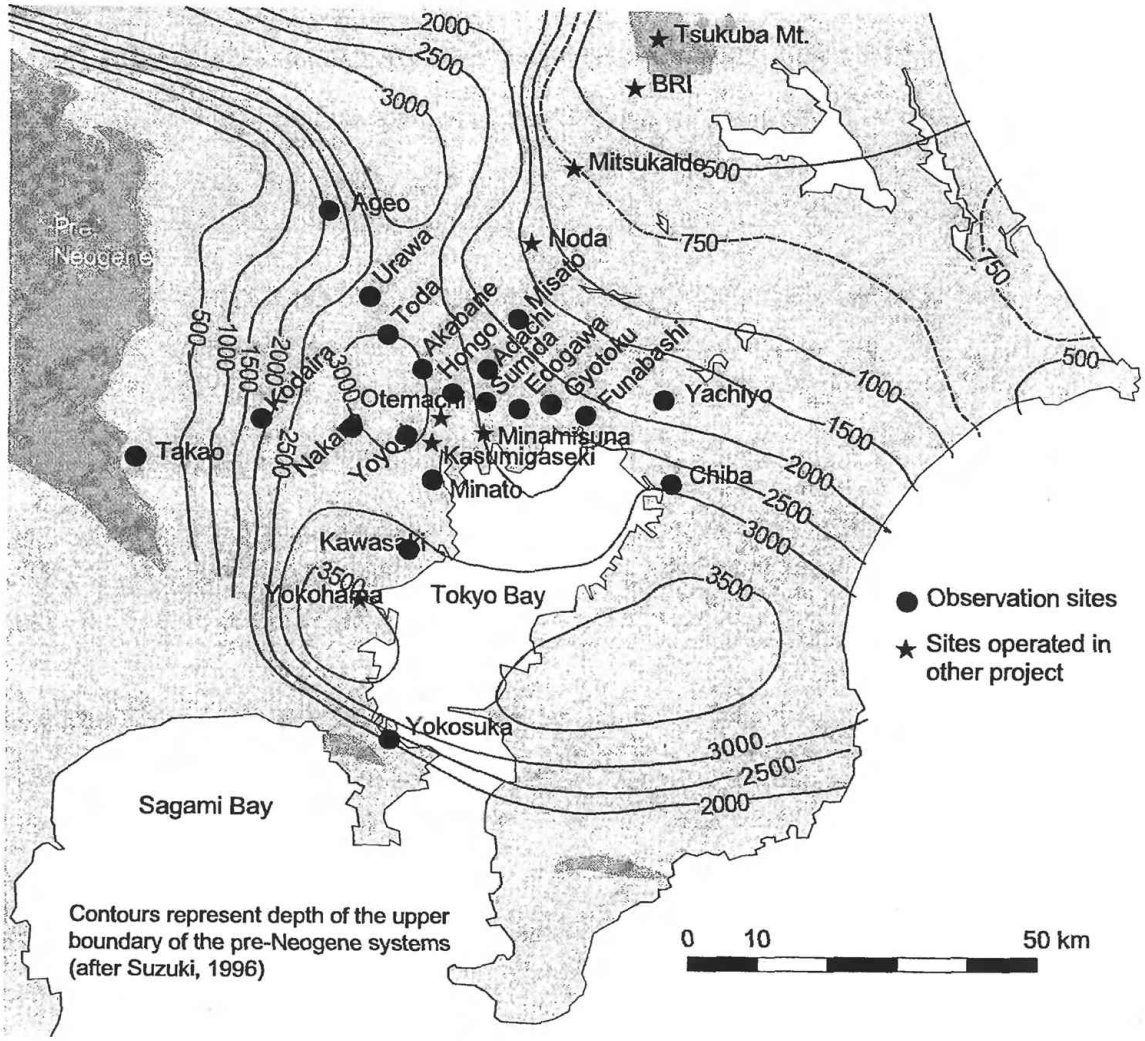

Fig. 5 Strong Motion Instrument Network in Tokyo Metropolitan Area

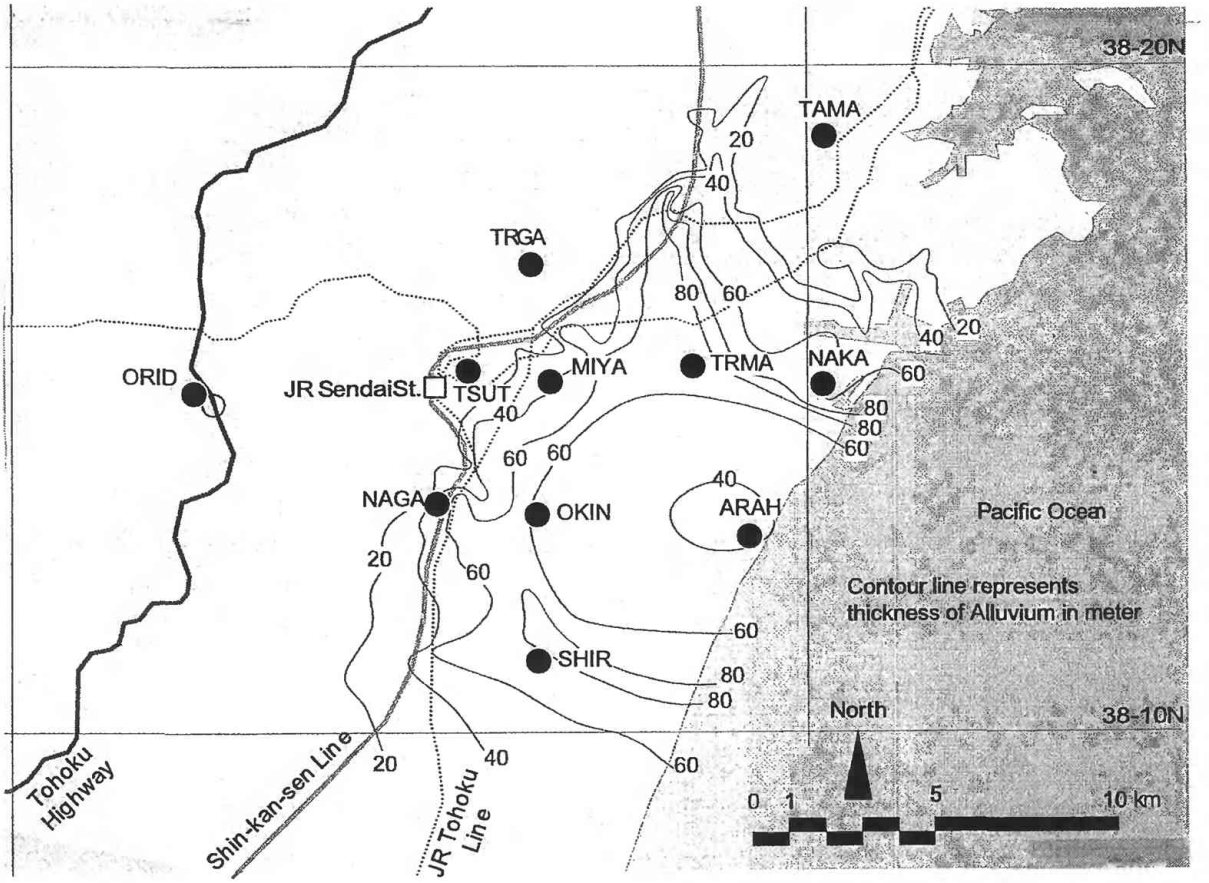

Fig. 6 Locations of Earthquake Recording in Underground of Sendai

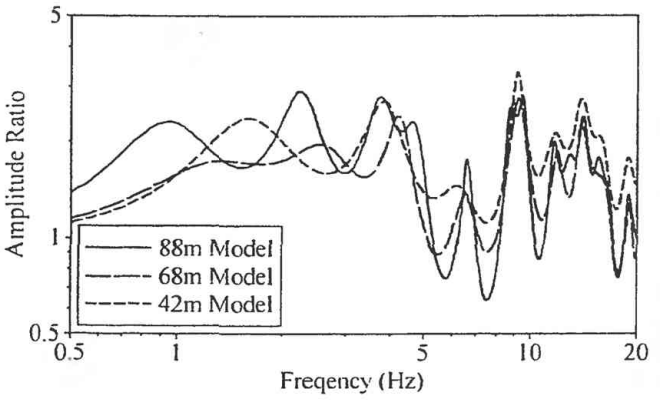

Fig.7 Transfer Function of the S-wave in Surface Ground (Surface/Incident*2)

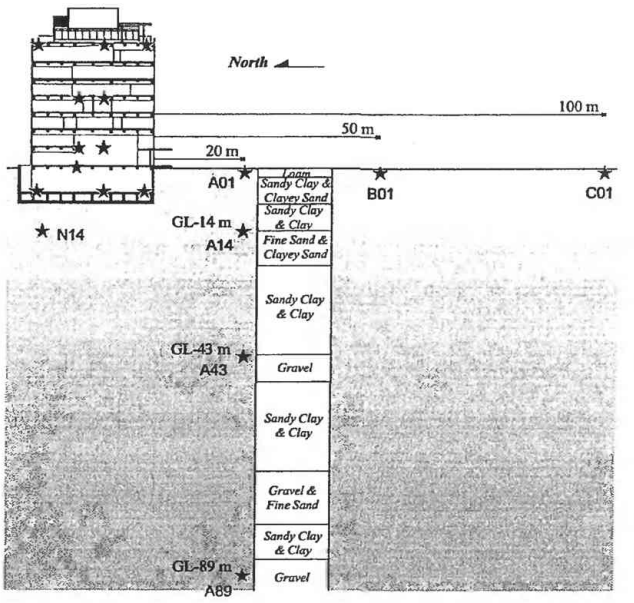

Fig.8 Cross-sectional configuration of recording points for dense instrument array in the Building Research Institute Campus, Tsukuba

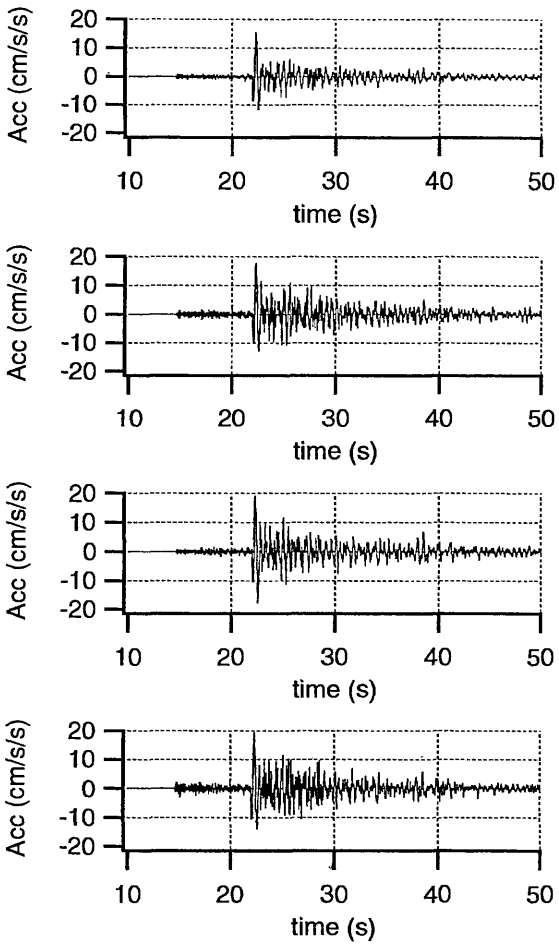

Fig.9 Recorded Motions in 1st Floor, C01, B01, A01 from the above.

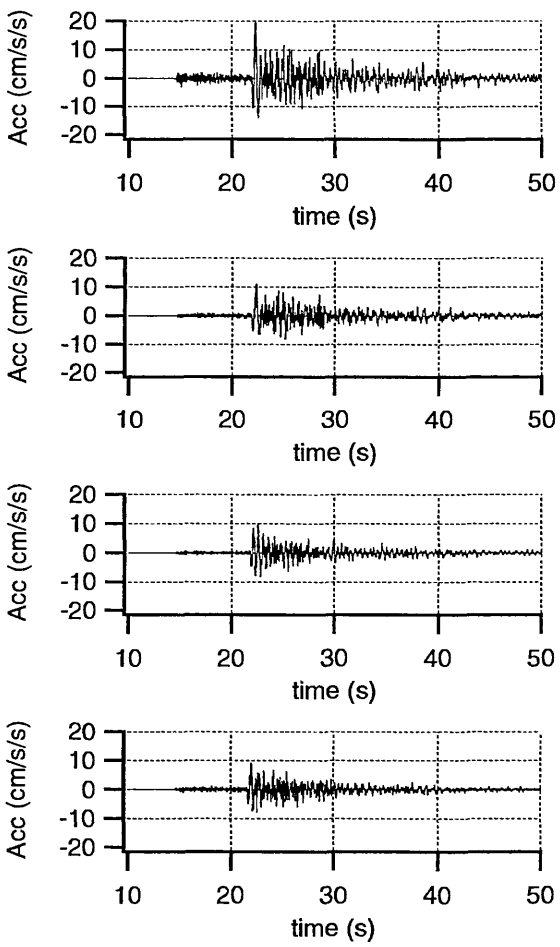

Fig.11 Recorded Motions in underground, GL-1m, GL-14m, GL-43m, GL-89m from the above.

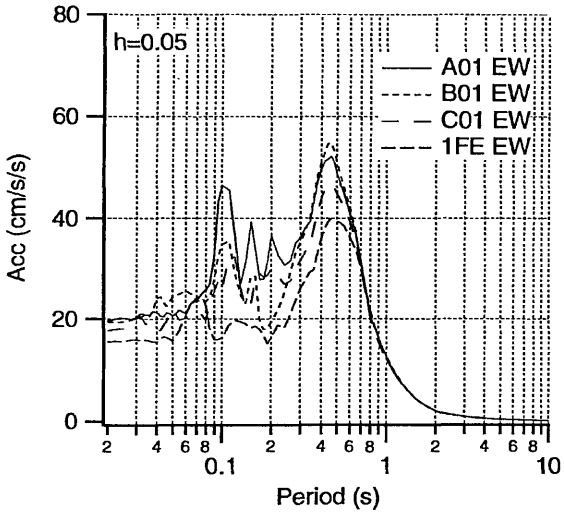

Fig.10 Comparison of Acc. Response Spectra between Recorded Motions in the Ground Surface Level including 1st Floor inside the Building (EW component)

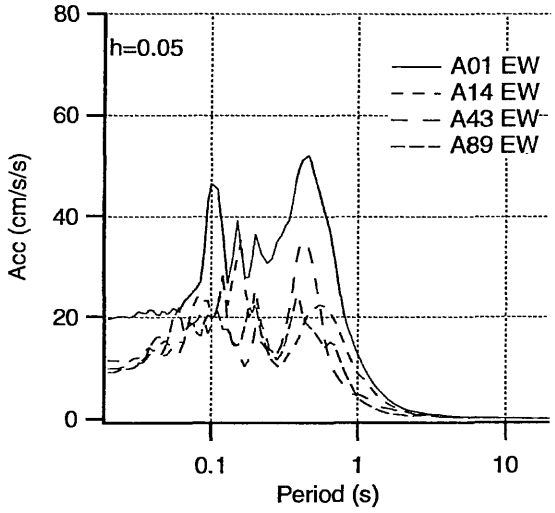

Fig.12 Comparison of Acc. Response Spectra between Recorded Motions in the Ground (EW component)

PLANNING AND IMPLEMENTATION OF A SOIL-STRUCTURE INTERACTION EXPERIMENT

by

Mehmet Çelebi[1]

ABSTRACT: The significant parameters in developing a soil-structure interaction experiment are reviewed. These parameters were described within five major recommendations determined during a workshop held in 1992. Recommendations of that workshop are presented. A project following the guidelines is currently underway, and its current status is discussed.

1. INTRODUCTION

The objectives of this paper are (a) to introduce the background information in establishing a special purpose array in a seismically active region of the United States specifically for studies of the effect of soil-structure interaction, (b) to review and define the parameters and details of a soil-structure experiment, and (c) to describe the current state of implementation.

In the past, during design/analysis processes of engineered structures, it was assumed that the foundation of a structure was fixed to a rigid underlying medium. In the last four decades, however, it has been recognized that soil-structure interaction (SSI) alters the response characteristics of a structural system. In important engineered structures, detailed numerical and closed-form-solution methods have been applied to SSI analyses. To date, the strong-motion data from instrumented buildings are insufficient to confirm the validity of the soil-structure interaction analysis methods and procedures as applied to structures other than nuclear power plant structures. Soil-structure interaction analysis procedures are now included in various codes (*e.g.* ATC--3, NEHRP--1985).

Since 1978, during several workshops and technical meetings, specific recommendations have been repeatedly made to instrument a building for soil-structure interaction studies (*e.g.* Lee, 1978; Iwan, 1978; Iwan 1981). As recently as November 4--5, 1991, during the NSF workshop on ``Experimental Needs for Geotechnical Earthquake Engineering," held in Albuquerque, New Mexico, strong-motion instrumentation for soil-structure interaction was given a high priority (Higgins, 1992). U.S. Geological Survey (a) Circular 947 describes a general SSI scheme (Çelebi et al, 1987) and (b) Circular 1079 spells out priority recommendations for special purpose arrays including those that will facilitate soil-foundation interaction studies (Page et al, 1992).

A workshop held in 1992 resulted in a set of recommendations (upon which this paper is based) to define the needs for and the parameters essential for implementation of a soil-structure interaction experiment. During that workshop, beneficial and adverse effects of soil-structure interaction were discussed

[1] Research Civil Engineer, Earthquake Hazards Team, U.S. Geological Survey, Menlo Park, Ca., USA 94025

(Çelebi, Lysmer and Luco, 1992). Prior to this workshop, there have been no meetings that directly addressed the detailing of a soil-structure interaction experiment except the ones related to the critical structures of nuclear power industry [*e.g.* the Lotung Array] (Tang, 1987, Tang et al, 1987a, 1987b, 1990, 1991).

2. MOTIVATION

Although, currently, there are over 200 instrumented structures in the United States, there is no instrumented structure that will allow detailed calibration and/or confirmation of the validity of the soil-structure interaction analysis methods. The significant sets of data acquired during the 1987 Whittier, 1989 Loma Prieta and 1994 Northridge earthquakes provide insight into structural responses and clearly show that soil-structure interaction took place in several instrumented buildings; however, the data set is insufficient to calibrate soil-structure interaction methods or to quantify the significant parameters related to it. That is, to date, we do not have strong-motion response data from instrumented structures complete enough to carry out detailed studies of the methods and procedures used in soil-structure interaction analyses, and, in turn, assess their impact on design codes and related analysis procedures. Examples of deficiencies in existing instrumented building systems are as follows:

(a) The strong-motion instrumented structures do not have pressure transducers and accelerometers around the periphery of the foundation system (1) to check the horizontal and vertical dynamic pressures and the variation of the forces, and (2) to quantify rocking and uplifting during strong-motion events.

(b) There are no downhole arrays below the foundation or in the vicinity of a building to carry out studies related to vertical spatial variation of motions to calibrate convolution and deconvolution processes and applications. (The only building with a tri-axial downhole instrument is in Norwalk, California. However, the downhole instrument is within a caisson (of a cluster of caissons) only 30 feet below the basement level. Recent data shows that its motion is same as the basement of the building; Çelebi, 1993a and b). The cluster of caissons has altered the soil condition by making it stiffer than it was. Therefore, the foundation and the caissons have very similar motions.

(c) There are no horizontal spatial arrays in the vicinity of a building to specifically study free-field motions and how these motions are altered by interaction with the foundation of a building structure. Specific question as to at what distance from a building the ground motion is unaffected by the interaction of a building has not yet been answered.

3. IDEAL SOIL-STRUCTURE INTERACTION EXPERIMENTAL SCHEME

An ideal layout of arrays that includes soil-structure interaction instrumentation is provided in Figures 1 and 2 (Çelebi et al, 1977; Çelebi and Joyner, 1978). Such a layout should have four main arrays:

1. Superstructure array
2. Soil-structure interaction array
3. Vertical Spatial array
4. Horizontal Spatial array.

These arrays are depicted schematically in both Figures 1 and 2.

4. LOTUNG AND HUALIEN EXPERIMENTS

The most detailed soil-structure interaction

(SSI) experiment to date was implemented in 1985 by EPRI at Lotung. The purpose of the Lotung experiment was to facilitate the study of SSI for a 1/4- and 1/12-scale, reinforced-concrete, cylindrically-shaped nuclear power plant containment models under strong ground motion earthquakes (EPRI, 1989; Tang , 1987 and Tang *et al*, 1987a, b 1990). The Lotung experiments provided insight into the SSI response of a very stiff structure (fixed-based frequency on the order of 7--10 Hz and SSI frequency of 2.7 Hz) on an extremely soft soil condition (shear wave velocity of the top layer between 300--1000 ft./sec. (100-330 m/s). The results of the Lotung experiment showed that the response of the structure was mainly in the rocking mode (rigid-body rotation) and that the SSI effect in structural deformation and seismic wave spatial variation under stiffer soil conditions were not addressed. To remedy those shortcomings, another experiment at a stiffer soil site, Hualien, has been implemented (Tang et al, 1991). The shear wave velocity of the top layer at this site is approximately 1200 ft./sec. (~400 m/s). Some of the lessons learned from the Lotung experiment and from the instrumentation schemes of both the Lotung and Hualien arrays can be used in the study of soil-structure interaction for regular building structures. However, the natural frequencies of the containment structures of both the Lotung and Hualien experiments are much higher than those of regular buildings, the subject of the SSI experiment discussed herein.

5. RECOMMENDATIONS OF THE 1992 WORKSHOP

5.1 Recommendation 1: (Needs and Motivation)

A field experiment should be implemented to observe the structural behavior of and the soil-structure interaction (SSI) effects for a typical (and regular) building (hereinafter referred to as typical building) during strong-motion earthquakes. This principal recommendation is motivated by the fact that there is still great uncertainty as to the significance of seismic soil-structure interaction (SSI) for typical structures. There may be both beneficial and adverse effects of soil-structure interaction. However, in many cases, SSI is simply ignored in design without establishing whether it will increase or decrease the response of the structure. The additional detailed recommendations to follow provide guidelines for the design of an experiment, which, if activated by a strong earthquake, will remove some of the above uncertainties.

It is necessary to consider what is currently known about SSI effects and what can realistically be observed and analyzed by current methods. For example, it is known that a major manifestation of SSI is a contribution to the rocking motion of the structure and perhaps to local deformations of the foundation of the structure. Thus, the instrumentation should be designed to observe these effects. Observations which can be checked against the results of numerical calculations are much more valuable than observations for which such comparisons cannot be made. Thus, the building, its foundation system, and the site configuration should be relatively simple --- thus the need for a typical and regular building.

The motivations for an SSI experiment can be itemized as:

(a) To improve the state-of-the-art of formulations and procedures for the evaluation of SSI effects.

(b) To provide a clear and useful guidance as to when SSI should be incorporated in the

analysis of a building, and, when necessary, how it should be done.

(c) To check the accuracy of numerical prediction of SSI and, in particular, of the rocking of the foundation since there is not yet great confidence in specific numerical predictions of the amount of rocking -- a major contributor to SSI.

5.2 Recommendation 2: (Site Location and Soil Conditions)

The test site should be located in an area with relatively high seismicity, and should be easily accessible for installation and maintenance of the instrumentation.

The following areas are identified by the USGS as having the highest earthquake probabilities (WGCEP, 1988, 1990):

(i) The San Francisco Bay Area [Faults: San Andreas, Hayward and Rogers Creek],

(ii) Southern California (Upland, Redlands, San Bernardino) [Faults: San Jacinto and San Andreas].

In order for the SSI effects to be significant the test site should be a soil site rather than a rock site. Also, the geometry and ground water conditions of the site should be relatively simple such that the incident wave field can be well-defined and analyzed. This leads to the following recommendations:

(a) The site should not be too shallow. Rock should be located at an appreciable depth (*e.g.* more than 50 feet below the foundation level of the candidate structure).

(b) A firm alluvial site is preferable. Such a site would consist of sands and gravels with shear-wave velocities V_s in the range of 500--1000 fps (~150--300 m/s) within the upper 50 feet of the site.

(c) The site should be level and essentially horizontally layered. This is a critical requirement if observations are to be compared with analytical results.

(d) The site should not be liquefiable and should have a stable ground water level.

(e) A detailed site investigation should be performed before the site is selected. The investigation should include several borings to establish stratigraphy, { in situ} shear-wave velocity measurements, laboratory tests on undisturbed samples and ground water observations.

(f) Permanent open space around the building must be ensured for long-term observation of free-field motions. This requirement is a ``must" and the chances of it being satisfied are probably highest if a public building is chosen for the experiment.

5.3 Recommendation 3: (Foundation)

The foundation system of the candidate structure should be as simple as possible and should not inherently minimize SSI effects. Thus:

(a) The preferred foundation type is a stiff box or mat foundation. The contact surface with the underlying soil should be approximately plane.

(b) A 1- or 2-story basement is acceptable. However, the foundation system should not be fully compensated since this will tend to minimize the inertial SSI effects, one of the effects that is desirable to observe. (A fully compensated foundation system is one for which the weight of the displaced soil is equal to the weight of the entire structure including the basement).

(c) The initial experiment should exclude pile supported structures.

5.4 Recommendation 4: (Superstructure)

It is preferable that a new building (before construction starts) can be identified for instrumentation as part of the SSI experiment rather than using an existing building. It is further recommended that the building (to be instrumented for an SSI experiment) have the following general characteristics:

(a) The geometry and load-carrying system of the structure should be as simple and regular as possible. A building which is symmetric about two axes is preferable. The design of the building should fall within the scope of current seismic design codes. It should also be amenable to accurate analysis.

(b) It is desirable that the structure have different stiffnesses in its two principal directions. However, the aspect ratio of its plan dimensions should not exceed 3 to 1 (preferably 2 to 1). Furthermore, to insure that there is reasonable radiation damping, the building should not be too slender. On the other hand, The in-plan dimensions of the building should not be large to cause horizontal wave length interactions.

(c) The structure should not be too light, since this would minimize SSI effects. A reinforced concrete structure or a steel structure with concrete walls is preferable.

(d) The fixed-base natural period of the superstructure should be of the order 0.5 seconds. This corresponds to a 5- to 10-story building, depending on the building type.

(e) If at all possible, a new, yet-to-be-constructed, building should be chosen. With access to the structure during construction, the load-carrying system of the structure can be clearly defined and instrumentation can be more easily installed. This is especially important if pressure cells or other instruments are to be installed on the external basement walls or in the backfill.

5.5 Recommendation 5: (Instrumentation)

Several types of instrumentation should be employed to record forces, motions and local deformations in the structure and the surrounding soil.

5.5.1. Superstructure Instrumentation:

The main instrumentation in the superstructure should be digital accelerometers with a common time base. Enough instruments should be installed to determine the translational, torsional and rocking motions at least at three levels of the structure, including the base level and the top floor. The exact location of the instruments should be determined only after extensive analytical response studies and ambient and forced vibration tests of the structure. Additional sensors should be installed within the structure to measure story drifts and slab deformations at several levels.

5.5.2. Foundation Instrumentation:

In addition to accelerometers, other sensors (linear variable displacement transducers [LVDT] or other instruments) should be installed to record local deformations of the foundation system. This is especially important if the foundation mat is flexible or if shear walls are founded on independent foundations. It is also desirable to be able to record dynamic contact pressures on basement walls and the foundation slab. Unfortunately, currently available pressure cells are not reliable for observations that extend over several years. Also, they are virtually impossible to install in an existing

backfill. Direct recording of contact pressures may therefore not be practical. It may, however, be possible, and it is certainly desirable, to install rugged instruments that can record wall/soil separation or foundation uplift.

5.5.3. Free-field Instrumentation:

A minimum of three boreholes should be instrumented to record free-field motions. The boreholes should surround the instrumented building and should be located far enough away from all existing and planned structures to ensure that the records obtained are not contaminated by SSI effects. However, the boreholes should not be so far away from each other that incoherency effects destroy the coherency between the motions observed in the different boreholes. At least three triaxial accelerometers should be installed in each borehole: at the surface, at mid-depth, and at a depth deeper than the foundation level of the candidate building. If the bedrock is within a depth of 300 feet (~100 m) an additional instrument should be installed at the soil/rock interface in each boring.

The surface instruments in the three borehole sets will double as a surface array. However, it is recommended that additional surficial instruments be deployed closer to the building to detect any changes in motion due to SSI and/or due to the presence of the backfill.

6. CURRENT STATUS

6.1 Selection of Hardware

In selecting hardware, priority was given to those that will be deployed below and in the periphery of the foundation and basement. These are:

(a) Downhole accelerometers: Triaxial downhole accelerometers have been selected and purchased. The intent is to deploy these immediately below the foundation of the building at least at two but preferably at three vertical locations. In addition, at a distance away from the building, another downhole array containing 2-3 downhole accelerograps will be deployed.

(b) Pressure Transducer Systems: In selecting pressure transducer system, consultations with technical staff of USGS and other institutions led to the concept of combinations of flatjack and differential pressure transducer system (Kilgore, Johnston and Warrick, personal communication, 1996). Figure 3 depicts a conceptual schematic of the deployment of the flatjack and the differential pressure transducer combination system. Several flatjacks will be buried between sand layers below the foundation system and outside of the side walls. Each flatjack will be connected to a valve inside the building. The connection will lead from the valve to a differential pressure transducer (DPT) and a dummy flatjack. Thus differential variation of the pressure below the foundation and on the side walls of the building will be realized. With the use of flatjacks, it will be possible to record the average differential pressure over a larger area than the usually smaller area that pressure transducer covers.

(c) Structural Array Hardware: Currently, we plan to deploy only accelerometers throughout the superstructure. However, laser technology allows deployment of displacement transducers although, at present, these are very costly to acquire and deploy.

(d) Recording Systems: We intend to use a

standard digital recording systems that works on ±2.5 volt signal. The DPT, accelerometers and downhole accelerographs work with this signal.

6.2 Selection of Site

We are in contact with the officials of City and County of San Bernardino. These officials will assist us in identifying a project that is on the drawing table and meets our requisite parameters. We expect this to occur within the next 12 months.

7. MANAGEMENT AND OTHER BENEFITS OF THE EXPERIMENT

When implemented, the experiment will be managed and maintained by the USGS National Strong Motion Program (NSMP). The data acquired through the experiment will be open to all investigators. It is anticipated that the data will be used as key research material related to soil-structure interaction methods. Future workshops may be held to discuss the data and related researches.

8. CONCLUSIONS

This paper present requisite parameters for a soil-structure-interaction experiment. The parameters were established during a 1992 workshop. Current status of the project is described.

9. ACKNOWLEDGMENTS

This paper is based on input from the participants of the 1992 workshop (USGS – Open File Report No. 92-295 [Çelebi, Lysmer and Luco, 1992]). Guidance and advice provided by J. Lysmer, E. Luco and J. Roesset and others are appreciated. In designing the pressure transducers systems, B. Kilgore, M. Johnston and R. Warrick, all of USGS, provided valuable input. Finally, the author thanks the officials of County ansd City of San Bernardino for their willingness to assist in developing the experiment.

10. REFERENCES

Çelebi, M., Lysmer, J., and Luco, E., *(compilers)*, 1992, Recommendations for a Soil-Structure Interaction Experiment (Report based on a workshop held at San Francisco, Ca on February 7, 1992), USGS, OFR: 92--295, April 1992.

Çelebi, M., and Joyner, W., 1987, Instrumentation for spatially varying ground response integrated with structural response in a seismically active region, PROC., Joint IASPEI/IAEE Working Group on ``Effects of Surface Geology on Seismic Motion," IUGG XIX General Assembly, Vancouver, B.C., August 1987.

Çelebi, M., etal , 1987, Integrated instrumentation plan for assessing the seismic response of structures---a review of the current USGS program, USGS Circular 947.

Çelebi, M., 1993a, Seismic response of two adjacent buildings with downhole and free -field recordings (Part I: Data and Analysis), *Journal of Structural Division*, American Society of Civil Engineers, v. 119, no. 8, pp.2461-2476, August 1993.

Çelebi, M., 1993b, Seismic response of two adjacent buildings with downhole and free -field recordings (Part II: Interaction), *Journal of Structural Division*, American Society of Civil Engineers.v. 119, no. 8, pp. 2477-2492, August 1993.

EPRI, 1989, Proceedings: EPRI/NRC/TPC Workshop on Seismic Soil-Structure Interaction Analysis Techniques Using Data

from Lotung, Taiwan, Volumes 1 and 2, EPRI NP--6154.

Higgins, C. J., 1992 (editor), PROC. NSF Workshop---Experimental Needs for Geotechnical Earthquake Engineering, Albuquerque, New Mexico, November 4--5, 1991 (in preparation).

Iwan, W. D., ed., 1978, Proceedings of the International Workshop on Strong Motion Instrument Arrays, May 1978, Honolulu, Hawaii.

Iwan, W. D., ed., 1981, Proceedings of the U.S. National Workshop on Strong-Motion Earthquake Instrumentation, April 1981, Santa Barbara, California.

Lee, K. L., W. F. Marcuson, K. H. Stokoe, and F. Y. Yokel, editors, 1978, Research needs and priorities for geotechnical earthquake engineering applications, Workshop at the University of Texas, Austin, June 1978.

Page, R., Boore, D. M., Bucknam, R. C., and Thatcher, W. R., 1992, Goals, Options, and Priorities for the USGS Earthquake Hazards Reduction Program: 1991--1995, USGS Circular 1079, February 1992.

Tang, H. T., 1987, Large-scale soil-structure interaction, EPRI NP--5513--SR.

Tang, H. T., etal , 1987a, A large-scale soil structure interaction experiment: Part I--Design and construction, SMIRT 9, Vol. K2, 177--182.

Tang, Y. K., etal , 1987b, A large-scale soil-structure interaction experiment: Part II--EPRI/NRC Research Program on Method Validation, SMIRT 9, Vol. K2, 183--188.

Tang, H. T., etal , 1990, Lotung large-scale seismic experiment and soil-structure interaction method validation, Nuclear Engineering and Design, 123, 397--412.

Tang, Y. K., etal , 1991, The Hualien large-scale seismic test for soil-structure interaction research, SMIRT 11, Transactions, Vol. K, August 1991, 69--74.

WGCEP (Working Group on California Earthquake Probabilities), 1990, Probabilities of Large Earthquakes in the San Francisco Bay Region, California, U.S. Geological Survey Circular 1053.

WGCEP (Working Group on California Earthquake Probabilities), 1988, Probabilities of Large Earthquakes Occurring in California on the San Andreas Fault, USGS OFR: 88--398.

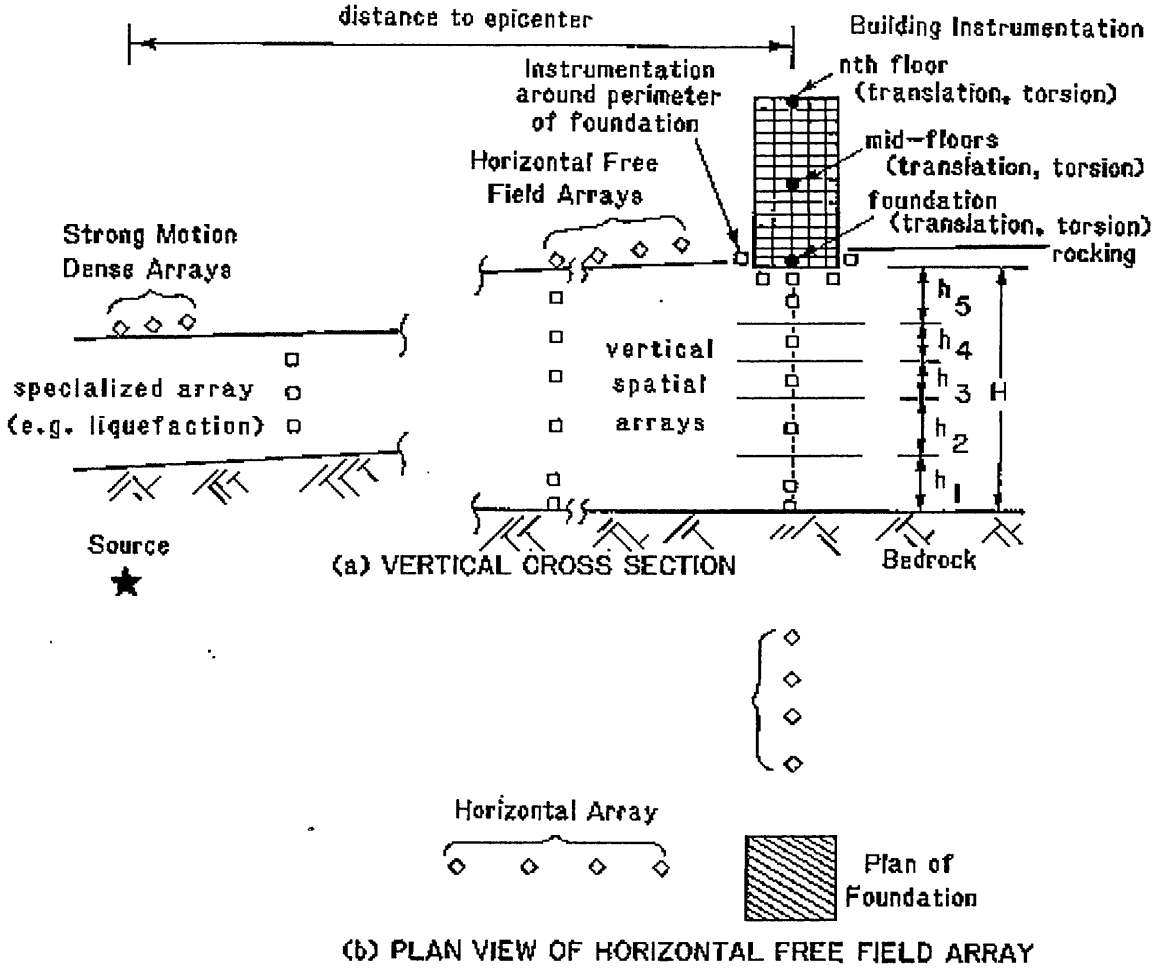

Figure 1. General Description of an Integrated Soil-Structure Interaction Experiment

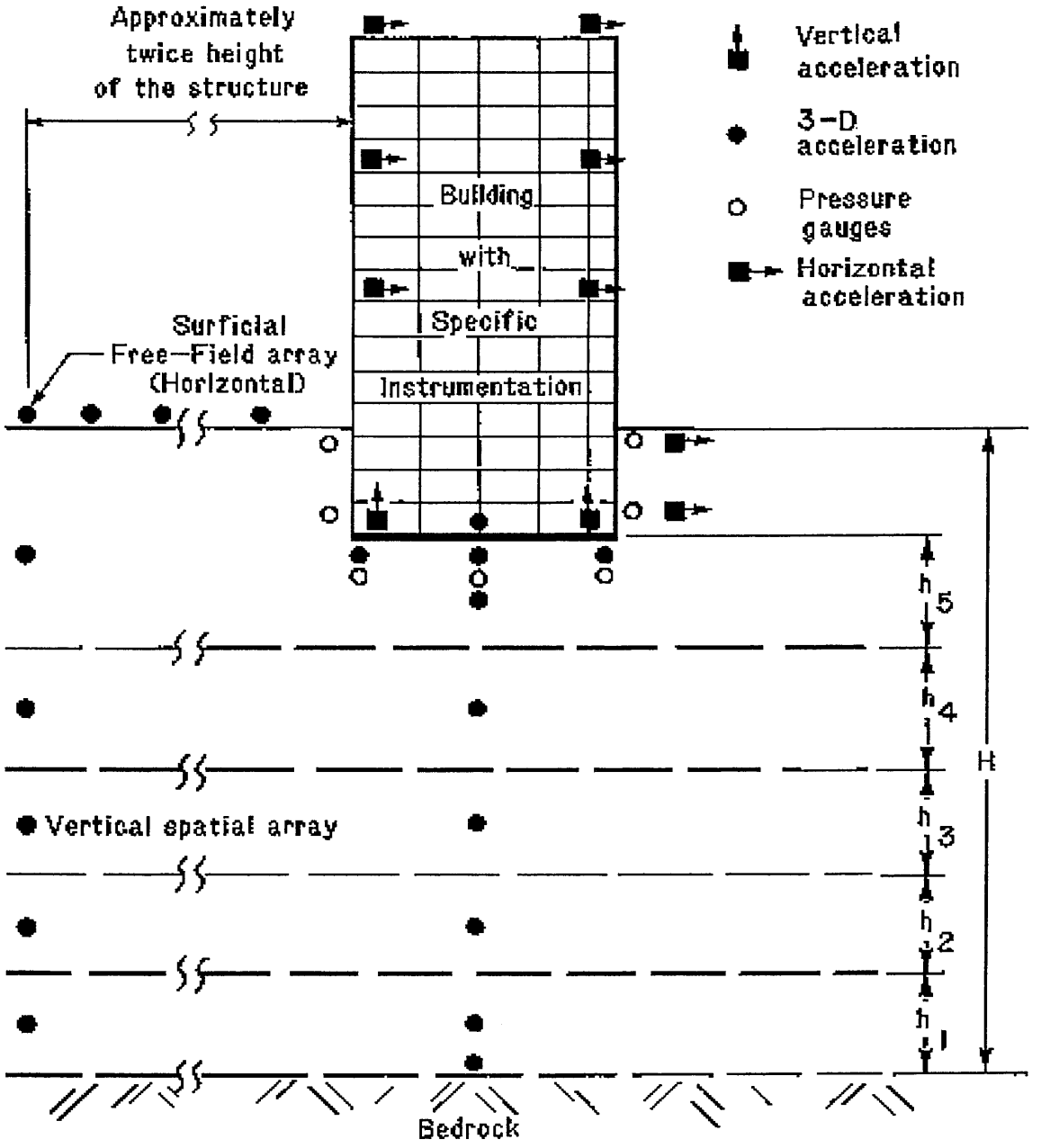

Figure 2. Details of Instrumentation in the Vicinity of the Building, Below and Around the Foundation of Soil-Structure Interaction Experiment

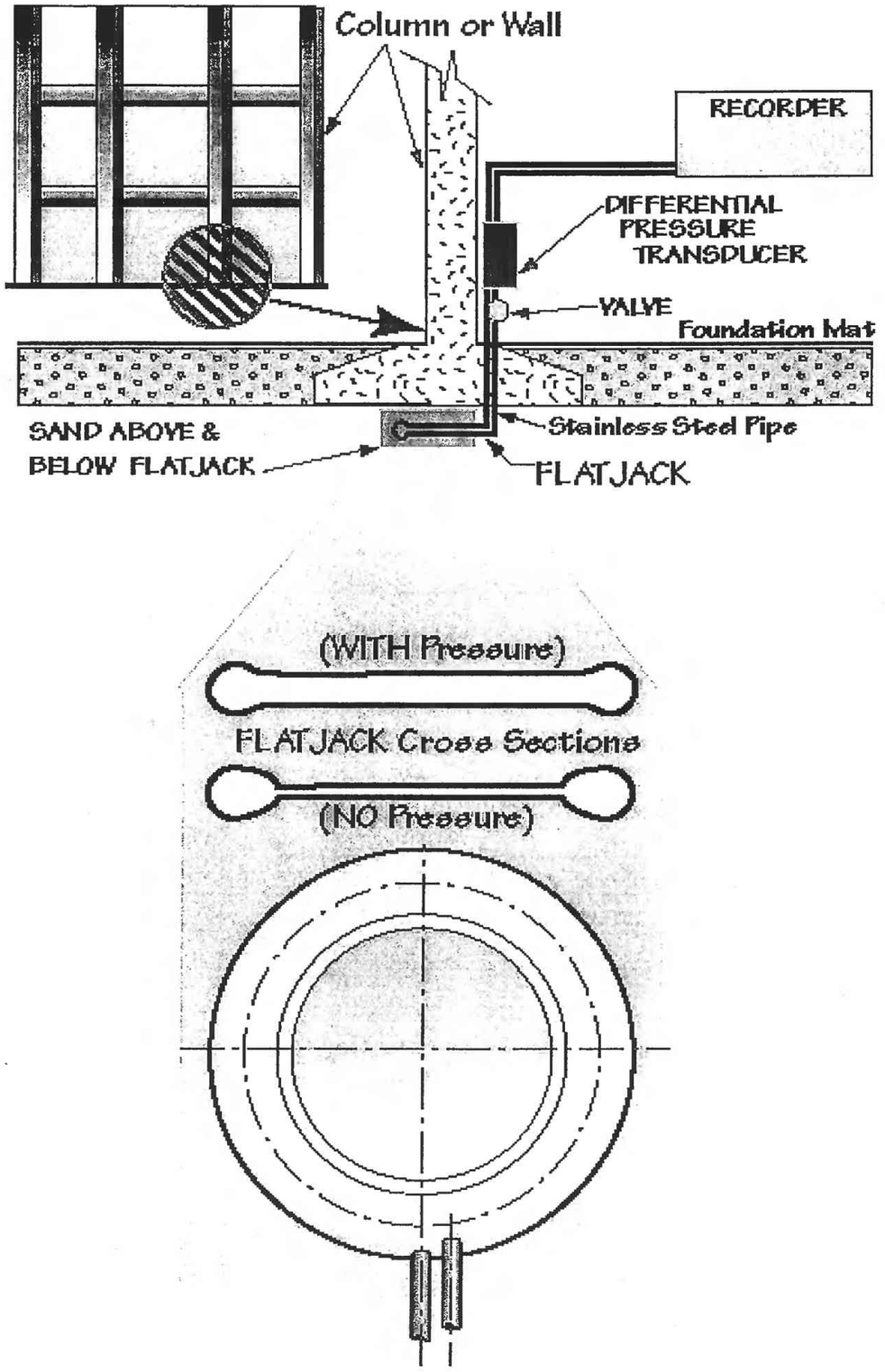

Figure 3. Flatjack and Differential Pressure Transducer Configuration around the Foundation of the Building

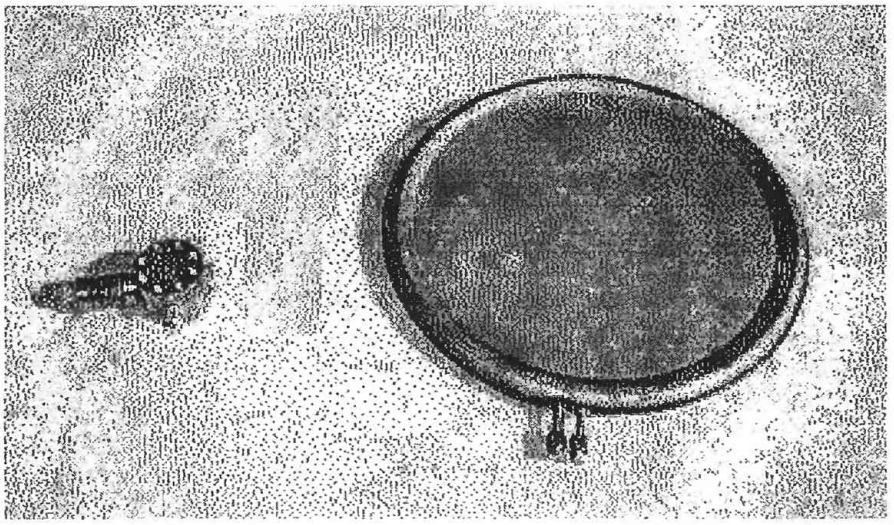

Figure 4. Actual Flatjack (50 cm in diameter) and Differential Pressure Transducer

EQUIVALENT 1-DOF MODEL FOR STRUCTURAL CONTROL INCLUDING SOIL-STRUCTURE INTERACTION EFFECTS

J. Enrique Luco

Department of Applied Mechanics and Engineering Sciences
University of California, San Diego, La Jolla, California 92093-0411.

ABSTRACT

A simple model for the seismic response of a one-storey structure subjected to active control in the presence of soil-structure interaction effects is presented. The approach is based on the successive use of equivalent 1-DOF oscillators which account for the effects of control and soil-structure interaction. Simple expressions for these oscillators based on exact analytical solutions of the control equations and approximate solutions of the interaction equations are presented. The study includes an evaluation of the effects of soil-structure interaction on the seismic response of actively controlled structures in which the control gains have been determined with and without inclusion of soil-structure interaction effects. A simple procedure to include the interaction effects on the control gains is also presented.

INTRODUCTION

In the last few years there has been increased interest in the study of the effects of soil-structure interaction (SSI) on the response of structures subjected to active control [Wong and Luco (1990, 1991, 1992), Sato et al (1991), Sato and Toki (1992), Alam and Baba (1991, 1993), Smith et al (1994), Wu and Smith (1995)]. These studies follow two lines of inquiry: the first line is concerned with the evaluation of the effects of soil-structure interaction on the response of structures with active control systems designed on the basis of conventional analyses which do not include the interaction effects; the second line considers the incorporation of the soil-structure interaction effects into the design of the control system and algorithms. These two issues were discussed by Wong and Luco (1991, 1992) for a structural model consisting of a shear beam supported on a rigid foundation embedded in a viscoelastic half-space. Control, in this case, was achived by an absorbing boundary located at the top of the building. Recently, Smith et al (1994) and Wu and Smith (1995) have considered the effects of SSI on the response of a one-storey actively-controlled structure supported on a rigid rectangular foundation resting on an elastic half-space. The analysis was based on the use of external control forces obtained by application of the linear optimal control theory to equations of motion which excluded or included the SSI effects.

Here, we reconsider the problem studied by Smith et al (1994) of the effects of SSI on the response of a one-storey structure subjected to active control. The approach differs from that of the previous authors in that elementary methods are used to derive equivalent oscillators which exactly account for the effects of control and approximately account for the effects of soil-structure interaction. By combination of these solutions it is possible to obtain simple expressions for the seismic response of the one-storey structure including the effects of control and SSI.

We start by summarizing approximate solutions of the interaction equations for a one-storey structure supported on a rigid surface foundation resting on a viscoelastic half-space when subjected to seismic excitation and to external and internal forces. The solution for seismic

excitation was initially presented by Bielak (1971) and Jennings and Bielak (1973) while that for external forces was presented by Luco et al (1986, 1987). The well known result of these approximate solutions is that the deformation of the one-storey structure including SSI effects can be calculated from the response of an equivalent or replacement oscillator supported on a rigid soil and characterized by a modified natural frequency and damping ratio. The equivalent oscillator is subjected to an effective ground acceleration and to an effective force at the top of the structure. The extension of the approximate solution to internal forces (or, more precisely, to internally reacted forces) reveals that the effective force acting on the equivalent oscillator depends on whether the actual forces correspond to internal or external forces. If the forces are internal (such as those on a diagonal tendon system) then they affect the equation controlling the deformation of the superstructure but do not appear in the global equations of motion of the structure-foundation system. On the other hand, external forces appear in the equation reflecting the deformation of the superstructure and in the global equations of motion for the system.

As a second preliminary step we consider the response of a damped 1-DOF system subjected to active control in the absence of SSI effects. In particular, we consider the optimal control of the free-vibration response of the oscillator for a quadratic performance index. An analytical solution for the control gains is obtained by elementary means which do not require consideration of Riccati's equation. In the particular case of an undamped oscillator, the resulting gains coincide with those obtained by Meirovitch and Öz (1980) and Meirovitch and Baruh (1982) by analytical solution of Riccati's steady-state equation. Clearly, the response of the oscillator including the effects of control can be assimilated to that of an equivalent (uncontrolled) oscillator with a modified natural frequency and damping. Simple expressions for the frequency and damping ratio of the equivalent oscillator are presented.

In a third stage we consider the seismic response of a one-storey structure supported on a flexible soil and subjected to active control by internal control forces with gains determined without inclusion of SSI effects. The solution starts by replacing the one-storey superstructure by a modified structure which exactly incorporates the effects of control. The modified one-storey

structure is then subjected to the seismic excitation in the presence of soil-structure interaction effects and an approximate solution to the interaction equations is obtained on the basis of an equivalent 1-DOF oscillator which includes both the effects of SSI and control.

Finally, a simple procedure to include the effects of soil-structure interaction on the determination of the control gains is presented. The procedure relies on representing the uncontrolled structure including SSI effects by an equivalent 1-DOF structure on a rigid soil. The optimal control gains for this equivalent structure are then obtained analytically. The original superstructure is then represented by an equivalent one-storey structure which includes the effects of control and the response of this modified structure to seismic excitation in the presence of SSI effects is obtained by the approximate solution summarized in the first part of the study.

EQUIVALENT OSCILLATOR FOR SOIL-STRUCTURE INTERACTION EFFECTS

In here we summarize an approximate solution for the response of a structure subjected to internal and external forces and to seismic excitation when the effects of soil-structure interaction are included in the analysis. The case of seismic excitation was considered by Bielak (1971) and Jennings and Bielak (1973) while the case of an external force at the top of the structure was considered by Luco et al (1986, 1987).

We consider the in-plane vibrations of an elastic one-storey structure supported on a flat rigid foundation resting on an elastic half-space. The structure is characterized by its mass m_1, stiffness k_1, damping constant c_1 and height h_1. The foundation is characterized by its mass m_o and by its equivalent radius a. The underlying elastic half-space is determined by the density ρ, the shear-wave velocity β, the hysteretic damping ratio ξ_s and Poisson's ratio ν. The system is subjected to a vertically-incident plane SH-wave with total particle motion u_g on the ground surface in absence of the structure, *i.e.* for free-field conditions. With respect to forces acting on the structure we consider two cases. In the first case, a horizontal external force F_1 is applied at the top of the structure. In a second case, internal horizontal forces F_1 and $F_o = -F_1$ are applied at the top and base of the structure together with an internal moment $M_o = -F_1 h_1$ acting on the foundation. This self-balancing set of forces and moments may represent the case of an internal control system such as a tendon system.

The global equations of motion for the structure-foundation system and the equation of motion for the top mass for harmonic excitation with time dependence $e^{i\omega t}$ are

$$m_o\ddot{u}_o + m_1(\ddot{u}_o + h_1\ddot{\theta}_o + \ddot{u}_1) + K_H u_o = F_R - (m_1 + m_o)\ddot{u}_g \tag{1}$$

$$I_o\ddot{\theta}_o + h_1 m_1(\ddot{u}_o + h_1\ddot{\theta}_o + \ddot{u}_1) + K_R\theta_o = M_R - h_1 m_1\ddot{u}_g \tag{2}$$

$$m_1(\ddot{u}_o + h_1\ddot{\theta}_o + \ddot{u}_1) + c_1\dot{u}_1 + k_1 u_1 = F_1 - m_1\ddot{u}_g \tag{3}$$

in which u_o is the horizontal displacement of the foundation relative to the free-field ground motion, θ_o is the rocking rotation of the foundation and u_1 is the deformation of the structure. The terms K_H and K_R represent the frequency-dependent horizontal and rocking (complex) impedance fuctions for the foundation and I_o is the sum of the moments of inertia of the foundation and the top mass with respect to horizontal axes through their centroids. The terms F_R and M_R correspond to the resultant force and the resultant moment (with respect to the base) of all external forces (other than soil reactions) acting on the structure-foundation system. If only an external force F_1 acts at the top of the structure, then $F_R = F_1$ and $M_R = F_1 h_1$. For a system of self-equilibrating internal forces and moments, $F_R = F_1 + F_o = 0$ and $M_R = F_1 h_1 + M_o = 0$. In Eqs. (1) and (2) the effects of the coupling impedances $K_{HR} = K_{RH}$ have been neglected.

At this point, we introduce the notation

$$k_1 = \omega_1^2 m_1 \tag{4a}$$

$$c_1 = 2\omega_1 m_1 \xi_1 \tag{4b}$$

$$K_H = m_1 \omega_H^2 \{1 + 2i[\xi_s + (\omega/\omega_H)\xi_H]\} \tag{5a}$$

$$K_R = h_1^2 m_1 \omega_R^2 \{1 + 2i[\xi_s + (\omega/\omega_R)\xi_R]\} \tag{5b}$$

where

$$\omega_1 = \sqrt{k_1/m_1} \tag{6a}$$

$$\xi_1 = \frac{c_1}{2m_1\omega_1} \tag{6b}$$

$$\omega_H = \sqrt{\frac{\mathrm{Re}\, K_H}{m_1}} \tag{7a}$$

$$\xi_H = \frac{1}{2}\left(\frac{\omega_H}{\omega}\right)\left[\left(\frac{\mathrm{Im}\, K_H}{\mathrm{Re}\, K_H}\right) - 2\xi_s\right] \tag{7b}$$

$$\omega_R = \sqrt{\frac{\mathrm{Re}\, K_R}{m_1 h_1^2}} \tag{8a}$$

$$\xi_R = \frac{1}{2}\left(\frac{\omega_R}{\omega}\right)\left[\left(\frac{\mathrm{Im}\, K_R}{\mathrm{Re}\, K_R}\right) - 2\xi_s\right] \quad . \tag{8b}$$

The terms ω_1 and ξ_1 correspond to the fixed-base natural frequency and the fixed-base damping ratio for the structure, respectively. The frequencies ω_H and ω_R correspond to the characteristic frequencies for horizontal and rocking vibrations of a rigid structure on the flexible soil. The damping ratios ξ_H and ξ_R reflect radiation damping in horizontal and rocking vibrations. The hysteretic material damping in the soil is represented by the terms containing ξ_s in Eqs. (5a) and (5b).

By use of Eqs. (4) and (5), the equations of motion for the complete system can be rewritten in the symmetric form

$$[D(\omega)] \begin{Bmatrix} (\omega_H/\omega_1)u_o \\ (\omega_R/\omega_1)h_1\theta_o \\ u_1 \end{Bmatrix} = \begin{Bmatrix} [\epsilon F_1/m_1 + \omega^2 u_g]/\omega_1\omega_H \\ [\epsilon F_1/m_1 + \omega^2 u_g]/\omega_1\omega_R \\ [F_1/m_1 + \omega^2 u_g]/\omega_1^2 \end{Bmatrix} \tag{9}$$

where $\epsilon = 1$ for the case of an external force F_1 acting at the top of the structure. In the case of a self-equilibrating system of internal forces $\epsilon = 0$. The elements of the matrix $[D(\omega)]$ are given by

$$D_{11} = \left\{1 - \left(\frac{\omega}{\omega_H}\right)^2 + 2i\left[\xi_s + \left(\frac{\omega}{\omega_H}\right)\xi_H\right]\right\} \tag{10a}$$

$$D_{22} = \left\{1 - \left(\frac{\omega}{\omega_R}\right)^2 + 2i\left[\xi_s + \left(\frac{\omega}{\omega_R}\right)\xi_R\right]\right\} \tag{10b}$$

$$D_{33} = \left[1 - \left(\frac{\omega}{\omega_1}\right)^2 + 2i\left(\frac{\omega}{\omega_1}\right)\xi_1\right] \tag{10c}$$

$$D_{12} = D_{21} = -\left(\frac{\omega}{\omega_H}\right)\left(\frac{\omega}{\omega_R}\right) \tag{10d}$$

$$D_{13} = D_{31} = -\left(\frac{\omega}{\omega_H}\right)\left(\frac{\omega}{\omega_1}\right) \tag{10e}$$

$$D_{23} = D_{32} = -\left(\frac{\omega}{\omega_R}\right)\left(\frac{\omega}{\omega_1}\right) \quad . \tag{10f}$$

In writting Eq. (9), the terms m_o and I_o have been ignored when compared with m_1 and $m_1 h_1^2$, respectively.

The solution for the case of a rigid soil (*i.e.* in the absence of soil-structure interaction) can be obtained by considering the limiting case $\omega_H \to \infty$ and $\omega_R \to \infty$. In this case,

$$u_o = \theta_o = 0 \tag{11a}$$

and

$$u_1 = \frac{(\omega/\omega_1)^2 u_g + F_1/(m_1\omega_1^2)}{1 - (\omega/\omega_1)^2 + 2i(\omega/\omega_1)\xi_s} \quad . \tag{11b}$$

An approximate solution of Eq. (9) for the case of an *external* force F_1 acting at the top of the structure ($\epsilon = 1$) can be obtained by neglecting certain terms involving ξ_1, ξ_H and ξ_R and assuming that the system frequency $\tilde{\omega}_1$ is close to ω_1, *i.e.* assuming that the soil-structure interaction effects are small. The resulting solution is given by

$$\begin{Bmatrix} u_o \\ h_1\theta_o \\ u_1 \end{Bmatrix} = \frac{\left(\frac{\omega}{\tilde{\omega}_1}\right)^2 u_g + \left(\frac{F_1}{m_1\tilde{\omega}_1^2}\right)}{1 - \left(\frac{\omega}{\tilde{\omega}_1}\right)^2 + 2i\left(\frac{\omega}{\tilde{\omega}_1}\right)\tilde{\xi}_1} \begin{Bmatrix} (\tilde{\omega}_1/\omega_H)^2 \\ (\tilde{\omega}_1/\omega_R)^2 \\ (\tilde{\omega}_1/\omega_1)^2 \end{Bmatrix} \tag{12}$$

where

$$\frac{1}{\tilde{\omega}_1^2} = \frac{1}{\omega_1^2} + \frac{1}{\omega_H^2} + \frac{1}{\omega_R^2} \tag{13}$$

and

$$\tilde{\xi}_1 = \left(\frac{\tilde{\omega}_1}{\omega_1}\right)^3 \xi_1 + \left[1 - \left(\frac{\tilde{\omega}_1}{\omega_1}\right)^2\right] \xi_s + \left(\frac{\tilde{\omega}_1}{\omega_H}\right)^3 \xi_H + \left(\frac{\tilde{\omega}_1}{\omega_R}\right)^3 \xi_R \quad . \tag{14}$$

Equations (13) and (14) give approximate expressions for the system frequency $\tilde{\omega}_1$ and for the system damping ratio $\tilde{\xi}_1$.

If we compare the form of the solution for the relative displacement u_1 in Eq. (12) with the solution for an oscillator on a rigid soil given by Eq. (11b), we observe that the relative displacement response for an oscillator on a flexible soil can be calculated from the response of an equivalent oscillator on a rigid soil with frequency $\tilde{\omega}_1$ and damping ratio $\tilde{\xi}_1$ subjected to the effective ground motion $\tilde{u}_g$ and to the effective force at the top $\tilde{F}_1$ given, respectively, by

$$\tilde{u}_g = \left(\frac{\tilde{\omega}_1}{\omega_1}\right)^2 u_g \tag{15a}$$

and

$$\tilde{F}_1 = \left(\frac{\tilde{\omega}_1}{\omega_1}\right)^2 F_1 \quad . \tag{15b}$$

In the case of a system of *internal* forces (F_1 at the top, $F_o = -F_1$ at the base, and $M_o = -F_1 h_1$) the parameter $\epsilon = 0$ and the approximate solution is given by

$$\begin{Bmatrix} u_o \\ h_1\theta_o \\ u_1 \end{Bmatrix} = \frac{\left(\frac{\omega}{\tilde{\omega}_1}\right)^2 u_g + \left(\frac{\tilde{\omega}_1}{\omega_1}\right)^2 \left(\frac{F_1}{m_1 \tilde{\omega}_1^2}\right)}{1 - \left(\frac{\omega}{\tilde{\omega}_1}\right)^2 + 2i\left(\frac{\omega}{\tilde{\omega}_1}\right)\tilde{\xi}_1} \begin{Bmatrix} (\tilde{\omega}_1/\omega_H)^2 \\ (\tilde{\omega}_1/\omega_R)^2 \\ (\tilde{\omega}_1/\omega_1)^2 \end{Bmatrix} \tag{16}$$

in which $\tilde{\omega}_1$ and $\tilde{\xi}_1$ are also given by Eqs. (13) and (14). In this case of internal forces ($\epsilon = 0$), the equivalent oscillator on a rigid soil is subjected to the effective ground motion $\tilde{u}_g$ and to the effective force at the top $\tilde{F}_1$ given, respectively, by

$$\tilde{u}_g = \left(\frac{\tilde{\omega}_1}{\omega_1}\right)^2 u_g \tag{17a}$$

and

$$\tilde{F}_1 = \left(\frac{\tilde{\omega}_1}{\omega_1}\right)^4 F_1 \quad . \tag{17b}$$

It must be noted that the equivalent force at the top $\tilde{F}_1$ given by Eq. (17b) differs from that given by Eq. (15b).

For later use, we note that the impedance functions K_H and K_R are usually normalized in the form

$$K_H = \rho\beta^2 a(k_H + ia_o c_H) \tag{18a}$$

$$K_R = \rho\beta^2 a^3(k_R + ia_o c_R) \tag{18b}$$

where a is the equivalent radius of the foundation, $a_o = \omega a/\beta$ is a dimensionless frequency, k_H and k_R are the normalized horizontal and rocking stiffness coefficients, and c_H and c_R are the normalized horizontal and rocking damping coefficients. In general, the coefficients k_H, c_H, k_R and c_R depend on a_o, the soil damping ratio ξ_s and Poisson's ratio ν, To determine $\tilde{\omega}_1$ and $\tilde{\xi}_1$ by use of Eqs. (13) and (14) these coefficients should be calculated at $\tilde{a}_o = \tilde{\omega}_1 a/\beta$ and, consequently, an iterative process is required to determine $\tilde{\omega}_1$.

Substitution from Eqs. (16) into Eqs. (7) and (8) leads to

$$\frac{\omega_1}{\omega_H} = \left(\frac{\omega_1 a}{\beta}\right)\sqrt{\frac{(m_1/\rho a^3)}{k_H}} \tag{19a}$$

$$\xi_H = \frac{c_H - 2\xi_s k_H/a_o}{2\sqrt{(m_1/\rho a^3)k_H}} \tag{19b}$$

$$\frac{\omega_1}{\omega_R} = \left(\frac{\omega_1 a}{\beta}\right)\left(\frac{h_1}{a}\right)\sqrt{\frac{(m_1/\rho a^3)}{k_R}} \tag{20a}$$

$$\xi_H = \frac{c_R - 2\xi_s k_R/a_o}{2(h_1/a)\sqrt{(m_1/\rho a^3)k_R}} \quad . \tag{20b}$$

where $(m_1/\rho a^3)$ is the mass ratio and h_1/a is the slenderness ratio.

The variations of the system frequency $\tilde{\omega}_1$ normalized by the fixed-base frequency ω_1 and of the system damping ratio $\tilde{\xi}_1$ as a function of the relative stiffness parameter $a_1 = \omega_1 a/\beta$

are shown in Fig. 2 for two values of the slenderness parameter h_1/a. The results are based on a structure with a mass ratio $m_1/\rho a^3 = 1.0$ and with a fixed-base damping ratio $\xi_1 = 0.02$. The circular foundation of radius a rests on a viscoelastic half-space characterized by the shear-wave velocity β, Poisson's ratio $\nu = 1/3$ and material damping ratio $\xi_s = 0.02$ (it was assumed that the damping ratios for P- and S-waves were equal to ξ_s). The impedance functions for a circular foundation resting on an elastic half-space presented by Luco and Mita (1987) were used in the analysis after modification to account for the effects of material damping.

The information in Fig. 2 reflects the well known results that the system frequency is reduced and the system damping is generally increased as the soil becomes softer, *i.e.* as a_1 increases. The reduction of the system frequency is larger for the more slender structure while the increase in the system damping is smaller. (Indeed, if $\xi_s = 0$, the system damping ratio $\tilde{\xi}_1$ may be smaller than ξ_1 if the structure is very slender).

OPTIMAL CONTROL OF A SINGLE-DEGREE-OF-FREEDOM OSCILLATOR

We consider the optimal control of the free vibrations of a single-degree-of-freedom oscillator characterized by the mass m_1, the frequency ω_1 and by the damping ratio ξ_1. The equation of motion of the oscillator subjected to the control force $F_1(t)$ is given by

$$\ddot{u}_1 + 2\xi_1\omega_1\dot{u}_1 + \omega_1^2 u_1 = F_1(t)/m_1 \tag{21}$$

with appropriate initial conditions on $u_1(0)$ and $\dot{u}_1(0)$. The control force is selected in such a way that the quadratic performance index J, defined as

$$J = \int_0^\infty \{\gamma_1\dot{u}_1^2 + \gamma_2\omega_1^2 u_1^2 + r[F_1(t)/m_1]^2\}\, dt \tag{22}$$

is minimized subject to the constraining Eq. (21). In Eq. (22), γ_1, γ_2 and r are weighting factors. In particular, if $\gamma_1 = \gamma_2$ then the first two terms in the integrand are proportional to the sum of the kinetic and strain energy of the oscillator. The factor r is a measure of the cost of the control force.

Next, we write the control force $F_1(t)$ in the form

$$F_1(t) = -m_1[\omega_1^2 g u_1 + \omega_1 h\dot{u}_1] \tag{23}$$

where g and h are the normalized gains. Substitution from Eq. (23) into the performance index leads to

$$J = (\gamma_1 + \beta h^2)\int_0^\infty \dot{u}_1^2\, dt + \omega_1^2(\gamma_2 + \beta g^2)\int_0^\infty u_1^2\, dt - \omega_1\beta g h u_1^2(0) \tag{24}$$

in which $\beta = r\omega_1^2$.

Also, substitution from Eq. (23) into Eq. (21) allows us to write the equation of motion for the controlled oscillator in the form

$$\ddot{u}_1 + 2\xi_{1c}\omega_{1c}\dot{u}_1 + \omega_{1c}^2 u_1 = 0 \tag{25}$$

which corresponds to the equation of motion for free-vibrations of an equivalent oscillator of mass $m_{1c} = m_1$, frequency

$$\omega_{1c} = \omega_1 \sqrt{1+g} \tag{26}$$

and damping ratio

$$\xi_{1c} = (2\xi_1 + h)/2\sqrt{1+g} \quad . \tag{27}$$

Multiplying Eq. (25) by $\dot{u}_1(t)$ and $u_1(t)$ and integrating leads to

$$\int_0^\infty \dot{u}_1^2 \, dt = \left[\dot{u}_1^2(0) + \omega_{1c}^2 u_1^2(0)\right] / (4\xi_{1c}\omega_{1c}) \tag{28}$$

and

$$\int_0^\infty u_1^2 \, dt = \left[\int_0^\infty \dot{u}_1^2 \, dt + u_1(0)\dot{u}_1(0) + \xi_{1c}\omega_{1c} u_1^2(0)\right] / \omega_{1c}^2 \tag{29}$$

which upon substitution into Eq. (24) results in the following expression for the performance index

$$\begin{aligned} \omega_1 J(g,h) = {} & \left[\frac{\gamma_1 + \beta h^2 + G(g)}{2(2\xi_1 + h)}\right] \left[\dot{u}_1^2(0) + \omega_1^2 u_1^2(0)\right] \\ & + G(g)\omega_1 u_1(0)\dot{u}_1(0) + \frac{1}{2} G(g)(2\xi_1 + h)\omega_1^2 u_1^2(0) \\ & + g\left[\frac{\gamma_1 + \beta h^2 + G(g)}{2(2\xi_1 + h)} - \beta h\right] \omega_1^2 u_1^2(0) \end{aligned} \tag{30}$$

where

$$G(g) = \frac{\gamma_2 + \beta g^2}{1+g} \quad . \tag{31}$$

The optimal values for the gains g and h which minimize $J(g,h)$ are then obtained by setting the partial derivatives $\partial J/\partial g$ and $\partial J/\partial h$ equal to zero. It is found that the optimal gains satisfy the conditions

$$\frac{dG}{dg} = \frac{2\beta g}{1+g} - \frac{\gamma_2 + \beta g^2}{(1+g)^2} = 0 \tag{32}$$

and

$$\frac{\gamma_1 + \beta h^2 + G(g)}{2(2\xi_1 + h)} - \beta h = 0 \quad . \tag{33}$$

The resulting optimal gains are given by

$$g = \sqrt{1 + \alpha\gamma_2} - 1 \tag{34}$$

$$h = \sqrt{4\xi_1^2 + \alpha\gamma_1 + 2\sqrt{1 + \alpha\gamma_2} - 2} - 2\xi_1 \tag{35}$$

where $\alpha = 1/\beta = 1/(\omega_1^2 r)$ is the control parameter (The uncontrolled case corresponds to $\alpha = 0$). For the special case of $\gamma_1 = \gamma_2 = 1$ and $\xi_1 = 0$ the present results coincide with those obtained by Meirovitch and Öz (1980) and Meirovitch and Baruh (1982) by a procedure involving the solution of a Riccati equation.

The value of the performance index for the optimal gains is given by

$$J = \left\{ h\dot{u}_1^2(0) + 2g\omega_1 u_1(0)\dot{u}_1(0) + [h + g(2\xi_1 + h)]\,\omega_1^2 u_1^2(0) \right\} / \alpha\omega_1 \tag{36}$$

which can be confirmed to be a positive definite form of $u_1(0)$ and $\dot{u}_1(0)$.

Finally, substitution from Eqs. (34) and (35) into Eqs. (26) and (27) leads to the following expressions for the frequency ω_{1c} and damping ratio ξ_{1c} of the equivalent oscillator

$$\omega_{1c} = \omega_1 (1 + \alpha\gamma_2)^{1/4} \tag{37}$$

$$\xi_{1c} = \left\{ \frac{\xi_1^2}{\sqrt{1 + \alpha\gamma_2}} + \frac{1}{2} \left[1 - \frac{(1 - \alpha\gamma_1/2)}{\sqrt{1 + \alpha\gamma_2}} \right] \right\}^{1/2} \quad . \tag{38}$$

Some of the characteristics of the equivalent oscillator defined by Eqs. (37) and (38) need to be stated here:

(i) in the uncontrolled case ($\alpha = 0$) $\omega_{1c} = \omega_1$ and $\xi_{1c} = \xi_1$,

(ii) the equivalent frequency ω_{1c} is independent of γ_1 – the weighting factor for the velocity $\dot{u}_1$,

(iii) if $\gamma_2 = 0$, *i.e.* if the displacement u_1 is not included in the performance index, then $\omega_{1c} = \omega_1$ and only the effective damping ratio changes to $\xi_{1c} = [\xi_1^2 + (\alpha\gamma_1/4)]^{1/2}$, and

(iv) if $\gamma_1 = 0$, *i.e.* if the velocity $\dot{u}_1$ does not appear in the performance index, then $\xi_{1c} \to 1/\sqrt{2}$ as $\alpha \to \infty$ (*i.e.* as the cost r of control tends to zero).

The variations of ω_{1c}/ω_1 and ξ_{1c} against the control parameter $\alpha = 1/(\omega_1^2 r)$ are shown in Fig. 3 for different values of the weighting factors γ_1 and γ_2. The results in Fig. 3b correspond to the case $\xi_1 = 0$. The controlled frequency ω_{1c} remains unchanged (for $\gamma_2 = 0$) or increases slightly with α while the equivalent damping ratio ξ_{1c} increases strongly with α. For example, for $\gamma_1 = \gamma_2 = 1.0$, $\xi_1 = 0$ and $\alpha = 2$, the frequency ω_{1c} increases to $1.32\omega_1$ while the damping ratio ξ_{1c} becomes equal to 0.707.

RESPONSE OF A CONTROLLED 1-DOF OSCILLATOR WITH GAINS DETERMINED WITHOUT SSI EFFECTS

In this section we consider the effects of soil-structure interaction on the seismic response of an actively-controlled structure in which the gains have been determined without consideration of the interaction effects. For this purpose we consider a one-storey structure characterized by the parameters m_1, ω_1, ξ_1 and h_1 and subjected to an *internal* control force $F_1(t)$ acting on the top mass. It is assumed that the control force is given by Eq. (23) with the control gains g and h determined by minimizing the performance index given by Eq. (22) for free-vibrations of the structure with the foundation kept fixed. The resulting gains are given by Eqs. (34) and (35).

When the effects of soil-structure interaction are included, the equation of motion for the top mass is given by Eq. (3) in which the control force F_1 is given by Eq. (23). The resulting equation of motion for harmonic vibrations can be written in the form

$$m_1(\ddot{u}_o + h_1\ddot{\theta}_o + \ddot{u}_1) + 2m_1\omega_{1c}\xi_{1c}\dot{u}_1 + m_1\omega_{1c}^2 u_1 = -m_1\ddot{u}_g \tag{39}$$

in which ω_{1c} and ξ_{1c} are the effective controlled frequency and damping ratio given by Eqs. (37) and (38), respectively.

The global equations of motion for the structure-foundation system are given by Eqs. (1) and (2) with $F_R = M_R = 0$ ($\epsilon = 0$) since the control forces in this case are internal forces. The system of interaction equations for u_o, θ_o and u_1 corresponds to

$$[D_c(\omega)] \begin{Bmatrix} (\omega_H/\omega_{1c})u_o \\ (\omega_R/\omega_{1c})h_1\theta_o \\ u_1 \end{Bmatrix} = \left(\frac{\omega}{\omega_{1c}}\right)^2 u_g \begin{Bmatrix} (\omega_{1c}/\omega_H) \\ (\omega_{1c}/\omega_R) \\ 1 \end{Bmatrix} \tag{40}$$

in which the matrix $[D_c(\omega)]$ is given by Eq. (10) after the substitutions $\omega_1 \rightarrow \omega_{1c}$ and $\xi_1 \rightarrow \xi_{1c}$.

The approximate solution to Eq. (40) is given by

$$\begin{Bmatrix} u_o \\ h_1\theta_o \\ u_1 \end{Bmatrix} = \frac{\left(\frac{\omega}{\tilde{\omega}_{1c}}\right)^2 u_g}{1-\left(\frac{\omega}{\tilde{\omega}_{1c}}\right)^2 + 2i\left(\frac{\omega}{\tilde{\omega}_{1c}}\right)\tilde{\xi}_{1c}} \begin{Bmatrix} (\tilde{\omega}_{1c}/\omega_H)^2 \\ (\tilde{\omega}_{1c}/\omega_R)^2 \\ (\tilde{\omega}_{1c}/\omega_{1c})^2 \end{Bmatrix} \tag{41}$$

where

$$\frac{1}{\tilde{\omega}_{1c}^2} = \frac{1}{\omega_{1c}^2} + \frac{1}{\omega_H^2} + \frac{1}{\omega_R^2} \tag{42}$$

and

$$\tilde{\xi}_{1c} = \left(\frac{\tilde{\omega}_{1c}}{\omega_{1c}}\right)^3 \xi_{1c} + \left[1-\left(\frac{\tilde{\omega}_{1c}}{\omega_{1c}}\right)^2\right]\xi_s + \left(\frac{\tilde{\omega}_{1c}}{\omega_H}\right)^3 \xi_H + \left(\frac{\tilde{\omega}_{1c}}{\omega_R}\right)^3 \xi_R \quad . \tag{43}$$

The peak amplitudes of the transfer functions u_o/u_g, $h_1\theta_o/u_g$ and u_1/u_g at $\omega = \tilde{\omega}_{1c}$ are given by

$$|u_o/u_g| = \frac{(\tilde{\omega}_{1c}/\omega_H)^2}{2\tilde{\xi}_{1c}} \tag{44a}$$

$$|h_1\theta_o/u_g| = \frac{(\tilde{\omega}_{1c}/\omega_R)^2}{2\tilde{\xi}_{1c}} \tag{44b}$$

$$|u_1/u_g| = \frac{(\tilde{\omega}_{1c}/\omega_{1c})^2}{2\tilde{\xi}_{1c}} \quad . \tag{44c}$$

The corresponding amplitude of the control force at $\omega = \tilde{\omega}_{1c}$ is given by

$$|F_1/\omega_1^2 m_1 u_g| = \sqrt{g^2 + \left(\frac{\tilde{\omega}_{1c}}{\omega_1}\right)^2 h^2}\left[\frac{(\tilde{\omega}_{1c}/\omega_{1c})^2}{2\tilde{\xi}_{1c}}\right] \quad . \tag{45}$$

To illustrate the effects of soil-structure interaction and control on the seismic response of a one-storey structure we consider a structure characterized by $m_1/\rho a^3 = 1.0$, $h_1/a = 1$ or $h_1/a = 2$ and $\xi_1 = 0.02$. The foundation is modeled as a flat rigid disk foundation of radius a placed on a uniform half-space characterized by the shear-wave velocity β, density ρ, Poisson's ratio $\nu = 1/3$ and hysteretic material damping ratio $\xi_s = 0.02$. The control gains are determined for weighting factors of $\gamma_1 = \gamma_2 = 1.0$ and do not include SSI effects. The

results obtained are shown in Figs. 4 and 5. In particular, each figure shows the apparent system frequency $\tilde{\omega}_{1c}$ including the effects of SSI and control and the corresponding system damping ratio $\tilde{\xi}_{1c}$. Also shown are the amplitudes of the transfer functions u_1/u_g, $F_1/\omega_1^2 m_1 u_g$, u_o/u_g and $h_1\theta_o/u_g$ at the frequency $\tilde{\omega}_{1c}$. The results in Fig. 4 and 5 are presented versus the relative stiffness parameter $a_1 = \omega_1 a/\beta$ where ω_1 is the fixed-base natural frequency of the uncontrolled superstructure, a is the radius of the foundation and β is the shear-wave velocity of the soil. The results are shown for several values of the control parameter $\alpha = (\omega_1^2 r)^{-1}$ ranging from $\alpha = 0$ for the uncontrolled case to $\alpha = 2$ in which there is a large control force.

The results in Figs. 4 and 5 indicate that as control increases (*i.e.* as α increases) the system frequency $\tilde{\omega}_{1c}$, the system damping ratio $\tilde{\xi}_{1c}$ and the control force F_1 also increase while the deformation of the structure, the relative displacement of the base and the rocking of the base decrease significantly.

The effects of soil-structure interaction tend to reduce the system frequency $\tilde{\omega}_{1c}$ and the control force F_1 but the reductions are significant only for values of $a_1 > 0.25$. The interaction effects clearly increase the relative displacement and rocking motion of the base. The effects of SSI on the deformation of the structure depend on the amount of control acting on the structure. For a small amount of control ($\alpha < 0.02$), the system damping ratio $\tilde{\xi}_{1c}$ increases and the deformation of the structure u_1 decreases significantly as the soil becomes softer. On the other hand, if the amount of control is large ($\alpha > 0.02$), the system damping ratio $\tilde{\xi}_{1c}$ decreases with a_1 and a slight increase in the deformation u_1 of the structure can be obtained as the soil becomes softer. For fixed values of $a_1 = \omega_1 a/\beta$, $m_1/\rho a^3$ and α, the effects of interaction appear to be stronger as the slenderness ratio h_1/a increases.

RESPONSE OF A CONTROLLED 1-DOF OSCILLATOR WITH GAINS DETERMINED INCLUDING SSI EFFECTS

We consider now the seismic response of a one-storey structure subjected to active control in which the gains have been determined by approximately including the effects of soil-structure interation. To start, we recall from Eq. (16) that the relative displacement u_1 for a one-storey structure supported on a flexible soil and subjected to an *internal* force F_1 and to the seismic excitation u_g can be approximately obtained as the response of an equivalent 1-DOF structure on a rigid soil satisfying the equation of motion

$$\ddot{u}_1 + 2\tilde{\xi}_1\tilde{\omega}_1\dot{u}_1 + \tilde{\omega}_1^2 u_1 = \tilde{F}_1/m_1 - \ddot{\tilde{u}}_g \tag{46}$$

in which the equivalent frequency $\tilde{\omega}_1$ and damping ratio $\tilde{\xi}_1$ are given by Eqs. (13) and (14), respectively. The corresponding effective input ground motion $\tilde{u}_g$ and the effective force $\tilde{F}_1$ are given by Eqs. (17a) and (17b), respectively.

To derive the optimal control parameters for the equivalent oscillator we use again, for the purpose of comparison, the same performance index J

$$J = \int_0^\infty \left\{\gamma_1\dot{u}_1^2 + \gamma_2\omega_1^2 u_1^2 + r[F_1/m_1]^2\right\}\, dt \tag{47}$$

which we rewrite in the form

$$J = \int_0^\infty \left\{\gamma_1 u_1^2 + \tilde{\gamma}_2\tilde{\omega}_1^2 u_1^2 + \tilde{r}[\tilde{F}_1/m_1]^2\right\}^2\, dt \tag{48}$$

in which

$$\tilde{\gamma}_2 = (\omega_1/\tilde{\omega}_1)^2\,\gamma_2 \tag{49}$$

and

$$\tilde{r} = (\omega_1/\tilde{\omega}_1)^8\, r \quad . \tag{50}$$

To simplify the process of obtaining the optimal gains, the displacement u_1 is constrained to satisfy the equation of motion for the equivalent oscillator in the absence of seismic excitation.

Following Eqs. (23), (34) and (35), the optimal effective control force is given by

$$\tilde{F}_1 = -m_1 \left[\tilde{\omega}_1^2 \bar{g} u_1 + \tilde{\omega}_1 \bar{h} \dot{u}_1\right] \tag{51}$$

in which $\bar{g}$ and $\bar{h}$ are the effective gains

$$\bar{g} = \sqrt{1 + \tilde{\alpha}\tilde{\gamma}_2} - 1 \tag{52}$$

$$\bar{h} = \sqrt{4\tilde{\xi}_1^2 + \tilde{\alpha}\gamma_1 + 2\sqrt{1 + \tilde{\alpha}\tilde{\gamma}_2} - 2} - 2\tilde{\xi}_1 \tag{53}$$

where $\tilde{\alpha} = 1/(\tilde{\omega}_1^2 \tilde{r}) = (\tilde{\omega}_1/\omega_1)^6 \alpha$. The actual control force $F_1 = (\omega_1/\tilde{\omega}_1)^4 \tilde{F}_1$ is given by

$$F_1(t) = -m_1[\omega_1^2 g u_1 + \omega_1 h \dot{u}_1] \tag{54}$$

where the actual gains, including SSI, are:

$$g = (\omega_1/\tilde{\omega}_1)^2 \bar{g} \tag{55}$$

$$h = (\omega_1/\tilde{\omega}_1)^3 \bar{h} \quad . \tag{56}$$

The effects of SSI on the gains g and h are illustrated in Fig. 6 for the case $m_1/\rho a^3 = 1.0$, $h_1/a = 1$ (a, b) and $h_1/a = 2$ (c, d), $\xi_1 = 0.02$, $\xi_s = 0.02$, $\nu = 1/3$, $\gamma_1 = 1$ and $\gamma_2 = 1$. In this figure, the values of $g^* = (2g/\alpha)$ and $h^* = (h/\sqrt{2\alpha})$ are shown versus the relative stiffness parameter $a_1 = \omega_1 a/\beta$ for values of the control parameter $\alpha = (\omega_1^2 r)^{-1}$ of 0.002, 0.02, 0.2 and 2.0. It is apparent that the effects of SSI on g and h are significant only if $a_1 > 0.5$. The effects appear to be stronger for the more slender structure and when the control force is small.

To calculate the relative response of the controlled structure we have several possibilities. One approximation is to substitute from Eq. (51) into Eq. (46) leading to

$$\ddot{u}_1 + 2\tilde{\xi}_{1c}\tilde{\omega}_{1c}\dot{u}_1 + \tilde{\omega}_{1c}^2 u_1 = -\ddot{\tilde{u}}_g \tag{57}$$

in which now

$$\tilde{\omega}_{1c} = \tilde{\omega}_1 \left(1 + \tilde{\alpha}\tilde{\gamma}_2\right)^{1/4} \tag{58}$$

and

$$\tilde{\xi}_{1c} = \left\{ \frac{\tilde{\xi}_1^2}{\sqrt{1+\tilde{\alpha}\tilde{\gamma}_2}} + \frac{1}{2}\left[1 - \frac{(1-\tilde{\alpha}\gamma_1/2)}{\sqrt{1+\tilde{\alpha}\tilde{\gamma}_2}}\right]\right\}^{1/2} \quad . \tag{59}$$

In the frequency domain, the peak amplitude of the transfer function u_1/u_g for the oscillator defined by Eqs. (58) and (59) would occur at $\omega = \tilde{\omega}_{1c}$ and would be given by

$$\left|\frac{u_1}{u_g}\right| = \frac{(\tilde{\omega}_1/\omega_1)^2}{2\tilde{\xi}_{1c}} \quad . \tag{60}$$

The amplitude of the internal control force F_1 at $\omega = \tilde{\omega}_{1c}$ corresponds to

$$\left|\frac{F_1}{\omega_1^2 m_1 u_g}\right| = \frac{1}{2\tilde{\xi}_{1c}}\sqrt{\bar{g}^2 + \left(\frac{\tilde{\omega}_{1c}}{\tilde{\omega}_1}\right)^2 \bar{h}^2} \tag{61}$$

where $\bar{g}$ and $\bar{h}$ are given by Eqs. (52) and (53), respectively.

A second and preferable approximate approach to obtain the response of the controlled structure including soil-structure interaction effects is to substitute the internal control force $F_1 = (\omega_1/\tilde{\omega}_1)^4 \tilde{F}_1$ in which $\tilde{F}_1$ is given by Eq. (51) into Eq. (3), the equation of motion for the top mass. The resulting equation of motion is given again by

$$m_1(\ddot{u}_o + h_1\ddot{\theta}_o + \ddot{u}_1) + 2m_1\omega_{1c}\xi_{1c}\dot{u}_1 + m_1\omega_{1c}^2 u_1 = -m_1\ddot{u}_g \tag{62}$$

in which now

$$\omega_{1c} = \omega_1\sqrt{1+g} \tag{63}$$

and

$$\xi_{1c} = \left(\frac{\omega_1}{\omega_{1c}}\right)\left[\xi_1 + \frac{1}{2}h\right] \quad . \tag{64}$$

Thus, the superstructure subjected to an internal control force F_1 can be represented by an equivalent 1-DOF structure with frequency ω_{1c} and damping ratio ξ_{1c}. The response of this equivalent structure to the seismic excitation in the presence of soil-structure interation effects can then be obtained by use of Eq. (41) in which $\tilde{\omega}_{1c}$ and $\tilde{\xi}_{1c}$ are calculated from Eqs. (42) and (43) with ω_{1c} and ξ_{1c} given by Eqs. (63) and (64). The values of the transfer functions $|u_o/u_g|$, $|h_1\theta_o/u_g|$ and $|u_1/u_g|$ at the controlled system frequency $\omega = \tilde{\omega}_{1c}$ are again given by

Eqs. (44a), (44b) and (44c). The amplitude of the control force at $\tilde{\omega}_{1c}$ is also given by Eq. (45) where g, h, ω_{1c}, ξ_{1c}, $\tilde{\omega}_{1c}$, and $\tilde{\xi}_{1c}$ are now calculated by use of Eqs. (55), (56), (63), (64), (42) and (43), respectively. This second approach is used in the calculations that follow.

The effects of SSI on the seismic response of a one-storey structure subjected to active control by internal forces with gains determined including SSI effects are shown in Figs. 7 and 8. Again, the characteristics of the structure, foundation and control system correspond to $m_1/\rho a^3 = 1.0$, $h_1/a = 1$ (Fig. 7) and $h_1/a = 2$ (Fig. 8), $\xi_1 = 0.02$, $\xi_s = 0.02$, $\nu = 1/3$ and $\gamma_1 = \gamma_2 = 1$.

The results in Figs. 7 and 8 for the case of gains determined including SSI effects follow the same trends as those shown in Figs. 4 and 5 for the case of gains determined without SSI. For $a_1 > 0.5$, the peak values of the transfer fuctions u_1/u_g, u_o/u_g and $h_1\theta_o/u_g$ are slightly larger and the control force is slightly smaller when the SSI effects are included in the calculation of the gains.

CONCLUSIONS

A simple model for the seismic response of a one-storey structure subjected to active control in the presence of soil-structure interaction effects has been presented. The resulting representation in terms of a modified 1-DOF oscillator which includes the effects of control and soil-structure interaction offers insight into the problem and allows us to evaluate the effects of interaction on the seismic response of actively controlled structures in which the control gains have been determined with and without inclusion of SSI effects.

It has been found that control reduces not only the internal deformation of the structure but also the relative horizontal displacement and the rocking motion of the base. If the control forces are small, the effects of SSI tend to reduce the deformation of the structure and the control forces while increasing the relative displacement and rocking motion of the base. For large control forces, the SSI effects may lead to deformations of the structure slightly larger than those obtained when the interaction effects on the response are ignored. The effects of ignoring the interaction between the structure and the soil in the calculation of the control gains are small and result in an slightly lower response of the structure and the foundation at the expense of a slightly larger control force.

The present results for internal control are slightly less favorable than those found by Wong and Luco (1992) for an instance of external control. Similar advantages have been obtained by Wu and Smith (1995) in their comparison of externally and internally controlled systems.

ACKNOWLEDGMENTS

The work described here was supported by a grant from the Ohsaki Research Institute of Shimizu Corporation. The author wishes to acknowledge the contributions of Dr. F. C. P. de Barros to the calculation of the numerical results presented here.

REFERENCES

1. Alam, S. M. S. and S. Baba (1991). "Active Optimal Control for Earthquake Excited Structures Using Optimal Observer," *Second Joint Japan/US Conference on Adaptive Structures,* Nagoya, Nov. 1991, 211-226.

2. Alam, S. M. S. and S. Baba (1993). "A Robust Active Optimal Control Scheme Including Soil-Structure Interaction," *Journal of Structural Engineering, ASCE,* 119(9), 2533-2551.

3. Bielak, J. (1971). "Earthquake Response of Building-Foundation Systems," Report EERL-71-04, Earthquake Engineering Research Laboratory, California Institute of Technology, Pasadena, California.

4. Jennings, P. C. and J. Bielak (1973). "Dynamics of Building-Soil Interaction," *Bulletin of the Seismological Society of America,* 63, 9-48.

5. Luco, J. E., H. L. Wong and M. D. Trifunac (1986). "Soil-Structure Interaction Effects on Forced Vibration Tests," Report 86-05, Dept. Civil Engineering, University of Southern California, Los Angeles, California, Sept. 1986, 112 pp.

6. Luco, J. E., M. D. Trifunac and H. L. Wong (1987). "On the Apparent Change in Dynamic Behavior of a Nine-Storey Reinforced Concrete Building," *Bulletin of the Seismological Society of America,* 77, 1961-1983.

7. Luco, J. E. and A. Mita (1987). "Response of a Circular Foundation on a Uniform Half-Space to Elastic Waves," *Earthquake Engineering and Structural Dynamics,* 15, 105-118.

8. Meirovitch, L. and H. Öz (1980). "Active Control of Structures by Modal Synthesis." In *Structural Control,* H. H. E. Leipholz (Editor), North-Holland Publishing Co., Amsterdam, 505-521.

9. Meirovitch, L. and H. Baruh (1982). "Control of Self-Adjoint Distributed Parameter Systems," *Journal of Guidance, Control and Dynamics,* 5, 60-66.

10. Sato, T., K. Toki and H. Matsushima (1991). "Optimal Control of Structures Taking into Account the Dynamic Soil-Structure Interaction," *Colloquium on Control of Structures,*Tokyo, July 1991, 257-263 (in Japanese).

11. Sato, T. and K. Toki (1992). "Predictive Control of Seismic Response of Structures Taking into Account the Soil-Structure Interaction," *Proceedings First European Conference on Smart Structures and Materials,* Glasgow, Scotland, 245-250.

12. Smith, H. D., W-H. Wu and R. I. Borja (1994). "Structural Control Considering Soil-Structure Interaction Effects," *Earthquake Engineering and Structural Dynamics*, 23, 609-626.

13. Wu, W-H. and H. A. Smith (1995). "Comparison of SSI Effects on Externally and Internally Controlled Systems," *Smart Mater. Struct.*, 4, A158-A168.

14. Wong, H. L and J. E. Luco (1990). "Active Control of the Seismic Response of Structures in the Presence of Soil-Structure Interaction Effects," *Proceedings U.S. National Workshop on Structural Control Research,* Oct. 25-26, 1990, University of Southern California, Los Angeles, California, 231-235.

15. Wong, H. L and J. E. Luco (1991). "Structural Control Including Soil-Structure Interaction Effects," *Journal of Engineering Mechanics, ASCE,* 1, 2237-2250.

16. Wong, H. L and J. E. Luco (1992). "Effects of Soil-Structure Interaction on the Seismic Response of Structures Subjected to Active Control," *Proceedings Tenth World Conference on Earthquake Engineering,* Madrid, Spain, 2137-2142.

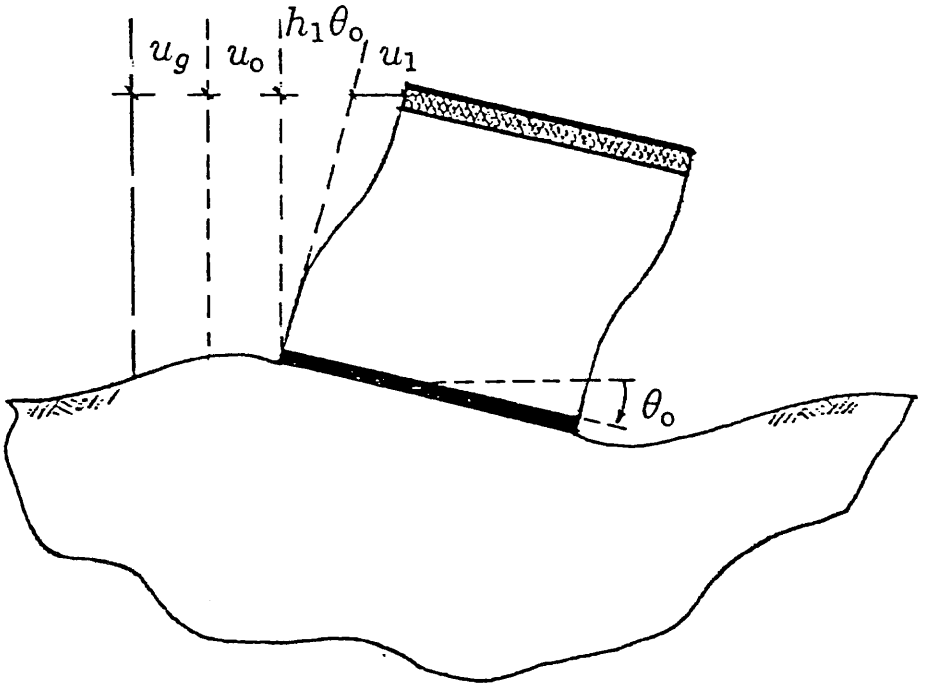

Figure 1. Model of One-Storey Structure.

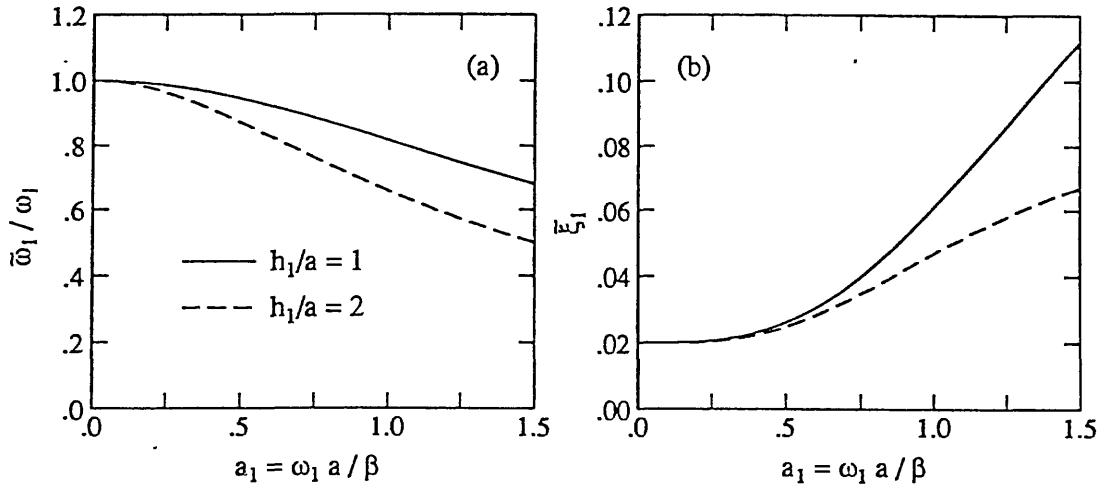

Figure 2. Normalized System Frequency $\tilde{\omega}_1/\omega_1$ and System Damping Ratio $\tilde{\xi}_1$ as a Function of the Relative Stiffness Ratio $a_1 = \omega_1 a/\beta$. [$m_1/\rho a^3 = 0.5$, $h_1/a = 1$ and 2, $\xi_1 = 0.02$, $\xi_s = 0.02$, $\nu = 1/3$].

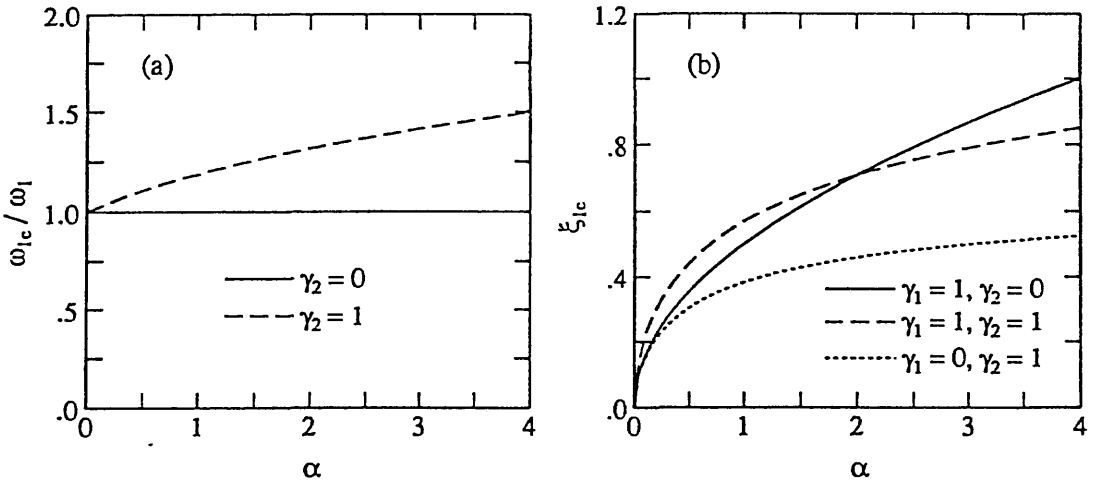

Figure 3. Normalized Frequency ω_{1c}/ω_1 and Damping Ratio ξ_{1c} of the Equivalent Oscillator as a Function of $\alpha = (\omega_1^2 r)^{-1}$ for Different Values of the Weights γ_1 and γ_2 ($\xi_1 = 0$).

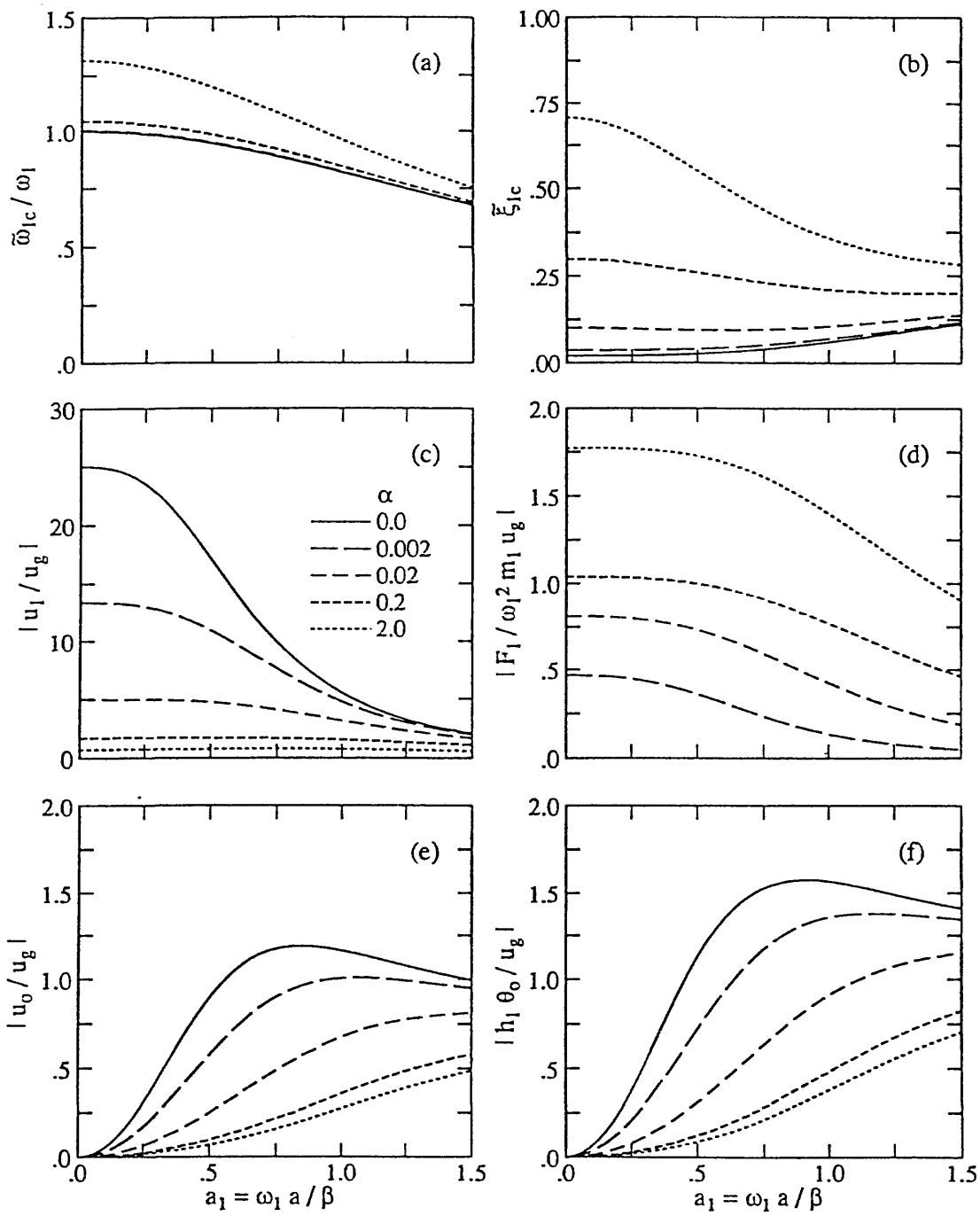

Figure 4. Effects of SSI on the Response of an Actively Controlled One-Storey Structure for the Case of Gains Determined without SSI. Results include: (a) $\tilde{\omega}_{1c}/\omega_1$, (b) $\tilde{\xi}_{1c}$ and (c) $|u_1/u_g|$, (d) $|F_1/\omega_1^2 m_1 u_g|$, (e) $|u_o/u_g|$ and (f) $|h_1\theta_o/u_g|$ at $\omega = \tilde{\omega}_{1c}$. Slenderness ratio $h_1/a = 1.0$.

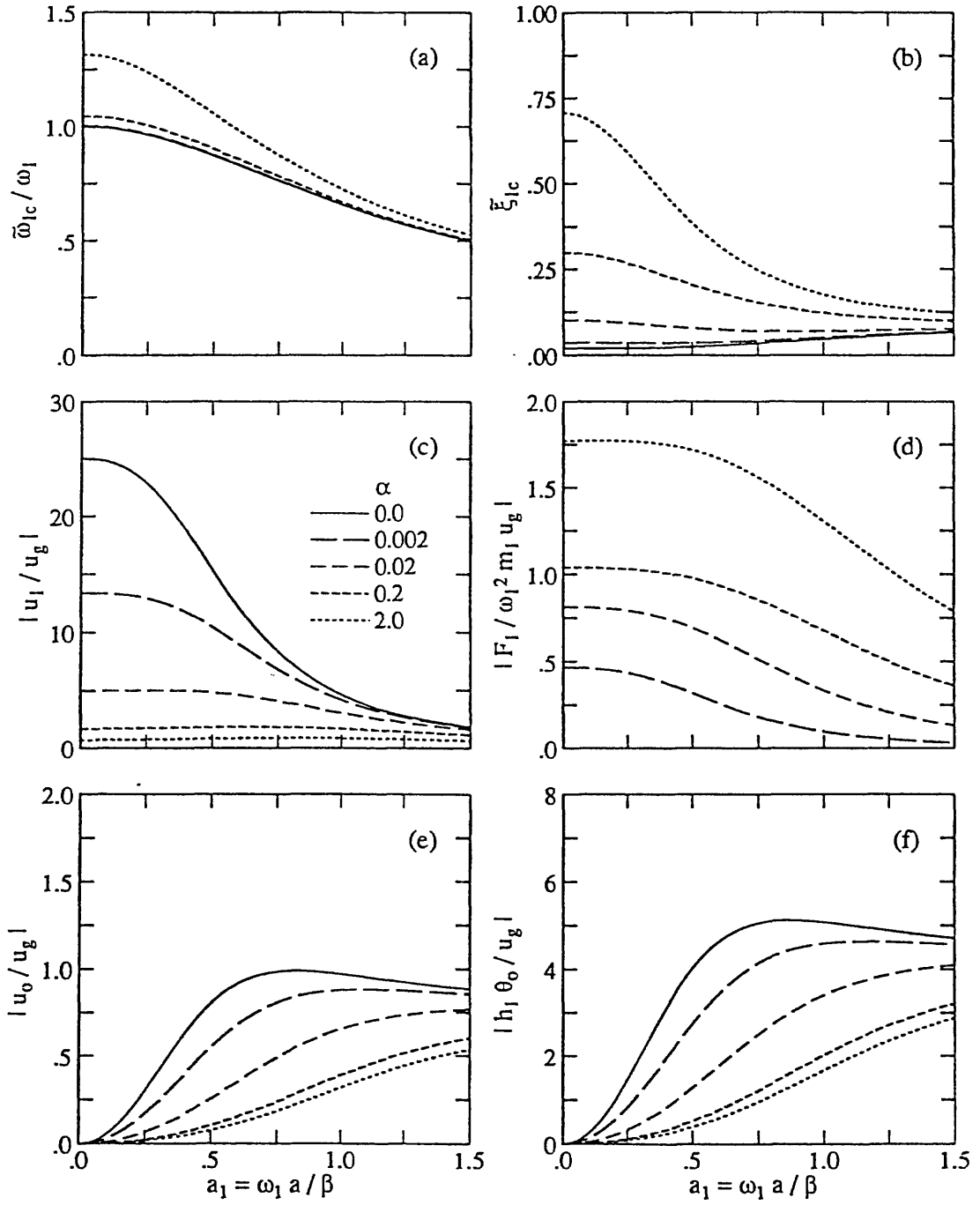

Figure 5. Effects of SSI on the Response of an Actively Controlled One-Storey Structure for the Case of Gains Determined without SSI. Results include: (a) $\tilde{\omega}_{1c}/\omega_1$, (b) $\tilde{\xi}_{1c}$ and (c) $|u_1/u_g|$, (d) $|F_1/\omega_1^2 m_1 u_g|$, (e) $|u_o/u_g|$ and (f) $|h_1\theta_o/u_g|$ at $\omega = \tilde{\omega}_{1c}$. Slenderness ratio $h_1/a = 2.0$.

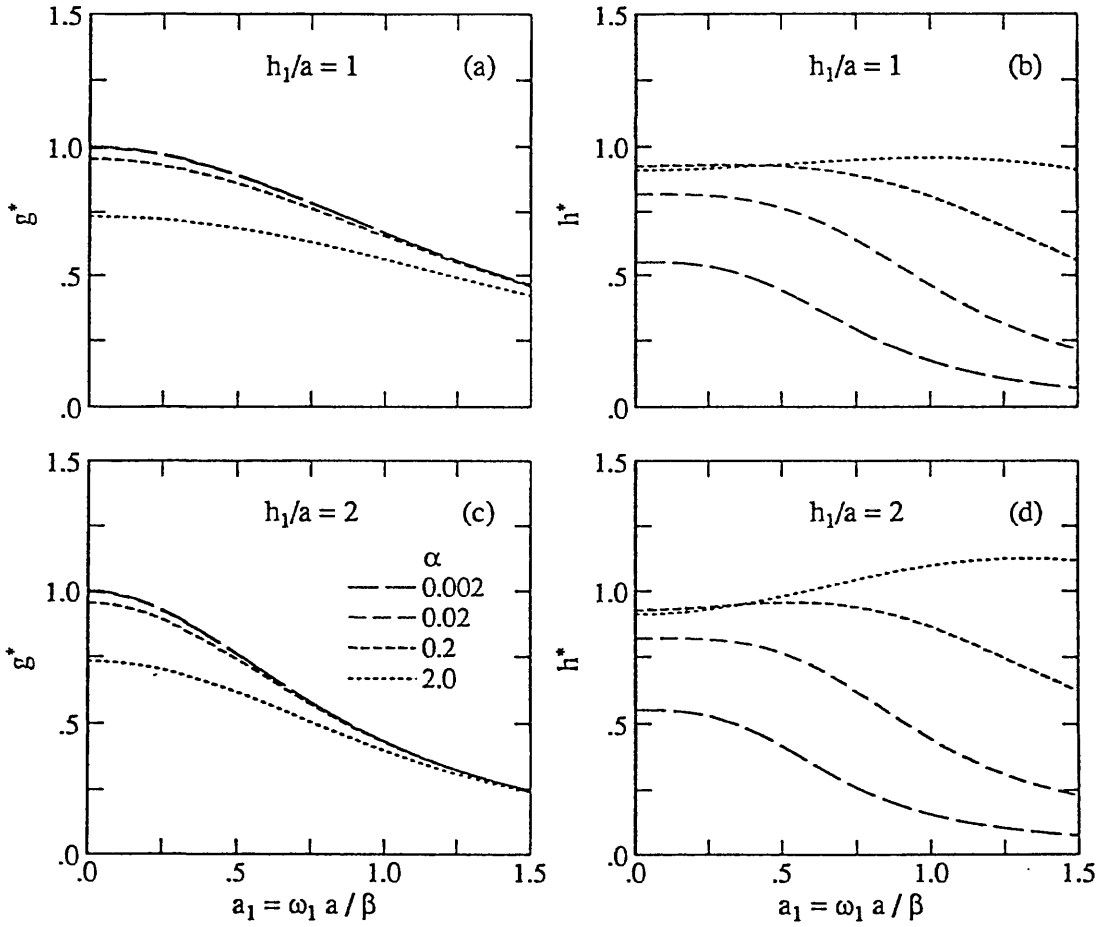

Figure 6. Effects of SSI on the Normalized Control Gains $g^* = (2g/\alpha)$ and $h^* = (h/\sqrt{2\alpha})$ for $h_1/a = 1$ (a, b) and $h_1/a = 2$ (c, d).

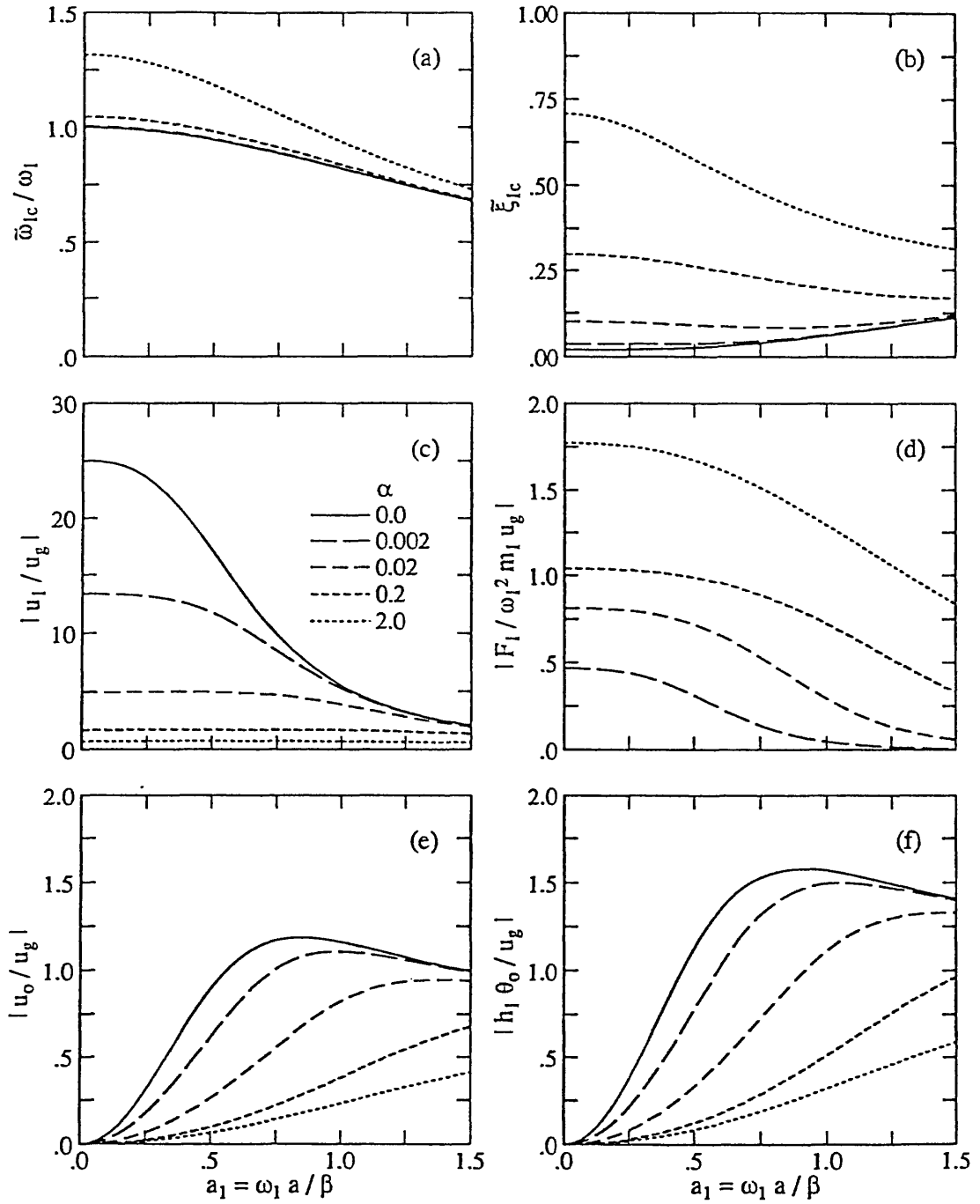

Figure 7. Effects of SSI on the Response of an Actively Controlled One-Storey Structure for the Case of Gains Determined with SSI. Results include: (a) $\tilde{\omega}_{1c}/\omega_1$, (b) $\tilde{\xi}_{1c}$ and (c) $|u_1/u_g|$, (d) $|F_1/\omega_1^2 m_1 u_g|$, (e) $|u_o/u_g|$ and (f) $|h_1\theta_o/u_g|$ at $\omega = \tilde{\omega}_{1c}$. Slenderness ratio $h_1/a = 1.0$.

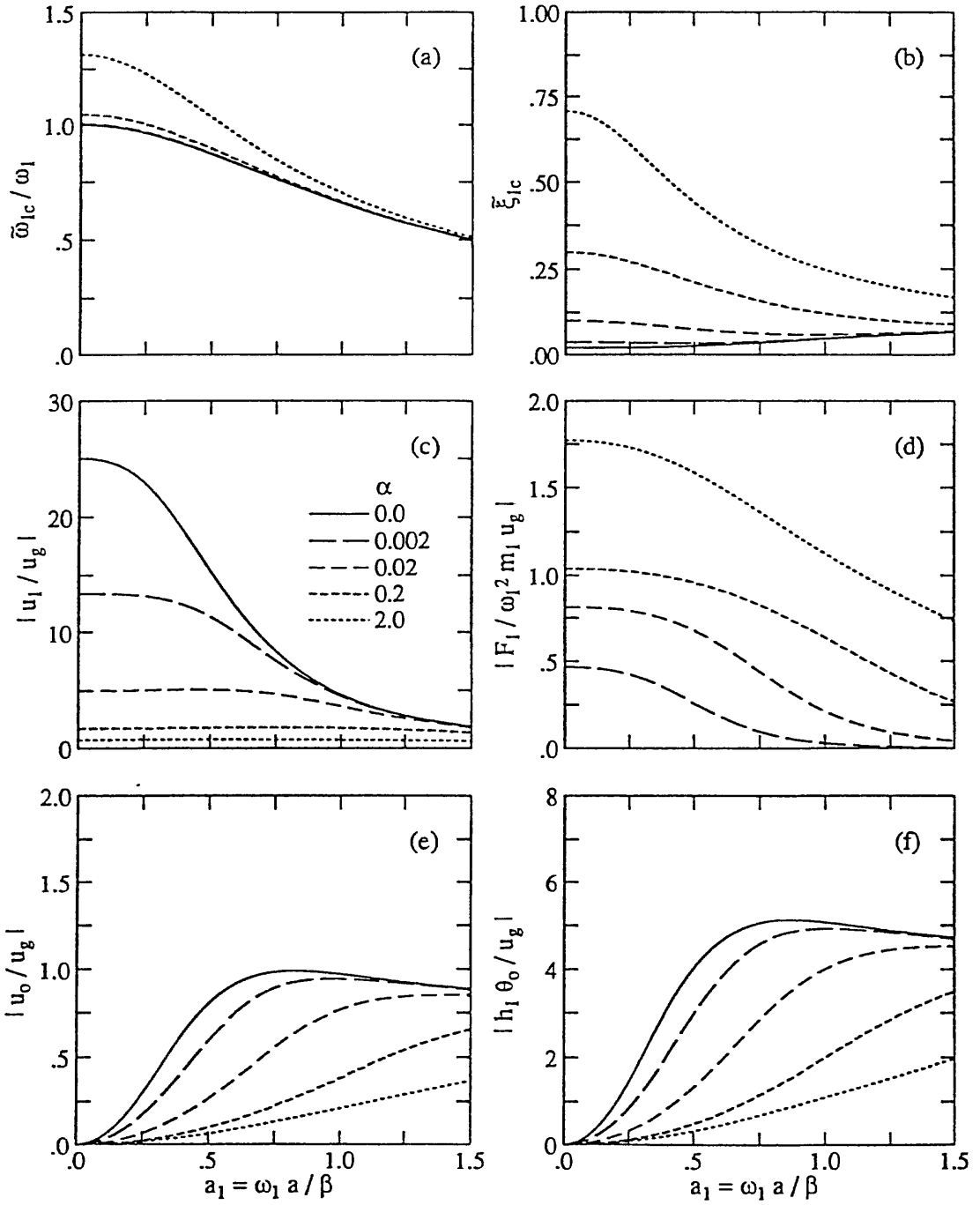

Figure 8. Effects of SSI on the Response of an Actively Controlled One-Storey Structure for the Case of Gains Determined with SSI. Results include: (a) $\tilde{\omega}_{1c}/\omega_1$, (b) $\tilde{\xi}_{1c}$ and (c) $|u_1/u_g|$, (d) $|F_1/\omega_1^2 m_1 u_g|$, (e) $|u_o/u_g|$ and (f) $|h_1\theta_o/u_g|$ at $\omega = \tilde{\omega}_{1c}$. Slenderness ratio $h_1/a = 2.0$.

SEISMIC RESPONSE OF A PIPELINE EMBEDDED IN A LAYERED MEDIUM

J. Enrique Luco[1] and Francisco C. P. de Barros[2]

(1) *Department of Structural Engineering, University of California, San Diego, La Jolla, California 92093-0411, USA.*

(2) *Departamento de Ciências Fundamentais, Radiações e Meio Ambiente, Instituto Militar de Engenharia, Praça General Tibúrcio 80, CEP 22290-270, Rio de Janeiro, Brasil.*

ABSTRACT

A method to obtain the three-dimensional harmonic response of a infinitely long pipeline of circular cross-section embedded in a layered viscoelastic half-space and subjected to harmonic plane waves impinging at an oblique angle with respect to the axis of the shell is presented. The procedure combines an indirect integral representation for the field in the exterior half-space with a model of the pipeline or tunnel based on Donnell shell theory. The integral representation for the soil is based on the use of moving Green's functions for the layered viscoelastic half-space. The accuracy of the formulation is tested by comparison of results obtained by use of different discretizations. Extensive comparisons with previous two- and three-dimensional results for the case of a shell embedded in a uniform half-space and some new numerical results for a pipeline embedded in a multilayered half-space are also presented.

INTRODUCTION

In this paper we consider the three-dimensional response of an infinitely long cylindrical shell of circular cross-section embedded in a horizontally layered half-space (Fig. 1 a, b). The shell representing a pipeline or a tunnel and the soil are excited by plane waves impinging at an oblique angle with respect to the axis of the shell (Fig. 1 a, c). Although the geometry of this model is two-dimensional, the response is fully three-dimensional.

Most of the previous work on the seismic response of pipelines or tunnels has been concentrated on two-dimensional models. In particular, the anti-plane shear case of a cylindrical shell of circular cross-section buried in a uniform elastic half-space and subjected to plane SH-waves normal to the axis of the shell has been considered by Lee and Trifunac (1979) and Balendra et al (1984). The solution is obtained by expanding the fields in both the exterior and interior region in series of cylindrical wave-functions. The coefficients of the terms in these series are obtained by truncating an infinite system of equations in the infinite number of unknown coefficients. The plane-strain case for P-, SV- and Rayleigh-wave excitation has been considered by El-Akily and Datta (1980, 1981), Datta et al (1983, 1984), Wong et al (1985) and Chin et al (1987). El-Akily and Datta (1980, 1981) considered a cylindrical shell of circular cross-section buried in a uniform half-space. The external field was represented by a series expansion in cylindrical wave-functions while the shell was modelled using Flügge's bending theory. Matched asymptotic expansions and a successive reflection technique were used to determine the coefficients in the expansion. Datta et al (1983,1984) considered a cylindrical pipe of circular cross-section lying in a concentric cylindrical region of soft soil buried in a uniform half-space. The fields within each of the three regions were expanded in series of wave-functions. The unknown coefficients in the expansion were obtained by truncating an infinite set of linear equations in the infinite number of unknown coefficients. Wong et al (1985) considered the two-dimensional response of a lined tunnel of non-circular cross section buried in a uniform elastic half-space by use of a technique involving wave-function expansion in the half-space combined with a finite element representation of the tunnel and its immediate cylindrical

vicinity. The same approach was used by Chin et al (1987) to study the response of a pipe of circular cross-section buried in a back-filled trench embedded in a uniform elastic half-space.

Three-dimensional models of infinitely long pipelines similar to those considered in this study have been considered previously by Datta and Shah (1982) for a full space and by Wong et al (1986a, 1986b) and Liu et al (1988) for a half-space. In particular, Wong et al (1986a, 1986b) have considered the response of a cylindrical pipeline of circular cross section buried in a uniform elastic half-space and subjected to obliquely incident plane P-, SV-, SH- and Rayleigh-waves. The solution was obtained by expansion into wave-functions in both the half-space and the shell and by truncation of the resulting infinite system of equations. Liu et al (1988) have obtained the three-dimensional response of an infinitely long pipeline buried in a backfilled trench embedded in a uniform half-space when subjected to obliquely incident P- and SV-waves. These authors have used a hybrid approach in which an internal region including the pipeline is modelled by finite elements while the exterior region is modelled by use of a boundary integral representation in terms of Green's functions for a uniform half-space.

In the present paper, a method of solution which combines an indirect integral representation for the exterior soil with a simplified shell theory (Donnell, 1933) for the internal pipeline or tunnel is presented (Luco and de Barros, 1994). The integral representation for the exterior domain is based on the moving Green's functions for a layered viscoelastic half-space obtained by de Barros and Luco (1992, 1994b). In this way, the physical three-dimensional problem is reduced to an essentially two-dimensional mathematical problem. The integral representation for the exterior domain, the solution for the shell and a discussion of the accuracy of the formulation is presented next. Detailed comparisons with previous two- and three-dimensional solutions for a shell in a uniform half-space and new numerical results describing the response of cylindrical shells embedded in layered media and subjected to obliquely incident P-, SV- and SH-waves are also presented (de Barros and Luco, 1994b). An extensive bibliography on the seismic response of pipelines and tunnels is included at the end of the paper.

FORMULATION

The geometry of the model is illustrated in Fig. 1. The external region representing the soil consists of $(N-1)$ horizontal viscoelastic layers overlying a viscoelastic half-space. The infinitely long shell of circular cross-section is parallel to the free surface of the half-space and is located at a depth H. Perfect bonding is assumed to exist between layers and between the shell and the exterior medium. Each of the media in the exterior half-space is characterized, for harmonic vibrations, by complex P- and S-wave velocities $\alpha_j = \bar{\alpha}_j(1 + 2i\xi_{\alpha_j})^{1/2}$ and $\beta_j = \bar{\beta}_j(1 + 2i\xi_{\beta_j})^{1/2}$ where $i = \sqrt{-1}$, and by the density ρ_j $(j = 1, N)$. The terms $\bar{\alpha}_j$ $\bar{\beta}_j$ represent (approximately) the real parts of the P- and S-wave velocities, and ξ_{α_j} and ξ_{β_j} represent the small hysteretic damping ratios for P- and S-waves, respectively. The shell is characterized by the centerline radius a, tickness h, Young's modulus E_o, Poisson's ratio ν_o and density ρ_o.

In what follows, the excitation and the response will have harmonic time dependence of the type $e^{i\omega t}$ where ω is the frequency. For simplicity, the factor $e^{i\omega t}$ will be dropped from all expressions.

Free-Field Ground Motion.

As a first step in the formulation, it is necessary to determine the ground motion and the stress components for free-field conditions, i.e., in the absence of the shell. The seismic excitation is represented by homogeneous plane P-, SV- or SH-waves, such that the normal to the wave front in the underlying half-space forms an angle θ_v with the vertical axis ($\theta_v = 0$ for vertical incidence). The projection of the normal to the wavefront on the horizontal plane forms the angle θ_h with the axis of the shell (x-axis).

To calculate the free-field ground motion it is convenient to consider the coordinate system x', y', z' $(z' = z)$ shown in Figs. 1a and 1c. Referred to this coordinate system, the

incident motion within the underlying exterior half-space is represented by

$$\{u'_{1N}\}_{\text{inc}} = A\{U'\}e^{-ik'x'+\nu'_N z'} \quad , \qquad z \geq z_N \tag{1}$$

where A is the amplitude of the incident displacement, $k' = (\omega/\beta_N)\sin\theta_v$ for S-waves and $k' = (\omega/\alpha_N)\sin\theta_v$ for P-waves. The term ν'_N is defined by

$$\nu'_N = \begin{cases} i\left(\dfrac{\omega}{\beta_N}\right)\cos\theta_v & \text{for S-wave excitation} \\ i\left(\dfrac{\omega}{\alpha_N}\right)\cos\theta_v & \text{for P-wave excitation} \end{cases} . \tag{2}$$

In Eq. (1), z_N is the depth of the last interface with the underlying half-space and $\{U'\}$ is the vector

$$\{U'\} = \begin{cases} (\sin\theta_v, 0, -\cos\theta_v)^T & \text{for P-wave excitation} \\ (\cos\theta_v, 0, \sin\theta_v)^T & \text{for SV-wave excitation} \\ (0, 1, 0)^T & \text{for SH-wave excitation} \end{cases} . \tag{3}$$

The total free-field ground motion satisfying all the continuity, free-surface and radiation conditions for the layered geometry shown in Fig. 1c can be calculated by the approach described by Luco and Wong (1987). The resulting free-field displacement and stress fields in the $x'y'z'$ - coordinate system are denoted here by

$$\{u'_{1\text{ff}}\} = \{U'_{1\text{ff}}(z')\}e^{-ik'x'} \tag{4}$$

$$[\sigma'_{1\text{ff}}] = [\Sigma'_{1\text{ff}}(z')]e^{-ik'x'} \tag{5}$$

where the elements of $U'_{1\text{ff}}(z')$ and $\Sigma'_{1\text{ff}}(z')$ are independent of y' and depend only on $z' = z$.

To impose boundary conditions at the interface between the layered half-space and the shell it is necessary to introduce the rotation of coordinates

$$\begin{Bmatrix} x' \\ y' \\ z' \end{Bmatrix} = \begin{bmatrix} \cos\theta_h & \sin\theta_h & 0 \\ -\sin\theta_h & \cos\theta_h & 0 \\ 0 & 0 & 1 \end{bmatrix} \begin{Bmatrix} x \\ y \\ z \end{Bmatrix} = [C]^T \begin{Bmatrix} x \\ y \\ z \end{Bmatrix} \tag{6}$$

leading to the free-field displacement and stress fields in the xyz-coordinate system:

$$\{u_{1\text{ff}}\} = \{U_{1\text{ff}}(\vec{x}_\text{o})\}e^{-ikx} \tag{7}$$

$$[\sigma_{1\text{ff}}] = [\Sigma_{1\text{ff}}(\vec{x}_\text{o})]e^{-ikx} \tag{8}$$

where $\vec{x}_\text{o} = (0, y, z)$, $k = (\omega/\beta_N)\sin\theta_\text{v}\cos\theta_\text{h}$ for S-wave excitation and $k = (\omega/\alpha_N)\sin\theta_\text{v}\cos\theta_\text{h}$ for P-wave excitation. In Eqs. (7) and (8),

$$\{U_{1\text{ff}}(\vec{x}_\text{o})\} = [C]\ \{U'_{1\text{ff}}(z)\}e^{-ik'y\sin\theta_\text{h}} \tag{9}$$

$$[\Sigma_{1\text{ff}}(\vec{x}_\text{o})] = [C]\ [\Sigma'_{1\text{ff}}(z)]\ [C]^T e^{-ik'y\sin\theta_\text{h}} \tag{10}$$

in which the y-dependence enters only in the last exponential factor.

The free-field traction vector $\{\overset{\nu}{t}_{1\text{ff}}(\vec{x})\}$ on the area that will be in contact with the shell can be written in the form

$$\{\overset{\nu}{t}_{1\text{ff}}(\vec{x})\} = \{\overset{\nu}{T}_{1\text{ff}}(\vec{x}_\text{o})\}e^{-ikx} \tag{11}$$

where

$$\{\overset{\nu}{T}_{1\text{ff}}(\vec{x}_\text{o})\} = [\Sigma_{1\text{ff}}(\vec{x}_\text{o})]\{\nu(\vec{x}_\text{o})\} \tag{12}$$

in which $\{\nu\} = (0, \nu_y, \nu_z)^T$ is the unit normal to the shell's boundary at $\vec{x}_\text{o}$ pointing into the shell. It is noted that the variable x appears only in the exponential factors $\exp(-ikx)$ affecting $\{u_{1\text{ff}}\}$, $[\sigma_{1\text{ff}}]$ and $\{\overset{\nu}{t}_{1\text{ff}}\}$.

Finally, it is convenient to recall for future reference that the incident ground motion in the underlying half-space referred to the (x, y, z) coordinate system is represented by the plane wave

$$\{u_{1N}\}_\text{inc} = A\{U\}\exp\left\{-i\frac{\omega}{v}\left[x\sin\theta_\text{v}\cos\theta_\text{h} + y\sin\theta_\text{v}\sin\theta_\text{h}\right] + \nu'_N z\right\} \tag{13}$$

where A is the amplitude of the incident displacement and the vector $\{U\}$ is given by

$$\{U\} = \begin{cases} (-\sin\theta_\text{h}, \cos\theta_\text{h}, 0)^T & \text{for SH-wave excitation,} \\ (\cos\theta_\text{h}\cos\theta_\text{v}, \sin\theta_\text{h}\cos\theta_\text{v}, \sin\theta_\text{v})^T & \text{for SV-wave excitation, and} \\ (\cos\theta_\text{h}\sin\theta_\text{v}, \sin\theta_\text{h}\sin\theta_\text{v}, -\cos\theta_\text{v})^T & \text{for P-wave excitation,} \end{cases} \tag{14}$$

in which θ_v and θ_h are the vertical and horizontal angles of incidence. The velocity v appearing in Eq. (13) corresponds to the (complex) velocity α_N in the underlying half-space for P-excitation and to β_N for SV- and SH-excitation.

It should be noted that if $\theta_h = 90°$ or if $\theta_v = 0°$, then, the incident displacement becomes independent of the coordinate x and the problem becomes two-dimensional.

Contact Problem.

In the presence of the shell, the total displacement vector $\{u_1(\vec{x})\}$ and the total traction vector $\{\overset{\nu}{t}_1(\vec{x})\}$ in the exterior region are written in the form

$$\{u_1(\vec{x})\} = \{u_{1\text{ff}}(\vec{x})\} + \{u_{1\text{s}}(\vec{x})\} \tag{15}$$

$$\{\overset{\nu}{t}_1(\vec{x})\} = \{\overset{\nu}{t}_{1\text{ff}}(\vec{x})\} + \{\overset{\nu}{t}_{1\text{s}}(\vec{x})\} \tag{16}$$

where $\{u_{1\text{s}}\}$ and $\{\overset{\nu}{t}_{1\text{s}}(\vec{x})\}$ are the scattered displacement and traction vectors, respectively. The exterior field satisfies the conditions of vanishing tractions on the free surface ($z = 0$) and the continuity conditions at layer interfaces. The exterior scattered field must also satisfy the radiation conditions at infinity. At the interface S between the shell and the exterior medium, the continuity conditions

$$\{u_1(\vec{x})\} = \{u_2(\vec{x})\} \tag{17}$$

$$\{\overset{\nu}{t}_1(\vec{x})\} = -\{\overset{\nu}{t}_2(\vec{x})\} \quad , \quad \vec{x} \in S \tag{18}$$

apply, in which $\{u_2(\vec{x})\}$ and $\{\overset{\nu}{t}_2(\vec{x})\}$ are the displacement and traction vectors for the shell. In here we assume that $\{u_2(\vec{x})\}$ and $\{\overset{\nu}{t}_2(\vec{x})\}$ can be related in the form

$$\{u_2(\vec{x})\} = \int_S [G_{22}(\vec{x}, \vec{x}')] \{\overset{\nu}{t}_2(\vec{x}')\} \, dS \tag{19}$$

where $[G_{22}(\vec{x}, \vec{x}')]$ is the 3×3 matrix of Green's functions for the shell.

To solve the boundary-value problem, the exterior scattered field is represented as resulting from the action of a distribution of concentrated loads moving in the direction of the x-axis with velocity $c = \omega/k$. These moving loads act in the layered exterior half-space (without the shell) on the surface S_1 (Fig. 1d) located within the region to be occupied by the shell. The scattered displacement field $\{u_{1s}(\vec{x})\}$ is, then, written in the form

$$\{u_{1s}\} = \{U_{1s}(\vec{x}_o)\}\, e^{-ikx} \tag{20}$$

where

$$\{U_{1s}(\vec{x}_o)\} = \int_{L_1} [G_{11}(\vec{x}_o, \vec{y}_o)]\, \{F(\vec{y}_o)\}\, dl(\vec{y}_o) \quad , \tag{21}$$

in which $[G_{11}(\vec{x}_o, \vec{y}_o)]$ is the 3×3 matrix of moving Green's functions (Barros and Luco, 1992, 1993). The first, second and third columns of the matrix G correspond to the displacement vector at $\vec{x}_o = (0, y, z)$ for a unit point load acting in the x, y and z-directions, respectively, and moving with velocity $c = \omega/k$ along a line parallel to the x-axis passing through the point $\vec{y}_o = (0, y_1, z_1)$ on S_1. The contour L_1 corresponds to the intersection of S_1 with the plane $x = 0$. The 3×1 vectors $\{F\}$ represent the unknown amplitudes of the j-th moving loads. The corresponding traction vector $\{\overset{\nu}{t}_{1s}(\vec{x})\}$ for the scattered field at the interface S with the shell can be written in the form

$$\{\overset{\nu}{t}_{1s}(\vec{x})\} = \left\{\overset{\nu}{T}_{1s}(\vec{x}_o)\right\} e^{-ikx} \tag{22}$$

where

$$\left\{\overset{\nu}{T}_{1s}(\vec{x}_o)\right\} = \int_{L_1} [H_{11}(\vec{x}_o, \vec{y}_o)]\, \{F(\vec{y}_o)\}\, dl(\vec{y}_o) \quad , \tag{23}$$

in which

$$\left[\overset{\nu}{H}(\vec{x}_o, \vec{y}_o)\right] = \begin{bmatrix} 0 & \nu_y & \nu_z & 0 & 0 & 0 \\ 0 & 0 & 0 & \nu_y & \nu_z & 0 \\ 0 & 0 & 0 & 0 & \nu_y & \nu_z \end{bmatrix} \begin{bmatrix} \sigma^x_{xx} & \sigma^y_{xx} & \sigma^z_{xx} \\ \sigma^x_{xy} & \sigma^y_{xy} & \sigma^z_{xy} \\ \sigma^x_{xz} & \sigma^y_{xz} & \sigma^z_{xz} \\ \sigma^x_{yy} & \sigma^y_{yy} & \sigma^z_{yy} \\ \sigma^x_{yz} & \sigma^y_{yz} & \sigma^z_{yz} \\ \sigma^x_{zz} & \sigma^y_{zz} & \sigma^z_{zz} \end{bmatrix} \tag{24}$$

In Eq. (24) $(\nu_y(\vec{x}_o), \nu_z(\vec{x}_o))$ are the direction cosines of the normal to the surface S of the shell, and $\sigma^x_{xx}(\vec{x}_o, \vec{y}_o)$, $\sigma^y_{xx}(\vec{x}_o, \vec{y}_o), \ldots$, are the stresses at $\vec{x}_o = (0, y, z)$ induced by the moving unit point loads acting in the x, y and z-directions.

The continuity conditions (17), (18) and Eqs. (7), (11), (20) and (22) indicate that $\{u_j(\vec{x})\}$ and $\{\overset{\nu}{t}_j(\vec{x})\}$ can be written in the form

$$\{u_j(\vec{x})\} = \{U_j(\vec{x}_o)\}\ e^{-ikx} \qquad (j = 1, 2) \tag{25}$$

$$\left\{\overset{\nu}{t}_j(\vec{x})\right\} = \left\{\overset{\nu}{T}_j(\vec{x}_o)\right\}\ e^{-ikx} \qquad (j = 1, 2) \quad . \tag{26}$$

The relation (19) is then given by

$$\{U_2(\vec{x}_o)\} = \int_L \left[\tilde{G}_{22}(\vec{x}_o, \vec{x'_o})\right] \left\{\overset{\nu}{T}_2(\vec{x'_o})\right\}\ dl(\vec{x'_o}) \tag{27}$$

where the contour L corresponds to the intersection of S with the plane $x = 0$, and

$$\left[\tilde{G}_{22}(\vec{x}_o, \vec{x'_o})\right] = \int_{-\infty}^{\infty} \left[G_{22}(\vec{x}, \vec{x'})\right]\ e^{-ik(x-x')}\, dx \quad . \tag{28}$$

By use of Eqs. (15), (16), (21), (23), (25), (26) and (27) the displacement fields $\{U_1(\vec{x}_o)\}$ and$\{U_2(\vec{x}_o)\}$ at the interface S between the shell and the soil can be written in the form

$$\{U_1(\vec{x}_o)\} = \{U_{1\text{ff}}(\vec{x}_o)\} + \int_{L_1} [G_{11}(\vec{x}_o, \vec{y}_o)]\, \{F(\vec{y}_o)\}\, dl_1(\vec{y}_o) \tag{29}$$

$$\begin{aligned}\{U_2(\vec{x}_o)\} = &- \int_L \left[\tilde{G}_{22}(\vec{x}_o, \vec{x'_o})\right] \left\{\overset{\nu}{T}_{1\text{ff}}(\vec{x'_o})\right\}\ dl(\vec{x'_o}) \\ &- \int_L \int_{L_1} \left[\tilde{G}_{22}(\vec{x}_o, \vec{x'_o})\right] \left[\overset{\nu}{H}_{11}(\vec{x'_o}, \vec{y}_o)\right] \{F(\vec{y}_o)\}\ dl_1(\vec{y}_o) dl(\vec{x'_o})\end{aligned} \tag{30}$$

At this point, we use a weighted version of the displacement continuity condition and require that

$$\int_L \left[\overset{\nu}{H}_{11}(\vec{x}_o, \vec{y'_o})\right]^T (\{U_1(\vec{x}_o)\} - \{U_2(\vec{x}_o)\})\ dl(\vec{x}_o) = 0 \quad . \tag{31}$$

Substitution from Eqs. (29), (30) into Eq. (31) leads to

$$\int_{L_1} \left[B(\vec{y_o'}, \vec{y_o})\right] \{F(\vec{y_o})\}\ dl_1\,(\vec{y_o}) = \left\{D(\vec{y_o'})\right\} \tag{32}$$

where

$$\left[B(\vec{y_o'}, \vec{y_o})\right] = \left(\int_L \left[\overset{\nu}{H}_{11}(\vec{x_o}, \vec{y_o'})\right]^T [G_{11}(\vec{x_o}, \vec{y_o})]\ dl(\vec{x_o}) + \right.$$

$$\left. \int_L \int_L \left[\overset{\nu}{H}_{11}(\vec{x_o}, \vec{y_o'})\right]^T \left[\tilde{G}_{22}(\vec{x_o}, \vec{x_o'})\right] \left[\overset{\nu}{H}_{11}(\vec{x_o'}, \vec{y_o})\right] dl(\vec{x_o}) dl(\vec{x_o'}) \right) \tag{33}$$

and

$$\left\{D(\vec{y_o'})\right\} = -\left\{ \int_L \left[\overset{\nu}{H}_{11}(\vec{x_o}, \vec{y_o'})\right]^T \{U_{1\text{ff}}(\vec{x_o})\}\ dl(\vec{x_o}) + \right.$$

$$\left. \int_L \int_L \left[\overset{\nu}{H}_{11}(\vec{x_o}, \vec{y_o'})\right]^T \left[\tilde{G}_{22}(\vec{x_o}, \vec{x_o'})\right] \left\{\overset{\nu}{T}_{1\text{ff}}(\vec{x_o'})\right\} dl(\vec{x_o}) dl(\vec{x_o'}) \right\}. \tag{34}$$

Eq. (32) represents an integral equation for the unknown distribution of forces $\{F(\vec{y_o})\}$.

The kernel $[B]$ and the right-hand-side $\{D\}$ of Eq. (32) depend on the moving Green's function matrix $\left[\tilde{G}_{22}(\vec{x_o}, \vec{x_o'})\right]$ for the shell. These Green's functions are derived in the next section.

MOVING GREEN'S FUNCTIONS FOR A CYLINDRICAL SHELL

The equations of motion for harmonic vibrations of the cylindrical shell are given by

$$-\omega^2 \rho_o h \{\bar{u}_2'\} - K_o[L]\{\bar{u}_2'\} = \{\overset{\nu}{t}_{2e}{}'\} \tag{35}$$

where $\{\bar{u}_2'\} = (\bar{u}, \bar{v}, \bar{w})^T$ represents the midsurface displacement vector in the local coordinates shown in Fig. 2, $\{\overset{\nu}{t}_{2e}{}'\}$ is the effective traction vector also referred to the local coordinates, ρ_o is

the density of the shell, h the tickness, $K_o = E_o h/(1-\nu_o^2)$ in which E_o is the Young's modulus and ν_o is the Poisson's ratio. The operator matrix $[L]$ has for elements (Donnell, 1933)

$$
\begin{aligned}
L_{11} &= \frac{\partial^2}{\partial x^2} + \frac{(1-\nu_o)}{2a^2}\frac{\partial^2}{\partial \theta^2} \\
L_{22} &= \frac{(1-\nu_o)}{2}\frac{\partial^2}{\partial x^2} + \frac{1}{a^2}\frac{\partial^2}{\partial \theta^2} \\
L_{33} &= -\frac{h^2}{12}\left(\frac{\partial^4}{\partial x^4} + \frac{2}{a^2}\frac{\partial^4}{\partial x^2 \partial \theta^2} + \frac{1}{a^4}\frac{\partial^4}{\partial \theta^4}\right) - \frac{1}{a^2} \\
L_{12} &= L_{21} = \frac{1+\nu_o}{2a}\frac{\partial^2}{\partial x \partial \theta} \\
L_{13} &= -L_{31} = \frac{\nu_o}{a}\frac{\partial}{\partial x} \\
L_{23} &= -L_{32} = \frac{1}{a^2}\frac{\partial}{\partial \theta} \quad .
\end{aligned}
\tag{36}
$$

The effective traction vector $\{\overset{\nu}{t}_{2e}{}'\}$ is related to the actual traction vector $\{\overset{\nu}{t}_2{}'\}$ on the outside surface ($r = r_o = a + h/2$) of the shell through the relation

$$
\left\{\overset{\nu}{t}_{2e}{}'\right\} = \begin{bmatrix} 1 & 0 & 0 \\ 0 & 1+\frac{h}{2a} & 0 \\ \frac{h}{2}\frac{\partial}{\partial x} & \frac{h}{2a}\frac{\partial}{\partial \theta} & 1 \end{bmatrix} \left\{\overset{\nu}{t}_2{}'\right\} \quad . \tag{37}
$$

To solve Eq. (35) we make explicit the exponential x-dependence and write

$$
\{\bar{u}_2'(x,\theta)\} = \left\{\bar{U}_2'(\theta)\right\} e^{-ikx} \tag{38a}
$$

$$
\left\{\overset{\nu}{t}_2{}'(x,\theta)\right\} = \left\{\overset{\nu}{T}_2{}'(\theta)\right\} e^{-ikx} \quad . \tag{38b}
$$

Applying the Finite Fourier transform

$$
w_n = \frac{1}{2\pi}\int_0^{2\pi} w(\theta) e^{-in\theta}\, d\theta \tag{39a}
$$

$$
w(\theta) = \sum_{n=-\infty}^{\infty} w_n e^{in\theta} \tag{39b}
$$

to Eq. (35) leads to

$$\frac{E_o h}{a^2}\,[A_n]\,\{\bar{U}'_{2n}\} = [B_n]\left\{\overset{\nu}{T}_{2n}{}'\right\} \tag{40}$$

where

$$[A_n] = -\left(\frac{1}{1-\nu_o^2}\right)[\bar{L}_n] - \left(\frac{\omega a}{\sqrt{E_o/\rho_o}}\right)^2 [I] \tag{41}$$

in which $[I]$ is the 3×3 unit matrix. The elements of the matrix $[\bar{L}_n]$ are given by

$$\begin{aligned}
\bar{L}_{11} &= -\left[(ka)^2 + \left(\frac{1-\nu_o}{2}\right) n^2\right] \\
\bar{L}_{22} &= -\left[\left(\frac{1-\nu_o}{2}\right)(ka)^2 + n^2\right] \\
\bar{L}_{33} &= -\frac{1}{12}\left(\frac{h}{a}\right)^2 \left[(ka)^4 + 2(ka)^2 n^2 + n^4\right] - 1 \\
\bar{L}_{12} &= \bar{L}_{21} = \left(\frac{1+\nu_o}{2}\right)(ka)\, n \\
\bar{L}_{13} &= -\bar{L}_{31} = -i\,\nu_o\,(ka) \\
\bar{L}_{23} &= -\bar{L}_{32} = i\,n \quad .
\end{aligned} \tag{42}$$

The matrix $[B_n]$ is given by

$$[B_n] = \begin{bmatrix} 1 & 0 & 0 \\ 0 & 1+\frac{h}{2a} & 0 \\ -\frac{i}{2}\left(\frac{h}{a}\right)(ka) & \frac{i}{2}\left(\frac{h}{a}\right) n & 1 \end{bmatrix} \tag{43}$$

Solving Eq. (40) and inverting the Finite Fourier transform leads to

$$\{\bar{U}'_2(\theta)\} = a \int_0^{2\pi} [G'_{22}(\theta,\theta')] \left\{\overset{\nu}{T}_2{}'(\theta')\right\} d\theta' \tag{44}$$

where

$$[G'_{22}(\theta,\theta')] = \frac{1}{2\pi}\frac{1}{E_o}\left(\frac{a}{h}\right) \sum_{n=-\infty}^{\infty} [A_n]^{-1}\,[B_n]\; e^{in(\theta-\theta')} \tag{45}$$

To impose the continuity conditions at the interface between the shell and the external medium we must consider not the midsurface displacements $\{\bar{U}_2'(\theta)\}$ but the displacements $\{U_2'(\theta)\}$ on the outside boundary $r = r_o = a + h/2$. These displacements are related by

$$\{u_2'\} = \begin{bmatrix} 1 & 0 & -\frac{h}{2}\frac{\partial}{\partial x} \\ 0 & 1+\frac{h}{2a} & -\frac{h}{2a}\frac{\partial}{\partial \theta} \\ 0 & 0 & 1 \end{bmatrix} \{\bar{u}_2'\} \quad . \tag{46}$$

The resulting expression for the outside displacement vector in terms of the tractions is

$$\{U_2'(\theta)\} = a \int_0^{2\pi} \left[\bar{G}_{22}'(\theta,\theta')\right] \left\{\overset{\nu}{T}_2'(\theta')\right\} d\theta' \tag{47}$$

where

$$\left[\bar{G}_{22}'(\theta,\theta')\right] = \frac{1}{2\pi}\frac{1}{E_o}\left(\frac{a}{h}\right) \sum_{n=-\infty}^{\infty} [D_n]\,[A_n]^{-1}\,[B_n]\; e^{in(\theta-\theta')} \tag{48}$$

in which

$$[D_n] = \begin{bmatrix} 1 & 0 & i\left(\frac{ka}{2}\right)\left(\frac{h}{a}\right) \\ 0 & 1+\frac{h}{2a} & -i\frac{n}{2}\left(\frac{h}{a}\right) \\ 0 & 0 & 1 \end{bmatrix} \quad . \tag{49}$$

Some of the stresses of interest are given by

$$\begin{Bmatrix} \bar{\sigma}_x \\ \bar{\sigma}_\theta \\ 2\bar{\sigma}_{x\theta}/(1-\nu_o) \end{Bmatrix} = \frac{K_o}{h} \left(\begin{bmatrix} \frac{\partial}{\partial x} & \frac{\nu_o}{a}\frac{\partial}{\partial \theta} & \frac{\nu_o}{a} \\ \nu_o\frac{\partial}{\partial x} & \frac{1}{a}\frac{\partial}{\partial \theta} & \frac{1}{a} \\ \frac{1}{a}\frac{\partial}{\partial \theta} & \frac{\partial}{\partial x} & 0 \end{bmatrix} \right.$$
$$\left. -\bar{z} \begin{bmatrix} 0 & -\frac{\nu_o}{a^2}\frac{\partial}{\partial \theta} & \left(\frac{\partial^2}{\partial x^2} + \frac{\nu_o}{a^2}\frac{\partial^2}{\partial \theta^2}\right) \\ 0 & -\frac{1}{a^2}\frac{\partial}{\partial \theta} & \left(\frac{1}{a^2}\frac{\partial^2}{\partial \theta^2} + \nu_o\frac{\partial^2}{\partial x^2}\right) \\ 0 & -\frac{1}{a}\frac{\partial}{\partial x} & \frac{2}{a}\frac{\partial^2}{\partial x \partial \theta} \end{bmatrix} \right) \{\bar{u}_2'(x,\theta)\} \quad . \tag{50}$$

where $\bar{z} = r - a$ [$\bar{z} = h/2$ on the outside wall ($r = r_o$) and $\bar{z} = -h/2$ on the inside wall ($r = r_i$)]. By writting

$$\begin{Bmatrix} \bar{\sigma}_x \\ \bar{\sigma}_\theta \\ 2\bar{\sigma}_{x\theta}/(1-\nu_o) \end{Bmatrix} = \begin{Bmatrix} \Sigma_x \\ \Sigma_\theta \\ 2\Sigma_{x\theta}/(1-\nu_o) \end{Bmatrix} . e^{-ikx} \tag{51}$$

it is found that

$$\left\{ \begin{array}{c} \Sigma_x \\ \Sigma_\theta \\ 2\Sigma_{x\theta}/(1-\nu_o) \end{array} \right\} = a \int_0^{2\pi} [H_{22}(\theta,\theta')] \left\{ \overset{\nu}{T_2}'(\theta') \right\} d\theta \tag{52}$$

where

$$[H_{22}(\theta,\theta')] = \frac{1}{2\pi a} \left(\frac{1}{1-\nu_o^2} \right) \left(\frac{a}{h} \right) \sum_{n=-\infty}^{\infty} [E_n] [A_n]^{-1} [B_n] \, e^{in(\theta-\theta')} \tag{53}$$

in which

$$[E_n] = \begin{bmatrix} -i(ka) & i\nu_o n & \nu_o \\ -i\nu_o(ka) & in & 1 \\ in & -i(ka) & 0 \end{bmatrix} + \left(\frac{\bar{z}}{a} \right) \begin{bmatrix} 0 & i\nu_o n & (ka)^2 + \nu_o n^2 \\ 0 & in & \nu_o(ka)^2 + n^2 \\ 0 & -ika & -2(ka)n \end{bmatrix} \quad . \tag{54}$$

The relation between displacements and tractions given by Eq. (47) involves the displacement and traction vectors referred to the local (cylindrical) coordinates. To connect the displacements and tractions on the shell with those of the soil it is necessary to refer these vectors to the global cartesian coordinates (x, y, z). Denoting by $\{U_2\}$ and $\{\overset{\nu}{T_2}\}$ the vectors $\{U_2'\}$ and $\{\overset{\nu}{T_2}'\}$ when referred to the global coordinate system we have

$$\{U_2\} = [C_o] \{U_2'\} \tag{55a}$$

and

$$\left\{ \overset{\nu}{T_2}' \right\} = [C_o]^T \left\{ \overset{\nu}{T_2} \right\} \tag{55b}$$

where

$$[C_o] = \begin{bmatrix} 1 & 0 & 0 \\ 0 & -\sin\theta & \cos\theta \\ 0 & -\cos\theta & -\sin\theta \end{bmatrix} \quad . \tag{56}$$

The relation between the displacement and the traction can now be written in the form

$$\{U_2(\theta)\} = a \int_0^{2\pi} \left[\tilde{G}_{22}(\theta,\theta') \right] \left\{ \overset{\nu}{T_2}(\theta') \right\} d\theta' \tag{57}$$

where

$$\left[\tilde{G}_{22}(\theta,\theta') \right] = [C_o(\theta)] \left[\bar{G}'_{22}(\theta,\theta') \right] [C_o(\theta')]^T \tag{58}$$

NUMERICAL APPROACH

The integral equation (32) is discretized by replacing the unknown distributed forces $\{F(\vec{y}_o)\}$ by a set of unknown concentrated forces $\{F_{sj}\}$ $(j = 1, N_s)$ acting at N_s source points $\vec{y}_o = \vec{y}_{sj}$ on L_1 and by imposing Eq. (32) at the same set of discrete points $\vec{y}'_o = \vec{y}_{sj}$ $(j = 1, N_s)$. In addition, the integrals over L appearing in Eqs. (33) and (34) are discretized by use of numerical integration formulae involving a set of N_o observation points $\vec{x}_o = \vec{x}_{oi}$ $(i = 1, N_o)$ on L. The resulting set of linear algebric equations can be written in the form

$$[\bar{B}]\,\{\bar{F}\} = \{\bar{D}\} \tag{59}$$

where the 3×3 blocks of the $3N_s \times 3N_s$ matrix $[\bar{B}]$ correspond to $[B(\vec{y}_{si}, \vec{y}_{sj})]$, $\{\bar{F}\}^T = \left(\{F(\vec{y}_{s1}\}^T, \{F(\vec{y}_{s2}\}^T, \ldots\right)$ and $\{\bar{D}\}^T = \left(\{D(\vec{y}_{s1}\}^T, \{D(\vec{y}_{s2}\}^T, \ldots\right)$.

To reduce the possibility of ill-conditioning it is useful to write $\{\bar{F}\}$ in the form of a finite Fourier expansion with respect to the angular coodinates $\theta_j = \arctan\left[(H - z_{sj})/x_{sj}\right]$ of the source points $\vec{y}_{sj}$ $(j = 1, N_s)$. In this case,

$$\{\bar{F}\} = [M]\,\{F_o\} \tag{60}$$

where the $i^{\underline{th}}$ row of 3×3 blocks of $[M]$ is given by $\left([I],\ \cos\theta_i\,[I],\ \sin\theta_i\,[I],\ \cos 2\theta_i\,[I],\ \sin 2\theta_i\,[I],\ \ldots,\ \cos\frac{N_s}{2}\theta_i\,[I]\right)$ in which $[I]$ is the 3×3 identity matrix, N_s is assumed to be even and $\theta_1 = 0$. The coefficients $\{F_o\}$ in the expansion are obtained from Eq. (59) in the form

$$\{F_o\} = \left([M]^T[\bar{B}][M]\right)^{-1}[M]^T\{D\} \quad . \tag{61}$$

Once the forces $\{\bar{F}\}$ have been calculated by use of Eqs. (60) and (61), the displacement fields in the external medium and in the shell can be calculated from Eqs. (29) and (30).

CONVERGENCE OF THE NUMERICAL APPROACH

The numerical results obtained by the procedure described in the previous section depend in principle on the location and number of source points (N_s) and on the number of observation

points (N_o) used. The first step is to test the convergence of this approach. For this purpose we consider a concrete circular shell ($\rho_o = 2,240\,kg/m^3$, $E_o = 1.6 \times 10^{10}\,N/m^2$, $\nu_o = 0.2$, $h = 0.1r_i = 0.0909r_o$) buried to a depth $H = 5.0r_i = 4.545r_o$ in a uniform half-space ($\rho_1 = 2,664\,kg/m^3$, $\bar{E}_1 = 7.567 \times 10^9\,N/m^2$, $\nu_1 = 0.333$, $\xi_\alpha = \xi_\beta = 0.001$). The half-space is subjected to non-vertically incident ($\theta_v = 30°$) P- and SV-waves propagating in the direction of the shell ($\theta_h = 0°$). The frequency of the excitation is such that $\eta = \omega r_o/\pi\bar{\beta}_1 = 0.105$.

Numerical results for the normalized displacement components at a few points on the ground surface ($z = 0$) and at a few points on the external wall of the shell ($r = r_o$) are presented in Table 1 for different numbers of sources and observers (N_s, N_o). Also shown are some values for the normalized hoop stress on the centerline ($r = a$) of the shell. In all cases, the sources are equally spaced on a circle of radius $a' = r_o - 3(2\pi r_o/N_o)$ ($N_o \geq 20$). Thus, as the number of observation points increases, the sources move closer to the actual boundary $r = r_o$.

The displacement amplitudes $U_i = |u_i/A|$ are normalized by the amplitude A of the incident displacement vector on the ground surface. The normalized hoop stress is given by $\Sigma_{\theta\theta} = |\sigma_{\theta\theta}(a)/\omega\rho_1\bar{\beta}_1 A|$. The numerical results presented for source/observer combinations (N_s, N_o) of (20, 40) and (40, 80) show that the procedure is very stable as the number of source and observation points increases. It appears that 20 source points and 40 observation points are sufficient for most applications.

VALIDATION AND CRITICAL COMPARISONS

In the comparisons that follow the displacements are normalized by the amplitude A of the incident displacement field. All of the stress components with the exception of $\sigma_{x\theta} = \sigma_{\theta x}$ are normalized by $\omega\bar{\rho}\bar{\beta}A = (\omega r_o/\bar{\beta})\bar{\mu}(A/r_o)$ where $\bar{\rho}$, $\bar{\beta}$ and $\bar{\mu} = \bar{\beta}^2\bar{\rho}$ are the density, shear wave velocity and shear modulus of reference and r_o is a length of reference corresponding to the external radius of the circular shell. The shear stress $\sigma_{\theta x}$ is normalized by $(1 - \nu_o)\omega\bar{\rho}\bar{\beta}A/2$ where ν_o is the Poisson's ratio of the shell. The reference quantities $\bar{\rho}$, $\bar{\beta}$ and $\bar{\mu}$ are taken to

correspond to those of the underlying half-space (which correspond to ρ_1, $\bar{\beta}_1$ and $\bar{\mu}_1$ in the case of a uniform half-space). In judging the comparisons it must be kept in mind that the present results include a small amount of attenuation in the soil $\xi_\alpha = \xi_\beta = 0.001$ and no attenuation in the shell ($\xi_{\alpha o} = \xi_{\beta o} = 0$) while the results by other authors typically do not include any attenuation.

Finally, the present results have been calculated using $N_s = 20$ source points equally spaced on a circle of radius $r_s = r_o - 6\pi r_o/N_o$ where $N_o = 40$ is the number of observation points equally spaced along the external shell boundary ($r = r_o$).

Two-Dimensional Anti-Plane Shear Cases.

A first comparison is made with results presented by Lee and Trifunac (1979) for a circular cylindrical shell of external radius r_o, internal radius $r_i = 0.9r_o$, thickness $h = 0.1r_o$ and embedment depth $H = 1.5r_o$ subjected to a vertically incident SH-wave with particle motion along the axis of the pipeline ($\theta_h = 90°$, $\theta_v = 0°$). The shell is characterized by shear modulus $\bar{\mu}_o$, shear wave velocity $\bar{\beta}_o$ and density ρ_o ($\bar{\mu}_o = \bar{\beta}_o^2\rho_o$) and the surrounding uniform half-space is characterized by $\bar{\mu}_1$, $\bar{\beta}_1$ and ρ_1. Lee and Trifunac (1979) present results for $\bar{\mu}_o/\bar{\mu}_1 = 3$ but do not state the value for ρ_o/ρ_1 or $\bar{\beta}_o/\bar{\beta}_1$. In here we assume (Lee, personal communication) that $\rho_o/\rho_1 = 3$ and, consequently, $\bar{\beta}_o/\bar{\beta}_1 = 1$. The present results were calculated by assuming a small amount of attenuation $\xi_{\beta 1} = 0.001$ in the half-space and no attenuation in the shell $\xi_{\beta o} = 0$. The results of Lee and Trifunac correspond to purely elastic media. Finally, the comparisons were made for the dimensionless frequency $\eta = \omega r_o/\pi\bar{\beta}_1 = 0.5$.

Figs. 3a and 3b show the comparisons for the amplitudes of the normalized displacements $U_x = |u_x/A|$ on the surface of the half-space ($z = 0$) and on the external boundary of the shell ($r = r_o$). These displacements are normalized by the amplitude A of the incident SH-wave at $z = 0$. Fig. 3c shows the comparisons for the amplitude of the normalized stress $\Sigma_{rx} = |\sigma_{rx}/\omega\rho_1\bar{\beta}_1 A|$ on the external wall of the shell ($r = r_o$). The results in Figs. 3a and

3b show excellent agreement between the present results and the results of Lee and Trifunac (1979) for the surface displacements ($z = 0$) and for the displacements on the external pipe wall ($r = r_o$). The results of Lee and Trifunac (1979) for the normalized contact stress Σ_{rx} on $r = r_o$ differ in shape and amplitude from the present results (Fig. 3c). The peak value for $|\Sigma_{rx}|$ obtained by Lee and Trifunac is about 6 times larger than our result.

As a second comparison we consider the results presented by Balendra et al (1984) for a concrete circular shell ($r_o = 3\,m$, $r_i = 2.7\,m$, $h = 0.3\,m$, $\bar{\mu}_o = 8.4\,GPa$, $\bar{\beta}_o = 1,870\,m/sec$, $\rho_o = 2,410\,kg/m^3$, $\nu_o = 0.2$) buried to a depth $H = 2.5r_o = 7.5\,m$ in a uniform half-space ($\bar{\mu}_1 = 0.111\,GPa$, $\bar{\beta}_1 = 260\,m/sec$, $\rho_1 = 1,640\,kg/m^3$). The medium is subjected to a non-vertically incident ($\theta_v = 30°$) SH-wave propagating normal to the axis of the shell with a frequency of $10.61\,Hz$. In this case, the dimensionless frequency η takes the value $\eta = \omega r_o/\pi\bar{\beta}_1 = 0.245$. Comparisons for the amplitudes of the normalized displacement $U_x = |u_x(r_i)/A|$, and normalized shear stresses $\Sigma_{rx} = |\sigma_{rx}(r_o)/\omega\rho_1\bar{\beta}_1 a|$ and $\Sigma_{\theta x} = |2\sigma_{\theta x}(r_i)/[(1-\nu_o)\omega\rho_1\bar{\beta}_1 a]|$ are presented in Figs. 4a, 4b and 4c, respectively. The figures show excellent agreement between the present results and those obtained by Balendra et al (1984). The small differences for $\Sigma_{\theta x}$ can be attributed to the fact that the present calculation is based on a thin shell theory which in the 2-D case ($ka = 0$) leads to a shear stress $\sigma_{\theta x}$ which does not vary across the tickness of the shell.

As a final comparison for the two-dimensional anti-plane shear case we consider the results presented by Liu et al (1991) for a concrete circular shell ($\rho_o = 2.24 \times 10^3\,kg/m^3$, $E_o = 1.6 \times 10^{10}\,N/m^2$, $\nu_o = 0.2$, $h = 0.1r_i = 0.0909r_o$) embedded to a depth $H = 5r_i = 4.545r_o$ in a uniform half-space ($\rho_1 = 2.664 \times 10^3\,kg/m^3$, $E_1 = 7.567 \times 10^9\,N/m^2$, $\nu_1 = 0.333$) and subjected to a vertically incident SH-wave (Fig. 8d in paper in reference). The corresponding comparison for the amplitude of the normalized displacement $U_x = |u_x(r_o)/A|$ for a dimensionless frequency $\eta = \omega r_o/\pi\bar{\beta}_1 = 0.105$ is shown in Fig. 5. The agreement betweeen the two sets of results is excellent.

Two-Dimensional Plane-Strain Cases.

As a first test for the plane strain case we consider the results presented by Datta et al (1983) [see also Datta et al (1984)] for a concrete circular shell ($\rho_o = 2.24 \times 10^3\, kg/m^3$, $E_o = 1.6 \times 10^{10}\, N/m^2$, $\nu_o = 0.2$, $h = 0.1r_i = 0.0909r_o$) buried to a depth $H = 8.33r_i = 7.573r_o$ in a uniform half-space ($\rho_1 = 2.665 \times 10^3\, kg/m^3$, $E_1 = 6.9 \times 10^8\, N/m^2$, $\nu_1 = 0.45$). The medium is subjected to vertically incident P- and SV-waves with a dimensionless frequency $\eta = \omega r_o/\pi\bar{\beta}_1 = 0.132$.

Comparisons for the normalized amplitudes of the radial displacements $U_r = |u_r(r_o)/A|$ on the external wall of the pipe are presented in Fig. 6a and 6b for vertically incident P- and SV-waves, respectively. There is a excellent agreement between the present results and those presented by Datta et al (1983). To make these comparisons it was necessary to renormalize the results presented by Datta et al (1983) for P- and SV-waves by multiplying these results by factors of 1.362 and 2.0, respectively. These factors correspond to the ratio of the peak free-field radial displacements at $r = r_o$ to the amplitude A of the incident waves. These peaks occur at $\theta = 90°$ and $\theta = 0°$ for P- and SV-waves, respectively.

The corresponding comparisons for the normalized hoop stresses $\Sigma_{\theta\theta}(r_o)$ for P- and SV-waves are shown in Figs. 6c and 6d, respectively. The agreement between the two sets of results is very good. The results of Datta et al (1983) shown in Figs. 6c and 6d were renormalized by multiplying by factors of 5.434 and 0.629 which correspond to the peak values of the normalized hoop stresses $\Sigma_{\theta\theta}(r_o)$ in the free-field. Also shown in Figs. 6c and 6d are the normalized hoop stresses $\Sigma_{\theta\theta}(a)$ on the centerline of the shell (segmented lines). The significant differences between the stresses at $r = r_o$ and $r = a$ indicate a significant amount of bending of the shell.

As a second test for the plane strain case we consider the results presented by Wong et al (1986) for a concrete circular shell ($\rho_o = 2,240\, kg/m^3$, $E_o = 16 \times 10^9\, N/m^2$, $\nu_o = 0.2$, $h = 0.1r_i = 0.0909r_o$) embedded to a depth $H = 2.0r_i = 1.818r_o$ in a uniform half-space ($\rho_1 = 2,665\, kg/m^3$, $E_1 = 0.69 \times 10^9\, N/m^2$, $\nu_1 = 0.45$). Values for the hoop stress $\Sigma_{\theta\theta}(r_o)$

and for the longitudinal stress $\Sigma_{xx}(r_o)$ at $r = r_o$ were presented for nonvertically incident ($\theta_v = 10°$) P- and SV-waves for $\eta = \omega r_o/\pi\bar{\beta}_1 = 0.132$.

Comparisons for the normalized hoop $\Sigma_{\theta\theta}(r_o)$ and longitudinal $\Sigma_{xx}(r_o)$ stresses at $r = r_o$ for both P- and SV-waves are shown in Fig. 7. The agreement between the present results and those of Wong et al (1986) for $\Sigma_{\theta\theta}$ is very good. Some small differences for $\Sigma_{xx}(r_o)$ (Figs. 7c and 7d) can be attributed to the present use of a simplified shell theory in which Σ_{rr} is considered to be much smaller than $\Sigma_{\theta\theta}$ and Σ_{xx}. The results of Wong et al (1986) shown in Fig. 7a, 7b, 7c and 7d were renormalized by multiplying by factors of 2.026, 1.856, 1.840 and 0.5764, respectively. These factors correspond to the peak values of the corresponding normalized stresses in the free-field.

Also shown in Figs. 7a, b, c, d are the normalized stresses (segmented lines) calculated by the present approach on the centerline $r = a$ of the shell. It is apparent, particularly for SV-excitation, that the bending effects are significant.

As a third test for the plane strain case we consider the results presented by Liu et al (1991) for a concrete circular shell ($\rho_o = 2.24 \times 10^3\, kg/m^3$, $E_o = 1.6 \times 10^{10}\, N/m^2$, $\nu_o = 0.2$, $h = 0.1r_i = 0.0909r_o$) buried to a depth $H = 5.0r_i = 4.545r_o$ in a uniform half-space ($\rho_1 = 2.664 \times 10^3\, kg/m^3$, $E_1 = 7.567 \times 10^9\, N/m^2$, $\nu_1 = 0.333$). The medium is subjected to vertically incident P- and SV-waves with dimensionless frequency $\eta = \omega r_o/\pi\bar{\beta}_1 = 0.105$.

The amplitudes of the normalized radial displacements $U_r = |u_r(r_o)/A|$ on the external wall of the pipe are compared in Figs. 8a and 8b for vertically incident P- and SV-waves, respectively. To compare both sets of results it was necessary to renormalize the results presented by Liu et al (1991) by multiplying by the factors 1.667 and 0.424 which correspond to the peak values of the normalized amplitudes of the free-field radial displacements at $r = r_o$ for P- and SV-waves, respectively. In this case, the peak values of $u_r(r_o, \theta)$ in the free-field occur at $\theta = 135°$ and $\theta = 90°$ for P- and SV-wave, respectively.

Comparisons for the normalized hoop stresses $\Sigma_{\theta\theta}(a)$ on the centerline of the shell are shown in Figs. 8c and 8d. For the purpose of the comparison the results of Liu et al (1991) for $\Sigma_{\theta\theta}$ have been renormalized by multiplying by 2.766 and 1.974 corresponding to our peak values for $\Sigma_{\theta\theta}(a)$ in the free-field. It is appparent from Fig. 8 that excellent agreement exist between the two sets of results. We note that Liu et al (1991) present two sets of results, one labeled "analytic" and a second set calculated by a hybrid approach. The comparisons in Fig. 8 refer to the "analytic" results. The agreement with the hybrid results of Liu et al (1991) is also good but not as close as that shown in Fig. 8.

Three-Dimensional Case.

To test the results in the three-dimensional case of waves impinging on the shell at angles other than 90° we consider first the results presented by Wong et al (1986) for a concrete circular shell ($\rho_o = 2,240\,kg/m^3$, $E_o = 16 \times 10^9\,N/m^2$, $\nu_o = 0.2$, $h = 0.1r_i = 0.0909r_o$) embedded to a depth $H = 2.0r_i = 1.818r_o$ in a uniform half-space ($\rho_1 = 2,665\,kg/m^3$, $E_1 = 0.69 \times 10^9\,N/m^2$, $\nu_1 = 0.45$). Values for the hoop $\Sigma_{\theta\theta}(r_o)$ and longitudinal $\Sigma_{xx}(r_o)$ stresses on the pipewall ($r = r_o$) were presented for obliquely incident P-, SV- and SH-waves characterized by $\theta_h = 30°$ and $\theta_v = 10°$ for $\eta = \omega r_o/\pi\bar{\beta}_1 = 0.132$.

Comparisons for the amplitudes of the normalized stress $\Sigma_{\theta\theta}(r_o)$ for P-, SV- and SH-wave are presented in Figs. 9a, 9b and 9c, respectively. The corresponding comparison for $\Sigma_{xx}(r_o)$ are presented in Figs. 9d, 9e and 9f. Clearly, there is good agreement between the two sets of results. The results of Wong et al (1986) in Figs. 9a, b, c, d, e and f have been renormalized by factors of 1.941, 1.082, 1.466, 1.834, 1.076 and 0.284, respectively, corresponding to our peak values for the normalized stresses on $r = r_o$ in the free-field.

Figs. 9a to 9f also show with segmented lines the normalized stresses $\Sigma_{\theta\theta}(a)$ and $\Sigma_{xx}(a)$ on the centerline $r = a$ of the shell. In is apparent that large differences exist between $\Sigma_{\theta\theta}(r_o)$ and $\Sigma_{\theta\theta}(a)$ for SV- and SH-waves indicating the importance of bending of the shell.

As a second test of the results in the three-dimensional case we consider the results presented by Liu et al (1991) for a concrete circular shell ($\rho_o = 2.24 \times 10^3\, kg/m^3$, $E_o = 1.6 \times 10^{10}\, N/m^2$, $\nu_o = 0.2$, $h = 0.1r_i = 0.0909r_o$) buried to a depth $H = 5.0r_i = 4.545r_o$ in a uniform half-space ($\rho_1 = 2.664 \times 10^3\, kg/m^3$, $E_1 = 7.567 \times 10^9\, N/m^2$, $\nu_1 = 0.333$). The medium is subjected to non-vertically incident ($\theta_v = 30°$) P- and SV-waves impinging in the direction of the pipeline ($\theta_h = 0°$). The dimensionless frequency corresponds to $\eta = \omega r_o/\pi\bar{\beta}_1 = 0.105$.

The amplitudes of the normalized radial $U_r(r_o)$ and longitudinal $U_x(r_o)$ displacements at $r = r_o$ and of the normalized hoop stress $\Sigma_{\theta\theta}(a)$ on the centerline $r = a$ are compared in Fig. 10. The results of Liu et al (1991) for P-waves were renormalized by multiplying by factors of 1.428, 0.573 and 2.325 which correspond to the peak values of U_r, U_x and $\Sigma_{\theta\theta}$ on the free-field. The corresponding results for SV-waves were renormalized by factors 0.937, 2.482 and 1.621, respectively. Significant differences can be seen between the present results and those of Liu et al (1991). The discrepancies are smaller for the dominant displacement components [U_r for P-waves, Fig. 10a and U_x for SV-waves, Fig. 10e] than for the secondary displacements [U_x for P-waves, Fig. 10b and U_r for SV-waves, Fig. 10d]. The discrepancies between the two sets of hoop stresses $\Sigma_{\theta\theta}(a)$ for SV-waves (Fig. 10f) are particularly large.

The differences shown in Fig. 10 between our results and those of Liu et al (1991) for the three-dimensional case are somewhat surprising considering the excellent agreement found between the two sets of results for two-dimensional cases (Figs. 5 and 8). To confirm our results we have recalculated our three-dimensional results by use of a hybrid approach which combines a finite element model for the shell with an indirect boundary formulation for the external half-space (FE/IBF, Luco and Barros, 1993b). In this case the shell is represented by four concentric layers including 160 triangular elements in each layer. The displacements on the contact area $r = r_o$ calculated by the hybrid FE/IBF approach coincide almost exactly with the results obtained by use of the present approach (DT/IBF). The moving Green's functions (Barros and Luco, 1992, 1993) which have been used in both the DT/IBF and FE/IBF approaches have

been carefully tested. Calculations for the three-dimensional response of a cylindrical canyon embedded in a uniform half-space and subjected to obliquely incident waves (Luco et al, 1990) based on the use of the same Green's functions have been validated by subsequent calculations by Zhang and Chopra (1991). Also, our three-dimensional results appear to agree with the earlier results of Wong et al (1986) (Fig. 9). These considerations tend to reinforce the validity of our present three-dimensional results. We note that the comparison with Liu et al (1991) involves a case in which the three-dimensional effects are much stronger than in the comparison with Wong et al (1986). The apparent horizontal speed of the excitation along the shell for SV-waves in the case considered by Liu et al ($\theta_h = 0°$, $\theta_v = 30°$) is $c/\bar{\beta}_1 = 2.0$ while the corresponding apparent speed for the case considered by Wong et al ($\theta_h = 30°$, $\theta_v = 10°$) is 6.65.

NUMERICAL RESULTS FOR A LAYERED MEDIUM

As an example we consider the response of a cylindrical concrete shell of circular cross section embedded in a layered viscoelastic half-space. The shell of external radius $r_o = 2.5\,m$ and thickness $h = 0.25\,m$ is characterized by $E_o = 2.646 \times 10^{10}\,N/m^2$, $\nu_o = 0.167$ and $\rho_o = 2,500\,kg/m^3$. The soil is represented by four viscoelastic layers overlying a viscoelastic half-space. The properties of the model are listed in Table 2. Two locations of the shell are considered. In the first and second cases the centerline of the shell is located at depths $H = 11.5\,m$ ($H/r_o = 4.6$, first layer) and $H = 42\,m$ ($H/r_o = 16.8$, third layer), respectively. Excitations in the form of non-vertically incident P-, SV- and SH-waves ($\theta_v = 30°$) impinging normal ($\theta_h = 90°$) and along ($\theta_h = 0°$) the axis of the shell are considered. All calculations were performed for a frequency of $10\,Hz$ corresponding to a dimensionless frequency $\eta = \omega r_o/\pi\bar{\beta}_5 = 0.098$. The response is normalized by the amplitude A of the incident displacement field at an outcropping with the same properties as the underlying half-space. The normalized amplitudes $U_x = |u_x/A|$, $U_y = |u_y/A|$ and $U_z = |u_z/A|$ on the free-field ground surface ($x = y = z = 0$) in absence of the shell are listed in Table 3.

The response in the two-dimensional case of P-, SV- and SH-waves impinging normal to the axis of the shell ($\theta_h = 90°$) is illustrated in Fig. 11 for $\theta_v = 30°$. The results shown include the amplitudes of the normalized displacements $U_r(r_o)$, $U_\theta(r_o)$ and $U_x(r_o)$ on the interface between the shell and the soil ($r = r_o$) and the amplitudes of the normalized hoop $\Sigma_{\theta\theta}(a)$ and shear $\Sigma_{\theta x}(a)$ stresses on the centerline $r = a$.

Results for the three-dimensional case of non-vertically incident ($\theta_v = 30°$) P, SV and SH-waves impinging along the axis of the shell ($\theta_h = 0°$) are shown in Figs. 12 and 13. The results in Fig. 12 include the amplitudes of the normalized longitudinal $U_x(r_o)$, tangential $U_\theta(r_o)$ and radial $U_r(r_o)$ displacements on the soil-shell interface ($r = r_o$). The results in Fig. 13 include the amplitudes of the normalized logitudinal $\Sigma_{xx}(a)$, tangential (hoop) $\Sigma_{\theta\theta}(a)$ and shear $\Sigma_{\theta x}(a)$ stresses on the centerline of the shell ($r = a$)

CONCLUSIONS

A procedure has been presented to calculate the three-dimensional response of a cylindrical pipeline of infinite length embedded in a layered viscoelastic half-space and subjected to obliquely incident waves. The procedure combines an indirect integral representation for the field in the exterior half-space with a simplified Donnell shell theory for the pipeline or tunnel. The procedure has been tested by comparison with previous solutions for a shell embedded in a uniform half-space. The effects of layering have been illustrated by a set of new numerical results for the two- and three-dimensional response of shells embedded in multilayered media and subjected to P-, SV- and SH-waves.

Comparisons for the particular two-dimensional case of excitation impinging normal to the axis of the shell indicate that the present results are consistent with earlier results of Lee and Trifunac (1979), Balendra et al (1984) and Liu et al (1991) for SH-waves and with those of Datta et al (1983, 1984), Wong et al (1986) and Liu et al (1991) for P- and SV-waves. These comparisons confirm the accuracy of the present approach in the two-dimensional case. In the

three-dimensional case the situation is more controversial. The present results do agree very closely with three-dimensional results for the stresses within the shell presented by Wong et al (1986) but do not agree with the three-dimensional results of Liu et al (1991). However, the present results for the three-dimensional case considered by Liu et al (1991) agree very closely with a second set of results obtained by the authors by use of an hybrid approach (Luco and Barros, 1993b) in which the shell was represented by a finite element model while the exterior region was accounted for by means of an indirect boundary formulation based on moving Greens's functions. The comparisons with the work of Wong et al (1986) and the confirmatory results obtained by a second method suggest that the present approach is also valid in the three-dimensional case.

ACKNOWLEDGMENTS

The work conducted here was supported by a Grant from California Universities for Research in Earthquake Engineering (CUREe) as part of a CUREe-Kajima Project.

Table 1. Normalized Displacement Components for Non-Vertically Incident ($\theta_v = 30°$) P- and SV-Waves Propagating in the Direction of the Axis of a Shell ($\theta_h = 0°$) for Different Numbers of Source (N_s) and Observation (N_o) Points.

Variable	Location	P-Wave (N_o, N_s) (20, 40)	P-Wave (N_o, N_s) (40, 80)	SV-Wave (N_o, N_s) (20, 40)	SV-Wave (N_o, N_s) (40, 80)
U_x ($z = 0$)	$y/r_o = 0$	1.0347	1.0347	3.4015	3.4015
	$y/r_o = \pm 1$	1.0303	1.0303	3.4013	3.4013
	$y/r_o = \pm 3$	1.0036	1.0036	3.4007	3.4007
U_y ($z = 0$)	$y/r_o = \pm 1$	0.0520	0.0520	0.0087	0.0087
	$y/r_o = \pm 3$	1.0216	1.0215	0.0167	0.0167
U_z ($z = 0$)	$y/r_o = 0$	2.0071	2.0070	0.0846	0.0846
	$y/r_o = \pm 1$	1.9884	1.9884	0.0874	0.0873
	$y/r_o = \pm 3$	1.8881	1.8881	0.1093	0.1093
U_x ($r = r_o$)	$\theta = 0°$	0.3565	0.3565	2.0488	2.0487
	$\theta = 45°$	0.6606	0.6606	2.4959	2.4959
	$\theta = 90°$	0.7847	0.7847	2.6699	2.6699
U_θ ($r = r_o$)	$\theta = 0°$	1.2737	1.2737	0.8990	0.8990
	$\theta = 45°$	1.1403	1.1404	0.5430	0.5430
U_r ($r = r_o$)	$\theta = 0°$	0.0239	0.0238	0.2444	0.2446
	$\theta = 45°$	1.2153	1.2153	0.7654	0.7656
	$\theta = 90°$	1.8732	1.8733	0.8865	0.8865
$\Sigma_{\theta\theta}$ ($r = a$)	$\theta = 0°$	10.141	10.140	2.9166	2.9204
	$\theta = 45°$	5.6199	5.6198	3.4289	3.4314
	$\theta = 90°$	1.6686	1.6684	5.4410	5.4436
	$\theta = 270°$	2.0929	2.0921	5.1771	5.1800

Table 2. Properties of the Layered Soil Model.

Medium	H	$\bar{\beta}$	$\bar{\alpha}$	ρ	$\xi_\alpha = \xi_\beta$
	m	m/sec	m/sec	kg/m^3	
1	23	185	827	1,900	0.01
2	11	305	1,304	1,800	0.01
3	16	370	1,428	1,800	0.01
4	28	443	1,478	1,800	0.01
5	∞	510	1,634	1,800	0.01

Table 3. Normalized Amplitudes of Free-Field Displacements on the Ground Surface ($x = y = z = 0$) for NonVertically Incident P-, SV- and SH-waves ($\theta_v = 30°$) for $\theta_h = 90°$ and $\theta_h = 0°$.

Wave	$[\theta_h = 90°]$			$[\theta_h = 0°]$		
	U_x	U_y	U_z	U_x	U_y	U_z
P	0	0.473	3.036	0.473	0	3.036
SV	0	3.366	0.073	3.366	0	0.073
SH	2.870	0	0	0	2.870	0

BIBLIOGRAPHY

Buried Pipelines and Lined Tunnels

1. Mow, C. C. and W. L. McCabe (1963). Dynamic Stresses in an Elastic Cylinder, *Journal of the Engineering Mechanics Division, ASCE,* 89, EM3, 21-41.

2. Mente, L. J. and F. W. L. French (1964). Response of Elastic Cylinders to Plane Shear Waves, *Journal of the Engineering Mechanics Division, ASCE,* 90, EM5, 103-118.

3. Kuesel, T. R. (1969). Earthquake Design Criteria for Subways, *Proc. ASCE,* 95, ST6, 1213-1231.

4. Sakurai, A. and Takahashi (1969). Dynamic Stresses of Underground Pipelines During Earthquakes, *Proc. 4th World Conference on Earthquake Engineering,* Santiago, Chile, January, Vol. 2, B4-81 to B4-96.

5. Duke, C. M. (1971). Damage of Water Supply Systems, *The San Fernando, California Earthquake of Feb. 9,1971, Geological Survey Professional Paper 733,* U.S.G.S. and NOAA, 225-240.

6. King, P. V. and J. M. Betz (1972). Earthquake Damage to a Sewer System, *Journal of Water Pollution Control Federation,* (WPCF), May, 859-867.

7. Aoki, Y. (1973). Seismic Design Spectra for Trench Type Tunnel, *Proc. Japan Society of Civil Engineering,* No. 211.

8. Kubo, K. (1973). Behaviour of Underground Waterpipes During an Earthquake, *Proc. of the Fifth World Conference on Earthquake Engineering,* Roma, Vol. 1, 569-587.

9. NOAA/EERI Subcommittee on Water and Sewerage Systems (1973). Earthquake Damage to Water and Sewer Facilities, San Fernando Earthquake of 1971, *Vol. 2 - Utilities, Transportation and Sociological Aspects,* (Editor: C. M. Murphy), National Oceanic and Atmospheric and Administration, 73-193.

10. Okamoto, S. and C. Tamura (1973). Behavior of Subaqueous Tunnels During Earthquakes, *Earthquake Engineering and Structural Dynamics,* 1, 253-266.

11. Pao, Y. H. and C. C. Mow (1973). *The Diffraction of Elastic Waves and Dynamic Stress Concentration,* Crane and Russak, New York.

12. Richardson, C. B. (1973). Damage to Utilities, The Great Alska Earthquake of 1964 - Engineering, Written by Committee of Alaska Earthquake, National Academy of Science, 1034-1073.

13. Toki, K. and S. Takada (1974). Earthquake Response Analysis of Underground Tubular Structures, *Bulletin of Disaster Prevention Research Institute,* Kyoto University, Vol. 24, June, 107-125.

14. Yeh, G. C. K. (1974). Seismic Analysis of Slender Buried Beams, *Bulletin Seismological Society of America,* 64, 1551-1562.

15. Katayama, T., K. Kubo and N. Sato (1975). Earthquake Damage to Water and Gas Distribution Systems, *Proc. of U.S. National Conference on Earthquake Engineering,* Ann Arbor, Michigan, EERI, 396-405.

16. Newmark, N. M. and W. J. Hall (1975). Pipeline Design to Resist Large Fault Displacement, *Proc. of U.S. National Conference on Earthquake Engineering,* Ann Arbor, Michigan, EERI, 416-425.

17. Parmelee, R. and C. Ludtke (1975). Seismic Soil-Structure Interation of Buried Pipelines, *Proc. of U.S. National Conference on Earthquake Engineering,* Ann Arbor, Michigan, EERI, 406-415.

18. Patel, Y. A., F. L. Cho and A. P. Dimopoulos (1975). Pipeline Designs for Earthquake Zones, *Pipeline and Gas Journal,* December.

19. Tamura, C., S. Okamoto and M. Hamada (1975). Dynamic Behavior of Submerged Tunnel During Earthquakes, *Report of the Institute of Industrial Science,* 24, 169-246.

20. ASME Guide for Gas Transmission and Distribution Piping Systems, New York, 1976.

21. Katayama, T. (1976). Effect of Ground Conditions on Seismic Damage to Buried Pipelines, *Proc. of the U.S.-Japan Seminar on Earthquake Engineering Research with Emphasis onLifeline Systems,* November, Tokyo, 197-210.

22. Narita, K. (1976). Study on Pipeline Failure due to Earthquakes, *Proc. of the U.S.-Japan Seminar on Earthquake Engineering,* (Editors: K. Kubo and P. C. Jennings), 157-176.

23. Popelar, C., A. S. Rosenfield and M. F. Kanninen (1976). Steady State Crack Propagation in Pressurized Pipelines, *ASME Paper No. 76-PVP-7,* September 1976.

24. Kennedy, R. P. and R. A. Williamson (1977). Fault Movement Effects on Buried Oil Pipeline, *Transportation Engineering Journal, ASCE,* 103(TE5), 617-633.

25. Kennedy, R. P., A. C. Darrow and S. A. Short (1977). General Considerations for Seismic Design of Oil Pipeline Systems, Lifeline E. E., The Current State of Knowledge, *Proc. of ASCE Specialty Conference,* Los Angeles, 252-266.

26. Kubo, K., T. Katayama and A. Ohashi (1977). Present State of Lifeline Earthquake Engineering in Japan, Lifeline E. E., The Current State of Knowledge, *Proc. of ASCE Specialty Conference,* Los Angeles, 118-133.

27. Shinozuka, M. and H. Kawakami (1977). Underground Pipe Damages and Ground Characteristics, *Proc. of ASCE Specialty Conference on Lifeline Earthquake Engineering,* Los Angeles, August, 293-307.

28. Shinozuka, M. and H. Kawakami (1977). Ground Characteristics and Free-Field Strains, *Technical Report No. CU-2,* Columbia University.

29. Wang, L. R. L. and M. O'Rourke (1977). State of the Art of Buried Lifeline Earthquake Engineering, *Proc. of the Current State of Lifeline Earthquake Engineering,* ASCE, 252-266.

30. Nelson, I. and P. Weidlinger (1978). Dynamic Seismic Analysis of Long Segmented Lifeliness, *Trans. of ASME, Jopurnal of Pressure Vessel Technology,* Paper No. 78-WA/PVP-4, December, 1-11.

31. Novak, M. and A. Hindy (1978). Dynamic Response of Buried Pipelines, *Proc. of the 6th European Conference on Earthquake Engineering,* Dubrovnik, Yugoslavia, September, 1978 2, 533-540.

32. Sanchez-Sesma, F.J. and J. A. Esquivel (1978). Difracción de Ondas SH por Túnels, *Instituto de Ingenieria , UNAM,* Mexico.

33. Wang, L. and K. Cheng (1978). Seismic Response Behaviour of Buried Pipelines, *ASME Annual Winter Convention,* San Francisco, California, December, 11-15.

34. Ariman, T. and G. E. Muleski (1979). Recent Developments in Seismic Analysis of Buried Pipelines, *Proc. of the U. S. National Congress on Earthquake Engineering,* Stanford University, 643.

35. Ariman, T., S. C. Liu and R. E. Nickell (Eds.) (1979). *Lifeline Earthquake Engineering - Buried Pipelines, Seismic Risk and Instrumentation,* AMES, New York, 285.

36. Constantopoulos, I. V. et al (1979). Dynamic Analysis of Tunnels, *Proc. 3rd Int. Conf. Num. Methods in Geomechanics,* Aachen, Germany, 2, 841-848.

37. Hindy, A. and M. Novak (1979). Earthquake Response of Underground Pipelines, *Earthquake Engineering and Structural Dynamics,* 7, 451-476.

38. Lee, V. W.. and M. D. Trifunac (1979). Stresses and Deformations near Circular Underground Tunnels Subjected to Incident SH-Waves, *J. of the Engineering Mechanics Division, ASCE,* 105, 643-659.

39. Muleski, G. E., T. Ariman and C. P. Auman (1979). A Shell Model of a Buried Pipe in a Seismic Environment, *Journal of Pressure Vessel Technology,* Transaction of the ASME, 101(1), 44-50.

40. Nelson, I. and P. Weidlinger (1979). Dynamic Seismic Response of Long Segmented Lifelines, *Journal of Pressure Vessel Technology,* Transactions of the ASME, 101(1), 10-20.

41. Novak, M. and A. Hindy (1979). Seismic Response of Buried Pipelines, *Proc. of the Third Canadian Conference on Earthquake Engineering,* June, Montreal.

42. O'Rourke, M. and L. R. L. Wang (1979). Earthquake Response of Buried Pipeline, *Proc. of the ASCE Specialty Conference on Earthquake Engineering and Soil Dynamics,* Pasadena, California, June, 720-731.

43. Constantopoulos, I. V. et al (1980). Seismic Analysis of Buried Tunnels, *Proc. 7th World Conf. on Earthquake Engineering,* Istanbul, Turkey, 8, 193-200.

44. Datta, S. K. and N. El-Akily (1980). Seismic Response of a Buried Pipe in an Infinite Medium, paper presented at the *Century 2 ETC Pressure Vessel and Piping Technology Conference,* August 12-15, San Francisco, California.

45. El-Akily, N. and S. K. Datta (1980). Response of Circular Cylindrical Shell to Disturbances in a Half-space, *Earthquake Engineering and Structural Dynamics,* 8, 469-477.

46. Hindy, A. and M. Novak (1980). Response of Pipelines to Random Ground Motion, *Jornal of the Engineering Mechanics Division, ASCE.*

47. Lee, L. H. N., T. Ariman and C. C. Chen (1980). Axisymmetric Buckling of Buried Pipelines by Seismic Excitations, *Technical Report No. 5, ERADUPS Project,* University of Notre Dame, December 1979 and ASME paper No. 80-C2/PVP-75.

48. Novak, M. and A. Hindy (1980). Seismic Analysis of Underground Tubular Structures, *Proc. of the 7th World Conf. on Earthquake Engineering,* Istanbul, Turkey, 8, 287-294.

49. Takada, S. (1980). Seismic Response Analysis of Buried PVC and Ductile Iron Pipelines, *Recent Advances in Lifeline Earthquake Engineering in Japan,* (Editors: H. Shibata, T. Katayama and T. Ariman), ASME, 23-32.

50. Ariman, T. and G. E. Muleski (1981). A Review of the Response of Buried Pipelines under Seismic Excitations, *Earthquake Engineering and Structural Dynamics,* 9, 133.

51. Datta, S. K., A. H. Shah and N. El-Akily (1981). Dynamic Behavior of a Buried Pipe in a Seismic Environment, *Journal of Applied Mechanics,* 49, 141-148.

52. Datta, S. K., A. H. Shah and N. El-Akily (1981). Dynamic Behavior of Embedded Pipelines, in Seismic Risk Analysis and Its Application to Reliability Based Design of Lifeline Systems, *Proc. of Review Meeting of the U.S.-Japan Cooperative Research,* Honolulu, Hawaii, 143-172.

53. El-Akily, N. and S. K. Datta (1981). Response of Circular Cylindrical Shell to Disturbances in a Half-space: Numerical Results, *Earthquake Engineering and Structural Dynamics,* 9, 477-489.

54. Muleski, G. E. (1981). Seismic Response and Fracture of Buried Pipelines, *Ph. D. Dissertation,* submitted to the University of Notre Dame.

55. Parnes, R. and P. Weidlinger (1981). Dynamic Interaction of an Embedded Cylindrical Rod under Axial Harmonic Forces, *Int. Journal of Solids and Structures,* 17, 915-924.

56. Wang, L. R. L. (1981). Seismic Evaluation Model for Buried Lifelines, *Proc. of the Second Specialty Conf. on Lifeline Earthquake Engineering,* ASCE, 335-347.

57. Wang, L. R. L., T. Okubo, E. Kuribayaski, T. Iwasahi and O. Ueda (1981). Lifeline Earthquake Engineering Literatures in Japan, *Technical Report CEE - 8025172, School of Engineering and Environmental Science,* University of Oklahoma, Norman, Oklahoma.

58. Datta, S. K. and A. H. Shah (1982). Dynamic Response of Buried Pipelines and Tunnels,*Earthquake Ground Motion and Its Effects on Structures,* (Editor: S. K. Datta), ASME, New York, 53, 181-197.

59. Christiano, P. P. et al (1983). Response of Buried Tunnels to Earthquake Excitation, *Trans. 7th Int. Conf. Struct. Mech. Reactor Technology,* Vol. K, 287-294.

60. Datta, S. K., T. Chakraborty and A. H. Shah (1983). Dynamic Responses of Pipelines to Moving Loads, *Earthquake Behavior and Safety of Oil and Gas Storage Facilities, Buried Pipelines and Equipment,* (Editor: T. Ariman), ASME, New York, 77, 246.

61. Datta, S. K., A. H. Shah and K. C. Wong (1983). Dynamic Amplification of Stresses and Displacements Induced in a Buried Pipe in a Semi-Infinite Medium, *Technical Report CUMER-83-3, Dept. of Mechanical Engineering,* University of Colorado, Boulder, Colorado.

62. Muleski, G. E. and T. Ariman (1983). Improved Seismic Input and Soil Models and Quasi-Static Approximation in Buried Pipes, *Earthquake Behavior and Safety of Oil and Gas Storage Facilities, Buried Pipelines and Equipment,* (Editor: T. Ariman), ASME, New York, 77, 202-208.

63. Wang, L. R. L. (1983). Role and Development of Soil Parameters for Seismic Response of Buried Lifelines, *Earthquake Behavior and Safety of Oil and Gas Storage Facilities, Buried Pipelines and Equipment,* (Editor: T. Ariman), ASME, New York, 77, 312-323.

64. Balendra, T., D. P. Thambiratnam, C. G. Koh and S-L Lee (1984). Dynamic Response of Twin Circular Tunnels due to Incident SH-Waves, *Earthquake Engineering and Structural Dynamics,* 12, 181-201.

65. Datta, S. K., P. M. O'Leary and A. H. Shah (1984). Dynamic Responses of Buried Pipelines to Incident Longitudinal and Shear Waves, *Technical Report CUMER-84-3, Dept. of Mechanical Engineering,* University of Colorado, Boulder, Colorado.

66. Datta, S. K., A. H. Shah and K. C. Wong (1984). Dynamic Stresses and Displacements in Buried Pipe, *Journal of Engineering Mechanics,* 110(10), 1451-1466.

67. Franssens, G. R. and P. E. Lagasse (1984). Scattering of Elastic Waves by Cylindrical Obstacles, *Journal of the Acoustical Society of America,* 76, 1535-1542.

68. Gómez-Massó, A. and I. Atalla (1984). Finite Element versus Simplified Methods in the Seismic Analysis of Underground Structures, *Earthquake Engineering and Structural Dynamics,* 12, 347-367.

69. Wong, K. C., A. H. Shah, S. K. Datta and P. M. O'Leary (1984). Dynamic Amplification of Displacements and Stresses around Buried Pipelines and Tunnels,*Earthquake Source Modeling, Ground Motion and Structural Response,* (Editor: S. K. Datta), ASME, New York, 80, 147-161.

70. Datta, S. K., P. M. O'Leary and A. H. Shah (1985). Three-Dimensional Dynamic Response of Buried Pipelines to Incident Longitudinal and Shear Waves, *Journal of Applied Mechanics,* 52(4), 919-926.

71. Muleski, G. E. and T. Ariman (1985). A Shell Model for Buried Pipes in Earthquakes, *Soil Dynamics and Earthquake Engineering,* 4(1), 43-51.

72. O'Leary, P. M. and S. K. Datta (1985). Dynamic Response of a Buried Pipeline at Low Frequencies, *ASME Journal of Pressure Vessel Technology,* 107, 44-50.

73. O'Leary, P. M. and S. K. Datta (1985). Dynamics of Buried Pipelines, *Soil Dynamics and Earthquake Engineering,* 4, 151-159.

74. Wong, K. C., A. H. Shah and S. K. Datta (1985). Dynamic Stresses and Displacements in a Buried Tunnel, *Journal of Engineering Mechanics,* 111(2), 218-234.

75. Wong, K. C., S. K. Datta and A. H. Shah (1986). Three Dimensional Motion of a Buried Pipeline I. Analysis, *Journal of Engineering Mechanics,* 112(12), 1319-1338.

76. Wong, K. C., A. H. Shah and S. K. Datta (1986). Three Dimensional Motion of a Buried Pipeline II. Numerical Results, *Journal of Engineering Mechanics,* 112(12), 1338-1345.

77. Chin, Y. F., R. K. N. D. Rajapakse, A. H. Shah and S. K. Datta (1987). Dynamics of Buried Pipes in Back-Filled Trench, *Soil Dynamics and Earthquake Engineering,* 6, 158-163.

78. Singh, V. P., P. C. Upadhyay and B. Kishor (1987). On the Dynamic Response of Buried Orthotropic Cylindrical Shells, *Journal of Sound and Vibrations,* 113(1), 101-115.

79. Singh, V. P., P. C. Upadhyay and B. Kishor (1987). A Comparison of Thick and Thin Shell Theory Results for Buried Orthotropic Cylindrical Shells, *Journal of Sound and Vibrations,* 119(2), 339-345.

80. Liu, S. W., K. R. Khair and A. H. Shah (1988). Three Dimensional Dynamics of Pipelines Buried in Back-Filled Trenches due to Oblique Incidence of Body Waves, *Technical Report CUMER-88-4, Dept. of Mechanical Engineering,* University of Colorado, Boulder, Colorado.

81. Upadhyay, P. C. and B. K. Mishra (1988). Non-Axisymmetric Dynamic Response of Buried Orthotropic Cylindrical Shells, *Journal of Sound and Vibrations,* 121(1), 149-160.

82. Upadhyay, P. C. and B. K. Mishra (1988). Non-Axisymmetric Dynamic Response of Buried Orthotropic Cylindrical Shell Due to Incident Shear Waves, *Journal of Sound and Vibrations,* 125(2), 227-239.

83. Dwivedi, J. P. and P. C. Upadhyay (1989). Effect of Imperfect Bonding on the Axisymmetric Dynamic Response of Buried Orthotropic Cylindrical Shells, *Journal of Sound and Vibrations,* 135(3), 477-486.

84. Hadley, P. K., A. Askar and A. S. Cakmak (1989). Scattering of Waves by Inclusions in a Nonhomogeneous Elastic Half Space Solved by Boundary Element Methods, *NCEER-89-0027, National Center for Earthquake Research,* State University of New York at Buffalo,Vol 1.

85. Chen, H. L., S. P. Shah and L. M. Keer (1990). Dynamic Response of Shallow-Buried Cylindrical Structures, *Journal of Engineering Mechanics,* 116(1), 152-171.

86. Dwivedi, J. P. and P. C. Upadhyay (1990). Effect of Fluid Presence on the Dynamic Response of Imperfectly Bonded Buried Orthotropic Cylindrical Shells, *Journal of Sound and Vibrations,* 139(1), 99-110.

87. Balendra,T., C. G. Koh and Y. C. Ho (1991). Dynamic Response of Buildings due to Trains in Underground Tunnels, *Earthquake Engineering and Structural Dynamics,* 20, 275-291.

88. Dwivedi, J. P. and P. C. Upadhyay (1991). Effect of Imperfect Bond on the Dynamic Response of Buried Orthotropic Cylindrical Shells under Shear-Wave Excitation, *Journal of Sound and Vibrations,* 145(2), 333-337.

89. Liu, S. W., K. R. Khair and A. H. Shah (1991). Three Dimensional Dynamics of Pipelines Buried in Backfilled Trenches due to Oblique Incidence of Body Waves, *Soil Dynamics and Earthquake Engineering,* 10(4), 182-191.

90. Cheung, Y. K. and J. X. Zhu (1992). Dynamic Interaction Analysis of a Circular Cylindrical Shell of Finite Length in a Half-Space, *Earthquake Engineering and Structural Dynamics,* 21, 799-809.

91. Chua, K. H., T. Balendra and K. W. Lo (1992). Groundborne Vibrations due to Trains in Tunnels, *Earthquake Engineering and Structural Dynamics,* 21, 445-460.

92. Dwivedi, J. P., B. K. Mishra and P. C. Upadhyay (1992). Non-Axisymmetric Dynamic Response of Imperfectly Bonded Buried Orthotropic Pipelines Due to an Incident Shear Wave, *Journal of Sound and Vibrations,* 157(1), 81-92.

93. Navarro, C. (1992). Seismic Analysis of Underground Structures, *Proc. Tenth World Conf. on Earthquake Engineering,* Madrid, Spain, 3, 1939-1944.

94. Penzien, J., C. H. Chen, Y. J. Lee and W. Y. Jean (1992). Seismic Analysis of Retangular Tunnels in Soft Ground, *Proc. Tenth World Conf. on Earthquake Engineering,* Madrid, Spain, 3, 1619-1624.

95. Luco, J. E. and F. C. P. de Barros (1994). Seismic Response of a Cylindrical Shell Embedded in a Layered Viscoelastic Half-Space. I: Formulation, *Earthquake Engineering and Structural Dynamics,* 23, 553-567.

96. Barros, F. C. P. de and J. E. Luco (1994a). Seismic Response of a Cylindrical Shell Embedded in a Layered Viscoelastic Half-Space. II: Validation and Numerical Results, *Earthquake Engineering and Structural Dynamics,* 23, 569-580.

97. Luco, J. E. and F. C. P. de Barros (1993). Three-Dimensional Response of a Cylindrical Tunnel Embedded in a Layered Medium, (*to be submitted for publication*).

Additional References

1. Barros, F. C. P. de and J. E. Luco (1992). Moving Green's Functions for a Layered Viscoelastic Half-Space, *Report, Dept. of Appl. Mech. & Engng. Sci.*, University of California, San Diego, La Jolla, California, 210 pp.

2. Barros, F. C. P. de and J. E. Luco (1994b). Response of a Layered Viscoelastic Half-Space to a Moving Point Load, *Wave Motions,* 19, 189-210.

3. Donnell, L. H. (1933). Stability of Thin Walled Tubes under Torsion, *NACA Report, No. 479.*

4. Luco, J. E. and F. C. P. de Barros (1993). On the Appropriate Depth Dependence for Plane Waves Reflected in a Viscoelastic Half-Space, (accepted for publication).

5. Luco, J. E. and H. L. Wong (1987). Seismic Response of Foundations Embedded in a Layered Half-Space, *Earthquake Engineering and Structural Dynamics,* 15(2), 233-247.

6. Luco, J. E., H. L. Wong and F. C. P. de Barros (1990). Three-Dimensional Response of a Cylindrical Canyon in a Layered Half-Space, *Earthquake Enginnering and Structural Dynamics,* 19(6), 799-817.

7. Zhang, L. and A. K. Chopra (1991). Three-Dimensional Analysis of Spatially Varying Ground Motion around a Uniform Canyon in a Homogeneous Half-Space, *Earthquake Engineering and Structural Dynamics,* 20, 911-926.

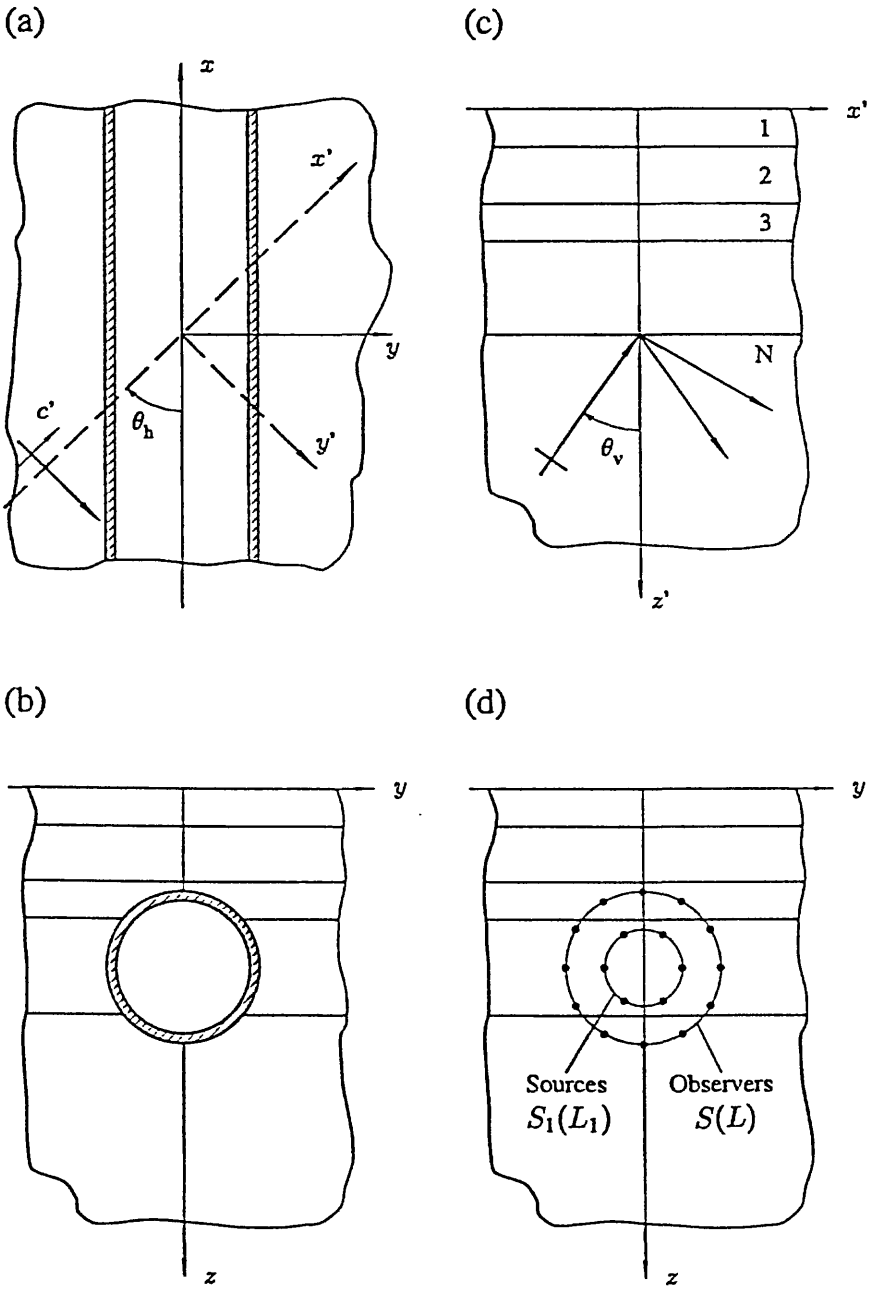

Figure 1. Schematic Representation of Cylindrical Shell Embedded in a Layered Half-Space. (a) Top view showing horizontal angle of incidence, (b) Cross section, (c) Free-field model showing vertical angle of incidence and (d) Location of sources and observers.

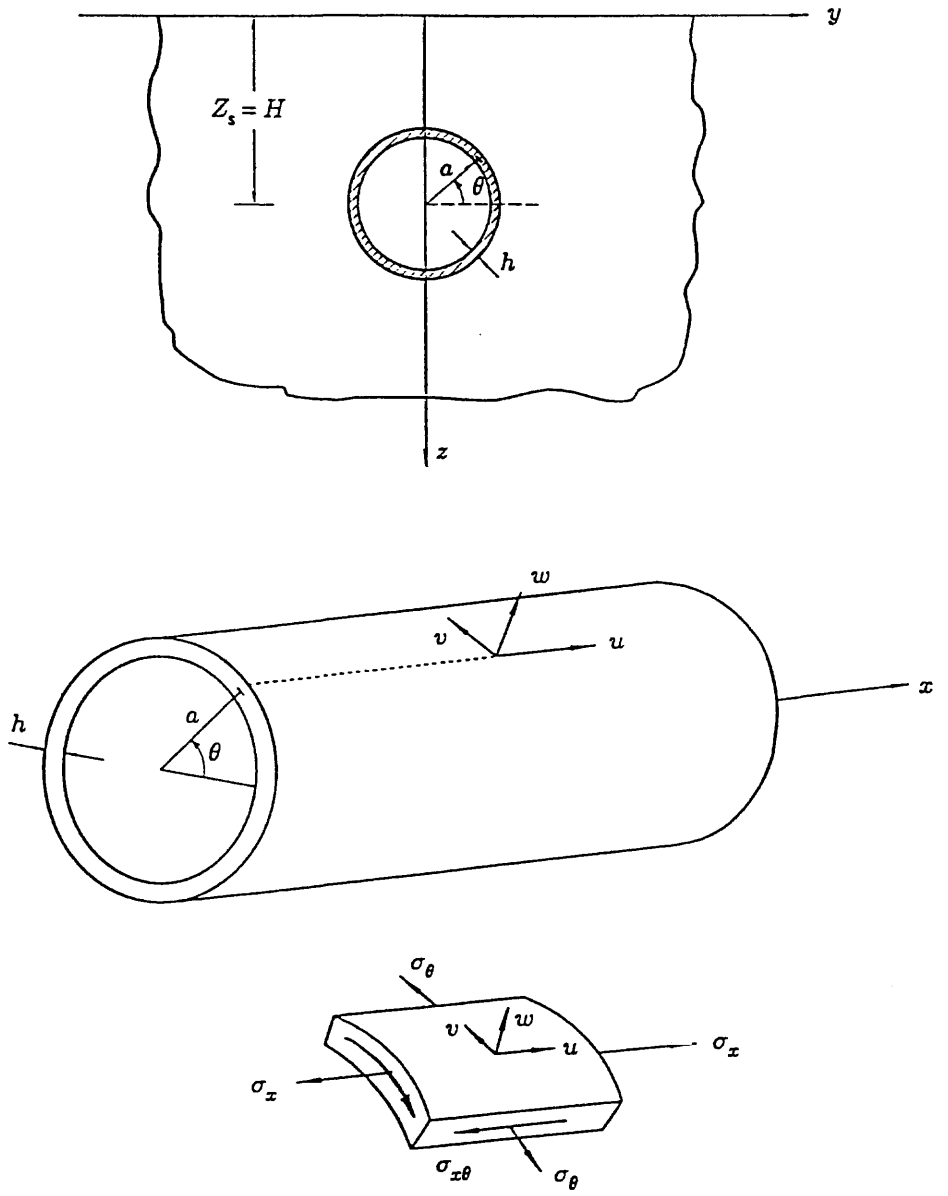

Figure 2. Schematic Representation of Shell Showing Local Coordinates.

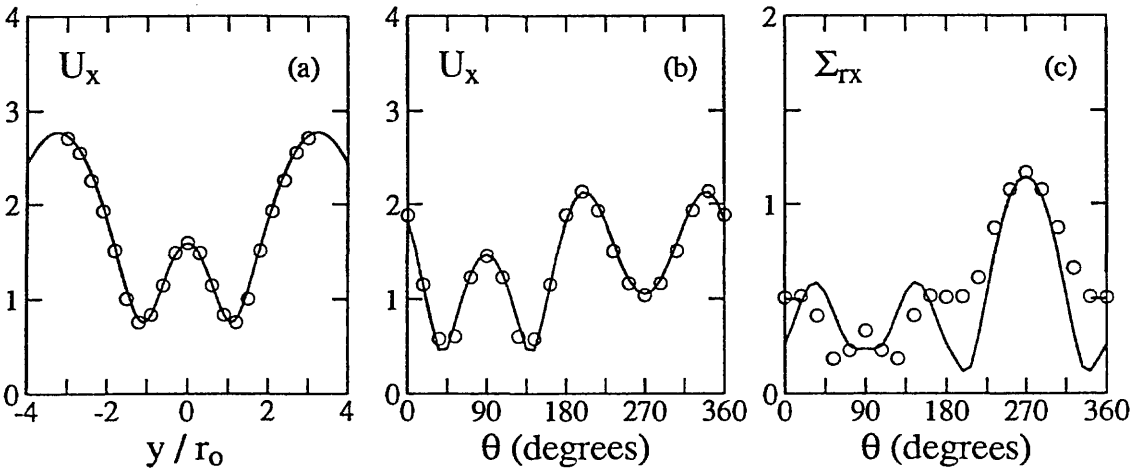

Figure 3. (a) Normalized Longitudinal Displacement U_x on the Ground Surface $z = 0$, (b) Normalized Displacement U_x on the Soil-Shell Interface $r = r_o$ and (c) Normalized Longitudinal Shear Stress Σ_{rx} on $r = r_o$ for a Vertically Incident SH-Wave ($\theta_h = 90°$, $\theta_v = 0°$) Impinging on a Shell ($h = 0.1r_o$) Embedded to a Depth $H = 1.5r_o$ in a Uniform Half-Space. Present results are shown with solid lines; the results of Lee and Trifunac (1979) are shown with open circles. In Fig. 2c the results of Lee and Trifunac have been divided by a factor of six ($\eta = 0.5$).

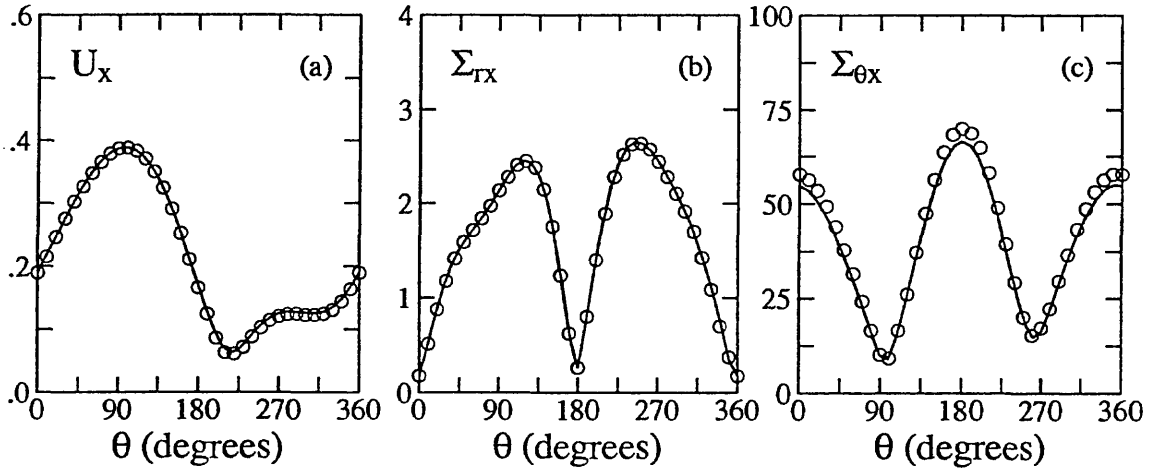

Figure 4. (a) Normalized Longitudinal Displacement U_x at $r = r_o$, (b) Tangential Stress Σ_{rx} at $r = r_o$ and (c) Shear Stress $\Sigma_{\theta x}$ at $r = r_i$ for a Nonvertically Incident SH-Wave ($\theta_v = 30°$) Impinging Normal ($\theta_h = 90°$) to a Shell ($h = 0.1r_o$) Embedded to a Depth $H = 2.5r_o$ in a Uniform Half-Space. Present results are shown with solid lines, those of Balendra et al (1984) are shown with open circles ($\eta = 0.245$).

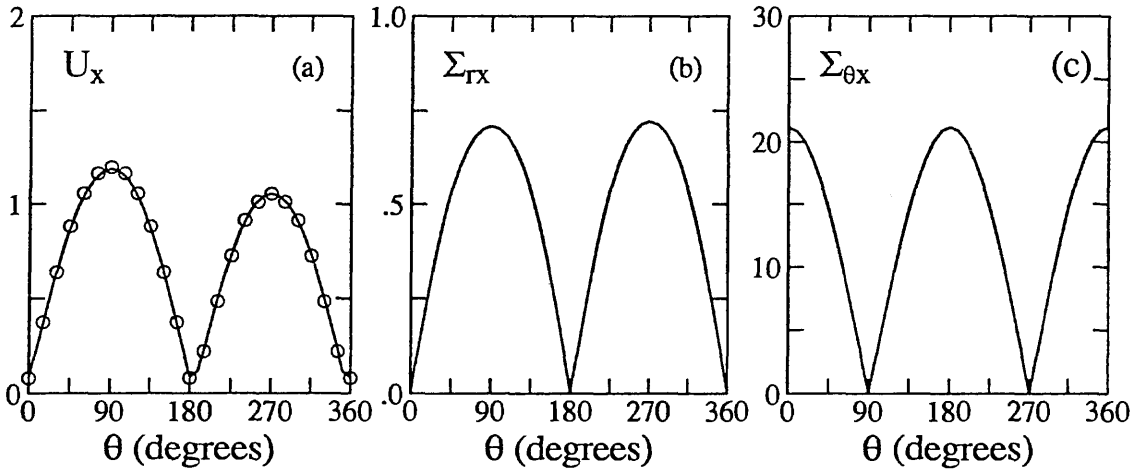

Figure 5. (a) Normalized Longitudinal Displacement U_x at $r = r_o$, (b) Tangential Stress Σ_{rx} at $r = r_o$ and (c) Shear Stress $\Sigma_{\theta x}$ at $r = r_i$ for a Vertically Incident SH-Wave ($\theta_v = 0°$) Impinging Normal ($\theta_h = 90°$) to a Shell ($h = 0.0909r_o$) Embedded to a Depth $H = 4.545r_o$ in a Uniform Half-Space. Present results are shown with solid lines, those of Liu et al (1991) are shown with open circles ($\eta = 0.105$).

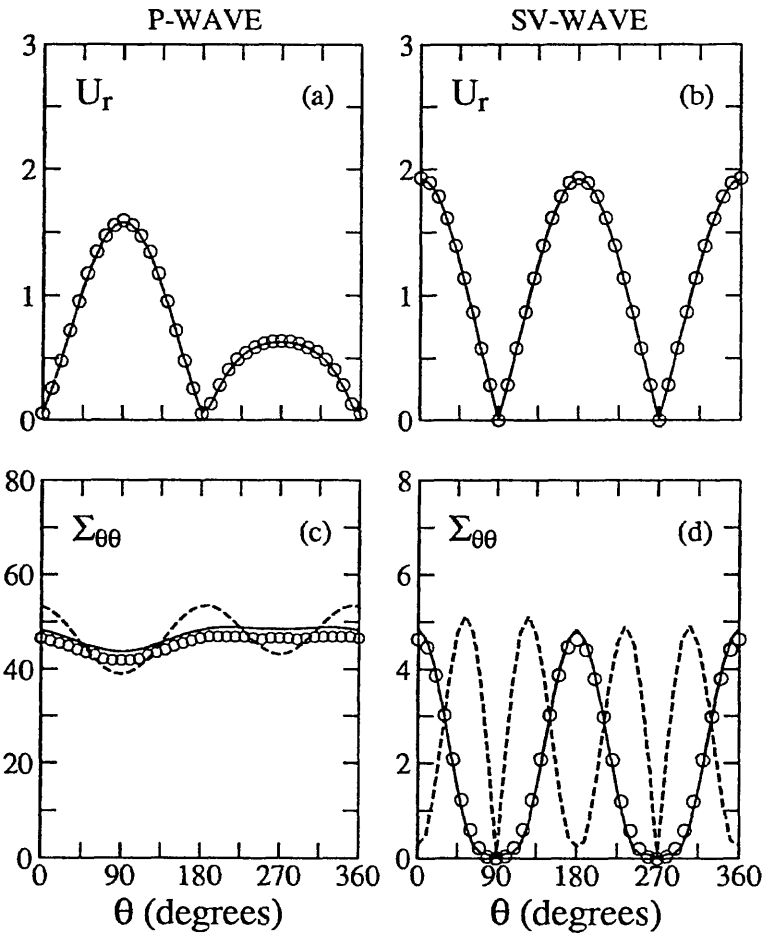

Figure 6. (a), (b) Normalized Radial Displacements U_r at $r = r_o$ and (c), (d) Normalized Hoop Stresses $\Sigma_{\theta\theta}$ at $r = r_o$ (solid lines) and $r = a$ (segmented lines) for Vertically Incident ($\theta_v = 0°$) P- and SV-Waves Impinging Normal ($\theta_h = 90°$) to a Shell ($h = 0.0909r_o$) Embedded to a Depth $H = 7.573r_o$ in a Uniform Half-Space. Present results are shown with solid lines or segmented lines, results of Datta et al (1983) are shown with open circles ($\eta = 0.132$).

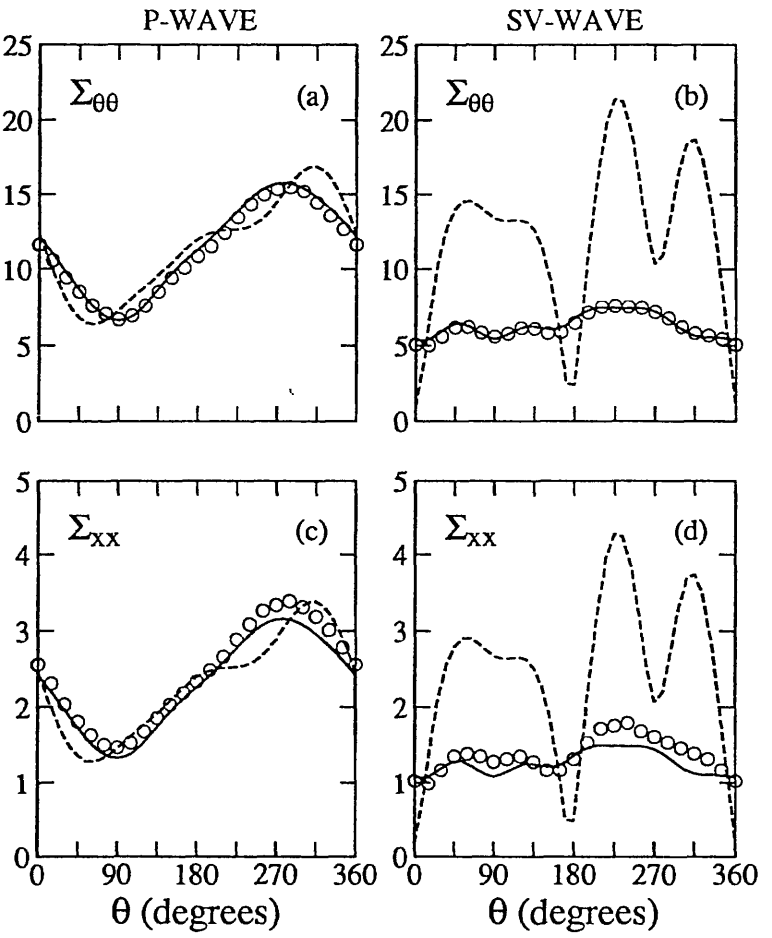

Figure 7. (a), (b) Normalized Hoop Stresses $\Sigma_{\theta\theta}$ at $r = r_o$ (solid lines) and $r = a$ (segmented lines) and (c), (d) Normalized Longitudinal Stresses Σ_{xx} at $r = r_o$ (solid lines) and $r = a$ (segmented lines) for Nonvertically Incident ($\theta_v = 10°$) P- and SV-Waves Impinging Normal ($\theta_h = 90°$) to a Shell ($h = 0.0909r_o$) Embedded to a Depth $H = 1.818r_o$ in a Uniform Half-Space. Present results are shown with solid lines or segmented lines, results of Wong et al (1986) for $r = r_o$ are shown with open circles ($\eta = 0.132$).

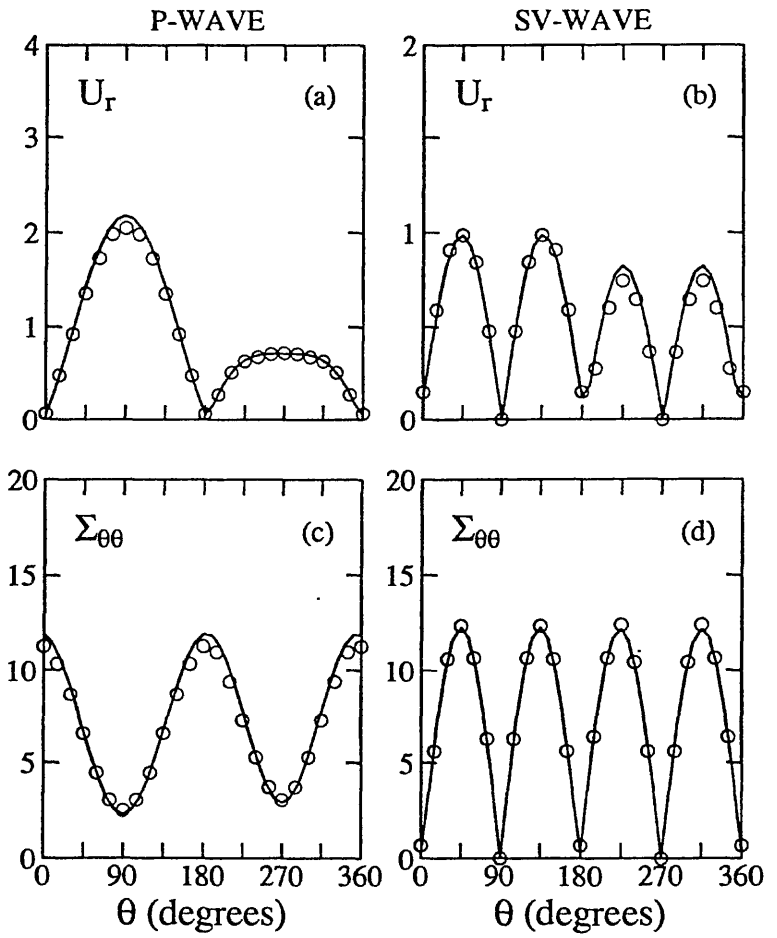

Figure 8. (a), (b) Normalized Radial Displacements U_r at $r = r_o$ and (c), (d) Normalized Hoop Stresses $\Sigma_{\theta\theta}$ at $r = a$ for Vertically Incident ($\theta_v = 0°$) P- and SV-Waves Impinging Normal ($\theta_h = 90°$) to a Shell ($h = 0.0909r_o$) Embedded to a Depth $H = 4.545r_o$ in a Uniform Half-Space. Present results are shown with solid lines; the results of Liu et al (1991) are shown with open circles ($\eta = 0.105$).

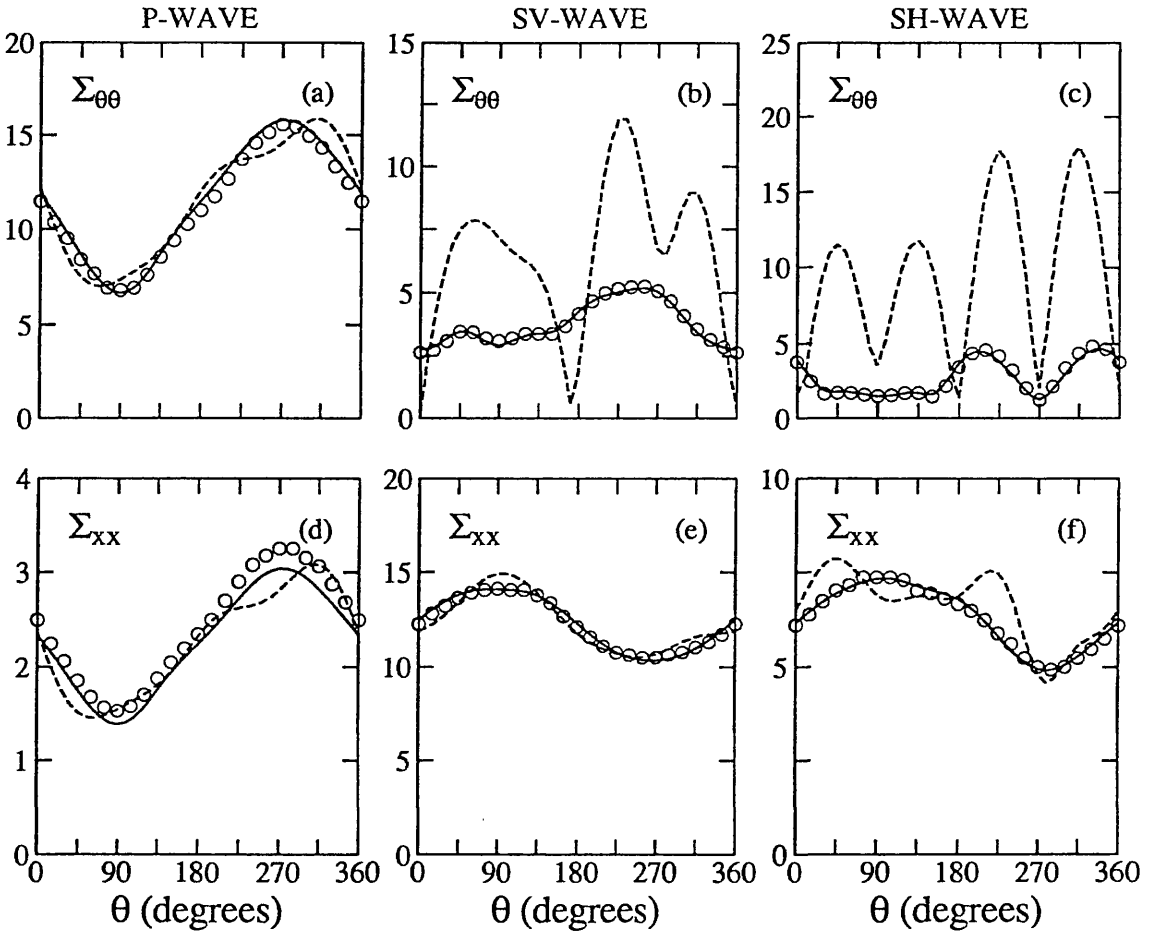

Figure 9. (a), (b), (c) Normalized Hoop Stresses and (d), (e), (f) Normalized Axial Stresses Σ_{xx} for Nonvertically Incident ($\theta_v = 10°$) P- ,SV- and SH-Waves Impinging Obliquely ($\theta_h = 30°$) on a Shell ($h = 0.0909r_o$) Embedded to a Depth $H = 1.818r_o$ in a Uniform Half-Space. The present results at $r = r_o$ are shown with solid lines while those at $r = a$ are shown with segmented lines. The results of Wong et al (1986) at $r = r_o$ are shown with open circles ($\eta = 0.132$).

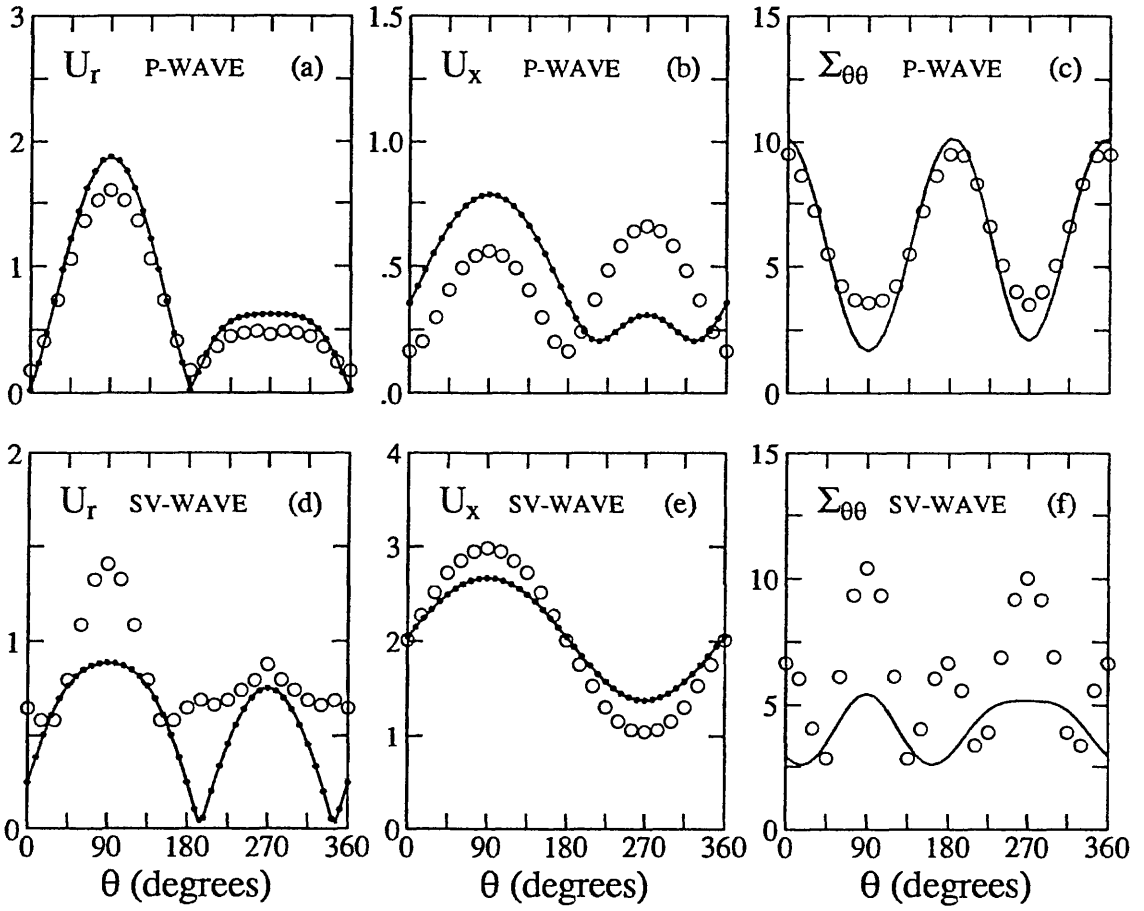

Figure 10. (a), (d) Normalized Radial Displacements U_r at $r = r_o$, (b), (e) Normalized Axial Displacement U_x at $r = r_o$ and (c), (f) Normalized Hoop Stresses $\Sigma_{\theta\theta}$ at $r = a$ for Nonvertically Incident ($\theta_v = 30°$) P- and SV-Waves Impinging with Angle $\theta_h = 0°$ on a Shell ($h = 0.0909r_o$) Embedded to a Depth $H = 4.545r_o$ in a Uniform Half-Space. Present results are presented by solid lines (DT/IBF) and solid dots (FE/IBF). The results of Liu et al (1991) are shown with open circles ($\eta = 0.105$).

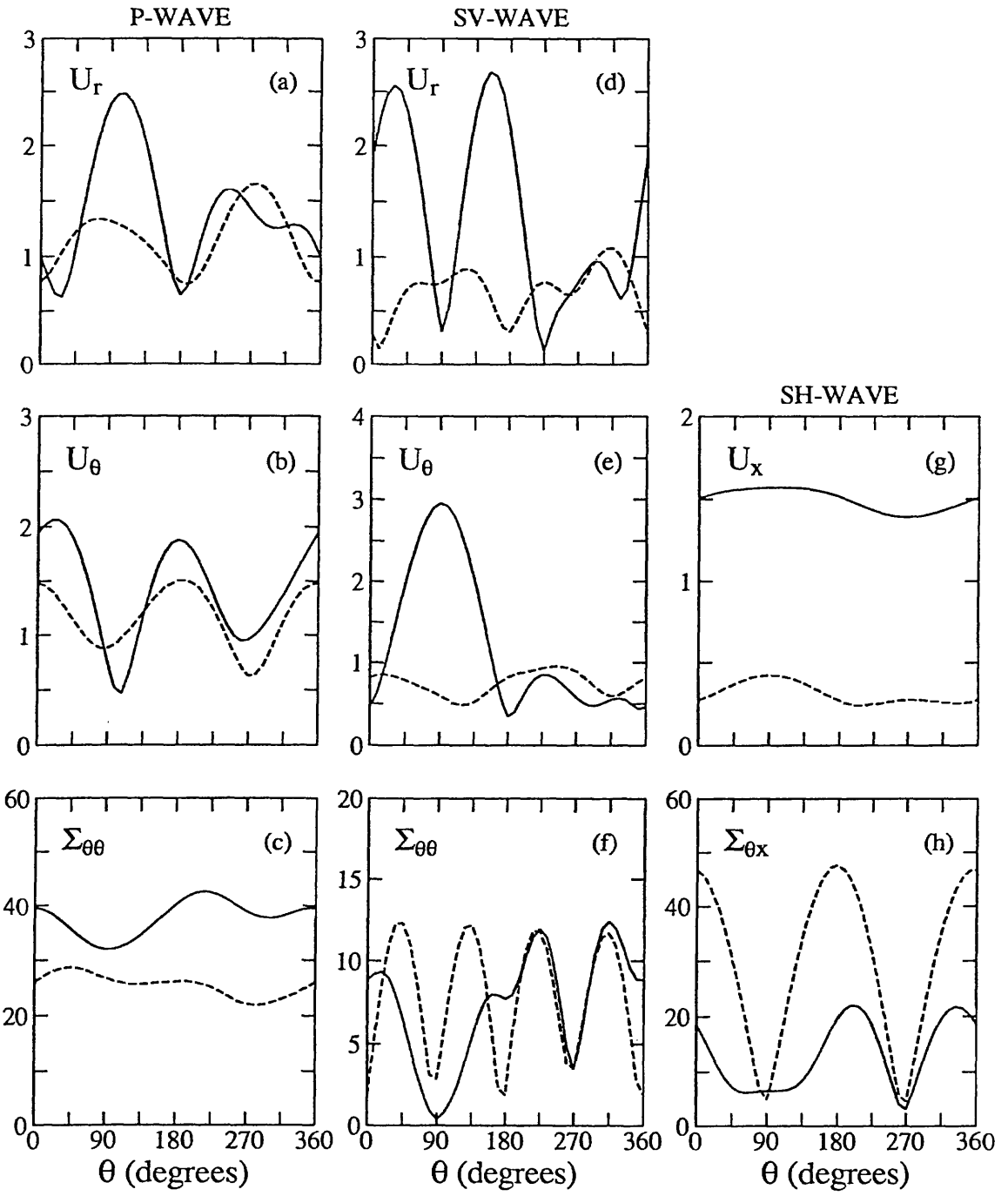

Figure 11. Normalized Radial U_r, Tangential U_θ, and Longitudinal U_x Displacements at $r = r_o$ and, Hoop Stresses $\Sigma_{\theta\theta}$ and Shear Stresses $\Sigma_{\theta x}$ at $r = a$ for Nonvertically Incident P-, SV- and SH-Wave ($\theta_v = 30°$) Impinging Normal ($\theta_h = 90°$) to a Shell ($h = 0.1r_o$) Embedded to Depths $H/r_o = 4.6$ (segmented lines) and 16.8 (solid lines) in a Multilayered Half-Space ($\eta = 0.098$).

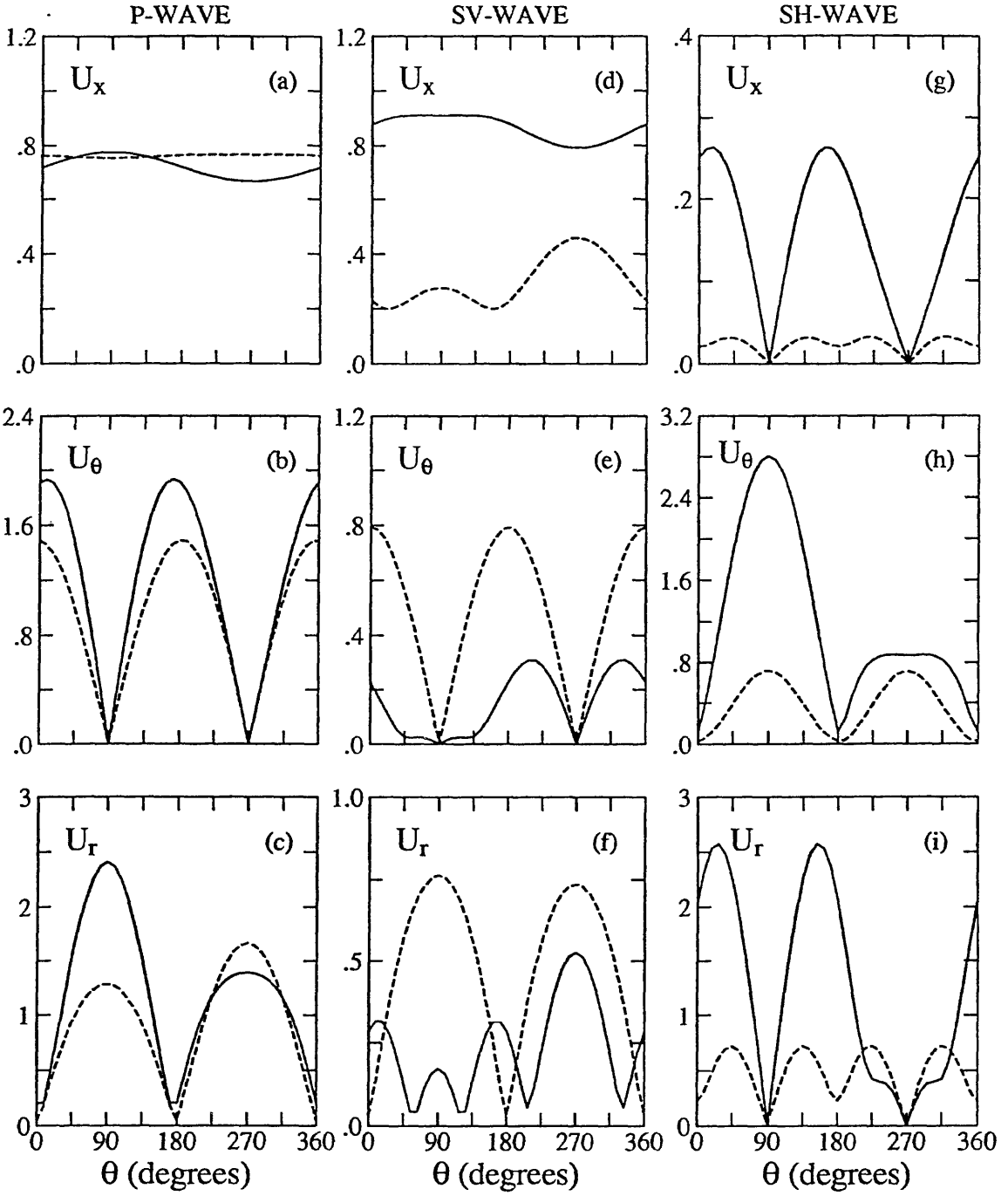

Figure 12. Normalized Longitudinal U_x, Tangential U_θ, and Radial U_r Displacements at $r = r_o$ for Nonvertically Incident ($\theta_v = 30°$) P-, SV- and SH-Wave Impinging with Angle $\theta_h = 0°$ on a Shell ($h = 0.1r_o$) Embedded to Depths $H/r_o = 4.6$ (segmented lines) and 16.8 (solid lines) in a Multilayered Half-Space ($\eta = 0.098$).

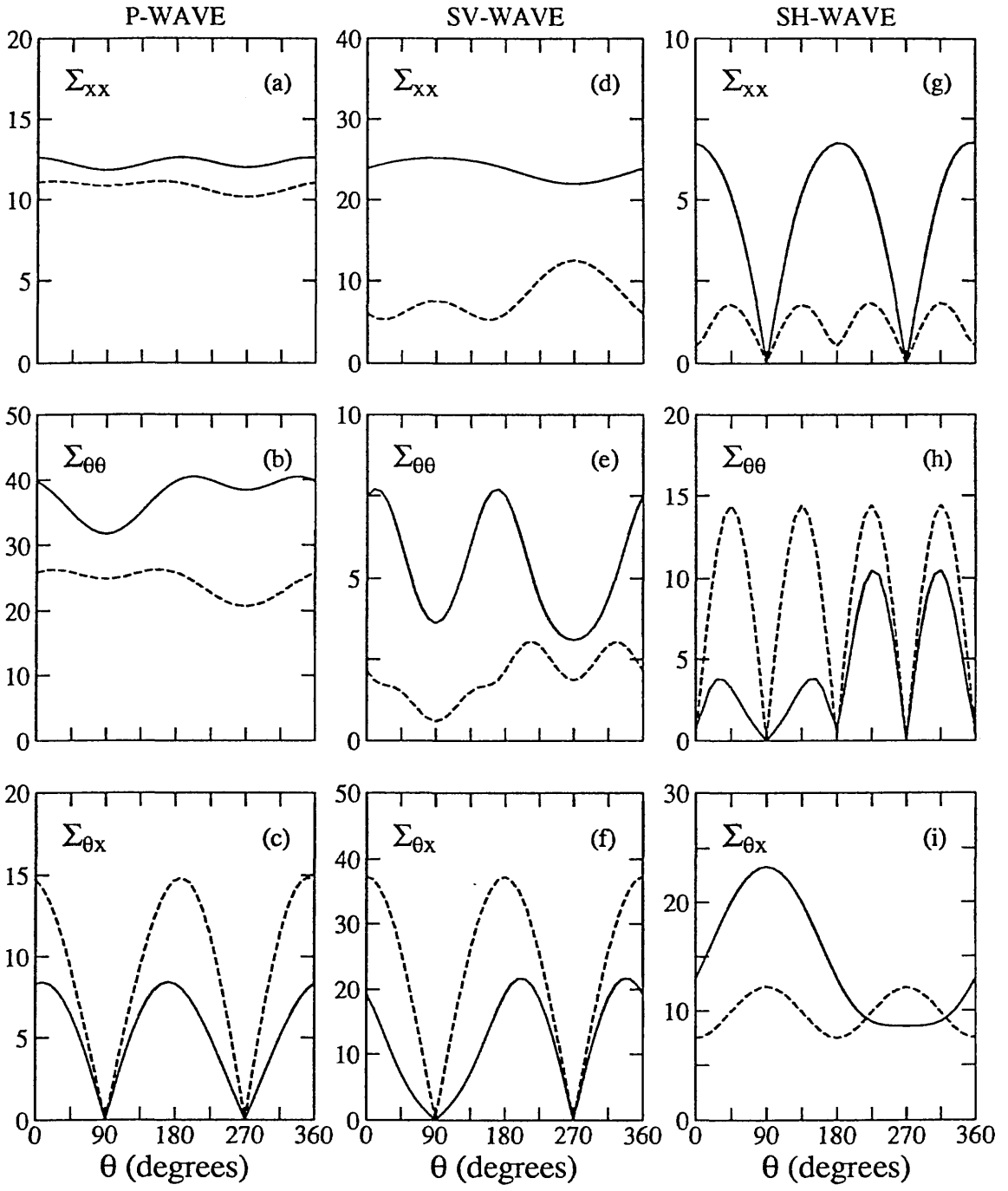

Figure 13. Normalized Axial Σ_{xx}, Hoop $\Sigma_{\theta\theta}$, and Shear $\Sigma_{\theta x}$ Stresses for Nonvertically Incident ($\theta_v = 30°$) P-, SV- and SH-Wave Impinging with Angle $\theta_h = 0°$ on a Shell ($h = 0.1r_o$) Embedded to Depths $H/r_o = 4.6$ (segmented lines) and 16.8 (solid lines) in a Multilayered Half-Space ($\eta = 0.098$).